

THE JOURNAL OF PHYSICAL CHEMISTRY

(Registered in U. S. Patent Office)

CONTENTS

SYMPOSIUM ON RECENT ADVANCES IN THE STUDY OF CONTACT CATALYSIS San Francisco, Calif., April 14-18, 1958

A Symposium Honoring Professor Paul H. Emmett, Recipient of the Kendall Award in Colloid Chemistry, American Chemical Society

Paul H. Emmett: Adsorption and Catalysis	449
Terrell L. Hill: Relations between Different Definitions of Physical Adsorption	456
J. T. Kummer: The Chemisorption of Oxygen on Silver	460
J. N. Wilson, H. H. Voge, D. P. Stevenson, A. E. Smith and L. T. Atkins: Physical Techniques in the Study of Silver Catalysts for Ethylene Oxidation	463
Robert Gomer: Adsorption and Diffusion of Argon on Tungsten	468
T. J. Gray, C. C. McCain and N. G. Masse: Defect Structure and Catalysis in the TiO ₂ System (Semi-conducting and Magnetic Properties)	472
A. I. M. Keulemans and H. H. Voge: Reactivities of Naphthenes over a Platinum Reforming Catalyst by a Gas Chromatographic Technique	476
Ralph A. Beebe and Eric R. Camplin: Heats of Adsorption of Hydrogen on a Singly Promoted Iron Catalyst	480
D. S. MacIver, R. C. Zabor and P. H. Emmett: The Adsorption of Normal Olefins on Silica-Alumina Catalysts	484
R. G. Haldeman and M. C. Botty: On the Nature of the Carbon Deposit of Cracking Catalysts	489
J. F. Shultz, M. Abelson, K. C. Stein and R. B. Anderson: Studies of the Fischer-Tropsch Synthesis. XVIII. Influence of Catalyst Geometry on Synthesis on Iron Catalysts	496
Harold W. Kohn and Ellison H. Taylor: The Effect of Ionizing Radiation upon γ -Al ₂ O ₃ as a Catalyst for H ₂ -I ₂ Exchange	500
Francis J. Cheselske, W. E. Wallace and W. Keith Hall: The Exchange of Deuterium Gas with the Hydrogen Associated with Solid Catalysts. I. The Model Tantalum-Hydrogen System	505
Harold L. Pickering and Hartley C. Eckstrom: Heterogeneous Reaction Studies by Infrared Absorption	512
M. V. C. Sastri, T. S. Viswanathan and T. S. Nagarajan: The Influence of a Chemisorbed Layer of Carbon Monoxide on Subsequent Physical Adsorption	518
D. S. Villars: A Method of Successive Approximations for Computing Combustion Equilibria on a High Speed Digital Computer	521
Reuben E. Wood: Experiments with the Cell Bi, Bi ₂ O ₃ , ZnCl ₂ /ZnCl ₂ /ZnCl ₂ , Zn between 450 and 510°	525
P. H. Lewis: Structure and Gas Adsorption Sites of a Synthetic Zeolite Determined by Fourier Radial Analysis	527
D. P. Ames, R. R. Irani and C. F. Callis: The Agreement between Independent Methods for Particle Size Distribution Measurements on Finely Divided Powders Including Phosphates	531
Graham Williams: The Measurement of Dielectric Constant and Loss Factor of Liquids and Solutions between 250 and 920 Mc./s. by Means of a Coaxial Transmission Line	534
Graham Williams: The Evaluation of Dielectric Data for Liquids and Solutions	537
John R. Lotz, B. P. Block and W. Conrad Fernelius: A Thermodynamic Study of some Coordination Compounds of Metal Ions with Amines Containing Oxygen	541
R. Nelson Smith, James Swinehart and David Lesnini: The Oxidation of Carbon by Nitric Oxide	544
Richard N. Work: A Convenient New Form of Onsager's Equation for the Dielectric Constant of Polar Solutions	548
D. Stüger and Terrell L. Hill: Theory of the Donnan Membrane Equilibrium. II. Calculation of the Osmotic Pressure and of the Salt Distribution in a Donnan System with Highly Charged Colloid Particles	551
J. H. Stern and N. W. Gregory: Vaporization Characteristics of <i>p</i> -Dibromobenzene	556
R. N. Sen Sarma, Edward Anders and J. M. Miller: Deviations from Plate Theory in the Ion-exchange Separation of Technetium and Rhenium	559
H. J. Bernstein: The Effect of Adjacent Bonds on Bond Distances in Hydrocarbons	565
Robert E. Connick and Richard E. Pouison: F ¹⁹ Nuclear Magnetic Resonance of Various Metal-Fluoride Complexes in Aqueous Solution	568
Donald G. Miller: Ternary Isothermal Diffusion and the Validity of the Onsager Reciprocity Relations	570
M. E. Milberg: Carbon Formation in an Acetylene-Air Diffusion Flame	578
Donald A. Pitt and Charles P. Smyth: Microwave Absorption and Molecular Structure in Liquids. XXVI. The Dielectric Relaxation Times of Two Large Oblate Ellipsoidal Molecules in Benzene Solution	582
B. D. Pollock: Dissociation Pressure and Stability of Beryllium Carbide	587
J. Rex Goates, Ralph J. Sullivan and J. Bevan Ott: Heats of Mixing in the System Carbon Tetrachloride-Cyclohexane-Benzene	589
A. C. Makrides and Norman Hackerman: Heats of Immersion. I. The System Silica-water	594
N. W. Taylor, H. F. Zobel, N. N. Hellman and F. R. Senti: Effect of Structure and Crystallinity on Water Sorption of Dextrans	599
Robert G. Charles and Alois Langer: Heat Stabilities and Volatilities of Some Metal Chelates Derived from 3-Hydroxyquinoline	603
Mary F. Koehler and J. P. Coughlin: Heats of Formation of Ferrous Chloride, Ferric Chloride and Manganous Chloride	605
S. V. R. Mastrangelo: Equation of Solubility of Non-electrolytes which Possess a Specific Interaction	608
Peter J. Dunlop: Data for Diffusion in Concentrated Solution of the System NaCl-KCl-H ₂ O at 25°: A Test of the Onsager Reciprocal Relation for this Composition	612
John A. Perri, Ira Binder and Ben Post: Rare Earth "Disilicides"	616
A. W. Czanderna and J. M. Hong: Interaction of Oxygen with Titanium Dioxide	620
Richard F. Porter and Richard C. Schoonmaker: A Mass Spectrometric Study of the Vaporization of Ferrous Bromide	626
M. J. Kronman and Serge N. Timasheff: Light Scattering Investigation of Ordering Effects in Silicotungstic Acid Solutions	629
Raymond M. Fuoss: The Velocity Field in Electrolytic Solutions	633
J. H. Simons and Ellison H. Taylor: The Action of Reactor Radiation on Saturated Fluorocarbons	636
Robert S. Hansen: Film and Substrate Flow in Surface Channels	637
M. E. Reichmann: Effect of Polydispersity of Non-Newtonian Viscosity of Polymeric Solutions	638
Communication to the Editor	
R. N. Keller, Jesse M. Cleveland and Frank Burlingame: Two Liquid Scintillators	640

THE JOURNAL OF PHYSICAL CHEMISTRY

(Registered in U. S. Patent Office)

W. ALBERT NOYES, JR., EDITOR

ALLEN D. BLISS

ASSISTANT EDITORS

A. B. F. DUNCAN

EDITORIAL BOARD

C. E. H. BAWN

G. D. HALSEY, JR.

R. G. W. NORRISH

R. W. DODSON

S. C. LIND

A. R. UBBELOHDE

PAUL M. DOTY

H. W. MELVILLE

E. R. VAN ARTSDALEN

JOHN D. FERRY

EDGAR F. WESTRUM, JR.

Published monthly by the American Chemical Society at 20th and Northampton Sts., Easton, Pa.

Second-class mail privileges authorized at Easton, Pa. This publication is authorized to be mailed at the special rates of postage prescribed by Section 132.122.

The *Journal of Physical Chemistry* is devoted to the publication of selected symposia in the broad field of physical chemistry and to other contributed papers.

Manuscripts originating in the British Isles, Europe and Africa should be sent to F. C. Tompkins, The Faraday Society, 6 Gray's Inn Square, London W. C. 1, England.

Manuscripts originating elsewhere should be sent to W. Albert Noyes, Jr., Department of Chemistry, University of Rochester, Rochester 20, N. Y.

Correspondence regarding accepted copy, proofs and reprints should be directed to Assistant Editor, Allen D. Bliss, Department of Chemistry, Simmons College, 300 The Fenway, Boston 15, Mass.

Business Office: Alden H. Emery, Executive Secretary, American Chemical Society, 1155 Sixteenth St., N. W., Washington 6, D. C.

Advertising Office: Reinhold Publishing Corporation, 430 Park Avenue, New York 22, N. Y.

Articles must be submitted in duplicate, typed and double spaced. They should have at the beginning a brief Abstract, in no case exceeding 300 words. Original drawings should accompany the manuscript. Lettering at the sides of graphs (black on white or blue) may be pencilled in and will be typeset. Figures and tables should be held to a minimum consistent with adequate presentation of information. Photographs will not be printed on glossy paper except by special arrangement. All footnotes and references to the literature should be numbered consecutively and placed in the manuscript at the proper places. Initials of authors referred to in citations should be given. Nomenclature should conform to that used in *Chemical Abstracts*, mathematical characters marked for italic, Greek letters carefully made or annotated, and subscripts and superscripts clearly shown. Articles should be written as briefly as possible consistent with clarity and should avoid historical background unnecessary for specialists.

Notes describe fragmentary or incomplete studies but do not otherwise differ fundamentally from articles and are subjected to the same editorial appraisals as are articles. In their preparation particular attention should be paid to brevity and conciseness. Material included in Notes must be definitive and may not be republished subsequently.

Communications to the Editor are designed to afford prompt preliminary publication of observations or discoveries whose value to science is so great that immediate publication is

imperative. The appearance of related work from other laboratories is in itself not considered sufficient justification for the publication of a Communication, which must in addition meet special requirements of timeliness and significance. Their total length may in no case exceed 500 words or their equivalent. They differ from Articles and Notes in that their subject matter may be republished.

Symposium papers should be sent in all cases to Secretaries of Divisions sponsoring the symposium, who will be responsible for their transmittal to the Editor. The Secretary of the Division by agreement with the Editor will specify a time after which symposium papers cannot be accepted. The Editor reserves the right to refuse to publish symposium articles, for valid scientific reasons. Each symposium paper may not exceed four printed pages (about sixteen double spaced typewritten pages) in length except by prior arrangement with the Editor.

Remittances and orders for subscriptions and for single copies, notices of changes of address and new professional connections, and claims for missing numbers should be sent to the American Chemical Society, 1155 Sixteenth St., N. W., Washington 6, D. C. Changes of address for the *Journal of Physical Chemistry* must be received on or before the 30th of the preceding month.

Claims for missing numbers will not be allowed (1) if received more than sixty days from date of issue (because of delivery hazards, no claims can be honored from subscribers in Central Europe, Asia, or Pacific Islands other than Hawaii), (2) if loss was due to failure of notice of change of address to be received before the date specified in the preceding paragraph, or (3) if the reason for the claim is "missing from files."

Subscription Rates (1959): members of American Chemical Society, \$8.00 for 1 year; to non-members, \$16.00 for 1 year. Postage free to countries in the Pan American Union; Canada, \$0.40; all other countries, \$1.20. Single copies, current volume, \$1.35; foreign postage, \$0.15; Canadian postage \$0.05. Back volumes (Vol. 56-59) \$15.00 per volume; (starting with Vol. 60) \$18.00 per volume; foreign postage, per volume \$1.20, Canadian, \$0.15; Pan-American Union, \$0.25. Single copies: back issues, \$1.75; for current year, \$1.35; postage, single copies: foreign, \$0.15; Canadian, \$0.05; Pan-American Union, \$0.05.

The American Chemical Society and the Editors of the *Journal of Physical Chemistry* assume no responsibility for the statements and opinions advanced by contributors to THIS JOURNAL.

The American Chemical Society also publishes *Journal of the American Chemical Society*, *Chemical Abstracts*, *Industrial and Engineering Chemistry*, *Chemical and Engineering News*, *Analytical Chemistry*, *Journal of Agricultural and Food Chemistry*, *Journal of Organic Chemistry* and *Journal of Chemical and Engineering Data*. Rates on request.

THE JOURNAL OF PHYSICAL CHEMISTRY

(Registered in U. S. Patent Office) (© Copyright, 1959, by the American Chemical Society)

VOLUME 63

APRIL 16, 1959

NUMBER 4

ADSORPTION AND CATALYSIS

By PAUL H. EMMETT

Chemistry Department, The Johns Hopkins University, Baltimore, Md.

Received October 7, 1958

When Berzelius in 1836 coined the word "catalysis" and used it to describe a number of observations that had already been recorded in the literature, he clearly recognized that the reacting components in catalytic reactions were held to the surface or adsorbed during the period in which they were reacting. In the intervening years since Berzelius gave birth to this new field of science, many studies have been reported under the general title of "Adsorption and Catalysis." This occasion seems to be a suitable one for pointing out the many ways in which adsorption has now become related to catalytic action and to the study of catalysts, and also for calling attention to the general direction along which progress is being made toward establishing a firm scientific explanation for the behavior of catalysts.

The existence of two types of adsorption of gases on solids has been recognized for many years.¹⁻³ One type, now commonly called physical adsorption, is non-specific and in general occurs between all gases and all solids. It is capable of forming monolayers and even multilayers of adsorbed gas on solids close to the boiling point of a gaseous adsorbate. The other type commonly known as chemical adsorption or activated adsorption is specific in nature and occurs under conditions in which the gaseous adsorbate might be expected to combine chemically with the surface of the solid adsorbent. Both types of adsorption are now considered to be useful and important in the study of catalysts.

Physical Adsorption.—Two distinct uses for physical adsorption in studying catalysts have now been developed. One of them is concerned with the measurement of the surface areas of finely divided catalysts; the other, with the measurement of the pore size of catalytic materials.

The method for measuring surface areas by the physical adsorption of gases is now so well known as to require little comment.⁴⁻⁶ Briefly, it involves measuring the adsorption isotherms of suitable inert adsorbates at temperatures close to the boiling points of the gases and determining by appropriate plots the point on the isotherms corresponding to the volume of gas required to form a single close-packed layer on the catalyst surface. By assuming a suitable cross-sectional area for the adsorbate molecules, one can then calculate the absolute surface area of the catalyst in square meters per gram. By these techniques, the relative surface areas of a number of catalysts or other solid adsorbents can be determined quite accurately. The absolute value of the surface area is, of course, subject to the accuracy with which one can estimate the area covered by each molecule in a close packed layer of physically adsorbed gas. It is probably safe to assume that the absolute surface area of solids can now be measured within an uncertainty of $\pm 30\%$ by these gas adsorption techniques, but relative surface areas for a series of solids can probably be estimated within a few per cent. The gas adsorption method is now universally used for specifying the surface areas of catalytic materials.

An equally or perhaps more important application of physical adsorption in catalysis has to do with measuring the pore size of the tiny capillaries that are present in most catalysts. Wheeler⁷ was the first to point out that by taking into account the formation both of multilayers of adsorbed gas and the capillary condensation of adsorbate in the tiny capillaries one could, in principle, calculate the size distribution of capillaries in solid adsorbents.

(1) I. Langmuir, *J. Am. Chem. Soc.*, **38**, 2221 (1916).

(2) A. F. Benton, *ibid.*, **45**, 887, 900 (1923).

(3) H. S. Taylor, *ibid.*, **53**, 578 (1931).

(4) P. H. Emmett and S. Brunauer, *ibid.*, **59**, 1553 (1937).

(5) S. Brunauer, P. H. Emmett and E. Teller, *ibid.*, **60**, 309 (1938).

(6) P. H. Emmett, "Catalysis," Vol. I, Chap. 2, Reinhold Publ. Corp., New York, N. Y., 1954.

(7) A. Wheeler, Gordon Research Conference, 1945 and 1946.

Barrett, Joyner and Halenda⁸ following this suggestion, arrived at a detailed procedure that could be used for making such calculations without making any arbitrary assumptions as to the nature of the size distribution curves for the capillaries in the solid catalysts. Using this procedure, one can now calculate the pore distributions over the range 10 to 2000 Å. diameter with a fair degree of assurance that the distribution so calculated is a good approximation to the true distribution. Confirmation of the pore distribution so calculated has been obtained on a number of solids by use of the mercury porosimeter⁹⁻¹¹ method by which the pressure necessary to force mercury into the various capillaries is used in calculating pore distributions. By a combination of the gas adsorption and mercury porosimeter method, one can obtain a fairly reliable distribution curve for the pore size of a given solid and can obtain an even more reliable value for the average pore size.

Wheeler¹² has also pioneered the development of the theory for interpreting the influence of pore size on many characteristics of the behavior of a catalyst toward various reactants. In particular, he has shown that pore distribution can affect the apparent order of the catalytic reaction, the temperature coefficient, the fraction of the surface participating in and contributing to the catalytic reaction,¹³ the specificity of the catalyst, and the behavior of the catalyst after it is exposed to various poisons. In a word, he has shown that for a given catalytic reaction, a particular catalyst can be tailor made by appropriate alteration of the method of preparation to yield a surface area and a pore distribution that will be optimum for a particular gas reaction. This makes it possible to put catalysis on a much more quantitative and scientific basis than has heretofore been possible.

For a good many years, physical adsorption was considered to involve such weak binding forces with the solid adsorbents as not to cause any alteration or change in the adsorbent. After five years ago, Cook, Pack and Oblad¹⁴ pointed out the possibility that even physical adsorption could distort the atomic arrangement in the surface of the catalyst. In 1954, Yates¹⁵ furnished proof of this effect by showing that the adsorption of inert gases such as nitrogen, krypton and argon on a sample of porous glass¹⁶ caused an appreciable expansion in the porous glass. This expansion was detectable even when only a few per cent. of the surface was covered with adsorbed gas. Although these observations are still not completely explained, they leave no doubt that physical adsorption, even at the tem-

perature of liquid nitrogen is capable of altering the surface energy of solid adsorbents and of causing either the expansion or contraction of the solid depending upon the particular gas-solid combination that is being used.

It is generally assumed that chemical and not physical adsorption is a form that is directly involved in catalytic reactions. Even this view may require some modification. For example, there are many catalytic reactions in which only one of two or more reactants apparently has to be chemisorbed as a pre-requisite to the occurrence of a catalytic reaction. It is entirely possible that the other components are merely physically adsorbed on the catalyst at the time of reaction. Furthermore, the very nice work of Becker¹⁷ and Ehrlich¹⁸ on the chemisorption of nitrogen on tungsten seems to indicate that the nitrogen molecules are first physically adsorbed and then are transformed over to a type of chemical adsorption. If this is generally true, then, physical adsorption may be a forerunner to catalytic reactions and to the chemical adsorption that is usually considered to be involved as a basic and essential part of catalytic reactions.

Chemical Adsorption—Chemical adsorption traditionally has found two applications in the study of catalysts. To begin with it has been found very useful in measuring the fraction of a catalyst surface which consists of the catalytically active component compared to the portion which consists of material that either acts as a support or as a promoter to the principal catalyst. For example, it has been found possible to measure the fraction of the surface of an iron synthetic ammonia catalyst that consists of metallic iron,¹⁹ by the study of the low temperature chemisorption of carbon monoxide. Similarly, if these catalysts are promoted with alkaline oxides, one can measure the concentration of such alkaline promoters on the surface of the catalyst by determining the chemisorption of carbon dioxide on the promoter at -78° . Properly designed experiments using isotopic forms of the adsorbate can even give information as to the extent to which the surface appears to be homogeneous and the extent to which it appears to be heterogeneous. Such work has been done, for example, using non-radioactive carbon monoxide and radio-active carbon monoxide on iron catalysts.^{20,21}

By far the biggest application of chemisorption is related to the part it plays in actual catalytic reactions. Two examples will suffice as illustrations. For many years, the chemisorption of hydrocarbons on standard silica-alumina cracking catalysts could not be detected. Volumetric measurements seemed to indicate that less than 0.1% of the surface of these catalysts was covered by chemisorbed hydrocarbons during cracking reactions.²² Recently,

(8) E. P. Barrett, L. G. Joyner and P. P. Halenda, *J. Am. Chem. Soc.*, **73**, 373 (1951).

(9) L. G. Joyner, E. P. Barrett and R. E. Skold, *ibid.*, **73**, 3155 (1951).

(10) E. W. Washburn, *Phys. Rev.*, **17**, 273 (1921).

(11) H. L. Ritter and L. C. Drake, *Ind. Eng. Chem., Anal. Ed.*, **17**, 782 (1945).

(12) A. Wheeler, "Catalysis," Vol. II, (P. H. Emmett, ed.), Reinhold Publ. Corp., New York, N. Y., 1955, Chap. 2.

(13) E. W. Thiele, *Ind. Eng. Chem.*, **31**, 916 (1939).

(14) M. A. Cook, D. H. Pack and A. G. Oblad, *J. Chem. Phys.*, **19**, 367 (1951).

(15) D. J. C. Yates, *Proc. Roy. Soc. (London)*, **224A**, 525 (1954).

(16) M. E. Nordberg, *J. Am. Ceramic Soc.*, **27**, 299 (1944).

(17) J. A. Becker, "Advances in Catalysis," Vol. VII, Academic Press, New York, N. Y., 1955, p. 135.

(18) G. Ehrlich, *J. Phys. Chem. Solids*, **1**, 3 (1956).

(19) P. H. Emmett and S. Brunauer, *J. Am. Chem. Soc.*, **59**, 310 (1937).

(20) J. T. Kummer and P. H. Emmett, *J. Chem. Phys.*, **19**, 289 (1951).

(21) R. P. Eischens, *J. Am. Chem. Soc.*, **74**, 6167 (1952).

(22) R. C. Zabor and P. H. Emmett, *ibid.*, **73**, 5639 (1951).

(23) D. S. MacIver and P. H. Emmett, *THIS JOURNAL*, **62**, 935 (1958).

by the use of radioactive techniques, it has been possible to show that chemisorption of such hydrocarbons as isobutane does actually occur on the silica-alumina catalysts but is restricted to a very small fraction (about 0.01%) of the total surface. It now appears therefore that this catalyst as well as all other known catalysts, function through the chemisorption of at least one of the reactants on the catalyst surface.

A second example, the chemisorption of nitrogen on iron is of especial interest because of the enormous amount of work that has been done upon it. The catalytic synthesis of ammonia over iron catalysts became a commercial process forty-five years ago. Since that time a good deal of interest has been shown in attempting to deduce the mechanism of the synthesis of ammonia from the mixture of hydrogen and nitrogen. Measurements of the rate and quantity of nitrogen adsorbed by active iron catalyst led to a conclusion many years ago that the slow step in the synthesis of ammonia was the chemisorption of nitrogen by the surface of the catalyst.²⁴ This result was generally accepted until a few years ago when Horiuti^{25,26} and his colleagues came to the conclusion that the slow step could not possibly be the chemisorption of nitrogen on iron. Their conclusion was based on their theory of the "stoichiometric number" of the individual steps in a catalytic reaction. Space does not permit a review of the theory of this stoichiometric number in the present article. It will perhaps suffice to point out that according to their ideas the stoichiometric number of the adsorption of nitrogen on iron would have to be unity if the slow step were to be the chemisorption of nitrogen. By a combination of kinetic measurements of the rate of synthesis of ammonia over iron catalysts close to equilibrium, and the rate of isotopic exchange of N¹⁵ between gaseous nitrogen and ammonia, the Japanese were able to calculate a value for this stoichiometric number; they reported a value of two rather than a value of one and concluded that the slow step in the synthesis had to be something other than the chemisorption of nitrogen. This would present a major disturbance in attempts to connect chemisorption and catalysis, if it were experimentally verified by other workers in the field. It so happens, however, that repetition of the work by Van Heerden, Zwietering²⁷ and their colleagues in Holland has led to results that contradict those obtained by the Japanese. These workers find a stoichiometric number of one and therefore conclude that the slow step in the synthesis may well be the chemisorption of nitrogen. Furthermore, by additional measurements of the rate of nitrogen adsorption during actual synthesis, they show²⁸ that at and above 250° excellent agreement is obtained between the rate of nitrogen chemisorption and the rate of synthesis that occurs over an iron catalyst.

(24) P. H. Emmett and S. Brunauer, *J. Am. Chem. Soc.*, **56**, 35 (1934).

(25) S. Enomoto and J. Horiuti, *J. Res. Inst. Cat., Hokkaido Univ.*, **2**, 87 (1955); *Proc. Japan Acad.*, **28**, 99 (1955).

(26) S. Enomoto, J. Horiuti and Y. Kobayashi, *J. Research Inst. Cat.*, **3**, 185 (1955).

(27) C. Bokhoven, M. J. Gorgels and P. Mars, private communication.

(28) J. J. F. Scholten and P. Zwietering, private communication.

This classic and long extended study of the chemisorption of nitrogen on iron accordingly serves as an excellent example of the way in which chemisorption can be related to the mechanism of a catalytic reaction.

A consideration of chemisorption would be incomplete without recording some of the spectacular advances that are being made in obtaining detailed information as to the nature of the chemisorption complex. Foremost among these new tools is the use of infrared absorption.²⁹ Pliskin and Eischens³⁰ have shown that it is possible to study by infrared the detailed nature of the binding of molecules such as carbon monoxide, acetylene, ethylene and hexene on finely divided metals supported on a finely divided silica. The method seems capable of giving information that could be correlated with the catalytic activity of the particular metals involved and in some cases can apparently even be used to obtain information as to the nature of the intermediate that is formed in catalytic reactions.³¹ This spectacular development of a method for measuring the infrared absorption spectra of a few chemisorbed molecules appears capable of giving us an insight into the details of chemisorption that, a few years ago, we would never have expected to be possible.

A second important set of tools for the study of the nature of the chemisorption of molecules on surfaces is the use of magnetic and conductivity measurements. Selwood³²⁻³⁵ has shown that when gases such as hydrogen, ethylene, acetylene and benzene are chemisorbed on the surface of metallic nickel, the specific magnetization of the finely divided nickel is lowered in such a way as to indicate a decrease in the number of d-band vacancies in the nickel as a result of the adsorption. Specifically, he concludes that hydrogen on nickel appears to contribute one electron per hydrogen atom to the nickel crystal. Ethylene and ethane contribute, respectively, about two and about four electrons per chemisorbed molecule. Selwood, at first, suggested that these magnetic results were consistent with the observations of Suhrmann³⁶ to the effect that the adsorbed hydrogen increased the conductivity of nickel. More recent measurements,³⁷ however, have indicated that the first exposure of the fresh nickel surface to hydrogen results in a decrease and not an increase in conductivity. When sufficient hydrogen has been taken up, the trend apparently reverses itself and begins to yield an increase in conductivity. The latest conclusion³⁶ as to hydrogen chemisorbed on metallic surfaces such as nickel is that it forms primarily a covalent bond with the nickel. Slight polarization of

(29) W. A. Pliskin and R. P. Eischens, *J. Chem. Phys.*, **24**, 482 (1956).

(30) R. O. French, M. E. Wadsworth, M. A. Cook and I. B. Cutler, *THIS JOURNAL*, **58**, 805 (1954).

(31) R. P. Eischens, *Z. Elektrochem.*, **60**, 782 (1956).

(32) P. W. Selwood, *J. Am. Chem. Soc.*, **78**, 3893 (1956).

(33) P. W. Selwood, *ibid.*, **79**, 3346 (1957).

(34) P. W. Selwood, "Advances in Catalysis," Vol. IX, Academic Press, New York, N. Y., 1957, p. 93.

(35) P. W. Selwood, *J. Am. Chem. Soc.*, **79**, 4637 (1957).

(36) R. Suhrmann, "Advances in Catalysis," Vol. VII, Academic Press, New York, N. Y., 1955, p. 303.

(37) J. J. Broeder, L. L. van Rijn, W. M. H. Saeltler and G. C. A. Schuit, *Z. Elektrochem.*, **60**, 838 (1956).

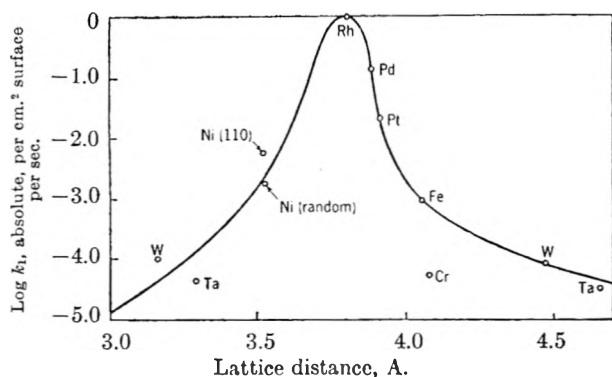


Fig. 1.—Activity at 0° of a series of thin metallic films per unit surface as a function of the distance between particular pairs of atoms in the lattice.⁴⁰

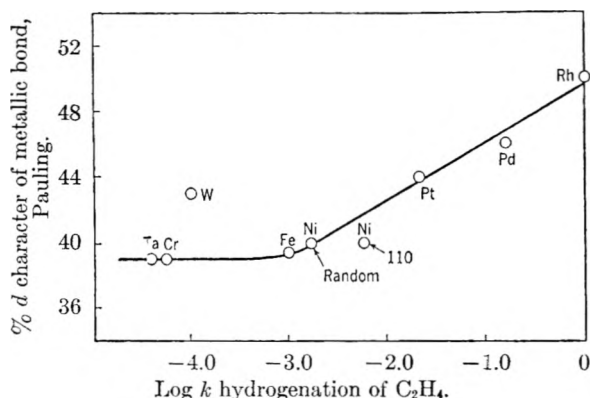


Fig. 2.—Plot of the per cent. of d-character of a series of metals (by Pauling's theory) against the logarithm of the activity of the metals per unit area for hydrogenating ethylene.⁴³

the bond occurs but the adsorbed atom is considered to be held in the surface primarily by covalent and not by ionic bonding. This interpretation is believed³⁶ to be consistent with both the magnetic data and the new conductivity data. There can be no doubt but that the combination of infrared measurements, magnetic measurements and conductivity measurements for gases on metals is going to give us a much more precise idea of catalytic action than we have been able to obtain in the past.

Chemisorption studies on semi-conductors have also received a great deal of attention. Some³⁸ have suggested that the word chemisorption of reacting gases on semi-conductors should really be called "ionisorption." This reflects the idea that on semi-conductors, most of the adsorbed particles are either positive or negative ions. There can be no question but that the chemisorption of gases on semi-conductors results in marked changes in conductivity. There may, however, still be considerable question as to whether the true reactants in catalysis over these semi-conductors are the completely ionized species that affect the conductivities or other types of chemisorbed gas including polarized molecules or molecules held by covalent bonds.

In summary, then, one can say that the chemisorption of gases on catalysts is receiving very intensive study at the present moment. A combina-

(38) K. Hauffe, "Advances in Catalysis," Vol. VII, Academic Press, New York, N. Y., 1955, p. 213.

tion of infrared, magnetic and conductivity studies appears capable of giving us as complete a picture of the details of molecular interaction on solids as we now have for reaction between ions, radicals, atoms and molecules in the gas phase and in solution.

Catalysis.—For many years catalysis has been correctly classified as an art. Only within the last few years has evidence been developing to indicate that a firm scientific basis is being laid to explain catalytic phenomena. In the past, we have selected our catalysts by trying thousands of combinations of catalysts and promoters until we found one that worked. In the future, it seems quite probable that our job of selecting catalysts will be made much easier and that a knowledge of the fundamental properties of reacting gases and the electronic properties of the solid catalysts will go far toward narrowing our choice to a few promising solids. Some of the newer ideas and techniques that are helping to elucidate the mechanism of catalytic reactions and to throw light on the basic properties of catalysts will now be reviewed.

Dowden³⁹ has suggested that in view of the importance of the electronic factor catalysts might well be classified as conductors, semi-conductors and insulators. Conductors can be illustrated by metallic catalysts such as nickel, platinum and iron. Semi-conductors, by well known commercial catalysts such as zinc oxide, chromium oxide, molybdenum oxide and vanadium pentoxide. Insulator type catalysts may include such compounds as aluminum oxide and alumina-silica cracking catalysts. For the sake of illustrating the new approach catalytic hydrogenation over metallic catalysts will perhaps suffice.

During the period 1934–1948, Beeck^{40–43} and his co-workers carried out their classical experiments on the study of the catalytic hydrogenation of ethylene over metallic films. They reached the conclusion that the activity of these metallic films for this reaction was apparently related to certain inter-atomic spacings in the metal. Their results for a number of metals, for example, were plotted according to the scheme shown in Fig. 1.⁴³ These results seemed to indicate that the spacing of atoms in rhodium was optimum for the ethylene hydrogenation reaction. In line with this, the activity of the rhodium per unit surface area was found to be some three orders of magnitude greater than that of nickel.

In the spring of 1950, Beeck⁴³ pointed out that these results could also be interpreted on the basis of the per cent. d-character of the various metals as defined by the theory of Pauling.⁴⁴ A plot of the data for the metallic films interpreted on this basis is shown in Fig. 2. Thus, Beeck and his co-workers suggested an electronic interpretation that suited

(39) D. A. Dowden, *J. Chem. Soc.*, 242 (1950).

(40) O. Beeck, *Rev. Modern Phys.*, **17**, 61 (1945).

(41) O. Beeck, A. E. Smith and A. Wheeler, *Proc. Roy. Soc. (London)*, **A177**, 62 (1940).

(42) O. Beeck, "Advances in Catalysis," Vol. II, Academic Press, New York, N. Y., 1950, p. 151.

(43) O. Beeck, *Disc. Faraday Soc.*, **8**, 118 (1950).

(44) L. Pauling, *Proc. Roy. Soc. (London)*, **A196**, 343 (1949).

their data equally as well as the geometric interpretation.

About this same time Dowden and Reynolds⁴⁵ carried out a series of studies on the catalytic hydrogenation of styrene, benzene and a few other gases over nickel-copper and nickel-iron alloys. The results for styrene are illustrated in Fig. 3. Dowden³⁹ predicted that when enough copper was added to nickel to fill completely the d-band vacancies, one would probably destroy the catalytic activity of the nickel toward the hydrogenation of styrene. His prediction was beautifully confirmed by the experimental results illustrated in Fig. 3. The activity of a catalyst for the hydrogenation of styrene decreased steadily with an increase in the copper content and reached substantially a zero value when 38% copper was incorporated into the nickel. The addition of iron to nickel lowered the catalytic activity in spite of the fact that it increased the number of d-band vacancies. This led Dowden and Reynolds to suggest that some other electronic properties such perhaps as the density of electronic levels in the catalysts were also important.

Although the results of Dowden and Reynolds for the hydrogenation of styrene seemed to suggest a firm correlation between the electronic properties of the metallic catalysts and the activity toward this reaction, later experiments with other reactions have indicated that the problem is quite complicated. Specifically, Best and Russell⁴⁶ reported that catalysts containing 30–60% copper were many times more active than nickel for the catalytic hydrogenation of ethylene. The results seem to indicate definitely that the explanation for the alloy effect is not the same for all hydrogenation reactions.

Hall⁴⁷ recently completed a detailed study of the hydrogenation of ethylene and of C_6H_6 ^{47b} over a series of nickel-copper alloy catalysts. His results like those of Best and Russell show that the addition of copper increases rather than decreases the activity toward the hydrogenation of ethylene until more than 80 atom % copper has been added (Fig. 4). Furthermore, he found that hydrogen added in the temperature range 100 to 300° acts as a promoter to the copper-nickel catalysts but as an inhibitor for pure nickel (Fig. 5). A theoretical explanation of the results is not yet forthcoming; it seems certain, however, that any satisfactory theory must explain the influence of the added copper and hydrogen on the proportionality factor A in the equation

$$\text{Rate} = Ae^{-E/RT}$$

as well as on the energy of activation E .

Very recently Kokes and the writer^{48,49} have completed a study of Raney nickel catalysts and obtained results that throw additional light on the question of the action of alloying constituents on the activity of metallic catalysts. It has long been

(45) D. A. Dowden and P. W. Reynolds, *Disc. Faraday Soc.*, **8**, 172 (1950).

(46) R. J. Best and W. W. Russell, *J. Am. Chem. Soc.*, **76**, 838 (1954).

(47) (a) W. Keith Hall, Thesis, University of Pittsburg, 1956;

(b) W. Keith Hall and P. H. Emmett, *THIS JOURNAL*, **62**, 816 (1958).

(48) R. J. Kokes and P. H. Emmett, to be published.

(49) R. J. Kokes and P. H. Emmett, to be published.

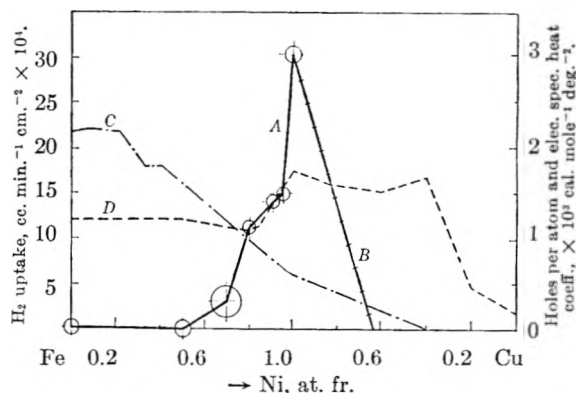


Fig. 3.—The variation with composition of the activity of a series of Fe-Ni (curve A) and Ni-Cu alloys (curve B) for the hydrogenation of styrene. The number of d-band vacancies per atom of Ni and the coefficient of the low-temperature electronic specific heat term are also shown (curves C and D, respectively).⁴⁵

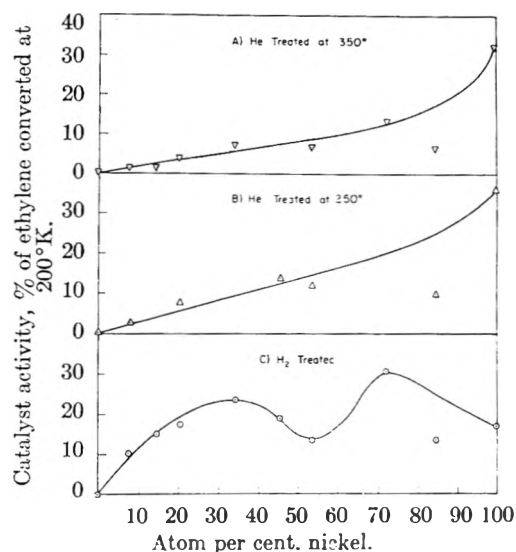


Fig. 4.—Catalytic activity of a series of nickel-copper alloys at 200°K. for the hydrogenation of ethylene.⁴⁷

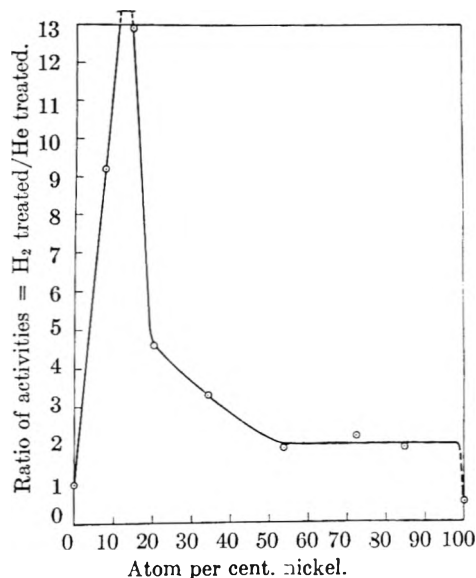


Fig. 5.—The promoting effect of pre-adsorbed hydrogen on the rate of hydrogenation of ethylene as a function of catalyst composition.⁴⁷

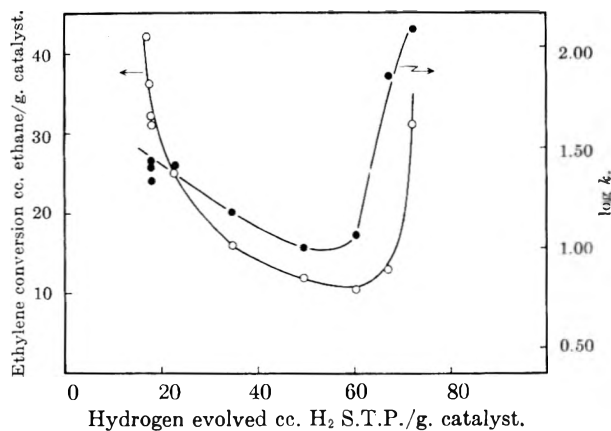


Fig. 6.—The activity of a Raney nickel catalyst for ethylene hydrogenation and for the ortho-parahydrogen conversion at -78° .⁴⁹

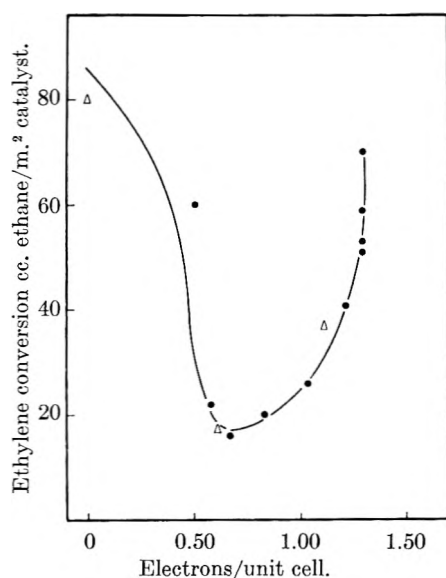


Fig. 7.—Activity per sq. m. of surface area for the hydrogenation of ethylene over a Raney nickel catalyst⁴⁹ and over a nickel-copper alloy⁴⁷ at -78° as a function of the number of electrons added by alloying components per unit cell. Each copper atom and each hydrogen atom is assumed to contribute one electron; each aluminum atom, three electrons. For the Ni-Cu alloys, the atom per cent. copper is 0, 15.2 and 27.3%, respectively, for the three points shown as triangles.⁴⁷ The solid line is for the Raney nickel catalyst.⁴⁹

known that active Raney nickel catalysts contain a considerable amount of dissolved hydrogen. A few years ago Smith and his co-workers⁵⁰ pointed out that the removal of this dissolved hydrogen tended to destroy the activity of the nickel catalysts. In checking up on this relation for the ethylene hydrogenation, Kokes and the writer have now obtained the data shown in Fig. 6. The results indicate that as the dissolved hydrogen content of the original Raney catalysts is gradually removed, the activity falls. However, it reaches a minimum and again increases as a last portion of the dissolved gas is removed from the nickel catalyst. We were at first inclined to believe that the rise of activity during the removal of the last part

(50) H. A. Smith, A. J. Chadwell, Jr., and S. J. Kirslis, *THIS JOURNAL*, **59**, 820 (1953).

of dissolved hydrogen might be the result of removing traces of oxygen poison from the surface of the nickel. However, a comparison with the results obtained by Hall for the addition of copper to nickel seems to indicate that the hydrogen is influencing the activity of the nickel because of some electronic factor. This is illustrated by the fact that a plot of catalytic activity per unit surface area for the nickel-copper catalysts against the atom per cent. copper in the alloy as measured by Hall⁴⁷ yields the three points shown as triangles on the curve in Fig. 7. It is, of course, fully realized that when the metallic surface of the Raney catalysts has been measured by carbon monoxide chemisorption one probably will find that the curve for the Raney nickel catalyst per unit surface area of nickel will be shifted upwards from the present curve which is based on total surface area. Nevertheless, the shape of the curve for the Raney nickel catalyst as a function of hydrogen content will still remain essentially the same as the shape of the curve for the catalytic activities as a function of copper content. This suggests that electronic factors are involved in both instances.

The nature and amount of added hydrogen in the copper-nickel series studied by Hall is not yet known. However, for Raney catalysts a combination of magnetic measurements, differential thermal analysis and density measurements (by helium) as a function of the amount of hydrogen pumped out of the samples seem to afford strong evidence that the hydrogen promoter is present in the form of a substitutional solid solution with the nickel. Thus, the number of nickel vacancies as estimated from the density of the catalyst is very closely the number needed to account for the hydrogen content if one atom of hydrogen is present in each lattice vacancy.

In summary, one can say that catalytic hydrogenation appears to be related to electronic properties of the metallic catalysts; however, we are still far from reaching definite conclusions as to the exact way in which this electronic factor enters into the different types of catalytic hydrogenation reactions.

Space does not permit a review of the very interesting work that is now being carried out in the field of semi-conductors as catalysts. It can perhaps be summarized by saying the catalysts such as zinc oxide, chromium oxide, nickel oxide and cuprous oxide appear to exert their catalytic activity by transferring electrons to the reactant gases on the surface or accepting electrons from them.^{51,52} Furthermore, both the semi-conductors and the metallic catalysts may have a considerable portion of their activities located in surface defects⁵³ and dislocations. Exact correlations are still few and far between but as methods become more exact for assaying the number and nature of these surface defects and dislocations, more quantitative correlations probably will follow.

One aspect of the electronic theory of catalysis

(51) W. E. Garner, "Advances in Catalysis," Vol. IX, Academic Press, New York, N. Y., 1957, p. 169.

(52) "Advances in Catalysis," ed. G. W. Frankenburg, Vol. VII, Academic Press, New York, N. Y., 1955.

(53) A. L. G. Rees, "Chemistry of the Defect Solid State," John Wiley and Sons, Inc., New York, N. Y., 1954.

merits a special mention. One might be inclined to say that the lattice defects and dislocations are merely specific forms of the "active points" postulated many years ago by Taylor.⁵⁴ In a measure this also could be said of the interfaces between promoter molecules and the catalytic substances. There is however one electronic concept that is very different from any involved in the early active point hypothesis. Volkenstein⁵⁵ has suggested that one variety of "active point" may actually be created on a homogeneous surface by the adsorption of a gas molecule or a gas atom. This idea has been utilized by Taylor and Thon⁵⁶ in explaining the kinetics of adsorption of gases on surfaces. They contend that the application of the Elovitch equation to such adsorption phenomena is an example of the way in which active adsorption sites can be created by the adsorption of the gaseous adsorbate and that the slowing down of the adsorption as a function of coverage during such an adsorption experiment can be best explained by the mutual self-destruction of these active points originally created by the adsorption of gases on the surface. Regardless of whether this picture of the creation of active sites by the adsorption of gases survives the test of time, there can be no question but that the analogous poisoning effect of various gases on surfaces may very logically and reasonably be interpreted on such a basis. As early as 1928, Brewer,⁵⁷ for example, pointed out that a single oxygen atom adsorbed on the surface of metal could be considered to poison the surface not by virtue of its occupying an active point by the influence that it exerted on the electronic properties of the metal for a number of molecular diameters around the adsorbed oxygen. Accordingly, the general idea of the importance of the electronic influence of gas molecules on solids is an accepted idea in catalysis, even though many are still skeptical of the evidence as to the creation of active sites by the chemisorption of gases on solids.

Two other research tools useful in the study of catalysts should be mentioned. The first of these is the use of isotopes in studying catalytic mechanisms. Many reactions are being studied with the help of the isotopes of hydrogen, nitrogen, oxygen and carbon. These can be illustrated by the extensive measurements that have been made with the help of carbon-14 in studying the mechanism of Fischer-Tropsch synthesis over iron and cobalt catalysts. By the addition of suspected intermediates in the form of radioactive compounds, it has been possible⁵⁸⁻⁶² to arrive at some fairly definite conclusions in regard to the various steps involved in the complicated synthesis of hydrocar-

bons over metallic catalysts. Up to the present time the radioactive compounds added in small amounts to carbon monoxide hydrogen feed-gas in such experiments include radioactive methanol, formaldehyde, ethyl alcohol, *n*-propyl alcohol, isopropyl alcohol, isobutyl alcohol, ethylene and carbon dioxide. Very recently to this list has been added experiments involving the use of radioactive ketene, C¹⁴H₂CO.⁶³ These results combine to suggest that the carbon monoxide-hydrogen reaction forming higher hydrocarbons over metallic iron or cobalt catalysts probably proceeds through the formation of an oxygen surface complex similar to those that can be formed by the chemisorption of the alcohols or molecules such as ketene on the surface of the catalysts.

Attention should also be called to the tremendous importance of gas chromatography⁶⁴ as a new tool in studying catalytic reactions. As an analytical tool gas chromatography⁶⁵⁻⁶⁷ makes possible a detailed analysis of products obtained in conventional catalyst test units with a speed and completeness far in excess of any heretofore obtainable. One particular type of set up emerging from this work and known as the micro-catalytic-chromatographic technique,⁶⁸ perhaps should be mentioned in closing. It has now been established that if a micro-quantity of reactant is added to a stream of carrying gas and passed through a small catalyst converter and directly onto a chromatographic column, detailed information can be obtained rapidly as to the quality and quantity of products formed by the particular catalyst with the particular added reactants. This technique promises to give valuable information in regard to the behavior of catalysts during the first fraction of a second of exposure to gaseous reactants as well as detailed information on the kinetics of catalytic reactions⁶⁹ and on the behavior of catalysts as judged by the use of radioactive reactants.

Space does not permit a complete enumeration of all the new tools that are being brought to bear in an endeavor to elucidate the way in which metallic, semi-conductor, or insulator catalysts exert their influence on reactants brought in contact with them. Not only the magnetic, conductivity and infrared measurements already mentioned but in addition nuclear magnetic resonance, contact potential, X-ray and electron microscope measurements will in the future be utilized or are at present being utilized in attempting to unravel the many facets of catalysis. One may venture the prediction that the next ten years or so will witness more progress in putting catalysis on a truly scientific basis than has been made in all work up to the present time.

Acknowledgements.—The writer here wishes to

(54) H. S. Taylor, *Proc. Roy. Soc. (London)*, **A108**, 105 (1925).
 (55) F. F. Volkenstein, *J. Phys. Chem. U.S.S.R.*, **23**, 917 (1949).
 (56) H. A. Taylor and N. Thon, *J. Am. Chem. Soc.*, **74**, 4169 (1952).
 (57) A. K. Brewer, *This Journal*, **32**, 1006 (1928).
 (58) J. T. Kummer, H. H. Podgurski, W. B. Spencer and P. H. Emmett, *J. Am. Chem. Soc.*, **73**, 564 (1951).
 (59) J. T. Kummer, T. W. De Witt and P. H. Emmett, *ibid.*, **70**, 3632 (1948).
 (60) W. Keith Hall, R. J. Kokes and P. H. Emmett, *ibid.*, **79**, 2983 (1957).
 (61) R. J. Kokes, W. Keith Hall and P. H. Emmett, *ibid.*, **79**, 2989 (1957).
 (62) W. Keith Hall, R. J. Kokes and P. H. Emmett, to be published.

(63) G. Blyholder and P. H. Emmett, to be published.
 (64) A. T. James and A. J. P. Martin, *Biochem. J.*, **60**, 679 (1952).
 (65) A. I. M. Keulemans, "Gas Chromatography," Reinhold Publ. Corp., New York, N. Y., 1957.
 (66) "Vapor Phase Chromatography," ed. D. H. Desty, Butterworths, London, 1957.
 (67) "Gas Chromatography," D. H. Desty, Butterworths, London, 1958.
 (68) R. J. Kokes, H. Tobin, Jr., and P. H. Emmett, *J. Am. Chem. Soc.*, **77**, 5860 (1955).
 (69) H. H. Voge and A. I. M. Keulemans, to be published.

acknowledge the valuable assistance of his many co-workers and collaborators with whom during the past 35 years he has been studying the properties of catalysts and the nature of catalytic processes. He is glad also to acknowledge gratefully the support of his work by the Gulf Oil Company in the form of funds for the Multiple Petroleum Fel-

lowship at the Mellon Institute; and direct and indirect support of his work at the Johns Hopkins University by W. R. Grace Company and the Davison Chemical Company. Finally, he wishes to thank the Kendall Company for the award, this year and for its continued support of the Kendall Award in colloid chemistry.

RELATIONS BETWEEN DIFFERENT DEFINITIONS OF PHYSICAL ADSORPTION^{1,2}

BY TERRELL L. HILL

Department of Chemistry, University of Oregon, Eugene, Oregon

Received October 7, 1958

The conventional two dimensional definition, a mechanical (or "bound" molecule) definition, and the correct Gibbs (surface excess) definition of physical adsorption are compared in the Henry's law region in terms of "effective" solid-gas molecule potentials. The differences are considerable. Also, the Gibbs definition is put in the form of an exact "two dimensional" virial expansion (surface pressure expanded in powers of excess surface density) and compared with the approximate virial expansion according to the two dimensional definition. The exact "two dimensional" treatment does not lead to a law of co-responding states or a pair-wise additive intermolecular potential as usually assumed.

I. Introduction

The object of the present paper is to compare three different definitions of physical adsorption for an idealized system consisting of a classical monoatomic gas in contact with a solid possessing a mathematically uniform surface (Fig. 1b), the ξ , η plane. The centers of the atoms of the solids are assumed to be distributed with uniform number density n in the region $\zeta \leq 0$. We consider the low gas pressure region only, where the first monolayer is just beginning to form.

The three definitions, which we consider in detail below, are the following.

(1) The actual interaction between a gas molecule and the solid is replaced by a parabolic potential function having the correct potential energy minimum (at $\zeta = \zeta_0$) and curvature at the minimum. A molecule trapped in this parabolic potential well is "adsorbed." The molecule carries out simple harmonic ζ -motion. Treatment of the motion in the ξ , η directions is simplified by assuming that it is independent of or separable from the ζ -motion and restricted to the plane $\zeta = \zeta_0$; thus, as far as the ξ , η directions are concerned, the adsorbed molecules are treated as a strictly two dimensional gas. This is the conventional definition of or model for mobile monolayer adsorption. We shall refer to it as the *two dimensional* definition.

(2) If, at any instant, the ζ contribution to the kinetic energy, $p_\zeta^2/2m$, of a given gas molecule is less than the negative of the potential energy of interaction between the molecule and the solid, then the molecule is considered "adsorbed" (or, the ζ -motion is "bound"). This is the *mechanical* definition of adsorption.³

(3) Finally, the number of adsorbed molecules can be defined as a surface excess, following Gibbs.

(1) This work was supported in part by a grant from the National Science Foundation.

(2) Presented at the San Francisco meeting of the American Chemical Society, April, 1958.

(3) T. L. Hill, *J. Chem. Phys.*, **16**, 181 (1948).

In Fig. 1, we obtain the number of adsorbed molecules by subtracting the number of molecules in V in Fig. 1a from the number in V in Fig. 1b. We shall call this the *Gibbs* definition.

From a rigid thermodynamic point of view,⁴ none of the above definitions can be made both exact and operational for a real system. However, the Gibbs definition resembles in principle the conventional operational definition (measurement of "dead space" by helium adsorption). Certainly, for the idealized system being considered and for theoretical purposes, the Gibbs definition should be regarded as correct. Incidentally, unlike the Gibbs definition, definitions (1) and (2), without modification, become obviously unrealistic in multilayer adsorption.

II. Two Dimensional Definition of Adsorption

The canonical ensemble partition function for N molecules can be written here as

$$Q_N = \frac{q_v^N Z_N^{(2)}}{N! \Lambda^{2N}} \quad (1)$$

where

$$\Lambda = h/(2\pi mkT)^{1/2} \quad (2)$$

and

$$Z_N^{(2)} = \int_{\mathcal{G}} \exp(-U_N^{(2)}/kT) dr_1^{(2)} \dots dr_N^{(2)} \quad (3)$$

The superscript (2) refers to the two dimensions ξ and η ($\zeta = \zeta_0$ plane). $U_N^{(2)}$ is the interaction potential energy between N gas molecules in the plane $\zeta = \zeta_0$. \mathcal{G} is the surface area. To obtain q_v , we have to discuss first $u(\zeta)$, the interaction potential between a gas molecule and the solid. If the potential energy of interaction with a single atom of the solid at a distance r is taken to be

$$-2\epsilon \left(\frac{r^*}{r}\right)^6 + \epsilon \left(\frac{r^*}{r}\right)^{12}$$

(4) E. A. Guggenheim, reviewed by T. L. Hill, *Advances in Catalysis*, **4**, 211 (1952), pp. 251-255.

then the interaction with the entire solid is^{3,5}

$$\frac{u(\zeta)}{kT} = \frac{3}{2\sqrt{5}} \frac{u_0}{kT} \left[\left(\frac{r^*}{\zeta}\right)^3 - \frac{1}{15} \left(\frac{r^*}{\zeta}\right)^9 \right] \quad (4)$$

where

$$\frac{u_0}{kT} = - \frac{2\sqrt{5}}{9} \frac{\epsilon r^{*3} \pi n}{kT} \quad (5)$$

The minimum in eq. 4 occurs at

$$u/kT = u_0/kT, \zeta/r^* = \zeta_0/r^* = 5^{-1/3} = 0.7647$$

If we expand eq. 4 about $\zeta = \zeta_0$, we find

$$\frac{u_{HO}}{kT} = \frac{u_0}{kT} \left[1 - \frac{27\sqrt{5}}{2r^{*2}} (\zeta - \zeta_0)^2 \right] \quad (6)$$

where $u_{HO}(\zeta)$ is the harmonic oscillator approximation to $u(\zeta)$. Then

$$q_v = (r^*/\Lambda) I_{HO} \quad (7)$$

where

$$I_{HO} = \int_0^{+\infty} e^{-u_{HO}/kT} d(\zeta/r^*) \quad (8)$$

$$= e^{-u_0/kT} \left[\frac{2\pi}{27\sqrt{5} (-u_0/kT)} \right]^{1/2}$$

Whether one writes the lower limit in eq. 8 as 0 or $-\infty$ is immaterial. The well-known expression

$$q_v = e^{-u_0/kT} \frac{kT}{h\nu}$$

relates the vibrational frequency ν to the parameters used above.

The grand partition function is

$$\Xi = \sum_{N \geq 0} Q_N e^{N\mu/kT} = \exp(\varphi Q/kT)$$

$$= \sum_{N \geq 0} \frac{Z_N^{(2)}}{N!} \bar{\delta}^N \quad (9)$$

$$z = q_v e^{\mu/kT} / \Lambda^2$$

where φ is the two dimensional pressure, and $\bar{\delta}$ is an activity defined so that $\bar{\delta} \rightarrow \Gamma = \bar{N}/Q$ as $\Gamma \rightarrow 0$. That is, in the Henry's law region ($\Gamma \rightarrow 0$), the amount of adsorption is given by

$$\Gamma = \bar{\delta} = \frac{r^* I_{HO} e^{\mu/kT}}{\Lambda^2} \quad (10)$$

Of course μ is determined by the fugacity of the gas in equilibrium with the adsorbed phase.

By standard methods⁶ we find the virial expansion

$$\frac{\varphi}{kT} = \Gamma + B_2^{(2)} \Gamma^2 + B_3^{(2)} \Gamma^3 + \dots \quad (11)$$

$$B_2^{(2)} = - \frac{1}{2Q} (Z_2^{(2)} - Q^2) \quad (12)$$

etc. If $u_{12}(\rho)$ is the intermolecular pair potential, then

$$B_2^{(2)} = - \pi \int_0^\infty [e^{-u_{12}(\rho)/kT} - 1] \rho d\rho \quad (13)$$

We will assume that $u_{12}(\rho)$ has the Lennard-Jones form

$$u_{12}(\rho) = - 2\epsilon_0 \left(\frac{r_0}{\rho}\right)^6 + \epsilon_0 \left(\frac{r_0}{\rho}\right)^{12} \quad (14)$$

Equations 9-13 represent the beginnings of a two-dimensional version of Mayer's imperfect gas the-

(5) T. L. Hill, *Advances in Catalysis*, **4**, 211 (1952).

(6) See, for example, T. L. Hill, "Statistical Mechanics," McGraw-Hill Book Co., Inc., New York, N. Y., 1956, pp. 134-136, 143-144.

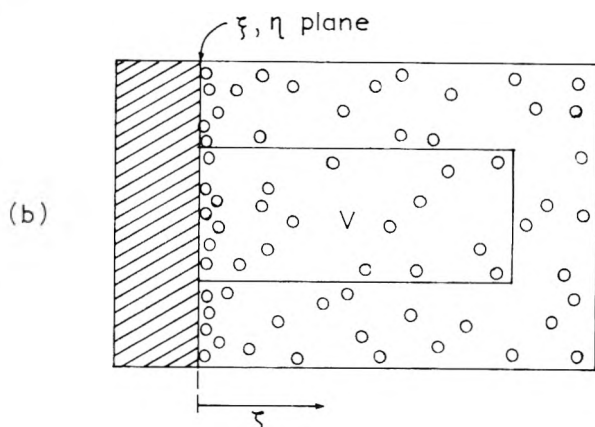
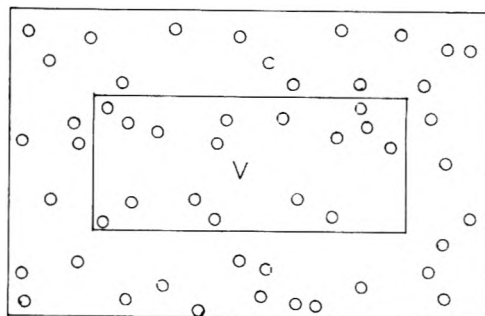


Fig. 1.—(a) Reference system—no adsorbing surface; (b) "real" system with adsorbing surface.

ory. At higher surface densities, approximate van der Waals⁷ and Lennard-Jones-Devonshire⁸ theories are available. A two dimensional law of corresponding states is of course obeyed if $U_N^{(2)}$ is pairwise additive and u_{12} has only two parameters as in eq. 14.

III. Mechanical Definition of Adsorption

We limit ourselves in this section to the Henry's law region (adsorbed molecules independent of each other). The partition function for a single molecule in the volume V (Fig. 1b) is (after integrating over ξ, η, p_ξ and p_η)

$$q = \frac{Q}{h\Lambda^2} \int_0^V \int_0^Q e^{-u(\zeta)/kT} d\zeta \int_{-\infty}^{+\infty} e^{-p_\zeta^2/2mkT} dp_\zeta \quad (15)$$

Now if we define³ an adsorbed molecule as one whose ζ -motion is bound

$$p_\zeta^2/2m < -u(\zeta)$$

then the partition function q_M for a single adsorbed molecule is, instead of eq. 15

$$q_M = \frac{Q}{h\Lambda^2} \int_{u(\zeta) < 0} e^{-u(\zeta)/kT} d\zeta$$

$$\times \int_{-\sqrt{-2mu(\zeta)}}^{+\sqrt{-2mu(\zeta)}} e^{-p_\zeta^2/2mkT} dp_\zeta$$

$$= \frac{Q}{\Lambda^2} \int_{u(\zeta) < 0} e^{-u(\zeta)/kT} \text{erf} \sqrt{-u(\zeta)/kT} d\zeta \quad (16)$$

If we define an effective potential $u_M(\zeta)$ by

$$e^{-u_M(\zeta)/kT} = e^{-u(\zeta)/kT} \text{erf} \sqrt{-u(\zeta)/kT} \quad u(\zeta) < 0$$

$$= 0 \quad u(\zeta) > 0 \quad (17)$$

(7) T. L. Hill, *J. Chem. Phys.*, **14**, 441 (1946).

(8) A. F. Devonshire, *Proc. Roy. Soc. (London)*, **163A**, 132 (1937).

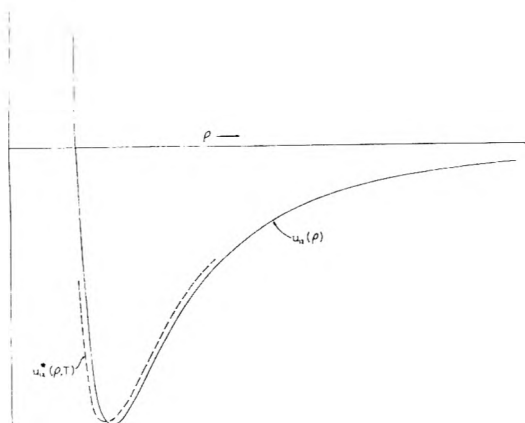


Fig. 2.—Relationship between $u_{12}(\rho)$ and $u_{12}^*(\rho, T)$ (schematic).

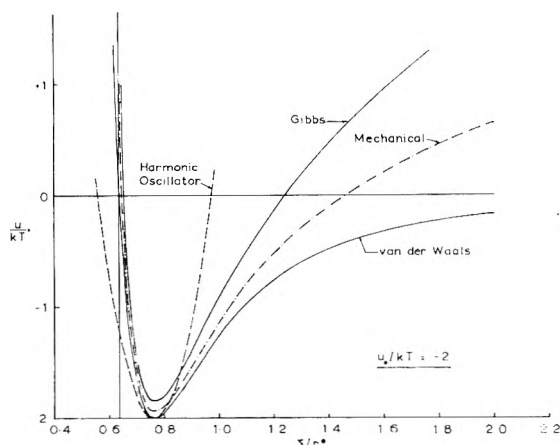


Fig. 3.—Comparison of actual van der Waals potential with three "effective" potentials for $u_0/kT = -2$.

then

$$q_M = \frac{\mathcal{Q}}{\Lambda^3} \int_0^\infty e^{-u_M(\zeta)/kT} d\zeta$$

We have

$$Q_N = \frac{1}{N!} q_M^N$$

$$\ln \Xi = \ln \sum_{N \geq 0} Q_N e^{N\mu/kT} = q_M e^{\mu/kT}$$

$$\Gamma = \frac{\bar{N}}{\mathcal{Q}} = \frac{kT}{\mathcal{Q}} \frac{\partial \ln \Xi}{\partial \mu} = \frac{q_M e^{\mu/kT}}{\mathcal{Q}} = \frac{r^* I_M e^{\mu/kT}}{\Lambda^3} \quad (18)$$

where

$$I_M = \int_0^\infty e^{-u_M/kT} d(\zeta/r^*) \quad (19)$$

Equations 18 and 19 are formally similar to eq. 10 and 8, respectively.

This treatment resembles a discussion⁹ of cluster formation in an imperfect gas using a "mechanical" definition of a cluster.

IV. The Gibbs Definition of Adsorption

Various aspects of this problem already have been discussed by Wheeler, Ono, Freeman and Halsey and Hill.¹⁰ The amount of adsorption (surface excess) can be expressed as a power series in the gas pressure or fugacity, etc. The new feature which

(9) Reference 6, pp. 152-164.

(10) See, for example, pp. 424-425 of reference 6. The other references are given there.

we wish to emphasize here is that this basically three dimensional treatment can be recast in two dimensional form, and can thus be compared directly with Section II. For example, φ can be expanded in powers of Γ with exact "two dimensional" virial coefficients.

In the absence of a surface (Fig. 1a), we have¹⁰

$$\frac{pV}{kT} = \ln \Xi^0 = \sum_{j \geq 1} V b_j^0 z^j \quad (20)$$

$$1! V b_1^0 = Z_1^0 = V, \quad b_1^0 = 1$$

$$2! V b_2^0 = Z_2^0 - V^2$$

$$Z_2^0 = \int_V e^{-u_{12}/kT} dr_1 dr_2$$

$$z = e^{\mu/kT}/\Lambda^3$$

etc. The average number of molecules in the system is

$$\bar{N}^0 = \sum_{j \geq 1} V j b_j^0 z^j \quad (21)$$

In the presence of a surface (Fig. 1b)

$$\frac{pV}{kT} + \frac{\varphi \mathcal{Q}}{kT} = \ln \Xi = \sum_{j \geq 1} V b_j z^j \quad (22)$$

$$1! V b_1 = Z_1$$

$$2! V b_2 = Z_2 - Z_1^2$$

$$Z_1 = \int_V e^{-u(\zeta_1)/kT} dr_1$$

$$Z_2 = \int_V e^{-[u(\zeta_1) + u(\zeta_2) + u_{12}(\zeta_1, \zeta_2)]/kT} dr_1 dr_2$$

etc. The average number of molecules in the system is

$$\bar{N} = \sum_{j \geq 1} V j b_j z^j \quad (23)$$

We subtract eq. 20 from 22 and 21 from 23 to find

$$\frac{\varphi \mathcal{Q}}{kT} = \ln (\Xi/\Xi^0) = \sum_{j \geq 1} V (b_j - b_j^0) z^j \quad (24)$$

$$\bar{N} - \bar{N}^0 = \sum_{j \geq 1} V j (b_j - b_j^0) z^j \quad (25)$$

As $z \rightarrow 0$

$$\frac{\varphi \mathcal{Q}}{kT} \rightarrow V (b_1 - 1) z \quad (26)$$

$$\bar{N} - \bar{N}^0 \rightarrow V (b_1 - 1) z \quad (27)$$

or

$$\varphi \rightarrow \Gamma kT \text{ where } \Gamma = (\bar{N} - \bar{N}^0)/\mathcal{Q}$$

In the Henry's law region

$$\Gamma = \frac{V (b_1 - 1) z}{\mathcal{Q}} = \frac{r^* I_G e^{\mu/kT}}{\Lambda^3} \quad (28)$$

where

$$I_G = \int_0^\infty (e^{-u/kT} - 1) d(\zeta/r^*)$$

If we define an effective potential $u_G(\zeta)$ by

$$e^{-u_G(\zeta)/kT} = e^{-u(\zeta)/kT} - 1 \quad (29)$$

then

$$I_G = \int_0^\infty e^{-u_G/kT} d(\zeta/r^*) \quad (30)$$

Equations 28 and 30 are analogs of eq. 10 and 8, and of 18 and 19, respectively. When $u > 0$, $e^{-u_G/kT} < 0$ and u_G is complex. Γ (and φ) can be

negative with the Gibbs definition of adsorption, but not according to the other two definitions. It should be noted that Gibbs' definition of adsorption is closely related to Mayer's definition of a cluster.¹¹

In view of eq. 26 and 27, we define a "two-dimensional" activity \bar{z} by

$$\bar{z} = \frac{V(b_1 - 1)z}{\Omega} = z \int_0^\infty [e^{-u(\zeta)/kT} - 1] d\zeta \quad (31)$$

so that $\bar{z} \rightarrow \Gamma$ as $\Gamma \rightarrow 0$ (as in Section II). If we define q_v by the relation

$$\bar{z} = q_v e^{\mu/kT} / \Lambda^2 = z q_v \Lambda \quad (32)$$

as in eq. 9, then

$$q_v = \frac{1}{\Omega} \int_0^\infty [e^{-u(\zeta)/kT} - 1] d\zeta \quad (33)$$

$$= V(b_1 - 1) / \Omega \Lambda$$

We use eq. 32 to replace z by \bar{z} , and eq. 24 becomes

$$\frac{\varphi}{kT} = \sum_{j \geq 1} b_j^{(2)} \bar{z}^j \quad (34)$$

where

$$b_j^{(2)} = \frac{V(b_1 - b_1^0)}{\Omega (q_v \Lambda)^j} \quad (35)$$

The usual relations⁶

$$\begin{aligned} 1! \Omega b_1^{(2)} &= Z_1^{(2)} = \Omega; \quad b_1^{(2)} = 1 \\ 2! \Omega b_2^{(2)} &= Z_2^{(2)} - \Omega^2 \\ 3! \Omega b_3^{(2)} &= Z_3^{(2)} - 3\Omega Z_2^{(2)} + 2\Omega^3 \end{aligned} \quad (36)$$

etc., then serve to define the $Z_N^{(2)}$. We find, for example

$$Z_2^{(2)} = \frac{\Omega^2(Z_2 - 2Z_1V - Z_2^0 + 2V^2)}{(Z_1 - V)^2} \quad (37)$$

The "two dimensional" virial expansion⁶ according to the Gibbs definition of adsorption is then

$$\frac{\varphi}{kT} = \Gamma + B_2^{(2)} \Gamma^2 + B_3^{(2)} \Gamma^3 + \dots \quad (38)$$

with $B_2^{(2)}$ given by eq. 12, etc.

Let us define an *effective* "two dimensional" intermolecular potential u_{12}^* by the equation

$$Z_2^{(2)} - \Omega^2 = \int \int_{\Omega} (e^{-u_{12}^*/kT} - 1) dr_1^{(2)} dr_2^{(2)} \quad (39)$$

Then from eq. 37 we find that

$$e^{-u_{12}^*(\rho, T)/kT} - 1 = \frac{\int_0^\infty \int_0^\infty [e^{-u(\zeta_1)/kT} e^{-u(\zeta_2)/kT} - 1] [e^{-u_{12}(r)/kT} - 1] d\zeta_1 d\zeta_2}{\left\{ \int_0^\infty [e^{-u(\zeta)/kT} - 1] d\zeta \right\}^2} \quad (40)$$

where

$$\begin{aligned} r^2 &= \rho^2 + (\zeta_2 - \zeta_1)^2 \\ \rho^2 &= (\xi_2 - \xi_1)^2 + (\eta_2 - \eta_1)^2 \end{aligned}$$

Thus, in an exact treatment, $u_{12}(\rho)$ in eq. 13 must be replaced by $u_{12}^*(\rho, T)$. Since u_{12}^* for a given gas will be different for different adsorbents, a two dimensional law of corresponding states cannot be strictly obeyed. Also, consideration of $Z^{(2)}$ shows, as might be expected, that the *effective* potential u_{12}^* is not strictly pair-wise additive (assuming that the actual intermolecular potential is pair-wise additive).

To get an approximate idea of the difference between $u_{12}^*(\rho, T)$ and $u_{12}(\rho)$ in eq. 40, we make the

(11) See p. 162, reference 6.

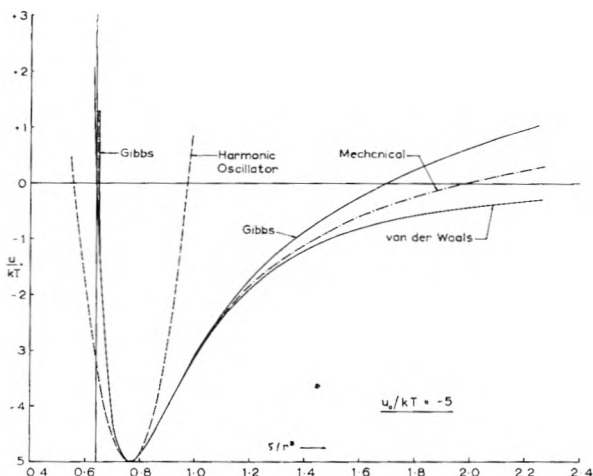


Fig. 4.—Comparison of actual van der Waals potential with three "effective" potentials for $u_0/kT = -5$.

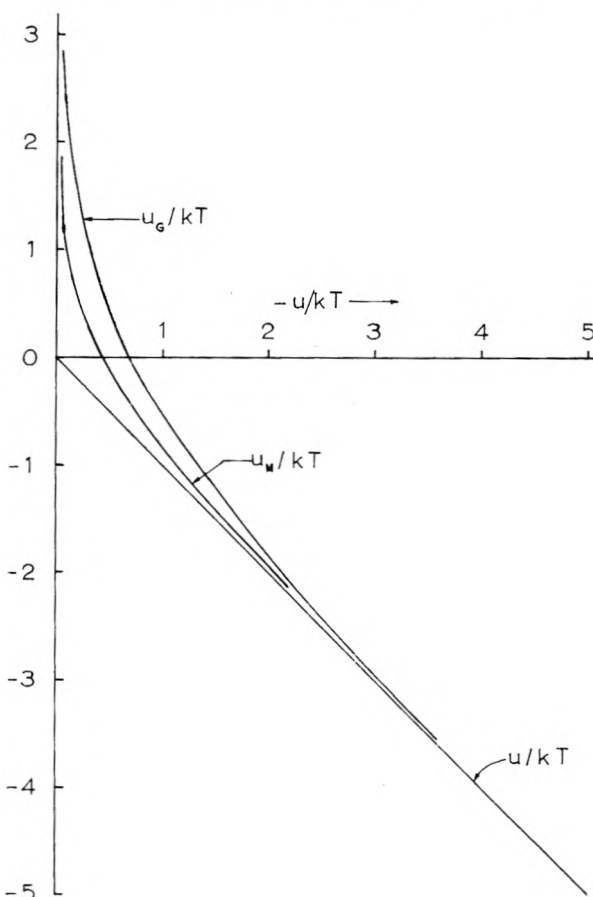


Fig. 5.—Gibbs and mechanical "effective" potentials as functions of van der Waals potential.

following first-order calculation (which will underestimate the difference). First, we use the parabolic approximation, eq. 6, to $u(\zeta)$, neglect unity compared to $e^{-u/kT}$, and expand $e^{-u_{12}/kT}$ about $r = \rho$ in powers of $x = \zeta_2 - \zeta_1$:

$$\begin{aligned} e^{-u_{12}(r)/kT} &= e^{-u_{12}(\rho)/kT} + bx^2 + cx^4 + \dots \\ b &= -\frac{1}{2\rho} e^{-u_{12}(\rho)/kT} \frac{u_{12}''(\rho)}{kT} \\ c &= \frac{e^{-u_{12}(\rho)/kT}}{8\rho^3} \left\{ \rho \left[\frac{u_{12}''(\rho)}{kT} \right]^2 - \rho \frac{u_{12}''(\rho)}{kT} + \frac{u_{12}''(\rho)}{kT} \right\} \end{aligned}$$

Then

$$e^{-u_{12}^*(\rho, T)/kT} = \frac{\int_{-\infty}^{+\infty} e^{-ax_1^2} e^{-ax_2^2} [e^{-u_{12}(\rho)/kT} + b(x_2 - x_1)^2 + c(x_2 - x_1)^4] dx_1 dx_2}{\left(\int_{-\infty}^{+\infty} e^{-ax_1^2} dx_1\right)^2} = e^{-u_{12}(\rho)/kT} + (b/a) + (3c/a^2) \quad (41)$$

where

$$x_1 = \zeta_1 - \zeta_0, x_2 = \zeta_2 - \zeta_0 \\ a = \frac{27\sqrt{5}}{2r^{*2}} \left(-\frac{u_0}{kT}\right)$$

If we substitute the expressions for b and c in eq. 41, factor out $e^{-u_{12}(\rho)/kT}$, take the logarithm of both sides, expand each of the terms on the right-hand side about $\rho = r_0$ up to $(\rho - r_0)^2$, and finally locate the minimum in the resulting expression for $u_{12}^*(\rho, T)$, we find

$$\rho_{\min} = r_0 \left(1 - \frac{\alpha}{12} + \dots\right) \\ u_{12}^*(\rho_{\min}) = -\epsilon_0 \left(1 - \frac{\alpha^2}{2} + \dots\right) \quad (42)$$

where

$$\alpha = \frac{6}{ar_0^2} = \frac{4}{9} \left(\frac{\zeta_0}{r_0}\right)^2 \left(-\frac{u_0}{kT}\right)^{-1}$$

The function $u_{12}^*(\rho, T)$ is compared schematically with $u_{12}(\rho)$ in Fig. 2. The general relationship shown in this figure results from the fact that oscillations, perpendicular to the surface, of two molecules a distance ρ apart in the ξ, η directions will necessarily make their average separation somewhat greater than ρ . Also, an average over u_{12} will necessarily lead to a minimum in u_{12}^* above the minimum in u_{12} itself.

If, for simplicity, a strictly two dimensional treatment (virial expansion, two dimensional condensation, critical properties, etc.) as in Section II is used, the theory will be improved by the use of the adjusted parameters of eq. 42 rather than r_0 and ϵ_0 themselves.

V. Discussion

The solid-gas molecule potentials u_{HO}, u_M and u_G are compared in Figs. 3 and 4 with u (eq. 4), for $u_0/kT = -2$ and -5 , respectively. It is clear that the Gibbs and mechanical definitions provide effective "bound" potentials just as does the harmonic oscillator model. Figure 5 shows u_M and u_G plotted against $-u$.

In the Henry's law region, the amount of adsorption, according to the three definitions, is given by eq. 10, 18 and 28. The three values of Γ differ only through the integral I (eq. 8, 19 and 30). I_{HO} can be evaluated analytically; we also have calculated values of I_M and I_G by numerical integration (and analytical integration for large ζ) for $u_0/kT = -2$ and -5 . These results are shown in Table I.

TABLE I
RELATIVE AMOUNTS OF ADSORPTION

	2	$-\frac{u_0}{kT}$ 5	∞
I_{HO}	1.93	24.5	∞
I_M	4.83	34.3	∞
I_G	1.81	30.2	∞
I_{HO}/I_G	1.07	0.81	1.00
I_M/I_G	2.67	1.13	1.00

I_M is much larger than I_G for $u_0/kT = -2$. The excess arises as follows: 0.6 in the interval 0 to 0.64 (in which I_G has a negative contribution and I_M none); 0.9 in the interval 0.64 to 2.75; and 1.5 in the interval 2.75 to ∞ . The negative contribution to I_G just referred to becomes relatively less important as $-u_0/kT$ increases. This effect is responsible for the reversal in relative magnitude of I_{HO} and I_G seen in the table.

It is apparent from Table I that significant errors can be made in estimating theoretically the amount of adsorption in the Henry's law region by not using the correct (Gibbs) definition of adsorption.

Finally, it should be mentioned again that classical rather than quantum mechanics has been used throughout.

The author is indebted to Dr. Dirk Stigter for his interest and assistance.

THE CHEMISORPTION OF OXYGEN ON SILVER

BY J. T. KUMMER

The Dow Chemical Company, Midland, Michigan

Received October 7, 1958

The silver-oxygen system has been studied by measuring the change in surface potential of a silver surface produced by oxygen chemisorption, and by measuring the paramagnetism of a silver surface after oxygen chemisorption. The change in surface potential was obtained by measuring the current flow into or out of a condenser consisting of gold and silver plates at $\sim 220^\circ$ when oxygen is admitted to the system. The change in surface potential is negative ~ 0.2 volt. The surface paramagnetism was measured by ortho-para hydrogen conversion, and the surface after oxygen chemisorption is slightly paramagnetic, corresponding to one unpaired electron per 150 \AA^2 .

The catalytic oxidation of ethylene to ethylene oxide over a silver surface occurs by the reaction between gas phase or weakly adsorbed ethylene and oxygen chemisorbed on the surface.¹ In order to

understand the catalytic reaction more thoroughly, we have measured the surface potential of a silver-oxygen surface relative to a silver surface and have measured its paramagnetism. The silver-oxygen bond in Ag_2O is largely covalent in character and the

(1) G. H. Twigg, *Trans. Faraday Soc.*, **42**, 284 (1946).

covalent radius of oxygen is approximately one-half the silver radius. If one pictures the oxygen as chemisorbed on top of the surface plane of silver atoms then one would expect the silver surface to become more negative to the extent of a few tenths of a volt. Brewer,² however, using a photoelectric technique concluded that the silver surface became more positive with the adsorption of oxygen and only became more negative than a silver surface when exposed to atomic oxygen which formed a layer of Ag_2O . The latter result was confirmed by Weissler and Wilson.³ The change in the surface potential of silver on chemisorption of oxygen has been measured by a number of other investigators. Finch and Stimson⁴ and Bradford⁵ measured the potential of a silver plate exposed to oxygen using an electrometer with a reference surface of glass. Finch and Simpson found the silver oxygen surface more positive than silver and Bradford found a more negative surface. Fianda and Lange⁶ studied the work function of an abraded silver surface exposed to oxygen at room temperature and found that oxygen reduced the work function and so presumably produced a positive surface. The result obtained by some of the investigators that oxygen adsorption causes the silver surface to become more positive was difficult to reconcile with known electronegative nature of oxygen (assuming oxygen did not penetrate the Ag lattice and lie below the silver atoms) so we have repeated the work as described below.

The apparatus used for our measurements consisted of a silver sheet formed into a cylinder $\sim 7/8''$ dia. and 4'' high (weight = 14.5 g.) surrounded by a gold cylinder $\sim 1 1/8''$ dia. and 7'' high all inclosed in a Vycor tube contained in a furnace (see Fig. 1). The gold cylinder was grounded and the silver cylinder was grounded through a 2×10^{10} ohm resistor. A vibrating reed electrometer measured the voltage drop across the resistor as oxygen was admitted to the sheet or the surface oxide was reduced. Since gold does not^{7,8} chemisorb oxygen it is assumed that the surface potential of the gold sheet does not change on admission of oxygen and that the current flow in or out of the silver sheet is due only to the change in surface potential of the silver. Knowing the capacity of the system and the total charge in coulombs in or out of the sheet one can calculate the surface potential. This method is useful only when the surface potential changes rapidly enough (as it was in this case) so that the area under the curve of current against time can be evaluated accurately. The electrometer sensitivity was $1/10$ of a millivolt (5×10^{-15} amp.) per scale division (~ 2.5 mm.). The recorder was a 1 sec. recorder and the time constant of the electrometer was made 2 sec. When oxygen is added to a reduced silver sheet at 220° in our apparatus there is observed a sharp peak on the electrometer recorder of ~ 15 second base width indicating a flow of electrons from ground to the silver sheet. If after brief evacuation hydrogen is added there is observed on the recorder a similar peak of opposite polarity indicating a reduction of the oxide by hydrogen.

The polycrystalline silver sheet was annealed in air at 900° and etched with nitric acid before use. The impurities were 8-16 p.p.m. Al, 10-20 p.p.m. Cu, 50-100 p.p.m. Fe, 3-6 p.p.m. Mg. The copper and iron impurities are as-

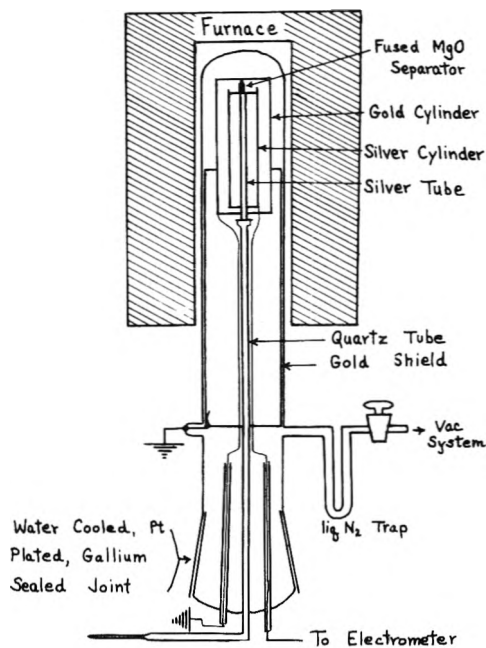


Fig. 1.

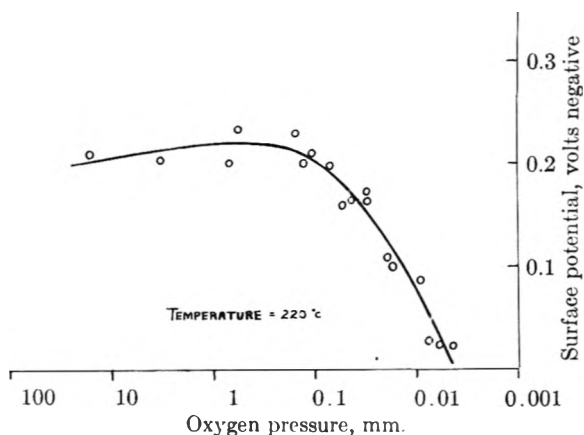


Fig. 2.

sumed to be in solid solution after reduction at 500° and the oxygen is added at 200° for only several min. in order to obtain the surface potential. Care was exercised to avoid long exposure to oxygen which might cause these impurities to accumulate on the surface. The grain size was ~ 1 mm., the sheet being one crystal thick, and the surface plane had a 110 preferred orientation due to rolling. The silver sheet was reduced overnight with hydrogen at 530° , cooled to room temperature and treated with CO for several days in an effort to remove any iron or nickel that may have been present (see Table I). After the CO was evacuated, the sample was re-reduced and evacuated at 530° . The silver sample was protected at all times from stopcock grease and mercury by a liquid nitrogen trap.

Results

We have found that the chemisorption of oxygen on silver gives a negative surface dipole which increases with surface coverage to ~ 0.2 volt at high oxygen pressures (see Fig. 2). Some difficulty was encountered with earlier results in which at low oxygen pressures a positive surface was observed. This was attributed to impurities in the gold sheet which chemisorbed oxygen (giving a negative dipole on the gold surface and thus looking like a positive silver surface) since on repeated heating to

(2) A. K. Brewer, *J. Am. Chem. Soc.*, **56**, 1909 (1934).
 (3) G. L. Weissler and T. N. Wilson, *J. App. Phys.*, **134**, 208 (1953).
 (4) G. I. Finch and J. C. Stimson, *Proc. Roy. Soc. (London)*, **A116**, 379 (1927).
 (5) B. W. Bradford, *J. Chem. Soc.*, 1276 (1934).
 (6) F. Fianda and E. Lange, *Z. Elektrochem.*, **55**, 237 (1951).
 (7) N. Bortner and G. Parravano, *J. Am. Chem. Soc.*, **78**, 4533 (1956).
 (8) B. M. W. Trapnell, *Proc. Roy. Soc. (London)*, **A218**, 566 (1953).

500° and etching with HNO₃ of the gold sheet the positive peak on the recorder (electrons flowing from the silver sheet to ground upon oxygen addition) disappeared. We are unable to offer an explanation as to why our results differ in sign from Brewer's photoelectric results, unless Brewer's silver surface was not clean but was coated with impurity oxide behaving like a semi-conductor.

TABLE I
EFFECT OF CO TREATMENT ON ORTHO-PARA H₂ CONVERSION
AT -195°

Pure silver catalyst, no oxygen treatment	Time of half conversion, min.
Sample reduced 53 hr., 520°	268
Sample reduced an additional 48 hr., 540°	144
Sample CO treated 20 hr., 1 atm., room temperature. CO evacuated and sample reduced 6 hr., 500°	2400

In Twigg's expression for the oxidation of ethylene to ethylene oxide over silver catalysts, he finds the rate of the side reaction to form carbon dioxide and water to be proportional to the square of the surface concentration of oxygen atoms, and concludes from this that two oxygen atoms chemisorbed side by side are necessary in order to form carbon dioxide and water. It is possible that the species responsible for the carbon dioxide and water formation could be a chemisorbed oxygen molecule (O₂⁻ ion),⁸ the concentration of which on the surface would also be proportional to the square of the surface coverage of oxygen atoms. DeBoer and Fortuin⁹ have postulated the presence of O₂⁻ ions on silver surfaces in order to explain the catalysis by silver of the reaction between cumene and oxygen to form cumene hydroperoxide. Recent work¹⁰ at the Shell Laboratories using oxygen-18 has shown that oxygen is adsorbed on silver at 200° initially as molecules which may be followed by dissociation into atoms. As pointed out by these investigators the chemisorbed oxygen molecules have a life-time on the surface at least comparable with the rate of ethylene oxidation and may be responsible for the carbon dioxide production. Their experiments however left unanswered the question as to whether a silver-oxygen surface at a low temperature on which the rate of oxygen adsorption and desorption is low, contains any appreciable concentration of chemisorbed oxygen molecules. We have looked for this steady-state concentration of chemisorbed oxygen molecules using the method of Sandler.

Sandler¹¹ has described a method for determining the concentration of paramagnetic species on diamagnetic or weakly paramagnetic surfaces using the rate of ortho-para hydrogen conversion as a measure of the paramagnetism of the surface. We have applied this method to a silver surface onto which oxygen has been chemisorbed in order to find evidence for O₂⁻ ions (paramagnetic) on the silver surface. Both silver and Ag₂O are diamagnetic. The silver surface used was made by decomposing Ag₂CO₃ (made from solutions of C.P. silver nitrate and ammonium carbonate) in a stream of hydrogen. The silver sample analyzed by weight 10 p.p.m. Al, 5-10 p.p.m. Ca, 1 p.p.m. Cu, 20 p.p.m. Fe, 5-10 p.p.m. Mg, 100-200 p.p.m. Si. The total sample

weight was 76 g., its nitrogen surface area 1.5 square meters and its oxygen adsorption at room temperature 0.3 cc. (S.T.P.). Reductions were carried out at 450-550° in a flow of oxygen-free hydrogen of ~100 cc. S.T.P. per min.

After a prescribed treatment with either oxygen or hydrogen, the silver sample was cooled to -195° in helium. The helium was evacuated and 20 cc. (S.T.P.) of normal nitrogen-free hydrogen was added to a pressure of 120 mm. The rate of ortho-para conversion was measured by withdrawing small samples at specified times, measuring the para content by a thermal conductivity gage and calculating the times of half conversion from the slope of the plot of log V_t/V_0 against time where V_t is the difference between the parahydrogen concentration at time t and the equilibrium parahydrogen concentration and V_0 is that difference at the start of the experiment. The amount of physical adsorption of hydrogen on the pure silver catalyst at -195° and 120 mm. hydrogen pressure was not measured because it is too small to measure. From data in the literature of physical adsorption (as separate from chemisorption) on iron catalysts of higher area it can be estimated that the 1.5 m.² area of the pure silver catalyst would physically adsorb 0.04 cc. S.T.P. of hydrogen. This gives a ratio of gas phase hydrogen (20 cc.) to adsorbed hydrogen of 500. The true half-lives would then be ~1/500 as large as the observed half-lives for this catalyst.

When the sample was reduced long periods of time with hydrogen the ortho-para conversion activity increased, apparently due to appearance of Ni or Fe at the surface. It was necessary to treat such reduced samples with CO at room temperature in order to remove the Ni or Fe as the carbonyl. After subsequent reduction the ortho-para conversion was lowered as can be seen in Table I.

Results

Using the method of Sandler¹¹ we have physically adsorbed oxygen on the silver surface in order to obtain a relation between the number of unpaired electrons on the surface and the ortho-para conversion rate. The data are given in Table II.

TABLE II

	Time of half conversion, min.
Silver sample reduced and evacuated 500°	~1500
Silver sample reduced and evacuated at 500°. Cooled to -195° in helium and evacuated. 0.09 cc. (S.T.P.) of oxygen physically adsorbed at -195° before addition of hydrogen.	41 ^a ± 3
Same as above except that a total of 0.22 cc. S.T.P. of oxygen physically adsorbed	13 ^a ± 2

^a Initial values. $t_{1/2}$ increased with time in the presence of hydrogen.

If the pure silver sample is reduced and evacuated at 500°, cooled to room temperature in helium, contacted oxygen at room temperature, evacuated, cooled to -195° in helium and used for the ortho-para hydrogen conversion it is found that the oxygen treatment lowers the time of half conversion as compared to the sample before oxygen treatment as shown in Table III from ~1500 to ~230 min. Using the data in Table II that 0.09 cc. of physically adsorbed oxygen gives a time of half conversion of 41 min. one can calculate that the first-order rate constant K is: $K = 0.46 \times 10^{-3} + 184 \times 10^{-3} \gamma$ l/min. where γ is cc.(S.T.P.) of oxygen on the surface. A time of half conversion of 230 min. ($K = 3 \times 10^{-3}$) would be caused by 0.0136 cc. of oxygen on the surface so that the observed paramagnetism of the silver surface produced by oxygen chemisorption would be equivalent to a surface on which 0.0136 cc. of oxygen was

(9) J. H. DeBoer, "Advances in Catalysis," Vol. 8, Academic Press, New York, N. Y., p. 79.

(10) "Second International Congress of Surface Activity," Vol. II, p. 299.

(11) Y. A. Sandler, THIS JOURNAL, 58, 54 (1954).

TABLE III

	Time of half conversion, min.
Silver sample reduced and evacuated at 500°	1700
Reduced and evacuated at 500° and then contacted oxygen at 1000 mm. for 100 hr. at 25°. Oxygen evacuated 1 hr. at 25°	200
Silver sample reduced and evacuated at 450°	1500
Reduced and evacuated at 500° and then contacted oxygen at 1000 mm. for 24 hr. at 25°. Oxygen evacuated 1 hr. at 25°	220
Silver sample reduced and evacuated 500°	1300
Reduced and evacuated at 500° and then contacted oxygen at 100 mm. for 11 days at 25°. O ₂ evacuated 1 hr. at 25°	290
Silver sample cooled from 240 to -78° in 500 mm. of oxygen. O ₂ evacuated at -78°	220

chemisorbed. Since the surface is 1.5 m.² this is

equivalent to 1 impaired electron per 150 Å.² using $\frac{3}{8}$ (¹¹) as the ratio of the square of the magnetic moment of the electron to the oxygen molecule. The paramagnetism observed could not come from physically adsorbed oxygen; however, since this would be removed by evacuation at room temperature (or -78°), so we have ascribed it to the presence of chemisorbed oxygen molecules on the surface (the presence of divalent silver on the surface would seem unlikely). Since the surface chemisorbs 0.3 cc. of oxygen at room temperature, then if one assumes the 0.0136 cc. of oxygen were equivalent to ~0.036 cc. of oxygen molecule ions (using the factor $\frac{3}{8}$ again)¹¹ one would say that 5% of the species present on the surface are chemisorbed oxygen molecules (O₂ assumed to give two chemisorbed atoms). These results give evidence for the existence of a small steady state concentration of chemisorbed oxygen molecules on silver surface covered with chemisorbed oxygen.

PHYSICAL TECHNIQUES IN THE STUDY OF SILVER CATALYSTS FOR ETHYLENE OXIDATION

BY J. N. WILSON, H. H. VOGEL, D. P. STEVENSON, A. E. SMITH AND L. T. ATKINS

Shell Development Company, Emeryville, California

Received October 7, 1958

To investigate whether different crystal planes of silver give different results in the catalytic oxidation of ethylene to ethylene oxide with air, several types of evaporated silver film were used. By evaporating *in vacuo* or in 1 mm. of nitrogen or hydrogen, films containing crystals randomly oriented or with the 110 plane parallel to the glass support were obtained. Both types were about equally active and selective. Most significantly, it was found that use of an oriented film for ethylene oxidation at 250–280° caused recrystallization to randomly oriented material in 2–4 hours. Thus, unusual crystal faces would not be expected to persist in use. Disorientation did not occur when similar films were heated in air at 250°. Detection of volatile impurities in silver catalysts was done by heating to near-fusion temperature in a small chamber connected to the inlet reservoir of a mass spectrometer. Appreciable amounts of carbon, oxygen, hydrogen and sulfur compounds were shown to be present in silver made by reduction of the oxide or by chemical deposition from solution. Fractional monolayers could be detected on catalysts with surface areas of 0.2 m.²/g. Another measurement of possible utility was that of surface potential relative to a gold electrode in air. Values for powdered silver catalysts held in a flat tray ranged from -500 to +500 mv. and were reproducible to about 10 mv. Chemisorption of phosphorus, sulfur or chlorine compounds made the values more negative.

The oxidation of ethylene with air or oxygen over silver catalysts is an important industrial process. Although many practical and fundamental studies of this reaction system have been made,^{1,2} much remains to be learned, both about mechanism and the nature of the catalyst. In some respects the silver catalysts are ideally suited to basic studies, for pure silver, unsupported and unpromoted, is an effective catalyst. Surface areas are very low, however, often falling in the range 0.02 to 0.2 m.²/g., and the surfaces are poisoned easily. The present paper describes some fundamental studies of silver catalysts using three special physical techniques. The first, electron diffraction observations on evaporated silver films before and after use, has given a definite answer to one of the basic questions concerning this system. The other two, detection of impurities by flashing into a mass spectrometer, and measurement of surface potentials, show real promise for applications but are described here only

as methods of wide possible utility for the study of catalysts.

Part I. Recrystallization of Silver under Influence of the Reaction

A silver catalyst that consists of a collection of small silver crystals may expose various crystal planes to the gas phase. It was thought that different faces might have different activities and different selectivities for the formation of ethylene oxide. To examine this question, evaporated silver films were used. By controlling evaporation conditions one can prepare films in which the crystals are randomly oriented, and others in which the crystals are oriented with the 110 plane parallel to the glass surface where the film is deposited. If different faces are exposed in the two types of film, and if different faces give different catalytic results, then catalytic tests on the films should show a difference. There was thus a chance that tests on evaporated films would supply evidence regarding the effect of crystal face on the reaction. Actually, however, another answer, of equal significance, was obtained from the experiments. It was found that

(1) G. H. Twigg, *Proc. Roy. Soc. (London)*, **188A**, 92, 105, 123 (1946).

(2) A. Orzechowski and K. E. MacCormack, *Can. J. Chem.*, **32**, 388, 415, 432, 443 (1954).

under the influence of the reaction the silver recrystallized so that an oriented film became randomly oriented. This implies that in prolonged operation of a silver catalyst a preferred face or combination of faces will form, and that preparation so as to favor a particular face will not have lasting effect.

Recently Kummer³ has observed ethylene oxidation on different faces of silver single crystals. He did not find any clear cut catalytic difference. It is conceivable that there was a surface recrystallization to bring all his faces to the same state. It is also possible that the faces he examined (211, 111, 110) do give the same results.

Experimental

Silver films were prepared by evaporation from an electrically heated silver filament or from a tungsten filament wrapped with silver wire. They were evaporated onto about 18 cm. of the inside surface of a Pyrex glass tube 4 cm. in diameter. A small holder carrying a flat, polished glass plate, 1 cm. by 2.5 cm., also was exposed to the evaporating silver. During evaporation both the glass plate and the tube were cooled to about 20°. Evaporations were *in vacuo* or in about 1 mm. of H₂ or N₂. Total weights of films were from 50 to 150 mg.

After the evaporation the tube was opened to the air, the filament was removed, and the plate was transferred to an electron diffraction apparatus for structure determination by diffraction of 32-35 kv. electrons at grazing incidence. Then the plate was again placed in the tube, and the entire tube and plate were made the reactor for a flow-system apparatus for the oxidation of ethylene. After use the tube was cooled and the plate again was transferred to the diffraction apparatus for structure determination. Transfer could be repeated as desired.

Ethylene oxidation over the evaporated films was carried out at 250-276° and atmospheric pressure. A mixture of 10 parts air and one part ethylene was passed through a guard tube containing cold granular silver catalyst and into the top of the tube containing the film. Total flow rate was 110 cc./min., for volumes measured at 0° and 760 mm. The reaction gases leaving the bottom of the tube were periodically passed through a simple absorption train for analysis. The train consisted of two bubblers containing 0.02 N HCl saturated with MgCl₂ to absorb ethylene oxide, a drying tube containing Drierite and a weighed tube containing Ascarite for collection of CO₂. Since ethylene oxide and CO₂ are the only major products, this train gave an adequate analysis. From the amounts of ethylene oxide and CO₂ found and the known sampling period and inlet flow rate, the following were calculated

$$\% \text{ reacted} = \frac{\text{moles ethylene consumed}}{\text{moles ethylene fed}} \times 100$$

$$\text{Selectivity, \%} = \frac{\text{moles C}_2\text{H}_4\text{O produced}}{\text{moles ethylene consumed}} \times 100$$

The percentage reaction over silver films was only 0.3-1.0%, and with this small amount of reaction the selectivity determinations were not very accurate. Nevertheless, trial tests made with small amounts of bulk silver catalysts of known characteristics showed that selectivities could be measured within 10% at this level of reaction. In these trial tests the bulk silver catalysts were supported loosely on glass wool placed in the otherwise empty 4 × 45 cm. evaporation tube.

Results

Silver differs from other face-centered cubic metals previously investigated by electron diffraction-observations of evaporated films in this Laboratory.⁴ In the past work, nickel, palladium, gold and platinum were found to form oriented films readily by evaporation in the presence of an inert

gas. It is much more difficult to obtain highly oriented films with silver. Evaporation conditions and structures observed for five silver films are given in Table I. We did not attempt to define closely the conditions needed for obtaining a film of a given type. It was sufficient for the present purposes that films of several types were obtained.

TABLE I

EVAPORATED SILVER FILMS

Evaporation was onto glass at about 20°. Orientation planes are parallel to the glass support.

Film no.	Evaporation conditions Atmosphere	Speed	Weight, mg.	Crystal structure of film by electron diffraction
2	1 mm. N ₂	Slow	21	Cubic Ag medium oriented 110
3	0.75 mm. N ₂ + 0.002 mm. H ₂	Slow	80	Cubic Ag oriented 110. Some oriented X crystals
4	Vacuum, 10 ⁻⁵ mm.	Rapid	81	Cubic Ag random and oriented. Some X random and oriented
5	0.84 mm. N ₂	Slow	77	X mostly oriented
6	Vacuum, 10 ⁻⁶ mm.	Slow	150	Cubic Ag oriented 110

In addition to face-centered cubic silver, another crystalline material was observed in some of the films. Although this material has not been identified definitely, there is evidence that it may be a hexagonal interstitial compound of nitrogen (or argon) in silver. This material, which is designated as "X" in the tables, was oriented if the silver was oriented. It disappeared on heating in hydrogen or during the use of a film for the oxidation of ethylene. It did not disappear on heating in air at 250° for 7 hours. Films 2 and 6 did not contain appreciable amounts of this unidentified material.

Table II describes changes of the films on heating

TABLE II

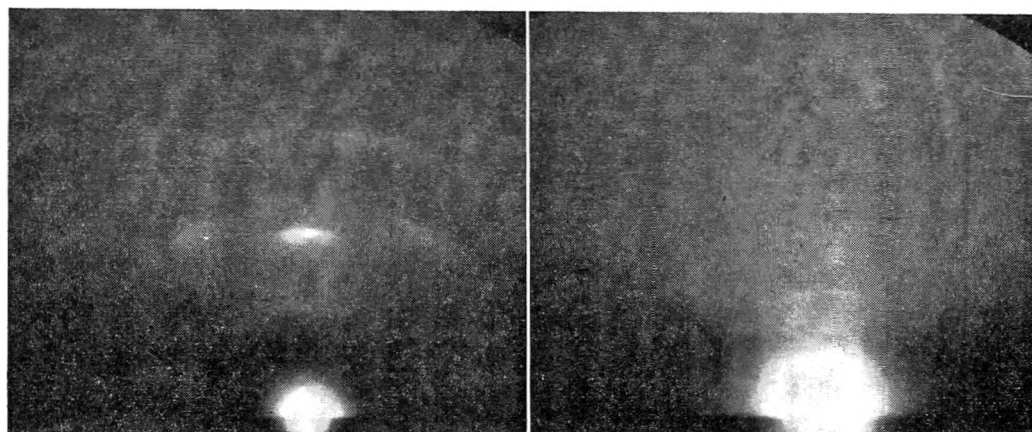
CHANGES OF EVAPORATED SILVER FILMS

Film no.	Exposure of film	Structure by electron diffraction
Exposures of films were applied in sequence, as listed		
2	None	Cubic Ag oriented 110
	Vacuum, 1 hr., 250°	As above, little change
	Air-C ₂ H ₄ , 2 hr., 250°	Much of orientation gone
	Air-C ₂ H ₄ , 6 hr., 250°	All orientation gone. Cubic Ag random
3	None	Cubic Ag oriented 110, plus X oriented
	Air, 7 hr., 250°	As above, little change
	Hydrogen, 1 hr., 250°	Cubic Ag oriented 110. X gone
	Air-C ₂ H ₄ , 5 hr., 250°	Almost all orientation gone
4	None	Cubic Ag random and oriented, plus X random and oriented
	Air-C ₂ H ₄ , 2 hr., 250°	Cubic Ag random. X gone. Some unidentified material

or use. Heating *in vacuo* or hydrogen for one hour at 250° did not destroy orientation of the silver, nor did heating in air for 7 hours at 250°. Use for ethylene oxidation, however, completely destroyed the orientation in 2-5 hours. Examples of the

(3) J. T. Kummer, THIS JOURNAL, 60, 666 (1956).

(4) O. Beeck, A. E. Smith and A. Wheeler, Proc. Roy. Soc. (London), 177A, 62 (1940).



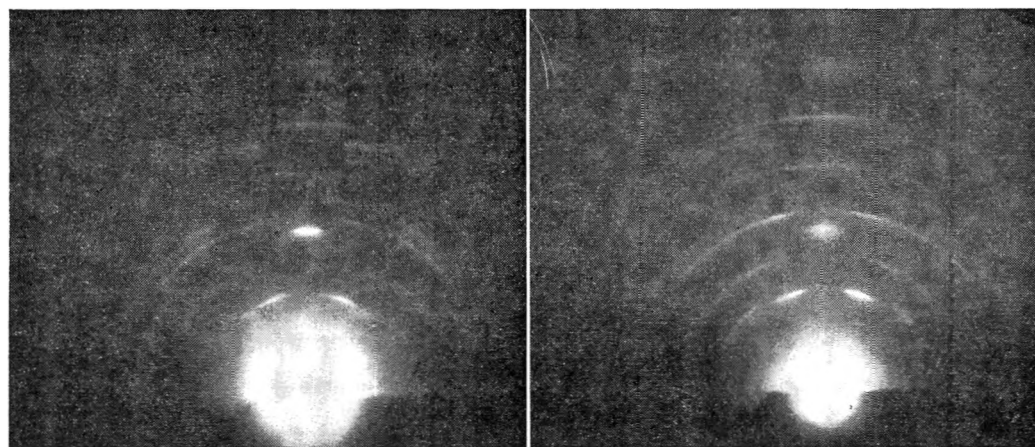
(a) Original silver film deposited in 1.0 mm. N_2 (b) Same film after use for ethylene oxidation for 8 hr.

Fig. 1.—Electron diffraction patterns from film no. 2.



(a) Original silver film deposited in 0.75 mm. N_2 . (b) Same film after heating in air 7 hr., H_2 1 hr., and use for ethylene oxidation for 5 hr.

Fig. 2.—Electron diffraction patterns from film no. 3.



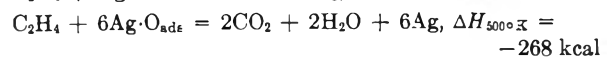
(a) Original silver film deposited in 0.75 mm. N_2 (the electron beam was at a lower angle of incidence to the film than in Fig. 2 and therefore surface features such as "X" lines show more strongly). (b) Same film after heating in air at 250° (same beam angle as in (a)).

Fig. 3.—Additional diffraction patterns for film no. 3.

change of structure in use are shown in Figs. 1 and 2 for films 2 and 3. The ineffectiveness of heating in air is shown in Fig. 3. Although the pictures are rather blurred, it is evident that the bright spots

characteristic of oriented crystals are gone after use, and only the rings for random cubic silver remain. The strong effect of reaction on the crystal structure is similar to that found by Leidheiser

and Gwathmey⁵ for copper single crystal faces used to catalyze the $H_2 + O_2$ reaction. We can visualize it as an effect of the repeated adsorption of oxygen followed by removal by reaction. The heat of adsorption of oxygen on silver is 16 kcal./mole according to Berton and Drake.⁶ The heats of reaction of this adsorbed oxygen with ethylene are considerably greater. Thus we estimate



Such amounts of energy, when released locally, can evidently cause considerable movements of the silver atoms. The relatively rapid surface rearrangement that occurs shows that initial differences in the crystal faces exposed cannot be held responsible for lasting differences in catalytic properties of practical silver catalysts.

Table III gives some catalytic results with the silver films. Activities were the same, within a factor of two, for all the films. There was no correlation between activity or selectivity and the types of film present at the start of a test. For the most part, selectivities fell in the range 30–50%, as observed by Kummer.³ The higher selectivities observed with film 3 and with film 4 in the last sample probably result from partial poisoning of the films with impurities from the reaction system. It is well known that certain impurities cause an increase in the selectivity of silver catalysts for this reaction.

TABLE III

ACTIVITY TESTS OF EVAPORATED SILVER FILMS

Air at 100 cc./min. plus ethylene at 10 cc./min. passed over film at atmospheric pressure

Film no.	Temp., °C.	Hr. use	% Reacted	Selectivity, %	Type of film at start
3	250	1.5	0.6	62	Oriented cubic Ag,
		5	0.3	84	some oriented X
4	250	1.5	1.0	41	Random cubic Ag,
		8	0.5	49	some X
5	276	10.5	.5	59	
		1	.3	44	Oriented X
6	256	4.5	.5	46	
		0.1	.9	29	Oriented cubic Ag
		3	.7	35	
		7	.7	32	

Part II. Detection of Impurities in Silver Catalysts

In part I it was shown that oriented films of silver are not stable under reaction conditions and therefore particular crystal planes cannot be made responsible for the observed catalytic differences often met among various silver catalysts. We are left with adsorbed or contained impurities as the most likely cause of such differences. Conventional analyses are of some help in detecting such materials, but since surface areas of silver catalysts are quite low, small amounts of impurities can have large effects, and sensitive methods of detection are desirable. One such method is a flashing technique combined with mass spectrometric analysis. This has been applied to a number of nearly pure silver

catalysts to show the presence of sulfur, carbon and oxygen compounds in amounts sufficient to form up to ten monolayers on the surface. Amounts of sulfur as low as 0.05 part per million were detected; this could cover only 0.0005 of a monolayer. Another technique that shows promise of rapidly detecting effects of certain types of adsorbed materials is the surface potential with respect to a reference electrode. Normally this is measured on bulk metals in a vacuum system. We have obtained results that appear to be significant by using silver powders in air.

Experimental

The flashing technique was applied to fresh or used "pure" silver catalysts in granular form. The sample of 1–5 g. was placed in a small quartz vessel attached to the inlet system of a mass spectrometer. Normally the catalyst was first evacuated 30 minutes at 25°. Then the vessel was connected to the inlet system and the sample was rapidly heated to about 800° with an induction furnace or a small resistance furnace. The composition and amount of the evolved gas were determined by the mass spectrometer.

Surface potentials were measured in the conventional way, using a vibrating gold electrode that formed one plate of a condenser while the grounded sample near it formed the other plate. The alternating current produced by the changing capacity was displayed on an oscilloscope. A counter potential was imposed on the condenser, and the magnitude needed to minimize the alternating current was taken as the surface potential. Similar apparatus has been described by Zisman.⁷ The silver catalysts had ample conductivity for this measurement. The granules were ground to a powder below 60 mesh and were put into a holder having an aluminum bottom 3.8 × 6 cm. and glass sides 1.5 mm. high. The loose powder was levelled and pressed down with a ten pound weight. The first reading was taken after about one minute. Further observation showed a slow drift in the potential, normally ranging from zero to 15 mv./min. The humidity of the atmosphere influenced the drift rate. Here only initial values of the potential are considered. In any further work of this kind, measurements could be refined by more rigorous pretreatment of samples and by better control of the ambient atmosphere.

Three types of silver catalyst were used, namely, precipitated silver, reduced silver oxide and silver from the lactate supported on Alundum.

Precipitated silver catalysts were prepared by adding a 50% KOH solution to a 9% silver nitrate solution containing dextrose. Quantities were 355.5 g. of $AgNO_3$ and 45 g. of dextrose in 4500 ml. of water, and 250 g. of KOH in 250 ml. of water. The addition took 12 to 17 minutes. The reduction of the precipitated silver oxide was completed by stirring for 45 minutes at room temperature and then heating to 70–75° during the course of another 45 minutes. The silver powder formed was filtered, washed and dried at about 120°. The powder was then pressed into a porous cake and this was broken into 10–20 mesh granules for use. Many such preparations were made; the catalysts were highly active for the oxidation of ethylene at 200° when tested with 100 cc./min. air and 10 cc./min. ethylene passed over 7 cc. of catalyst at atmospheric pressure (percentage reacted 20–80%).

Reduced silver oxide catalysts were made by the reduction of granular silver oxide in a stream of 9% H_2 , 91% N_2 at 170–220°. Silver oxide was prepared by adding a 9.1% KOH solution to a 9.1% $AgNO_3$ solution. Addition was normally at room temperature over a period of 10–30 minutes. In some cases stoichiometric KOH was used; in others an excess. The precipitate stood for one hour, and then was filtered, washed and dried. Usually the filter cake could be broken into granules of adequate strength for reduction and use. These catalysts were of about the same activity as the precipitated silver catalysts.

Silver from lactate on Alundum was prepared by impregnating Alundum pellets from the Norton Company with a hot solution of silver lactate. This then was decomposed in a stream of nitrogen at 400° for about eight hours.

(5) H. Leidheiser and A. T. Gwathmey, *J. Am. Chem. Soc.*, **70**, 1200 (1948).

(6) A. F. Benton and L. C. Drake, *ibid.*, **56**, 255 (1934).

(7) W. A. Zisman, *Rev. Sci. Instr.*, **3**, 367 (1932).

TABLE IV
GASES FLASHED FROM CATALYSTS AT HIGH TEMPERATURE
Samples were pre-evacuated to 25°, except as noted. Analyses by mass spectrometer.

No.	Type	Catalyst		Area, m. ² /g. ^a	CO ₂	Gases obtained, cc. cm. ³ /g. of catalyst			
		History				O ₂	CO + N ₂	H ₂	SO ₂
244a	Ppt. Ag	Fresh ^b		0.16	11.8	0.2	1.8	2.2	0.06
244a	Ppt. Ag	Used		.14	4.7	4.2	1.2	0.7	.05
248	Ppt. Ag	Fresh ^b		..	10.2	3.1	1.7	0.7	.003
244a	Ppt. Ag	Fresh		.16	53.2	2.9	3.0
244a	Ppt. Ag	Fresh		.16	50.6	4.0	3.3	0.0	...
152	Ppt. Ag	Fresh		.17	19.8	0.0	14.4	26.5	...
285	Redcd. Ag ₂ O	Fresh		.42 ^c	16.6	0.03	3.5	6.0	...
288	Redcd. Ag ₂ O	Fresh		..	18.6	0.02	2.8	0.3	...
273	Redcd. Ag ₂ O	Fresh		..	8.2	0.05	3.4
273	Redcd. Ag ₂ O	Used		.18	5.5	3.8	2.9
311	Redcd. Ag ₂ O	Fresh		..	2.5	32.7	1.8	..	.02

^a Surface area by B.E.T. method, using Kr gas adsorbed at -195°. ^b Pre-evacuated at 120°. Therefore gave relatively less gas. ^c Area value for a used sample of Catalyst No. 285.

Catalysts were made up to contain 10-15% silver by weight. These catalysts were somewhat less active than the others, requiring of the order of 220-240° for equivalent conversions.

Results

Some data obtained by flashing gases from catalysts are given in Table IV. The large quantities of gas are remarkable. These catalysts had surface areas of the order of 0.2 m.²/g., and 3.5 cc. cm. of N₂ will form a monolayer on a gram of such material. The evolution of up to 20 times this amount of gas, chiefly CO₂, O₂ or H₂, suggests that bulk materials like silver carbonate or materials trapped within the silver were present. This technique is clearly useful in showing the presence of such impurities. The smallest quantity detected, 0.003 cc. cm./g. of SO₂ from one catalyst, corresponds to only 0.0005 of a monolayer, assuming one sulfur atom for each surface silver atom, and an average area per silver atom like the 100 face (8.31 Å.²).

Large amounts of gases (CO₂, CO, and H₂ or O₂) were evolved from the precipitated silver catalysts, and these no doubt derived from the dextrose used for reduction. It is likely that most of the impurities were present as bulk materials or were trapped within the silver and were not actually adsorbed on the surface. Small amounts of hydrocarbons were obtained from these catalysts, including C₂ to C₄ hydrocarbons and benzene. Less gas was produced by the reduced silver oxides, though in one example a considerable quantity of oxygen appeared, suggesting that the catalyst had not been reduced completely. Some adsorbed oxygen is expected after exposure to O₂ or air, as in use. The CO₂ from reduced Ag₂O may derive from Ag₂CO₃ or from adventitious organic matter. Hydrogen from the reduced Ag₂O may represent trapped water. The hydrogen was eliminated very slowly by either evacuation at 200° or heating in oxygen at 200°. There were no hydrocarbons from the silver oxide catalysts.

Use for ethylene oxidation did not introduce new materials into the evolved gases and in general diminished the total amount evolved. Most of the catalysts produced a small amount of a mass 30 ion, not identified and not listed in the table, but perhaps representing NO derived from the silver

TABLE V
SURFACE POTENTIALS OF SILVER CATALYSTS
Measurements relative to a gold electrode in air

No.	Type	Catalyst		Surface potential, mv. Δ	
		History			
152	Ppt. Ag	Fresh		-215	
152	Ppt. Ag	Used, S poisoned		-455	-240
225	Ppt. Ag	Used, S poisoned		-491	
244a	Ppt. Ag	Fresh		-382	
262	Ppt. Ag	Fresh, 70° prepn.		-415	
269d	Ppt. Ag	Fresh, 1 hr. 350° in air		-424	
269d	Ppt. Ag	Used, C ₂ H ₆ in feed		-296	
215	Lactate	Fresh		+98	
215	Lactate	Used, S poisoned		-215	-315
220	Lactate	Fresh		+530	
220	Lactate	Used, Cl poisoned		+313	-220
239	Lactate	Fresh		+278	
239	Lactate	Used, poisoned		-59	
239	Lactate	Used, S poisoned		-34	-310
282	Lactate	Fresh		-101	
282	Lactate	Used, P poisoned		-161	
273	Redcd. Ag ₂ O	Fresh		-330	
293	Redcd. Ag ₂ O	Fresh, O ₂ treated		-515	
293	Redcd. Ag ₂ O	Fresh, H ₂ treated		-410	
304	Redcd. Ag ₂ O	Fresh, AgNO ₃ added		-380	
304	Redcd. Ag ₂ O	Used		-412	
305	Redcd. Ag ₂ O	Fresh, standard prepn.		-113	
306	Redcd. Ag ₂ O	Fresh, meagre washing		-415	
308	Redcd. Ag ₂ O	Fresh, repeat of 306		-351	
309	Redcd. Ag ₂ O	Fresh, excess KOH		-379	
309	Redcd. Ag ₂ O	Used		-374	

nitrate used in preparation. The maximum sulfur dioxide observed was only enough to cover 0.02 of the surface, assuming one sulfur atom per surface silver atom.

Surface potential data are collected in Table V. According to the extensive and valuable work of Mignolet,³ surface potential tells us much about the nature of adsorbed gases, being related to the elec-

tric moment of the adsorbed molecules and to their concentration on the outer surface. According to Mignolet, chemisorption normally makes the potential more negative. The data of Table V represent a cursory survey of some catalysts by this method. No systematic study was attempted, but it was clear from the wide range of values that this is a sensitive and potentially valuable tool. The potentials ranged from -500 to $+500$ mv., relative to the gold reference electrode. Most of the values were negative. Some observations from the data are given.

Adsorption of compounds of phosphorus, sulfur

or chlorine on catalysts made the surface potentials more negative by 20 to 250 mv. Although measurements were reproducible to within about 10 mv. in successive measurements on the same sample, there was no clear correlation between surface potential and catalytic activity or selectivity. When catalysts were allowed to stand in closed containers for several days, the surface potential did not change.

Acknowledgment.—Thanks are due to R. G. Meisenheimer for assistance in some of the degassing experiments and for observations on the slow removal of hydrogen from catalysts.

ADSORPTION AND DIFFUSION OF ARGON ON TUNGSTEN¹

By ROBERT GOMER

Institute for the Study of Metals and Department of Chemistry, The University of Chicago, Chicago 37, Illinois

Received October 7, 1958

A field emission method for studying the adsorption and diffusion of A on W is described. It is found that the first adsorbed layer decreases the work function of W by 0.8 volt. Multilayer adsorption is observed by the decrease in emission caused by layers beyond the first. Estimates for the heat of adsorption and the activation energy of diffusion in the first layer are obtained. The behavior of the multilayer adsorbate is discussed in terms of its physical and electrical properties.

The study of physical adsorption on clean single crystals of known orientation eliminates the smearing out of effects unavoidable with conventional adsorbents and permits fairly detailed observations. A field emitter² makes an ideal adsorbent since it is a small, almost perfect single crystal simultaneously exposing several faces. Observation of adsorbed layers is visual and made possible by changes in electron emission, which often can be converted into work function changes.

A field emission technique for the study of adsorption and diffusion of chemisorbates³ has been modified for similar studies with physically adsorbed gases. This paper presents some of the findings for the system argon-tungsten. A preliminary report of this and related work has appeared.⁴ Since it was started the author has learned of very similar investigations by Ehrlich.⁵

Experimental

The method consists of evaporating the gas to be studied onto a field emitter from one side with the body of the tube at 4.2°K. Rebounds of gas molecules from the walls do not occur at this temperature, so that only the portions of the emitter "seeing" the gas source receive a deposit.³ The source used here has not been described in detail previously.⁶ It is shown schematically in Fig. 1 and consists of a Pt sleeve, 1 mm. in diam. and 1 cm. long constructed of 0.001" Pt foil. This mortar is open at the end pointing to the tip and spotwelded to a W rod at the other. The

latter is sealed into a glass well as shown. A smaller W rod and Pt wire provide contact so that the mortar may be heated electrically. The latter is loaded by piping liquid He into the glass well through a fine rubber hose while the rest of the field emission tube is at 77°K. The mortar is cooled rapidly by conduction so that any gas contained in the tube condenses there preferentially. After the source has been loaded, liquid He is allowed to spill over from the well into the body of the cryostat and to surround the entire emission tube.

In order to prevent cooling of the glass wall of the well before condensation in the mortar is complete, a Teflon tube is fitted snugly over the press seal P. A glass funnel fitted into the upper end of this tube provides for some storage of liquid He before spill-over into the cryostat occurs. He is piped into the source by fitting a transfer tube⁷ into a Teflon coupling whose lower end terminates in a rubber hose leading into the source.

At 4.2°K. pressures below 10^{-15} mm. within the tube are assured no matter what gas (except He) it contains. Preferential condensation in the source which is not hit by the electron beam from the field emitter, permits operation with large currents and also with high pressures (at room temperature) of gas in the tube. The source described here can be used with almost any gas and can be reloaded indefinitely.

In the present experiments a field emission tube, described in detail elsewhere³ was filled with 30 mm. of Airco Spectroscopic Grade Argon, purified only by passage over liquid N₂.

Tip temperatures were found from the resistance of the W loop to which it was spotwelded. Calibration points of 4.2, 20.4, 63 and 77.8°K. were used. It was found that a plot of $\log R$ vs. $\log T$ was linear in this range if the (very low) 4.2°K. residual resistance was subtracted from the resistance values. This plot is shown in Fig. 2. Temperatures below 20.4°K. were estimated by using the curve of Fig. 2.

Average values of work functions and field strengths were found from the slopes of Fowler-Nordheim plots in the usual manner.³ Tip radii were calculated from the approximate relation³

$$E = V/5r \quad (1)$$

where E is the electric field, V the applied potential and r the tip radius. In the diffusion experiments a tip of radius 1.5×10^{-5} cm. was used.

(1) This research was supported in part by a grant from the Petroleum Research Fund administered by the American Chemical Society. Grateful acknowledgment is hereby made to the donors of this fund.

(2) A summary of field emission work through 1955 is given in R. H. Good and E. W. Müller, *Handbuch Physik*, XXI, 196 (1956).

(3) Details of the method are to be found in R. Gomer, R. Wortman and R. Lundy, *J. Chem. Phys.*, **26**, 1147 (1957). Other pertinent papers: Wortman, Gomer and Lundy, *ibid.*, **27**, 1099 (1957); Gomer and J. K. Hulm, *ibid.*, **27**, 1363 (1957).

(4) R. Gomer, *J. Chem. Phys.*, **29**, 441, 443 (1958).

(5) G. Ehrlich, T. W. Hickmott and F. G. Hudda, *ibid.*, **28**, 977 (1958), and private communications.

(6) R. Gomer, *ibid.*, **28**, 168 (1958).

(7) J. W. Stout, *Rev. Sci. Instr.*, **25**, 929 (1954).

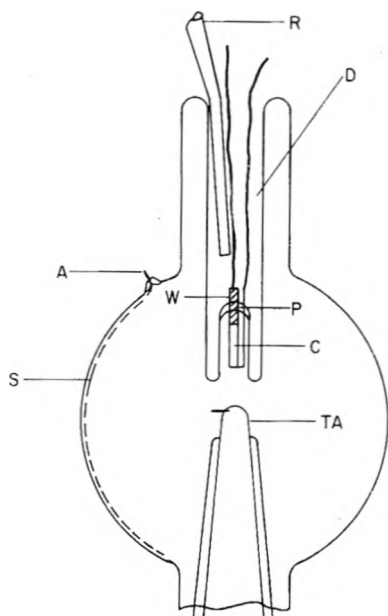


Fig. 1.—Schematic diagram of field emission tube for surface diffusion studies with universal gas source: S, fluorescent screen; A, anode lead; TA, tip assembly; D, glass Dewar well; R, rubber hose guiding liquid He into D; C, Pt mortar; W, heavy tungsten lead spotwelded to C for rapid cooling; P, press seal.

Results

When small amounts of A were evaporated onto the tip enhancement of emission occurred. Diffusion of such doses was complete at 18°K. in 60 seconds. The appearance of the pattern corresponding to this state is shown in Fig. 3. It will be noticed that brightening is most pronounced around the 100 faces. The work function decrease on adsorption has a maximum value of 0.8 volt.

When larger amounts of A were evaporated the region of deposit was darkened, as shown in Fig. 4. Under these conditions some diffusion occurred again at 18°K. and led to enhanced emission on the originally clean portions of the tip. On raising the temperature to 21–22°K. more diffusion occurred, with sharp boundaries and in waves, or layers. There was a time lag of a few seconds between some of these waves, making it possible to see several simultaneously, as shown in Fig. 5. As many as 4 waves could be counted, each leading to a further decrease in emission. At maximum coverage (~5 layers or waves) the apparent work function increased from the minimum of 3.7 to a value of 4.3 volts.

If the tip was heated to 26–28°K. evaporation occurred, with concentric sharp boundaries, which shrank at different rates toward the center of the tip. The innermost boundary, enclosing the darkest region, shrank most rapidly and the outermost one corresponding to highest emission least so. The process required about 10 seconds at 28°K. and left the tip in a state identical to that resulting from a light A deposit, with a work function of 3.7 volts. If the tip was now heated to 30–35°K. this adsorbate evaporated, leading to the pattern and work function (4.5 volts) of clean W. It was possible to obtain a plot of $1/T$ vs. log of desorption time, shown in Fig. 6. A value of 1870 ± 300 cal. was

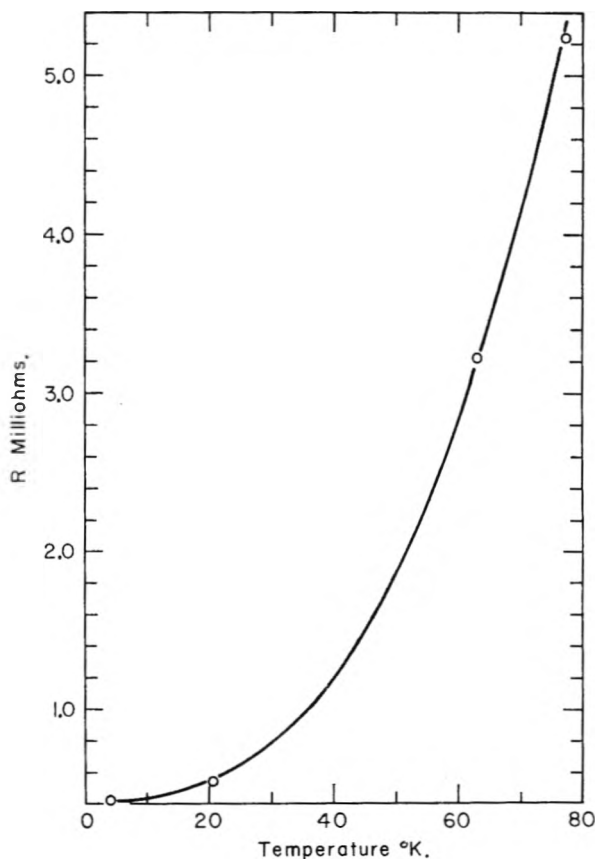
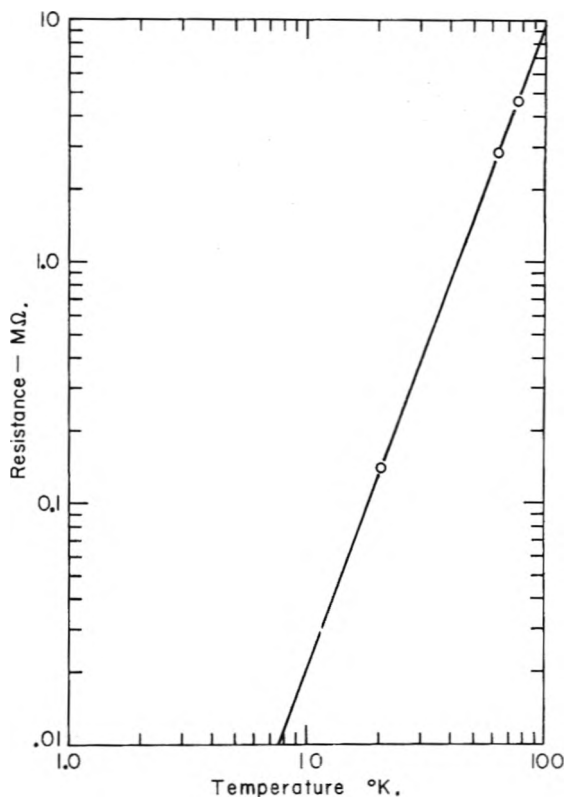


Fig. 2.—(a) Plot of log resistance vs. log absolute temperature for a tungsten loop. The 4 2°K. residual resistance has been subtracted from the R values in making this plot. (b) Plot of resistance vs. temperature for the W loop of Fig. 2a.

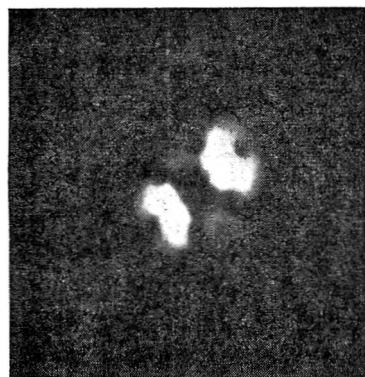


Fig. 3.—Field emission pattern from a W tip covered with a monolayer of A. Note the emission enhancement around the 100 faces.

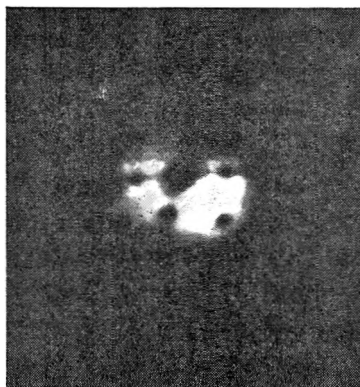


Fig. 4.—Appearance of W emission pattern when a heavy dose of A is evaporated onto upper half of tip.

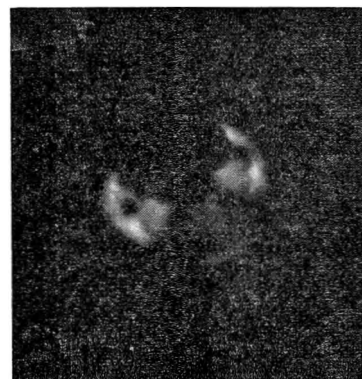


Fig. 5.—Multilayers flowing over W tip. Two boundaries can be seen inundating the surface; $T \cong 22^\circ\text{K}$.

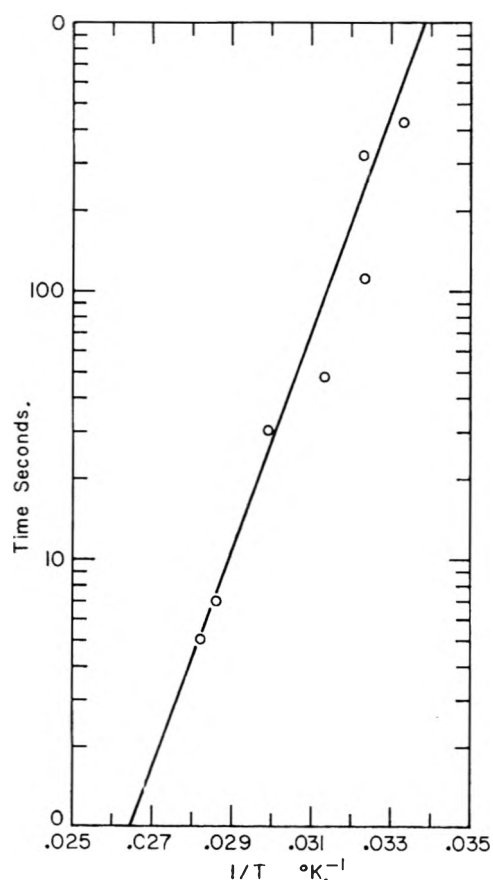


Fig. 6.—Plot of $1/T$ vs. log desorption time for a monolayer of A on W.

calculated for the activation energy. Evaporation of that fraction of the adsorbate which enhanced emission occurred without boundaries.

When enough A to reduce emission was adsorbed two field effects were noticed. At 25°K . an increase in the field above 3.7×10^7 volts/cm. resulted in pulling the adsorbate cap into the center of the tip as shown in Fig. 7 from the original position shown in Fig. 8. After a few seconds spontaneous relaxation occurred and the adsorbate flowed away from the center. Further increases in field led to a repetition of the cycle until the state of Fig. 3 with a

work function of 3.7 volts resulted. With each cycle some increase in emission occurred.

For the highest coverages a spontaneous breakdown of the layers was noted at 4.2°K . and high currents ($\sim 10^7$ amperes). This showed up as the formation of bright patches which could grow spontaneously to large size. Heating to $\sim 20^\circ\text{K}$. healed these breaks.

Successive decreases in resolution with increasing coverage were noted until the pattern was almost totally smeared out at maximum coverage as shown in Fig. 8.

Discussion

These facts are most consistently interpreted as follows. At sufficiently low temperatures mono- and multi-layer physical adsorption of A on W takes place even at zero pressure. Monolayer formation is accompanied by a decrease in work function, probably because of charge transfer from the adsorbate to the substrate. This was first observed by Mignolet on evaporated metal films by a vibrating condenser method.⁸ The magnitude of this contact potential, 0.8 volt, corresponds to a dipole moment per ad-atom of 0.43 Debye, assuming a maximum coverage of 10^{15} A atoms/cm.² of surface. This results in relatively strong dipole-dipole repulsions between atoms in the first layer, making the latter a two-dimensional gas. This accounts for the absence of boundaries in the diffusion or evaporation of this layer. It is interesting to note that such boundaries are observed with Ne in the first layer, where the dipole moment per ad-atom is very small, so that repulsive forces are weak.⁴

The first layer is nearest the substrate and hence most tightly bound. This is in accord with the finding that the fraction of the adsorbate leading to enhanced emission evaporates at a higher temperature than the rest. It therefore seems safe to identify this portion with the first and the remainder with higher layers.

Charge transfer or any other plausible mechanism responsible for the contact potential is bound to be of short range, so that higher layers are unlikely

(8) J. C. P. Mignolet, *Rec. trav. chim.*, **74**, 685 (1955). References to previous work by this author are given there.

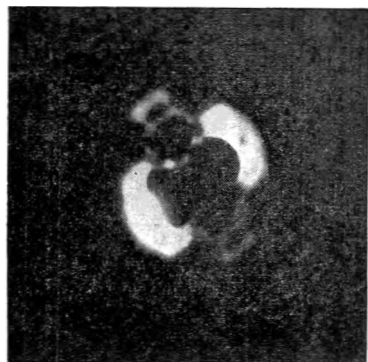


Fig. 7.—Multilayer adsorbate (dark) being pulled toward center of W tip by a field $E > 3.7$ volts/cm. at 25°K . Bright portion corresponds to monolayer of A.

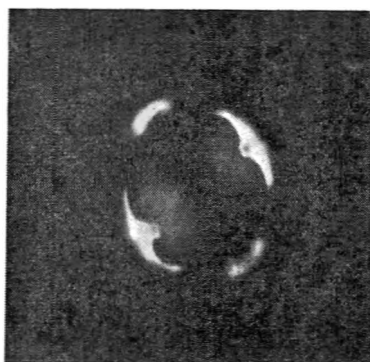


Fig. 8.—Multilayer adsorbate of A on W at a field < 3.7 volts/cm. Note almost complete lack of resolution.

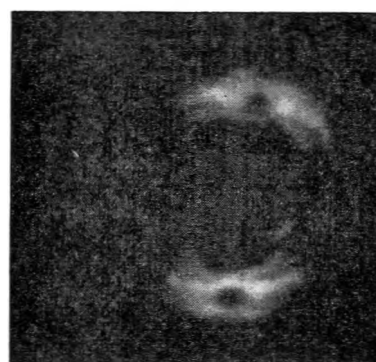


Fig. 9.—Evaporation of multilayer adsorbate of Ne on W at $\sim 5^\circ\text{K}$. Note concentric layer boundaries. Darkest area corresponds to maximum number of layers.

to participate in it. The consequent absence of strong dipoles in these layers should allow cohesive forces between ad-atoms to come into play. The observed boundaries are interpreted as layer edges, resulting from ad-atom attractions.

Layers beyond the first should behave as dielectrics. This will affect the emission in several ways.⁴

(1) It can be shown that a thin shell of dielectric reduces the field within it by $1/\kappa$, where κ is the dielectric constant.

(2) There will be scattering from the adsorbate, leading to decreased resolution and to a reduction in the pre-exponential term of the Fowler-Nordheim equation.

(3) There will be a reduction in image potential by $1/\kappa$.

(4) The ad-atoms will act as short-range potential wells for tunneling electrons, making the barrier more transparent.

Of these effects only the last enhances emission and is not able to compensate for the others, so that a net decrease in emission is observed for heavy coatings of all inert gases studied.⁴ Layers higher than the first should therefore show up visually by successive decreases in emission, as observed.

Evaporation should occur from layer edges where ad-atoms are least tightly bound. During evaporation layers should appear to shrink with the preservation of boundaries at their edges. The layer farthest from the substrate should be least tightly bound and hence evaporate most rapidly, the next layer, slightly less so, and so on. Thus the picture of shrinking concentric boundaries with least emission from the central area, observed during evaporation, is explained. The phenomenon is difficult to photograph with argon but not with neon. Figure 9 shows layers of neon evaporating slightly above 4.2°K .

The melting point of bulk argon is 84°K . It is remarkable that the ad-layers behave almost like two-dimensional liquids below 30°K . This is probably explained as follows. The lattice structure of the substrate is transmitted to the adsorbate layer by layer. Up to a point this prevents the latter from assuming its own bulk structure and thus introduces a great deal of local disorder, or a very large number of grain boundaries. Thus the layers possess only short range order and are liquids for all

practical purposes. Since the disruptive influence of the substrate must decrease with increasing distance the adsorbate will appear as an anisotropic liquid, somewhat like a liquid crystal.

Beyond a certain distance from the substrate, its disordering effect on the A lattice will cost more in the loss of A-A interaction than is gained by interaction with the substrate. The multilayered adsorbate should therefore become metastable with respect to A crystallites. The spontaneous brightening observed at 4.2°K . and high currents indicates that this occurs, and that formation of A crystallites denudes the adsorbed layers. Apparently a small increase in temperature suffices to melt these crystallites. It is interesting that the temperature for this is the same as that necessary for initiation of multilayer flow from an initial heavy deposit. Since the latter may very well consist of microcrystallites, it may be that onset of multilayer diffusion depends on melting these. It is not clear what causes the nucleation of crystallites from multilayers. It has been suggested by Ehrlich that the cause is connected with ion bombardment of the tip at high currents.⁵

The tidal pull of the field on the adsorbate can be interpreted as follows. There will be an interaction energy U_E between the dielectric medium and the field given by

$$U_E = 2\pi r^2(1 - \cos \theta_0)t_0 \left(\frac{\kappa - 1}{8\pi}\right) E_0^2 \int_0^\theta (1 - k\theta)^2 d\theta \quad (2)$$

where r is the tip radius, θ the polar angle of the adsorbate edge, κ the dielectric constant, E_0 the field at the tip apex, and k a constant describing the (assumed linear) decrease of E with θ . For most emitter geometries $k = 0.127$. t_0 is the film thickness at an arbitrary polar angle θ_0 . While t is a function of θ it will be noted that the combination $(1 - \cos \theta)t$ is not, so that it may be designated by a subscript to indicate its independence of θ .

Since E is a maximum near the apex the field will tend to pull the adsorbate toward the center. This tendency will be counteracted by the wetting energy of the multilayers on the first one. At equilibrium

$$\partial U / \partial \theta = 0 \quad (3)$$

so that the difference between the wetting energy of argon on argon covered tungsten and the surface energy of the outermost layer can be found from equations 2 and 3. Designating this quantity by γ we have

$$\gamma = (1 - \cos \theta_0) \epsilon_0 \left(\frac{K-1}{8\pi} \right) E_0^2 (1 - k\theta)^2 / \sin \theta \quad (4)$$

Substitution of $E_0 \cong 3.7 \times 10^7$ volts/cm. and $\theta = \theta_0 \cong 45^\circ$ results in a value of $\gamma \cong 12$ ergs/cm.² for a 20 Å. thick deposit.

When the field is increased the deposit is pulled toward the center. This results in a thickening, since the same number of atoms are based on a smaller area than before. At moderate temperatures the outermost layer will therefore evaporate faster than before pull-in. When this happens the energy stored in the dielectric will no longer balance the spreading tendency and θ will increase, *i.e.*, the adsorbate will flow out. Further increases in field will lead to a repetition of the cycle until all but the first layer have been desorbed in this way.

The activation energy of desorption of the first layer can be interpreted as its heat of adsorption if it is assumed that this process is not activated. There is a great deal of evidence that even chemisorption on clean metals requires no activation energy. It is probably safe to assume that the average heat of adsorption $E_{ad} = 1870 \pm 300$ cal. for the first layer. A very rough guess for the corresponding values for the second and subsequent layers can be made by assuming that the desorption

process is first order and that the pre-exponential term is equal to that for the first layer. Values of 1600 and 1520 cal. are estimated in this way for the second and higher layers. No attempt to differentiate between the third and higher layers is warranted by the data. It is interesting to compare these values with the heat of sublimation of A, 1500 cal.

If the mean distance x traversed by a diffusing argon atom is adequately represented by²

$$x = \sqrt{Dt} \quad (5)$$

where t is time and D the surface diffusion coefficient, and if the latter may be assumed to be

$$D = \nu a^2 e^{-E_s/kT} \quad (6)$$

where ν is a jump frequency of the order of 10^{12} sec.⁻¹ and a a jump length 3×10^{-8} cm., the activation energy for surface diffusion of A on clean W can be estimated to be $E_d \cong 600 \pm 200$ cal. since $x \cong 10^{-5}$ cm. The ratio $E_d/E_{ad} \cong 0.3$ for this case. This is comparable to the value found for O₂ on oxygen covered tungsten.³

Conclusion

The findings reported here are rather direct visual evidence for multilayer adsorption. It appears that liquid-like behavior below the bulk melting point of the adsorbate occurs for several layers. Finally it is interesting that the interaction of a perfectly clean metal surface with an inert gas leads to a heat of adsorption very similar to that found on other adsorbents, despite the presence of large electronic effects.

DEFECT STRUCTURE AND CATALYSIS IN THE TiO₂ SYSTEM (SEMI-CONDUCTING AND MAGNETIC PROPERTIES)

BY T. J. GRAY, C. C. MCCAIN AND N. G. MASSE

State University of New York College of Ceramics, at Alfred University, Alfred, New York

Received October 7, 1958

Considerations relating to the correlation between defect structures and catalysis indicate that the enhancement of n-type character in an oxide such as TiO₂ would be beneficial for processes such as hydrogenation, cracking and Fischer-Tropsch reactions. Such enhancement of semi-conducting character can be achieved by the introduction of pentavalent ions, notably niobium. It has been demonstrated that TiO₂, which in the very pure stoichiometric condition is not an active catalyst for cracking processes or Fischer-Tropsch synthesis, can be converted to a highly active material by niobium doping with a corresponding change from insulating properties to those of a typical n-type semi-conductor. The activation energy for the conduction process is considerably reduced as is that for the catalytic process. A very precise method for measuring semi-conducting properties as the surface component of the a.c. dielectric loss over a wide frequency range has been developed for use with powdered materials under conditions that facilitate gas access. Either fixed temperature or controlled rising/falling temperature operation is employed under dynamic reaction conditions using simple "type" reactions, notably the formic acid decomposition and the hydrogenation of benzene. Magnetic susceptibility measurements have confirmed the concentration of defects in the surface regions and indicate a very substantial divergence from bulk constitution. Furthermore, it has been demonstrated that desorption of product may frequently be rate controlling as during the reduction process. The results obtained indicate additional features; firstly, they demonstrate the use of magnetic susceptibility and semi-conductivity measurements as indirect methods for observing and studying hydrate or similar transformations. These are observed as peaks on the dielectric loss curves against temperature. Secondly, the results further substantiate the premise previously advanced, that a spinel structure is advantageous to catalytic processes. Thus, it is found that lithium titania spinel enhances the catalytic activity out of all proportion to the concentration in which it is present. The importance of this phase may be due to its half-inverted nature thereby being analogous to the θ -alumina previously reported.

Introduction

The correlation between the defect constitution of solids and their catalytic activity first proposed approximately simultaneously and independently by Garner, Gray and Stone,^{1,2} Volkenshtein,³ and

Hauffe⁴ is now widely accepted as a formal basis to

(1) W. E. Garner, T. J. Gray and F. S. Stone, *Proc. Roy. Soc. (London)*, **A197**, 294 (1949).

(2) T. J. Gray, *ibid.*, **A197**, 314 (1949).

(3) F. F. Volkenshtein, *J. chim. Fiz. (U.S.S.R.)*, **23**, 917 (1949).

explain the details of the catalytic process. These considerations have been applied to catalysis in the TiO_2 system.

In a condition of extreme purity and close to stoichiometry, TiO_2 is not an active hydrogenation catalyst. However, some activity can be induced by partial reduction by hydrogen at elevated temperatures. The material turns blue-gray and its electrical conductivity rises sharply. Similar activity may be imparted by the introduction of pentavalent cations, notably Nb^{5+} which induces an equivalent number of Ti^{4-} ions to revert to the Ti^{3+} condition. However, in this latter material, there is less oxygen deficiency and the material has a higher permanence of operating character. Catalytic activity was established during this investigation with respect to the Fischer-Tropsch process for which stoichiometric TiO_2 is inactive, whereas the Nb^{5+} doped material is a satisfactory catalyst in the range from atmospheric pressure to 400 p.s.i. and temperatures from 150 to 300°

The application of magnetic susceptibility measurements to indicate the icnization state of a catalyst material has long been established in the extensive work of Selwood.⁵ An extension of these measurements to dynamic systems originated by Gray² has been employed to confirm the existence of a univalent oxygen ion on the surface of certain oxide materials during the adsorption of oxygen. Refinements to the dynamic measurements have enabled the change in susceptibility occasioned by the adsorption of oxygen and hydrogen on the surface of platinum to be studied in detail.⁶

The present investigation relates to the reduction and oxidation of the TiO_2 system by dynamic measurements of susceptibility simultaneously with classical adsorption measurements and in association with measurements of semi-conductivity and electric properties. Direct evidence is presented of a lag in the desorption step of the reaction which is probably rate controlling. The susceptibility measurements established that there is a very large local concentration of Ti^{3+} ions in the surface region which the associated semi-conductivity measurements will demonstrate as inducing n-type semi-conductivity and even pseudo-metallic (essentially free electron) constitution in the surface regions.

Experimental

The material used in all pertinent investigations was obtained by the hydrolysis of highly purified titanium tetrachloride which was refluxed for an extended period over C.P. copper in the presence of a heavy metal soap and then distilled into a prepared container for conversion to the hydroxide. The hydroxide was decomposed at 450° under a hard vacuum and reoxidized with purified oxygen at high temperature. Difficulty is experienced if ammonia has been employed owing to the exchange with water molecules in the hydrated titania.⁷ The resulting oxide with a surface area of 22.6 m.²/g. was analyzed by X-rays to be 20% anatase and 80% rutile. Samples with surface areas up to

250 m.²/g. can be obtained by less severe heating and re-oxidation and contain a higher proportion of anatase. Detailed spectroscopic analysis failed to show any transition metal impurities (less than 1 p.p.m.) and only very faint traces (below 0.001%) of silicon and sodium. Although there will be differences in absolute value of the magnetic susceptibility dependent on the anatase/rutile and other variations in structure,⁸ this will have no significance in the present investigation which relates only to changes occurring during reduction and adsorption of gases on particular specimens of material.

Measurements of semi-conductivity were performed by an a.c. method previously described by Gray² together with the essential analysis to derive bulk and surface contribution. Dielectric loss characteristics at fixed frequency are employed to indicate details of hydrate formation and also serve to demonstrate the relaxation phenomena induced by various impurities.

The dynamic measurement of small changes in magnetic susceptibility using a modified Gouy balance system has been described by Gray.² Changes in mass and susceptibility are followed as their equivalent current changes in a solenoid maintaining a silicone resin-coated, vacuum-mounted, analytical balance in equilibrium at all times. Operation of the balance maintained in the continuously equilibrium position enables measurements to be made rapidly with and without the magnet field in operation, giving directly the mass changes as well as the corresponding susceptibility change for any instant. Ultimate long-term accuracy is dependent on the electronic current regulator which sets the accuracy to one part in 10⁶, while one order of magnitude improvement is attainable for periods of several hours.

Results

Magnetic Susceptibility.—The uniform samples of titanium dioxide used in these experiments gave an initial magnetic susceptibility of 0.075×10^{-6} c.g.s. units independent of temperature and magnetic field (0 to 10 kgauss). This value is significantly lower than that recorded by Reyerson⁹ or by Ehrlich¹⁰ which was 0.088×10^{-6} c.g.s. unit and closely approaches the values obtained by Raychandhuri and Sengupta.¹¹ This indicates a closer approach to stoichiometry and probably a higher state of purity. Although diamagnetic values have been reported by certain authors¹²⁻¹⁴ it is improbable that their samples were completely dehydrated so that the values are suspect. The kinetics of the reduction process as a function of weight loss were determined and indicated that at lower temperatures there is an induction period before the desorption of water is observed. After correction for initial susceptibility, the corresponding changes in magnetic susceptibility were compared with changes anticipated from the weight loss curves. When the amount of hydrogen adsorbed as determined volumetrically is compared with the weight change it is observed that the weight change lags the adsorption of hydrogen in the early stages of reduction but coincides during later stages. This clearly establishes the slow desorption of water.

After reduction the temperature was raised to 575° and the sample strongly evacuated for 24 hours

(8) K. E. Zimens and J. A. Hedval, *Svensk Kem. Tid.*, **53**, 12 (1941); *Trans. Chalmers Univ. Tech.*, **9**, 3 (1942).

(9) L. H. Reyerson and J. M. Honig, *J. Am. Chem. Soc.*, **75**, 3920 (1953).

(10) P. Ehrlich, *Z. Elektrochem.*, **45**, 362 (1939).

(11) D. P. Raychandhuri and P. N. Sengupta, *Ind. J. Phys.*, **10**, 253 (1936).

(12) S. Berkman and H. Zoher, *Z. physik. Chem.*, **124**, 322 (1926).

(13) G. F. Huttig, *Z. anorg. allgem. Chem.*, **224**, 225 (1935).

(14) F. N. Hill and P. W. Selwood, *J. Am. Chem. Soc.*, **71**, 2522 (1949).

(4) K. Hauffe, *Ann. Physik.*, **8**, 201 (1950); "Reaktionen in Festen Stoffen," Springer, Berlin, 1955.

(5) P. W. Selwood, "Magnetochemistry," Interscience Publishers, Inc., New York, N. Y., 1956.

(6) T. J. Gray and C. C. McCain, "Second International Congress on Surface Activity," Butterworths, London, 1957.

(7) W. Biltz, G. A. Lehrer and O. Rahlfs, *Z. anorg. allgem. Chem.*, **244**, 281 (1940).

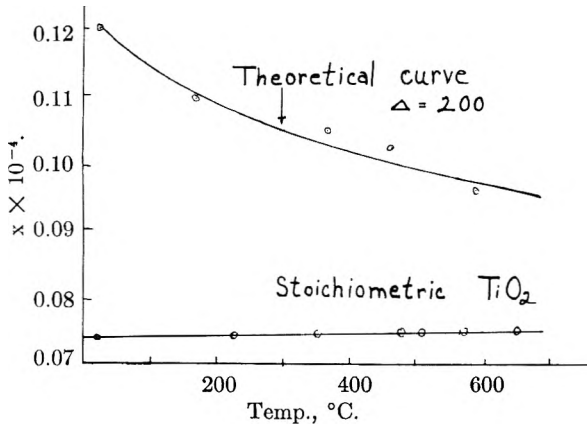


Fig. 1.—Variation in magnetic susceptibility with temperature for near stoichiometric and reduced TiO_2 ; reduced TiO_2 (0.603×10^{-4} g. ion Ti^{3+} /g.).

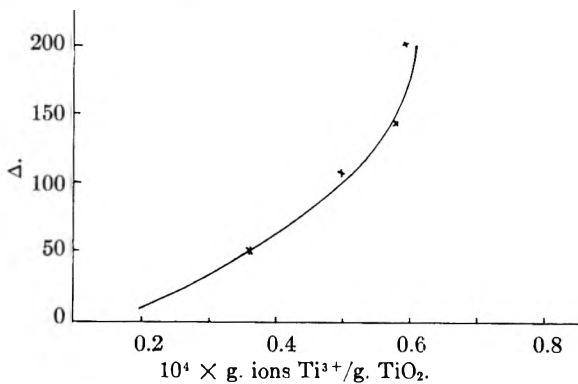


Fig. 2.—Variation of Weiss constant with degree of reduction; $10^4 \times \text{g. ions } Ti^{3+}/\text{g. } TiO_2$.

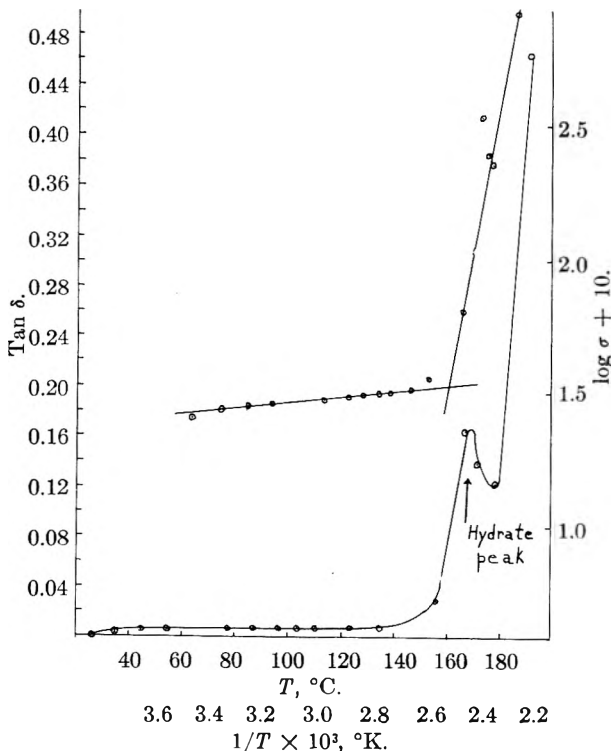


Fig. 3.—Semi-conductivity of pure TiO_2 ; $\tan \delta$ vs. T ; $\log \sigma$ vs. $1/T$.

at 10^{-7} mm. to determine whether any further water could be removed. A weight loss of 0.2 mg. and magnetic susceptibility decrease of 0.003×10^{-6} c.g.s. units indicated that some hydrogen was removed with the reoxidation of some Ti^{3+} ions to Ti^{4+} .

An investigation of the variation of magnetic susceptibility of the specimens of TiO_2 with temperature showed a marked contrast between the initial material and reduced specimens. This is shown in Fig. 1 which illustrates the comparison between the reduced sample and highly evacuated original material. Taking the normal Curie-Weiss law

$$\chi_m = \frac{C_m}{T + \Delta}$$

for the particular sample which contains 0.603×10^{-4} g. ion of Ti^{3+} per gram of sample, excellent agreement with experimental results is achieved using a Weiss constant of 200.

The relationship between Weiss constant and extent of reduction is given in Fig. 2, and while further data obviously are necessary, the general upward trend is apparent.

These results can be compared with those of Ehrlich⁹ which indicated an increase in spin interaction between the Ti^{3+} ions as the concentration increases. Using his results these data may be calculated.

Composition	Mole % Ti^{3+}	Δ for 20° results	Δ for -183° results
$TiO_{1.97}$	6	191	126
$TiO_{1.95}$	10	225	142
$TiO_{1.9}$	20	330	257

For comparison with these results the typical sample under investigation had a composition of $Ti_{1.9976}$ with 0.48 mole % giving a Weiss constant of 332. This would tend to confirm a considerable increase in concentration of Ti^{3+} ions near the surface with a corresponding rise in interaction.

During the adsorption of oxygen on previously reduced titanium dioxide, similar results were obtained although the quantitative agreement is not good. This is hardly surprising, considering the nature of the measurements and the probable complication due to even very small concentrations of O^- ion capable of providing a very large paramagnetic contribution (Gray,² Fensham¹⁵).

ΔX g. reduced $TiO_2 \times 10^6$	ΔX g. atoms oxygen adsorbed per 1 g. $TiO \times 10^4$	ΔX g. due to adsorbed oxygen $\times 10^6$	Weiss constant
0.041	0.159	-0.019	320°
.046	.154	-.023	218
.040	.129	-.026	76
.040	.128	-.021	125

The Weiss constants have been calculated on the basis that the paramagnetic contribution from two Ti^{3+} ions is removed per atom of oxygen absorbed.

It is important to note that the assumption that there is a direct correlation between the number of Ti^{3+} ions produced during reduction and the amount of oxygen adsorbed cannot be sustained. There is evidently a structure-sensitive effect and in the range from 20 to 600° the oxygen removed by

(15) P. W. Fensham, Ph.D. Thesis, Bristol University, 1952.

reduction cannot be entirely replaced. At room temperature, only about one-third of the oxygen is replaced. In contrast to carbon monoxide which shows a small reversible adsorption at room temperature, oxygen is irreversibly adsorbed. No susceptibility change occurs during the adsorption of carbon monoxide which, on this basis, could be considered as physically adsorbed. Oxygen is adsorbed to a very limited extent on the unreduced material with no measurable effect on the susceptibility.

The general character of conductivity changes during the adsorption/reduction are particularly interesting, indicating a separate adsorption stage at lower temperatures. Owing to the protracted times involved, it is not realistic to develop adsorption and reduction kinetics by the analysis previously established by Darby and Gray¹⁶ for other oxides. However, desorption of hydrogen from the oxide at lower temperatures (up to 125°), leads to a decrease in conductivity thereby establishing adsorption characteristics as distinct from reduction which is characterized by increasing conductivity on desorption of the adsorbed water. Desorption at somewhat higher temperatures confirms the magnetic susceptibility results, indicating desorption of water as being the slow step.

Oxygen adsorption after partial reduction takes place with a drop in surface conductivity but only to an extent considerably less than would be equivalent to the reduction. Not more than about 30–50% of the oxygen can be replaced.

The activation energy for the conduction process under various conditions is deduced from Fig. 3 which emphasizes the pseudo-metallic condition of the surface due to a relatively very high concentration of Ti^{3+} ions. Ti_2O_3 has been described by Morin¹⁷ as a metallic conductor which is in accord with this observation since the surface may well approximate this composition in the surface monolayer and immediately adjacent to it.

The semi-conductivity measurements also lead to further information provided by the peak in the dielectric loss curve at approximately 180°. This is associated with the decomposition of a tenacious hydrate and the rate of disappearance of the peak

which occurs at higher temperatures readily could be employed to determine the kinetics of hydrate decomposition.

Conclusions

The most important contribution offered by the magnetic susceptibility and semi-conductivity measurements is that they demonstrate conclusively the localization of a relatively high concentration of Ti^{3+} ions in the vicinity of the surface, these ions being directly associated with the catalytic activity of the material. Their concentration is such that there is considerable "pseudo-metallic" character in this region alternately explained by the overlapping of discrete impurity states or by the local formation of a few layers of Ti_2O_3 which may, in many respects, be "metallic" in character providing essentially free conduction electrons.

It has been demonstrated that the desorption process during reduction is rate controlling and it is suggested that this also holds during hydrogenation or similar processes. Slow desorption of hydrogen also occurs at temperatures below that necessary for reduction. There is no direct correlation between the subsequent adsorption of oxygen on a partially reduced material but it is established that only a small portion of the oxygen removed by reduction can be replaced readily.

Identical catalytic activity can be achieved either by partial reduction or by valence control; however, in the former case, the stability of the material is severely limited. The presence of small amounts of lithium promoting a local constitution closely analogous to an inverted spinel further stabilizes the material and improves catalytic properties, probably as a function of the directional character of potential surface bonding with the adsorbed species and the limitations to electron spin direction at these sites controlled by spin coupling with adjacent sites in a spinel lattice.

It has been indicated that dynamic magnetic susceptibility and semi-conductivity measurements readily may be applied to the investigation of other kinetic relationships such as dehydration of solids.

Acknowledgment.—The authors wish to acknowledge the generous support of the M. W. Kellogg Company and Cities Service Research and Development Company under whose sponsorship this program has been conducted.

(16) P. W. Darby and T. J. Gray, *THIS JOURNAL*, **60**, 201, 209 (1956).

(17) F. J. Morin, *Bell System Tech. J.*, **37**, 1047 (1958).

REACTIVITIES OF NAPHTHENES OVER A PLATINUM RE-FORMING CATALYST BY A GAS CHROMATOGRAPHIC TECHNIQUE

BY A. I. M. KEULEMANS AND H. H. VOGÉ*

Koninklijke/Shell-Laboratorium, Amsterdam, Netherlands (N. V. De Bataafsche Petroleum Maatschappij)

Received October 7, 1958

A micro-reactor coupled directly with a gas chromatographic analysis apparatus comparable to that of Kokes, Tobin and Emmett, was used to determine reactivities of thirty individual C_5 - C_8 naphthenes. Tests were made over a platinum-alumina-halogen catalyst at 350° and atmospheric pressure, using excess hydrogen. It was found that cyclopentanes and 1,1-dimethylcyclohexane are converted to aromatics much more slowly than are ordinary cyclohexanes. To explain reactivities of cyclopentanes, it is supposed that cyclopentanes first dehydrogenate to olefins which then migrate to form carbonium ions on acidic sites. Skeletal isomerization of the carbonium ions to cyclohexyl structures is taken to be the slow step in the series of reactions leading to aromatic hydrocarbons. Relative rates of alternative paths are given by simple ratios for relative carbonium ion stabilities, multiplied by the number of possible paths. In this way, rates of aromatization and the amounts of specific aromatic isomers formed are explained. Two adjustable parameters suffice for fitting the data for 21 cyclopentanes.

Heterogeneous catalysis is recognized as one of the most difficult branches of chemical kinetics. Knowledge about the reaction intermediates is hard to obtain because these intermediates exist as transitory fractional monolayers on surfaces of ill-defined nature. In fact, the intermediates must in many cases consist of actual chemical compounds between the reacting molecules and groups of atoms of the solid, but unfortunately we seldom know the formulas or chemical properties of these compounds. In this situation, progress in understanding can only be made by systematically varying the catalyst, the reaction conditions or the reactants, and by establishing correlations between the observed reactions and the properties that are varied. The making of such studies has been greatly expedited by the gas chromatographic technique for catalysis, which has been described by Kokes, Tobin and Emmett.¹ In the following paragraphs we describe an application of this technique to the re-forming of a series of naphthenes. The data so obtained have led us to a theory which gives insight into the nature of this important type of catalysis.

The re-forming of gasolines for octane number improvement is today largely carried out over platinum-alumina-halogen catalysts. Some reactions in "Platforming" are described by Haensel and Donaldson.² The major conversion in this process is that of naphthenes (cycloalkanes) to aromatics. Among the reactions that occur, some, such as isomerization of paraffins and the conversion of methylocyclopentane naphthenes to aromatics, require an acidic catalyst function as well as metal dehydrogenation sites. Both types of site are present in the bifunctional platinum-alumina-halogen catalysts. Mills and co-workers³ have shown that olefins are probable intermediates in conversions of cyclopentanes. It also has been demonstrated, by Mills,⁴ and by Weisz and Swegler,⁵ that the platinum sites and the acidic sites can act independently, for paraffin isomerization and methylocyclopentane conver-

sion are obtained with physical mixtures of platinum catalysts and acidic catalysts. This latter finding is consistent with the appearance of olefins in the vapor phase as intermediates. In none of this work, however, has a systematic series of hydrocarbons been investigated. With the aid of the gas chromatographic technique we have been able to study such a series, using very small amounts of the excellent pure hydrocarbon samples from the American Petroleum Institute. The results illustrate the great power of this method of investigation. The theoretical interpretation of the results indicates that the slow step in re-forming of cyclopentanes under our conditions is not the formation of the olefin intermediate nor the migration of this intermediate to the acid sites, but is the skeletal isomerization of the olefin at the acid site. Furthermore, there is quantitative satisfaction in the theory developed from these data.

Experimental

A micro-reactor was placed in the hydrogen line leading to a gas chromatographic column. This reactor contained one gram of catalyst, which gave a volume of nearly 2 cc. For an experiment the naphthene feed was injected as a small shot through a serum cap directly into the hydrogen stream prior to the reactor. The hydrogen served to carry the feed through the reactor, to maintain the catalyst in the proper condition, to hydrogenate the major fraction of the olefins as in normal re-forming, to carry all the products into the chromatographic column, and to elute the fractions from the column. The usual feed shot was 4-5 microliters, or about 3 mg. The hydrogen flow rate of 3 liters per hour gave a residence time in the catalyst zone of about 2 seconds. Temperature was varied from 300-400°, but for the most part only results at 350° are shown. Pressure was atmospheric plus the small amount of pressure drop through the column.

Hydrocarbons.—The naphthenes used were all from the American Petroleum Institute.⁶ For the most part, these have been prepared by the A.P.I. Project 45.⁶ Gas chromatographic analyses verified the high purities of these samples.

Catalyst.—The platinum-alumina-halogen catalyst was ground and sieved to 40-60 mesh. Since the activity of a fresh catalyst changes rapidly, it was stabilized by use with a sulfur-containing feed at 400° before the experiments were done. All the runs were made with a single catalyst charge. Its activity was periodically measured by feeding 1,1-dimethylcyclohexane under standard conditions and was found to be virtually constant.

(6) American Petroleum Institute, Standard Samples of Hydrocarbons, Chemical and Petroleum Research Laboratory, Carnegie Institute of Technology, Pittsburgh 13, Penna. See also publications of A.P.I. Project 45, by C. E. Boord and co-workers.

* Shell Development Co., Emeryville, Calif.

(1) R. J. Kokes, H. Tobin, Jr., and P. H. Emmett, *J. Am. Chem. Soc.*, **77**, 5860 (1955).

(2) V. Haensel and G. R. Donaldson, *Ind. Eng. Chem.*, **43**, 2102 (1951).

(3) G. A. Mills, H. Heinemann, T. H. Milliken and A. G. Oblad, *ibid.*, **45**, 134 (1953).

(4) G. A. Mills, *Advances in Catalysis*, **IX**, 639 (1957).

(5) P. B. Weisz and E. W. Swegler, *Science*, **126**, 31 (1957).

Chromatographic Column.—A U-shaped glass column 1.8 m. long and 6 mm. i.d. was used. It was packed with 30–100 mesh firebrick coated with an ester prepared from dinitrodiphenic acid and C₅–C₆ oxo alcohols. The ratio of support to column liquid was 100/±0. This column was used at 120°. It had excellent stability and good selectivity for separation of saturates and aromatics. Toluene emerged just after the highest boiling C₈ naphthenes. The detector made use of the ionization by Sr-90 β-rays. An integrating recorder was employed. With the radiological detection, the area of an elution peak is directly proportional to the weight of the component, and detailed calibration is not necessary.⁷

Results

Data for cyclohexanes treated at 350° are given in Table I. The dehydrogenation to the expected aromatic compound was 96–100% complete, except with 1,1-dimethylcyclohexane. The latter compound reacted only to the extent of 34% and gave almost exclusively *o*-xylene. The low reactivity of 1,1-dimethylcyclohexane was expected from the fact that the geminal dimethyl grouping blocks direct dehydrogenation to an aromatic.

TABLE I

CONVERSIONS OF CYCLOHEXANES OVER PLATINUM-ALUMINA-HALOGEN CATALYST
Temperature 350°; excess H₂ at slightly above atmospheric pressure

Compound	B.p., °C.	Wt. % of total effluent— Unconverted	Reaction products
Cyclohexane	80.7	4	Benzene 96
Methylcyclohexane	100.9	2	Toluene 98
Ethylcyclohexane	131.8	0	Ethylbenzene 100
1- <i>cis</i> -2-Dimethylcyclohexane	129.7	0	<i>o</i> -Xylene 100
1- <i>trans</i> -2-Dimethylcyclohexane	123.4	0	<i>o</i> -Xylene 100
1- <i>trans</i> -3-Dimethylcyclohexane	124.5	0	<i>m/p</i> -Xylene 100
1- <i>cis</i> -4-Dimethylcyclohexane	124.3	0	<i>m/p</i> -Xylene 100
1,1-Dimethylcyclohexane	119.5	66	Toluene 1.3; <i>o</i> -xylene 32.7 (calcd. <i>o</i> -xylene 44)

Results from C₅–C₇ cyclopentanes are summarized in Table II. Conversions to aromatics varied from 1.4 to 25% and there were traces of cracking. Data for C₈ cyclopentanes are given in Table III. These were converted to the extent of 3 to 43.6%, but again amounts of cracking were quite small except for isopropylcyclopentane, for which cracking was 15.4%.

When it was possible, extensive *cis*–*trans* isomerization occurred in both C₇ and C₈ compounds. Some data on the *cis*–*trans* isomerizations are collected in Table IV. It appears that in many cases an equilibrium was reached. The *cis*–*trans* isomerizations are very much faster than isomerizations involving the shift of a methyl group from one carbon to another. This is consistent with the theory developed below.

Experiments not tabulated were done at 300 and 400°. Even at 300° dehydrogenation of cyclohexanes was 95% or more, except for values of 89% for ethylcyclohexane, 78% for methylcyclohexane, 64% for cyclohexane and only 13% for 1,1-dimethylcyclohexane. Conversions of the cyclopentanes under the same conditions were less than 5%, except for a value of 7.7% for isopropylcyclopentane. Thus it is possible that an analytical method for distinguish-

ing cyclopentanes from cyclohexanes could be based on the dehydrogenation reaction over a platinum catalyst at about 300°. Such an analysis would put geminally substituted cyclohexanes largely into the cyclopentane group. At 400° the cyclohexanes were 100% converted, except for 1,1-dimethylcyclohexane, 93.7%. At this temperature conversions of cyclopentanes ranged from 6 to 76%. Clearly, 300° is better for an analytical scheme.

Discussion

It is well known that platinum re-forming catalysts are bifunctional, for they display characteristics that can be attributed to metal sites and other characteristics that can be attributed to acid sites (halogen on alumina). It has been shown many times that simple dehydrogenation reactions, such as the conversion of cyclohexane to benzene, require only the participation of metal sites. Other typical re-forming reactions, however, such as conversion of methylcyclopentane to benzene, or the isomerization of *n*-heptane, require action of sites of both types. In these reactions olefins formed on the metal sites presumably migrate to the acid sites where the isomerization occurs. It often has been thought that the low concentration of olefins, or the slow migration of the olefins, sets a limit to the rate of reactions requiring cooperation of both sites. However, our results demonstrate that the rate-controlling step, under our conditions, is the isomerization at the acid site. This is most clearly shown by the great difference in rate of reaction of different cyclopentanes. It is reasonable to think that rates of dehydrogenation to olefin are about the same for all these cyclopentanes. Likewise, equilibrium concentrations of olefins, and rates of migration to the acid sites, should be relatively constant. We are left with isomerization as the crucial slow step. This conclusion has consequences that are well borne out by the experimental results.

Cyclohexanes, except for the geminally substituted members like 1,1-dimethylcyclohexane, can be directly dehydrogenated to aromatics on the metal sites. They are converted rapidly at 350° and atmospheric pressure, with no change in carbon skeleton, to almost the full extent permitted by equilibrium, which is essentially 100%. We need no further theory for these compounds.

Cyclopentanes, on the other hand, must be isomerized before they can be dehydrogenated to aromatics. The same applies for the geminally substituted cyclohexanes. The isomerization occurs on the acid sites, and is closely akin to isomerizations that take place on acidic cracking catalysts. The reactions on cracking catalysts can be explained by reactions of postulated intermediate species called carbonium ions held on a surface adjacent to a counter-ion. The carbonium ions split and rearrange according to definite rules.⁸ Similar rules applied to the isomerizations of the cyclopentenes on the acid sites of reforming catalysts explain reactivities and predict the major products. This is further evidence that the isomerization is the slow step.

(7) C. H. Deal, J. W. Otvos, V. N. Smith and P. S. Zucco, *Anal. Chem.*, **28**, 1958 (1956); H. Boer in D. H. Desty, "Vapor Phase Chromatography" Butterworths Scientific Publications, London, 1956.

(8) B. S. Greensfelder, H. H. Voge and G. M. Good, *Ind. Eng. Chem.*, **41**, 2573 (1949).

TABLE II
CONVERSIONS OF C₅-C₇ CYCLOPENTANES OVER PLATINUM-ALUMINA-HALOGEN CATALYST
Temperature 350°; excess H₂ at slightly above atmospheric pressure

Compound	B.p., °C.	Unconverted	Products, wt. % of effluent				Other
			Benzene		Toluene		
			Obsd.	Calcd.	Obsd.	Calcd.	
Cyclopentane	49.3	99.3	^b
Methylcyclopentane	71.8	96.0	2.6	1.4	^c
Ethylcyclopentane	103.5	74.0	25.0	21.9	^d
1,1-Dimethylcyclopentane	87.8	98.0	2.0	2.7	..
1-cis-2-Dimethylcyclopentane	99.5	97.1 ^a	2.9	2.7	..
1-trans-2-Dimethylcyclopentane	91.9	96.1 ^a	3.9	2.7	..
1-cis-3-Dimethylcyclopentane	90.8	98.6 ^a	1.4	2.7	..
1-trans-3-Dimethylcyclopentane	91.7	98.5 ^a	1.5	2.7	..

^a *cis-trans* isomerization occurred, but is not counted as conversion. ^b 0.7% *n*-pentane formed. ^c 1.4% *n*-hexane formed. ^d 1.0% *n*-heptane formed.

TABLE III
CONVERSIONS OF C₈ CYCLOPENTANES OVER PLATINUM-ALUMINA-HALOGEN CATALYST
Temperature 350°; excess H₂ at slightly above atmospheric pressure

Compound	B.p., °C.	Unconverted	Products, wt. % of effluent						Other
			Ethylbenzene		<i>m/p</i> -Xylene		<i>o</i> -Xylene		
			Obsd.	Calcd.	Obsd.	Calcd.	Obsd.	Calcd.	
<i>n</i> -Propylcyclopentane	130.9	73.2	26.4	21.9	0	0	0	0	^b
Isopropylcyclopentane	126.4	56.4	0	0	0	0	28	43.8	^c
1-Methyl-1-ethylcyclopentane	121.5	79.9	1.1	1.4	3.4	0	15.6	21.9	
1-Methyl- <i>cis</i> -2-ethylcyclopentane	128.1	81.4 ^a	2.5	1.4	8.5	10.9	7.6	10.9	
1-Methyl- <i>trans</i> -2-ethylcyclopentane	121.2	82.0 ^a	1.7	1.4	9.1	10.9	7.5	10.9	
1-Methyl- <i>cis</i> -3-ethylcyclopentane	121.1	83.4 ^a	0.2	1.4	16.4	21.9	0	0	
1-Methyl- <i>trans</i> -3-ethylcyclopentane	121.1	70.3 ^a	0.3	1.4	29.4	21.9	0	0	
1,1,2-Trimethylcyclopentane	113.7	95.6 ^a	0	0	3.4	1.4	0.9	2.7	
1,1,3-Trimethylcyclopentane	104.9	97.0 ^a	0	0	2.4	2.7	0.6	1.4	
1- <i>cis</i> -2- <i>cis</i> -3-Trimethylcyclopentane	123.0	95.3 ^a	0	0	2.8	1.4	1.9	2.7	
1- <i>cis</i> -2- <i>trans</i> -3-Trimethylcyclopentane	117.5	95.1 ^a	0	0	2.9	1.4	2.0	2.7	
1- <i>trans</i> -2- <i>cis</i> -3-Trimethylcyclopentane	110.2	96.7 ^a	0	0	2.1	1.4	1.2	2.7	
1- <i>cis</i> -2- <i>trans</i> -4-Trimethylcyclopentane	116.7	95.9 ^a	0	0	3.5	2.7	0.6	1.4	
1- <i>trans</i> -2- <i>cis</i> -4-Trimethylcyclopentane	109.3	95.4 ^a	0	0	3.6	2.7	1.0	1.4	

^a *cis-trans* isomerization occurred, but is not counted as conversion. ^b 0.4% toluene. ^c 0.2% methane, 15.2% octane.

TABLE IV
cis-trans ISOMERIZATION OF CYCLOPENTANES

The table shows the compositions of some recovered cyclopentanes after treatment at 350°

Compound treated	Composition of recovered material
Dimethylcyclopentanes	
1- <i>cis</i> -2	35% 1- <i>cis</i> -2; 65% 1- <i>trans</i> -2
1- <i>trans</i> -2	15% 1- <i>cis</i> -2; 85% 1- <i>trans</i> -2
Methylethylcyclopentanes	
1 <i>M</i> , <i>cis</i> -2 E	16% 1 <i>M</i> , <i>cis</i> -2 E; 84% 1 <i>M</i> , <i>trans</i> -2 E
1 <i>M</i> , <i>trans</i> -2 E	13% 1 <i>M</i> , <i>cis</i> -2 E; 87% 1 <i>M</i> , <i>trans</i> -2 E
Trimethylcyclopentanes	
1- <i>cis</i> -2- <i>ci</i> -3	60% 1- <i>trans</i> -2- <i>cis</i> -3; 30% 1- <i>cis</i> -2- <i>trans</i> -3; 10% 1- <i>cis</i> -2- <i>cis</i> -3
1- <i>cis</i> -2- <i>trans</i> -3	56% 1- <i>trans</i> -2- <i>cis</i> -3; 40% 1- <i>cis</i> -2- <i>trans</i> -3; 4% 1- <i>cis</i> -2- <i>cis</i> -3
1- <i>trans</i> -2- <i>cis</i> -3	72% 1- <i>trans</i> -2- <i>cis</i> -3; 24% 1- <i>cis</i> -2- <i>trans</i> -3; 4% 1- <i>cis</i> -2- <i>cis</i> -3
1- <i>cis</i> -2- <i>trans</i> -4	73% 1- <i>trans</i> -2- <i>cis</i> -4; 25% 1- <i>cis</i> -2- <i>trans</i> -4; 2% 1- <i>cis</i> -2- <i>cis</i> -4
1- <i>trans</i> -2- <i>cis</i> -4	83% 1- <i>trans</i> -2- <i>cis</i> -4; 16% 1- <i>cis</i> -2- <i>trans</i> -4; 1% 1- <i>cis</i> -2- <i>cis</i> -4

The chief steps in the conversion of a cyclopentane to an aromatic are: (1) dehydrogenation to olefin on a metal site; (2) migration of the olefin to an acid site; (3) addition of a proton at the acid site to form a carbonium ion; (4) isomerization of the ion by carbon skeleton rearrangement; (5) release and migration of a new olefin; (6) dehydrogenation of the new olefin to an aromatic at a metal

site. In this complex set of reactions, many carbonium ions have to be considered in steps 3 and 4. Simplifications result, however, from the facts that step 4 is slow and that many carbonium ions produce no new dehydrogenation products. But before we proceed with our analysis of step 4, some comment on the other steps is needed.

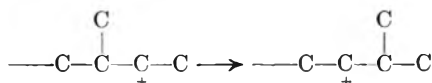
Dehydrogenation to olefin in step 1 is rapid. Evidence for this is found in the high rate of conversion of cyclohexanes, where cyclohexenes are presumably intermediates. We shall postulate that cyclopentenes are in equilibrium with cyclopentanes. We shall also postulate that the migration of step 2 is rapid, either through the vapor phase or across the catalyst surface. Step 3 is the initial formation of a carbonium ion. There are a number of possible carbonium ions of unchanged carbon skeleton. The high observed rate for double-bond shift isomerizations over cracking catalysts⁹ and the rapidity of hydrogen exchange reactions in similar systems both suggest that equilibrium will prevail among these various ions of the same carbon skeleton. Since tertiary carbonium ions are most stable, secondary next, and primary least stable, we may take their abundances in that order. These values are used: tertiary/primary carbonium ion ratio, 32;

(9) H. H. Vogel, G. M. Good and B. S. Greensfelder, *ibid.*, **38**, 1033 (1946).

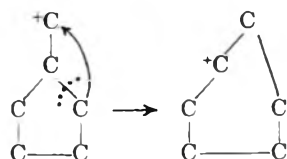
secondary/primary carbonium ion ratio, 16.

Steps 5 and 6 are fast for the same reasons that 1 and 2 are fast. They have no influence on product distribution. Step 6, the dehydrogenation of suitable olefins to aromatics, removes these olefins from the system, and thus permits more of the same structure to form. The completeness of this dehydrogenation reaction, determined by thermodynamics, causes aromatics to be the major products rather than isomerized naphthenes. If there is extensive cracking, lower paraffins can also be major products.

In step 4 several types of isomerization of the carbonium ion at the acid site can occur, as well as cracking. The new olefins that return to the metal sites may be dehydrogenated to aromatics or hydrogenated to paraffins or to isomerized naphthenes. We can expect some of each, but since cracking is not extensive under mild re-forming conditions, aromatics that can form readily will predominate as stable end products. Thus we can restrict attention to those ions and isomerizations that lead to aromatics. In the isomerization of a carbonium ion, a group attached to the carbon atom adjacent to the carbonium-ion carbon moves over to the carbonium-ion carbon. This shifting group is visualized as carrying a negative charge.



This shift is closely related to the beta fission rule that explains the products of catalytic cracking over acid catalysts.⁸ The same type of shift can change a 5-ring to a 6-ring.



The 6-ring goes readily to an aromatic. The ring enlargement is essentially like one of the steps proposed by Pines and Shaw¹¹ to explain movement of a tagged carbon from the side chain to the ring in treatment of ethylcyclohexane over another bifunctional catalyst, nickel on alumina-silica.

The rate of the series of reactions leading to a particular product will be given by the relative amount of the carbonium ion multiplied by one factor for the rate of the step 4 isomerization and another for the number of equivalent isomerization paths (statistical factor). As a simple assumption, we take the rate of isomerization as a constant (empirical factor) in this series of closely related compounds. For example, consider 1-methyl-2-ethylcyclopentane. The two ions that can produce aromatics are in the tabulation, with calculations. The empirical factor here is chosen to fit the average total aromatics formed from the trimethylcyclopentanes. The same empirical factor is used for all the cyclopentanes. Probably this is somewhat of an oversimplification for in certain isomerizations two successive rearrangements are necessary

EXAMPLE OF CALCULATION

Ion	Product	Relative amount of ion	Statistical factor	Empirical factor	Rate of formation
	Ethylbenzene	1	2	0.684	1.4
	<i>o</i> -Xylene	16	1	.684	10.9
	<i>m</i> -Xylene	16	1	.684	10.9

to produce a structure dehydrogenatable to an aromatic. This occurs when a 1,1-dimethylcyclohexane structure is formed by the primary isomerization, and then the final product is predicted to be *o*-xylene. However, use of additional rate factors for such cases introduces too many adjustable parameters.

In Tables II and III the calculated amounts of various products are given for comparison with the experimental amounts. The average amounts of aromatics from various classes are summarized below.

AROMATIC CONTENTS OF PRODUCTS AT 350°

Compound or class	No.	Av. aromatics, % wt. Obsd.	Calcd.
Methylcyclopentane	1	2.6	1.4
Ethylcyclopentane	1	25	22
Dimethylcyclopentanes	5	2.3	2.8
<i>n</i> -Propylcyclopentane	1	27	22
Methylethylcyclopentanes	5	21	23
Trimethylcyclopentanes	7	4.1	4.1
1,1-Dimethylcyclohexane	1	34	44

In this summary table, only two adjustable parameters are involved, namely, 16/1 and 0.684. Conversions have been taken as proportional to rates, which is reasonable at conversion levels below 30%. The agreement between observed and calculated amounts is quite good considering the simplifications that have been introduced into the theory. The calculated value for 1,1-dimethylcyclohexane is also of the right order of magnitude. Isopropylcyclopentane is the only compound of the series in which a tertiary carbonium ion has been postulated. Because of the double isomerization necessary in converting isopropylcyclopentane to *o*-xylene, as well as because of the extensive cracking that occurred, the parameter of 32, used with this compound only, is probably too low. In other cases some double isomerization may account for appearance of a product not predicted, such as *m*-xylene from 1-methyl-1-ethylcyclopentane.

The aromatic products did not ever appear to be at equilibrium. At 350° the approximate equilibrium composition is 22% *o*-xylene, 50% *m*-xylene, 22% *p*-xylene, 6% ethylbenzene.

Re-forming is normally carried out at 20–40 atmospheres rather than at near atmospheric pressure as in these experiments. Nevertheless, the higher temperature of re-forming, about 480°, means that equilibrium olefin concentrations are not much different than at 350° and atmospheric pressure. There is no evidence of which we are

(10) H. Pines and A. W. Shaw, *J. Am. Chem. Soc.*, **79**, 1474 (1957).

aware to say that the present picture would not hold under commercial re-forming conditions, although naturally the parameters will be somewhat different, and the isomerization step will be faster because of the higher temperature. Our conclusion that the isomerization step is rate limiting agrees

(11) P. B. Weisz and C. D. Prater, *Advances in Catalysis*, **IX**, 575 (1957).

with the evidence of Weisz and Prater¹¹ who found acid activity usually limited octane improvement in re-forming.

Acknowledgment.—We wish to thank the Bataafsche Petroleum Maatschappij for permission to publish this paper, Dr. H. Bau who designed and constructed the apparatus, and H. van Kranen for experimental work.

HEATS OF ADSORPTION OF HYDROGEN ON A SINGLY PROMOTED IRON CATALYST

BY RALPH A. BEEBE AND ERIC R. CAMPLIN

Department of Chemistry, Amherst College, Amherst, Mass.

Received September 15, 1958

Early work by Emmett and Harkness has indicated the presence of two types of chemisorption of hydrogen on iron catalysts. These types, designated as A and B, proceed fairly rapidly at temperatures around 0 and 200°, respectively. More recently Kummer and Emmett have shown that "singly promoted iron catalysts, unlike doubly promoted catalysts, rapidly catalyze the hydrogen-deuterium exchange reaction at -195°." On the basis of this observation and of the adsorption data for the hydrogen-iron system, these authors postulate a third kind of chemisorption, called Type C, occurring in the low temperature region. At Emmett's suggestion, we have undertaken the calorimetric measurement of the heats of adsorption of hydrogen on the singly promoted iron catalyst at temperatures selected to sort out the three types of chemisorption. We have achieved satisfactory calorimetric measurements at 0° and at -195°. At these two temperatures the heat values range from 16.5 to 8.0 (at 0°) and from 5.4 to 1.6 kcal. per mole (at -195°) for successive increments of hydrogen. Rather crude measurements at 200° indicate heats ranging from 27 to 15 kcal. per mole. In particular the calorimetric results at -195° confirm the prediction of Emmett and Kummer that the heat of Type C adsorption would be "considerably greater than that of the heat of adsorption of physically adsorbed hydrogen, but at the same time considerably smaller than the heat of adsorption of either Type A or Type B hydrogen adsorption."

Introduction

The work of Emmett and Harkness¹ has indicated the presence of two types of chemisorption of hydrogen on a doubly promoted iron catalyst and on a "pure" iron catalyst. These types designated as A and B were found to occur in the temperature ranges -78 to 0° and +100 to 460°, respectively. The evidence for types A and B chemisorption is based on the shapes of the isobars and also upon the relative poisoning effects of these two types on the ortho-para hydrogen conversion at -190°, Type B being a much more effective poison. In addition to the two chemisorption processes, there was a physical adsorption in the -195 to 183° range; however there was no evidence for any significant amount of chemisorption in this low temperature region.

More recently Kummer and Emmett² have extended the previous work to include a singly promoted iron catalyst and to test the activity of both the doubly and singly promoted catalysts for the hydrogen-deuterium exchange reaction as well as the ortho-para hydrogen interconversion. These investigators found that, unlike the doubly promoted catalyst, the singly promoted material could effect a rapid hydrogen-deuterium exchange at -195°. Moreover the singly promoted catalyst differed in another respect in that it was not poisoned for the ortho-para hydrogen interconversion at -195° by the presence of Type B adsorption. On the basis of these observations and of the adsorption data for the hydrogen-iron system Kum-

mer and Emmett have suggested the existence of a third type of chemisorption, called Type C, on the singly promoted iron catalyst. On the basis of their observations, Kummer and Emmett conclude that the heat of binding of this third type of chemisorption "is apparently considerably greater than the heat of adsorption of physically adsorbed hydrogen but at the same time considerably smaller than the heat of adsorption of either Type A or Type B hydrogen adsorption."

At Professor Emmett's suggestion we have undertaken the calorimetric measurement of the heats of adsorption of hydrogen on the singly promoted iron catalyst at temperatures selected to sort out the three types of chemisorption. The temperatures selected were 0, 214 and -195° for Types A, B and C, respectively.

Experimental

Reduction of the Iron Catalyst.—The sample of singly promoted iron catalyst, designated as catalyst 198, was kindly supplied to us by Professor Emmett. This sample contained 5.50% Al₂O₃ and 70.73% Fe before reduction. The weight of this catalyst used in the calorimeter was 36.67 g. Approximately the same weight (36.12 g.) was used in the preliminary adsorption experiments. The specific surface area of the catalyst 198, as used in the preliminary experiments and computed from the nitrogen isotherm at -195° by the BET method, was 16.9 m.²/g. After the completion of the calorimetric work, the specific surface area of the sample was determined at 11.85 m.²/g.

Experience has shown¹⁻³ that the optimum conditions for activating these iron catalysts are achieved by reduction at 500° in a stream of pure hydrogen at high space velocity. For instance, Kummer and Emmett² used 1000 to 5000 cc. of hydrogen per hour per cc. bulk volume of catalyst. Special precautions are necessary to prevent traces of oxy-

(1) P. H. Emmett and R. W. Harkness, *J. Am. Chem. Soc.*, **57**, 1624 (1935).

(2) J. T. Kummer and P. H. Emmett, *This Journal*, **56**, 258 (1952).

(3) H. H. Podgurski and P. H. Emmett, *ibid.*, **57**, 159 (1953).

gen, water vapor or nitrogen from coming into contact with the iron surface. To meet these conditions we used a modification of the reduction schedule described in an earlier publication from this Laboratory.⁴ Tank hydrogen was passed over copper turnings at 500° to convert traces of oxygen to water vapor, then through a liquid air trap to remove water vapor, and finally through a charcoal trap at liquid air temperature to remove any small quantity of nitrogen that might be present in the original tank hydrogen.³ We used a space velocity of about 2200.

The Calorimeter.—Because of the necessity for reduction of the iron in the calorimeter in a hydrogen atmosphere at 500° we found it was not practicable to use the calorimeter design most recently employed in this Laboratory.^{5,6} In particular it was found that Kovar was attacked by hydrogen at 500° with the consequent failure of the Kovar-to-glass seal formerly used. The calorimeter employed in the present work consisted of an all Pyrex glass external assembly (Fig. 1a) with a platinum filler (Fig. 1b) which enhanced the heat distribution.

The complete calorimeter is shown in Fig. 1. The inner container (A) consists of a thin-walled glass cylinder, 9.5 cm. long, 1.8 cm. internal diameter, and about 1 mm. wall thickness. Surrounding the glass container is a glass jacket (B), the annular space being about 1 cm. The head of the calorimeter is fitted with a gas inlet tube (C), and an outlet (D) which extends to the bottom of the inner container. Four Kovar to glass seals, 1/8" in diameter, two of which are shown in the figure (E), are attached for thermocouple and heater leads from the interior of the calorimeter. A perforated copper disc (F) fits loosely on to the ring seal at the top of the inner container, and supports Pyrex glass beads (G) filling the space in the head of the calorimeter.

A platinum filler was close-fitted into the glass container. This unit is shown in Fig. 1b, and consists of six symmetrically spaced fins, riveted together (H). Notches are cut at the bottom of each fin to facilitate gas circulation. A single copper-constantan thermocouple (J), B and S Nos. 30 and 31, respectively, is spot welded to one of the fins, about half way down. The 60 ohm heater is wound from B and S No. 34 double glass covered "Advance" wire, on two thin strips of mica, approximately 7 cm. long and 6.5 mm. wide. These strips (K) are placed between more mica and bolted, top and bottom, to a pair of opposite fins on the filler. Both the heater and thermocouple wires are sleeved with thin-drawn glass capillaries and connected to short sections of heavier wire (B and S No. 18) which in turn are sealed through the Kovar side arms. Throughout the reduction schedule the Kovar-to-glass seals remained outside the furnace and so were not subjected to hydrogen at elevated temperatures.

This calorimeter has been employed successfully at both 0 and -195° using an ice-water mixture and liquid nitrogen, respectively, to obtain a constant temperature bath at these two temperatures. At both these temperatures, time-temperature curves have been obtained during calibration for heat capacity and during actual adsorption measurements. A treatment of these curves according to Newton's law of cooling has resulted in reconstructed curves which represent constant temperature with time. This indicates that the new calorimeter model is operating in a satisfactory way and that it may be used with confidence.

We have attempted to measure the heats of adsorption for the system hydrogen-iron at 214° (Type B adsorption). In this work we held the temperature as nearly constant as possible by means of an electric furnace. Because we had no temperature regulating device the experiments at 214° were of necessity rather crude, and most of the time-temperature curves did not conform exactly to Newton's law of cooling. Four experimental points are shown in Fig. 4, runs 7 and 8. It happened that the experimental data for the initial point of run 8, giving a differential heat of adsorption of 26 kcal. per mole, gave indication of excellent agreement with Newton's law; as a result we feel rather confident about this one point. We prefer however to consider all four points 7 and 8 as giving only qualitative evidence

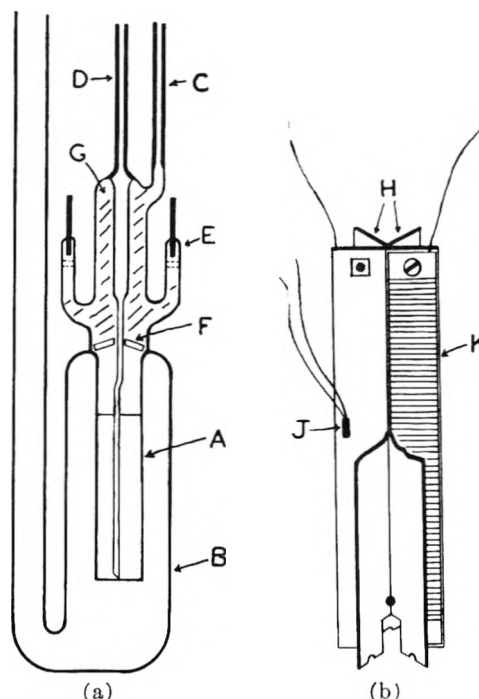


Fig. 1.—The calorimeter: inner Pyrex jacket, A; outer Pyrex jacket, B; inlet tube, C; outlet tube, D; Kovar-glass seal, E; copper disc, F; Pyrex glass beads, G; platinum fins, H; thermocouple, J; heater, K.

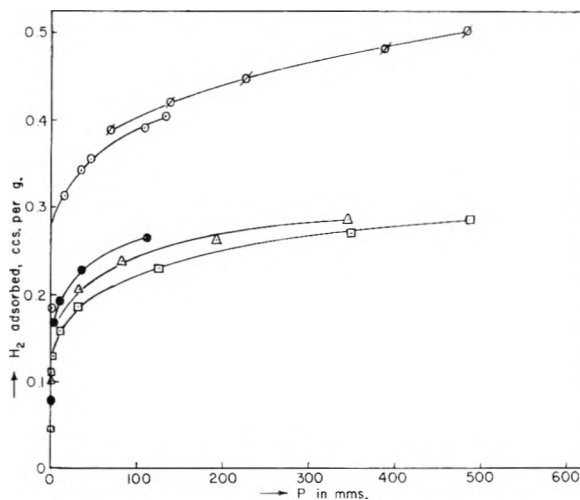


Fig. 2.—Isotherms at 0° for hydrogen on singly promoted iron catalyst: heat runs 1, 2 and 5, ●, △, □; adsorption runs A₁ and A₂, ○, ◊.

that the heat values for Type B adsorption are higher than for Type A.

Results and Discussion

The Isotherms for the Hydrogen-Iron System.

—In anticipation of the heats of adsorption measurements, the isotherms for hydrogen on iron catalyst 198 were first determined at 0 and -195° in a simple glass adsorption tube which had approximately the same capacity and dimensions as the inner chamber of the calorimeter. The results are shown in Figs. 2 and 3 as adsorption runs A₁ and A₂ at 0°, and adsorption run C at -195°. A second set of isotherms was determined along with the heat runs 1, 2 and 5 at 0° and heat runs

(4) R. A. Beebe and N. P. Stevens, *J. Am. Chem. Soc.*, **62**, 2134 (1940).

(5) C. H. Amberg, W. B. Spencer and R. A. Beebe, *Can. J. Chem.*, **33**, 305 (1955).

(6) R. A. Beebe and R. M. Dell, *This Journal*, **59**, 746 (1955).

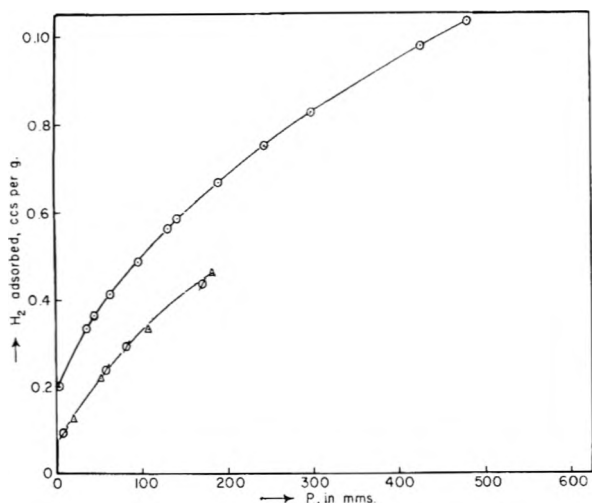


Fig. 3.—Isotherms at -195° for hydrogen on singly promoted iron catalyst: adsorption run C, O; heat runs 4 and 6, Δ , \emptyset .

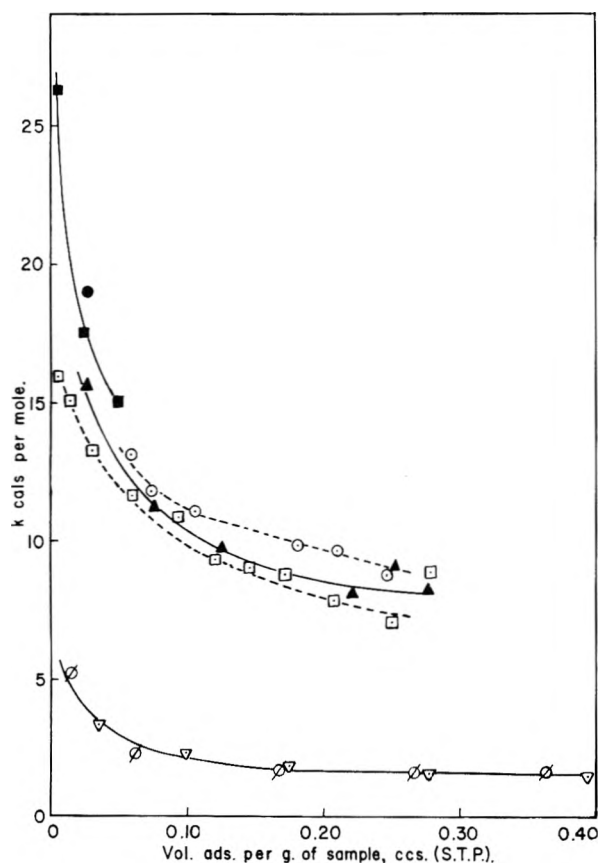


Fig. 4.—Calorimetric heats of adsorption for hydrogen on singly promoted iron catalyst: runs 4 and 6 at -195° , ∇ , \emptyset ; runs 1, 2 and 5 at 0° , O, \blacktriangle , \square ; runs 7 and 8 at 214° , \bullet , \blacksquare .

4 and 6 at -195° , and these also are shown in Figs. 2 and 3.

It is at once apparent that the adsorptive capacity of the catalyst for hydrogen adsorption in the calorimetric work was only about one-half that in the initial experiments in the simple glass adsorption tube. We can offer no explanation of this marked difference in the Type B hydrogen adsorption in the simple adsorption tube and in the calo-

rimeter since the schedule of space velocity of hydrogen gas flow and the temperature of reduction and outgassing was made as nearly identical as possible in the two sets of experiments. It could be in part due to a decrease in total surface since the specific surface area at the end of the heat measurements was down to $11.85 \text{ m}^2/\text{g}$. Unfortunately no check was kept on the BET surface area of the catalyst in the calorimeter during the course of the heat runs.

It is of interest to compare our Type C hydrogen adsorption isotherms at -195° on catalyst 198 with those of Kummer and Emmett² on a singly promoted iron catalyst although the catalysts used in our studies and in theirs are not identical. At "zero" pressure we found 0.2 and 0.09 cc./g. in our two sets of experiments (Fig. 3) whereas Kummer and Emmett² found 0.11 cc./g. (see Fig. 1 of their paper).

It is also to be noted that the isotherms at 0° are not very reproducible. The heat runs and concomitant isotherm measurements were carried out in the order listed from run 1 to run 6. (Run 3 was abandoned after only one or two initial increments because of temporary difficulty with the temperature recording device, and the results are not shown.) As a result of accidents, the catalyst was exposed to air at room temperature between heat runs 1 and 2 and again between heat runs 4 and 5. Of course each exposure to air necessitated the repetition of the high temperature reduction and outgassing procedure. It is to be noted that this history of the catalyst resulted in decreasing Type B adsorptive capacity for hydrogen at 0° from run 1 to 2 to 5, but that exposure to air and subsequent reduction between runs 4 and 6 caused no detectable change in the amount of Type C adsorption at -195° .

Types A and C adsorption of hydrogen on catalyst 198 proceed at a sufficient rate at 0 and -195° , respectively, to make calorimetric measurements practicable by our technique. For instance all the adsorption points shown in Figs. 2 and 3 represent equilibrium pressures which were reached within 10 minutes or less of the admission of the given increment of hydrogen. We also have investigated the adsorption for the hydrogen-iron system at -78° and at 200° . Confirming the results of Kummer and Emmett² we have found a very considerable "creep" at -78° , and as a consequence we did not make calorimetric measurements at this temperature. We also have found a definite "creep" in the Type B adsorption at 200° but since this creep in pressure did not represent more than a 15% change in the amount adsorbed up to about 0.06 cc. per g. we have found it practicable, so far as adsorption rate is concerned, to attempt the rough measurements represented by the four points given in runs 7 and 8. Any heat measurements for Type B adsorption at higher coverages than those shown in Fig. 4 would be precluded by the slow adsorption rate.

The Heat of Adsorption.—The heat values for Types A, B and C adsorption at 0, 214 and -195° , respectively, are shown in Fig. 4. For reasons already given, heat runs 7 and 8 for Type B adsorption at 214° have only qualitative significance.

Because of the relatively small increments of hydrogen adsorbed even on the large sample of catalyst (36.67 g.) we consider that heat runs 1, 2 and 5 at 0°, and runs 4 and 6 at 195° are satisfactory with respect to the spread of the experimental points.

From Fig. 4 it is at once apparent that Types A and C adsorption are sharply differentiated as regards the heat values which range, respectively, from 16.5 to 8.0 (at 0°) and from 5.2 to 1.6 kcal. per mole at -195°. The crude measurements at 214° indicate heats for Type B adsorption ranging from 27 to 15 kcal. per mole.

It is of interest that the differential heat values for Type A adsorption at 0° show a small decrease in the successive runs 1, 2 and 5, and that a corresponding decrease for these three runs is shown in the isotherms at 0° in Fig. 2. On the other hand, neither the heat data nor the isotherms for Type C adsorption at -195° show any observable differences in runs 4 and 6. From these observations we must conclude that Type B adsorption is rather sensitive to differences in the state of the surface caused by exposure to air and subsequent reduction at high temperature whereas Type C adsorption is comparatively insensitive to any effects of this history of the adsorbing surface. Our calorimetric data at -195° support the prediction of Kummer and Emmett² that the heat of binding for Type C adsorption is "considerably smaller than the heat of adsorption of either Type A or Type B hydrogen adsorption." On the other hand only a small fraction of the hydrogen adsorbed at -195° yields heats which are in excess of about 2.0 kcal. per mole. It is to be noted that this fraction represents that part of the isotherms which is adsorbed at pressures too small to observe on a regular mercury manometer (see Fig. 3). Since Kummer and Emmett² have presented strong evidence for a chemisorption process at -195°, we conclude that the initial increments in runs 4 and 6 shown in Fig. 4, perhaps up to about 0.10 cc. per g., are due to Type C chemisorption. According to Trapnell⁷ and to Schwab,⁸ any heats of adsorption for hydrogen which exceed 2.0 kcal. per mole must be attributed to chemisorption.

In previous publications from this Laboratory^{9,10}

(7) B. M. W. Trapnell, "Chemisorption," Academic Press, New York, N. Y., and Butterworth's Scientific Publications, London, 1955, p. 146.

(8) G. M. Schwab, "Proceedings of the Second International Congress of Surface Activity in Liege," Vol. II, Butterworth and Interscience, 1957.

we have reported the calorimetrically determined heats of adsorption for hydrogen and for deuterium on a chromic oxide adsorbent at -183°. Since the chromic oxide had a specific adsorptive capacity about thirty times that of the present iron catalyst, it was possible to obtain the heat values at low coverage in much greater detail than in the present work. Thus we see that it was possible to introduce nine increments of about 4.0 cc., each with only 1.2 mm. equilibrium pressure for the last increment. In the current work (run 4, Fig. 3) the equilibrium pressure after the first increment was already 3.0 mm. In the work of Beebe and Dowden it is seen (Fig. 3) that the heats for hydrogen on chromic oxide decrease from 5.2 to 3.2 kcal. per mole for the nine increments introduced. It is seen from Fig. 4 of the current work that the heats for the first four points from runs 4 and 6 fall in the range from 5.1 to 2.5 kcal. per mole. Thus on the basis of the heats and of the residual pressures we may consider the range represented by these four experimental points as being comparable to the whole range of points studied for the hydrogen-chromic oxide system.¹¹

In a previous publication⁹ from this Laboratory the work of Gould, Bleakney and Taylor¹² on the catalysis by chromic oxide of the hydrogen-deuterium exchange reaction at -183° has been cited, and it was concluded that the heat values for the hydrogen-chromic oxide system varying from 5.2 to 3.2 kcal. per mole^{9,10} must represent a chemisorption process. It seems admissible to draw a similar conclusion in the present case for Type C adsorption having heats in excess of 2.0 kcal. per mole. It should be noted that Schwab⁸ argues that it is incorrect to suppose that the chemisorbed state is necessarily identical with the activated state in catalytic reaction. Thus it seems worthwhile to present the heat data for Type C adsorption as supporting evidence for chemisorption in the iron-hydrogen system.

(9) R. A. Beebe and H. M. O'feld, *J. Am. Chem. Soc.*, **59**, 1627 (1937).

(10) R. A. Beebe and D. A. Dowden, *ibid.*, **60**, 2912 (1938).

(11) It is unfortunate that we could not obtain more detailed information in the present work, but this was impracticable because of the small quantity of hydrogen adsorbed on iron catalyst 198. It should be mentioned that the abscissae of Fig. 4 are plotted at the mid-point of each increment. A more accurate use of the data would involve plotting total heat evolved against total volume adsorbed and then calculating the differential heats from the slope of this line. This has not been done because of the small number of experimental points involved in the region of decreasing differential heats.

(12) A. J. Gould, W. Bleakney and H. S. Taylor, *J. Chem. Phys.*, **2**, 1627 (1937).

THE ADSORPTION OF NORMAL OLEFINS ON SILICA-ALUMINA CATALYSTS

BY D. S. MACIVER, R. C. ZABOR AND P. H. EMMETT¹

Mellon Institute, Pittsburgh, Pa.

Received October 7, 1958

The adsorption of 1-butene and 1-octene on silica-alumina catalysts has been studied in an attempt to elucidate the mechanism of catalytic cracking. It was found that 1-butene was strongly chemisorbed by silica-alumina at temperatures as low as -78° and that this adsorption was very sensitive to pretreatment of the catalyst. It also was found that the adsorption passed through a maximum as water was added back to a catalyst previously evacuated at 760° . Further, the amount of adsorption decreased when the surface protons of the catalyst were replaced with barium ions. 1-Butene, when chemisorbed below about 100° , underwent a slow surface polymerization to form what appeared to be a C_3 complex. At higher temperatures this complex started to decompose in a manner suggesting that the complex must exist, at least partially, as a carbonium ion. With further increase in temperature, there was a gradual accumulation of hydrocarbonaceous deposit. While the adsorption characteristics of 1-octene were less thoroughly studied, they appeared in general to be similar to those of 1-butene. From the olefin adsorption measurements between -78 and 500° it appeared that some stable catalyst-olefin complex was formed throughout the entire temperature range although the nature of the complex undergoes a gradual transition from a chemisorbed olefin at -78° to a coke-like hydrocarbon at 500° . On the basis of these and other observations it was concluded that carbonium ion formation is not the rate-determining step in the catalytic cracking of olefins. Instead, it appears that the slow step is the rate at which the carbonium ions break up into smaller fragments and desorb from the catalyst surface.

Introduction

It is generally accepted that the decomposition or cracking of hydrocarbons over silica-alumina catalysts involves the formation of a carbonium ion which is intimately associated with the catalyst surface. Few data are available, however, for judging the actual extent of such carbonium ion formation or chemisorption. In previous work,^{2,3,4} it has been shown that alkanes such as butane, heptane and octane cover only a very small fraction (less than 0.5%) of the surface with carbonium ions even at the temperature at which rapid decomposition is observed. From these results it was concluded that the step controlling the over-all decomposition rate was the actual formation of carbonium ions. The present paper reports the results of an extension of these chemisorption studies to two olefins, 1-butene and 1-octene, and presents conclusions based on these experimental observations.

Experimental

The apparatus used for olefin adsorption measurements was essentially the same as that employed in the study of the adsorption of saturated hydrocarbons.³ It included a volumetric system for adsorption measurements at low pressures (four mm.) and a flow-type gravimetric system for adsorptions at higher pressures and at temperatures above those at which decomposition is initiated. Two essential modifications were made in the flow system. Both a water saturator and a reduced copper oxide bed were installed in the entrance side of the flow system. The saturator permitted the vaporization of about 30 mm. of water vapor into a nitrogen stream. This saturated nitrogen then could be passed over the catalyst to adjust the extent of rehydration of a catalyst sample partially dried by prior evacuation at high temperature. The extent of rehydration was determined from the weight increase of the catalyst sample. The bed of reduced copper oxide, maintained at about 300° , was used to remove trace impurities of oxygen from the hydrocarbon feed.

Two catalysts were employed in this study. The first of these was a commercial synthetic silica-alumina cracking catalyst obtained from the Houdry Process Corporation

and designated by them as M-46. It contained 12.5% Al_2O_3 and had a BET surface area of $262 \text{ m}^2/\text{g}$. The other was a barium-exchanged silica-alumina prepared by contacting M-46 pellets with a 1.5 molar barium acetate solution for 66 hours at 30° , washing thoroughly, and drying at 110° . The final catalyst contained 0.46 meq. Ba^{++}/g . and had a surface area of $228 \text{ m}^2/\text{g}$. About 6 g. of catalyst was used for each run in the volumetric system and about 10 g. in the flow system. In all cases, 20 to 30 mesh particles were employed.

The 1-butene and 1-octene were pure grade hydrocarbons obtained from the Phillips Petroleum Co. and Humphrey-Wilkinson, Inc., respectively.

Results

1-Butene.—Volumetric adsorption measurements quickly showed that butene, unlike the saturated hydrocarbons,^{3,4} was strongly chemisorbed by the catalyst even at room temperature or below, and that its adsorption was very sensitive to the pretreatment of the catalyst. This sensitivity is well illustrated by a series of four isobars of 1-butene at 4 mm., shown in Fig. 1. The four runs were made consecutively on the same catalyst sample with varying pretreatment. Before run one, the sample had been used for a number of adsorption measurements and had been regenerated repeatedly by heating in dry air at 500° . Finally, it was evacuated at 500° for 10 hours following a regeneration and then permitted to adsorb 1.8 cc. (STP) of water vapor per g. at 450° . Before run two, the sample from run one was treated at 500° for two hours with a stream of dry air to remove all carbonaceous material, evacuated at 500° , and allowed to adsorb 0.8 cc. (STP) of water vapor per g. at 470° . Runs three and four were made after the catalyst from run two had again been regenerated and evacuated at 500° without any water having been added back to the catalyst. Evacuation prior to run three was for about 10 hours; that preceding run four about 64 hours. This technique, then, produced a series of catalysts of decreasing water content. In general, the four runs seem to indicate that the adsorption of 1-butene is sensitive to the amount of adsorbed water vapor.

It became apparent during the course of run one that both decomposition products and water were being evolved as the temperature reached about

(1) Johns Hopkins University, Baltimore, Maryland.

(2) R. C. Zabor and P. H. Emmett, *J. Am. Chem. Soc.*, **72**, 5639 (1951).

(3) D. S. MacIver, University of Pittsburgh, Ph.D. Thesis, 1957.

(4) Also D. S. MacIver and P. H. Emmett, *THIS JOURNAL*, **62**, 935 (1958).

100°. Accordingly, a rough correction has been made for this gas evolution in runs two, three and four. The portion of the gas phase that did not condense in a trap cooled to -195° was called "cracked product" and presumably consisted of hydrogen and methane, while the material condensing at -78° was termed "water." As will be noted in this series of runs, the volume of cracked product was rather small in run two, but increased with successive experiments until in run four the total volume of cracked products amounted to about 0.6 cc. (STP)/g. Thus, in a strict sense, the curves in Fig. 1 do not represent true equilibrium isobars for butene, because at temperatures of 100° and above, although the total pressure was 4 mm., the partial pressure of butene in the gas phase was in all cases less than four mm.

Evidence that 1-butene chemisorbs on silica-alumina in the form of a stable complex having the characteristics of a carbonium ion was obtained from a mass spectrographic analysis of the hydrocarbon fraction of the gas phase at 130° in a typical adsorption run in which 1-butene was used as adsorbate. The results of this analysis are shown in Table I.

TABLE I
ANALYSIS OF HYDROCARBON FRACTION OF GAS PHASE

Components	Mole %
Methane	0.8
Ethane	1.1
Propane	1.4
Butenes	39.5
Isobutane	16.8
Pentenes	18.5
Isopentane	18.8
C ₆ and higher hydrocarbons	Some

From the analysis of these gases, it is apparent that a variety of hydrocarbon reactions including decomposition, alkylation and isomerization have occurred in this temperature range. Inasmuch as these reactions are thought to proceed *via* a carbonium ion mechanism, these data may be taken as indicative of carbonium ion formation from olefins even at these low temperatures. Samples of gases taken at higher temperatures contained greater amounts of cracked products and smaller amounts of butenes.

As a check on the butene adsorption values at low pressure, a run was made in the gravimetric flow system at 100° on a sample of Houdry M-46 flushed with dry nitrogen for 16 hours at 500° . Points were taken as a function of time, the partial pressure of butene being maintained at about 5, 20 and 100 mm. Traces of water evolved during the runs were measured by means of a $Mg(ClO_4)_2$ drying tube. The adsorption values in these and all subsequent flow type experiments were corrected for any weight changes due to the loss of water. Plots of these data are given in Fig. 2. As is evident, the adsorption at 5 mm. gradually increased with time, reaching a value of about 4.5 cc. (STP)/g. at the end of eight hours. This value is in fair agreement with that shown in run four of Fig. 1. Due to the apparent dependence of adsorption upon catalyst water content, exact agreement is not

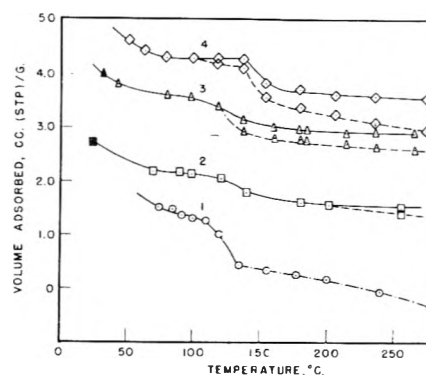


Fig. 1.—Adsorption isobars of 1-butene on silica-alumina cracking catalyst at 4 mm. pressure. Open symbols represent initial adsorption; closed symbols, re-adsorption after cooling from 100° . — represents the isobar corrected for cracked products and water; - - - - - represents the isobar corrected for water; ······ represents the uncorrected isobar.

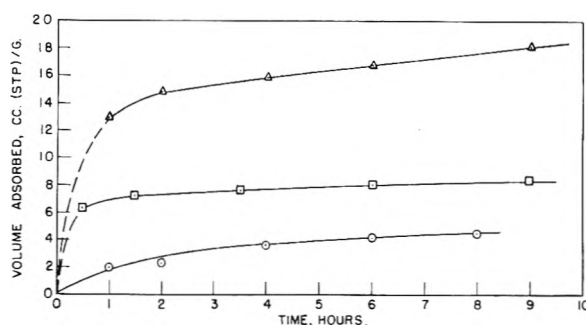


Fig. 2.—Rate of adsorption of 1-butene at 100° on silica-alumina: Δ , adsorption at 100 mm.; \square , at 20 mm.; \circ , at 5 mm.

to be expected. Adsorption values at 20 mm. and 100 mm. also appear to increase gradually with time, indicating the possibility of slow polymerization under these temperature and pressure conditions, the product of this polymerization also being adsorbable. At 100 mm., the adsorption corresponds to slightly less than a monolayer. It should be pointed out that these three runs of Fig. 2 were made successively on the same sample of silica-alumina rather than on three different samples. Thus, the rate curves for the two higher pressures are shown as dotted curves up to the first adsorption point, inasmuch as the sample had been equilibrated at the next lower pressure of the previous experiment.

The results shown in Fig. 1 made it evident that the chemisorption of butene was dependent upon the state of hydration of the catalyst. This suggested a series of butene chemisorption experiments on catalysts of varying but known water content. Accordingly, a number of catalyst samples having different water contents were prepared by evacuation at 760° and rehydration to equilibrium (reached in about 30 minutes) with water carried at a known partial pressure in a nitrogen stream. The extent of rehydration was controlled by proper selection of the rehydration temperature. Butene chemisorption values for such samples measured at 100° and 5 mm. pressure after six hours of gas flow are shown in Fig. 3 as a function of the amount of water added back to the catalyst. The curve

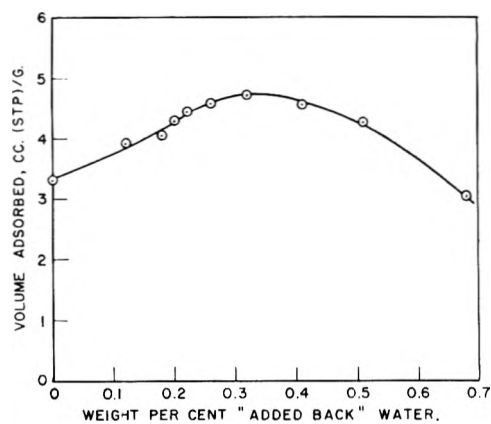


Fig. 3.—1-Butene adsorption at five mm. and 100° on silica-alumina vs. catalyst water content.

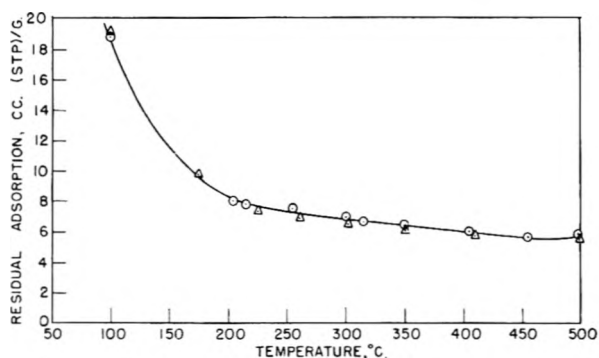


Fig. 4.—Residual weight, calculated as cc. butene per g., after nitrogen flushing vs. temperature: O, 1-butene on silica-alumina; Δ, Cu treated 1-butene on silica-alumina.

shows that the adsorption values increased with increasing water content over and above the water content after the evacuation pretreatment. The adsorption reached a maximum value of about 4.7 cc.(STP)/g. at a content of added water of about 3.2 mg./g. The curve then dropped off rapidly with an additional increase in water content.

In a separate experiment, the total amount of water on a similar catalyst was determined by evacuation up to 1300°. From this work it was possible to show that the water remaining associated with the catalyst after a 760° evacuation (the treatment used in the above experiments) amounted to about 1.0%.⁵ The total water content of the catalyst showing maximum butene chemisorption was therefore approximately 1.3% by weight.

An adsorption run of still another type was carried out at one atmosphere pressure by passing pure 1-butene for six hours over a sample of the catalyst previously flushed with nitrogen overnight at 500°. At 100° the sum of the physical and chemical adsorption amounted to 49.6 cc.(STP)/g. This is equivalent to about two layers of butene over the entire surface on the basis of a measured surface area of 262 m.²/g. To differentiate between physical and chemical adsorption, the sample was flushed overnight with nitrogen at 100°. The

(5) Work completed in recent months has indicated that the measured water content per unit weight of catalyst after a given period of evacuation at some specified temperature will depend upon the volume of catalyst being evacuated. Water contents as low as 0.3 to 0.8% are obtained upon evacuation at 500°, provided only one or two pellets are used.

removable butene amounted to 30.8 cc.(STP)/g. This was thought to be mainly physically adsorbed. The residual butene amounting to 18.8 cc.(STP)/g. is presumably chemisorbed. It is equivalent to somewhat less than a monolayer and is equal to less than two butene molecules per H⁺, if we estimate the latter to be 0.5 to 0.6 meq./g. by the usual base exchange procedure. The flushing with nitrogen was continued as the temperature was increased by steps to 500°; at the same time, at successively higher temperatures, the residual material on the catalyst was determined gravimetrically. A plot of the weight of this residual material, calculated as cc.(STP) butene/g., is shown in Fig. 4 as a function of the temperature. Over the higher part of the temperature range this residue on the catalyst is probably existent not as butene, but as a layer of coke.

Also shown in Fig. 4 is a curve obtained in a similar manner showing the adsorption on silica-alumina of 1-butene, treated with hot copper for trace oxygen removal. This run indicates that either no oxygen was present in the unpurified butene or that the adsorption of olefins is not as sensitive to traces of oxygen as is the adsorption of paraffins.³

Considerable work has been done on the low temperature adsorption characteristics of 1-butene in which attempts have been made to differentiate between physical adsorption, chemisorption and polymerization in the temperature range from -78° to room temperature. With 1-butene as the adsorbate, two consecutive isotherms were run in the volumetric system on the silica-alumina catalyst at -78° where 1-butene has a vapor pressure of 13.5 mm. Pretreatment of the catalyst consisted of a 16 hour evacuation at 500°. Between these two isotherms, which are shown in Fig. 5, the sample was warmed to room temperature and equilibrium established under these conditions before the second isotherm was run. In the first adsorption curve, the adsorption at a relative pressure of 0.5 corresponded to about three molecular layers, on the basis of a butene monolayer of approximately 25 cc.(STP)/g. This adsorption has been estimated to consist of about two layers of physically adsorbed butene, as predicted by the BET theory,^{6,7} and a monolayer of chemisorbed butene. At relative pressure 0.96, the adsorption increased to about five molecular layers. The desorption portion of the first adsorption curve showed a hysteresis loop which failed to close, and the equilibrium adsorption at zero relative pressure, even after evacuation, amounted to 25.1 cc.(STP)/g. This has been interpreted as indicating the chemisorption of approximately a monomolecular layer of 1-butene.

After the catalyst was warmed to room temperature and recooled to -78°, the second adsorption curve was run. This isotherm showed behavior similar to that of the first isotherm. The adsorption at relative pressure of 0.95 was 132.5 cc.(STP)/g., corresponding to somewhat more than five molecular layers of 1-butene. The desorption curve of this second isotherm was quite similar in shape to

(6) S. Brunauer and P. H. Emmett, *J. Am. Chem. Soc.*, **59**, 2682 (1937).

(7) S. Brunauer, P. H. Emmett and E. Teller, *ibid.*, **60**, 309 (1938).

that of the first isotherm, again yielding a hysteresis loop which failed to close. The final adsorption value after evacuation at -78° amounted to 38.4 cc.(STP)/g. of tightly bound 1-butene. This represents an increase in chemisorption of about a half layer. The additional chemisorption has been interpreted as resulting from a rearrangement of the chemisorbed butene on the surface, this rearrangement occurring at room temperature between the determination of the two isotherms. This rearrangement or migration may result in concentrated piles of butene molecules or polymerized butene molecules at the most active portions of the heterogeneous surface. It also apparently causes the barring of fresh portions of the somewhat less active surface, portions still capable of accumulating additional chemisorption at -78° .

To check this interpretation, a similar set of two isotherms was run at -73° on a fresh sample of pretreated catalyst without the intervening heating to room temperature. The results are shown in Fig. 6. The second isotherm at -78° was, in general, sigmoidal in shape and typical of Type IV isotherms.⁸ The desorption curve again showed a hysteresis loop which in this instance closed at a relative pressure of about 0.1. At the completion of the run, 24.0 cc.(STP)/g. remain chemisorbed. This value agrees closely with the quantity of butene initially present at the beginning of the second isotherm, indicating that the adsorption occurring in the second isotherm was quite reversible. This behavior can be accounted for as resulting from physical adsorption of 1-butene, this adsorption merely covering over the monomolecular layer of 1-butene.

Inasmuch as the observed adsorption was thought to be physical adsorption in this second isotherm, the data from the adsorption portion of the curve, up to a relative pressure of 0.35, were treated by the BET method. A good straight line was obtained, and a value for V_m , the butene volume corresponding to monolayer coverage, was found to be 27 cc.(STP)/g., a value in good agreement with the amount of chemisorption observed at -78° . This monolayer coverage was observed at a relative pressure of 0.26.

This second isotherm also emphasizes the essential correctness of the initial interpretation concerning the difference in behavior of chemisorbed butene at -78° and room temperature. The apparent rearrangement or polymerization observed at room temperature does not occur as rapidly at -78° , so that subsequent readsorption at -78° results only in physical adsorption and not in increased chemisorption.

By similar adsorption studies, an attempt was made to determine the behavior of 1-butene on silica-alumina at a temperature intermediate between -78° and room temperature, namely, 0° . An isotherm of 1-butene showed greatly increased adsorption values characterized by a very slow approach to equilibrium. Upon desorption it was found that 97 cc.(STP)/g. remained bound quite strongly to the surface at a relative pressure of es-

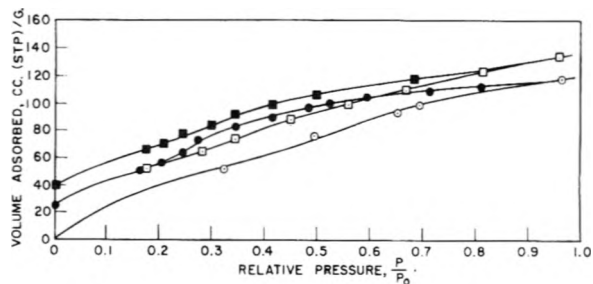


Fig. 5.—1-Butene adsorption at -78° on silica-alumina: open and solid circles, initial adsorption and desorption, respectively; open and solid squares, readsorption and desorption after equilibration at room temperature.

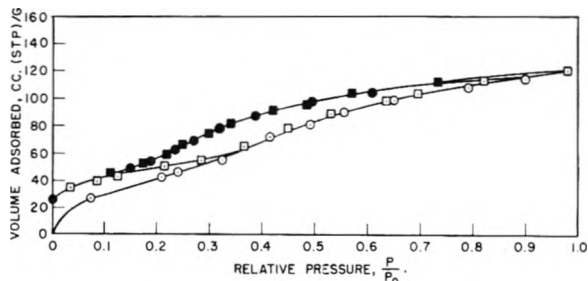


Fig. 6.—1-Butene adsorption at -78° on silica-alumina: open and solid circles, initial adsorption and desorption, respectively; open and solid squares, readsorption and desorption. Temperature was maintained at -78° between runs.

entially zero. This corresponds to nearly four layers of butene. Attempts to remove portions of this residual adsorbed material by evacuation at 0° resulted in the recovery of considerable hydrocarbon, which was identified by vapor pressure measurements to be mainly a C_8 hydrocarbon, probably octene. Thus the surface polymerization of butene occurs at 0° as well as at room temperature, and it is this molecular rearrangement on the surface which causes the increased adsorption values observed. At -78° , on the other hand, adsorption appears to be a combination of physical and chemical adsorption, and relatively little cumulative polymerization takes place. No C_8 hydrocarbon was detected in the gases desorbed at the lower temperature.

Despite the foregoing work, it was felt that even at -78° chemisorbed butene might undergo some change with time. Accordingly, experiments were performed in which a monolayer of butene was chemisorbed at -78° and allowed to remain on the catalyst at this temperature for a specified period of time. The catalyst then was warmed to room temperature; the desorbed gases were trapped at -195° and measured volumetrically. The results of three such experiments are shown in Table II. A fresh sample of catalyst was used in each run. These data would seem to be suggestive of a slow surface polymerization of the chemisorbed butene at -78° .

It is well known that the catalytic activity of a silica-alumina can be poisoned by base exchanging the surface protons with alkali metal or alkaline earth ions.^{9,10} Further, it has been shown⁵ recently

(9) J. D. Danforth, *This Journal*, **68**, 1030 (1954).

(10) R. G. Haldeman and P. H. Emmett, *J. Am. Chem. Soc.*, **78**, 2922 (1956).

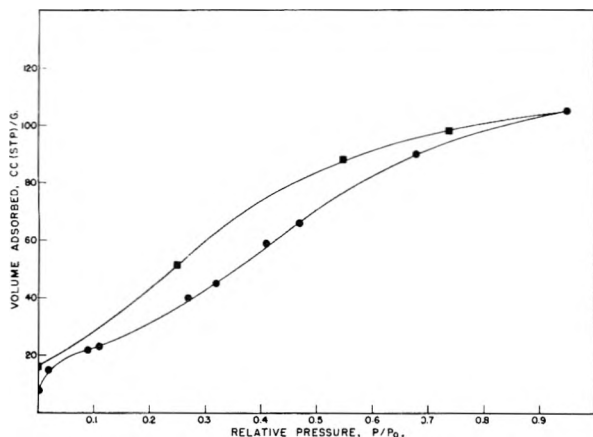


Fig. 7.—1-Butene adsorption at -78° on barium exchanged silica-alumina: circles, adsorption; squares, desorption.

TABLE II

AGING OF CHEMISORBED 1-BUTENE AT -78°

Time adsorbed at -78° , days	% of chemisorbed butene desorbed at room temp.
1	70
8	62
21	33

that the ability of a catalyst to chemisorb isobutane is also decreased by this treatment. It was of interest, therefore, to determine whether a similar effect is operative in the case of 1-butene chemisorption. Accordingly, an adsorption isobar was measured at -78° on a sample of the Houdry M-46 which had been base exchanged with 0.46 meq. $\text{Ba}^{++}/\text{g.}$; the result is shown in Fig. 7. Before the run, the catalyst was evacuated for 16 hours at 500° . As can be seen, the isotherm showed a behavior similar to that found for the unexchanged catalyst (Fig. 6) except that in the present case only about 16 cc.(STP)/g. remained adsorbed at the completion of the run. This corresponds to about 0.74 of a monolayer, as compared to about a complete layer for the unexchanged material, indicating a definite poisoning of the catalyst by the barium ions.

1-Octene.—Because of the sensitivity of the catalyst to pretreatment and particularly to the amount of adsorbed water vapor on its surface, no extensive adsorption measurements were made for 1-octene. The few experiments that were carried out, however, showed clearly that octene was chemisorbed in slightly greater quantities than was butene at a partial pressure of four mm. However, octene differed from butene in that it began to decompose quite extensively at temperatures lower than those at which butene decomposition took place.

Discussion

The experiments with butene show that unsaturated hydrocarbons are chemisorbed very rapidly by the surface of cracking catalysts even at -78° . This observation seems to be consistent with information available in the literature. For example, Hansford and co-workers¹¹ report that when

unsaturated hydrocarbons are let into a reaction vessel containing a cracking catalyst covered with D_2O , the pressure drops to a very low value (about one mm.) at -30° , and the adsorbed butene exchanges its hydrogen atoms at an appreciable rate with the adsorbed deuterium oxide on the surface of the catalyst. In interpreting their experiments, they present the reasonable conclusion that the exchange probably occurs as a result of butene molecules forming carbonium ions by addition to the deuterium ions of the catalyst.

It is interesting to compare the maximum observed in butene chemisorption as a function of water content (Fig. 3) with similar maxima found by other workers. Hansford, *et al.*,¹¹ report a maximum in the exchange rate of hydrogen between isobutane and adsorbed D_2O on silica-alumina at an "added back" D_2O content of 0.25%. Hindin, Mills and Oblad,¹² in a somewhat similar study, found an exchange rate maximum at 0.2–0.3% "added back" water. The same authors also have investigated the effect of catalyst water content on the isomerization and cracking of a number of alkanes over silica-alumina and observed the highest rate when water was added to the dried catalyst in amounts varying from 0.05 to 0.1%. Finally, Haldeman and Emmett,^{10,13} in an extensive study of the isobutane exchange reaction, found that the optimum "added back" water content ranged from 0.13 to 1.0%, depending upon the prior history of the catalyst.

Thus there seems to be ample evidence that the surface characteristics of silica-alumina are strongly dependent upon the state of hydration of the catalyst, and it is not surprising that the chemisorption of butene should be a function of the amount of "added back" water. Because of the complexity of the system, however, it is difficult to develop a detailed, mechanistic picture of this dependency; and only a qualitative explanation seems possible at this time.

The work of Haldeman and Emmett^{10,13} suggests that most of the active sites on silica-alumina catalysts are in the form of Lewis acids after evacuation at 500° ; Brønsted acids apparently predominate on the hydrated catalyst. If it can be assumed that the addition of water to the evacuated catalyst regenerates the Brønsted acid and that the olefin reacts most readily with this form, then the initial rise in butene adsorption as shown in Fig. 3 becomes reasonable. The decline in chemisorption with further increase in the amount of added water could then result from excessive hydration of protons which might render them less active for carbonium ion formation. That protons are involved in the chemisorption of an olefin seems to be indicated by the observed decrease in adsorption when some of the protons are replaced by barium ions.

Initial 1-butene adsorption experiments made in the volumetric system, the results of which are shown in Fig. 1, yielded adsorption values considerably lower than those corresponding to the maximum adsorption of Fig. 3 and discussed above. It

(11) R. C. Hansford, P. G. Waldo, L. C. Drake and R. E. Honig, *Ind. Eng. Chem.*, **44**, 1108 (1952).

(12) S. G. Hindin, G. A. Mills and A. G. Oblad, *J. Am. Chem. Soc.*, **73**, 278 (1951).

(13) R. G. Haldeman and P. H. Emmett, *ibid.*, **78**, 2917 (1956).

is believed that, due to the less severe dehydration treatment of catalysts in the volumetric system (500° as compared to 760°), these catalysts had water contents correspondingly higher than those showing maximum adsorption in Fig. 3. Accordingly, the observed volumetric adsorption values were low.

From olefin adsorption measurements at -78, 0, 100° and higher, it is obvious that, even though some stable catalyst-olefin complex is formed throughout the entire temperature range, differences exist in the nature of the complex at these various temperatures. The stable 1-butene adsorption of 25 cc.(STP)/g. at -78° amounts to roughly two butene molecules for each proton. This behavior suggests either two butene molecules or one octene molecule in the immediate vicinity of each acid site. As the temperature is increased to 0° and further to room temperature, polymerization to octene seems to occur, as evidenced by detection of gas phase octene. This polymerization is presumably accompanied by rearrangement of molecular positions on the surface inasmuch as fresh surface is bared for further adsorption at -78°. Finally, at temperatures of 100° and higher, it becomes even more difficult to suggest the exact composition of the stable complex. However, since reaction products are continually observed, the complex must exist, at least partially, as a carbonium ion. This agrees with the usual concept of a carbonium ion mechanism for olefin polymerization reactions.^{14,15} There is a gradual accumulation of hydrocarbonaceous deposit as temperature is increased

further. Hence, from the adsorption results and other observations, the exact nature of the complex cannot be defined more closely than to say it displays the characteristics of a carbonium ion, and it appears to undergo gradual transition from a chemisorbed olefin at -78° to a coke-like hydrocarbon at 500° as the temperature is raised.

In conclusion, it may be well to summarize the way in which the present olefin adsorption results fit into the picture of catalytic cracking. The formation of a carbonium ion involves a considerably smaller energy of activation for olefins than for paraffins, inasmuch as ion formation involves only sharing or donating of the electrons of the double bond as opposed to bond breaking in the case of paraffins. As judged by values for the chemisorption of olefins the formation of carbonium ions accordingly appears to take place even at temperatures far below those at which decomposition is observed. On the basis of these facts, then, it is believed that carbonium ion formation is not the rate-controlling step of olefin decomposition. Instead, the rate at which carbonium ions break up into small fragments and desorb from the silica-alumina surface is envisioned as the step controlling the over-all reaction rate. From these postulates it is clear that the rate of decomposition of paraffins is much slower than the corresponding decomposition rate of olefins because of the comparative rates of controlling steps in these reactions. Carbonium ion formation from paraffins is considerably slower than carbonium ion decomposition.

Acknowledgment.—This work was sponsored by Gulf Research and Development Company as a part of the research program of the Multiple Fellowship on Petroleum.

(14) F. C. Whitmore, *ibid.*, **26**, 961 (1934).
 (15) L. Schmerling and V. N. Ipatieff, "Advances in Catalysis," Vol. II, Academic Press, New York, N. Y., pp. 28-78.

ON THE NATURE OF THE CARBON DEPOSIT OF CRACKING CATALYSTS

BY R. G. HALDEMAN AND M. C. BOTTY

American Cyanamid Company, Stamford, Conn.

Received October 7, 1958

Regeneration kinetics, X-ray diffraction, low temperature nitrogen adsorption, and light and electron microscopical studies were used to characterize the carbon (coke) deposit of silica-alumina catalysts. A technique in electron microscopy was developed which permits examination of identical fields before and after regeneration. These studies indicate that the carbon deposit is a finely divided, highly dispersed phase present within the ultimate pore structure of the catalyst. X-Ray diffraction studies indicate that the coke deposit consists largely of pseudo-graphitic structures together with considerable amounts of poorly organized carbonaceous material. A model of the coked structure is proposed which is consistent with observed regeneration kinetics.

Introduction

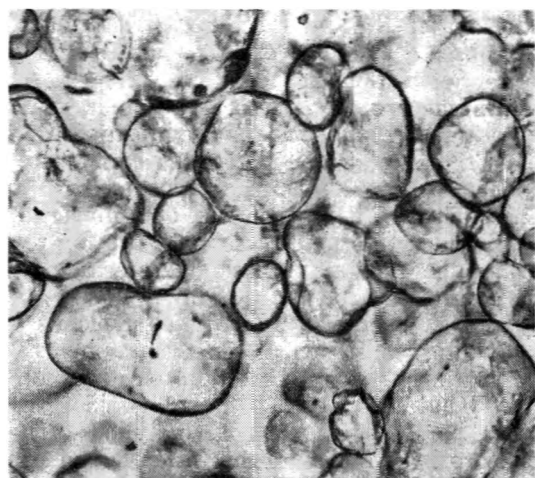
The characterization of the carbonaceous material which forms on a cracking catalyst when it is exposed to hydrocarbons at elevated temperatures is a problem of considerable challenge to the colloid chemist and the microscopist. Whereas carbon (coke) in the catalyst at a level of a few tenths per cent. is detected by the unaided eye, a most careful examination on the electron microscopical scale is required to resolve it even at a concentration of 5-15%.

The scientist can bring other tools into play which permit characterization of the carbon deposit: *i.e.*, low temperature nitrogen adsorption,

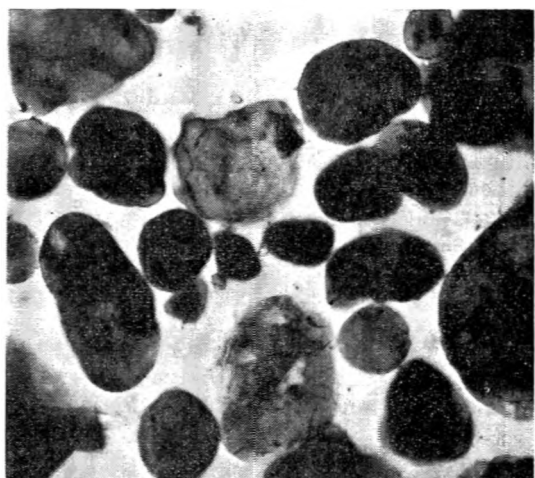
X-ray diffraction and kinetics studies of the combustion of the carbonaceous phase. All of these approaches supply information which allow a picture of the coke deposit to be constructed. It is the purpose of this paper to summarize our knowledge of the nature of this elusive material.

Experimental

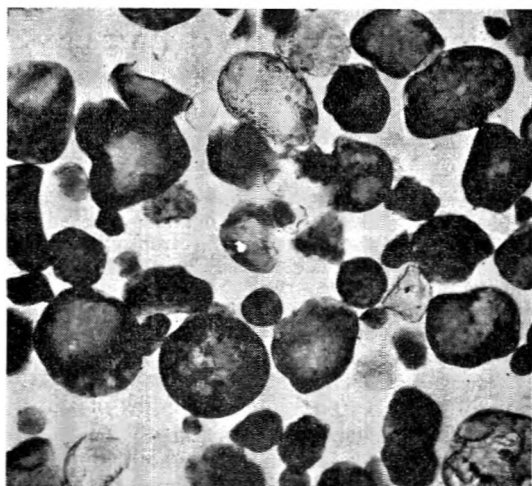
The catalysts studied were manufactured by the American Cyanamid Company. They included fresh microspheroidal 13% Al₂O₃-87% SiO₂ (MSA-1) catalyst, surface area 544 m.²/g., pore volume 0.71 cc./g.; steamed (artificially aged) MSA-1, surface area 100 m.²/g., pore volume 0.38 cc./g. and plant-aged (or equilibrium) MSA-1, low metals contamination (0.1% Fe and <100 p.p.m. Ni + V), surface area



(a) Uncoked.



(b) Coked, uncontaminated.



(c) Coked, contaminated with 0.15 nickel.

Fig. 1.—Thin sections of commercial catalyst (magnification 250 diameters).

143 m.²/g., pore volume 0.42 cc./g. Average granule size in each case was 50–60 μ .

Coke was deposited on the catalysts in a shallow, 3 in.-diameter, fixed-bed, Pyrex glass reactor by contact at 482° with Mid-Continent gas-oil. Carbon level was regulated by time of exposure.

The carbon phase was isolated for direct examination by leaching of the catalyst phase. This was accomplished by contacting the coked catalyst with a concentrated KOH

solution (100 g. KOH/100 cc. H₂O) for several hours. The carbon phase floated on the liquid surface and could be removed by decantation. It was added to a large volume of distilled water in which it slowly settled. Washing was continued by decantation until the wash water was neutral. After acidification with dilute HCl, washing was continued until the filtrate was chloride-free. The final aqueous concentrate was examined directly or was first freeze-dried. Recovery of carbon amounted to about 50% of that originally present in the catalyst. Ash determinations on the coke samples indicated 1–5% non-volatile material.

Electron microscopical studies were made on the RCA Model EMU-1. In order to observe a given field before and after catalyst regeneration, a thermally stable substrate was needed. Vacuum evaporation of α -Al₂O₃ produced films which proved satisfactory. These substrates were stable even when heated to 600°.

X-Ray studies of the carbon phase were made with a Norelco wide range diffractometer using Cu K α radiation under essentially the same conditions as described by Alexander and Sommer.¹

Catalyst regeneration studies were carried out in a 2 in. diameter fluidized bed under essentially differential reaction conditions.² The products of combustion were analyzed continuously for CO₂, CO and water, so that instantaneous rates of carbon and hydrogen combustion could be calculated. These data could be integrated to obtain total carbon and hydrogen as a function of time.

Results and Discussion

Light Microscopical Examination.—Considerable information can be gained about the distribution of the carbonaceous phase in a catalyst granule by examination of coked cracking catalyst in the light microscope. For this purpose plane-parallel thin sections ground to 25–30 μ thickness were prepared from catalyst samples mounted in a resin.³ This method of preparation was desirable because it permitted direct observation of carbon distribution by transmitted light.

Photomicrographs of uncoked catalyst granules showed that the catalyst was essentially transparent to the incident light, and that some subgranular structure was present, as shown in Fig. 1a. Coked catalyst samples had a brownish color throughout. The intensity of color is thought to be directly related to the concentration of carbon in a given element of volume. A photomicrograph of plant-aged catalyst containing 3% carbon is shown in Fig. 1b. Within a given granule and among granules of the catalyst there was considerable variation in color intensity. In steam aged catalyst the color intensity was more uniform both within and among the granules. This difference between plant and steam aged catalyst is attributed to more uniform aging of the latter material. Plant aged catalyst normally contains granules of widely different age and activity.⁴

A most significant observation is that in catalyst of low metal content and in steam-aged catalyst there are no apparent preferential locations of carbon deposition within the granules. Variations appear to be random. Thus, it seems that all regions of the catalyst are capable of carbon formation, and it follows that the carbon phase is normally well dispersed within the granules, at least at the level of resolution of the light microscope.

(1) L. E. Alexander and E. C. Sommer, *THIS JOURNAL*, **60**, 1646 (1956).

(2) R. G. Haldeman and M. C. Botty, "Gordon Research Conference on Catalysis," 1956, to be published.

(3) Prepared by Mr. G. Rev, Columbia University.

(4) C. R. Adams and H. H. Voge, *THIS JOURNAL*, **61**, 722 (1957).

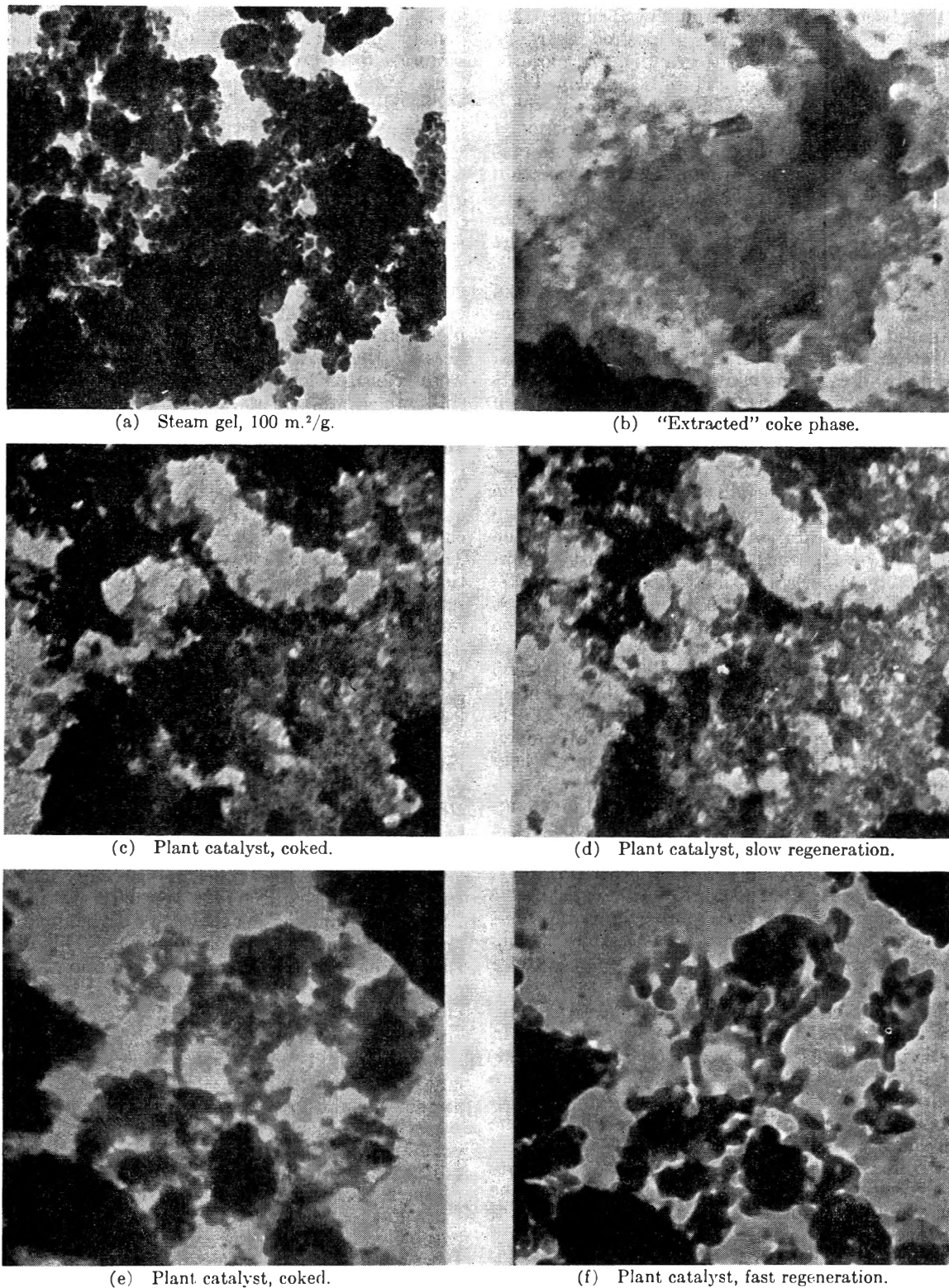


Fig. 2.—Electron micrographs of silica-alumina gel and coke phase (magnification 75,000 diameters).

The presence of metal contamination can markedly alter the carbon distribution in the coked catalyst. Nickel (0.15%) was deposited on the plant-aged catalyst by passing gas-oil vapor containing nickel naphthenate over the catalyst at 370°. The catalyst was examined for carbon distribution and then was regenerated and recoked.

The contaminated catalyst, both with original and with redeposited carbon present, showed a marked tendency for preferential deposition of carbon near the periphery of the catalyst granules. This condition is illustrated for the redeposited carbon in Fig. 1c, whereas the uncontaminated catalyst in Fig. 1b shows only a random distribution of carbon

and the absence of dark circumferential rings. It is believed that the nickel was deposited near the sites of first impact with the granule, *i.e.*, close to the geometrical surface. This is confirmed by abrasion studies on the contaminated catalyst which showed that about 50% of the nickel was removed when the outer 10% of radius of the catalytic material was attrited. Thus, the nickel contamination leads directly to increased coke formation in its environs. This preferential deposition supplements the normal carbon formation within the catalyst granules.

Preferential deposition has been observed also, although to a lesser degree, in some heavily contaminated plant aged catalysts.

Electron Microscopical Examination.—Uncoked catalysts and catalysts containing various amounts of carbon were pulverized and examined electron microscopically. It was observed that the granules and sub-granules consisted of aggregates of very small particles, the majority of which ranged in size from 50 to 300 Å., depending on the history of the catalyst. Figure 2a shows the typical appearance of a steam-aged catalyst containing no coke. The clearly defined, porous fragments consist of approximately spherical ultimate particles of 200–300 Å. diameter. Micrographs of fresh catalyst indicated ultimate particles of about 50 Å. average diameter. The plant-aged catalyst consisted of ultimate particles of diameter in the range 100–200 Å. An excellent discussion of silica-alumina catalyst structure and an elucidation of the effects of thermal and steam aging on structure is given by Adams and Voge.⁴ Pioneering work in the field was done by Ashley and Innes.⁵

The presence of as much as 3% carbon in a sample did not appreciably alter the appearance of the particulate structure and therefore the carbonaceous phase could not be identified with certainty. However, as the carbon content was increased above 3%, the fragments appeared more opaque and resolution of the ultimate structure was less clear. Still, the differences were too subtle to allow interpretation to be very certain.

In order to characterize the carbonaceous phase directly, samples of coked catalyst were leached in caustic to remove the $\text{Al}_2\text{O}_3\text{-SiO}_2$ phase. The residual carbonaceous sediments (*ca.* 95% carbon) were dispersed by stirring and by agitation during drying on the Formar substrates. Figure 2b shows the coke phase from the equilibrium catalyst which had been coked to 3% carbon. The carbon particles are characterized by a much lower density to the electron beam than are silica-alumina particles of the same thickness. Most of the coke consisted of thin, filmy, aggregates of particles of less than 100 Å. size. Uranium shadowing showed that these particles were less than 100 Å. in thickness. There were also considerable areas of very thin fragments showing essentially no structure and indicating dimensions smaller than could be resolved by our microscope.

These observations on the nature of the carbon phase, and the observation that the opacity of the catalyst structure increases with coke deposition,

lead to the postulate that the carbon phase is intimately dispersed within the ultimate particulate structure of the catalyst. This concept can be tested directly by comparison of a given field of highly dispersed coked catalyst before and after regeneration.

Accordingly, the plant-aged catalyst was pulverized and coked to 15% carbon. The sample was dispersed on a refractory supporting film which was made by vacuum evaporation of $\alpha\text{-Al}_2\text{O}_3$. Characteristic fields were micrographed. The specimen was removed from the microscope and slowly heated in a furnace to 450° for one hour to cause removal of the carbonaceous phase by combustion. Complete removal of carbon was indicated by the whiteness of the catalyst specimen. The same fields were relocated and again micrographed. The results are shown in Fig. 2c and d. The decrease in opacity in many zones as the result of heating is believed to be due to the removal of coke by oxidation.

It is estimated from calculations based on pore volume and skeletal density of the "extracted" carbon phase that 15% by weight of coke would occupy about 25% of the interparticle pore space. Taking into account that considerable local variation of carbon content probably occurs, the observed difference in porosity between coked and regenerated catalyst seems reasonable.

When identical fields of a catalyst containing only 3% carbon were examined before and after regeneration, there was no significant change in porosity. Thus, the coke phase could not be identified.

When mounts of a heavily coked catalyst were rapidly heated in a furnace to 600°, sintering of the catalyst occurred as evidenced by its loss of fine structure and its transition to a glassy appearance as observed in the electron microscope. This is illustrated in Fig. 2e and f. Apparently autooxidation occurred so that much higher local temperatures were reached. The specimen retained a greyish color, indicating that some carbon had been trapped in the fused catalyst phase. This clearly shows how excessive thermal deactivation may occur in a commercial regenerator if heat transfer facilities are inadequate.

Klemenok and Shekhter⁶ made an electron microscopical study of the deposition of coke in the cracking of isoöctane on silica-alumina. They examined an uncoked fragment of catalyst, then repeatedly exposed it to isoöctane at 500° and re-examined the fragment in the electron microscope. No experimental details are available. Comparison of their micrograph for the final stage of coking with that for their uncoked fragment seems to indicate an extremely heavy coating of carbon around the periphery of the fragment and larger micropores, although they claim an over-all carbon concentration of only 0.6%. A possible explanation of their results is that contamination by deposition of amorphous material occurred during repeated exposures in the electron microscope. This can be a major problem in high resolution electron microscopy.⁴ On the other hand, in our comparative experiments the problem of contamination in the

(5) K. D. Ashley and W. B. Innes, *Ind. Eng. Chem.*, **44**, 2857 (1952).

(6) B. V. Klemenok and A. B. Shekhter, *Doklady Akad. Nauk (S.S.S.R.)*, **83**, 109 (1952).

electron beam is largely removed since we are studying specimens under essentially identical conditions before and after removal of the carbon phase.

Nitrogen Adsorption Studies.—Our microscopic studies lead to the conclusion that coke deposition normally occurs at the level of the ultimate particles and associated pore spaces.

These observations seem to be confirmed also by low temperature nitrogen adsorption studies. Adsorption-desorption isotherms were carefully determined for a typical sample of the plant-aged catalyst, uncoked and coked to 6% carbon, in the laboratory cracking unit.

The data for the coked catalyst were corrected to an uncoked weight basis since it was desired to study pore volume differences resulting from deposition in the pores of a given weight of uncoked catalyst. (We are tacitly assuming that the volume of the alumina-silica aggregates does not change significantly as the result of coking.) Surface area and pore volume data are shown in Table I.

TABLE I

NITROGEN ADSORPTION DATA ON PLANT-AGED CATALYST (COKE-FREE BASIS)

	Surface area, m. ² /g.	Pore vol., cc./g.
Uncoked	143	0.420
Coked	138	.380
Difference		.040
Difference, calcd. for $d_c = 1.6$ g./cc.		.038

The skeletal density of extracted carbon was determined by helium displacement to be 1.6 g./cc. The calculated volume that would be occupied by 6% carbon is then 0.038 cc./g., which agrees well with the observed difference of 0.040 cc./g. These results indicate that in this catalyst there is no significant occlusion of catalyst pore space by carbon, *i.e.*, there is no appreciable formation of carbon barriers around aggregates of ultimate particles, sealing off their interstitial space.

In contrast, Ramser and Hill⁷ have reported considerable occlusion of catalyst pore space and surface area by coke deposited on a rather highly deactivated plant-aged catalyst. From their data we calculate that the presence of 2.2% carbon reduced pore volume by 22% and surface area by 27%. We further calculate the theoretical pore volume reduction for their catalyst, assuming negligible occlusion and a coke density of 1.6 g./cc., to be about 10%. The physical properties of their catalyst (surface area 61 m.²/g., pore volume 0.147 cc./g., and average pore diameter 37 Å.) indicate the presence of extensively sintered, glassy regions together with minor regions of structure closely resembling fresh catalyst. These properties are characteristic of a thermally deactivated catalyst.⁴ The occlusion of pore space may be due largely to heavy deposition of coke at sites of metal contamination near the boundaries of the active regions, thus partially isolating them from the gas phase.

From the desorption isotherms of uncoked and coked catalyst containing 6% carbon, pore volume-pore diameter data were calculated according

(7) J. N. Ramser and P. B. Hill, *Ind. Eng. Chem.*, **50**, 117 (1958).

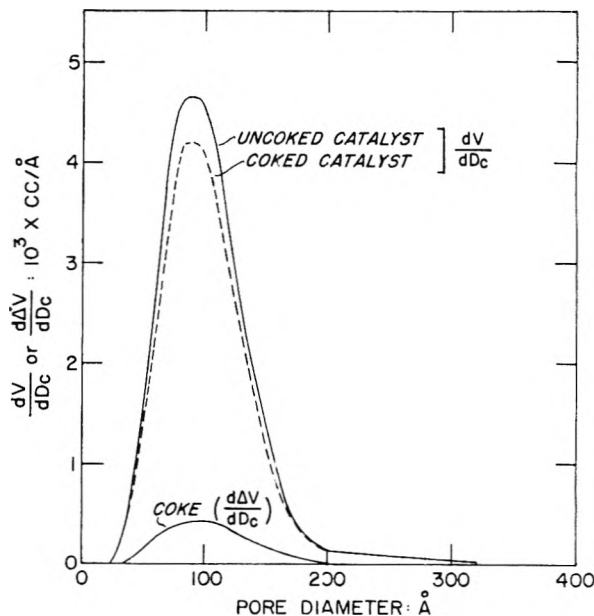


Fig. 3.—Pore size distribution for uncoked and coked catalyst.

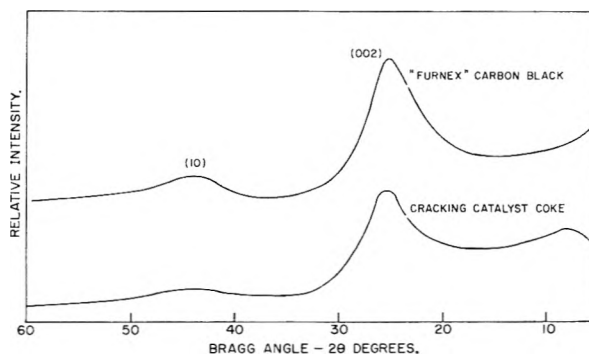


Fig. 4.—X-Ray diffraction pattern of cracking catalyst coke and Furnex carbon black.

to the method of Barrett, Joyner and Halenda.⁸ This method is based on the cylindrical pore model of catalyst structure. Although this model is only a rough approximation, it is believed to lead to a reasonable estimate of the size distribution of the interstices between the fundamental building blocks of catalyst structure.⁹

The pore volume distribution functions, dV/dD_c , for coked and uncoked catalysts are plotted in Fig. 3. The most probable capillary diameter, \bar{D}_c , corresponding to $(dV/dD_c)_{\max}$ is seen to be essentially unchanged by coking, *i.e.*, about 90 Å. The difference between the curves, $d\Delta V/dD_c$ may be taken as a measure of the distribution of carbon in the pores. Thus, it appears that the carbon is deposited largely in the most probable pore spaces, *i.e.*, the interstices between the ultimate particles.

A small decrease in surface area (5 m.²/g.) was observed as the result of deposition of 6% carbon. Based on the spherical model of the ultimate particle system it is evident that if the carbon were to plug completely interparticle pore spaces, the reduction in surface area would be approximately

(8) E. P. Barrett, L. C. Joyner and P. P. Halenda, *J. Am. Chem. Soc.*, **73**, 373 (1951).

(9) A. Wheeler, "Catalysis," Vol. II, P. H. Emmett, ed., Reinhold Publ. Corp., Baltimore, Md., 1955, p. 124.

proportional to the reduction in pore volume, *i.e.*, about 15 mg.²/g. If coke were present as thin films adhering to the ultimate particles, a slight increase in area would be expected. A third case might be random, non-adherent, thin films extending throughout the pore space. This situation would result in a fairly large increase in surface area. Actually, the observed small decrease favors the first postulate but suggests that considerable irregularity or roughness exists in the packing of the carbon phase.

It should be pointed out that in contrast to the Ramser and Hill catalyst, the physical properties of our plant-aged catalyst indicate that aging of the structure has occurred largely through the process of growth of the ultimate particles, a process which is characteristic of low temperature steam aging.⁴

X-Ray Studies.—Further information about the nature of the carbonaceous phase may be gained from X-ray diffraction studies of the "extracted" coke. A number of samples were examined with a Norelco wide-range diffractometer using Cu K α radiation. Figure 4 shows the spectrum of carbon from a freshly coked catalyst compared with that of Furnex carbon black. From the X-ray diffraction data for cracking catalyst carbon, structural parameters were calculated by the method developed by Alexander and Sommer.¹ The results are compared in Table II with the data of the latter authors for Furnex carbon black.¹

TABLE II
X-RAY ANALYSIS OF CRACKING CATALYST COKE AND FURNEX CARBON BLACK

		Furnex	Cracking catalyst coke
Fraction disorganized material	(<i>D</i>)	0.09	0.40–0.50
Fraction single layers	(<i>F</i>)	0.06	0.12
Av. no. of layers in parallel layer groups	(<i>N_e</i>)	3.83	4.9
Mean inter-layer spacing within pseudo-crystallites	(<i>d_m</i>), Å.	3.55	3.47
Dimensions of av. pseudocrystallite, A.:			
Normal to layers	(<i>L_c</i>)	15.0	17
In plane of layers	(<i>L_a</i>)	13.6	10–12

There is a general similarity in the X-ray structure of the two carbon samples except with regard to the higher fraction of disorganized material in cracking catalyst carbon. The term "disorganized" material refers to aggregates of atoms having so little order as to be incapable of yielding distinct X-ray interferences. Thus, 40–50% of the X-ray scattering in our sample is of this continuous type. It is due not only to the strictly amorphous fragments present, but also to the terminal groups which bound the individual layers and probably as well to a significant amount of carbon present in the form of very small ring systems.

The diffraction patterns of both carbons are characteristic of a turbostratic, or random layer lattice.^{10,11} Hence, there is no three-dimensional, or true, crystallinity although the individual layers are similar to those in graphite. Compared to the

carbon black, pseudo-crystallites of the cracking catalyst carbon appear to have a slightly higher degree of organization normal to the layers (4.9 *vs.* 3.8 layers)—but are possibly less well-developed in the direction parallel with the layers (10–12 Å. *vs.* 13.6 Å.).

Carbon-hydrogen ratio data for our cracking catalyst carbon, as determined in regeneration studies, are consistent with the X-ray analysis. Values for a well-purged coked catalyst usually fall in the range 2.0–2.6, depending on the exact pretreatment conditions. Uniform condensed aromatic ring systems of about 10 Å. diameter with each peripheral carbon atom containing a hydrogen atom would have C/H of about 3. A similar system of about 14 Å. diameter would have a C/H of about 4. The experimental values suggest that a considerable fraction of aliphatic or alicyclic fragments (C/H *ca.* 1/2) is present in the deposit. Because of its negligible volatility, this material probably consists largely of appendages to the condensed aromatic systems.

The experimental skeletal density of the extracted carbon is also consistent with the X-ray structure. The observed value of 1.6 g./cc. indicates considerable development of pseudo-graphitic structures.

Regeneration Studies.—The kinetics of the combustion of the carbonaceous deposit furnish further information about its structure. The details of our kinetic studies will be published elsewhere.² These experiments were made in a small fluid bed converter under essentially differential reaction conditions. Over the range of conditions oxygen partial pressure (*P*) 0–0.6 atm., initial carbon concentration (*C₀*) 0.5–6%, temperature (*T*) 773–853°K. (500–580°), using initially dry combustion gas, and specified coke pretreatment conditions, regeneration kinetics can be expressed as

$$-d(C/C_0)/dt = f(C/C_0)P^{0.75} \exp(-34,500/RT)$$

Under these terms $f(C/C_0)$ is a fundamental property of the catalyst carbon deposit. Its shape for a thoroughly-aged carbon deposit is indicated by curve A, Fig. 5. A thoroughly-aged coked catalyst is one which has been purged with inert gas approximately at regeneration temperature until essentially a steady state has been reached, as indicated by constancy of regeneration characteristics. The time may vary from 15–30 minutes at the upper temperatures to several hours at the low temperatures.

The fact that $f(C/C_0)$ is independent of carbon concentration over the range 0.5–6% implies that the carbonaceous phase exists in approximately the same state of aggregate regardless of initial concentration. If massive deposition occurred in relatively few areas, it seems likely that oxygen accessibility, and, therefore, relative burning rate $-d(C/C_0)/dt$, would depend on the size of the aggregates.

Conversely, the $f(C/C_0)$ curve suggests that some degree of aggregation, or unit structure, exists. Thus, the nearly constant burning rate over the range 0.9–0.5 C/C_0 suggests the development of inner surface as the carbon phase is consumed during oxidation. It has been shown² in studies of "extracted" coke that carbon burning rate is proportional to the B.E.T. surface area of the coke

(10) B. E. Warren, *Phys. Rev.*, **9**, 693 (1941).

(11) J. Bischoff and B. E. Warren, *J. App. Phys.*, **13**, 364 (1942).

after the initial 10–20% of combustion. It is believed that a similar situation exists for the carbon phase within the catalyst pores, and that a small increase in coke surface area or porosity occurs even within a highly dispersed, minutely aggregated carbon deposit.

Curve A of Fig. 5 is essentially temperature independent, *i.e.*, it is a limiting curve. It would be obtained, for example, on regeneration at 524° of the catalyst which had been coked at 482°, then purged for 90 minutes at 524°. Under conditions of relatively mild aging, *e.g.*, 10 minutes at 524°, curve B is obtained, which differs from curve A by considerably faster burning rates over the first 50% of regeneration. The same limiting slope is reached in either case. In the latter region, combustion is approximately first order in carbon, as indicated by curve C.

Associated with the transformation from curve B to curve A of Fig. 5 is the loss of hydrogen by the coke phase. Curve B corresponds to an initial C/H of 1.8 to 2.0; curve A to a value in the range 2.4–2.6. During aging considerable hydrogen, methane and small amounts of other low molecular wt. hydrocarbons are evolved. It appears that this aging process involves aromatization reactions together with condensation and organization of aromatic systems by loss of hydrogen and small alkyl groups. The changes which occur under the above range of conditions, however, are not sufficient to be detected readily by X-ray examination of the "extracted" carbon phases.

It is of interest that when combustion is started hydrogen-rich areas of the coke deposit are attacked preferentially (*cf.* ref. 12). Analysis of the initial combustion gas indicates a C/H of roughly 0.5 for the first material gasified. Although this is an average figure for the over-all combustion process in its initial stages, it suggests preferential attack at alkyl or naphthenic regions. The number of such hydrogen-rich sites should have a direct bearing on the rate of attack of the over-all coke structure and the development of porosity in the coke phase.

Conclusions

The electron microscopical and the nitrogen adsorption studies indicate the carbon phase to be distributed in the fine pore systems of the catalyst, *i.e.*, in the interstices between the ultimate particles. The light microscopical and regeneration studies indicate that the carbon phase is well dispersed in the catalyst, although high local carbon concentrations were observed in regions of heavy-metals contamination.

X-Ray diffraction studies show that approximately 50% of the carbon phase exists in pseudo-graphitic, or turbostratic structures. The remainder probably consists of relatively unorganized aromatic systems and of aliphatic and alicyclic appendages to polynuclear aromatic systems.

A model of a coked equilibrium catalyst is proposed and shown in Fig. 6. The spheres represent ultimate particles of the catalyst (in this case, of approximately 175 Å. average diameter) which appear packed in a loose, roughly hexagonal configura-

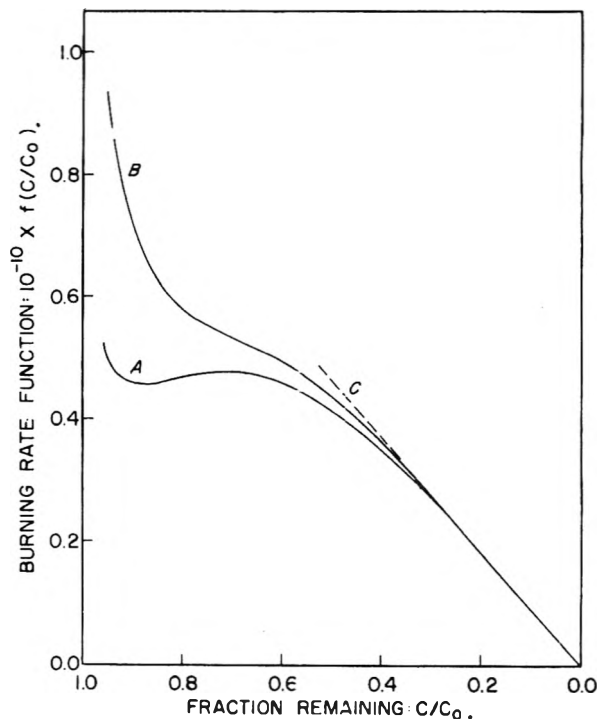


Fig. 5.—Regeneration of silica-alumina catalyst: A, thoroughly aged coke deposit; B, mildly aged deposit; C, first-order kinetics.

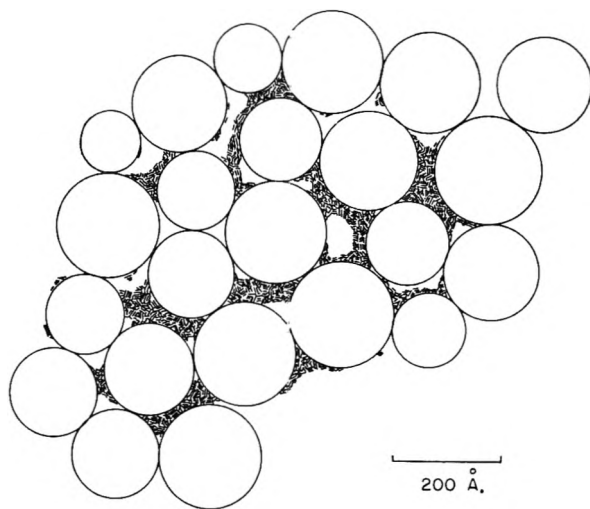


Fig. 6.—Model of coked cracking catalyst: spheres; catalyst phase, hatched areas; carbon phase.

tion. The interstitial spacings between particles are in the range 50–200 Å. The carbon phase which is present in the interstitial spaces is represented by the hatched lines and indicates the presence of pseudo-graphitic crystallites together with disorganized carbonaceous material.

Regeneration studies indicate preferential attack of hydrogen-rich sites and the development of porosity in the interstitial carbon.

Acknowledgment.—Many persons made important contributions to this research. We are particularly indebted to L. E. Alexander, of the Mellon Institute of Industrial Research, who interpreted the X-ray data on cracking catalyst carbon.

(12) A. D. Reichle, Doctoral Dissertation, University of Wisconsin, 1948.

We are indebted to several others for their contributions: G. C. Castellion (adsorption studies), T. F. Comiskey (regeneration experiments), J. Byrne (attrition studies), E. Thomas (light micro-

scopical examination), W. Doughman (X-ray spectra) and F. Horvath (photography). We also express appreciation to the American Cyanamid Company for permission to publish this work.

STUDIES OF THE FISCHER-TROPSCH SYNTHESIS. XVIII. INFLUENCE OF CATALYST GEOMETRY ON SYNTHESIS ON IRON CATALYSTS

By J. F. SHULTZ,¹ M. ABELSON, K. C. STEIN¹ AND R. B. ANDERSON¹

Bureau of Mines, Region V, Pittsburgh, Pa.

Received October 7, 1958

The influence of catalyst geometry on activity of reduced and reduced-and-nitrided fused iron catalysts in the Fischer-Tropsch synthesis was studied by the Bureau of Mines by varying (a) the particle size, (b) the depth of reduced layer and (c) the average pore radius. For catalysts reduced at 400 and 450° the activity curves may be approximated by assuming that only the outer layers of the particles to a depth of 0.01–0.02 cm. are active. When the average pore radius was varied, the activity of 6- to 8-mesh particles remained essentially constant, despite the fact that the surface area varied in an inverse manner to pore radius. Apparently the depth of effective catalyst increased sufficiently to compensate for the decreased surface area. Changes in the composition of the catalyst during synthesis and product distribution are considered with respect to a simplified picture of transport phenomena in pores.

Introduction

Diffusion in the pores of catalysts is intimately related to the reactions at the surface, as the concentration gradients required for diffusion are produced by the catalytic reaction. Several investigators^{2–4} have solved differential equations for simple hypothetical catalytic reactions in which diffusion in pores was coupled with reaction at the surface. Wheeler^{5,6} has summarized and extended this work to include consideration of selectivity and poisoning in porous catalysts and an appraisal of well known catalytic reactions. Weiss and Prater⁷ have treated dehydrogenation reactions on this basis, and Bokhoven and associates⁸ have considered diffusion and reactions in iron catalysts. Koelbel, Ackermann and Engelhardt⁹ considered mass transport in the Fischer-Tropsch synthesis with emphasis on liquid-cooled reactor synthesis.

A previous paper¹⁰ has shown that the pore geometry of fused-iron catalysts can be "tailor-made" within certain limits by varying the extent and temperature of reduction: (a) at all temperatures studied, 400 to 625°, the pore volume and porosity increase linearly with extent of reduction; (b) the reduction, at least on a macroscopic scale, proceeds uniformly inward from the external surface; (c) the average pore diameter of the reduced portion of the catalyst increases with increasing temperature of reduction.

The influence of the geometry of reduced and reduced-and-nitrided, fused-ammonia synthesis catalyst on rate of the Fischer-Tropsch reactions was studied by varying (a) the particle size, (b) the extent of reduction, and (c) the reduction temperature. Catalytic activity and composition changes were determined for all three series. In the present paper these data are interpreted by simple computations, and in a subsequent paper a special solution of the differential equations of Wheeler is applied.

Experimental

These tests employed our standard fused-iron catalyst, D-3001, containing 67.4% by weight of iron, 4.61 MgO, 0.57 K₂O, 0.71 SiO₂ and 0.65 Cr₂O₃. The original material of about 4- to 8-mesh was crushed in a roller mill and sieved into the desired size fractions. The catalyst was reduced in hydrogen at temperatures varying from 400 to 625°, as desired, in a metal block reactor,¹¹ and for nitrided catalysts the sample was subsequently treated with ammonia at 350° in this unit. The catalyst-testing units and mode of operation have been described in previous papers.^{11,12}

Tests were made with 1H₂ + 1CO gas at 21.4 atmospheres. The space velocity was held at about 300 hr.⁻¹, and the temperature of the reactor was varied to maintain the apparent CO₂-free contraction at about 65%. The activity, in terms of volume of synthesis gas reacted per hour per gram of iron at 240°, was computed by an empirical rate equation.¹³ Experiments at a constant temperature with the flow rate varied to maintain a constant conversion would have been preferable; however, experiments at constant reactor temperature would require more than fivefold variations of total gas conversion, and localized over-heating of the catalyst probably would have occurred at the higher space time yields. Although the use of an empirical equation with a constant energy of activation¹³ is incorrect, fortunately the errors introduced do not change the interpretation of the results, as will be shown in the next paper. Reproducibility of catalytic activity as computed by the empirical equation was fairly good, as shown by duplicate tests of nitrided catalysts. Condensed products from the synthesis were divided into several fractions by simple one-plate distillation.¹¹ The reproducibility of product characterizations

(1) Physical Chemist, Region V, Bureau of Mines, U. S. Department of the Interior, Pittsburgh, Pa.

(2) E. W. Thiele, *Ind. Eng. Chem.*, **31**, 916 (1939).

(3) C. Wagner, *Z. Physik. Chem.*, **A193**, 1 (1943).

(4) G. Damkohler, *ibid.*, **A193**, 16 (1943).

(5) A. Wheeler, in "Advances in Catalysis," Vol. III, edited by W. G. Frankenburg, V. I. Komarewsky and E. K. Rideal, Academic Press, Inc., New York, N. Y., 1951, p. 250.

(6) A. Wheeler, in "Catalysis," Vol. II, edited by P. H. Emmett, Reinhold Publ. Corp., New York, N. Y., 1955, p. 105.

(7) P. B. Weiss and C. D. Prater in ref. 5, Vol. VI, 1954, p. 143.

(8) C. Bokhoven, C. van Heerden, R. Westrik and P. Zwietering in ref. 6, p. 265.

(9) H. Koelbel, P. Ackermann and F. Engelhardt, *Erdoel und Kohle*, **9**, 153 (1956).

(10) W. K. Hall, W. H. Tarn and R. B. Anderson, *J. Am. Chem. Soc.*, **72**, 5436 (1950); *THIS JOURNAL*, **56**, 688 (1952).

(11) R. B. Anderson, J. F. Shultz, B. Seligman, W. K. Hall and H. H. Storch, *J. Am. Chem. Soc.*, **72**, 3502 (1950).

(12) R. B. Anderson, A. Krieg, R. Seligman and W. E. O'Neill, *Ind. Eng. Chem.*, **39**, 1548 (1947).

(13) R. B. Anderson, B. Seligman, J. F. Shultz, R. E. Kelly and M. A. Elliott, *ibid.*, **44**, 391 (1951).

Mesh size	Average activity per g. Fe for weeks 2-6
6-8	75
	77
42-60	207
	222

was less satisfactory, and these data are used only to show major trends.

In some experiments a sizable fraction of the catalyst disintegrated into finer particles during the pretreatment. On this basis the pretreated catalysts for the particle-size series were sieved to the desired mesh size under liquid heptane. Suitable precautions were taken to preclude oxidation of the catalyst in this manipulation. When this procedure was adopted, the extent and temperature of reduction series was nearly completed; however, a few additional experiments with sieved catalysts were made to show that the trends observed in the earlier tests were essentially correct.

It was desired to select a value for activity at a suitable period after steady conditions were attained. The activity was somewhat erratic in the first two or three days of synthesis, but in the remaining period of synthesis the activity was relatively constant. The deviations (absolute) of the average activities of the second to sixth week from the activity in the second week averaged only 6% for all tests considered. On this basis the average value for the second to sixth weeks was used as an expression of activity.

In subsequent considerations the particles will be assumed to be smooth spheres. A hypothetical spherical radius was computed from the average weight per particle of raw catalyst and the real density of this material. It is further assumed that the pore geometry of the pretreated catalyst may be used in activity correlations, despite the fact that these catalysts are oxidized to a large extent during synthesis.^{14,15} Subsequent sections considering reaction and mass transport in pores and oxidation of catalyst largely justify this postulate.

The three groups of experiments for both reduced and reduced-and-nitrided samples are reported:

A. Particle Size Series.—The first group of catalysts was virtually completely reduced at 450° and sieved after pretreatment. Catalysts of 6- to 8-mesh and 28- to 32-mesh were tested after reduction at 600°.

B. Reduction Temperature Series.—Six- to 8-mesh samples were reduced essentially completely at 450, 500, 550, 600 and 625°, and tested in the synthesis. Particles of 28- to 32-mesh were completely reduced at 450 and 600°. Most of the tests were made without sieving catalyst after pretreatment.

C. Extent of Reduction Series.—To ensure uniform reduction throughout the catalyst bed, 6- to 8-mesh particles were reduced at 400°; at this temperature the rate of reduction is low. Catalysts were not sieved after pretreatment.

The geometry of the reduced catalyst per gram of raw (unreduced) catalyst may be described as: A. Hypothetical spherical radius:

Mesh size	Particle radius, R , cm.
4-6	0.151
6-8	.116
12-16	.0508
28-32	.0225
42-60	.0135

B. Properties that are independent of reduction temperature:

- (1) external vol. of catalyst = 0.20 cc./g.
- (2) pore vol. = 0.089 f cc./g., where f is the extent of reduction
- (3) porosity = $\frac{0.089}{0.20} f = 0.445f$
- (4) depth of reduced zone from external surface = $R\{1 - (1 - f)^{1/2}\}$ where R is the particle radius

(14) R. B. Anderson, L. J. E. Fifer, E. M. Cohn and B. Seligman, *J. Am. Chem. Soc.*, **73**, 944 (1951).

(15) J. F. Shultz, B. Seligman, J. Lecky and R. B. Anderson, *ibid.*, **74**, 637 (1952).

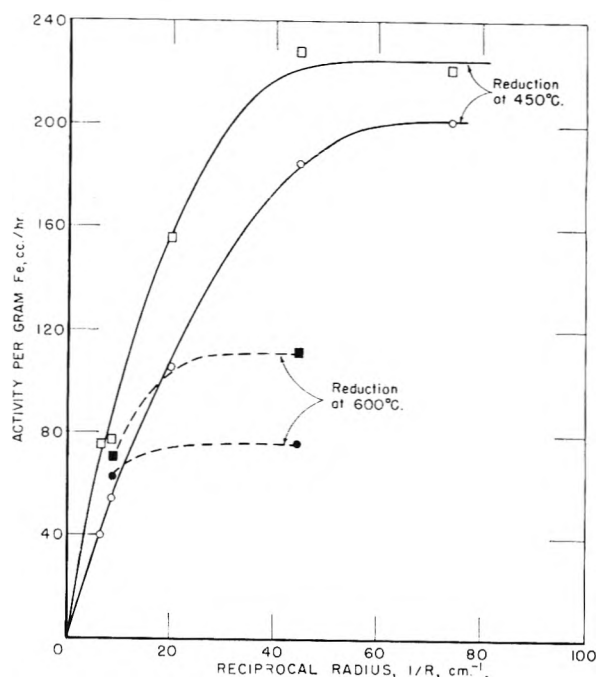


Fig. 1.—Variation of activity with particle size: circles, reduced catalysts; squares, nitrided catalysts.

C. Properties dependent on reduction temperature:

1. For completely reduced catalysts

Reduction temp., °C.	Surface area, m. ² /g.	Average pore radius, r , Å.
400	15.7	113
450	9.3	194
500	6.4	278
550	3.5	508
600	1.6	1112
625	1.6	1112

2. For partly reduced catalysts, surface area = $S_0 f$, where S_0 is the area of the completely reduced catalyst.

For nitrided catalysts the same relationship holds, except that the external volume and pore volume are about 15% larger than for the reduced catalyst; however, to simplify calculations, the pore geometry data for reduced catalysts have been used for both reduced and nitrided samples. For nitrided catalysts of the extent of reduction series, the catalyst was reduced at 400° to the desired extent and then nitrided in ammonia at 350°. At this temperature ammonia nitrides only the reduced part of the catalyst and does not reduce or nitride any of the remaining magnetite.

Activity as a Function of Catalyst Geometry.—Tables I, II and III present activity data for the particle size, extent of reduction and temperature of reduction series, respectively. Figure 1 shows the variation of activity with particle size.

According to Fig. 1, activity increases rapidly with reciprocal particle radius, which is proportional to external area per gram. With increasing values of $1/R$, the slope decreases and eventually becomes zero. For catalysts reduced at 600°, the slope apparently becomes zero at a larger particle size than for samples reduced at 450°. These curves should become flat when the particle is sufficiently small so that the entire particle is effective.

To illustrate the magnitude of the depth of the effective catalyst layer from the external surface, a simple calculation was made assuming (a) hypothetical spherical particles, and (b) that the catalytic activity was constant in the surface layers to a depth ΔR and was zero at depths greater than ΔR . On this basis the activity, A , is proportional to the weight of material in this active zone per unit weight of catalyst, and for values of $R \geq \Delta R$

$$A = 3k \frac{\Delta R}{R} \left\{ 1 - \frac{\Delta R}{R} + \frac{\Delta R^2}{3R^2} \right\}$$

TABLE I
VARIATION OF ACTIVITY WITH PARTICLE SIZE
(Catalysts sieved after pretreatment)

Particle radius, R , cm.	Reduced catalyst		Nitrided catalyst		Atomic ratio N/Fe
	Extent of reduction, f	Activity, A^a	Extent of reduction, f	Activity, A^a	
A. Reduction temp. = 450°, av. pore radius, $\bar{r} = 1.94 \times 10^{-6}$ cm.					
0.151	0.915	40	0.915	75	0.35
.116	.971	54	.971	77	.40
.0508	.977	105	.977	156	.40
.0225	.995	185	.995	228	.43
.0135	1.00	210	.979	222	.42
B. Reduction temp. = 600°, av. pore radius, $\bar{r} = 11.12 \times 10^{-6}$ cm.					
0.116	1.00	62	0.914 ^b	70 ^b	0.49
0.0225	1.00	76	1.00	111	0.47

^a Activity A defined as cc. (S.T.P.) of $H_2 + CO$ converted per gram of iron per hour at 240°. ^b This sample not sieved.

TABLE II
VARIATION OF ACTIVITY WITH EXTENT OF REDUCTION
(Reduction temp. = 400°, particle radius, $R = 0.116$ cm., av. pore radius, $\bar{r} = 1.13 \times 10^{-6}$ cm.)

Extent of reduction, f	Reduced		Nitrided		Atomic ratio N/Fe ^c
	Depth of reduced layer, cm.	Activity, A^a / A^{fb}	Extent of reduction, f	Depth of reduced layer, cm.	
A. Catalyst not sieved after pretreatment					
0	0	2	0	0	0
0.082	0.336	39	0.090	0.360	45
.125	.522	52	.192	.80	62
.280	1.205	75	.399	1.82	68
.546	2.67	63	.577	2.90	84
B. Catalyst sieved after pretreatment					
0.350	1.57	50	0.430	2.01	55
0.975	8.36	54	0.713	3.94	59

^a Activity defined as cc. (S.T.P.) of $H_2 + CO$ converted per gram of iron per hour at 240°. ^b Activity per gram of active layer. ^c These values give atomic ratio N/Fe for the reduced layer.

TABLE III
VARIATION OF ACTIVITY WITH TEMPERATURE OF REDUCTION
(Particle radius, $R = 0.116$ cm.)

Temp. of reduction, °C.	Pore radius, $\bar{r} \times 10^{-4}$, cm.	Reduced catalysts		Nitrided catalysts		Atomic ratio N/Fe
		Extent of reduction, f	Activity, A^a	Extent of reduction, f	Activity, A^a	
A. Catalysts not sieved after pretreatment						
450	1.94	0.964	73	0.964	98	0.42
500	2.78	.971	79	.987	98	.49
550	5.08	.977	69	.964	95	.47
600	11.12	.995	76	.914	70	.49
625	11.12	1.00	66	1.00	50	.44
B. Catalysts sieved after pretreatment						
450	1.94	0.977	51	0.975	70	0.38
600	11.12	1.00	62			

C. Influence of temperature of reduction on smaller particles shown in Table I.

^a Activity defined as cc. (S.T.P.) of $H_2 + CO$ converted per gram of iron per hour at 240°.

The constants k and ΔR were evaluated by a graphical method using a log-log plot of $(3\Delta R/R)(1 - \Delta R/R + \Delta R^2/3R^2)$ as a function of $\Delta R/R$. Activity data, super-

imposed on the log-log plot in Fig. 2, indicate that the equation above represents the experimental results satisfactorily. The values for the constants were

	Reduction temp., °C.	ΔR , cm.	k
Reduced catalyst	450	0.0110	211
Nitrided catalyst	450	.0175	221
Reduced catalyst	600	~ .05	~ 76
Nitrided catalyst	600	~ .03	~ 110

The values for reduction at 600°, based on only two points each, probably are not very accurate and are shown only to illustrate the direction of change in these parameters with increasing reduction temperature. It should be noted that ΔR is an average depth of useful catalyst for a hypothetical system in which the activity is constant in the effective zone and is zero beyond this depth. Actually the effectiveness decreases rapidly with distance from the surface, as shown in Table II for the extent of reduction series; however, the quantity ΔR is useful in discussing the data in a simple manner. With reduced catalysts the activity ceased to increase at an extent of reduction of about 28%, corresponding to a depth of reduced layer of 0.012 cm. in good agreement with values above; however, for nitrided catalysts this depth must be taken as 0.026 cm. These values should be regarded as tentative, being based on catalysts that were not sieved after pretreatment.

In the reduction temperature series (Table III) for 6- to 8-mesh reduced catalysts no definitive change in activity was observed, although the average pore radius increased fivefold and the surface area decreased correspondingly. For nitrided catalysts activity was constant for reduction temperatures of 450–550°, but decreased significantly for 600 and 625°. As the pore geometry of catalysts reduced at 600 and 625° was essentially identical, the lower activity at the higher temperature cannot be attributed to a smaller surface area. With 28- to 32-mesh catalysts a marked decrease in activity was observed for both reduced and nitrided catalysts when the reduction temperature was increased from 450 to 600°.

Reduction temp., °C.	Ag. cm. ³ of $H_2 + CO$ converted per g. of Fe per hr. at 240°	
	450	600
Reduced catalyst	185	76
Nitrided catalyst	228	111

Discussion

In the medium-pressure synthesis at the temperatures used in the present study the pores of iron catalysts are filled with liquid hydrocarbons,¹⁶ and mass transfer involves dissolution in and diffusion through oil films and oil in pores. From the data of Tables I, II and III this summary relating to catalyst geometry is made

Variable	How varied	Variation of activity
(1) External area	Particle Size	Large
(2) Area of pore openings		
(3a) Surface area	Reduction temp.	Slight
(3b) Surface area	Extent of reduction	Large
(4) Pore volume	Extent of reduction	Large
(5) Av. pore radius	Reduction temperature	Slight
(6) Depth of pores	Extent of reduction	Large

The general aspects of items 1, 2, 3a and 5 could be explained by assuming that the slow step is the rate of dissolution and diffusion through oil films at the external surface of the particle; however, the large variations in 3b, 4 and 6 require a more complicated mechanism, probably involving diffusion

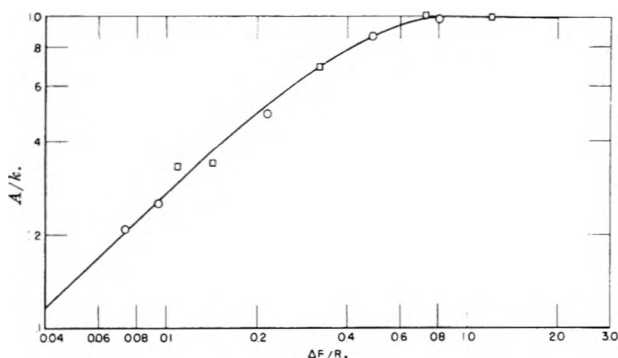


Fig. 2.—Log-log plot of data for reduced \circ and reduced-and-nitrided \square catalysts in particle size series. Catalysts reduced at 450° .

in oil-filled pores coupled with reaction at the catalyst surface.

The present results indicate that the average depth of effective catalyst on the periphery of the particle is of the order of 0.01–0.02 cm. for samples reduced at 400 and 450° and for samples reduced at 600° of the order of 0.04 cm. Thus, the average depth of effective catalyst increases with increasing pore radius. For larger particles the increase of effective depth appears sufficient to compensate rather exactly for the decreased surface area, and the rate remains essentially constant as the temperature of reduction is increased from 450 to 550° . For smaller particles a sufficient depth of ineffective catalyst is apparently not available to compensate for the decrease in surface area as the reduction temperature was increased from 450 to 600° .

A generalized picture of catalyst pores during synthesis is proposed, based on the data presented, and these hypotheses were examined with respect to changes of catalyst composition that occur during synthesis and selectivity. A typical simplified pore as shown in Fig. 3 is filled with liquid hydrocarbon, and the average and ultimate depths of active layer are shown by dotted lines. Hydrogen and carbon monoxide dissolve in the oil and diffuse into the pore; the concentration gradients that cause diffusion are produced by the reaction on the walls of the pores. Synthesis products—water, carbon dioxide and hydrocarbons—dissolve in the liquid hydrocarbons in the pore and diffuse to the pore mouth. As the solubilities of gaseous hydrocarbons, water and carbon dioxide in oil exceed those of the reactants, it is not necessary to postulate the presence of a gas phase within the pores. High molecular weight oils produced in the pore cause a small net flow of oil out of the pore.

The concentrations of hydrogen and carbon monoxide, as shown by a single curve in Fig. 3, decrease rapidly with increasing distance from the pore mouth from values in equilibrium with the gas phase until the concentration is sufficiently low so that the rate is zero due to either kinetic or thermodynamic limitations. The concentrations of water and carbon dioxide increase from values in equilibrium with the gas phase to high constant values at the point where the concentration of reactants becomes so low that synthesis does not occur. On this basis optimum conditions for oxidation of iron are found in the interior of the particle

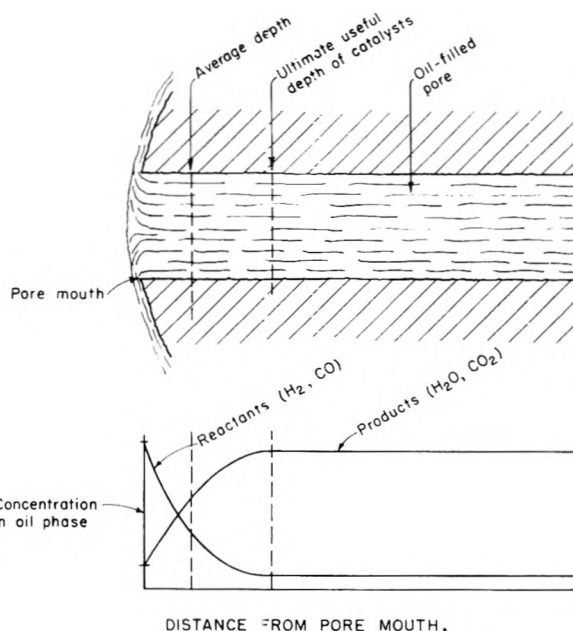


Fig. 3.—Schematic representation of a pore in a Fischer-Tropsch catalyst.

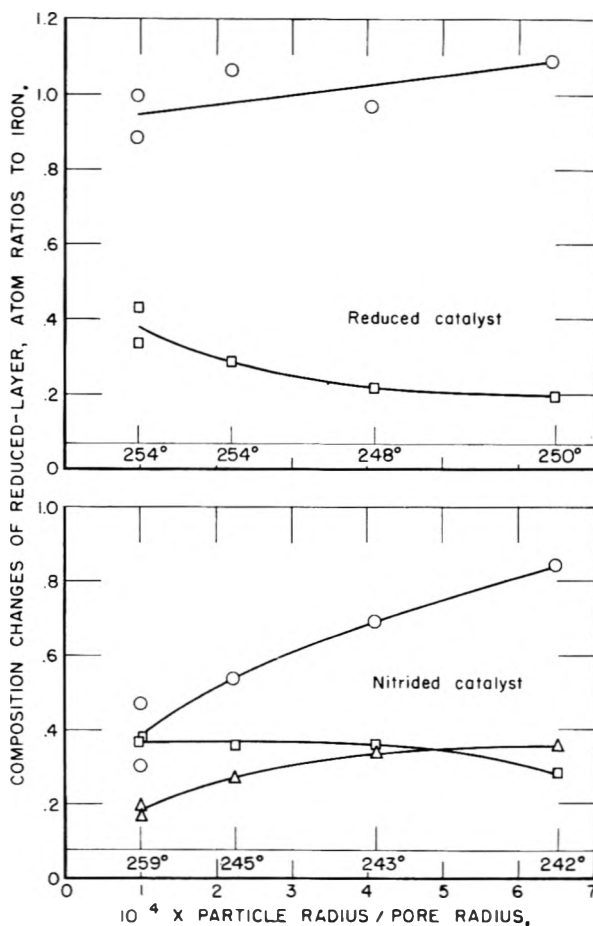


Fig. 4.—Changes in catalyst composition in six weeks of synthesis expressed as charge of atom ratios to iron of oxygen \circ , carbon \square , and nitrogen \triangle , divided by extent of reduction, f , as a function of particle radius divided by average pore radius for reduction temperature series. Synthesis temperatures are shown on graphs.

beyond the effective depth, and optimum conditions for formation of carbide and free carbon occur in the effective layer.

In the present experiments with $1\text{H}_2 + 1\text{CO}$ gas carbon monoxide is used in greater amounts than hydrogen (the over-all usage ratio $\text{H}_2:\text{CO}$ is about 0.7); thus the liquid hydrocarbon in the pores in the ineffective portion of the catalyst should contain sizable quantities of dissolved hydrogen, as well as dissolved water, carbon dioxide and light hydrocarbons. In the ineffective zone, hydrocracking reactions leading to a decrease in molecular weight may occur.

In the experiments described in Tables I, II and III representative samples of the entire catalyst charge were taken after six weeks of synthesis. After extraction to remove adsorbed hydrocarbons, entire particles were analyzed for iron, carbon, nitrogen and oxygen, and the changes in concentration of oxygen, carbon and nitrogen are expressed as differences of atom ratios with respect to iron. For all of the experiments, the changes in atom ratios are divided by the initial extent of reduction.

In the next paper it will be shown that the depth of effective catalyst is approximately proportional to the average pore radius. On this basis the ratio of total pore length (particle radius or depth of reduced zone) to average pore radius was taken as a measure of the relative amounts of ineffective and effective catalyst, and the selectivity and composition change data were plotted against this quantity.

Despite a number of complicating factors, the data show the following trends as the ratio of ineffective to effective catalyst was increased: (a) the oxidation of the catalyst increased, (b) the deposition of carbon and elimination of nitrogen (if present) decreased, and (c) the average molecular weight of the product decreased. Data for the temperature of reduction series in Fig. 4 are shown as an example of composition changes.

The present postulates provide qualitative ex-

planations for a number of observations on the Fischer-Tropsch synthesis at temperatures below about 290° .

1. As synthesis temperature is increased, the depth of the effective layer should decrease, and this is consistent with available data showing that the rate of oxidation of the catalyst increases and the average molecular weight of the product decreases with increasing synthesis temperature.

2. The activity and selectivity of reduced or nitrated fused catalysts^{13-15,17} remains essentially constant for long periods, although the composition of the catalyst changes drastically. For example, the percentage of iron as oxide in reduced catalysts increases from zero to 80 in six weeks of synthesis at 21.4 atmospheres. These data can be explained by the postulate that the catalyst oxidizes predominantly at the interior of the particle.

3. Surface layers of activated steel lathe turning¹⁸ and steel spheres,¹⁹ a thickness of active material of about 0.006 cm. on a core of massive iron, oxidized very much slower than fused catalyst, despite the fact that the massive iron catalysts were operated at temperatures as high as 290° compared with a maximum of 270° for fused catalysts.

These postulates certainly will not explain all aspects of the synthesis. The relative rates of reactions for chain growth, chain termination and hydrocracking probably do not increase at the same rate with increasing temperature, and the rates of reactions with the catalyst, such as oxidation and carburization, probably increase with increasing temperature. Finally, the occurrence of hydrocracking reactions to a significant extent on iron catalysts may be questioned in view of the observations of Koch and Titzenthaler.²⁰

(17) J. F. Shultz, M. Abelson, L. Shaw and R. B. Anderson, *Ind. Eng. Chem.*, **49**, 2055 (1957).

(18) H. E. Benson, J. F. Field, D. Bienstock and H. H. Storch, *ibid.*, **46**, 2278 (1954).

(19) J. F. Shultz and M. Abelson, unpublished data of Bureau of Mines.

(20) H. Koch and E. Titzenthaler, *Brennstoff-Chem.*, **31**, 212 (1950).

THE EFFECT OF IONIZING RADIATION UPON $\gamma\text{-Al}_2\text{O}_3$ AS A CATALYST FOR $\text{H}_2\text{-D}_2$ EXCHANGE

BY HAROLD W. KOHN AND ELLISON H. TAYLOR

*Chemistry Division, Oak Ridge National Laboratory, Oak Ridge, Tennessee
(Operated by Union Carbide Corporation for the U. S. Atomic Energy Commission)*

Received October 7, 1958

Relatively small doses of γ -rays at -78° have been found to enhance the $\text{H}_2\text{-D}_2$ exchange activity of $\gamma\text{-Al}_2\text{O}_3$. The enhancement by radiation depends upon the presence of a catalyst poison, H_2O , H_2 or C_2H_4 , and in the case of H_2O is a function of the extent of poisoning, being greatest for the most highly poisoned samples. However, Al_2O_3 not activated by high temperature treatment is not made active by prolonged irradiation. The enhancement in activity produced by radiation decays fairly rapidly at room temperature and above, and appreciable decay can be noted in some samples (highly poisoned ones, highly sensitive to radiation) even at -78° . Reactor radiation (fast neutrons and γ -rays) and radon produce similar enhancement, but in this case the effect does not decay markedly at room temperature. Although it is not yet possible to assign these effects surely to electron trapping (for gammas) and atom displacement (for heavy particles), these are the most attractive hypotheses at present. In any case, it appears likely that further study of these phenomena will help to clarify the importance for catalysis of various crystal imperfections.

Introduction

The modification by ionizing radiation of the activity of heterogeneous catalysts has been sought

for a number of years, originally, probably, as an empirical possibility, more recently with some plausible reasons for expecting such a phenomenon.

The earlier experiments, generally negative or inconclusive, were reviewed by Günther,¹ but since his review appeared in an uncommon journal, his references are repeated here,² with three additions.³ Several recent experiments, using adequate doses and non-metallic catalysts capable of storing electronic energy, apparently have demonstrated the existence of such an effect, and the range of behavior observed has been such as to encourage further study.⁴⁻⁷

The experiments at this Laboratory were undertaken with the hope that the electronic dislocations produced by high-energy electromagnetic radiation could be shown to affect catalytic activity, and that, therefore, some of the resulting special electronic configurations could be identified with, or related to, the centers responsible for catalysis. The strong correlations between catalytic activity and semi-conduction and between catalytic activity and paramagnetism suggested that the trapping of radiation-ejected electrons might well create, destroy or modify catalytic activity in such substances as metallic oxides. In the first experiments, with ZnO, the hydrogenation of ethylene was used as an index of activity. The lowest convenient temperature for this reaction was about 0°, although considerations of electron trapping suggested holding the catalyst at as low a temperature as possible. At this temperature (and somewhat above) a small effect of radiation (a decrease in activity with irradiation) was observed.⁴ The effect required so large a dose, however, as to differentiate it rather sharply from those phenomena (coloration, electrical conductivity, luminescence) which can generally be interpreted by fairly simple assumptions about trapping of electrons (or of holes) at pre-existing defects, and which reach saturation at the dose rate used in hours rather than months. As soon as possible, therefore, experiments were begun with H_2 - D_2 exchange in the hope that the lower temperature of reaction would bring to light more striking effects. This indeed proved to be the case, for irradiation of γ - Al_2O_3 at -78° with as little as 5×10^{18} e.v./g. caused approximately a tenfold increase in catalytic activity for H_2 - D_2 exchange measured at -78° .⁶ The similarity to phenomena attributed to electron trapping was further indicated by a ready annealing of the extra activity when the irradiated catalyst was raised to room temperature.

(1) P. Günther, *Ergeb. tech. Röntgenkunde*, **4**, 100 (1934).

(2) R. Schwarz and M. Klengenfuss, *Z. Elektrochem.*, **28**, 473 (1922); **29**, 470 (1923); G. L. Clark, P. C. McGrath and M. C. Johnson, *Proc. Nat. Acad. Sci.*, **11**, 646 (1925), P. H. Emmett and E. J. Jones, *THIS JOURNAL*, **34**, 1102 (1930); G. Harker, *J. Soc. Chem. Ind., Chem. and Ind. Transac.*, **51**, 314 (1932); S. Gözky and P. Günther, *Z. physik. Chem.*, **B26**, 373 (1934).

(3) G. Harker, *J. Cancer Res. Comm. Univ. Sydney*, **4**, 109 (1932); L. Pizarzhevskii, S. Chrelashvili and G. Savchenko, *Acta Physicochim. U. R. S. S.*, **7**, 289-294 (1937); L. F. Heckelsberg, A. Clark and G. C. Bailey, Joint Symposium on Mechanisms of Homogeneous and Heterogeneous Hydrocarbon Reactions, Kansas City A.C.S. Meeting (Spring, 1954).

(4) E. H. Taylor and J. A. Wethington, Jr., *J. Am. Chem. Soc.*, **76**, 971 (1954).

(5) P. B. Weisz and E. W. Swegler, *J. Chem. Phys.*, **23**, 1567 (1955).

(6) E. H. Taylor and H. W. Kohn, *J. Am. Chem. Soc.*, **79**, 252 (1957).

(7) R. W. Clarke and E. J. Gibson, *Nature*, **180**, 140 (1957).

Experimental

Preparation of Catalysts.—The catalysts used in the present research were prepared from commercially available types of aluminum oxide by evacuation at temperatures between 200 and 650°. The first such preparation was made as a blank for a series of catalysts supported on alumina and was moistened with water to simulate the solution impregnation technique used in that series. The satisfactory activity of that preparation led to the adoption of moistening prior to evacuation as a standard method of preparation. Moistening was later shown to be unnecessary, and was abandoned. Alumina that was not evacuated at about 200° or above was inactive. Some properties of the types of alumina used are given in Table I.

Measurement of Activity.—The reaction between H_2 and D_2 was used as a measure of catalytic activity. It was carried out in a cylindrical Pyrex vessel about 15 cm. long by 1.4 cm. i.d. (ca. 23 cm.³) connected through a ground joint and appropriate stopcocks to the gas supply and pumps and protected from H_2O and Hg by a trap at -196° . The gas mixture (approximately 1:1) was made up in advance from D_2 (Stuart Oxygen Co.) and H_2 (tank, electrolytic), each purified before mixing by passage through a heated palladium valve. The mixture was admitted to a pressure of 15 (occasionally 20) mm., allowed to react for a predetermined time, and expanded into a sample bulb of about 60 cm.³.

The effect of pressure was studied between 10 and 200 mm. Above about 35 mm. the first-order rate constant began to fall off, presumably because of the reduced rate of diffusion relative to reaction.

Analysis for exchange was by mass spectrometer. Unreacted samples yielded $4.0 \pm 0.3\%$ HD by exchange in the mass spectrometer; a proportionate correction was made for this, depending upon the observed distance from equilibrium. The fraction of HD to be expected at equilibrium was calculated from the equilibrium constant $K = (HD)^2 / (H_2)(D_2)$ at the temperature of the reaction (3.2 at 25°, 2.9 at -78° , 2.7 at -126°).⁸ The results were expressed either as half-times for the given volume of gas with 1 g. of catalyst (calculated as if first order in catalyst weight) or as first-order rate constants for the same situation.

Preliminary Experimental Survey.—The first step in the present work was a series of experiments with a variety of oxides known^{9,10} to possess catalytic activity for H_2 - D_2 exchange. Among several showing an increase in activity upon irradiation (Al_2O_3 , ZnO, TiO_2 , MgO), γ - Al_2O_3 was chosen for detailed study because of ease of preparation and satisfactory reproducibility.

Some of the first results on γ - Al_2O_3 , shown in Table II, demonstrate the relatively large effect of a short irradiation and the ease with which the induced excess activity is removed by exposure to room temperature. Since the activity itself was known to be a function of the temperature of the activating evacuation,⁹ a series of experiments was performed in which this temperature was varied from sample to sample between 200 and 650°. The results in Table III show that not only is the activity thus affected, but likewise the sensitivity to radiation, the catalyst prepared at the lowest temperature being the most sensitive and that at 525° the least. The small decrease upon irradiation shown at 650° has been observed more than once and appears to be real. The anomaly in the radiation sensitivity at 300° and in the activity itself at 450° have not been examined further and may well be spurious.

Since the most obvious difference between catalysts evacuated to different temperatures is in the amount of residual water, the influence of water content was studied at a single temperature of evacuation by adding H_2O to a catalyst evacuated at 525°. After heating with the H_2O vapor to develop the poisoning,⁹ the previously insensitive sample was found to be sensitive to radiation, as shown in Table IV. To determine whether the temperature of evacuation had an effect beyond the regulation of the residual H_2O , a sample was evacuated exhaustively at one temperature (400°) with periodic determinations of activity and radiation sensitivity. After prolonged evacuation the catalyst reached a state in which its activity was insensitive

(8) H. C. Urey and D. Rittenberg, *J. Chem. Phys.*, **1**, 137 (1933); A. J. Gould, W. Bleakney and H. S. Taylor, *ibid.*, **2**, 362 (1934).

(9) S. W. Weller and S. G. Hindin, *THIS JOURNAL*, **60**, 1506 (1956).

(10) V. C. F. Holm and R. W. Blue, *Ind. Eng. Chem.*, **43**, 501 (1951).

TABLE I
 CHARACTERISTICS OF ALUMINA SAMPLES

Sample	Type by X-ray	Surface area by N ₂ , m. ² /g.	Spectroscopic anal., %			
			0.1-1	0.01-0.1	0.001-0.01	0.0001-0.001
Adsorption alumina Fisher Sci. Co.	γ	210	Na	Ca, Fe, Ga, Mg, Si	B, Ti	Cu
α-Alumina J. T. Baker Co.	α	14	(not analyzed)			
Polishing alumina B Linde Air Prod. Co.	α ^a	75	Si			

^a γ-Al₂O₃ by electron diffraction.

 TABLE II
 EFFECT OF RADIATION ON CATALYTIC ACTIVITY OF ALUMINA
 (Fisher adsorption alumina; H₂-D₂ exchange)

Treatment before activity measurement	Temp. of exchange, °C.	Half-time, min., g.
Evacuate at 450°	-78	8.5
Age 7 days, room temp.	-78	24
Age 0.5 hr., 200°	+25	570
Irradiate 45 m.n., -78°	-78	9.4
Age 2 hr., -78°	-78	14.5
Age 7 days, room temp.	+25	356
Irradiate 45 m.n., -78°	-78	13.4
Age 1 hr., -78°	-78	24.4
Age 1 hr., -78°	-78	42.8
Age 1 hr., -78°	-78	170
Age 1 day, -78°	-78	ca. 300

 TABLE III
 EFFECT OF TEMPERATURE OF EVACUATION OF RADIATION
 SENSITIVITY OF γ-Al₂O₃
 (Samples evacuated overnight at indicated temperature.
 H₂-D₂ exchange at -78°)

Evacuation temp., °C.	Ratio of activities (postirradiation/preirradiation)	Preirradiation activity (first-order rate constant) for 1 g. catalyst, g. ⁻¹ min. ⁻¹
200	200	3.5 × 10 ⁻⁴
300	4	3.6 × 10 ⁻³
350	...	1.8 × 10 ⁻²
400	10	3.5 × 10 ⁻²
450	9	1.0 × 10 ⁻²
520	1	7.0 × 10
650	0.5	14.0 × 10

 TABLE IV
 EFFECT OF RADIATION ON WATER-POISONED ALUMINA
 (Fisher adsorption alumina; H₂-D₂ exchange)

Treatment before activity measurement	Half-time at -78°, min., g.	Half-time at -126°, min., g.
Evacuate 16 hr., 520°		0.40
Age 3 days, room temp.		1.41
Age 0.5 hr., 300°		5.32
Evacuate 2 days, 520°		0.42
Heat 0.3 hr., 300°		0.51
Add 0.3 mg. H ₂ O, age 0.3 hr., 300°	3.3	49.6
Irradiate 70 min., -195°		9.9
Age 2 days, room temp.	1.85	24
Irradiate 1 hr., -195°	1.12	14.5
Add 0.3 mg. H ₂ O, heat at 350° 0.3 hr.	276	
Irradiate 1 hr., -78°	7.9	
Age 2 days, room temp.	420	
Irradiate 66 min., -78°	1.6	
Age 1-3 hr., -78°	3.6	
Age 3-6 hr., -78°	8.2	

to radiation, contrary to the results of a shorter evacuation at this temperature. Hence the principal effect of temperature (in this range) is to alter the rate of removal of H₂O.

Discussion and Further Results

Three general hypotheses can be suggested to explain the results just described: (1) that the catalytic activity is affected by the concentration of trapped electrons or holes, which are altered by ionizing radiation and by subsequent annealing. (2) That the catalytic activity is associated with particular atomic distances or configurations in the lattice, and that the atom displacements brought about (at a low rate) by the γ-rays produce new sites of favorable spacing and configuration. (3) That the radiation acts radiolytically upon the poison (H₂O), either to remove it and thus regenerate activity or to yield products which act as promoters for the catalytic reaction.

The first hypothesis, which will be referred to as electron trapping, appears to be favored by the rate of introduction of the effect and by the ready annealing at moderate temperatures, both being similar to those of other phenomena which do result from electron trapping. Thus, marked coloration of alkali halide crystals occurs in the present radiation source in a half hour or less, and the coloration is approximately saturated in several hours.

Interatomic spacing in catalysts has sometimes been suggested as a determining factor in catalytic activity.¹¹ While current theories minimize the importance of lattice spacing, there appears no reason to reject this factor completely. Although the cross-section for atom displacement by gamma rays is very small, some properties sensitive to displacements have been shown to be affected by gamma irradiation. Thus, Thompson and Holmes¹² found an initial rate of change in Young's modulus of a copper single crystal of about 1% per hour in a γ-ray flux about equal to the present one. This is markedly lower than the rate of change of catalytic activity observed in the present work, but one might postulate a very much greater sensitivity for this property than for the change in Young's modulus in copper.

The obvious way to study the effect of atomic displacements is to employ a source of massive energetic particles, so that the displacements will be a major fraction of the events. Separate samples of γ-alumina were irradiated with neutrons in the

(11) A. A. Balandin, *Z. physik. Chem.*, **B2**, 289 (1929); **B3**, 167 (1932); O. Beeck, A. E. Smith and A. Wheeler, *Proc. Roy. Soc. (London)*, **A177**, 62 (1940).

(12) D. O. Thompson and D. K. Holmes, *J. Phys. Chem. Solids*, **1**, 275 (1957).

ORNL graphite reactor and with α -particles from radon adsorbed on the sample. Marked increases in activity were shown in each case, as detailed in Table V. The noteworthy point, however, is that the increase was observed after a long period of annealing at room temperature (because of the necessity of allowing the added or the induced radioactivity to decay). In the case of γ -irradiation of similarly prepared samples, such an annealing would have restored nearly the original activity. Thus, the results with massive particles differ in kind from those with gamma rays. Since the essential difference between the effects of the two types is the large fraction of atomic displacements in the heavy particle bombardments, it is natural to suggest that the displaced atoms or the vacancies are in this case the seat of the added activity. The more labile enhancement by γ -rays is then less likely to be the result of atomic disordering.

TABLE V
EFFECT OF HEAVY PARTICLE IRRADIATION ON γ - Al_2O_3

Treatment	$t_{1/2}$, min., g.		
	-78°	-95°	-126°
Sample I, 0.1 g.			
Pump 16 hr. at 500°			6.7
Repeat activity measurement			7.2
Irradiate 16 hr. with neutrons and age 14 days			1.6
Repeat activity measurement			2.6
Age 2 days at 25°			2.1
Sample II, 0.2 g.			
Pump 3 hr. at 400°	28		
Age 1 day at 25°	37		
Irradiate 16 hr. with neutrons and age 11 days	<6		
Age 1 day at 25°	1.4		
Age 9 days at 25°	1.0		
Sample III, 1 g., previously studied with γ -rays			
Pump 1.3 hr. at 400°	11.7		
Age 17 days at 25°	8.8		150°
Irradiate 102 days with 150 mc. Rn	<4, <6		
Age 8 days at 25°		1.3, 3.0	
Age 5 days at 25°			<12, <50
Age 1 day at 25°			5.5
Age 6 days at 25°			1.8
Pump 1 hr. at 100°	3.6, 0.5		2.7
Pump 1 hr. at 200°	600		

* Calculated using $\Delta E^* = 3.5$ kcal./mole.

Since the magnitude of the radiation effect proved to depend so strongly upon the water content of the alumina, it is natural to inquire whether the effect does not result simply from the removal by radiation of the poisoning water. A calculation of the possible rate of such removal can be made easily, but the validity of the necessary assumptions is not clear. It is necessary to assume a value for $G(-H_2O)$, the number of H_2O molecules decomposed per 100 e.v. of energy absorbed, and to decide whether the absorption of energy by the H_2O alone or by the H_2O plus catalyst is effective for H_2O removal. For the first assumption, it seems preferable to use the G for H_2O vapor rather than for liquid, since H_2O - H_2O interactions are probably

negligible on the surface (1% covered for 0.3 mg. H_2O /g. Al_2O_3 with surface of 2×10^6 cm.²/g. Al_2O_3). Thus, $G(-H_2O)$ is taken to be 1.7¹³ rather than 4.5.¹⁴ The most favorable assumption for H_2O removal is that all of the energy absorbed by the Al_2O_3 is somehow transferred to the adsorbed H_2O . Caffrey and Allen have observed partial transfer of this sort with pentane adsorbed on certain solids, such as silica gel.¹⁵ The present assumption is an unlikely limiting case. For a 50-minute irradiation at 2×10^{17} e.v. g.⁻¹, min.⁻¹ absorbed and $G = 11.7$, the total water removed per g. Al_2O_3 is calculated to be 1.2×10^{18} molecules, or 12% of the approximately 1×10^{19} molecules adsorbed per gram. Unless the energy is preferentially transferred to those H_2O molecules covering especially active sites, then the explanation by H_2O removal is quite untenable.

Although calculation thus indicates the improbability of a H_2O -removal mechanism, the indefinite state of theory in this area suggested an experimental search for decomposition products of H_2O . Two 1-g. samples of γ - Al_2O_3 showing exchange half-times of 7 to 10 min. at -78° were irradiated for 1.15 hr. at -78° in helium at 0.5 atm. After irradiation, the He was analyzed mass spectroscopically for H_2 , HDO, HD and H_2O . No such impurity above the background (0.01% H_2) was found, although the total adsorbed water equaled some 30% of the helium added. Again barring a very specific removal of part of the water, radiation-removal of poison seems an unlikely mechanism for the effect.

The second proposed mechanism involving radiation decomposition of water postulates the production of a promoter or sensitizer, for instance an adsorbed decomposition fragment (H or OH) or final product (H_2 , O_2 or H_2O_2). The most obvious mechanism for an enhancement of activity in this way would be for the adsorbed fragment to constitute part of a new reaction path, presumably by itself exchanging hydrogen with the reaction mixture. The data in Table VI indicate that this does not occur, since the 3-g. sample of Al_2O_3 , pre-equilibrated with D_2O , exchanged D far too slowly under irradiation for this path to be important. This experiment does not, of course, rule out a mechanism in which an active center is in some way produced in the Al_2O_3 by adsorption of a fragment such as OH.

A qualitative connection between catalyst preparation and the thermal stability of the radiation enhancement already has been noted.⁶ A more detailed study of the thermal stability of a single catalyst was made by irradiating it at successively lower temperatures (from 25 to -78°) and measuring the activity at -78° after each irradiation. Since the radiation-induced enhancement remaining at any temperature is a balance between its rate of introduction (constant) and its rate of removal (temperature-dependent), a plot of the logarithm of the enhancement ($\Delta K =$ rate constant after irradiation minus rate constant before) versus the reciprocal

(13) R. F. Firestone, *J. Am. Chem. Soc.*, **79**, 5593 (1957).

(14) A. O. Allen, *Radiation Research*, **1**, 85 (1954).

(15) J. M. Caffrey, Jr., and A. O. Allen, *THIS JOURNAL*, **62**, 33 (1958).

TABLE VI
EXCHANGE BETWEEN H₂ AND D₂O ON Al₂O₃
(3 g. of Al₂O₃ equilibrated with D₂O and evacuated 2 hr. at 400°)

H ₂ pressure, mm.	Reaction temp., °C.	Time	Remarks	% D in gas	% Equilibrium
34	-78	41 min.	0.25	2
101	-78	30 min.	Pump 1 hr. before run	.14	1
25 (0.14% D)	-78	30 min.	Irradiate during exchange	.29	2
34	25	27 days	Assumed to be at equilibrium	13.9	100

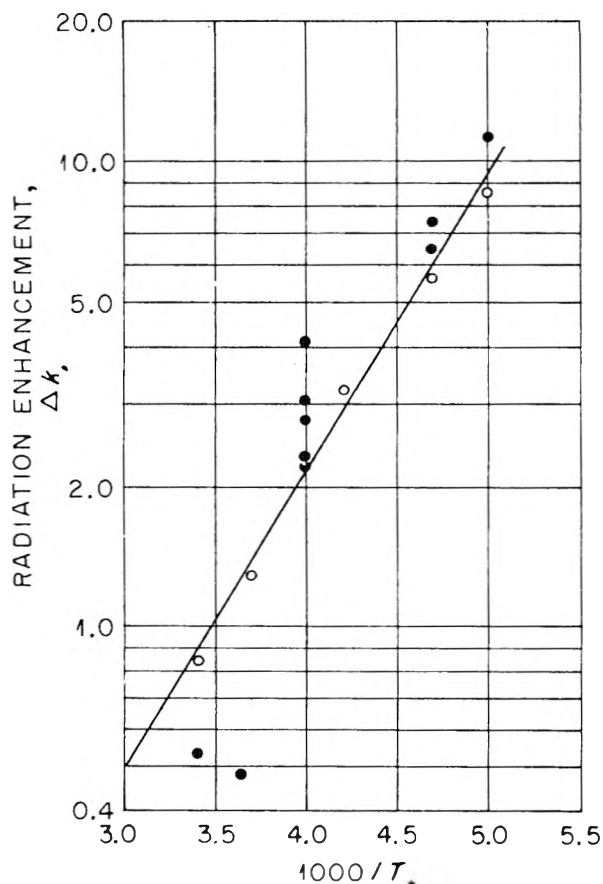


Fig. 1.—Radiation effect vs. temperature of irradiation, Al₂O₃ evacuated at 520°, then H₂O-poisoned.

absolute temperature of irradiation should give an indication of the activation energy for removal. Figure 1 shows an approximately linear relation, as expected, and an activation energy of about 3 kcal./mole. This is a reasonable value for release of trapped electrons or holes, but does not absolutely preclude a mechanism involving displaced atoms or migration of H₂O or its decomposition products.

The important role of H₂O in the radiation enhancement of activity led to examination of other known poisons for the exchange. Table VII shows that both H₂ and C₂H₄ adsorbed on a well-pumped, radiation-insensitive catalyst produced in it a sensitivity to radiation. In the case of C₂H₄ it was shown that the radiation did not produce measurable exchange between the poison and the gas phase nor liberate detectable amounts of poison. A 3-g. sample of Al₂O₃ was equilibrated with 0.25 atm. C₂H₄ at 25° for 2-3 days. It then was irradiated 4.8 hr. in He at -78°. The He was removed and substituted by D₂. After standing 16 hr. a sample of D₂ was removed, the remainder was irradiated

TABLE VII
RADIATION SENSITIVITY OF Al₂O₃ POISONED WITH H₂ OR WITH C₂H₄

Treatment	Reaction time, min.	% to equilibrium	t _{1/2} , min., g. at -78°
Sample I, 0.1 g.			
Heat in dry H ₂ stream, 520°, 2.5 hr.	36	2.9	~85
Age 1 week, room temp.	3617	8.1	~300
Irradiate 1 hr., -78°	87	24.9	21.1
Anneal, room temp., 4 days	151	5.5	~125
Irradiate 1 hr., -78°	150	24.0	38
Irradiate 16 hr., -78°	90	71.1	5
Heat 16 hours in dry H ₂ stream, 520°	380	36.1	58.2
Pump overnight, 520°	25	85.3	0.9
Sample II, ^a 0.01 g.			
Pump 16 hr., 520°. Heat 16 hr. in dry H ₂ stream, cool to -78°			
in H ₂ , pump -78°	972	6.0	10.9
Age 1 day, room temp.	1060	~1.5	~50
Irradiate, 1 hr., -78°	150	11.9	0.82
Sample III, 0.1 g.			
Heat in dry H ₂ stream 6 hr., 520°, cool to -78°, pump -78°	1105	69.8	65
Irradiate, -78°, 1 hr.	122	97.6	2.2
Sample IV, ^a 0.1 g.			
Pump 16 hr., 520°	65	52.0	0.6
Second activity measurement	990	100	<1.8 ^b
Poison with 1/2 atm. C ₂ H ₄ , 16 hr. at rm. temp., pump off	60	0	Long
Second activity measurement	1237	4.8	~170
Age 2 weeks, room temp.	1140	0	Long
Irradiate 16 hr. during reaction	1000	100	<1.8 ^b
Repump at 520°, repositon with C ₂ H ₄ , age 2 weeks at room temp.	151	0	Long
Second activity measurement	1140	0	Long
Irradiate 50 min. during reaction	180	59.1	1.4
Age 1 week, room temp.	1140	4.4	~165

^a Linde B polishing alumina. ^b Assumes 100% reaction means more than five half-lives are completed during reaction time.

6.5 hr. at -78°, and a final sample was taken. None of the 3 samples showed an increase (over background) of H₂ or HD.

Since other modifications of alumina exist, it was natural to examine the catalytic properties of the principal one of these, α-Al₂O₃, corundum. A sample of Linde B Polishing Alumina, principally corundum, proved to be superficially γ-Al₂O₃ by electron diffraction, and exhibited the same catalytic behavior (including radiation enhancement) as γ-Al₂O₃.

Heating overnight at 1400°, which should convert the sample entirely to the α -form, destroyed the activity even if the exchange reaction was run at 200°. It was not regenerated by evacuation at 400° or by long irradiation with γ -rays or neutrons. It seems likely, therefore, that the activity in γ -Al₂O₃ is associated with the structure, and that the corundum lattice is not suitable. For that matter, the bulk γ -Al₂O₃ lattice might also be non-catalytic, and the activity might reside in some special surface structure derived from the hydrous oxide from which the γ -Al₂O₃ is prepared.

Although a comparison of changes in physical properties (electrical conductivity, etc.) with changes in catalytic activity is an obvious step in the use

of radiation damage to study catalysts, preference has so far been given to the exploration of chemical variables. Light emission has been observed as some of these irradiated catalysts have been warmed, showing that some of the radiation energy is stored electronically. This was expected from the observation of Rieke and Daniels on several kinds of alumina.¹⁶ Attempts to observe paramagnetic resonance lines attributable to trapped species were negative, but this does not constitute evidence against their existence, particularly in polycrystalline samples such as these.¹⁷

(16) J. K. Rieke and F. Daniels, *ibid.*, **61**, 629 (1957).

(17) R. Livingston, *Radiation Research*, scheduled for February, 1959.

THE EXCHANGE OF DEUTERIUM GAS WITH THE HYDROGEN ASSOCIATED WITH SOLID CATALYSTS. I. THE MODEL TANTALUM-HYDROGEN SYSTEM

BY FRANCIS J. CHESELSKE,¹ W. E. WALLACE AND W. KEITH HALL

Mellon Institute, Pittsburgh, Pa.

Received November 26, 1958

A study of the kinetics of the exchange reaction between pure deuterium gas and tantalum initially containing interstitial hydrogen has been made with a view to establishing the feasibility of the method for studies of the nature of the hydrogen content of solids, both with regard to the amount of hydrogen initially held by the solid, and also as to the energetics of the exchange reaction. The tantalum-hydrogen system was selected as a "model system" because the interstitial hydrogen occupies sites of equivalent energy approximating a model required for a simple, theoretical treatment; also, the exchange takes place at relatively high temperatures, minimizing the isotope effect. The kinetic experiments were made using both constant temperature and continuously rising temperature techniques. The results were found to be in good agreement, indicating that the rising temperature technique can be used advantageously to obtain the parameters of interest, the principal advantages being a large saving of time. From the isothermal data, it was possible to determine the true activation energy for the underlying rate process. The same data showed that the apparent activation energy and the true activation energy differed approximately by the heat of solution of hydrogen in tantalum. It is of interest to note that the true activation energy for the underlying rate process probably sets an upper limit on the activation energy for diffusion of hydrogen through the tantalum lattice. The results obtained in this investigation should serve to establish a criterion by which results obtained from systems of catalytic interest can be compared.

Introduction

Two parameters of interest can be determined in simple experiments where pure deuterium gas is exchanged with the hydrogen held by solid materials. These are the total amount of hydrogen initially associated with the solid and the temperature interval over which the exchange first starts to take place at an appreciable rate. The first of these is a thermodynamic quantity in the sense that it depends only upon the equilibrium situation at the end of the experiment, but the latter depends upon the kinetics of the process as well.

The principal objective of the work was to explore what could be learned about these parameters that might be useful in studies of catalysts. The tantalum-hydrogen system was selected as a "model" system, because the interstitial hydrogen resides in sites of equivalent energy allowing a simple theoretical treatment of the data and because the exchange takes place at relatively high temperatures, minimizing the "isotope effect." Another objective was to establish an upper limit to

the activation energy for diffusion of hydrogen through the tantalum lattice.

Earlier workers² have shown that the hydrogen content of solids can be determined by exchange with deuterium gas. Winter and co-workers³ have studied the kinetics of exchange of oxygen-18 with the oxygen content of various materials. More recently, Harrison, Morrison and Rudham⁴ have followed the exchange of chlorine gas with crystals of the alkali halides containing small amounts of radioactive chlorine and described their results in terms of anionic diffusion through the lattice. Also, Annis, Clough and Eley⁵ have reported on the kinetics of exchange of deuterium with glasses and have discussed these results by analogy with the ortho-para hydrogen conversion reaction, catalyzed by the same solids. In the present work, the system is treated as a box filled with hydrogen atoms; this

(2) (a) J. K. Lee and S. W. Weller, *Anal. Chem.*, **30**, 1057 (1958); (b) J. T. Kummer and P. H. Emmett, *This Journal*, **55**, 337 (1951).

(3) E. R. S. Winter, *J. Chem. Soc.*, 1509, 1517, 1522 (1954); 2726 (1955); "Advances in Catalysis," Vol. X, Academic Press, N. Y., 1958, p. 196 ff.

(4) L. G. Harrison, J. A. Morrison and R. Rudham, *Trans. Faraday Soc.*, **54**, 421 (1958).

(5) G. S. Annis, H. Clough and D. D. Eley, *ibid.*, **54**, 394 (1958).

(1) This work was submitted by Mr. Cheselske in partial fulfillment for the requirements of the degree of Master of Science at the University of Pittsburgh, 1958.

permits a particularly simple, yet general, treatment of the data.

Theory

It is generally agreed that the kinetics of all isotope exchange reactions are first-order in the distance from equilibrium provided that the small differences in isotopic reactivity may be neglected. With heavier elements such as those used by Winter³ and by Morrison,⁴ any "isotope effect" should be negligibly small, particularly at the relatively high temperatures used in their experiments; a maximum effect may be anticipated for the exchange of deuterium with hydrogen, particularly at low temperatures.

The first-order law provides a particularly simple and useful way to treat exchange data and as such it is widely used. A conceptually simple interpretation of this law follows directly from the theoretical developments of Duffield and Calvin⁶ and of Marcus.⁷ These workers have quite generally proved that, neglecting differences in isotopic reactivity, the apparent order of any isotope exchange reaction must be first order in the distance from equilibrium, regardless of its mechanism. These ideas are extended here to take into account a two-phase system. It may be noted that, although the present development is in several respects mathematically similar to that of Winter,³ it differs sufficiently in point of view to warrant restatement here, particularly as an understanding of the underlying ideas^{6,7} is important to a proper evaluation of our data.

As a model, consider the hydrogenated tantalum as a box filled with hydrogen atoms and surrounded by deuterium molecules. A mechanism for transport between the two phases is now established, *i.e.*, the system is brought to such a temperature that gas molecules permeate the box and the atoms inside the box recombine and enter the gas phase. The gas leaving the box will always contain hydrogen in proportion to its atom fraction inside the box and the gas entering the box from the gas phase likewise will contain hydrogen in proportion to its concentration (as atoms) in the gas phase. Thus, as reaction proceeds, the hydrogen content of the gas phase and the deuterium content of the box will increase until at equilibrium the atom fraction in both phases will be identical. Following Marcus,⁷ the transport process can be described by

$$V_g(dx/dt) = R(y - x) \quad (1)$$

where x and y are defined as the atom fraction H in the gas phase and in the solid phase, respectively, and R is defined as the underlying rate of the forward and/or backward equilibrium process which would be taking place if no tracer were present. Conservation of matter requires that

$$V^0_{H_2} = V_g y + V_s x = V_g y_\infty + V_s x_\infty \quad (2)$$

where V_g and V_s represent the total moles⁸ (as NTP

(6) R. B. Duffield and J. J. Calvin, *J. Am. Chem. Soc.*, **68**, 557 (1946).

(7) R. A. Marcus, *J. Chem. Phys.*, **23**, 1107 (1955).

(8) Although the separate phases are thought of in terms of atoms only, for convenience the convention has been adopted that the amounts (total moles) in the separate phases be measured as cc. (NTP) of H₂ and/or D₂, respectively.

volumes) of the hydrogen plus deuterium associated with the solid and with the vapor phase, respectively; $V^0_{H_2}$ is the corresponding amount of hydrogen initially associated with the solid and x_∞ and y_∞ are the values of these variables at $t = \infty$. Neglecting an isotope effect, the condition for equilibrium will be

$$y_\infty = x_\infty \quad (3)$$

Combining (1), (2) and (3), it is found that

$$V_g(dx/dt) = R(V_g/V_s + 1)(x_\infty - x) \quad (4)$$

There are two restrictions implied in (4). These are that differences in isotopic reactivity may be neglected and that all of the reacting species are equivalent in energy, *i.e.*, that the system can be described by only one value of R .

To take into account effects of differences in isotopic reactivity on the kinetics of the exchange process would require a treatment of considerable sophistication. Such a treatment is certainly not warranted here. It is possible, however, to obtain quite simply a limiting form of the equation which would result from such a treatment. This comes about as follows. If an isotope effect is not neglected, (2) would remain unchanged; however, for (3) it would be necessary to substitute

$$y_\infty = K'x_\infty \quad (5)$$

The correct form of (1) is, of course, unknown. Nevertheless, it follows from the work of Manes, Hofer and Weller⁹ that the rate of approach to equilibrium will remain first order in the displacement from equilibrium, *as equilibrium is approached*, regardless of whether an isotope effect is operative or not. This is important as it is seen that a linear first-order plot should be obtained as equilibrium is approached, but that deviations from this linear behavior may be expected in the early stages of the exchange process. Thus, for the situation of interest here

$$V_g(dx/dt)_{t \rightarrow \infty} = \beta(x_\infty - x) \quad (6)$$

Combining (2) with (5) and (6), yields

$$V_g(dx/dt)_{t \rightarrow \infty} = \beta \left(\frac{V_s}{V_g + K'V_s} \right) (y - K'x) \quad (7)$$

showing the correct form of the transport equation. It is now permissible to rewrite (7) as

$$V_g(dx/dt)_{t \rightarrow \infty} = R'(y - K'x) \quad (8)$$

so that (6) becomes

$$(dx/dt)_{t \rightarrow \infty} = R' \left(\frac{V_g + K'V_s}{V_g V_s} \right) (x_\infty - x) \quad (9)$$

It remains to identify R' . If (8) held over the whole course of the reaction, rather than just close to equilibrium, it would be possible to write

$$V_g(dx/dt)_{t \rightarrow 0} = R' \quad (10)$$

i.e., R' represents the rate of the underlying equilibrium process (with the equilibrium mixture of isotopes) as measured by the linear portion of the data taken near equilibrium. It is expected that R' will differ in magnitude from R as the latter represents the rate were no isotope present.

Equations 4 and 9 hold even though there may

(9) M. Manes, L. J. E. Hofer and S. W. Weller, *J. Chem. Phys.*, **18**, 1355 (1950).

be a net transport of gas from one phase to the other during the course of the reaction. Experimentally, however, it is usually not convenient to measure V_s or V_g independently as a function of time. These quantities are related to $V_{H_2}^0$, the volume of hydrogen initially associated with the solid, and $V_{D_2}^0$, the volume of deuterium gas initially measured out at the start of the experiment, by the parametric equations

$$\begin{aligned} V_g &= V_{D_2}^0 + \delta \\ V_s &= V_{H_2}^0 - \delta \end{aligned} \quad (11)$$

where δ cc. (NTP) are transferred from the solid to the gas phase during the course of the reaction. For experiments that are carried out at constant temperature and pressure, it is possible to ensure that $\delta = 0$ by a pre-equilibration and quenching procedure described in the Experimental Section. When this is the case, (4) becomes

$$(dx/dt) = R \left(\frac{V_{H_2}^0 + V_{D_2}^0}{V_{H_2}^0 V_{D_2}^0} \right) (x_\infty - x) \quad (12)$$

Combination of the volume term of (9) with (11) yields

$$\left(\frac{V_g + K'V_s}{V_g V_s} \right) = \left(\frac{V_{D_2}^0 + K'V_{H_2}^0 + \delta(1 - K')}{V_{D_2}^0 V_{H_2}^0 + \delta(V_{H_2}^0 - V_{D_2}^0) - \delta^2} \right) \quad (13)$$

This expression enables an evaluation of the errors which may accrue by assuming $K' = 1$ and $\delta = 0$. Also, from (2), (5) and (11) it is found that

$$V_{H_2}^0 = \frac{x_\infty [V_{D_2}^0 + \delta(1 - K')]}{(1 - K'x_\infty)} \approx \frac{V_{D_2}^0 x_\infty}{(1 - x_\infty)} \quad (14)$$

It should be noted that (14) is exact, *i.e.*, does not involve a transport equation. From (14), again it is possible to evaluate the magnitude of the error introduced by neglect of the two factors mentioned above. Calculations for a number of simple circumstances have been made and are presented in Table I.

TABLE I

EVALUATION OF POSSIBLE EFFECTS OF DIFFERENCES IN ISOTOPIC REACTIVITY AND/OR GAS TRANSPORT ON REACTION RATE AND ON MEASUREMENT OF THE AMOUNT OF HYDROGEN INITIALLY PRESENT IN THE SOLID

Combination no. ^a	K'	δ , cc. (NTP)	Right-hand member of (13)	$V_{H_2}^0$ (calcd. from 14) ^a
1	1.0	0	$4/V_{D_2}^0$	$0.333V_{D_2}^0$
2	0.75	0	$3.75/V_{D_2}^0$	$.333V_{D_2}^0$
3	1.25	0	$4.25/V_{D_2}^0$	$.333V_{D_2}^0$
4	1.0	$V_{H_2}^0/2$	$6.86/V_{D_2}^0$	$.333V_{D_2}^0$
5	0.95	$V_{H_2}^0/2$	$6.66/V_{D_2}^0$	$.336V_{D_2}^0$
6	0.75	$V_{H_2}^0/2$	$6.65/V_{D_2}^0$	$.347V_{D_2}^0$
7	1.25	$V_{H_2}^0/2$	$7.07/V_{D_2}^0$	$.320V_{D_2}^0$
8	1.0	$V_{H_2}^0/10$	$4.30/V_{D_2}^0$	$.333V_{D_2}^0$

^a In all cases, it is assumed that $V_{D_2}^0 = 3V_{H_2}^0$.

It has been convenient from the experimental standpoint always to measure out a volume of pure deuterium $V_{D_2}^0$, of such a size that the volume of hydrogen contained by the solid, $V_{H_2}^0$, amounts to an over-all isotopic composition of less than 25 atom % H; *i.e.*, $V_{H_2}^0 \approx V_{D_2}^0/3$. Under such circumstances, if $K' = 1$ and $\delta = 0$, then as shown by the first combination of variables in the table, the value of the right-hand member of (13) becomes $4/V_{D_2}^0$. Pro-

vided only that $\delta = 0$, large deviations from this value are not obtained. As shown by combinations 2 and 3, inconvincibly large deviations of K' from unity result in only relatively minor variations in the rate constant of (9). When any appreciable mass transport of gas between the two phases takes place, however, relatively large deviations from ideality may occur. This is demonstrated by combinations 4, 5, 6 and 7 where half of the gas originally held by the solid is supposed to have been transported into the gas phase in the course of an experiment. In all cases, extreme variations from the result of combination 1 are found and again it is observed that the effect of differences in isotopic reactivity is at least second order. Thus it would appear that under the experimental conditions selected, neglect of possible isotope effects is not likely to seriously affect values of the rate constants obtained, but that the effects of transport of gas cannot be neglected. Experimentally this difficulty has been circumvented by proper pre-equilibration techniques, ensuring that $\delta = 0$, in experiments carried out at constant temperature and by another development to be described separately for experiments carried out while the temperature is altered.

The effects of the two parameters, K' and δ , on the volumes of hydrogen calculated to be initially associated with the solids is quite interesting. As shown in the last column of Table I, if $K' = 1$, there is no effect of gas transport on the volume of hydrogen measured as being initially associated with the solid. Similarly, if there is an isotope effect, but no net transport of gas, there is no error introduced in the measurement of the initial hydrogen content. Only if both effects take place is an error introduced by ignoring both. In any case, it is virtually impossible for errors from these sources to be as large as 5%.

Experimental

Equipment.—An all-glass circulating system in the form of a circular loop was attached to a conventional high-vacuum system. The loop, starting with an all-glass circulating pump, included in order: the Vycor sample tube, a 500-ml. mixing chamber, a small volume trap filled with small glass beads, a pair of thermostated thermal conductivity gauges and a pump. The Vycor tube was attached to Pyrex stopcocks with graded seals, and the tube itself to the system by ground glass joints. The mixing chamber was sufficiently large (the order of 500 ml.) to contain about 95% of the total volume of the circulating system. This was large enough so that the data could be treated as though it were taken in a static reactor. Also, its size minimized the fluctuations in pressure due to changes in temperature and in solubility of hydrogen in tantalum in the rising temperature experiments. The small volume trap was kept immersed in liquid nitrogen to prevent traces of water vapor (from whatever source) from reaching the thermal conductivity gauges. This was important in that Kummer and Emmett^{2b} have shown that a substantial blank can be obtained by a cyclic process involving exchange of small traces of water with the glass apparatus. The liquid nitrogen trap incorporated into our system reduced any such blank to a negligible level.

The conductivity gauges were constructed of Pyrex glass, using the glass-covered filaments removed from Leeds and Northrup Model 3284 cells. Using these cells, the gas could be circulated directly over the filaments without creating any unbalance in the d.c. bridge circuit. The latter was of standard design, but constructed of high quality materials with a view to minimizing thermal effects. The unbalance created by the bridge between pure hydrogen

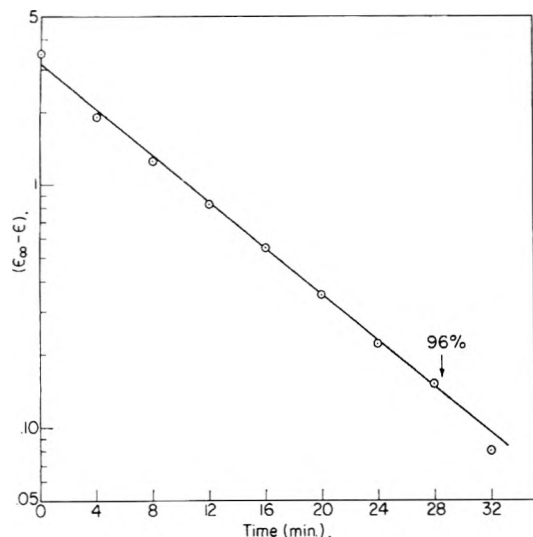


Fig. 1.—First-order plot for Ta_2H system, 625° .

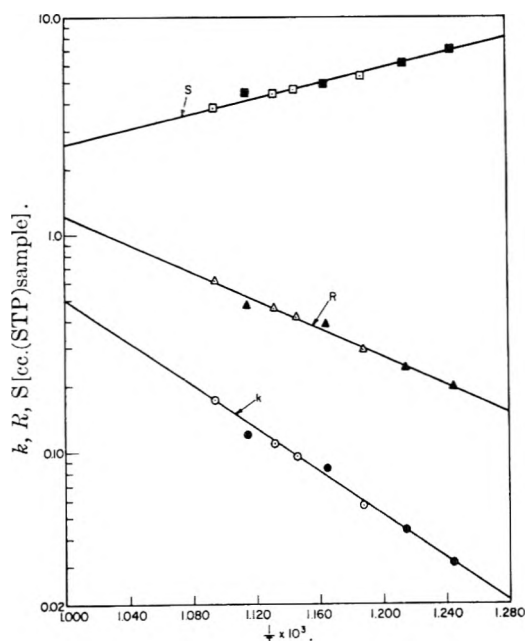


Fig. 2.—Temperature dependence of solubility, true and apparent rate constant, R and k .

and deuterium was about 70 mv.; the noise level was less than 0.1 mv. The bridge unbalance was recorded continuously on a Leeds and Northrup Azar recorder. For gas compositions of equilibrium mixtures of the hydrogen isotopes containing less than about 30 atom % hydrogen, the unbalance, ϵ , recorded was directly proportional to the atom fraction hydrogen, x , in the gas. Consequently, for convenience, the experiments were designed so as to obtain final equilibrium mixtures between 10 and 30 atom % hydrogen. This made the treatment of the kinetic data particularly simple as the rate constant could be determined as the slope of plots of $\log(\epsilon_\infty - \epsilon)$ versus time rather than the corresponding functions of x . Not only did this immensely decrease the labor involved in the calculations, but it had an additional advantage in that the slope parameter relating x and ϵ became irrelevant as it entered into the intercept of the first-order plots rather than affecting the values of the calculated first-order rate constants. This also eliminated the necessity of making corrections for the slight changes in isotope distributions (among H_2 , HD , and D_2) with temperature for given initial compositions.

The cells were immersed in a mercury bath which in turn was thermostated in an oil-bath to $\pm 0.01^\circ$. The glass

pump was of the conventional two-valve piston design. At STP it had a capacity of 135 ml. per minute. Under the conditions of these experiments (100 ml. pressure), it was estimated that the volume contained in the mixing bulb was displaced at least once every five minutes. Since the kinetic measurements were made over considerably longer periods, the results obtained were independent of pumping speed.

Auxiliary equipment included furnaces that could be controlled to $\pm 0.1^\circ$ for constant temperature experiments and a high temperature furnace that could be driven from room temperature to 1000° with a linear rate of rise of about 2° per minute. A Toepler pump was attached through a stopcock to the circulating system; this could be used in the calibration of the thermal conductivity cells.

Materials.—The tantalum used in this investigation was purchased from the Fansteel Metallurgical Corporation, North Chicago, Illinois. The metal was in the form of 15 mil wire and was reported to be at least 99.9% pure. The wire was abraded with an emery cloth to remove the surface film and was washed with ether. The wire was weighed and rapidly sealed into an appropriate Vycor tube where it was reduced in hydrogen at 650 to 1000° overnight. In this process, a solid solution of hydrogen in tantalum was formed, the composition of which was adjusted by equilibrating at the temperature and pressure at which the exchange experiment was to be carried out for a time sufficiently long so that no further hydrogen absorption could be noted. This required up to 20 hours.

The hydrogen used in these experiments was, before further purification, better than 99.8% pure. It was further purified by passage through a train consisting of a "Deoxo" purifier, anhydrous magnesium perchlorate, platinized asbestos at 360° , another magnesium perchlorate column, and finally a trap containing 30 grams of high-area charcoal maintained at the temperature of liquid nitrogen. The deuterium gas was supplied by the Stewart Oxygen Company and was initially of a similar purity. This was further purified by passage through a Pd thimble.

Experimental Method.—The experimental procedures have already been more or less indicated. These differed slightly, depending upon whether the experiments were to be carried out at constant temperature and pressure, or were to be carried out using the rising temperature technique. In constant temperature experiments, following the equilibration, the stopcocks on the sample tube were closed, the furnace removed, and the sample quenched to the temperature of liquid nitrogen. At this temperature, the gas phase was removed and replaced by deuterium gas. After circulation of the latter was commenced, the furnace, which was brought into control at the appropriate temperature, was quickly replaced around the sample. Temperature equilibrium was re-established within the first several minutes. Any errors introduced by this short heating period were neglected in the treatment of the data. When the rising temperature experiments were carried out, the tantalum samples were cooled slowly in flowing hydrogen gas from the pretreatment temperature (1000°) to the temperature of liquid nitrogen, and the gas phase was replaced as before. The tube then was warmed to room temperature and placed in the rising temperature furnace. Circulation was commenced at room temperature and the temperature program was started immediately. As essentially no exchange took place below about 250° , this procedure was found satisfactory.

Results

Constant Temperature Experiments.—The pre-equilibration and quenching procedure, described above, made it possible to carry out the exchange experiments without a net mass transport of gas between the two phases, *i.e.*, it ensured that δ of (11) remained zero. Defining

$$k \equiv R \left(\frac{V_{H_2}^0 + V_{D_2}^0}{V_{H_2}^0 V_{D_2}^0} \right) \quad (15)$$

the integrated form of (12) becomes

$$-\ln(x_\infty - x) = kt + \text{Const.} \quad (16)$$

Typical data are plotted in Fig. 1, according to (16).

TABLE II
SUMMARY OF CONSTANT TEMPERATURE EXPERIMENTS

Experiment no.	Reaction temp., °C.	Vol. ^a D ₂ , cc. (STP)	Vol. ^b H ₂ /sample cc. (STP)	Alloy comp. atom % hydrogen	k ^c (min. ⁻¹)	R ^e cc. (STP) min.	Reduction ^d Temp., °C.	Time, hr.	Equilibration ^e Temp., °C.	Time, hr.
1	530	73.46	6.96	6.14	0.030	0.193	650 ^d	16	530	18
2	550	73.78	6.07	5.39	.043	.240	550	60	550	16
3	585	72.96	4.91	4.41	.083	.382	585	17	585	16
4	625	72.95	4.49	4.06	.110	.463	625	60	625	16
9	610	72.97	4.41	3.98	.107	.447	775	17	610	16
10	567	72.42	5.37	4.82	.056	.280	805	17	567	16
11	600	72.75	4.60	4.14	.094	.407	805	16	600	16
12	640	72.68	3.82	3.47	.170	.610	800	17	640	16

^a Initial volume of D₂ measured out at STP. ^b Volume of hydrogen (STP) contained in the solid as measured by the exchange experiment. ^c Defined by equation 15; see text. ^d The tantalum (1.718 g.) was treated initially at 650° in pure hydrogen (50 cc./min. at 1 atm.). The remaining reduction temperatures indicate the temperature at which deuterium (remaining in the sample from the previous experiment) was removed by hydrogen (50 cc./min. at 1 atm.). ^e The sample was equilibrated in hydrogen at a pressure of 100 mm.

(Actually, $\log(\epsilon_{\infty} - \epsilon)$ is plotted.) It is clear that a first-order dependence on the distance from equilibrium is operative over most of the range of the variable. As k can be determined from the slope of such plots and as $V^0_{D_2}$ and $V^0_{H_2}$ are known, respectively, from the volume of deuterium initially measured out at the start of the experiment and from the volume of hydrogen calculated to be initially associated with the tantalum from the equilibrium situation, it is possible to calculate R , the rate of the underlying process at the particular temperature and pressure in question. Thus, two activation energies can be obtained. These are (a) the apparent activation energy, E_a , corresponding to the temperature coefficient of k and also (b) the true activation energy, E_0 , corresponding to the rate process, R . The data obtained from experiments carried out at the various temperatures are listed in Table II and are plotted in Fig. 2, along with the values of $V^0_{H_2}$ obtained from the same experiments. The latter quantity is in reality the solubility of hydrogen in tantalum; hence, the slope of this curve is directly related to the heat of solution.

It should be noted that if at the end of any experiment, the sample is again quenched and the equilibrium gas phase removed, the magnitude of the isotope effect can be determined by measuring the isotope ratio in the gas remaining in the solid. This experiment was carried out as it afforded an opportunity of evaluating the magnitude of K' . For clarity, one such experiment will be described in detail. Actually the experiment has been carried out on four separate occasions yielding $K' = 1.08 \pm 0.06$.

An approximately five-gram sample of tantalum was equilibrated with pure hydrogen gas at 500° for about 20 hours at 100 mm. pressure; the pretreatment and exchange were carried out as described for constant temperature experiments. The results obtained from the exchange are listed in the first row of Table III. The 30.2% H observed as the equilibrium gas phase composition corresponds to x_{∞} . Following the exchange, the stopcocks on the tube were again closed, and the sample was quenched to the temperature of liquid nitrogen and the gas phase removed. A Toepler pump then was turned on the sample at an initial pressure of 10^{-6} mm. and the temperature was raised slowly to 500°. After

24 hours at 500°, the evolved gas was measured volumetrically; pumping was then continued as the temperature was raised to 650° to accelerate removal of the gas still held by the tantalum. After 60 hours at this temperature, over 95% of the expected amount was obtained. Because of the small increment in the final period, the experiment was stopped at this point.

The composition of the evolved gas was determined using the thermal conductivity cell. The final result, 31.9% H = y_{∞} , may be compared to the observed value of x_{∞} . The data show quite clearly that a small isotope effect is involved. The ratio of the observed concentrations yields a value of 1.06 for the equilibrium constant. This is about the magnitude and in the direction expected.

Rising Temperature Experiments.—A set of experiments, such as that described above for the constant temperature method, is quite laborious and time consuming. Further, when any new composition of matter is selected for examination, a number of preliminary experiments is required to locate the temperature range over which kinetic measurements can be made. During the course of this work, it was realized that a particularly simple solution of these problems could be obtained utilizing the rising temperature reactor technique of Bridges and Houghton¹⁰ and/or Kofstad¹¹ and the equations already developed. If (4) is written in the form of

$$V_g(dx/dt) = A(x_{\infty} - x)e^{-E_a/RT} \quad (17)$$

where E_a is the apparent activation energy obtained in the constant temperature experiments and A is the collection of temperature independent factors, the behavior to be expected becomes obvious. Suppose that D₂ gas is being exchanged with the hydrogen contained in or on a solid while the temperature is being raised according to a linear program. Measurement of temperature and the atom fraction of hydrogen in the gas phase as a function of time yields results such as are shown schematically in Fig. 3. The sigmoid shape of the x versus time curve results because, as the temperature is increased, the reaction will proceed immeasurably

(10) J. M. Bridges and G. Houghton, *J. Am. Chem. Soc.*, **81**, 1334 (1959).

(11) P. Kofstad, *Nature*, **179**, 13E2 (1957).

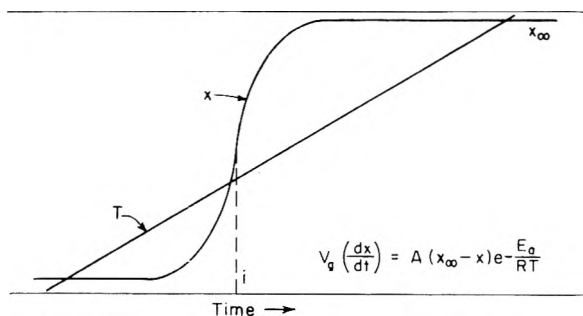


Fig. 3.—Record of data obtained automatically by the rising temperature technique.

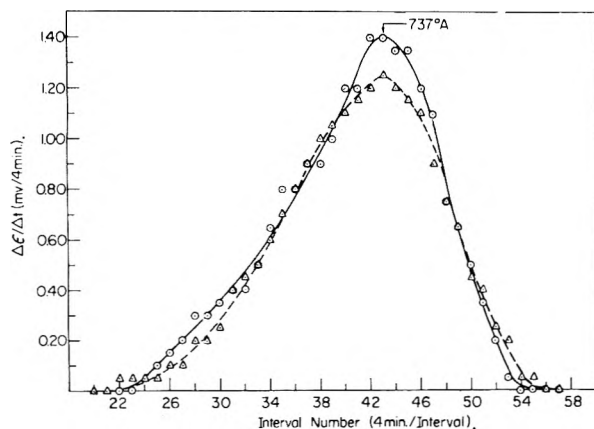


Fig. 4.—Differential plot of rising temperature kinetic data for Ta-H system.

slowly until the exponential function of (17) increases to such ε value that the rate can become appreciable; as the temperature increases further, the rate will increase exponentially and become a maximum at the point of inflection, after which the rate must decrease again due to the decreasing magnitude of the factor describing the distance from equilibrium. At the inflection point, the second derivative of x with respect to time is zero. Performing this operation on (17) yields

$$E_a = \frac{RT_i^2 (dx/dt)_i}{(x_\infty - x)_i (dT/dt)_i} \quad (18)$$

where the subscripts "i" indicate that the value of the variable must be selected at the point of inflection. It may be seen from the magnitude of the various parameters entering into the right-hand member of (18) that the temperature at the point of inflection is the dominant factor in determining the activation energy so that the temperature interval over which the reaction rate just starts to become appreciable has a simple interpretation in terms of the activation energy for the rate determining step.

The parameters required for the evaluation of the right-hand member of (18) can most accurately be obtained by differentiation of the sigmoid curve obtained when per cent. conversion is plotted (automatically) versus time. Data obtained in two duplicate experiments are plotted in Fig. 4. The maxima in the curves appear at the points of inflection of the sigmoid curves and the values of the abscissae at the maxima fix the temperatures at the inflection points. Actually, the ordinate and the abscissa of Fig. 4 are the incremental change in electrical unbalance with respect to time and the chart

interval number from the start of the experiment, respectively. These units are, of course, proportional to those of the desired parameters and the proportionality constants cancel out in (18).

The average value of E_a calculated from these data is listed in Table IV, where it is compared with the corresponding figure obtained from the constant temperature experiments. The agreement is striking. In the constant temperature experiments, the value found experimentally for E_0 differs from that found for E_a by the temperature coefficient of the volume factor of (15). This is listed in Table IV as ΔH_0^0 and has a value of 7.4 kcal./mole. When this result is compared to our experimentally determined temperature coefficient of V_{H_2} (8.0 kcal./mole), it is seen that the temperature coefficient of the volume term of (15) arises mainly from the change in solubility of hydrogen in tantalum. That this result might have been expected for this particular system is shown in Appendix I. Its usefulness is illustrated with the rising temperature data. Here the only experimental result obtained, $E_a = 22.9$ kcal./mole, may be corrected by the heat of solution of hydrogen in tantalum taken from the literature¹² to obtain an approximate value of E_0 which is in excellent agreement with the value found by the more laborious constant temperature method. It should be noted that it does not follow that this sort of behavior should be expected for hydrogen associated with the surfaces of catalytic materials.

TABLE III
ISOTOPE EFFECT FOR TANTALUM-HYDROGEN-DEUTERIUM SYSTEM AT 500°

H ₂ content from D ₂ exchange, cc. (NTP)	Isotopic Composition of phases, atom % H	Gas recovery by Toepler pump, cc. (NTP)	Temp. of exchange or recovery, °C.	Exchange or recovery period (hr.)	Fractional recovery (based on D ₂), %	K'
27.5	30.2	..	500	30		
..	31.5	26.0	500	24		
..	31.9	26.4	650	60	96	1.06
Av. of four experiments = 1.08 ± 0.06.						

TABLE IV
PARAMETERS OBTAINED FOR Ta₂H SYSTEMS FROM KINETIC EXPERIMENTS

Rising temp. reactor	Constant temp.
$E_a = 22.9$ kcal./mole	$E_a = 22.3$ kcal./mole
$\Delta H_0^0 = 7.8$ kcal./mole°	$\Delta H_0^0 = 7.4$ kcal./mole
$E_0 = 15.1$ kcal./mole	$E_0 = 14.9$ kcal./mole

° Taken from data on solubility of hydrogen in tantalum found in "Hydrogen in Metals," by D. P. Smith, University of Chicago Press, 1948, p. 173.

Contaminated Samples.—Four experiments were omitted in the preparation of Fig. 2. The eight points plotted are made up two sets of four each, as distinguished by the open and solid points. After the first four experiments (solid points) had been carried out, the tube containing the partially-deuterated tantalum was stored under vacuum for a period of several months, while other research was carried out. When the experiments were finally

(12) D. P. Smith, "Hydrogen in Metals," The University of Chicago Press, Chicago, Ill., 1948, p. 29 ff.

resumed, it was found that the measured exchange rates fell below those previously obtained and that the amounts of hydrogen found associated with the solid appeared to be a little higher than the accepted solubility. As successive experiments were carried out at 610°, the solubility data and the apparent rate constant data approached more closely the curves established by the earlier work. By the time the ninth experiment had been carried out, both the solubility and the rate data agreed with the earlier work, not only at 610°, but also at the remaining temperatures plotted. In an effort to obtain some insight into what could be wrong, attempts were made to remove the hydrogen held by the sample by collection of the gas with a Toepler pump at the conclusion of experiments 7 and 8, as had previously been done in determining the isotope effect discussed in connection with Table III. These experiments showed that only 75 and 76%, respectively, of the hydrogen content measured by the deuterium exchange could be removed by prolonged pumping at temperatures as high as 650°. As earlier experiments had consistently yielded well over 90% of the hydrogen determined by deuterium exchange under similar conditions, these low results were totally unexpected. It now seems likely that the sample left standing *in vacuo* picked up oxygen during the several months storage period. This oxygen was evidently in a form that was removed only with great difficulty, so that the samples approached the initial reproducible condition only after repeated treatment with H₂. If interstitially held, this oxygen might explain the apparent enhancement of the solubility of hydrogen into the tantalum and the incomplete removal of the hydrogen on evacuation. It is of interest to note that whatever the nature of the "poison," the tantalum evidently is not susceptible to its action before the lattice is "opened up" by hydrogen.

Discussion and Conclusions

A theory has been developed to describe the apparent kinetics of the exchange reaction between a gas phase initially containing pure deuterium gas and a solid phase initially containing hydrogen in one form or another. This treatment was adapted from the more general one of Marcus⁷; it delineates the most favorable experimental conditions and in certain instances defines the manner in which experiments must be carried out to obtain interpretable results. In its present form, there are two experimental limitations. These are that the small differences in isotopic reactivity are neglected and the assumption that the underlying rate process is single valued, *i.e.*, that only one value of R is required to describe the kinetics.

It has been demonstrated that the rising temperature technique may be employed advantageously in many cases to obtain most of the information that can be found by the more laborious conventional method. This method should be particularly useful with refractory oxides from which hydrogen cannot be removed at any temperature and where water is evolved only at temperatures much above those required for equilibrium to be obtained with deuterium gas.

From the constant temperature experiments, it

was possible to unambiguously determine E_0 , the true activation energy for the underlying rate process. Its value (14.9 kcal./mole) for the Ta₂H system probably sets an upper limit for the activation energy of diffusion of hydrogen through the tantalum lattice.

It was possible to obtain solubility data and, therefore, the heat of solution of hydrogen in tantalum concomitant with the rate measurements in the constant temperature experiment. The values so obtained are in fair agreement with those published elsewhere.¹²

Finally, it has been demonstrated experimentally that the apparent activation energy, E_a , and the true activation energy for the underlying rate process, E_0 , differ approximately by the heat of solution of hydrogen in tantalum. An explanation for this behavior is offered in Appendix I.

Appendix I

The Relationship between E_a , E_0 and ΔH_s^0 .— E_a and E_0 differ because of the temperature coefficient of the quantity $[(V_g + V_s)/V_g V_s]$. The numerator is independent of temperature for a given (rising temperature) experiment and may be kept nearly constant in a series of related (constant temperature) experiments by making $V_{D_2} \gg V_{H_2}$. The temperature dependence of the denominator can be shown to be given approximately by the expression

$$V_g V_s \approx B e^{-\Delta H_s^0/RT} \quad (I-1)$$

Consider the reaction



for which the equilibrium condition can be approximately written as Siever's law,¹² *i.e.*

$$K_s = \frac{a_H}{a^{1/2}_{(H_2)} a_{(Ta)}} \approx \frac{N_H}{P^{1/2}_{H_2}} = e^{-\Delta F_s^0/RT} \quad (I-3)$$

where N_H is the atom fraction of hydrogen in the hydrogen-tantalum solution and P_{H_2} is the pressure of the hydrogen gas. Also, for the dilute solution used

$$N_H \approx b V_s \quad (I-4)$$

where b is a constant; further, for the gas phase

$$V_g = (22,400) \frac{PV}{RT} \quad (I-5)$$

where V is the actual volume of the system which remains constant. In this connection, it should be pointed out that the volume in the hot zone (within the furnace) is a very small fraction of V , so that the temperature of the gas phase also may be taken as a constant. Thus, combining (I-4) and (I-5) with (I-3) and rearranging leads to

$$V_g V_s = \left(\frac{22,400 P^{1/2}}{RT b} \right) e^{\Delta S_s^0/RT} e^{-\Delta H_s^0/RT} \quad (I-6)$$

Since under the conditions of the experiment, the pressure cannot increase by more than about 10% due to gas transport (from solid to gaseous phase), it is seen immediately that a relationship of the required form is obtained. Actually, the standard state entropy change is not expected to be completely temperature independent and would tend to operate in such a direction as to partially compensate for the small error introduced by the increasing

pressure. From (4), (I-2) and (I-6), it is immediately obvious that

$$E_a = E_0 + \Delta H^0 \quad (\text{I-7})$$

It is, therefore, clear why the agreement noted earlier, between the results obtained by the rising

temperature and the constant temperature technique was obtained.

Acknowledgment.—This work was sponsored by the Gulf Research & Development Company as a part of the research program of the Multiple Fellowship on Petroleum.

HETEROGENEOUS REACTION STUDIES BY INFRARED ABSORPTION¹

BY HAROLD L. PICKERING AND HARTLEY C. ECKSTROM

Contribution from Pan American Petroleum Corporation, Tulsa, Oklahoma

Received July 9, 1958

An experimental apparatus and procedure were developed for obtaining the infrared spectra of substances which are adsorbed on the surface of freshly evaporated metal surfaces. In addition, this equipment may be used either to observe changes in the reflectivity of the metal surfaces or to observe changes in gaseous components while a reaction is taking place. The basis of the equipment is the use of a multiple reflection cell whose front surfaced mirrors are covered by freshly evaporated catalyst metal. When ethylene is added in excess to new rhodium mirrors, it is adsorbed with dissociation to produce ethane and an adsorbed substance. Evidence was obtained which indicates this substance is composed of paired carbon atoms which probably are present on the catalyst surface. This adsorbed substance may be hydrogenated to ethane at room temperature and at hydrogen pressures of less than 1 mm. No direct evidence was found for hydrogen-carbon bonds in the adsorbed molecules. The ethylene adsorption is accompanied by a small decrease in film reflecting power while the hydrogenation step is accompanied by a similar increase in reflectivity. When the CO pressure over new rhodium mirrors is 1 mm., an infrared absorption band at 4.854 μ is observed. A band of increased reflectivity is also observed at 4.785 μ . Upon evacuation, the absorption band shifts to 4.914 μ , whereas the band of increased reflectivity remains unchanged. When CO is added to new nickel mirrors, a large infrared absorption band is observed at 4.859 μ , corresponding to gaseous nickel carbonyl. However, no other nickel carbonyl bands are observed. The 4.859 μ band disappears upon evacuation. These results show that the CO is more strongly adsorbed on the rhodium catalyst than on the nickel catalyst. The positions of the infrared absorption bands suggest that the CO is chemisorbed as single linear molecules. When hydrogen is added to new rhodium mirrors, a decrease in film reflecting power occurs. Only a fractional recovery in reflectivity occurs upon evacuation. As many as 23 absorption bands are observed which may be attributed to hydrogen on the rhodium surface.

Introduction

Direct evidence bearing on the structure of adsorbed molecules has been reported by Sheppard and Yates² for physically adsorbed molecules and by Eischens, *et al.*,³ and Yang and Garland⁴ for chemisorbed molecules using infrared absorption techniques. In these cases, the spectra were obtained in transmission for finely divided, infrared-transparent solids. In the latter two cases, the solid particles served as a support for metallic catalysts. Another method for obtaining direct structural evidence about adsorbed molecules involves obtaining the infrared spectra in reflection from evaporated metal films which have gases adsorbed. Such experiments also may simultaneously provide information about the film reflectivity and about the presence of gaseous molecules in the system.

This paper describes the experimental equipment which is used to obtain infrared absorption spectra of molecules adsorbed on films of nickel and rhodium.

Preliminary results obtained with this equipment are reported for the systems: (1) ethylene and hydrogen over rhodium films, (2) hydrogen over rhodium films, (3) carbon monoxide over rhodium films and (4) carbon monoxide over nickel films.

(1) Presented at the 134th National A.C.S. meeting in Chicago, September 10, 1958, as a part of the "Symposium on the Nature of the Chemisorbed Species."

(2) N. Sheppard and D. J. C. Yates, *Proc. Roy. Soc. (London)*, **238A**, 69 (1956).

(3) R. P. Eischens, S. A. Francis and W. A. Pliskin, *This Journal*, **60**, 194 (1956).

(4) A. C. Yang and C. W. Garland, *ibid.*, **61**, 1504 (1957).

Experimental

Equipment.—The equipment consists essentially of a source of infrared, two matched cells and a prism monochromator with detector, amplifier and recorder. The source radiation alternately enters a catalyst cell and a comparison cell. This is accomplished by means of semicircular plane mirrors rotating at 13 cycles per second. The radiation transmitted by either cell illuminates the entrance slit of a Perkin-Elmer Model 83 prism monochromator for dispersion. The prism calibration method was that as outlined by McKinney and Friedel.⁵ Calibrations were made in the spectral region for investigation on the same day that experimental data were obtained.

A thermocouple was used for detection of the dispersed radiation in most experiments. In a few cases, at wave lengths shorter than about 2 μ , a lead sulfide detector, operating at room temperature, was used. The detector signal, because of the optical chopping, is 13 cycle alternating current. It is amplified by a Perkin-Elmer Model 81 tuned amplifier. This amplified signal feeds a Leeds and Northrup recording potentiometer. This instrument produces data in strip chart form and also drives an analog-to-digital converter for automatic data recording in punched card form. Scanning rates were adjusted so that 6 to 8 thermocouple output voltages per spectral slit were recorded in punched card form.

The optical path in both the comparison and catalyst cells is of the multiple reflection type described by White.⁶ From 15 to 35 surface reflections were used during measurements. The mirrors were ground from 5" diameter blanks. The radius of curvature of the mirrors was 294 mm. The comparison cell and spectrometer housing were maintained at a steady reference condition during measurements by continuous flushing with nitrogen. The catalyst cell is equipped with connections to a high vacuum and gas supply system and with an internal tungsten filament from which metal can be evaporated onto the mirror surfaces. The

(5) D. S. McKinney and R. A. Friedel, *J. Opt. Soc. Am.*, **38**, 222 (1948).

(6) J. U. White, *ibid.*, **32**, 285 (1942).

catalyst cell is also provided with an electrical heating system for degassing the cell (upper limit 250°) and with cooling coils for operations below room temperature (lower limit -50°). Access to either cell between experiments is provided by flanged closures. In the case of the heated catalyst cell, a tongue and groove closure with an annealed aluminum ring is used. The catalyst cell is further provided with a surrounding vacuum jacket which is sealed in place by means of Apiezon W wax. This vacuum jacket provided adequate insulation when the interior cell was being heated and also made the vacuum seal requirement to the inner cell much less severe.

Materials. Hydrogen: electrolytic hydrogen was further purified by diffusion through a hot palladium tube.

Nitrogen: compressed nitrogen was dried by cooling to the sublimation point for Dry Ice.

Ethylene: Phillips Research grade ethylene was stored in a glass container at or below atmospheric pressure. The walls of the container were coated with metallic sodium for removal of traces of water or oxygen.

Carbon monoxide: reagent grade formic acid was added dropwise to hot phosphoric acid to produce carbon monoxide. The gas was passed through a glass wool trap at 0° and over soda lime, calcium chloride and phosphorus pentoxide at room temperature. This carbon monoxide was collected on activated charcoal (surface area = 100 sq. m. g.) cooled to the boiling point of liquid nitrogen. The carbon monoxide for the experiments was that which could be obtained by warming the charcoal to about -78°.

Tungsten: wire of 0.020 in. diameter was obtained from Sylvania Electric Products, Tungsten and Chemical Division, Towanda, Pa.

Rhodium: wire of 0.015 in. diameter and assaying 99.5% rhodium was from A. D. Mackay, Inc., New York, N. Y.

Nickel: wire of 0.020 in. diameter and assaying 99% nickel was obtained from the Malin Company of Cleveland, Ohio.

Procedure.—Mirrors for the catalyst cell were cleaned by heating in the presence of fuming sulfuric acid, washing in distilled water, with "Orvus" solution in distilled water and finally with freshly distilled acetone. After the mirrors were installed in the catalyst cell, a tungsten filament with interwoven catalyst metal wire for deposition on the mirrors was installed. The mirrors used in the comparison cell have front surfaces of the same catalyst metal to produce a radiation path whose reflectivity characteristics vary with wave length in a manner similar to the catalyst cell. After the catalyst cell was degassed by heating under vacuum at 250°, the tungsten filament bearing the catalyst metal was heated, at first briefly, and finally for several hours to remove "dissolved" gases from the tungsten and catalyst. The process of evaporation of catalyst metal onto the mirrors was performed by short filament heating periods to temperatures above the melting point of the catalyst metal. The heating was stopped if the mirror temperature rose as high as 115° or if the cell pressure rose to 8×10^{-4} mm.; the heating was resumed when the mirror temperature dropped to 80° and the pressure decreased to 1×10^{-5} mm. Rhodium surfaces with reflectivity of 93% at a wave length of 3 microns and nickel mirrors with reflectivity of 89% at the same wave length were obtained in this way. The deposited metal amounted to from 0.2 to 0.6 g. corresponding to film areas of from 2.6 to 7.8 sq. m.

Once the mirror preparation was completed, background scans of the spectral region to be studied were made. These data were punched into IBM cards as they were obtained. A gas component then was admitted to the cell. During this addition either gas composition data or radiation reflecting power data may be obtained by proper selection of a monitoring wave length. These data were recorded in strip chart form only. In the systems studied, a period of two to five minutes was required for the system to reach a steady state after the gas addition. Once steady state was reached, a series of scans was made in the same spectral region in which the background scans had been made. These data were recorded in punched card form. The gas in the catalyst cell was removed by evacuation. During this evacuation, as was the case during the addition, either gas composition data or radiation reflecting power data may be obtained by proper choice of monitoring wave length. These data were recorded in strip chart form only. During the gas removal, samples could be taken for mass spectrometric analyses. Once the evacuation was com-

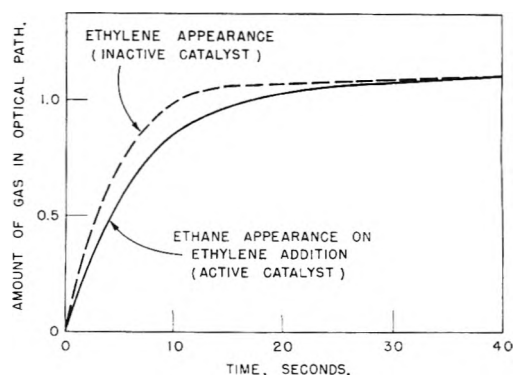


Fig. 1.—Ethylene addition with fresh rhodium surfaces.

pleted (usually to a pressure of 1×10^{-3} mm.), a series of scans again was made in the same spectral region in which the background scans had been made. These data were recorded in punched card form. Several gas addition and removal cycles could be made with the same catalyst film.

The strip charts were used directly for identification of gaseous components. Also, by comparing strip chart scans before any gas was added with those when gases were present, it was possible to determine relative amounts of ethane and of ethylene when only these two gases were present.

Computer processing of the punched card data was adopted to obtain the most favorable chance for observing the small radiation absorptions which would be expected from molecules adsorbed on the surfaces of the catalyst cell mirrors. The background scans were combined by point by point averaging to produce a single averaged background or reference curve. All the scans of a series with gas present in the cell were combined by point by point averaging to produce an averaged data curve. Difference curves between each averaged data curve and the averaged background curve were formed by point by point subtraction. Further noise filtering was performed using cross correlation with functions of type derived from the application of communications theory to a spectrometer of finite aperture by King, *et al.*⁷ The final results of this analysis were in a punched card form which could be used for plotting with an IBM accounting machine.

Results and Discussion

1. Ethylene and Hydrogen over Rhodium Films.—In these experiments, ethylene and hydrogen were added at room temperature alternately to the catalyst cell with rhodium films. Between additions, the catalyst cell was evacuated to less than 1×10^{-3} mm. The amounts of ethylene added were such that the system pressure after addition was from 0.1 to 0.3 mm.; the amounts of hydrogen added were about twice the previous ethylene addition.

When ethylene was being added, ethane was formed rapidly. Typical results are shown in Fig. 1 where the amount of each gas in relative units is plotted against time. These data were obtained by monitoring at a wave length of 3.342μ for ethane and at 3.204μ for ethylene in separate additions. The dashed curve is for ethylene appearance into the cell in a separate experiment with an inactive catalyst. It may be noted that, over active rhodium films, ethane formation occurs at a rate comparable with the rate of arrival of ethylene in the system. If the 2.84μ wave length was monitored, a small decrease ($\sim 0.001\%$) in reflectivity was detected. This decrease at a wave length at which the gases present are transparent corresponds to a

(7) G. W. King, E. H. Blanton and J. Frawley, *J. Opt. Soc. Am.*, **44**, 400 (1954).

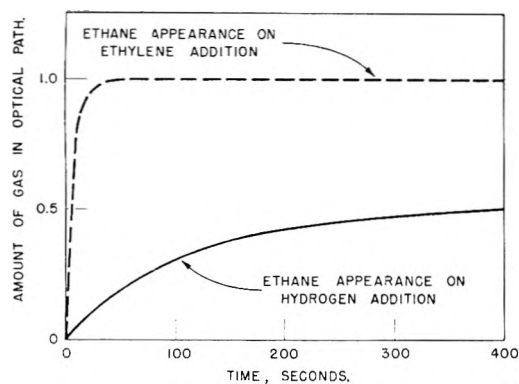


Fig. 2.—Hydrogen addition with rhodium surfaces after exposure to ethylene and evacuation.

decrease in the reflecting power of the rhodium surface because of adsorbed ethylene.

Infrared absorption data from 2.84 to 3.67 μ , taken after the amount of ethane in the system became constant, indicated that the only new gaseous hydrocarbon present was ethane. This result was verified by mass spectrometer analysis.

Infrared data, obtained after the evacuation of the ethylene and ethane, and processed by the computer, revealed no absorptions which could be attributed to surface structure in the wave length intervals 1.6 to 2.4 μ , 2.8 to 5.4 μ , and 8.6 to 11.7 μ . These were regions where carbon-hydrogen or carbon-carbon absorptions might be expected for adsorbed molecules. During evacuation no change in reflectivity was observed.

The results of hydrogen addition after ethylene evacuation are given in Fig. 2. These data were obtained by monitoring the 3.342 μ wave length during the hydrogen addition. The coordinates are the same as for Fig. 1, except that a longer time axis has been used. The dashed curve corresponds to the formation of ethane during the previous ethylene addition. If the 2.84 μ wave length is monitored during hydrogen addition, an increase in reflectivity is observed. The increase is approximately equal to the decrease observed during ethylene addition. Infrared absorption data from 2.86 to 3.67 μ , taken after the amount of ethane in the system became constant, indicated that the only gaseous hydrocarbon present was ethane. Mass spectrometer analysis of these gases showed only hydrogen and ethane to be present.

Because the hydrogen to produce ethane could only come from the ethylene during the ethylene addition, the quantity of ethane formed is a measure of the amount of ethylene reacted. To produce this ethane, some fragments of ethylene must be left on the surface, because no acetylene was formed. The amount of ethane produced during the hydrogenation step is a measure of the amount of "carbon" left on the surface during the previous step, because the ethylene fragments on the surface are the only source of carbon at this step. The ratio of the amount of ethane formed during the ethylene addition step to the amount formed during the hydrogen addition step is shown in column three of Table I. Column one shows the experiment designation and column two the cycle number. A complete cycle includes the steps: (a) addition

of ethylene, (b) evacuation of ethylene, (c) addition of hydrogen, and (d) evacuation of hydrogen. In most of the experiments, enough data were available after steps (a) and (c) for each cycle to compute the ratio shown in column three.

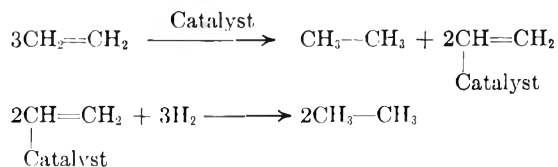
TABLE I

Exp.	Cycle	Ratio $\frac{C_2H_6 \text{ from } C_2H_4}{C_2H_6 \text{ from } H_2}$
A	2	2.0
A	3	2.1
B	1	1.7
B	2	2.0
B	3	1.9
B	6	2.1
C	1	1.8
C	2	2.2
C	3	2.4
C	4	2.3
D	1	1.0 (1.2)
D	2	1.9 (2.3)
D	3	1.9 (2.0)

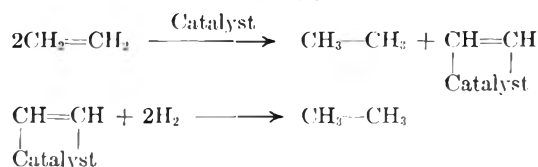
The ratio for cycle 1 of experiment D is far enough from the average to justify exclusion from the set with less than one chance in a hundred that it should be included. The average ratio, excluding that point, is 2.02 with a standard deviation of 0.22. The results in parentheses for experiment D were based on mass spectrometer analyses combined with pressure data. The remaining ratios were derived from infrared absorption data taken during the experiments. Although the precision is not high, the two methods of analysis are in agreement.

Plausible mechanisms for self-hydrogenation of ethylene, followed by hydrogenation of the surface complex, may be pictured as

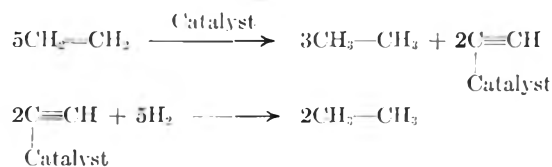
MECHANISM 1



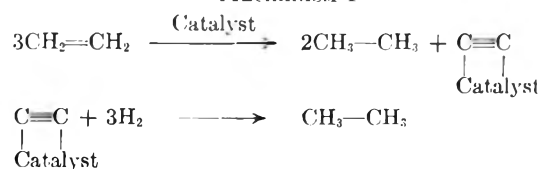
MECHANISM 2



MECHANISM 3



MECHANISM 4



For these four mechanisms, the ratio of ethane produced on the ethylene addition step to that produced on the hydrogen step varies from 0.5 to 2.0. Because the data presented in Table I indicate a ratio of 2.02 with a standard deviation of 0.22, it would appear that the net self-hydrogenation of ethylene over rhodium reaction may be *via* Mechanism 4. The fact that only ethane is formed in the hydrogenation step supports the hypothesis that the final surface complex when ethylene is adsorbed on rhodium is a pair of carbon atoms. Assuming Mechanism 4 and using the data of Fig. 2, the concentration of surface complex was calculated as a function of time. With excess hydrogen in the system, it was found that the rate of ethane formation was first order with respect to surface complex concentration, *i.e.*, $dY/d\theta = K(N - Y)$ where

$$\begin{aligned} Y &= \text{moles of ethane formed at time } \theta \\ K &= \text{rate constant} \\ \theta &= \text{time} \\ N &= \text{total ethane recoverable by hydrogenation} \end{aligned}$$

Additional data with improved signal-to-noise ratio are needed to evaluate the structure of the adsorbed substance formed when ethylene acts on rhodium.

2. CO Addition to Rhodium Mirrors.—When CO is added to new rhodium mirrors at a pressure of 0.65 mm. at room temperature, the spectrum shown in Fig. 3 was obtained. In this and the subsequent spectra presented, the absorption scale has an arbitrary zero value. The absorption band centered at 2.333 μ is interpreted as the first overtone of the CO fundamental frequency for physically adsorbed CO. The band disappears upon evacuation to 1×10^{-3} mm. At a CO pressure of 0.9 mm. on another film, the spectrum shown as the solid curve in Fig. 4 was obtained. Here the CO fundamental at the wave length observed for gaseous CO is resolved into two bands centered at 4.608 and 4.713 μ . The absorptions, however, are not much stronger than for the overtone band seen in Fig. 3. This weak fundamental supports the interpretation of the 2.333 μ band as due to physically adsorbed carbon monoxide, because the absorption for the first overtone in the gas phase would be expected to be very much smaller than for the fundamental. Returning to the solid curve in Fig. 4, it is further seen that an absorption band is present, centered at 4.854 μ together with a region of increased reflectivity with a minimum at 4.785 μ . After a 25 minute pumping period to 1×10^{-4} mm., the 4.854 μ band shifted to 4.915 μ while the position of the increased reflectivity extremum remained unchanged (see dashed curve in Fig. 4). No additional infrared absorptions which could be attributed to surface carbon monoxide were observed in the regions 1.7 to 2.6 μ , 4.3 to 5.3 μ or 5.9 to 7.1 μ .

Following the interpretation of Yang and Garland,⁴ it would appear that the absorption band at 4.854 μ corresponds to single linear CO molecules chemisorbed on rhodium atoms through the carbon atom. They also observed a small shift to longer wave lengths at low coverage. The region of increased reflectivity on the short wave length

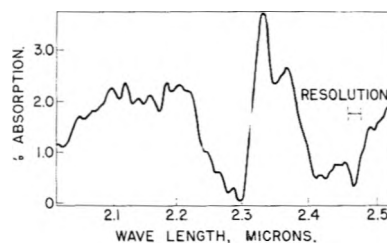


Fig. 3.—Spectrum of carbon monoxide over fresh rhodium surfaces; pressure = 0.65 mm.

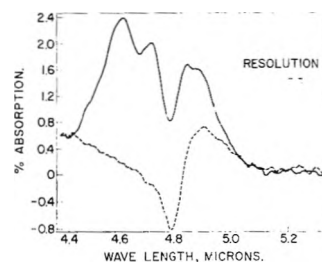


Fig. 4.—Spectra of CO over rhodium: —, pressure = 0.89 mm.; ---, pressure = 1×10^{-4} mm.

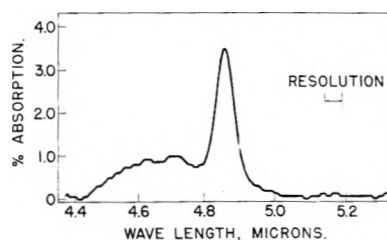


Fig. 5.—Spectrum of carbon monoxide over fresh nickel surfaces; pressure = 0.37 mm.

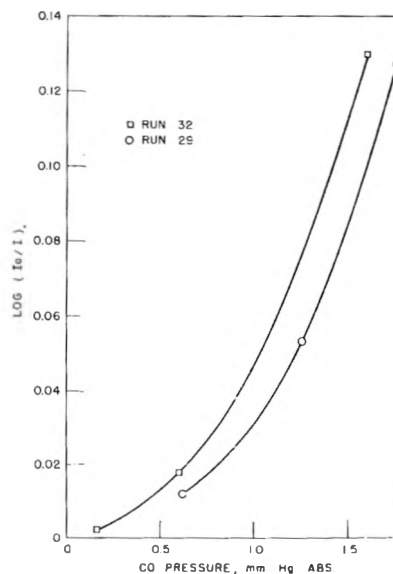


Fig. 6.—Carbon monoxide over fresh nickel surfaces. Optical density *vs.* pressure at a wave length of 4.859 μ .

side of an absorption band for reflection spectra of crystals is well known⁸ and may account for the 4.785 μ reflectivity maximum. The % absorption of radiation at 4.854 μ is so small that the observed band center is within a few thousandths of a micron of the actual wave length corresponding to the "adsorbed" CO frequency.

(8) Ivan Simon, *J. Opt. Soc. Am.*, **41**, 336 (1951).

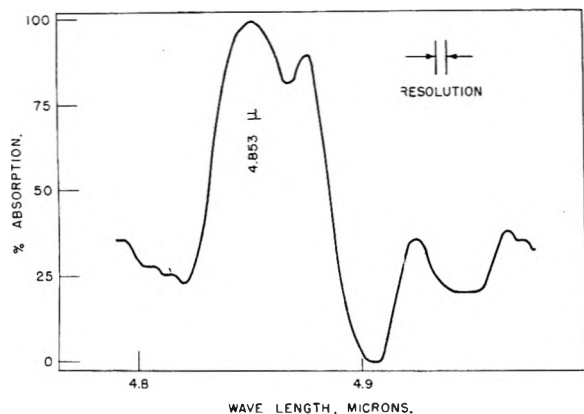


Fig. 7.—Spectrum of carbon monoxide over fresh nickel surfaces; pressure = 12.1 mm.

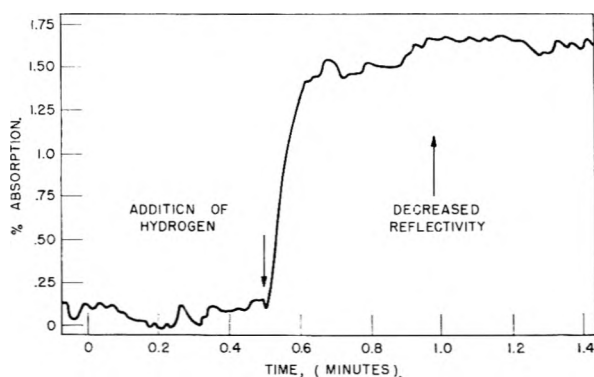


Fig. 8.—Hydrogen addition with fresh rhodium surfaces: % absorption vs. time at wave length of 1.731 μ .

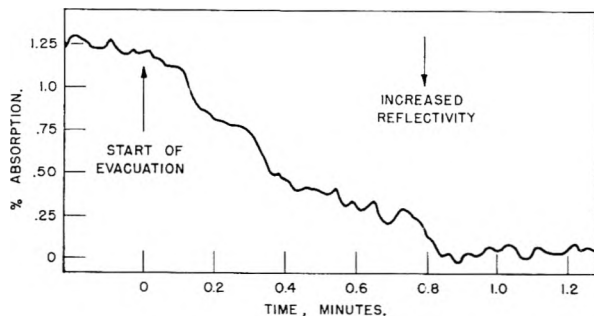


Fig. 9.—Hydrogen removal by evacuation: % absorption vs. time at a wave length of 1.731 μ .

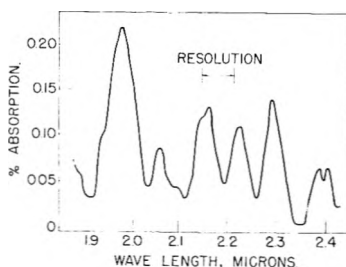


Fig. 10.—Spectrum of hydrogen over rhodium surfaces.

In another experiment with rhodium mirrors, hydrogen was added to the catalyst cell and then evacuated before the first CO addition. The addition of the CO did not produce the 4.854 μ band nor the increase in reflectivity at 4.785 μ . The hydrogen pretreatment apparently blocked the rhodium sites which are responsible for the production of the

component which gives the strong 4.854 μ absorption for CO on new rhodium mirrors.

3. CO Addition to Nickel Mirrors.—When CO is added to new nickel mirrors at room temperature, a large infrared absorption at 4.859 μ occurs. This is illustrated in Fig. 5 where it is also possible to see the resolved CO fundamental doublet at 4.608 and 4.713 μ . These bands all disappear upon evacuation. Figure 6 shows the optical density ($\log I_0/I$) at 4.859 μ as a function of pressure for two films to which batches of CO had been added. Clearly the optical density increases more than linearly with system pressure, but less than fourth power. The fourth power relationship would be applicable if the band observed were due to gaseous nickel tetracarbonyl and if the following assumptions are made: (1) the CO and nickel tetracarbonyl were in equilibrium *via* the mechanism $4\text{CO} + \text{Ni} \rightleftharpoons \text{Ni}(\text{CO})_4$ and (2) the amount of nickel carbonyl is small relative to the amount of CO.

In Fig. 7 a higher resolution spectrum of the band centered at 4.859 μ is shown for a 12 mm. CO pressure over new nickel mirrors. The band appears to be resolved into peaks at 4.877 and 4.853 μ . The small peak at 4.926 μ may be analogous to the "low coverage" CO reported by Yang and Garland⁴ for rhodium.

No other bands were observed in the regions 4.36 to 6.67 μ and 6.84 to 13.35 μ when CO was added to nickel mirrors.

Finally, all of the infrared absorptions shown in Figs. 5 and 7 disappeared upon evacuation to 1×10^{-3} mm. Thus the "adsorbed" CO on nickel is not as tightly bound as in the case for CO adsorbed on rhodium. The 4.859 μ peak is believed to be caused by "adsorbed" CO since no other nickel carbonyl bands were observed; furthermore, nickel tetracarbonyl could not be detected by mass spectrometric analyses of gases removed from the catalyst cell after CO addition.

4. Hydrogen Addition to Rhodium Mirrors.—Figure 8 shows the chart which was obtained when hydrogen was added to new rhodium mirrors at room temperature with the monochromator held at 1.731 μ . A decrease in energy of about 1.5% arriving at the detector was observed to occur rapidly; this was followed by a slower decrease which was complete after about 0.6 min. Because no infrared absorption is known for gaseous hydrogen at this wave length, and because subsequent scanning of this region showed no absorption of this magnitude which could be attributed to the surface hydrogen, the change must be the result of a change in reflectivity of the mirror surfaces. This latter effect could be a result of the change in electron density in the metal near the surface brought about by the presence of chemisorbed hydrogen.

Figure 9 shows the chart which was obtained during the hydrogen removal by evacuation. Again the record was made of the energy arriving at the detector at a wave length of 1.731 μ . The energy increased 1.2% over a 1-minute period. Although the final pressure was less than 1×10^{-3} mm., only about three-fourths of the reflectivity change previously noted was reversed. Assuming no irreversible change to the rhodium surface, these

TABLE II

Band center μ	Times observed	Interpretation	Band center μ	Times observed	Interpretation
4.560	1	H ₂	5.817	4	H ₂ O
4.572	2	H ₂	5.914	1	H ₂ O
4.645	1	H ₂	5.938	1	H ₂ O
4.671	1	H ₂	5.981	1	H ₂ O
4.693	1	H ₂	6.017	5	H ₂ O
4.726	2	H ₂	6.094	6	H ₂ O
4.771	3	H ₂	6.139	1	H ₂
4.817	2	H ₂	6.223	2	H ₂ O
4.907	3	H ₂ O	6.266	1	H ₂ O
4.946	3	H ₂ O	6.289	1	H ₂
5.025	1	H ₂ O	6.305	3	H ₂
5.086	3	H ₂ O	6.329	1	H ₂ O
5.200	2	H ₂ O	6.382	4	H ₂ O
5.216	3	H ₂ O	6.394	2	H ₂ O
5.271	3	H ₂ O	6.443	4	H ₂
5.333	1	H ₂	6.460	3	H ₂ O
5.411	3	H ₂ O	6.540	3	H ₂
5.453	2	H ₂ O	6.566	1	H ₂ O
5.470	3	H ₂	6.583	5	H ₂
5.549	1	H ₂ O	6.636	6	H ₂ O
5.571	2	H ₂ O	6.716	5	H ₂
5.583	3	H ₂	6.789	3	H ₂ O
5.627	1	H ₂ O	6.817	1	H ₂ O
5.647	3	H ₂ O	6.868	5	H ₂ O
5.675	1	H ₂ O	6.964	4	H ₂ O
5.757	2	H ₂ O	7.042	2	H ₂ O
5.784	1	H ₂ O	7.062	3	H ₂ O

results indicate that some of the adsorbed hydrogen had not been removed by evacuation.

The result of combining several spectra of rhodium mirrors to which hydrogen had been added is shown in Fig. 10. The six absorption bands indicated in the figure may be attributed to the presence of chemisorbed hydrogen. Figure 11 shows the spectrum for hydrogen on rhodium at the pressure indicated. Two bands are present which can be accounted for as water vapor. This was caused by a small decrease in the amount of water vapor left in the comparison cell which was being purged with nitrogen dried at -78° . The decrease of water in the comparison cell after the background data were obtained appears the same as water in the catalyst cell. In addition to the water absorptions, there are three absorptions which are too large to be considered accidental but which do not correspond with water spectra absorptions. Table II summarizes the results of several spectra over the wave length region 4.5 to 7.0 μ . The hydrogen pressure varied from 3×10^{-4} to 5 mm. for these results. No significant variation in absorption with pressure was observed.

Water spectra used in making the interpretations were those of Oetjen, *et al.*,⁹ and Jones.¹⁰ The positions of the water absorption agree with literature values to less than 0.010 μ . The completeness with which the water spectrum is obtained lends support to the hypothesis that the other bands observed are "real," *i.e.*, caused by some absorbing component in the system. Because the only gaseous component present in the catalyst cell is hydrogen, and

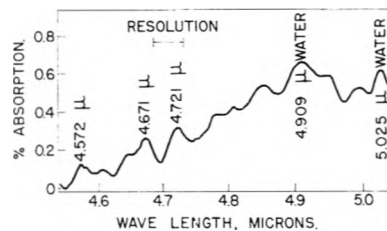


Fig. 11a.—Spectrum of rhodium surfaces after hydrogen addition and evacuation; pressure = 3×10^{-4} mm.

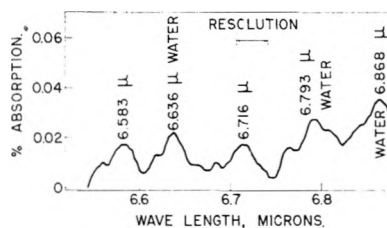


Fig. 11b.—Spectrum of rhodium surfaces after hydrogen addition and evacuation; pressure = 5×10^{-4} mm.

because gaseous hydrogen is transparent in the infrared in this region, these bands are attributed to adsorbed hydrogen on the rhodium mirror surfaces. More extensive data with improved signal-to-noise ratio would be required to provide firm enough data to attempt a detailed interpretation of the results.

Conclusion

The equipment which was designed and constructed permitted changes in gas composition and mirror surfaces to be observed readily. The sensitivity was high enough to permit observation of the spectra of adsorbed molecules on evaporated metal films with the systems comprising CO on nickel, CO on rhodium and H₂ on rhodium.

(9) R. A. Oetjen, C. L. Kao and H. M. Randall, *Rev. Sci. Instr.*, **13**, 515 (1942).

(10) L. H. Jones, *J. Chem. Phys.*, **24**, 1250 (1956).

THE INFLUENCE OF A CHEMISORBED LAYER OF CARBON MONOXIDE ON SUBSEQUENT PHYSICAL ADSORPTION¹

By M. V. C. SASTRI, T. S. VISWANATHAN AND T. S. NAGARJUNAN

Department of Applied Chemistry, Indian Institute of Technology, Kharagpur, India

Received July 18, 1958

Experiments reported in this paper show that, on cobalt catalysts, a part of the carbon monoxide chemisorbed at liquid nitrogen temperature is removed by evacuation at -78° . Thus two types of chemisorption of CO are visualized, one resisting desorption at -78° and the other desorbing at -78° . The former type suppresses the subsequent low temperature physisorption of nitrogen and carbon monoxide whilst the latter does not. The suppression is attributed to the positive charge gained by the metal surface as a result of CO chemisorption. These observations also show that low temperature CO chemisorption methods cannot be used, in all cases, to determine the extent of metal surface.

Introduction

The extent of the exposed metallic component on the surface of iron, cobalt and nickel has been estimated by several workers by the chemisorption of carbon monoxide at liquid nitrogen temperature. Since the total adsorption of carbon monoxide at this temperature comprises of physisorption as well as chemisorption, the amount of chemisorbed CO is estimated as the difference between the total CO adsorption and the physisorption of the same gas, assuming that the chemisorbed carbon monoxide does not affect the subsequent CO physisorption on the chemisorbed film.

To determine the amount of physisorption two methods have been used. In the first method proposed originally by Emmett and Brunauer,² the total CO adsorption is determined at -194° , followed by evacuation at -78° . Assuming that this evacuation removes only the physisorbed gas leaving the chemisorbed layer intact, the CO adsorption isotherm is redetermined on this surface at -194° so that the second isotherm gives the amount of CO physisorbed.

Finding that in certain cases evacuation at -78° removed part of the chemisorbed CO, Emmett and Skau³ later suggested that the difference between CO and N₂ isotherms at the same low temperature and relative pressure might be taken as the amount of CO chemisorbed, since the physical adsorption of CO and of N₂ are almost identical on most surfaces. This method later on was extensively used by Anderson.⁴ The assumption in this method is that the adsorption characteristics of the bare surface and of the chemisorbed film are the same. Recently however some doubt regarding the validity of the above assumption arose from the results of Stone and Tiley⁵ who reported that the presence of a chemisorbed layer of carbon monoxide on cuprous oxide suppressed the subsequent physisorption of nitrogen or krypton.

Besides, Joy and Dorling⁶ found that on a fused iron Fischer-Tropsch catalyst, a part of the carbon monoxide chemisorbed at -194° was removed by

evacuation at -78° . This enabled them to differentiate between two types of chemisorption of carbon monoxide, the first resisting desorption during evacuation at -78° and the other removed during this evacuation. This differentiation between strong and weak chemisorption of CO is arbitrary but useful. They found that the presence of strongly chemisorbed CO on the iron catalyst did not affect the subsequent physisorption of nitrogen. Similar results have been obtained by Srikant⁷ on iron synthetic ammonia catalyst. On the other hand, Sastri and Srinivasan⁸ observed that on Co catalysts physisorption of N₂ was suppressed in presence of chemisorbed CO. From these observations it would appear that the suppression effect is specific to the metal in question.

The present paper reports a more detailed investigation of the effect on cobalt catalysts particularly with reference to the relative effects of the so-called strongly and weakly chemisorbed carbon monoxide. Incidentally, the reliability of the method under review for the estimation of carbon monoxide chemisorbed on metal surfaces has been re-examined.

Experimental

The catalyst used in the present investigations was of the following composition: cobalt:thoria:kieselguhr 100:18:200, the surface area of kieselguhr used being 25.6 m.²/g. The catalyst was prepared from the corresponding nitrates by the simultaneous addition of kieselguhr and potassium carbonate. The catalyst was reduced by a rapid stream of carefully purified (described later) hydrogen till no more moisture could be detected in the exit gas by a liquid nitrogen trap.⁹ The reduction temperature was 350°. The results reported in this paper refer to adsorption by about 1.5 g. of unreduced catalyst.

The apparatus for the measurement of adsorption was essentially the same as that described in an earlier paper¹⁰ with an arrangement to permit continuous flow of gas through the catalyst tube whenever necessary without removing the catalyst tube. The gases used in the adsorption experiment were purified as follows.

Hydrogen, used for reduction, was prepared electrolytically and purified by passage through (a) metallic copper at 400° and (b) "Deoxo" purifier of Messrs. Baker & Co., London, which is an alumina-supported platinum catalyst active at room temperatures. Subsequently the gas was passed over anhydrous magnesium perchlorate and finally over silica gel cooled in liquid nitrogen to remove completely water vapor and gases heavier than hydrogen.

Carbon monoxide was prepared by adding formic acid

(1) Part of the work described in this paper is abstracted from the Ph.D. thesis of T.S.V. submitted to the Madras University in January, 1955.

(2) P. H. Emmett and S. Brunauer, *J. Am. Chem. Soc.*, **57**, 1754 (1935); **59**, 310, 1553 (1937).

(3) P. H. Emmett and N. Skau, *ibid.*, **65**, 1029 (1943).

(4) R. B. Anderson, W. K. Hall and L. J. E. Hofer, *ibid.*, **70**, 2465 (1948).

(5) F. S. Stone and P. F. Tiley, *Nature*, **167**, 654 (1951); **168**, 434 (1951).

(6) A. S. Joy and T. A. Dorling, *ibid.*, **168**, 433 (1951).

(7) H. Srikant, Ph.D. thesis accepted by the Madras University, in 1954.

(8) M. V. C. Sastri and V. Srinivasan, *Current Sci.*, **23**, 154 (1954).

(9) J. T. Kummer and P. H. Emmett, *This Journal*, **55**, 337 (1951).

(10) J. C. Ghosh, M. V. C. Sastri and T. S. Viswanathan, "Symposium on Contact Catalysis," *Bull. Natl. Inst. Sci.*, 1957 (in press).

dropwise to 85% phosphoric acid at 170° and removing acid spray and traces of CO₂ by KOH. The gas was purified by passage over hot copper followed by U tubes of potash pellets and anhydrous magnesium perchlorate, respectively.

Tank nitrogen was purified by passage over hot copper and anhydrous magnesium perchlorate. Tank helium of purity 99.5% was passed over hot copper, anhydrous magnesium perchlorate and finally through an activated charcoal trap cooled in liquid nitrogen.

After reduction by hydrogen, the catalyst was evacuated at the reduction temperature for 8 hours to remove adsorbed hydrogen, before nitrogen and carbon monoxide adsorptions at low temperature were carried out. After each CO adsorption run the catalyst was evacuated at 100° for two hours to remove as much of the carbon monoxide as possible. It was then treated with flowing hydrogen at 250° for two hours and later evacuated at the reduction temperature for 8 hours. This procedure was found to give a reproducible catalyst surface. The temperature of the liquid nitrogen bath was measured by means of an oxygen vapor pressure thermometer. Solid carbon dioxide-acetone and melting methylcyclohexane baths were used to obtain temperatures of -78° and -122°, respectively, which were read by a pentane-in-glass thermometer.

The adsorption results in each series of experiments were closely reproducible.

Sequence of Experiments

Influence of Strongly Chemisorbed CO on Physical Adsorption.—Experiments were carried out on cobalt-thoria-kieselguhr catalyst to investigate (a) the different types of chemisorption of CO on the catalyst surface and (b) their influence on subsequent physical adsorption of N₂ and CO.

The sequence of the experiments was as follows.

(1) Adsorption of nitrogen at -194° was determined on the bare surface of the thoroughly evacuated catalyst. The catalyst later was evacuated for two hours at 200° to remove the adsorbed nitrogen.

(2) Adsorption of carbon monoxide at -194° on the bare surface obtained after step (1).

(3) The catalyst was evacuated at -78° for one hour, after the adsorption in step (2). The catalyst then was cooled down to -194° and the adsorption of carbon monoxide on the surface determined at this temperature.

(4) After the CO adsorption in step (3), the catalyst was evacuated at -78° for one hour. It then was cooled back to -194° and the adsorption of nitrogen on the surface determined.

(5) After the carbon monoxide adsorption in step (2), the catalyst was evacuated at -122° for one hour. It then was cooled back to -194° and the adsorption of carbon monoxide on this surface measured at this temperature.

(6) After the adsorption in step (5), the catalyst was evacuated at -122° for one hour. It was then cooled back to -194° and nitrogen adsorbed at this temperature determined.

The catalyst then was evacuated and cleared of all the chemisorbed carbon monoxide as described before, and the entire cycle of operations noted above was repeated to check the reproducibility of the results.

These experiments also were performed on a catalyst of the same composition prepared with a calcined kieselguhr sample having a surface area of only 1.44 m.²/g. and with a cobalt-thoria-magnesia-kieselguhr catalyst. The results obtained with these were very similar to those pre-

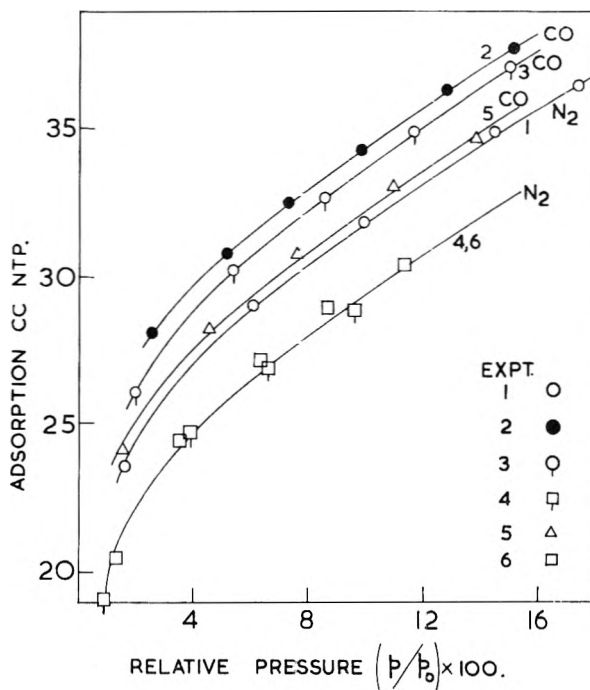


Fig. 1.—Suppression of physical adsorption of nitrogen.

sented below for one sample of cobalt-thoria kieselguhr catalyst.

Results

The results are represented graphically in Fig. 1, the numbers on the curves denoting the respective operations. It is seen that the repeat carbon monoxide isotherm (3) falls in between the carbon monoxide isotherm on bare surface (2) and the nitrogen isotherm (1). The difference between (2) and (3) gives the amount of CO strongly chemisorbed whilst the amount weakly chemisorbed is roughly given by the difference between (3) and (1). Hence low-temperature chemisorption of CO consists of (a) strongly chemisorbed CO resisting desorption at -78° and (b) weakly chemisorbed CO being desorbed at -78°. Also it is seen that due to the presence of a film of strongly chemisorbed CO, the physisorption of nitrogen is suppressed, the extent of suppression being given by the difference between (1) and (4).

To determine the influence of weakly chemisorbed CO on subsequent physisorption, the system after initial adsorption of CO at -194° was evacuated at -122° to leave behind a film of weakly chemisorbed CO and then the N₂ isotherm was determined at -194° (Fig. 1). The results show that the presence of weakly chemisorbed CO does not affect the subsequent physisorption of nitrogen.

Since the activation energy for low temperature CO chemisorption is very low, the activation energy for the desorption of the gas will be determined predominantly by the heat of adsorption. It may be estimated very roughly that gas adsorbed with a heat below 10 kcal. per mole would be removed by evacuation at -78° (Stone and Tiley give the figure of 12 kcal. as the maximum limit of the heat of adsorption of a gas removed by evacuation at -78°); while at -122° any gas adsorbed with a heat less than 7 kcal. is removed during evacuation.

Thus the presence of carbon monoxide chemisorbed with heat between 7 and 10 kcal. and presumably any gas chemisorbed with heat less than 7 kcal. also, is without effect on physisorption.

Discussion

The results show that less nitrogen is adsorbed in presence of a strongly chemisorbed film of CO left over at -78° than on the bare surface. Weaker chemisorption of CO which could be removed by evacuation at -78° did not produce any increase in the suppression. Since this work was completed, Srinivasan¹¹ has reported that on reduced cobalt oxide powder also, the physisorption of nitrogen is similarly suppressed in the presence of chemisorbed carbon monoxide.

Before attributing this suppression exclusively to the presence of the chemisorbed CO film it is necessary to examine if any (molecular) chemisorption of nitrogen occurred on the cobalt surface at -194° (besides physisorption). Because if it did occur, the observed suppression would then be due, at least in part, to the strongly chemisorbed CO, occupying sites which were otherwise available for nitrogen chemisorption. However, it would be difficult to account for more than two-fifths of the observed suppression (ca. 2.2 cc.) of nitrogen adsorption in this way, since the amount of strong CO chemisorption is only about 0.8 cc.

A simple experiment indicated the low order of energy associated with the adsorption of nitrogen. When, after determining the nitrogen adsorption isotherm on the bare Co surface at -195° the gas was pumped off for 1 hour at -78° and the nitrogen isotherm redetermined at -194° the previous isotherm was reproduced perfectly, thereby proving that the whole of the nitrogen adsorbed at low temperature was removed by the short evacuation at -78° . In other words, no part of the nitrogen adsorption was associated with an energy high enough (*i.e.*, ca. 8 kcal.) to make it resist desorption at -78° .

These observations, though not conclusive in eliminating altogether the possibility of N_2 -chemisorption occurring on the bare cobalt surface at -194° show clearly enough that this can at best be only a minor factor in the over-all suppression observed. The bulk of the suppression must be interpreted in terms of the influence of the strong CO-chemisorption on the physical adsorption of nitrogen over the bare surface and over the chemisorbed CO molecules. This is the purport of the following discussion.

Physisorption of non-polar gases on metals is caused by the co-operation of the two factors: (i) non-polar van der Waals forces arising out of interaction of induced dipoles in the metal with the (continually changing) inducing dipoles of the gas molecules; (ii) the polarization of the molecules by the metal. The metal surface acquires a positive charge with electrons projecting a short distance outside the surface. The approaching molecules are polarized by the metal surface with the positive end pointing away from the surface; it is assumed that the negative layer of electrons does not polarize the molecules.

The observed suppression of the physisorption isotherm is tantamount to decrease in the monolayer volume V_m , which by definition is the product of the surface area (A) and the limiting value of adsorption per unit area. The suppression effect could therefore be due to either or both of the following causes: (i) decrease in the total area A , say by "blocking" of the pores and also perhaps by localized chemisorption at the pore mouths ("poisoning" of the pore mouths) preventing the two-dimensional migration of the physisorbed molecules along the pore walls into the interior of the pores; (ii) decrease in the value of v_0 , representing the density of packing at saturation. As already mentioned, during physisorption, non-polar gas molecules are polarized with their positive ends pointing away from the surface. Due to this polarization, the magnitude of the attraction forces between the adsorbed molecules are less, resulting in a decrease in the two-dimensional van der Waals constant a_2 ; sometimes even a negative value for a_2 is obtained.¹²

In many cases of chemisorption normal covalent bonds are formed where an electron of the adsorbed atom and one of the metal form a pair. Since these bonds are partly ionic in character, the adatoms form dipoles on the surface of the metal, the direction of the dipoles depending upon the ionization potential of the adatom and the electron work function of the metal. In the case of CO chemisorbed over cobalt surface, the negative charges of the dipoles point away from the surface with a resultant decrease in the number of conduction electrons. The dipoles so formed tend to repel each other so that the chemisorbed layer is incomplete with patches of bare metal surface remaining exposed. Under such conditions, a molecule physisorbed subsequently comes directly into contact with the metal surface possessing enhanced positive charge. As a result, the polarization of the physisorbed molecule is more pronounced, thereby increasing the magnitude of the repulsive forces in the physisorbed layer. Similar results have been obtained by Mignolet,¹³ who observed that in presence of a chemisorbed film of hydrogen on nickel, the physisorption of nitrogen was suppressed to a large extent with a simultaneous increase in the surface potential of the physisorbed film. Therefore the molecules in the physisorbed layer are now more loosely packed so that v_0 is less than that on the bare surface. These arguments hold good in the case of a polar molecule (like CO) also. Regarding the method suggested by Emmett and Skau, the difference between CO and N_2 isotherms at the same low temperature and relative pressure would give a lower estimate of the metal surface, since the suppression of physisorption of CO by the chemisorbed CO has not been considered. Moreover, since the extent of suppression in physisorption of CO will be different from that of N_2 , it would be difficult to determine one with the help of the other.

Reference may now be made to the observed difference in behavior of strongly and weakly

(11) V. Srinivasan, *Proc. Ind. Acad. Sci.*, XLVI, Sec. A, 120 (1957).

(12) J. H. de Boer, *Adv. in Catalysis*, VIII, 38 (1956).

(13) J. C. P. Mignolet, *Disc. Faraday Soc.*, 8, 105 (1950).

chemisorbed CO toward subsequent physisorption. The initial rapid chemisorption of CO increases the electron work function of the metal considerably so that the subsequent chemisorption of CO occurs with less heat of adsorption. It is probable that the heat of chemisorption may be of the same order as that of physical adsorption. Therefore at -194° , CO adsorbed subsequently will be bound to the surface in a quasi-chemical way without significantly contributing to the magnitude of the positive charge on the metal. A further assumption that the extent of physisorption is the same over the weakly and strongly chemisorbed CO gives an explanation for the result that the presence of weakly chemisorbed CO does not add any more to the suppression already caused by the strong CO chemisorption.

Since the transition from physisorption to chemisorption is continuous and the heat of chemisorption at high coverages may be as low as that of physisorption, it is not possible to visualize any

temperature at which only the physisorbed molecules are removed by evacuation. Nor is there any theoretical justification for assuming tacitly that the amount of such weak chemisorption is inconsiderable in comparison with the amount held more strongly. Strictly speaking, therefore, it would not be possible to estimate accurately the true extent of the CO-chemisorption by the technique of evacuation at any temperature higher than that of liquid nitrogen and re-adsorption at the same temperature. Evacuation at liquid nitrogen temperature will not be any better, because it is bound to leave behind a considerable quantity of the physisorbed gas.

In view of the uncertainties caused on the one hand by the suppression effect and on the other hand by the desorbability of the chemisorbed gas over a range of low temperatures, neither of the procedures suggested in the paper of Emmett and Skau can be expected to give an accurate estimate of the surface metal sites on cobalt catalysts.

A METHOD OF SUCCESSIVE APPROXIMATIONS FOR COMPUTING COMBUSTION EQUILIBRIA ON A HIGH SPEED DIGITAL COMPUTER¹

BY D. S. VILLARS

Contribution from the Research Department, U. S. Naval Ordnance Test Station, China Lake, California

Received July 18, 1958

A procedure has been developed for rapidly solving complicated thermodynamic equilibria by a flexible iteration method which can be readily extended to include additional chemical elements. Changes in composition are computed for only one reaction at a time, neglecting the interaction of such changes in composition on the other equilibria. Current values of concentrations are used to calculate back all equilibrium constants. For the next computation the program selects that reaction showing the greatest discrepancy between calculated and given equilibrium constant. Discrepancies are then recalculated and another determination made of the reaction showing the greatest discrepancy. The process is repeated until the maximum discrepancy is reduced to a value less than an error, E , specified as a parameter of the problem. Speed of convergence may be maximized by expressing all species in terms of components existing in the largest concentrations at equilibrium. A subiteration procedure is utilized for solving the individual equations. This converges upon the solution by halving successive tentative intervals. For errors of 0.001% the JPN equilibrium at 2 atmospheres is computable with 28 iterations for 2500°K. and 43 for 4000°K. A composition involving excess solid carbon has been computed with 14 iterations for 2500°K. and 20 for 4000°K. Each iteration involves about 0.2 second machine time.

Introduction

It is well known² that the specific impulse I_{sp} of a propellant is calculable from flame temperature T_c , the average ratio of specific heats γ , and the average molecular weight M of the gaseous mixture

$$I_{sp} = (1/g)[(RT_c/M) \{2\gamma/(\gamma - 1)\} \{1 - (P_e/P_c)^{(\gamma-1)/\gamma}\}]^{1/2} \quad (A)$$

if equilibrium is frozen during expansion through the nozzle, or from the change in enthalpy at constant entropy ΔH_s , on adiabatic expansion between chamber and exit

$$I_{sp} = (-2\Delta H_s/M)^{1/2}/g \quad (B)$$

if the reaction mixture continually re-equilibrates during expansion. In the above equations g is the acceleration of gravity, R the molar gas constant, P_e the external pressure, and P_c the chamber pressure. Since the above averages are weighted in

proportion to the number of moles at equilibrium of each of the different species present, it is highly desirable to have an easy method of calculating the equilibrium composition

In order to discuss a concrete problem let us consider the typical propellant, JPN,³ which is a double base ballistite consisting of carbon, hydrogen, oxygen and nitrogen. At flame temperatures in a rocket chamber six equilibria produce 10 reaction species in appreciable concentrations. To solve for 10 mole fractions one requires 10 equations. Four of the 10 necessary equations are atom balances in the four elements and are linear. However, the six equilibrium constant equations are quite non-linear, several of them being cubic and others quadratic.

The only practical way of solving such a system of equations is by successive approximations. Such procedures are likely to be very laborious for desk machine calculations but with the recent availability of high speed digital computers which thrive on

(1) Presented in part before the Division of Physical and Inorganic Chemistry 131st Meeting of the American Chemical Society, Miami, April 12, 1957.

(2) S. S. Penner, "Chemistry Problems in Jet Propulsion," Pergamon Press, New York, N. Y., 1957, see Chapter 14.

(3) R. N. Wimpres, "Internal Ballistics of Solid-Fuel Rockets," McGraw-Hill Book Co., New York, N. Y., 1950, Table 2-1, p. 4.

multiple repetitions of simple arithmetical operations, the possibility is opened up of writing programs which can complete one of these problems in a few seconds machine time. The calculations of the equilibrium concentrations of gases which result from the combustion of materials of varying composition thus becomes quite feasible.

As to method of approximation to be used there is probably an infinite variety available. In the long run those methods will survive which combine simplicity and speed of operation with accuracy of results. The purpose of the present paper is to disclose an iterative procedure which rapidly gives results accurate to within the accuracy of the given equilibrium constants, yet is so simple that it is readily capable of extension to include additional chemical elements.

Space is not available to cite all approximation methods which have been developed for this problem. One important class of schemes involves linearization; ref. 4 one of the most elegant.⁴ Taylor's series expansions are made of the equations around differences between the solutions and "guestimates." On the assumption that the initial guestimates are good these differences will be small and higher powers than the first may be dropped. This enables one to solve the system as a set of linear equations. The writer independently applied the linearization method to the present problem in early 1950. However, although theoretically beautiful, the method is subject to breakdown under two sets of circumstances. For certain types of functions, the guestimates have to be quite good for the method to converge (in other words, higher powers which have been discarded often are not negligible). Also, if the matrix of coefficients approaches singularity, the solution is unstable. Because of these complications the linearization method was not considered foolproof enough for the present work.

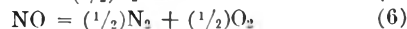
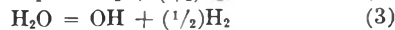
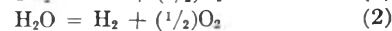
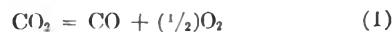
A different scheme used in this Laboratory was developed by McEwan⁵ and consisted of setting up a rigorous algebraic solution of the ten equations in terms of a parameter whose value had to be guessed and improved by trial and error. The procedure was coded for the IBM 701⁶ but the technique was such that a completely new derivation and reprogramming was required for extension to cases involving additional chemical elements.

Equilibrium Constant Equations

In order to distinguish between smoky and non-smoky flame we include



For the reacting elements, C, H, O and N, equilibria (1) to (6) are generally accepted as being of importance



Consider the general chemical equation

$$\sum_j b_j X_j = 0 \quad (C)$$

where X_j is the j th chemical species, products having positive coefficients b_j , reactants negative. According to the principles of conventional physical chemistry, changes in composition necessary to achieve equilibrium may be calculated by a formula of the general type

$$K_p[(S + yd)/P]^d = \prod_j (X_j^0 + b_j y)^{b_j} \quad (D)$$

where

$$S = \sum_j X_j^0 \quad (E)$$

(the superscript⁰ referring to initial concentrations) and

$$d = \sum_j b_j \quad (F)$$

The mathematical problem now is: given certain initial values of C, H, O and N, and the equilibrium constants at constant pressure, the pressure and temperature, find the final concentrations of the 10 reaction species that will satisfy all six equilibrium constant equations corresponding to reactions 1 through 6 when there is no excess carbon, or find the final amounts of the 11 reaction species when solid carbon is in excess. A further condition on the solution is that the total sum of atoms of each element is to be maintained unchanged. As stated at the outset, it is proposed to do this by solving the equations one at a time. In view of the fact that the number of individual types of equations which (D) represents is small, their solution may be conveniently programmed as subroutines. Or, better, the general type (D) may be programmed as a single subroutine. This allows us to capitalize upon the high speed potentiality of the digital computer which works best for repeated routine operations.

Iteration Procedure.—The proposed iterative procedure is to start immediately with the initial composition specified by the propellant under consideration, and calculate the complete change in composition for one reaction at a time, neglecting the interaction of such changes in composition on the other equilibria. Each time an equation is solved, the amounts listed for the different species are revised to accord with the new results and used for solving the next equation. Different variants of this procedure have been tried. In the first, a test sum, T , of the absolute values of the changes of all six reactions computed in succession was recorded and the computations repeated again and again until this test sum of changes per round became less than an error, E , specified as a parameter of the problem. This scheme gave results satisfactory

(4) H. J. Kandiner and S. R. Brinkley, Jr., *Ind. Eng. Chem.*, **42**, 850 (1950).

(5) U. S. Naval Ordnance Test Station: "Equilibrium Composition and Thermodynamic Properties of Combustion Gases," by William S. McEwan, China Lake, Calif., NOTS 26 May 1950. (NAVORD Report 1229, Part 1, NCTS 289).

(6) U. S. Naval Ordnance Test Station: "A Thermodynamic Investigation of the Product Gases of Carbon-Hydrogen-Oxygen-Nitrogen-Propellant Systems," by Mary M. Williams and William S. McEwan, China Lake, Calif., NOTS, 12 January 1955 (NAVORD Report 3421, Part 1, NCTS 1020).

for specific impulse calculation, but was shown by the referee of this paper to be defective in that it did not converge to correct answers as higher accuracy was specified.⁷ This procedure was modified by determining the fractional discrepancy between calculated and given equilibrium constants

$$D_i = (\text{calcd. } K_i / \text{given } K_i) - 1$$

and computing that reaction next which shows the greatest discrepancy. After concentrations are adjusted to the new values, the discrepancies are recomputed and that reaction again chosen for solution which corresponds to the greatest current discrepancy. This process is repeated until the maximum discrepancy is less than the error, E . (Each repetition will be referred to herein as an iteration). Such a procedure converges satisfactorily as smaller and smaller errors are specified.

Improvement of Rate of Convergence.—In the first iteration scheme used, over two thousand equilibria had to be computed to achieve an (absolute) error of $E = 10^{-6}$ for JPN at 2 atmospheres and 2500°K. To speed up convergence, use of an additional reaction, the water gas equilibrium, was suggested by Prof. K. S. Pitzer and independently by L. S. Kassel. The chemical equation corresponding to the latter equilibrium is the linear combination, (2)–(1). Inclusion of this reaction reduced the number of computations of equilibria to 66. The reason that convergence was so markedly affected, as pointed out by L. S. Kassel, is that (1) and (2) involve an intermediate (molecular oxygen) which at 2500°K. is present in such small amounts that even 100% consumption in each reaction computation accounts for such a very small change in CO, CO₂, H₂ and H₂O that a large number of calculations is required for any progress to be made. The water gas reaction does not involve this intermediate, so the complete change can be effected at once. This same effect shows its importance also in the computation of NO by reaction (6). It became of preponderant importance in calculations involving excess carbon where the oxygen mole fraction is of the order 10^{-13} .

It was ultimately realized (during discussions with Prof. Verner Schomaker) that the principle introduced by Kandiner and Brinkley⁴ to aid the convergence of their linearized equations is just as beneficial to the present iteration method and represents the key to rapid convergence. This is to guess which reaction species are likely to be present in highest concentrations in the final equilibrium mixture (call them "components") and express all other species in terms of reactions of formation from these components. By such a technique there is no question of trying to compute the formation of relatively high concentration species through intermediates existing only in low concentrations.

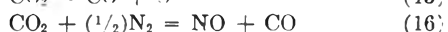
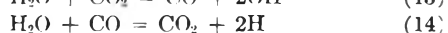
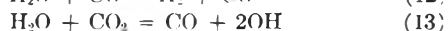
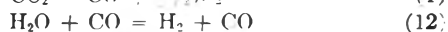
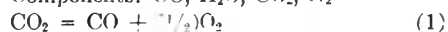
It may perhaps be objected that use of the Kandiner and Brinkley suggestion requires one to "know the answer before he gets it." While success with the linearization procedure often depends upon one providing the problem with fairly close quantitative

estimates of the final equilibrium concentrations, the present method only utilizes the attributive (qualitative) estimate of *which* constituents are to be considered as the components. Furthermore, the method does not require this information. Its provision is recommended only to reduce the number of iterations required for arriving at the final solution. Indeed, all of the components used below were obtained from preliminary runs which were carried out without benefit of use of components.

For JPN at 2500°K. it turns out that the species existing in greatest concentrations are CO, H₂O, CO₂ and N₂. Calling these the components, the reactions of formation of the other species are the following linear combinations

JPN 2500°K.

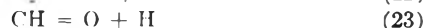
Components: CO, H₂O, CO₂, N₂



On the other hand the components indicated for 4000°K. are CO, H, O and N₂. The reactions of formation are accordingly

JPN 4000°K.

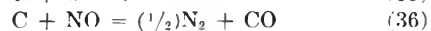
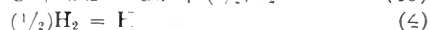
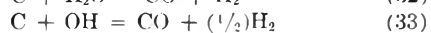
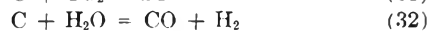
Components: CO, H, O, N₂



To test a composition giving excess carbon, JPN was modified by adding carbon. Preliminary results indicated the components are CO, H₂, N₂, and C for 2500° and CO, H, N₂ and C for 4000°. Since H₂ was still of the same order of magnitude (0.0626) as H (0.2826) at 4000°, the same set of components was used for both temperatures. The reactions of formation are

JPN modified, 2500°K.

Components: CO, H₂, N₂, C



Results

For input compositions and equilibrium constants listed, respectively, in Tables I and II results were obtained as given in Table III. It may be seen that the discrepancies listed at the bottom of Table III with which the final mole fractions reproduce the respective equilibrium constants are all less than the specified error, $E = 10^{-5}$. Specification of higher accuracy is meaningless in view of the number of significant figures of the given equilibrium constants. It may be seen that use of the Kandiner and Brinkley principle has brought the number of

(7) The author is indebted to the referee, L. S. Kassel, for the suggestion that this may have been due to internal round-off errors in the fixed point arithmetic used.

iterations to achieve this error down to 28 at 2500°K., 43 at 4000° for JPN; and to 14 at 2500° and 20 at 4000° for the soot case. In terms of machine time these problems are computed in the order of 3 to 9 seconds.

TABLE I
COMPOSITIONS, MOLE FRACTIONS

	JPN	Soot case
C	0.34523	0.70000
H ₂	.23075	.23075
O ₂	.32847	.32847
N ₂	.09556	.09556

TABLE II
EQUILIBRIUM CONSTANTS

	2500°K.	4000°K.
K _{p0}	0.71531 × 10 ⁷	0.69375 × 10 ⁶
K _{p1}	.037818	4.998
K _{p2}	.0062008	0.60159
K _{p3}	.0047528	.92132
K _{p4}	.02509	1.5933
K _{p5}	.015575	1.5528
K _{p6}	10.983	3.3565

TABLE III
RESULTS FOR 2 ATMOSPHERES PRESSURE

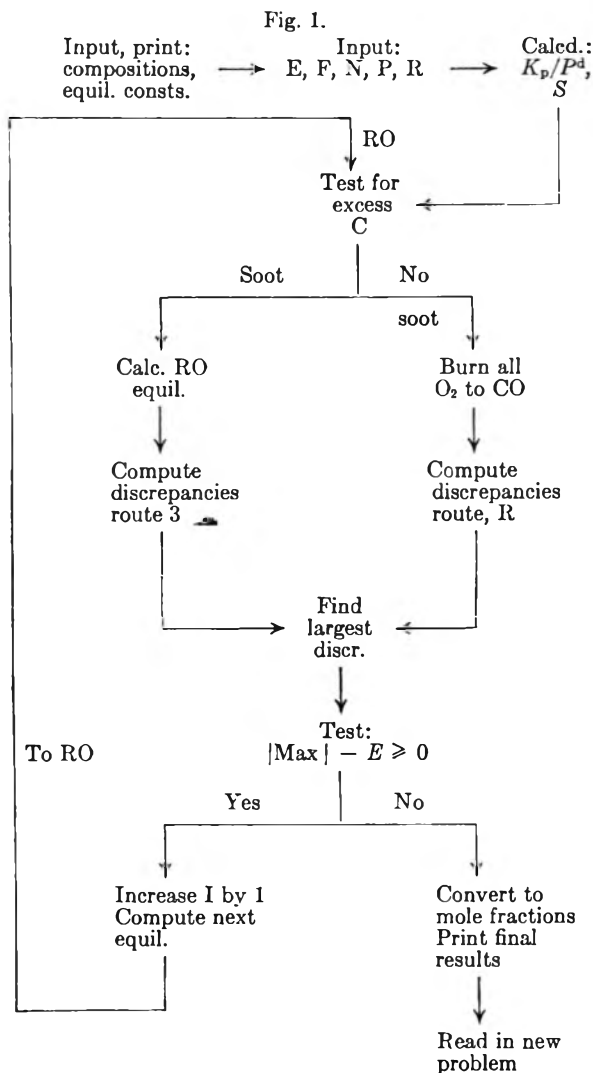
	JPN		Soot	
	2500°K.	4000°K.	2500°K.	4000°K.
Equilibrium mole fraction of gas				
O ₂	0.000258	0.022272	0.173 × 10 ⁻¹⁰	0.137 × 10 ⁻¹¹
O	.000177	.163861	.145 × 10 ⁻⁸	.000001
H ₂	.072454	.053543	.229434	.061793
H	.004775	.260696	.008498	.280059
OH	.003316	.052885	.483 × 10 ⁻⁷	.446 × 10 ⁻⁶
H ₂ O	.265538	.009843	.000007	.170 × 10 ⁻⁸
CO	.319592	.316061	.665282	.574568
CO ₂	.192100	.013346	.000003	.190 × 10 ⁻⁶
N ₂	.141455	.084707	.096773	.083577
NO	.000356	.012940	.241 × 10 ⁻⁸	.101 × 10 ⁻⁶
Residual C			(.043081)	(.043074)
Discrepancies × 10 ⁵ for error specification, E = 10 ⁻⁶				
0			0.004	0.004
1	0.031	0.153	.025	.639
2	.016	.159	.096	.006
3	.884	.007	.122	.057
4	.020	.536	.869	.498
5	.010	.060	.185	.153
6	.025	.328	.064	.745
No itrns.	28	43	14	20

The program was coded so that by means of a sense switch it is possible to print out the order in which the different reactions are selected. In the first run they went in the order: 1, 12, 1, 13, 14, 15, 16, 12, 1, 16, 14, 15, 13, 1, 16, 12, 1, 16, 14, 15, 13, 1, 16, 12, 1, 15, 14 and 15.

Program.—Principal steps of one variant of the program are shown in the flow diagram, Fig. 1. Only general functions are outlined. As indicated above, each solution of an equilibrium equation is achieved by invoking a subroutine. All calculations are in floating point arithmetic.

Before each computation of discrepancies a check is made of reaction (0) to determine whether or not carbon is in excess. Since the equilibrium constant for this reaction is of the order 10⁺⁶ up to 4000°K., this reaction has been coded for excess oxygen on the approximation of complete combustion of oxygen and carbon. Such an assumption is valid only for oxidizer-rich propellants. An ac-

tual calculation of the equilibrium is carried out when carbon is in excess.



Three methods of solution of the individual equations were coded before a practical one was devised. The third method which turned out to be quite satisfactory makes use of the knowledge that, in order to avoid negative concentrations and still have finite positive equilibrium constants, physically acceptable solutions for $x = -y$ in equation (D) have to lie between

$$(X_i^0/b_i)^*_{R} < x < (X_i^0/b_i)^*_{P}$$

where the lower limit of x is the quotient having smallest absolute value among the reactants (negative b_i 's) and the upper limit is the quotient having smallest absolute value among the products (positive b_i 's). Furthermore, the value of the right side of (D) changes monotonically as x is changed between these limiting values. Half their difference is therefore taken to define a starting value of a computation variable z and an initial value of x is set up equal to $z + (X_i^0/b_i)^*_{R}$. Values of X_i^0 are replaced with $X_i^0 + b_i y = X_i^0 - b_i x$ and the discrepancy, D_i , is computed (see Iteration Procedure). If D_i comes out +, the next value of x is set to be $+z$ (which in the meanwhile has been divided by

2); if D_i comes out $-$, x is set to equal $-z$. The procedure is repeated as many times as is necessary to get $|D_i| - F < 0$.

In the present work, solutions of the individual equilibria were carried out using the simplifying assumption that y in equation (D) is negligible compared with S . It is believed that avoidance of this assumption would have shortened the calculations only to a minor extent.

It is recommended that F , the subiteration error, be set an order of magnitude smaller than E , else there may be danger of an infinite loop occurring. Furthermore, E should not be specified with too small a value such that it represents digits beyond those carried by floating point numbers.

Extension to Additional Elements.—The exten-

sion of the present procedure to include additional (chemical) elements is quite simple. The first step, of course, is to decide which are the important reactions. Usually an estimate will be available from previous work as to the most reasonable species to choose as components. Then, after rewriting the chemical equations to correspond to reactions of formation of the other species from the components, one need merely provide for inclusion of the additional data and code in appropriate calling sequences for the new reactions. It is proposed to carry out such extensions in subsequent work.

Availability of Program.—The author will be pleased to reproduce a copy of the program for any one wishing to see it.

EXPERIMENTS WITH THE CELL Bi, Bi₂O₃, ZnCl₂/ZnCl₂/ZnCl₂, Zn BETWEEN 450 AND 510°

By REUBEN E. WOOD

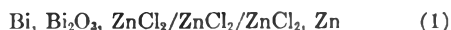
National Bureau of Standards, Washington 25, D. C.

Received July 21, 1958

As a part of a study of cells having a fused zinc chloride electrolyte, experiments were carried out on such a cell in which the negative electrode was liquid zinc and the positive electrode was liquid bismuth on top of which had been put some Bi₂O₃. The cell potentials are quite rapidly and accurately reproducible after temperature changes and after the passage of current. The cell potentials and temperature coefficient are reported. Phase equilibria in this system may be rather complicated and have not yet been studied.

Introduction

The calomel electrode has long been of interest and utility as a reference electrode in aqueous electrochemistry, but it is difficult to devise a close, fused-salt analog of this electrode because of the relatively high mutual solubility of the metal halides. As a possible basis for a satisfactory fused-salt reference electrode, similar if not exactly analogous to the aqueous calomel electrode, the use of bismuth and bismuth oxychloride in a suitable fused halide electrolyte suggested itself. The cell that was assembled and studied to test this idea may be represented as



What solid phases are present at the bismuth electrode when this cell is operating reversibly is not yet known. It seems unlikely that they include Bi₂O₃, more likely that they include bismuth oxychloride and zinc oxide or zinc oxychloride. In fact, although he did not report studies of systems containing zinc, Sillén's work¹ on two-metal oxyhalide compounds suggests the possibility that reaction between zinc chloride and bismuth and zinc oxides could produce a series of double oxychlorides. However, the above representation is used for the cell to indicate that Bi₂O₃ and the other substances shown were the only ones put into the cell. This cell was studied over the temperature range 450 to 510° and over a period of several weeks.

(1) L. G. Sillén, *Naturwissenschaften*, **30**, 318 (1942).

Apparatus and Procedures

The cell system used was similar to the conventional H cell except that there were three vertical tubes and two cross connections between each outside vertical tube and the middle vertical tube. The two lower cross connections provided the electrolyte path between the electrodes, the upper cross connections permitted the passage of helium which was maintained as an inert atmosphere above the cells. The purpose of having three vertical tubes was to allow the use of two Zn-ZnCl₂ reference electrodes against which to measure the potential of the bismuth electrode. One of these zinc reference electrodes was in the center tube, the other was in one of the outside tubes.

At the bottom of each vertical tube were approximately 4 ml. of molten metal, zinc in two tubes, bismuth in the other. 2.4 g. of Bi₂O₃ was placed above the bismuth and then about 100 g. of liquid ZnCl₂ was introduced into the cell. A glass-enclosed thermocouple junction dipped into the molten metal of each electrode. Electrical connection was made to the molten metals through graphite rods introduced into the cells through side arms so that these rods were not in contact with the electrolyte. Reagent-grade chemicals were used exclusively except that the zinc was an especially pure product asserted by the manufacturer to be 99.99% pure. The zinc chloride was dried by bubbling anhydrous HCl through it at about 500° for 10 hours, then dried oxygen for about two hours.

The cell was kept hot in a cylindrical electric furnace. This furnace was supplied with current from a constant-voltage transformer through a variable resistor system. No automatic temperature regulator was used but because of the constancy of power input and of the room temperature, the temperature conditions within the furnace remained quite static as long as it was undisturbed and the resistance was not changed. Under such conditions, gradual temperature variations at the rate of 0.5° per hour would be typical.

All potentials were measured with a Type K potentiometer using a standard cell calibrated in these laboratories. The thermocouples were calibrated only at the melting

point of zinc. The deviation from standard tables² found at this temperature (about 1.5°) was assumed to represent a satisfactory correction over the temperature range of these experiments to within the probable accuracy of the values of E and dE/dT reported here.

Experiments and Observations

The electrolyte over the bismuth electrode had the pale pink to lavender color which has been found to characterize all such electrodes. This is presumably the color of some bismuth-containing ion.

The potential difference observed between the two zinc electrodes was about 0.15 millivolt a few hours after the cell was assembled, and it gradually increased to about 0.45 millivolt during a period of two weeks. It varied between 0.41 and 0.52 millivolt during the next two weeks, at the end of which time the cell was disassembled. Temperature differences of as much as three degrees were observed from time to time among the three electrodes. By changing the position of the cell in the furnace the relative temperatures of the electrodes with respect to each other could be changed. However, whether the two zinc electrodes were at nearly the same temperature or whether the middle electrode was two degrees hotter or two degrees colder than the other one, the middle electrode was always negative with respect to the outer one, and any changes in the magnitude of this potential difference resulting from such temperature changes could not be distinguished from the random fluctuations of this potential difference within the ranges already stated. It was concluded from these facts that the temperature of the zinc electrodes had relatively little influence on the cell potentials.

In view of this conclusion, although the temperatures of all three electrodes were measured regularly only those of the bismuth electrode are recorded in Table I. The potentials recorded in Table I are those of the cell comprising the bismuth electrode and the outside zinc electrode. The zinc electrode is negative with respect to the bismuth electrode, of course. The outer zinc electrode was chosen as reference electrode for purposes of this tabulation mainly because contamination by diffusion from the bismuth electrode should have been less at the outer electrode than at the middle one. It may be borne in mind, however, that the choice is not very important because the maximum difference ever observed between the two zinc electrodes was 0.52 mv.

It was found that the potential of the cell could be represented by the equation

$$E = 0.6727 - 0.00055(t - 450) \quad (2)$$

where the potential is in volts and t is the temperature in degrees centigrade. The last column in Table I represents the deviation of the measured value from the value that would be calculated by this equation. Many more readings than those included in the table were recorded. The values are representative. They were chosen by the arbitrary rule of taking the last measurement on the indicated day or, on days when the furnace current was readjusted, the last reading before this readjustment.

The potentials of the Bi, Bi₂O₃, ZnCl₂/ZnCl₂/ZnCl₂, Zn cell were very steady and easily measurable to one hundredth of a millivolt. As can be seen from the data in Table I and from equation 2, the cell temperature coefficient is large but the temperature effects are quite reproducible and reversible. Most of the readings recorded in Table I were made at least one day after any previous major temperature change. However, the cell potentials followed the temperature changes quite rapidly even without stirring. In two instances the potentials were read every few minutes while the temperature was changing at the rate of about 10° per hour. In one of these instances the temperature was rising, in the other it was falling. In neither case did the potential lag by more than a millivolt behind the values corresponding to equation 2. Stirring seldom was resorted to. It has

(2) "Reference Tables for Thermocouples," Circular 561, National Bureau of Standards, 1955.

TABLE I
CELL POTENTIALS AT VARIOUS TEMPERATURES

Days ^a	t , °C.	$E_{\text{obsd.}}$, v.	$E_{\text{calcd.}}$, ^b v.	$\frac{E_{\text{obsd.}} - E_{\text{calcd.}}}{\text{mV.}}$
10	507.9	0.64029	0.6408	-0.5
11	509.0	.64066	.6402	+ .5
12	504.7	.64182	.6426	- .8
13	507.4	.64131	.6411	+ .2
14	507.6	.64158	.6410	+ .6
15	482.0	.65434	.6551	- .8
16	480.3	.65543	.6560	- .6
17	481.1	.65504	.6556	- .6
19	480.6	.65613	.6559	+ .2
21	452.1	.67167	.6716	+ .1
22	464.2	.66494	.6649	0
22	473.2	.66033	.6600	+ .3
23	482.6	.65431	.6548	- .5
24	491.1	.64983	.6501	- .3
26	500.4	.64590	.6450	+ .9

^a Since cell was assembled. ^b Calculated by equation 2.

the disadvantage of promoting diffusion of bismuth ions and temporarily aggravating the effect of any vertical temperature gradients in the furnace. When necessary, the stirring was done without exposing the electrodes to air. The potential of the bismuth electrode always fell with stirring. This may have been due at least in part to temporary unsaturation of the solution at the bismuth surface by dilution with unsaturated electrolyte from above. In any case, normal potential values (values consistent with equation 2) were restored within less than one-half hour after stirring.

The cell appears to be relatively non-polarizable. In one experiment a load of 1000 ohms was connected between the bismuth electrode and the adjacent zinc electrode. The potential difference between the bismuth electrode and the remote zinc electrode was observed. Before the load was applied this potential difference was 0.645 volt. Immediately upon application of the load it fell to 0.439 volt. It fell only 0.002 volt further during the 40 minutes the load was left on. Within one minute after the load was removed the measured potential difference had gone back to 0.644 volt. The temperature at the start of this experiment was 501° and it fell by about one-half degree during the experiment. The current drawn by the load was 0.42 ma. and the electrode current density about 0.25 ma. cm.⁻².

Summary

Until the phase equilibria in the system Bi-Bi₂O₃-ZnO-ZnCl₂ have been studied it would seem impossible to relate the cell potentials reported here to free energies and entropies of formation. The following two statements summarize the conclusions to which these experiments lead.

1. The measured potentials of the cell Bi, Bi₂O₃, ZnCl₂/ZnCl₂/ZnCl₂, Zn are reproducible with respect to temperature changes and after the flow of current. The reversible E of this cell at 450° is 0.6727 ± 0.0010 volt and $dE/dT = -0.00055 \pm 0.00001$ volt deg.⁻¹.

2. Within the stated temperature range at least, either electrode of this cell should serve as a reliable reference electrode in cells whose electrolyte is mainly fused zinc chloride.

Acknowledgment.—This work was done under a research contract with the Office of Ordnance Research, Ordnance Corp, U. S. Army.

STRUCTURE AND GAS PERSORPTION SITES OF A SYNTHETIC ZEOLITE DETERMINED BY FOURIER RADIAL ANALYSIS

BY P. H. LEWIS

Contribution from the Texaco Research Center, Beacon, New York

Received July 24, 1958

Distances between persorbed gas molecules, exchanged metal ions and the aluminosilicate framework determined by Fourier radial analysis are used to obtain the crystal structure common to the 4 and 5 Å. Linde synthetic zeolites. A cage structure, formed by 8-membered aluminosilicate rings on the faces of a 12.30 Å. cubic unit cell, confirms the previously reported work of Reed and Breck. In contrast to their work, metal ions are found to be situated on the axes of these rings, 2.5 Å. from the ring planes. In the 5 Å. zeolite, gases, for which hydrogen bonding is possible, occupy the centers of the octagonal rings; CO₂, H₂S and *n*-C₆H₁₃Br locate in the center of the cage. In the 4 Å. zeolite only H₂S occupies the center of the cage; CO₂, NH₃ and H₂O lie in the center of the octagonal rings.

Introduction

In early 1955 an X-ray study was begun to determine the distances between persorbed gas molecules, metal cations and the aluminosilicate framework of two Linde synthetic zeolites, useful as molecular sieves.¹ X-Ray powder photographs, used because no single crystal X-ray data were available, showed that the two zeolites were isomorphous and simple cubic. For materials of this crystal class a relatively large number of X-ray lines have other lines with different Miller indices superposed on them so Fourier projection methods, which depend on the intensities of discrete reflections, therefore could not be used. Differential radial analysis,² which does not require discrete X-ray reflections, therefore was applied to the intensity changes of diffraction lines in powder photographs of the zeolites caused by gas persorption or exchange of the metal cations. These analyses gave the scalar distances between the gas molecules and the metal cations introduced into the zeolite and its aluminosilicate framework.

It soon was realized that these distances in combination with known bond distances could be used to determine the skeletal structure of this aluminosilicate framework, that is, the structure exclusive of oxygen ions. The method for doing this might prove useful to others. The skeletal structure, independently found, subsequently was confirmed by publication by Reed and Breck³ who applied Fourier projection analysis to the discrete X-ray reflections from a rather small single crystal. The positions of the replaceable metal cations determined by the two methods are not the same.

The method of using radial analysis data for determining the structure, the positions of the replaceable cations and the positions that persorbed gas molecules occupy will be discussed in the remainder of the paper.

Experimental

A. Materials.—Type A zeolite materials, described as having effective channel widths of 4 and 5 Å. for persorption, were obtained from the Linde Air Products Company. Commercially available gases and liquids were used without further purification.

B. Properties.—The density of dehydrated 4 Å. zeolite,

1.73 g./cm.³, was determined by liquid displacement using xylene which cannot penetrate the zeolite crystals. Knowing this density, the mass contained within the cubic unit cell of lattice constant 12.30 Å. can be determined. This gives the number of molecules of Na₂O·Al₂O₃·2SiO₂ per unit cell as 6, the relative amounts of sodium, aluminum and silicon being established by chemical analysis. Similarly, the content of the isomorphous 5 Å. zeolite unit cell is 2Na₂O·4CaO·6Al₂O₃·12SiO₂.

C. Apparatus.—X-Ray data were obtained using a Philips Electronics source unit equipped with voltage and current stabilizers. Iron-filtered cobalt radiation (λ 1.7902 Å.) was employed. The samples were mounted on a Philips Electronics diffractometer equipped with a Geiger counter run at 1° (2θ) per minute and diffraction data were recorded graphically, the integration time constant being two seconds. The powder samples were spread on top of a simple, flat, wire wound heating unit with a gas tight enclosure equipped with Mylar windows.

D. Procedure.—Room temperature X-ray patterns were obtained after drying the sample at 300° for 30 minutes in a nitrogen stream and then 30 minutes after exposure at room temperature to the sample gas. The conditions are adequate for drying or saturating the sample. Water and hexyl bromide were added to the sample by means of a saturated nitrogen stream; other gases were taken directly from gas cylinders. The potassium zeolite used in determining metal ion positions was obtained by allowing the sodium 4 Å. zeolite to stand in a dilute, aqueous potassium chloride solution for 24 hours at room temperature. The exchange is 60–70% complete. The patterns of the ion exchanged zeolites studied in both the dry and wet states led to the same results for the positions of the metal ions.

E. X-Ray Analysis.—The peak values of the diffraction maxima corrected for background *I*_i were measured at Bragg angles θ_i. The changes in these intensities Δ*I*_i were used in radial analyses of the form

$$4\pi R^2 D(R) = R \sum_i \frac{\Delta I_i \sin \theta_i}{1 - \cos^2 2\theta_i} \sin \left(\frac{4\pi \sin \theta_i R}{\lambda} \right)$$

modeled after Finbak's work.⁴ Here *D*(*R*) is the radial distribution function. The summations were performed at intervals of 0.5 Å. in the radial distance *R*. Intensity differences scaled to a maximum change of intensity of 100 are listed in Table I. The small differences in intensity at high angles make the use of a series termination correction unnecessary. The fact that intensity changes of the Bragg reflections are observed after gas persorptions shows that molecules occupy relatively fixed rather than random positions within the zeolite structure.

In order to obtain some experience with applying the radial technique to zeolite type materials, it was applied to the known structure of analcite.⁵ This showed that peaks on the radial distribution vs. distance plot corresponded to distances between centers of electron density of groups; i.e., oxygen in water, silicon and aluminum within their respective oxygen tetrahedra, etc. This led to some confidence in applying the radial technique to an unknown structure of a zeolite type.

(1) R. M. Barrer, *J. Soc. Chem. Ind.*, **64**, 130 (1945).

(2) J. S. Lukeah, *Proc. Natl. Acad. Sci.*, **28**, 277 (1942).

(3) T. B. Reed and D. W. Breck, *J. Am. Chem. Soc.*, **78**, 5972 (1956).

(4) C. Finbak, *Acta Chem. Scand.*, **3**, 1279, 1293 (1949).

(5) W. H. Taylor, *Z. Krist.*, **74**, 1 (1930).

TABLE I

Zeolite Persorbate Index	d, Å.	INTENSITY DIFFERENCES									
		4 Å. H ₂ O	4 Å. NH ₃	4 Å. CO ₂	4 Å. H ₂ S	5 Å. H ₂ O	5 Å. NH ₃	5 Å. CO ₂	5 Å. n-C ₆ H ₁₃ Br	5 Å. H ₂ S	4 Å. K ⁺ /Na ⁺
100	12.1	-100	-70	-38	-100	-100	-100	-100	-100	-100	-71
110	8.6	-91	-100	-100	-66		-17	-12	-15	-14	-100
111	7.06	-19	-13	-8	-19	-5		-13	-15	-14	-61
200	6.13					+11					
210	5.50	-59	-51	-24	-37	-16	-3	-8	-11	-10	-78
211	5.01	-4			-4	-5	-4	-5	-4	-5	+2.2
220	4.34	-2	-3	-3		-6	-7	-3		-3	-4.5
300, 221	4.09	-6	+6	-6	-11	+3	-4	-5	+4	-14	-28
311	3.70	-13			-26			+3	-4	-12	-57
222	3.55			-3		+3	+4		+4		+2.2
320	3.40	+15	+12		-1	+6	+8		+4	+1	+4.6
321	3.29	+13	+18	+9	-15	+6		-6	+13		
400	3.25					+15	+9				-4.6
410, 322	2.98	+14	+22	+3	-19	-6	+8	-3	+4	-21	-27
411, 330	2.90	+2	+3		-2	-3		-3		-3	
420	2.75	+7	+9	+3	-3	+6	+4	-3	+5	-2	+10
421	2.68	+3		-3	-1	-6		-3		-4	-2.4
332	2.62	+9	+6	+3	-15	+7		-3	+9	-23	-37
422	2.51	+3	+3		-1	+3				+4	+2.6
500, 430	2.46	-7	-7	-3	-3					-4	-22
511, 333	2.36	-3			-1	-7					-8.2
521	2.24	-3	+3	+4	-3		-5				-2.9
440	2.18	+3	-7	+4	-1			-3			-2.9
522, 441	2.14		+4	+4	-1	-4	-5	-3		-5	-8.6
530, 433	2.11				-3			-3			-8.6
531	2.08				-1	-4	+5			+6	-3.1
600, 442	2.05	+3		-4	-3	-4	-5	-3	+5	-12	-15
621, 540, 443	1.92				-4						-13
541	1.90				-4	-4	-5	-4		-3	-13
630, 542	1.83									+7	
631						+4					
710, 550, 543	1.74	-6		-4						-15	-23
711, 551	1.72		+4				+6				
720, 641	1.70	+3	+13		-7					-8	-10
721, 633, 552	1.67					-4				+8	-3.5
722, 544	1.63	+3	+4	-5	-2	+4		-4		+4	-3.5
731, 553	1.60	+3	+9		+2	-4		-4	+2		-11
650, 643	1.57	+3	+5		-2	-5			+6	-9	+3.7
800	1.54										
821, 742	1.48	+4				+5				+5	
653	1.47									+5	+3.9
822, 660	1.45				-3	+5				-5	
831, 750, 743	1.43			+5	-3						
832, 654	1.40		-5	+5	-3		-6		+7	-6	-12

Results

The differential radial analysis of water in the 5 Å. zeolite shown in Fig. 1 is a typical example. The ordinate was not scaled to electronic units. The peak at 0.5 Å., a physically impossible interatomic distance, is small indicating that intensity measurement errors are small. The peak at 2.0-2.5 Å. is about right for the distance between a water molecule and a metal ion, the ion-water distance in chabazite⁶ being 2.32 Å. The large peak at 4.0 Å. was interpreted to be the distance between the water molecule and nearest aluminosilicate tetrahedra. This assignment (rather than to a water molecule-calcium ion distance) was made because it was figured that there would be a relatively large number of silicate groups near the

water molecule. No use was made of the peaks at higher values of R in the preliminary analysis. Subsequently it was found that they are compatible with the determined structure. The assignment of the first two radial peaks was made in the same fashion for a number of persorbed gases in both the 4 and 5 Å. zeolites and for the potassium ion exchanged 4 Å. zeolite, the results being given in Table II.

In the 5 Å. type zeolite the molecules most capable of forming hydrogen bonds, H₂O and NH₃, are located nearest to the aluminosilicate tetrahedra in contrast to *n*-C₆H₁₃Br (the center of electron density of this molecule is 3.34 Å. from the bromine atom along the chain axis), H₂S and CO₂. In the 4 Å. zeolite both H₂S and CO₂ appear to be closer to the aluminosilicate tetrahedra than in the 5 Å. zeolite.

(6) J. Wyart, *Bull. Soc. Min. Fr.*, **56**, 81 (1933).

TABLE II
RADIAL DISTANCES, R_{AB}

A	B	Zeolite, Å.	Distance, Å.
H ₂ O	Ca, Na	5	2.0
H ₂ O	Si, Al	4, 5	4.0
H ₂ O	Na	4	2.0
NH ₃	Ca, Na	5	2.0
NH ₃	Na	4	2.0
NH ₃	Si, Al	4, 5	4.0
Na	Si, Al	4	5.0
H ₂ S	Si, Al	5	6.5
H ₂ S	Ca, Na	5	2.5
H ₂ S	Si, Al	4	5.5
H ₂ S	Na	4	2.5
<i>n</i> -C ₆ H ₁₃ Br	Si, Al	5	7.0
<i>n</i> -C ₆ H ₁₃ Br	Ca, Na	5	3.5
CO ₂	Ca, Na	5	2.0
CO ₂	Si, Al	5	6.0
CO ₂	Si, Al	4	4.5
CO ₂	Na	4	3.0

Structure Determination

The radial analysis results in Table II can be represented geometrically as a collection of spheres. The center of each sphere is occupied by a persorbed molecule or exchanged cation. The aluminum and silicon neighbors to these are located somewhere on the surfaces of these spheres, or more exactly at the intersection of the spheres.

The scalar distances between the centers of the spheres are known from the radial analyses, but the relative orientation of these spheres needed to locate the aluminum and silicon neighbors must be devised. It was assumed that the aluminum and silicon ions of the zeolite form rings as in chabazite⁶ and sodalite⁷ and that the persorbed molecules and cations occupy sites on the axes of these rings. The validity of these assumptions is to be tested by the consistency of the results obtained. The analysis then reduces to the planar figure shown in Fig. 2. The aluminum and silicon ions lie on the circle whose plane is perpendicular to the plane of the paper and passes through the intersection of the three circles shown. Examination shows that the intersection is not perfect, small triangular figures being formed. Adjustments of a few tenths of an ångström of each radius would make the intersection perfect. The diameter of the circle on which the aluminum and silicon ions lie is 8.5 Å., reckoned between the centers of the small triangular areas. It is recognized that the determination of this diameter with three sets of data is overdone in that the intersection of but two circles is required. By overdoing the determination one sees that the assumptions lead to consistent results and one can appraise the experimental error.

The diameter of this circle passing through the aluminum and silicon atoms in the ring is somewhat larger than that of the hexagonal ring found in chabazite⁶ or sodalite,⁷ about 6 Å., and is close to that calculated for an octagonal figure, 8.1 Å., using the fact that in chabazite,⁶ 2.90 Å. sides alternate with 3.30 Å. sides in the hexagon. Density, lattice constant and chemical analysis data show

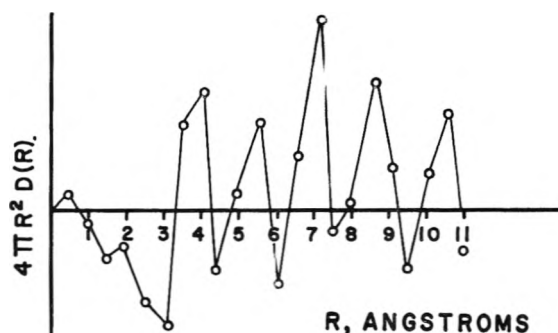


Fig. 1.—Radial analysis of H₂O in 5 Å. zeolite.

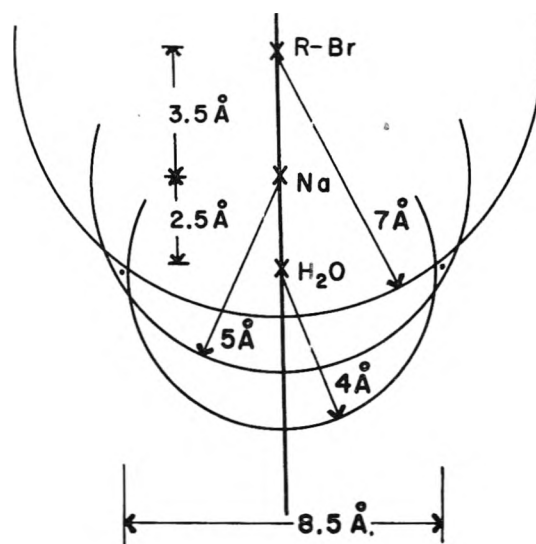


Fig. 2.—Analysis of radial analysis results.

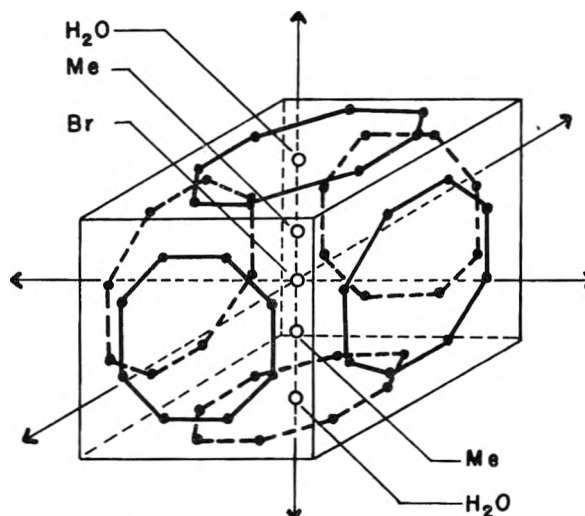


Fig. 3.—Structure of type A zeolite.

that there is a total of 24 aluminum and silicon ions per unit cell. A structure with 8-membered rings on the 6 faces of the cubic unit cell is consistent with all these data. It was encouraging that such 8-membered rings are known to exist in silicate structure.⁸

(7) L. Pauling, *Z. Krist.*, **74**, 213 (1930).

Discussion

The skeletal structure of the aluminosilicate framework common to the 4 and 5 Å. zeolites is shown in Fig. 3. Aluminum and silicon ions form 8-membered rings on the six faces of the cubic unit cell. Channels through which persorbed molecules diffuse are indicated by the arrows. To avoid confusion the sites that replaceable cations and persorbed molecules occupy are shown in only one of the three channels.

Only a fraction of the metal cations can be easily exchanged.³ Only the positions of these were determined in this radial analysis study. The positions suggested by Reed and Breck for the more fixed metal cations are consistent with the radial analysis results. The replaceable metal ion positions (Me in Fig. 3) are different from those of Reed and Breck.³ These authors place metal ions in the planes of the octagonal ring rather than on the ring axis, 2.5 Å. from the plane as found in this work. The radial data also indicate that at least some of these metal ion sites are occupied in both the 4 and 5 Å. zeolites. The difference in the size of molecule that can be persorbed in these is due to a lower probability of a molecule encountering metal cations on both sides of the octagonal ring in the 5 Å. zeolite than in the 4 Å. one.

The two proposed metal cation positions may be compared by determining the distances from them to the oxygen atoms located by Reed and Breck. The distance from these to the metal ion position in the plane of the ring is 2.1 Å., smaller than the 2.4 Å. calculated using ionic radii. The distance to the metal position outside the ring plane is 4.0 Å. Some basis for comparison can be established by examining metal ion-oxygen distances in known zeolite structures. In chabazite⁶ this distance is either 3.05 or 3.18 Å.; in sodalite⁷ 2.39 or 3.10 Å. These data favor a larger than calculated distance.

The following must be borne in mind in discussing the positions that gas molecules adopt in the zeolites. The data of Reed and Breck³ show that of the order of 20-30 gas molecules can be persorbed in a zeolite cage. The radial analysis results show that only the positions of a few of these affect X-ray line intensities. The rest move about the cage in a completely random way characteristic of a liquid. One would say the residence time of one of these molecules in any one position is very small. What

is being detected with the diffraction data are the few positions in which gas molecules have a relatively long residence time. Exchange between gas molecules occupying these sites and those in random motion is to be expected. Re-examination of Fig. 1 shows something else. It is true that the peaks at 4.0 and 7.0 Å. can be attributed to radial distances from a water molecule in a ring center to the aluminum and silicon ions of the cage. It is, however, difficult to tell whether the second peak might also be due to a water molecule 7.0 Å. or so from the aluminum, silicon ions of the cage, that is a water molecule located in the center of the cage. On the other hand, if the data indicate positioning of a molecule in the center of the cage, the possibility of location in the ring center is precluded.

Instead of the metal ions occupying the plane of the ring the work shows that H₂O and NH₃ molecules locate in the ring center (see Fig. 3). This seems entirely reasonable, for the tendency to locate in a site where hydrogen bonds can be formed in 16 directions should be enormous. Interatomic distances are reasonable for such a location, these molecules being 3.4-3.7 Å. from the Reed and Breck oxygen positions. The oxygen-oxygen distance is 3.4 Å. in calcium hydroxide⁹ and 3.50 Å. in analcite.⁵ The distance from H₂O or NH₃ to the metal ion is 2.5 Å., close to the 2.4 Å. expected. Nearness to these metal ions also seems to stabilize the position of H₂O and NH₃ in the ring.

In the 5 Å. zeolite H₂S, CO₂ and C₆H₁₃Br locate in the center of the aluminosilicate cage. This site is indicated by Br in Fig. 3. This is a site surrounded by 6 metal ion positions (not all occupied) about 3.5 Å. away. The reason for preferred location in such a site is not clear. Perhaps maximum coordination with metal ions is a factor. In contrast, CO₂ locates in the position central to the octagonal rings of the 4 Å. zeolite. Steric effects account for this. Molecules of H₂S for which steric effects would be smaller locate in the center of the cage.

Acknowledgment.—The author is indebted to Dr. L. C. Roess, R. P. Eischens, E. E. Sensel and members of the Physical Research Department of the Texaco Research Center for their helpful advice in preparing this paper. Mr. D. McNelly helped obtain the X-ray data and run the Fourier summations.

(8) W. L. Bragg, "Atomic Structure of Minerals," Cornell Univ. Press, Ithaca, N. Y., 1931, p. 144.

(9) R. E. Rundle and M. Parasol, *J. Chem. Phys.*, **20**, 1487 (1952).

THE AGREEMENT BETWEEN INDEPENDENT METHODS FOR PARTICLE SIZE DISTRIBUTION MEASUREMENTS ON FINELY DIVIDED POWDERS INCLUDING PHOSPHATES

By D. P. AMES, R. R. IRANI¹ AND C. F. CALLIS

Research Department, Inorganic Chemicals Division, Monsanto Chemical Company, St. Louis 24, Missouri

Received August 8, 1958

The particle size distributions of various powdered substances as measured by a microscopic electronic sizing and counting technique and by an automatized liquid sedimentation balance are shown to exhibit log normal distribution behavior. The results of these two independent methods are shown to agree with the predicted values based on the transformations involving log normal distribution behavior. Screen analysis is critically evaluated. The geometric mean diameters on a weight basis, M_g , for the samples investigated are in the size range 4–70 μ . The geometric standard deviations, σ_g , of these samples are found to lie between 1.3 and 3.5. The average deviation between the observed and calculated M_g and σ_g values are 6 and 5%, respectively.

Introduction

The interest in the measurement of particle size distributions has increased over the past few years²⁻⁸ due to the necessity for better characterization of powdered materials. This study was initiated in order to correlate independent methods for these measurements. In addition to making it possible to evaluate the soundness of these methods, such a correlation would further test the mathematical transforms involving log normal distribution.⁹⁻¹³ The methods chosen for this correlation are direct sizing and counting, liquid sedimentation and screen analysis.

The search for a direct sizing and counting method revealed that particle size distributions could be obtained automatically using flying spot scanning.^{6,14} Flying spot scanning is a method of converting a two dimensional density distribution into a varying voltage-time relationship. An intense light spot slowly scanning a cathode ray tube is optically imaged down through a conventional microscope. This imaged down light spot scans a fixed microscopic field. The transmitted spot intensity alteration as received by a photomultiplier is amplified, counted and monitored. Particle sizing is performed by pulse width selection; all pulses below the preset size are not recorded during the count.

Since the determination of particle size distributions by liquid sedimentation and screen analysis has been thoroughly reviewed by various authors,²⁻⁸ no additional description is necessary.

(1) Presented at the September, 1958, meeting of the American Chemical Society in Chicago.

(2) "Symposium on Particle Size Analysis," Suppl. to Trans. Inst. Chem. Engrs. (London), 1947.

(3) J. M. Dalla Valle, "Micromeritics," 2nd Ed., Pitman Publishing Co., New York, N. Y., 1948.

(4) G. Herdan, "Small Particle Statistics," Elsevier Publishing Co., New York, N. Y., 1953.

(5) J. J. Hermans, "Flow Properties of Disperse Systems," Interscience Publishers, Inc., New York, N. Y., 1953.

(6) "Conference on the Physics of Particle Size Analysis," Suppl. No. 3, *Brit. J. Appl. Phys.*, 1954.

(7) H. E. Rose, "The Measurement of Particle Size in Very Fine Powders," Chemical Publishing Co., New York, N. Y., 1954.

(8) R. D. Cadle, "Particle Size Determination," Interscience Publishers, Inc., New York, N. Y., 1955.

(9) H. Green, *J. Franklin Inst.*, **204**, 713 (1927).

(10) T. Hatch and S. P. Choate, *ibid.*, **207**, 369 (1929).

(11) T. Hatch, *ibid.*, **215**, 27 (1933).

(12) F. Kottler, *ibid.*, **250**, 339 (1950).

(13) F. Kottler, *ibid.*, **251**, 617 (1951).

(14) J. Z. Young and F. Roberts, *Nature*, **167**, 231 (1951).

Experimental

Sources of Materials.—All powdered samples investigated in this work were Monsanto preparations except for the glass beads, which were procured from the Minnesota Mining and Manufacturing Company. The solvents used as dispersion fluids were standard C.P. grade and no further purification was performed.

Procedures.—The particle number size distribution measurements were made with a Flying-Spot Particle Resolver manufactured by Cinema Television (Cintel) Co. Ltd. (London).¹⁴ The microscope utilized as an integral component of the resolver is a Baker Model 4, and the apochromatic optics were purchased from Bausch and Lomb Optical Company. Prior to making the measurements, the powder must be dispersed on a microscope slide. These dispersions were obtained by one of the following methods: (1) touching a powder coated brush to a clean slide, (2) evaporating the solvent from a liquid dispersion, (3) counting the particles as a dispersion on a covered slide. The instrument calibrations¹⁴ were checked (Fig. 1) by visually sizing and counting several powders as given by ASTM Designation E 20-51T, 1951. The resolving power of the "Cintel" is 0.6 μ and is a stable characteristic.

The reproducibility of the count and size measurements as obtained by the Flying-Spot Resolver is shown in Table I. Triplicate counts of different representative microscopic fields were made in all of the reported cases in this article.

TABLE I
CINTEL FLYING-SPOT RESOLVER REPRODUCIBILITY WITH
DICALCIUM PHOSPHATE DIHYDRATE^a

M_n (μ)	σ_n	Total no. of particles counted
2.28	2.07	940
2.68	2.00	680
2.58	1.98	720
2.78	1.96	1040
2.54	1.94	800
2.53	2.10	750
2.45	2.05	820
2.67	2.06	690
2.52	2.11	700
2.77	1.93	780
Av.	2.02	790
% stand. dev.	± 5.5	± 3.0

^a M_n and σ_n have the same meaning as defined by equations 5 and 6.

The particle-weight size distribution measurements were made by a Bostock¹⁵ type liquid sedimentation balance. The balance, manufactured by A. Gallenkamp and Company (London), was modified in order to omit the required continuous operator attention. The modifications are: (1) the core of 033S-L Schaevitz¹⁶ linear variable differential

(14) W. K. Taylor, page S173 of ref. 6.

(15) W. Bostock, *J. Sci. Instr.*, **29**, 209 (1952).

(16) Schaevitz Engineering, Camden, N. J., Bulletin AA-1A.

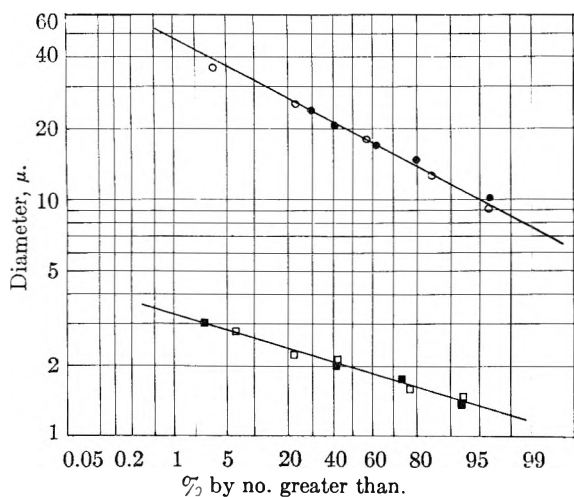


Fig. 1.—Cintel calibration check on two apatite sand samples: ○, Cintel data, sample 1; ●, microscopic counting based upon ASTM E20-51T, 1951, sample 1; □, Cintel data, sample 2; ■, microscopic counting based upon ASTM E20-51T 1951, sample 2.

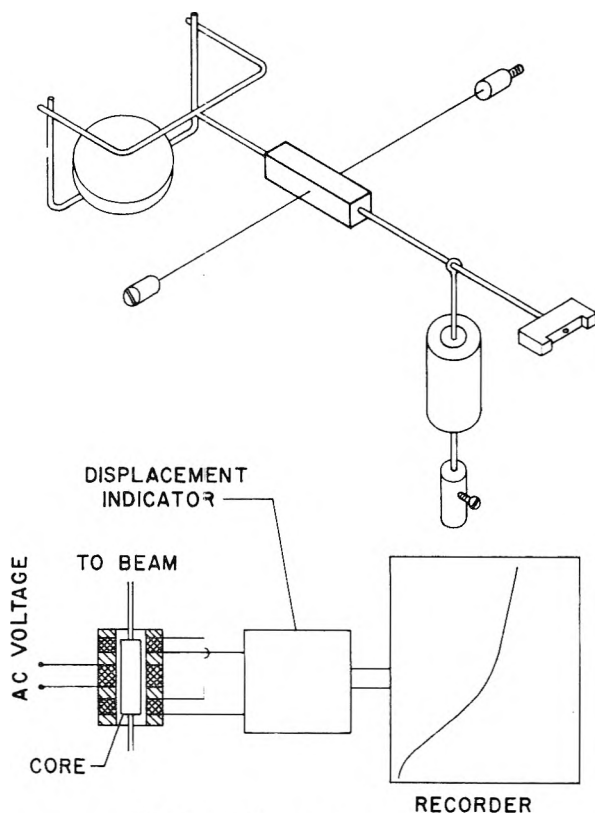


Fig. 2.—Sedimentation apparatus.

transformer is fastened to the balance beam, while the transformer body is attached to the balance assembly housing; (2) the output of the transformer secondary coils is amplified with a Daytronic¹⁷ Model 300 Displacement Indicator and recorded on a 0-100 MV Brown Electronik Minneapolis Honeywell recorder with the proper chart speed; (3) two solenoids and a sequence switching arrangement are installed to facilitate the operation of the balance and (4) the original aluminum balance pan was replaced with a stainless steel pan to avoid aluminum dissolution in alkaline media. The block diagram of the modified balance is shown in Fig. 2.

For the sedimentation experiments, the dispersions were obtained by the gradual dilution of the weighed sample powder, and examined microscopically to verify the de-

agglomeration of the powdered particles. The volume fraction of the powder in the dispersion was not allowed to exceed 0.2%. The inter-agreement in the particle size data when different solvents are employed further proves that proper deagglomeration is achieved (see Fig. 3). The reproducibility of a typical weight size measurement is shown in Table II. The particle densities were measured pycnometrically,¹⁸ and the fluid densities and viscosities were obtained from the International Critical Tables.

The screen analysis was performed with standard U. S. Screens and a "Ro-Tap Sieve Shaker."

TABLE II
THE REPRODUCIBILITY OF THE SEDIMENTATION APPARATUS WITH ANHYDROUS MONOCALCIUM PHOSPHATE IN ISOBUTYL ALCOHOL^a

$M_g(\mu)$	σ_g
43.3	1.48
41.8	1.58
43.1	1.45
40.9	1.55
41.8	1.58
43.5	1.60
41.8	1.62
39.2	1.58
43.1	1.67
39.3	1.70
Av.	41.8
% stand. dev.	±3.9
	±4.8

^a M_g and σ_g have the same meaning as defined by equations 5 and 6.

Treatment of the Data

The liquid sedimentation data were interpreted to give particle size distributions by the methods outlined by Oden¹⁹ and modified by Bostock¹⁵

$$W = P - \frac{dP}{d \ln t} \quad (1)$$

where P is the settled weight at time t , and W is the weight of that fraction of settled particles whose diameter d would allow sedimentation through the entire height of the column h as given by Stokes' equation

$$d = \sqrt{\frac{18\eta h}{(\rho_1 - \rho_2) g t}} \quad (2)$$

η and ρ_2 are the viscosity and density of the sedimentation fluid, respectively, g the acceleration due to gravity, and ρ_1 the particle density. For some of the powders investigated in this work, it was shown that the particle density is independent of particle size.

It was found that the recorder reading in the sedimentation set-up is linearly proportional to the settled weight; thus, it can be shown easily that the recorder reading may be used directly to calculate the size data without converting to actual weight.

Since the Flying-Spot Particle Resolver gives the number of particles greater than a chosen diameter, the various percentages of these particles readily are calculated by normalizing the total number of counted particles.

Results and Discussion

Electronic Sizing and Sedimentation Compari-

(18) F. Daniels, J. H. Mathews, J. W. Williams and Staff, "Experimental Physical Chemistry," 4th Ed., McGraw-Hill Book Co., Inc., New York, N. Y., 1949, p. 430.

(19) S. Oden, *Proc. Roy. Soc. Edinburgh*, **36**, 219 (1915).

(17) Daytronic Corporation, Dayton, Ohio.

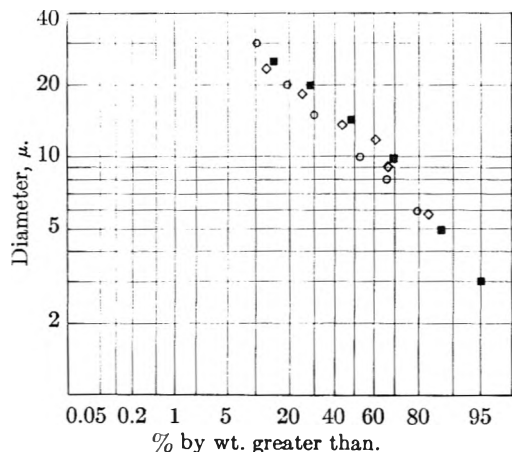


Fig. 3.—Insoluble sodium metaphosphate: O, sedimentation in ethyl alcohol; ■, sedimentation in hexane; ◇, sedimentation in isobutyl alcohol.

son.—The size frequency relationship of powdered substances ordinarily can be represented by a log-normal distribution

$$f(d) = \frac{1}{\sqrt{2\pi} \log \sigma} \exp\left[-\frac{1}{2} \left(\frac{\log d - \log M}{\log \sigma}\right)^2\right] \quad (3)$$

where $f(d)$ represents the probability of occurrence of a diameter d , and M is the geometric mean diameter

$$\sum_{d=0}^{\infty} f(d) = 1 \quad (4)$$

$$\log M = \frac{\sum n_i \log d}{\sum n_i} \quad (5)$$

The geometric standard deviation σ can be represented by

$$\log \sigma = \left[\frac{\sum n_i (\log d - \log M)^2}{\sum n_i} \right]^{1/2} \quad (6)$$

Furthermore, it can be shown readily from the following definite integrals that M may be evaluated by locating on a log probability plot, *e.g.*, Fig. 1, the diameter above which 50% of the particles lie; whereas, σ represents either of the ratios in equation 9

$$\int_0^M f(d) d \ln d = 1/2 \quad (7)$$

$$\int_{M\sigma}^M f(d) d \ln d = \int_M^{M/\sigma} f(d) d \ln d = 0.3413 \quad (8)$$

$$\sigma = \frac{\text{diameter at 15.87\% cumulative oversize}}{M} \quad (9)$$

$$= \frac{M}{\text{diameter at 84.13\% cumulative oversize}}$$

The geometric mean diameters on a number and weight basis, M_n and M_g , respectively, have been shown to be interrelated¹¹

$$\ln M_g = \ln M_n + 3 \ln^2 \sigma_n \quad (10)$$

It should be noted from equation 10 that the errors in M_n and σ_n are magnified when computing M_g .

Table III shows that the calculated values of M_g according to equation 10 agree very well with the measured ones for various powders. In addition, σ_g and σ_n are identical.

It is interesting to note that the majority of the particles for the calcium phosphates lie in the sub-

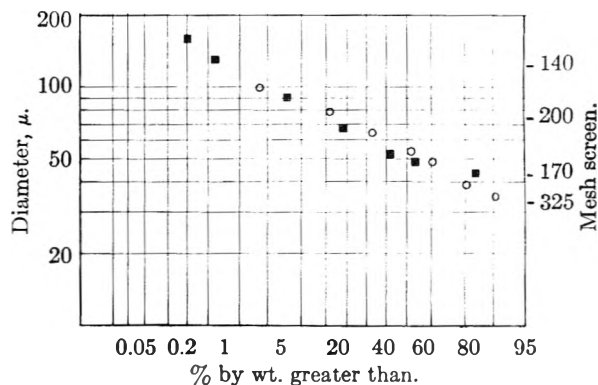


Fig. 4.—The particle size distribution of a sodium isethionate: □, screen analysis; ●, sedimentation data in 2-ethylhexanol.

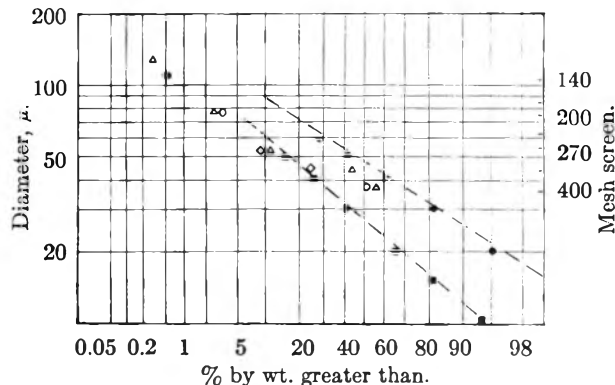


Fig. 5.—The comparison between screen analysis and the more precise methods on anhydrous monocalcium phosphate. Screening: ◇, sample no. 18; △, sample no. 3 sedimentation in isobutyl alcohol; ■, sample no. 18; ○ sample no. 3 --- Cintel data converted to weight.

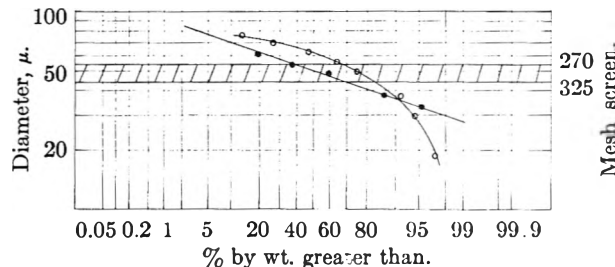


Fig. 6.—Screen classification: O, sedimentation data in 2-butanol for -270 mesh, +325 mesh anhydrous monocalcium phosphate; ●, sedimentation data in 2-ethylhexanol for -270 mesh, +325 mesh sodium isethionate.

sieve range with the exception of monocalcium phosphate monohydrate which has an M_g and σ_g of 71.5 μ and 3.54, respectively. For tricalcium phosphate, with an M_g of 4.4 μ , it was not feasible to employ sedimentation techniques due to the failure of Stokes' law for extremely fine particles.⁷

All the powders that were investigated in this work did not differ markedly from sphericity. Unless this was true an agreement between the sedimentation and the electronic sizing technique would not be expected; the sedimentation technique yields particle size by computing the diameter of a sphere that falls with the same velocity as the particle, while the direct counting technique yields a random average of the projections of diameters of a particle resting under equilibrium.

TABLE III
 AGREEMENT BETWEEN PARTICLE SIZE DISTRIBUTIONS FROM SEDIMENTATION AND ELECTRONIC SIZING

Powder	Dispersion fluid	Measured		Measured		Calcd. ^b	
		M_n^a	σ_n	M_g^a	σ_g	M_g^a	σ_g
Sand	Water	5.3	1.96	21.2	2.00	20.7	1.96
Glass beads	Butyl alcohol	23.6	1.38	31.0	1.34	32.5	1.38
Anhydrous monocalcium phosphate	Isobutyl alcohol	4.6	2.38	45.0	2.18	43.5	2.38
Monocalcium phosphate monohydrate	2-Ethylhexanol	0.61	3.54	70.0	3.50	71.5	3.54
Anhydrous dicalcium phosphate	Ethanol	2.5	2.22	18.8	2.22	16.8	2.22
Dicalcium phosphate dihydrate	0.1% Na hexametaphosphate in water	2.05	1.96	9.0	2.09	8.0	1.96
Tricalcium phosphate	Ethanol	1.16	1.95	4.4	1.95
Calcium pyrophosphate	Ethanol	2.08	1.95	8.4	2.15	7.9	1.95
Insoluble sodium metaphosphate	Ethanol	3.0	2.07	11.2	2.24	10.1	2.07

^a In microns. ^b Calculated from the measured M_n and σ_n and equation 10.

Sieve Analysis Evaluation.—For those powders where ca. 80% or more of the particles have diameters greater than 44 μ (325 mesh U. S. Screen), the particle size distributions as determined by sieving and sedimentation are identical, provided there is no significant amount of large particles to cause turbulent flow. Figure 4 demonstrates the agreement for a sodium isethionate sample. However, Fig. 5 shows that when ca. 35% or more of the particles of a powder have diameters smaller than 44 μ , sieve analysis is inaccurate and fails to show significant differences for two powders having different particle size distributions.

The results plotted in Fig. 6 offer a plausible explanation for the above described behaviors. Thus, for the case of sodium isethionate the geo-

metric mean diameter of a sieve cut as determined by sedimentation approximately equalled the average diameter of the two screen openings. However, for the anhydrous monocalcium phosphate sample investigated, the actual geometric mean diameter of a sieve cut is significantly different from the average diameter of the two screen openings. Figure 6 further shows that a significant portion of the powder lies outside the screen opening limits.¹¹ In addition, this figure demonstrates that exactly the same screens give different size classifications for different powders. Consequently, accurate sieve analysis is obtained only when the sieves are pre-calibrated against the more precise methods for the individual powder under investigation.

THE MEASUREMENT OF DIELECTRIC CONSTANT AND LOSS FACTOR OF LIQUIDS AND SOLUTIONS BETWEEN 250 AND 920 MC./SEC. BY MEANS OF A COAXIAL TRANSMISSION LINE

BY GRAHAM WILLIAMS

The Edward Davies Chemical Laboratories, University College of Wales, Aberystwyth, Wales

Received July 8, 1968

A coaxial line method of measuring the dielectric properties of liquid systems in the frequency range 250–1000 Mc./sec. (or higher) is described. The method is essentially that of Roberts, Westphal and von Hippel. Data are presented for typical systems of high and low ϵ' and ϵ'' values showing results which compare favorably with other methods in this region. Evaporation losses, access of moisture and temperature are readily controlled for the liquids.

The frequency range 100 to 1000 Mc./sec. has proved in the past to be a difficult region for the measurement of dielectric constant and loss factor. The difficulties arise from residual lead and electrode inductance, resistance and capacitance, and the correction of these factors. Measurements have been achieved using re-entrant cavities^{1–6} and parallel transmission lines^{7–11} and also by a modi-

fication of an impedance method of Cole¹² by Marcy and Wyman.¹³

However, elaborate equipment is required, and in some cases only moderate reproducibility of results could be achieved. The present apparatus offers an excellent alternative, since the effects of stray inductance and capacitance are eliminated by confining the electric field between the coaxial conductors and treating the system in terms of distributed circuits. The apparatus could be used for lower frequency work, the lower limit being fixed by the length of coaxial transmission line available, and the measurements could be extended

(1) C. N. Works, T. W. Dakin and F. W. Boggs, *Proc. Inst. Radio Eng.*, **33**, No. 4, 245 (1945).

(2) C. N. Works, *J. Appl. Phys.*, **18**, 605 (1947).

(3) S. J. Reynolds, *General Electric Rev.*, **50**, No. 9, 34 (1947).

(4) J. V. L. Parry, *Proc. Inst. Electr. Eng.*, **98**, pt. III, 303 (1951).

(5) D. L. Holloway and G. J. A. Cassidy, *ibid.*, **99**, pt. III, 364 (1952).

(6) J. H. Beardsley, *Rev. Sci. Instr.*, **24**, No. 2, 180 (1953).

(7) R. A. Chipman, *J. Appl. Phys.*, **10**, 27 (1939).

(8) W. L. G. Gent, *Trans. Faraday Soc.*, **50**, 383 (1954).

(9) H. Linhart, *Z. physik. Chem.*, **B38**, 23 (1937).

(10) J. B. Bateman and G. Potapenko, *Phys. Rev.*, **67**, 1185 (1940).

(11) W. P. Conner and C. P. Smyth, *J. Am. Chem. Soc.*, **64**, 1870 (1942).

(12) R. H. Cole, *Rev. Sci. Instr.*, **12** (6), 298 (1941).

(13) H. O. Marcy and J. Wyman, *J. Am. Chem. Soc.*, **63**, 3388 (1941).

up to 3000 Mc./sec. by means of commercially available oscillators, with a more accurate vernier scale on the coaxial line. The components used are commercially available and although we have used the most sensitive of the immediately procurable detecting systems, alternative simpler versions can be used when reduced accuracy would suffice.

Experimental

The arrangement of the apparatus is shown in Fig. 1.

The signal oscillator is a General Radio (G.R.) 1209 B unit oscillator operating in the range 250 to 920 Mc./sec. The line used is a G.R. 874 LBA slotted line, which is a 50 ohm, air dielectric coaxial transmission line, whose electric field is sampled by a probe that projects through a longitudinal slot in the line. The voltage induced in the probe is measured by means of a G.R. DNT3 detector. This comprises a G.R. 874 MR mixer rectifier, a G.R. 1209 B unit oscillator operating between 250 and 920 Mc./sec., and a G.R. 1216 A unit i.f. amplifier. The latter is a four-stage high gain intermediate frequency amplifier operating at 30 Mc./sec., with a band width of 0.7 Mc./sec. The meter is calibrated in a decibel and linear scale, and has a precision step attenuator for measuring relative signal levels. The cell for liquid dielectrics is a 30 cm. length of 50 ohm coaxial transmission line which fits on the slotted line by means of flanges. The lower end of the cell is shorted by means of a brass plate, and a small slot at the shorted end (0.37 cm. X 0.15 cm.) allows liquid to enter the coaxial line. Liquid depths are varied continuously by firmly fixing the glass cylindrical container for the liquid (A, Fig. 1), whose diameter is twice that of the air line (i.e., 2 X 1.5 cm.), on to a small table having a vertical rack-and-pinion movement. Depths are found by measuring the external liquid height relative to a reference mark on the cell, the distance between the reference and the physical end of the line being known: a long-focus travelling microscope or cathetometer readable to ±0.02 mm. is used for this purpose.

Variation in the liquid temperature can be achieved by a concentric jacket fused on to the glass cell (A of Fig. 1). Circulation of a thermostatically controlled transparent liquid (water or Nujol) allows ready control of the temperature. A is some 30 cm. in length and the depth of liquid is usually of the order of 5 cm. A Teflon ring acts as a stopper at the top of A, and serves to center the coaxial line in the cylindrical container A and to reduce evaporation losses; guard tubes or a dry air stream serve to prevent access of moisture when the liquid is hygroscopic.

Frequencies beyond 920 Mc./sec. can be measured by choice of suitable harmonics of the signal oscillator: for instance, fairly accurate measurements have been achieved at 1700 Mc./sec. using the second harmonic of 850 Mc./sec. The very small band width of the detector amplifier relative to the beat-frequency (30 Mc./sec.) allows this to be done for chosen harmonics. The purity of the standing-wave for the harmonic frequency can be checked from the symmetry of its pattern in the line and from the measured widths of the succession of nodal minima.

Method.—The method of measurement is due to Roberts and von Hippel.¹⁴ They obtain the relation

$$\frac{\tan h \gamma_2 d}{\gamma_2 d} = \frac{s - j \tan \beta_1 x_0}{j \beta_1 d \{1 - j s \tan \beta_1 x_0\}} \quad (1)$$

where γ_2 is the propagation constant of the liquid, d is the liquid depth, $s = E_{\min}/E_{\max}$ is the standing wave ratio, x_0 is the distance of the first node from the liquid surface, λ_1 is the wave length in the air portion of the line and $\beta_1 = 2\pi/\lambda_1$. Writing the right-hand side of equation 1 in the form $x + jy$

$$x = \frac{(s^2 - 1) \tan \beta_1 x_0}{\beta_1 d \{1 + s^2 \tan^2 \beta_1 x_0\}}; \quad y = -\frac{s(1 + \tan^2 \beta_1 x_0)}{\beta_1 d \{1 + s^2 \tan^2 \beta_1 x_0\}} \dots \quad (2)$$

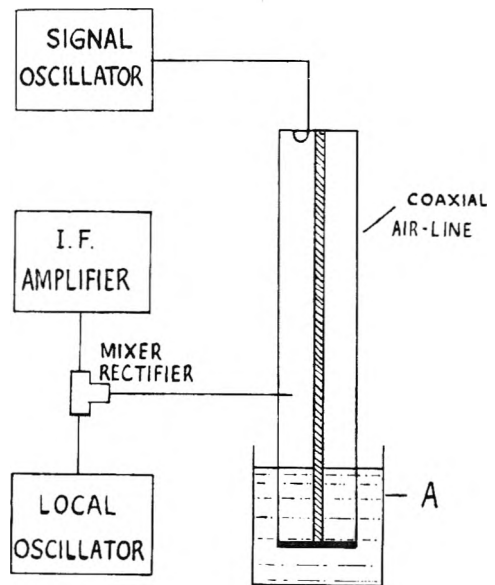


Fig. 1.

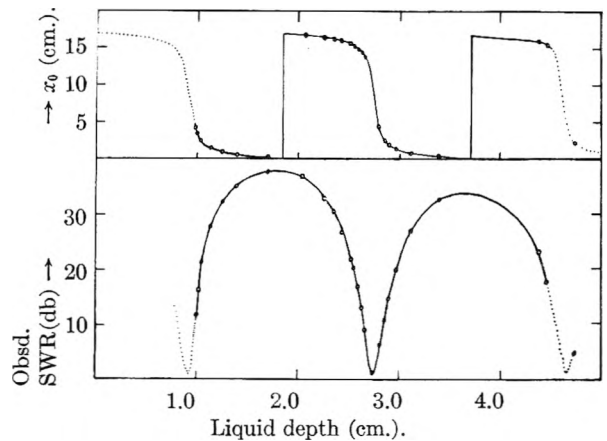


Fig. 2.—Water at 900 Mc. and 18.5°. Observed SWR = E_{\min}/E_{\max} ; x_0 = distance of first node from liquid surface.

x and y are determined from experimental data. Expressing $x + jy = Ce^{i\xi}$, we have

$$C = \sqrt{x^2 + y^2}; \quad \xi = \tan^{-1}(y/x)$$

Writing $\gamma_2 d = Te^{j\tau}$, then by means of correlation charts¹⁵ T and τ are found from C and ξ . Since $\gamma_2 = \alpha_2 + j\beta_2$ where α_2 is the attenuation constant and β_2 is the phase constant for the liquid, then

$$\alpha_2 = \frac{T \cos \tau}{d}; \quad \beta_2 = \frac{T \sin \tau}{d}$$

The real and imaginary factors of the dielectric constant are found by the relations

$$\epsilon' = n^2(1 - \alpha_2^2/\beta_2^2); \quad \epsilon'' = 2n^2(\alpha_2/\beta_2) \quad (3)$$

where n is the generalized index of refraction for the liquid and is equal to $\lambda_1 \beta_2 / 2\pi$.

For large s values, the direct decibel difference between maxima and minima was used, since

$$(\text{db response})_{\max} - (\text{db response})_{\min} = -20 \log s$$

For small values of s , the width of minimum method was used.¹⁵ A 3 db displacement from the voltage minimum as indicated by the amplifier,

(14) S. Roberts and A. R. von Hippel, *J. Appl. Phys.*, **17**, 610 (1946).

(15) W. B. Westphal, in "Dielectric Materials and Applications," Chapman and Hall, 1954, p. 67.

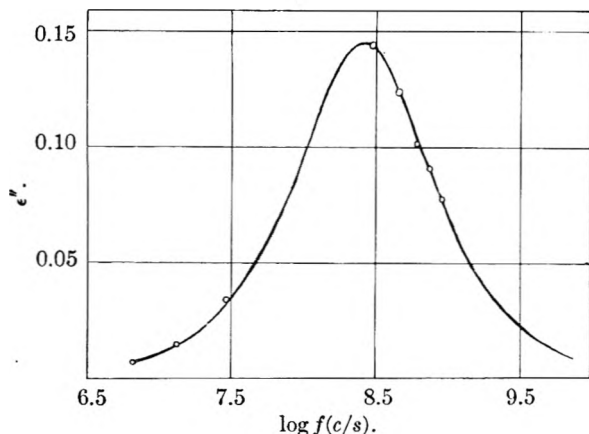


Fig. 3.— Bu_4NPic in dioxane: $1.03 \times 10^{-2} M$ at 17° . The curve is a calculated Debye function for $\epsilon'' = 0.145$; $\tau = 620 \times 10^{-12}$ sec. The experimental uncertainty in the observations is given by the diameter of the circles.

is required for the points of twice minimum power. Then

$$s = \pi\Delta/\lambda_1$$

where Δ is the distance between points of twice minimum power. If Δ is very small, then the points of four times minimum power may be employed. This corresponds to a 6 db displacement from the voltage minimum and $s = \pi\Delta'/\sqrt{3}\lambda_1$, where Δ' is the distance between points of four times minimum power.

The observed widths must be corrected for the air line attenuation.¹⁵

Some Typical Results. (1) **Water.**—Water provided a check of the accuracy of the apparatus and method for a high dielectric constant, medium loss liquid. The variation of s and x_0 with varying depth is shown in Fig. 2. A study of these curves which can be calculated for given dielectric parameters, serves to emphasize the variations in the accuracy of the results likely to be achieved with varying conditions, e.g., for different x_0 and d values. The evaluation of some of these results is shown in Table I.

TABLE I

VALUES OF ϵ' AND ϵ'' WITH VARYING LIQUID DEPTH FOR WATER AT 900 Mc. AND 18.5°

d (cm.)	ϵ'	ϵ''
2.625	84.4	4.5 ± 0.10
2.669	83.9	$4.1 \pm .10$
2.803	82.2	$3.76 \pm .16$
2.849	82.6	$3.90 \pm .10$
2.891	82.7	$3.91 \pm .10$
2.965	82.6	$3.96 \pm .10$
4.463	80.7	$3.70 \pm .10$

The uncertainty quoted for the loss factor is that involved in reading the von Hippel charts for this system. The deviation of the ϵ' values from 80.2^{16} arises principally from two factors: the error owing to the meniscus in the depth (d), and the air attenuation in the line which has not been taken into account in the calculation of these results. The former becomes less the greater the depth:

(16) E. H. Grant, T. J. Buchanan and H. F. Cook, *J. Chem. Phys.*, **26**, 156 (1957).

a 1% error in the liquid depth introducing an error of 1.3 to 3.5 % in ϵ' and of 0.6 to 1.6% in ϵ'' . The latter is more significant at small s values.

Using these data to calculate τ via

$$\epsilon'' = \frac{(\epsilon_0 - \epsilon_\infty)\omega\tau}{1 + \omega^2\tau^2} \quad (4)$$

gives with $\epsilon_\infty = 4.5^{16}$ a value $\tau = (8.9 \pm 0.2) \times 10^{-12}$ sec. If we take $\epsilon_0 = 80.8$,¹⁶ $\epsilon_\infty = 4.5$ and $\epsilon'' = (3.9 \pm 0.1)$ the value becomes $\tau = (9.0 \pm 0.2) \times 10^{-12}$ sec. At the same temperature, the best value in the literature is $(9.6 \pm 0.4)^{16}$; other values are 9.5 at 20° ¹⁷ and 8.5 at 21° .¹⁸ Thus it is evident that the experimental procedure and method are suitable for the measurement of large dielectric constants to an accuracy of about 2% and the loss factor to about 4%.

Water was also investigated at 800 Mc. using the procedure described by Little.¹⁹ The dielectric constant was accurate to $\pm 1.5\%$, the loss factor to $\pm 5\%$. The relaxation time calculated from the loss factor was $(9.8 \pm 0.5) \times 10^{-12}$ sec., which is in good agreement with the results quoted above. However, the experimental procedure is extremely tedious compared with the Roberts-von Hippel method, and cannot be recommended for general application.

(2) **Tetra-*n*-butylammonium Picrate in Dioxane.**—A $1.03 \times 10^{-2} M$ solution of the salt was examined as an example of a low dielectric constant, low loss medium. The dielectric constant values were accurate to $\pm 0.5\%$, and the loss factors to $\pm 1\%$. The frequency range 300 to 900 Mc. was covered, and using a Hartshorn-Ward dielectric test set, the range 6 to 30 Mc. also was measured. From the results it was found possible to construct a complete Debye curve corresponding to a single relaxation time. The accuracy of the relaxation time is dependent upon the accuracy of $(\epsilon_0 - \epsilon_\infty)$. The curve is shown in Fig. 3, where the measured $\epsilon''(\text{max})$ is found to coincide with $\frac{(\epsilon_0 - \epsilon_\infty)}{2}$ for the solution and τ is 620×10^{-12} sec.

(3) **Other Systems.** (i).—A $1.03 M$ solution of benzophenone in xylene was studied at 900 Mc. in order to test the reproducibility of ϵ' and ϵ'' as the liquid depth is varied for a low dielectric constant medium. The results are summarized in Table II. The relaxation time was calculated using the Debye dilute solution equation. The

TABLE II

1.03 M BENZOPHENONE IN XYLENE AT 900 Mc. AND 18°

d (cm.)	ϵ'	ϵ''	$10^{12} \times \tau$, sec. (calcd.)	$10^{12} \times \tau$, sec. (lit.)
2.99	3.65	0.230 ± 0.012	20.0	22 (20)
4.75	3.65	$.242 \pm .08$	21.0	18.1 (21)
5.32	3.65	$.254 \pm .10$	21.7	20.4 (22)

(17) C. H. Collie, J. V. Hasted and R. M. Ritson, *Proc. Phys. Soc., (London)*, **60**, 145 (1948).

(18) J. A. Saxton and J. A. Lane, *Proc. Roy. Soc., (London)*, **A213**, 400 (1952).

(19) V. I. Little, *Proc. Phys. Soc., (London)*, **66B**, 175 (1953).

(20) D. H. Whiffen and H. W. Thompson, *Trans. Faraday Soc.*, **42A**, 114 (1946).

(21) F. J. Cripwell and G. B. B. M. Sutherland, *ibid.*, 149 (1946).

(22) E. Fischer, *Z. Naturforschung*, **4a**, 707 (1949).

literature values refer to benzene as solvent; the viscosity difference from xylene is negligible.

(ii).—Pure chlorobenzene was studied over the frequency range 300 to 900 Mc. at 12°. The results are shown in Table III.

TABLE III
PURE CHLOROBENZENE AT 12° FOR DIFFERENT AIR WAVE LENGTHS (λ_1)

λ_1 (cm.)	ϵ'	ϵ''	$10^{10} \times \epsilon''/f$
33.32	5.90	0.275	3.06
42.94	5.86	.200	2.86
49.84	5.83	.172	2.86
74.73	5.81	.124	3.10
99.28	5.81	.093	3.10

Taking the mean ϵ''/f to be $(3.0 \pm 0.1) \times 10^{-10}$, and ϵ_∞ to be n_D^2 , i.e., $(1.522)^2 = 2.32$, then using equation 4, $\tau = (13.6 \pm 0.5) \times 10^{-12}$ sec.

Hennelly, Heston and Smyth²³ obtained $12.5 \times$

(23) E. J. Hennelly, W. M. Heston and C. P. Smyth, *J. Am. Chem. Soc.*, **70**, 4102 (1948).

10^{-12} sec. at 12° from the Cole-Cole circular arc. It is to be noted that their value for ϵ' at this temperature is 5.88 ± 0.02 , whilst the present work obtains 5.84 ± 0.03 . This indicates the accuracy to which low dielectric constants can be measured.

As this work was being completed the thesis of F. C. De Vos²⁴ was received. This describes similar measurements using a coaxial line with a number of fixed filled cells having Teflon windows. This thesis also provides an excellent survey of other high frequency dielectric methods.

Grateful thanks are offered to Messrs. Courtauld's Educational Trust Fund for a grant which has made this work possible. The author also wishes to thank Dr. Mansel Davies for his advice and constant encouragement during this work. A maintenance grant from the Department of Scientific and Industrial Research is gratefully acknowledged, and also helpful correspondence from Professor Böttcher and Dr. F. C. De Vos.

(24) F. C. De Vos, Thesis, Leiden, 1958.

THE EVALUATION OF DIELECTRIC DATA FOR LIQUIDS AND SOLUTIONS

BY GRAHAM WILLIAMS

The Edward Davies Chemical Laboratories, The University College of Wales, Aberystwyth, Wales

Received September 26, 1958

A number of useful modifications and correlations of current methods of evaluating the dielectric parameters for polar liquids and solutions are described and illustrated by examples. These include the comparison and correlation of the "dilute solution" and "pure liquid" equations for the relaxation time, simple graphical methods for determining the relaxation time and its distribution factor in the general cases, and the calculation of dipole moments *via* Guggenheim's relations using Smyth's dielectric parameters.

The Dilute Solution and Pure Liquid Equations for a Single Relaxation Time.—The general equations for the dielectric constant (ϵ') and loss factor (ϵ'') of a polar medium possessing a single relaxation time (τ) are

$$\epsilon' = \epsilon_\infty + \frac{\epsilon_0 - \epsilon_\infty}{1 + \omega^2\tau^2} \quad (1a)$$

$$\epsilon'' = (\epsilon_0 - \epsilon_\infty) \frac{\omega\tau}{1 + \omega^2\tau^2} \quad (1b)$$

Here ϵ_0 is the static dielectric constant of the medium and ϵ_∞ is its value at an angular frequency (ω) so high that all orientational polarization has vanished.

For a dilute solution of a solute having dipole moment μ in a non-polar solvent, Debye,¹ twenty-five years ago, made the approximation

$$\epsilon'' = \frac{(\epsilon_1 + 2)^2 N \pi \mu^2 c}{6750 kT} \times \frac{\omega\tau}{1 + \omega^2\tau^2} \quad (2)$$

In this relation ϵ_1 is the static dielectric constant of the non-polar solvent and c is the molar concentration.

We wish firstly to compare the relaxation times deduced by the use of equations 1 and 2 for the typical case of a $6.54 \times 10^{-2} M$ solution of tri-*n*-butylammonium picrate in *m*-xylene at 17°. Measurements in these laboratories from 196 kc./sec. to 1700 Mc./sec. show that this system,

after allowances for the small solvent absorption, is precisely defined by a single relaxation time. Of the various ways of evaluating the parameters of equations 1, three convenient procedures due to Cole may be quoted: (i) the circular arc plot of ϵ'' against ϵ' ; (ii) the linear plot of ϵ' against $\epsilon'' \times \omega$; (iii) the linear plot of ϵ' against ϵ''/ω . All gave $\tau = 353 \pm 6 \times 10^{-12}$ sec. and the corresponding value of $(\epsilon_0 - \epsilon_\infty) = 0.99 \pm 0.01$.

Comparison of (1b) and (2) gives

$$(\epsilon_0 - \epsilon_\infty) = K \frac{N \pi \mu^2 c}{6750 kT}$$

where $K = (\epsilon_1 + 2)^2$. Using the Debye dilute solution equations we obtained $\mu = 11.4 \pm 0.1 D$: Maryott² found for the same solute in benzene $\mu = 11.7 D$. Accordingly, using the above value of $(\epsilon_0 - \epsilon_\infty)$, $K = (\epsilon_0 - \epsilon_\infty)/5.89 \times 10^{-2} = 16.8$.

Equation 2, in which $K = (\epsilon_1 + 2)^2$, can be arrived at in various ways.³ In one of them ϵ_1 replaces ϵ' the real (and frequency dependent) dielectric constant of the solution; in another $(\epsilon_1 + 2)^2$ is substituted as an approximation for $(\epsilon_0 + 2)(\epsilon_\infty + 2)$. The values of these factors are $(\epsilon_1 + 2)^2 = 18.8$; $(\epsilon' + 2)^2 = 29.2$ to 19.6 over the measured frequency range; $(\epsilon_0 + 2)(\epsilon_\infty + 2) = 24.3$. It is clear that even the best of these factors (18.8) would give a τ -value 20% below that

(2) A. A. Maryott, *J. Research Natl. Bur. Standards*, **41**, 1 (1948).

(1) P. Debye, "Polar Molecules," Chemical Catalog Co., New York, N. Y., 1929, Chapter V.

(3) C. J. F. Böttcher, "Theory of Electric Polarisation," Elsevier Publishing Co., 1952, p. 374.

of the correct value from equations 1. Because of the large dipole moment involved, this example serves to emphasize the general conclusion that τ values arrived at *via* equation 2 or its equivalents can be markedly uncertain even at quite low concentrations.

One general difficulty in using equations 1 for dilute solutions is that $(\epsilon_0 - \epsilon_\infty)$ will be quite small and the accuracy of τ will be markedly dependent upon the value taken for ϵ_∞ , in which the uncertainty is accentuated by the difficulties of measuring ϵ' with sufficient precision at the highest frequencies. One approximation which can be (and has been) used for ϵ_∞ is, of course n_0^2 , where n_0 is the refractive index of the solution. The inadequacy of this particular approximation, and a better value for it, is deduced *via* the form of the Debye equation for the dipole moment of a solute in dilute solution advanced by Guggenheim⁴

$$\mu^2 = \frac{6750kT}{N\pi(\epsilon_1 + 2)(n_1^2 + 2)} \times \left(\frac{\Delta}{c}\right)_0 \quad (3)$$

n_0 and n_1 are the refractive indices of the solution and solvent, respectively; $\Delta = (\epsilon_0 - n_0^2) - (\epsilon_1 - n_1^2)$; and $(\Delta/c)_0$ is the value of this ratio on extrapolation to zero concentration, but we shall assume the solution to be sufficiently dilute to use the actual value of the ratio.

If, for the moment, we assume $(\epsilon_1 + 2) = (n_1^2 + 2)$ for the non-polar solvent, combination of equations 2 and 3 gives

$$\epsilon'' = \Delta \frac{\omega\tau}{1 + \omega^2\tau^2}$$

Comparison of this with the general equation 1b leads to

$$\begin{aligned} \epsilon_0 - \epsilon_\infty &= \Delta = (\epsilon_0 - n_0^2) - (\epsilon_1 - n_1^2) \\ \text{i.e., } \epsilon_\infty &= n_0^2 + (\epsilon_1 - n_1^2) \end{aligned} \quad (4)$$

Thus when equations 2 and 3 are simultaneously valid, equations 1 and 2 would give coincident τ values if $\epsilon_1 = n_1^2$ and $\epsilon_\infty = n_0^2$. Primarily these latter conditions reduce to $\epsilon_1 = n_1^2$, as for adequately dilute solutions the conditions $\epsilon_\infty = \epsilon_1$ and $n_0 = n_1$ are likely to be closely approximated. However, in practice ϵ_1 and n_1^2 can differ significantly even for the conventionally "non-polar" solvents;⁵ see Table I. For carbon tetrachloride the difference in these factors is nearly 5% and for dioxane it is 10%. This will be the source of discrepant τ values if the assumption $\epsilon_\infty = n_0^2$ is used.

TABLE I

Solvent	t, °C.	ϵ_1	n_1^2
Benzene	20	2.284	2.254
p-Xylene	20	2.270	2.236
Carbon tetrachloride	20	2.238	2.132
Tetrachloroethylene	25	2.300	2.270
p-Dioxane	20	2.209	1.991

As already emphasized, it frequently happens for solutions that the uncertainty in the ϵ' values leads to very appreciable error in $(\epsilon_0 - \epsilon_\infty)$. To eliminate this factor for cases where equation 1b applies

(4) E. A. Guggenheim, *Trans. Faraday Soc.*, **45**, 714 (1949).

(5) A. Weissberger, *et al.*, "Organic Solvents," Interscience Publishers, Inc., New York, N. Y., 1955.

the following procedure can be used to evaluate τ solely from the loss factor measurements. For $\omega\tau \ll 1$ equation 1b becomes

$$\begin{aligned} \epsilon'' &= (\epsilon_0 - \epsilon_\infty)\omega\tau \\ \tau &= \left(\frac{\epsilon''}{\omega}\right) \frac{1}{(\epsilon_0 - \epsilon_\infty)} = \frac{A}{(\epsilon_0 - \epsilon_\infty)} \end{aligned}$$

Here A is the "best" experimental value of ϵ''/ω for $\omega\tau \ll 1$. At the higher frequencies, $\omega\tau \gg 1$, the same equation 1b becomes

$$\epsilon'' = \frac{(\epsilon_0 - \epsilon_\infty)}{\omega\tau}$$

whence

$$\tau = \frac{(\epsilon_0 - \epsilon_\infty)}{\omega\epsilon''} = \frac{(\epsilon_0 - \epsilon_\infty)}{B}$$

and the "best" value of B is readily evaluated.

Clearly

$$\tau = (A/B)^{1/2}; (\epsilon_0 - \epsilon_\infty) = (AB)^{1/2}$$

As an example we may quote the results obtained for a $1.03 \times 10^{-2} M$ solution of tetra-*n*-butylammonium picrate in *p*-dioxane: we found $A = 1.83 \times 10^{-10}$ sec.; $B = 4.58 \times 10^8$ sec.⁻¹. Accordingly $\tau = 630 \times 10^{-12}$ sec. and $(\epsilon_0 - \epsilon_\infty) = 0.290$. As $\epsilon_0 = 2.53$ experimentally, we have $\epsilon_\infty = 2.24$. That this should be identical with the value $\epsilon_1 = 2.24$ we measured for our sample of the solvent is confirmed from equation 4 as the measured value of $(n_0^2 - n_1^2)$ was $(1.4248)^2 - (1.4241)^2 = +0.002$, *i.e.*, it is in this instance negligibly small.

The Relaxation Time and its Distribution Factor.

—Cole and Cole⁶ have provided one of the standard procedures for determining an empirical factor representing a distribution of relaxation times and Cole⁷ has described equally convenient means of graphically evaluating the relaxation time when there is no distribution involved. The following paragraphs show the application of the latter method to the general case.

For a spread of relaxation times, the complex dielectric constant is expressed as

$$\epsilon^* = \epsilon' - j\epsilon'' = \epsilon_\infty + \frac{\epsilon_0 - \epsilon_\infty}{1 + (j\omega\tau_0)^n} \quad (5)$$

Separating the real and imaginary parts

$$\epsilon' = \epsilon_\infty + \frac{(\epsilon_0 - \epsilon_\infty) \left[1 + (\omega\tau_0)^n \cos \frac{n\pi}{2} \right]}{1 + 2(\omega\tau_0)^n \cos \frac{n\pi}{2} + (\omega\tau_0)^{2n}} \quad (6)$$

$$\epsilon'' = \frac{(\epsilon_0 - \epsilon_\infty)(\omega\tau_0)^n \sin \frac{n\pi}{2}}{1 + 2(\omega\tau_0)^n \cos \frac{n\pi}{2} + (\omega\tau_0)^{2n}} \quad (7)$$

Let

$$\left[1 + (\omega\tau_0)^n \cos \frac{n\pi}{2} \right] = \alpha;$$

$$\left[1 + 2(\omega\tau_0)^n \cos \frac{n\pi}{2} + (\omega\tau_0)^{2n} \right] = \beta$$

$$\text{and } (\omega\tau_0)^n \sin \frac{n\pi}{2} = \gamma$$

Thus equations 6 and 7 are

$$\epsilon' = \epsilon_\infty + (\epsilon_0 - \epsilon_\infty) \frac{\alpha}{\beta}; \quad \epsilon'' = (\epsilon_0 - \epsilon_\infty) \frac{\gamma}{\beta}$$

(6) K. S. Cole and R. H. Cole, *J. Chem. Phys.*, **9**, 341 (1941).

(7) R. H. Cole, *ibid.*, **23**, 493 (1955).

Rewriting

$$\epsilon' = \frac{\epsilon_{\infty}(\beta - \alpha) + \epsilon_0\alpha}{\beta}$$

$$\epsilon_{\infty} = \frac{\epsilon' \beta - \epsilon_0\alpha}{(\beta - \alpha)}$$

Then

$$\epsilon'' = \left[\epsilon_0 - \frac{(\epsilon'\beta - \epsilon_0\alpha)}{(\beta - \alpha)} \right] \frac{\gamma}{\beta} = \frac{(\epsilon_0 - \epsilon')\gamma}{(\beta - \alpha)}$$

$$\epsilon'' \left[(\omega\tau_0)^{2n} + (\omega\tau_0)^n \cos \frac{n\pi}{2} \right] = (\epsilon_0 - \epsilon') (\omega\tau_0)^n \sin \frac{n\pi}{2}$$

$$\epsilon'' \left[(\omega\tau_0)^n + \cos \frac{n\pi}{2} \right] = (\epsilon_0 - \epsilon') \sin \frac{n\pi}{2}$$

Rearranging

$$\omega^n = \frac{1}{(\tau_0)^n} \left[\left(\frac{\epsilon_0 - \epsilon'}{\epsilon''} \right) \sin \frac{n\pi}{2} - \cos \frac{n\pi}{2} \right] \quad (8)$$

Equation 8 may be used conveniently by plotting ω^n against $(\epsilon_0 - \epsilon')/\epsilon''$ for various n values. The "correct" value of n is quickly found as that giving a straight line whose slope is $(\sin n\pi/2)/(\tau_0)^n$ and whose intercept is $(\cos n\pi/2)/(\tau_0)^n$. Not only do these factors provide values of τ_0 but their agreement in this respect provides (together with the linearity of the plot) a quantitative check of the adequacy of equation 5 in representing the data. A further check, is available by calculation of τ_0 at the different frequencies using the deduced "n" value.

From the role of the factor $(\epsilon_0 - \epsilon')/\epsilon''$ it is clear that the relation 8 will provide best discrimination in the region where the dispersion (or absorption) is appreciable.

Some alternative versions of (8) may be noted before its use is illustrated. If the departures from a single relaxation time, *i.e.*, $n = 1.00$, are small, it is convenient to write $n = (1 - d)$. With the approximations $\cos d\pi/2 \approx 1.00$; $\sin d\pi/2 \approx d\pi/2$ we then have

$$(\omega\tau_0)^{1-d} = \left(\frac{\lambda_0}{\lambda} \right)^{1-d} = \left[\left(\frac{\epsilon_0 - \epsilon'}{\epsilon''} \right) - \frac{d\pi}{2} \right]$$

Here λ_0 is the "critical" wave length (*i.e.*, for maximum ϵ'') and λ is the wave length corresponding to the ϵ' and ϵ'' values measured at the angular frequency ω . The logarithmic version is

$$(1 - d) \log \lambda_0 - (1 - d) \log \lambda = \log \left[\left(\frac{\epsilon_0 - \epsilon'}{\epsilon''} \right) - \frac{d\pi}{2} \right] \quad (9)$$

Plotting the r.h.s. (neglecting, in the first instance, $d\pi/2$) against $\log \lambda$ leads to $(1 - d)$ and λ_0 values but such log-log plots are notoriously poor methods of detecting departures from algebraic relations.

Reverting to (6) and (7) we have

$$(\epsilon' - \epsilon_{\infty}) = (\epsilon_0 - \epsilon_{\infty})(\alpha/\beta)$$

$$\epsilon'' = (\epsilon_0 - \epsilon_{\infty})(\gamma/\beta)$$

or

$$\left(\frac{\epsilon' - \epsilon_{\infty}}{\epsilon''} \right) = \frac{\alpha}{\gamma} = \frac{\left[1 + (\omega\tau_0)^n \cos \frac{n\pi}{2} \right]}{(\omega\tau_0)^n \sin \frac{n\pi}{2}}$$

With the same approximations as above, one finds

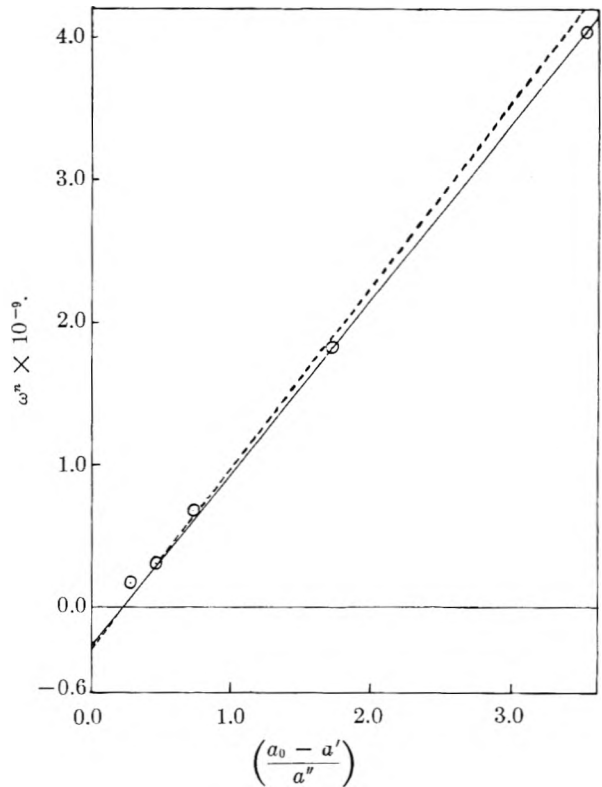


Fig. 1.—Anthrone in benzene (20°): \odot , experimental points. Full line corresponds to $n = 0.86$; $\tau_0 = 26.3 \times 10^{-12}$ sec.; dotted line corresponds to $n = 0.86$; $\tau_0 = 24.8 \times 10^{-12}$ sec. (Smyth, *et al.*⁹).

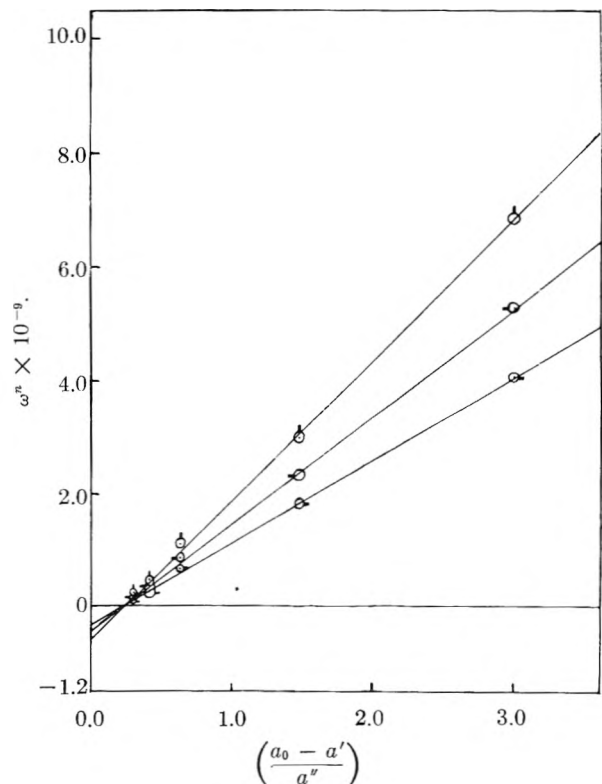


Fig. 2.—Fluorenone in benzene (20°): \odot , experimental points using $n = 0.88$; \square , experimental points using $n = 0.87$; \triangle , experimental points using $n = 0.86$.

$$(1 - d) \log \lambda - (1 - d) \log \lambda_0 = \log \left[\left(\frac{\epsilon' - \epsilon_\infty}{\epsilon''} \right) - \frac{d\pi}{2} \right] \quad (10)$$

This relation 10 is quoted by Grant, Buchanan and Cook⁸ and they have used it to obtain λ_0 from the log-log plot. However, this is a less generally useful version than (9) for, as those authors note, the value of ϵ_∞ has to be assumed, as well as the initial neglect of $d\pi/2$.

The use of equation 8 may now be illustrated with the data due to Smyth, *et al.*, who have represented their results for various solutions in the form

$$\begin{aligned} \epsilon' &= \epsilon_1 + a'f_2 \\ \epsilon_0 &= \epsilon_1 + a_0f_2 \\ \epsilon'' &= a''f_2 \end{aligned}$$

Here f_2 is the mole fraction of the polar solute; ϵ' is the frequency dependent dielectric constant of the solution, ϵ_1 and ϵ_0 the static d.c.s. of the solvent and solutions. Accordingly, equation 8 is tested by plotting ω^n against $(\alpha_0 - \alpha')/\alpha''$. Figure 1 shows such plots for anthrone in benzene⁷ at 20°. Pitt and Smyth have deduced $n = 0.86$ and $\tau_0 = 24.8 \times 10^{-12}$ sec. The plot using $\omega^{0.86}$ gives a good straight line whose slope and intercept correspond to $\tau_0 = 26.3 \times 10^{-12}$ sec.: the line for $n = 0.86$ and $\tau_0 = 24.8 \times 10^{-12}$ sec. is also shown. The slightly higher value of τ_0 is confirmed by individual calculations from equation 8 using $n = 0.86$: see Table II.

TABLE II

RELAXATION TIMES FOR ANTHRONE IN BENZENE (20°) CALCULATED AT VARIOUS AIR WAVE LENGTHS (λ) FROM EQUATION 8

λ (cm.)	1.25	3.22	10.00	25.00	50.0
$10^{12} \times \tau_0$, sec.	26.3	26.9	24.4	25.2	12

The poor value at 50 cm. emphasizes the uncertainty in $(\alpha_0 - \alpha')/\alpha''$ (*i.e.*, $(\epsilon_0 - \epsilon')$ and ϵ'' are small).

For fluorenone in benzene at 20° Pitt and Smyth find $n = 0.87$ and $\tau_0 = 19.9 \times 10^{-12}$ sec. Figure 2 shows plots of equation 8 for $n = 0.88, 0.87, 0.86$. The differentiation over $n = 0.87 \pm 0.01$ is not clear. The line drawn for $n = 0.87$ gave $\tau_0 = 20.9 \times 10^{-12}$ sec. from its slope: 20.4×10^{-12} sec. from its intercept. Accordingly Table III represents the variation in the τ_0 values calculated at various wave lengths for different n values. From this the best values appear to be $n = 0.87$, $\tau_0 = 20.7 \times 10^{-12}$ sec. in agreement with Pitt and Smyth's deductions, although $n = 0.88$, $\tau_0 = 21.5 \times 10^{-12}$ sec. is almost equally acceptable.

(8) E. H. Grant, T. J. Buchanan and H. F. Cook, *ibid.*, **26**, 156 (1957). *Cf.* Smyth, *et al.*, *J. Am. Chem. Soc.*, **72**, 3447 (1950).

TABLE III

RELAXATION TIMES (IN 10^{-12} SEC.) FOR FLUORENONE IN BENZENE (20°) CALCULATED AT VARIOUS AIR WAVE LENGTHS (λ) FOR ASSUMED VALUES OF n

n	1.00	0.90	0.88	0.87	0.86	0.84	0.80
λ (cm.)				τ_0			
1.25	19.9	20.8	20.9	20.9	20.9	21.2	21.2
3.22	25.2	22.9	22.4	21.8	21.4	20.8	19.1
10.00	33.7	23.0	20.4	19.6	18.20	16.1	12.6
25.00	54.1	28.0	22.9	20.4	18.20	14.0	6.3
50.0	79.5	29.8	20.9	17.4	13.2	6.1	-ve

For fluorenone in benzene at 40° Pitt and Smyth give $n = 0.88$, $\tau_0 = 14.9 \times 10^{-12}$ sec. The slope and intercept of the plot of $\omega^{0.88}$ against $(\alpha_0 - \alpha')/\alpha''$ each give $\tau_0 = 15.5 \times 10^{-12}$ sec.

Calculation of Dipole Moments from Smyth's Parameters.—In addition to the relations already quoted for the dielectric properties Smyth⁹ has used the relation

$$n^2_D = n^2_{D_1} + aDf_2$$

for the refractive indices (n_D) of solutions in terms of that of the solvent (n_{D_1}) and the mole fraction of solute (f_2). Smyth, *et al.*,¹⁰ then calculate the dipole moments from the Halverstadt and Kumler relations: we merely wish to indicate that they can, equally conveniently, be deduced from Guggenheim's version of the dilute solution equation, see equation 3. In that we now have

$$\Delta = (\epsilon_0 - n^2_D) - (\epsilon_1 - n^2_{D_1}) = (a_0 - aD)f_2$$

In the limit of very dilute solutions, $f_2 = cM_1/1000\rho$ where M_1 is the molecular weight of the solvent and ρ is its density. Thus, insofar as the Smyth parameters represent the dilute solutions and Δ/c is a constant, we have $\Delta/c = (a_0 - aD)(M_1/1000\rho)$. Some values for benzene solutions calculated in this way (μ_G) are given in Table IV together with those from Halverstadt and Kumler (μ_{H-K}).

TABLE IV

COMPARISON OF DIPOLE MOMENTS CALCULATED IN BENZENE SOLUTIONS (20°)

	μ_G , debyes	μ_{H-K} , debyes
1-Nitronaphthalene ¹⁰	4.00	4.00
Anthrone	3.62	3.63
Fluorenone	3.35	3.38
Phenanthraquinone	5.25	5.36

As both evaluations are based on the Debye equation which is of limited significance for solutions, the agreement is satisfactory.

Acknowledgments.—The author wishes to thank Dr. Mansel Davies for his discussion of these points and the D.S.I.R. for a Maintenance Award.

(9) D. A. Pitt and C. P. Smyth, *ibid.*, **80**, 1061 (1958).

(10) R. W. Rampolla and C. P. Smyth, *ibid.*, **80**, 1057 (1958); ref. 7.

A THERMODYNAMIC STUDY OF SOME COORDINATION COMPOUNDS OF METAL IONS WITH AMINES CONTAINING OXYGEN^{1,2}

BY JOHN R. LOTZ, B. P. BLOCK AND W. CONARD FERNELIUS

*Contribution from the Department of Chemistry, The Pennsylvania State University, University Park, Penna.**Received August 19, 1958*

Thermodynamic equilibrium constants have been determined by potentiometric titration at 10, 20, 30 and 40° for the reactions of ethanolamine (I), 2-methoxyethylamine (II), 2-aminoethyl-2'-hydroxyethyl sulfide (III), bis-(2-aminoethyl) ether (IV), 1,8-diamino-3,6-dioxaoctane (V) and 1,8-diamino-2-oxa-6-thiaoctane (VI) with H⁺ and Ag⁺; of III, IV, V and VI with Cu⁺⁺; and of IV and VI with Ni⁺⁺. The results indicate for the relative stability of metal-element bonds the series N > S > O. Heats of reaction were found to be more important than entropy changes in determining stability.

Introduction

A recent publication for this Laboratory³ summarized the literature on the formation constants of metal-amine complex ions and the kinds of problems which have received attention. Numerical values for such constants may be found in a recent compilation.⁴

In continuation of previous studies there are presented here values for ethanolamine, 2-methoxyethylamine, 2-aminoethyl-2'-hydroxyethyl sulfide, bis-(2-aminoethyl) ether, 1,8-diamino-3,6-dioxaoctane and 1,8-diamino-2-oxa-6-thiaoctane with several metal ions at 10, 20, 30 and 40°. From these data are calculated values for ΔF , ΔH and ΔS for the association reactions.

Experimental

Ethanolamine.—The technical material (Union Carbide Chemicals Co.) was twice distilled at reduced pressure, and the distillate boiling at 75–76° (19 mm.) collected as product. (The reported boiling point is 75–78° (15 mm.)).⁵ The neutral equivalent, determined by titration with standard acid, was 60.9 (calcd. 61.1).

2-Methoxyethylamine.—The amine was salted out of the 65–70% aqueous solution (Eastman Kodak Co.) with solid sodium hydroxide. Drying with solid barium oxide and distillation gave a product which boiled at 90.5° (727 mm.) (reported 95° (756 mm.)).⁶ Because of the extremely hygroscopic nature of this amine, no reliable neutral equivalent was determined.

2-Aminoethyl-2'-hydroxyethyl Sulfide.—Forty-three grams (one mole) of ethylenimine (Chemirad Co.) was added dropwise with mechanical stirring at room temperature to 78 g. (one mole) of 2-mercaptoethanol (Eastman Kodak Co.). Addition required about 1.25 hr. and stirring was continued for an additional 3 hr. The reaction mixture was distilled at 3 mm. and the material boiling at 116–120° (mainly 117–119°) was collected as product. The amine weighed 101.5 g. (83.9%) and had a neutral equivalent of 120.8 (calcd. 121.2).

Bis-(2-aminoethyl) Ether.—This amine was prepared from bis-(2-chloroethyl) ether by the Gabriel synthesis as modified by Ing and Manske.⁷ This compound proved to be difficult to isolate and purify, and reliable physical constants could not be determined. However, the dihydro-

chloride contained 40.3% Cl (calcd. 40.0%) as determined by the Fajans method.

1,8-Diamino-3,6-dioxaoctane.—This compound was synthesized from triethylene glycol through the dichloride and phthalimido compound. Since this amine was prepared, Dwyer and co-workers⁸ have given details of an essentially similar synthesis. The product boiled at 105–109° (6–7 mm.) (reported 95° (1 mm.)).⁹ The neutral equivalent was 75.1 (calcd. 74.1) and the picric acid melted at 94–96° (reported 97°).⁹

1,8-Diamino-2-oxa-6-thiaoctane.—This amine was prepared by the method of Dwyer, *et al.*⁸ The product boiled at 120–121° (2–3 mm.) and its dipicric acid melted at 157–158°. The reported values are 120–121° (1.5 mm.) and 157°, respectively.⁹

The preparation of reagents, the procedure for making the measurements, and the method of calculation were the same as previously reported.³

Results

Logarithms of equilibrium constants and thermodynamic quantities derived from the constants are presented in Table I. The logarithms of the constants are the average of four values, and the 95% confidence limits are given. The slope of the log K vs. $1/T$ curve, used in the evaluation of ΔH , was calculated by the method of least squares.

Dashes in the table indicate systems for which precipitation occurred. Mercuric ion solutions were titrated with all of the amines at all four temperatures. Attempts to calculate equilibrium constants gave values which depended upon which points were taken for the calculation. Data for mercury are therefore not reported, since it is apparent that its reactions with the amines used in this study are different from those of the other metals.

Discussion

The values of ΔF for the addition of a proton to an amine are nearly constant, and in all cases the entropy contributions are small. Thus it is evident that the strength of the N–H bond is not greatly influenced by the nature of the organic group bonded to the nitrogen, and that the stability of the protonated species is primarily due to the heat effect. Probably because of electrostatic repulsion, ΔF_2 for the diamines is slightly smaller than ΔF_1 . These observations are in agreement with McIntyre's work.⁹

Ethanolamine and 2-methoxyethylamine coordinated only with silver ion, and the ΔF values for these reactions are somewhat greater than half those for some typical diamines.³ The terminal

(1) This investigation was carried out under contract N6-onr 26913 between The Pennsylvania State University and The Office of Naval Research.

(2) A portion of a thesis presented by John R. Lotz in partial fulfillment of the requirements for the degree of Doctor of Philosophy, June, 1954.

(3) C. R. Bertsch, W. C. Fernelius and B. P. Block, *THIS JOURNAL*, **62**, 444 (1958).

(4) J. Bjerrum, G. Schwarzenbach and L. G. Sillen, "Stability Constants of Metal-Ion Complexes. Part I. Organic Ligands," Special Publication No. 6, The Chemical Society, Burlington House, London W 1, England, 1957.

(5) E. Abderhalden and H. Brockman, *Fermentforschung*, **10**, 159 (1928).

(6) W. Traube and E. Peiser, *Ber.*, **53**, 1507 (1920).

(7) H. R. Ing and R. H. F. Manske, *J. Chem. Soc.*, 2348 (1926).

(8) F. P. Dwyer, N. S. Gill, E. C. Gyarfás and F. Lions, *J. Am. Chem. Soc.*, **75**, 1526 (1953).

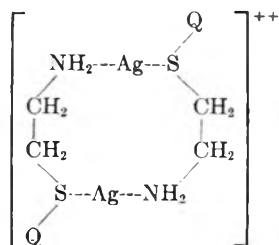
(9) G. H. McIntyre, Jr., Ph.D. Thesis, The Pennsylvania State University, 1953.

KNO_3 .¹⁰ Gonick¹¹ observed that the reverse is true in the reaction of $\text{CH}_3\text{SCH}_2\text{CH}_2\text{NH}_2$ with silver ion ($\log K_1 = 4.17$, $\log K_2 = 2.71$ at 30° in $1.0 M \text{KNO}_3$) and postulated chelate formation involving both nitrogen and sulfur. Table I shows a similar situation with $\text{HOCH}_2\text{CH}_2\text{SCH}_2\text{CH}_2\text{NH}_2$.

As is discussed later, oxygen appears to coordinate very weakly as compared to nitrogen. This is borne out in the apparent behavior as unidentate ligands of $\text{HOCH}_2\text{CH}_2\text{NH}_2$ and $\text{CH}_3\text{OCH}_2\text{CH}_2\text{NH}_2$ with silver ion. It is thus likely that the oxygen atom in $\text{HOCH}_2\text{CH}_2\text{SCH}_2\text{CH}_2\text{NH}_2$ is coordinated weakly as compared to nitrogen. It is probable, however, that the unusual behavior of both of these amines toward silver ion can be explained in terms of the common presence of the $-\text{SCH}_2\text{CH}_2\text{NH}_2$ group.

A 5-membered chelate ring, such as would be formed if both nitrogen and sulfur are coordinated, would be badly strained because of the normal 180° bond angle of the silver ion. Schwarzenbach¹² concluded that ethylenediamine and silver give the cyclic dimeric complex $[\text{Ag}_2(\text{H}_2\text{NCH}_2\text{CH}_2\text{NH}_2)_2]^{++}$ which should be essentially strainless.

It is reasonable to assume that amines such as $\text{CH}_3\text{SCH}_2\text{CH}_2\text{NH}_2$ or $\text{HOCH}_2\text{CH}_2\text{SCH}_2\text{CH}_2\text{NH}_2$ would behave similarly to give complexes with the structure



(where $\text{Q} = \text{CH}_3$ or HOCH_2CH_2), and that continued addition of ligand would open the ring (presumably at the $\text{Ag}-\text{S}$ bonds) to give the usual amine-silver complex, $[\text{Ag}(\text{H}_2\text{NCH}_2\text{CH}_2\text{SQ})_2]^+$.

Table II lists $\log K$ values for the reactions of silver and nickel ions with several amines analogous in structure to those used in this study. Thermodynamic constants would have been preferable to equilibrium constants, but were not available for all cases. Several of the systems were studied in neutral salt solution.

Size difference between oxygen and sulfur atoms might account for the different stabilities of the silver ion complexes with $\text{S}(\text{CH}_2\text{CH}_2\text{NH}_2)_2$ and $\text{O}(\text{CH}_2\text{CH}_2\text{NH}_2)_2$. Models of both complexes can be made, but the oxygen compound involves considerable strain if the usual 180° bond angle of the silver ion is to be satisfied. The slightly larger sulfur atom lengthens the chain just enough to relieve the strain.

The low K_1 for the reaction of $(-\text{CH}_2\text{SCH}_2\text{CH}_2\text{NH}_2)$ may be anomalous. With the other three amines of similar structure the constants are about

(10) G. A. Carlson, J. P. McReynolds and F. H. Verhoek, *J. Am. Chem. Soc.*, **67**, 1334 (1945).

(11) E. Gonick, W. C. Fernelius and C. E. Douglas, *ibid.*, **76**, 4671 (1954).

(12) G. Schwarzenbach, H. Ackermann, B. Maissen and G. Anderegg, *Helv. Chim. Acta*, **35**, 2337 (1952).

TABLE II

LOG K_n VALUES AT 30° IN THE ABSENCE OF NEUTRAL SALT UNLESS OTHERWISE NOTED

Amine	Ag^+ $\log K_1$	Ni^{++} $\log K_1$	Ag^+ $\log K_2$	Ni^{++} $\log K_2$
$\text{HN}(\text{CH}_2\text{CH}_2\text{NH}_2)_2$	5.1 ^a	10.81 ^b	...	8.14 ^b
$\text{S}(\text{CH}_2\text{CH}_2\text{NH}_2)_2$	7.00 ^c	7.27 ^c	...	6.10 ^c
$\text{O}(\text{CH}_2\text{CH}_2\text{NH}_2)_2$	5.31 ^d	5.54 ^d	...	3.19 ^d
$(-\text{CH}_2\text{NHCH}_2\text{CH}_2\text{NH}_2)_2$	7.7 ^e	14.34 ^b	...	5.63 ^b
$(-\text{CH}_2\text{SCH}_2\text{CH}_2\text{NH}_2)_2$	5.08 ^c	7.90 ^c
$(-\text{CH}_2\text{OCH}_2\text{CH}_2\text{NH}_2)_2$	7.71 ^d
$\text{CH}_2\text{OCH}_2\text{CH}_2\text{NH}_2$				
$\text{CH}_2\text{SCH}_2\text{CH}_2\text{NH}_2$	8.12 ^c	6.17 ^d		

^a Ref. 13; 20° ; in $0.1 M \text{KNO}_3$. ^b Ref. 14; in $1.0 M \text{KCl}-\text{KNO}_3$. ^c Ref. 11; in $1.0 M \text{KNO}_3$. ^d This work. ^e Ref. 15; in $0.1 M \text{NaNO}_3$.

the same, suggesting that only the nitrogen atoms are coordinated and that the chains are sufficiently long so that size differences between N, S and O atoms do not significantly affect the stability of the complexes.

Discussion of the nickel complexes is limited to comparison of $\log K_1$ values. The decrease in stability in the order $\text{N} > \text{S} > \text{O}$ is quite evident.

Table III lists $-\Delta H$ values for the coordination reactions of a number of amines with copper(II) ion. Using McIntyre's⁹ value of about 6 kcal. for a single metal-nitrogen bond as a standard, it is apparent that sulfur or oxygen bonds to copper are considerably weaker.

TABLE III

HEATS OF REACTION IN KCAL./MOLE FOR THE STEPWISE COORDINATION OF VARIOUS AMINES WITH Cu^{++} ION AT 30° Neutral salt absent unless otherwise noted.

Amine	$-\Delta H_1$	$-\Delta H_2$	Ref. and notes
$\text{HN}(\text{CH}_2\text{CH}_2\text{NH}_2)_2$	18.9	6.3	9
$\text{S}(\text{CH}_2\text{CH}_2\text{NH}_2)_2$	11	13	11; ^a
$\text{O}(\text{CH}_2\text{CH}_2\text{NH}_2)_2$	11.0	3.7	This work
$\text{S} \begin{cases} \text{CH}_2\text{CH}_2\text{NH}_2 \\ \text{CH}_2\text{CH}_2\text{OH} \end{cases}$	5.1	5.9	This work
$(-\text{CH}_2\text{NHCH}_2\text{CH}_2\text{NH}_2)_2$	22	..	14; ^b
$(-\text{CH}_2\text{SCH}_2\text{CH}_2\text{NH}_2)_2$	15.5	..	9
$(-\text{CH}_2\text{OCH}_2\text{CH}_2\text{NH}_2)_2$	7.9	..	This work
$\text{CH}_2\text{OCH}_2\text{CH}_2\text{NH}_2$			
$\text{CH}_2\text{SCH}_2\text{CH}_2\text{NH}_2$	13.1	..	This work

^a In $1.0 M \text{KNO}_3$. ^b In $1.0 M \text{KCl}-\text{KNO}_3$.

With both $\text{S}(\text{CH}_2\text{CH}_2\text{NH}_2)_2$ and $\text{O}(\text{CH}_2\text{CH}_2\text{NH}_2)_2$, $-\Delta H_1$ is approximately twice the value for a single $\text{Cu}-\text{N}$ bond. Thus it appears that neither sulfur nor oxygen is coordinated with strength comparable to nitrogen. With $\text{HOCH}_2\text{CH}_2\text{SCH}_2\text{CH}_2\text{NH}_2$, $-\Delta H_1$ is slightly less than the standard value for nitrogen alone. This amine apparently behaves here as a monodentate ligand, only the nitrogen being coordinated, and loses a small amount of bond strength through failure of chelation to occur.¹⁶

(13) J. E. Prue and G. Schwarzenbach, *ibid.*, **33**, 985 (1950).

(14) H. B. Jonassen, G. G. Hurst, R. B. LeBlanc and A. W. Meibohm, *THIS JOURNAL*, **56**, 16 (1953).

(15) G. Schwarzenbach, *Helv. Chim. Acta*, **33**, 974 (1950).

(16) Cf. C. G. Spike and R. W. Parry, *J. Am. Chem. Soc.*, **75**, 3770 (1953).

It should be possible to add a third and fourth molecule of this amine to the copper ion, but constants for these reactions could not be calculated. Probably the amine concentrations used in this study were too low to give appreciable concentrations of the tri- and tetraamine complexes.

The tetradentate amine $(-\text{CH}_2\text{NHCH}_2\text{CH}_2\text{NH}_2)_2$ shows normal Cu-N bond strengths. For its disulfur analog $(-\text{CH}_2\text{SCH}_2\text{CH}_2\text{NH}_2)_2$ $-\Delta H_1$ exceeds that for two Cu-N bonds by 3 or 4 kcal. On this basis, the strength of a Cu-S bond is of the order of 2 kcal. The mixed compound $\text{H}_2\text{NCH}_2\text{CH}_2\text{SCH}_2\text{CH}_2\text{OCH}_2\text{CH}_2\text{NH}_2$ has $-\Delta H_1$ greater by only 1 or 2 kcal. than that for two Cu-N bonds. This figure is in good agreement with the estimate of $-\Delta H$ just given for a single Cu-S bond, and suggests that, as was the case with $\text{O}(\text{CH}_2\text{CH}_2\text{NH}_2)_2$ and $\text{HOCH}_2\text{CH}_2\text{SCH}_2\text{CH}_2\text{NH}_2$, oxygen is not bound strongly enough to give a measurable $-\Delta H$.

The low $-\Delta H_1$ for $(-\text{CH}_2\text{OCH}_2\text{CH}_2\text{NH}_2)_2$ is somewhat surprising. Even if the oxygens are very weakly coordinated, a $-\Delta H_1$ of about 12 kcal. for the two nitrogens would have been predicted. It is possible that the 8-membered chain between the amine groups is flexible enough to allow rather free movement over a considerable area. This would tend both to weaken the Cu-N bonds and to hinder the approach of a second ligand molecule. The behavior of $\text{H}_2\text{NCH}_2\text{CH}_2\text{SCH}_2\text{CH}_2\text{OCH}_2\text{CH}_2\text{NH}_2$ is in line with this hypothesis. The Cu-S bond, even though comparatively weak, is sufficient to restrain free movement of the amine molecule with respect to the copper ion, and the strength of the Cu-N bonds is preserved.

Acknowledgment.—The authors are indebted to Miss Helen A. Carbone for assistance with the calculations involved in this work.

THE OXIDATION OF CARBON BY NITRIC OXIDE

BY R. NELSON SMITH, JAMES SWINEHART AND DAVID LESNINI

Contribution from the Chemistry Department, Pomona College, Claremont, California

Received August 13, 1958

Below 200° NO reacts with an ashless sugar charcoal to give N_2 and carbon-oxygen surface complexes, the reaction ceasing when the surface is saturated with complexes. In the temperature range 450–600° the reaction is first order, proceeds continuously, and yields N_2 , CO_2 , CO and carbon-oxygen surface complexes. The activation energy varies from 15.0–18.3 kcal./mole, depending on the nature of the surface. It is postulated that a NO molecule reacts with another adsorbed at the site of a surface oxygen complex to give N_2 and CO_2 , and an oxygen complex on an adjacent carbon atom. The new oxygen complex usually serves as a site for further adsorption of NO and continuing reaction, but its location may be unstable and CO may be the product instead. H_2 -treatment of the surface decreases the rate, and O_2 -treatment increases the rate of reaction.

A previous study¹ of the adsorption of nitric oxide on carbon showed that adsorption isotherms at temperatures above about -150° were without meaning because of the very rapid reaction of NO with the carbon to form N_2 gas and carbon-oxygen surface complexes. This paper reports a further study of this complicated reaction of NO with carbon at elevated temperatures where the additional reaction products are CO and CO_2 .

Experimental

The reaction system provided for the continuous circulation of NO through a heated bed of carbon, and in design it was much the same as that used in earlier work.² The major portion of the reaction proceeds with no pressure change and the reaction products vary with conditions so that rate measurements cannot be made manometrically. Instead, samples were removed at regular intervals for analysis by gas chromatographic methods.³ The decrease in pressure which would have occurred after the removal of each sample was prevented by adding an equal volume of mercury to a compensation bulb. The design of the compensation bulb and circulation system was such as to eliminate dead space. A small dead volume of about 2 ml. (in a system volume of about 600 ml.) existed where a manometer was connected to the system. This manometer was used to ascertain when a proper volume of mercury had been added in compensation for sample removal, and to follow any small changes in pressure which occurred during the course of the reaction.

An activated sugar charcoal of extremely low ash content (less than 0.005%) was prepared from Confectioners AA sugar furnished by the California and Hawaiian Sugar Refining Corporation, San Francisco, California. It is designated as Su-60 and the method of its preparation and activation is described elsewhere.² The BET nitrogen surface area is 1060 m.² per gram. An 0.85-g. sample was used. For many of the runs the sample was " H_2 -treated" prior to the addition of the nitric oxide. This hydrogen treatment consisted of three approximately 15-minute treatments with H_2 gas at 1000°. The H_2 was pumped out between each treatment and after the last treatment the sample was cooled slowly with continuous pumping.

Nitric oxide was prepared by the method of Marquoyrol and Florentin⁴ following a detailed procedure described elsewhere.¹ The analytical method used showed this gas to be pure NO. Initial pressures of 200 mm. or less were used in each run.

Carbon monoxide was obtained by dropping powdered, outgassed sodium formate onto outgassed concentrated sulfuric acid in an evacuated system. The CO so produced was passed through a Dry Ice trap before storing in a Pyrex reservoir. The analytical method used showed this gas to be pure CO.

Results

The rate of disappearance of NO is most rapid on an O_2 -treated surface (one which has been treated with O_2 and outgassed for several hours at the same temperature as the run), and least rapid on a H_2 -treated surface. Regardless of the nature of the carbon surface, the rate of disappearance of NO is first order with respect to the partial pressure of NO.

(1) R. N. Smith, D. Lesnini and J. Mooi, *THIS JOURNAL*, **60**, 1063 (1956).

(2) R. N. Smith and J. Mooi, *ibid.*, **59**, 814 (1955).

(3) R. N. Smith, J. Swinehart and D. Lesnini, *Anal. Chem.*, **30**, 1217 (1958).

(4) M. Marquoyrol and D. Florentin, *Bull. soc. chim. France*, [4] **11**, 804 (1912).

Figure 1 shows typical first-order plots for a variety of temperatures on a surface that had already been exposed to and had reacted with NO. This surface is designated as an "oxide surface" to distinguish it from a H₂-treated surface which has no carbon-oxygen complexes or an O₂-treated surface which has a very high concentration of carbon-oxygen complexes. The initial rate on an O₂-treated or an oxide surface is always somewhat greater than the first-order rate by which the reaction continues after this short initial period. Table I gives the rate constants for this reaction for a variety of temperatures at a variety of surface conditions. The activation energy for this reaction over the temperature range 450–600° varies from 15 kcal./mole on an O₂-treated surface to 18.3 kcal./mole on a H₂-treated surface. It should be emphasized that the rate constants for both the O₂-treated and the H₂-treated surfaces, as well as the activation energies calculated from them, must be considered as qualitative only since the nature of the surface is continually changing during the course of these runs. It is also of interest to note that at 600° the rate is substantially the same regardless of the form of surface pre-treatment.

TABLE I
RATE CONSTANTS

Type of surface	Temp. (°C)	k (sec. ⁻¹ g. ⁻¹) × 10 ⁶
O ₂ -treated	450	..
	500	19.2
	550	38.5
	600	38.9
Oxidized (Run after that on O ₂ -treated surface)	450	5.1
	500	13.0
	550	22.4
	600	36.7
H ₂ -treated	450	5.1
	500	7.2
	550	20.2
	600	35.6
Oxide (Run after that on H ₂ -treated surface)	450	..
	500	9.0
	550	19.1
	600	35.5

The products of the reaction of NO with carbon vary with temperature and the previous treatment of the carbon surface. From below Dry Ice temperatures to approximately 200° the sole products are N₂ gas and carbon-oxygen surface complexes (which can be removed from the surface only at higher temperatures in the form of carbon dioxide and carbon monoxide). With increasing temperature above 200°, more CO₂ gas appears as one of the major products and carbon-oxygen surface complexes become less important as a product. The approximate percentage of NO which is used in making oxygen complexes varies with temperature as follows: 200° and lower, 100%; 250°, 75%; 450°, 35%; 500°, 32%; 550°, 16%; 600°, 7%. If the carbon surface has been H₂-treated prior to the addition of NO, no gaseous products other than N₂ and CO₂ appear up to a temperature of 500°. At 550° and higher, CO also appears as a product; at 600° about one-tenth of the oxygen from the de-

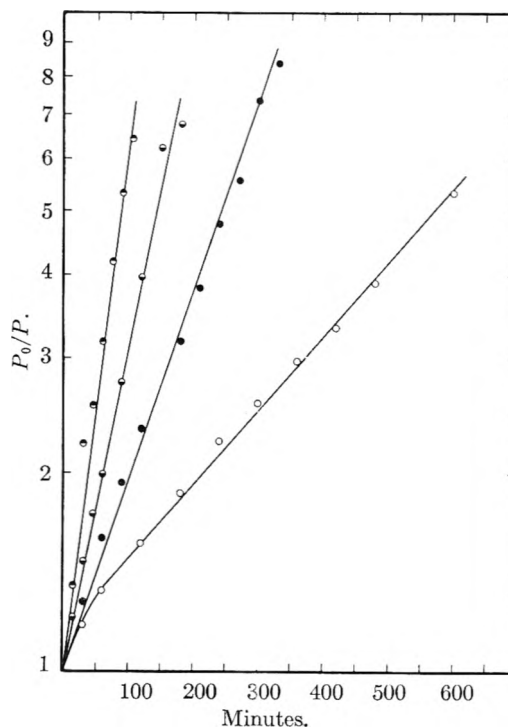


Fig. 1.—A typical semi-log plot of P_0/P vs. time showing, at various temperatures, the first-order nature of the reaction on an oxide surface. P_0 = initial pressure of NO and P = partial pressure of NO at time t . O, 450°; ●, 500°; ○, 550°; ●, 600°.

composed NO appears as CO. If the outgassed carbon surface possesses carbon-oxygen complexes as a result of previous reaction with NO, the addition of NO will cause production of some CO at temperatures as low as 450°. At 450°, 8% of the oxygen from the decomposed NO may be combined as CO, while at 600° there may be as much as 20% as CO. CO is formed even more readily if, prior to the addition of NO, the carbon surface has been treated with oxygen (and also outgassed). The ratio of CO to CO₂ is much greater in the initial stages of a reaction carried out over an oxidized surface than over a H₂-treated surface (see Fig. 2). It is not possible to make precise statements about the fraction of the NO which reacts to form CO because NO also reacts with CO at these temperatures in the presence of carbon surfaces to produce N₂ and CO₂. Thus during the course of a given run, the partial pressure of CO builds up rather rapidly during the early stages of the reaction, levels off during the middle portion, and then decreases during the later stages (see Fig. 3). An equimolar mixture of CO and NO passed over carbon at 550° reacts in such a manner that about one-half of the NO reacts with the carbon surface and one-half with the CO. Higher temperatures and excess CO favor the reaction with CO.

Discussion

Certain conclusions about the mechanism of the reaction of NO with carbon may be quickly drawn from the experimental observations.

1. The first step in the reaction must be the formation of carbon-oxygen surface complexes, for if these are not already present on the surface the

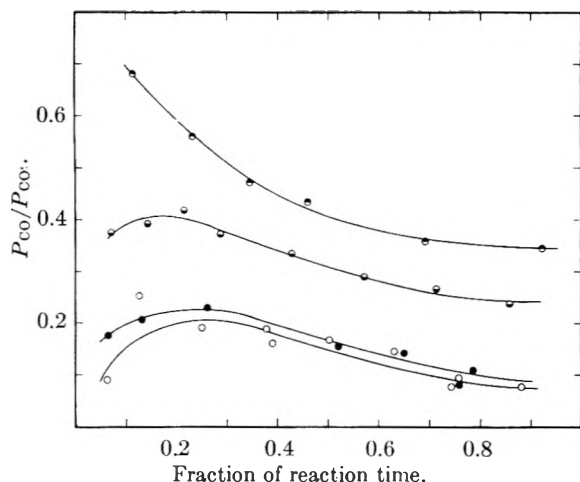


Fig. 2.—The ratio of the partial pressures of CO and CO₂ as a function of reaction time on a variety of surfaces at 550°: ●, O₂-treated surface; ●, run following a run on an O₂-treated surface; ●, oxide surface; ○, H₂-treated surface. There is essentially no difference between an oxide and a H₂-treated surface.

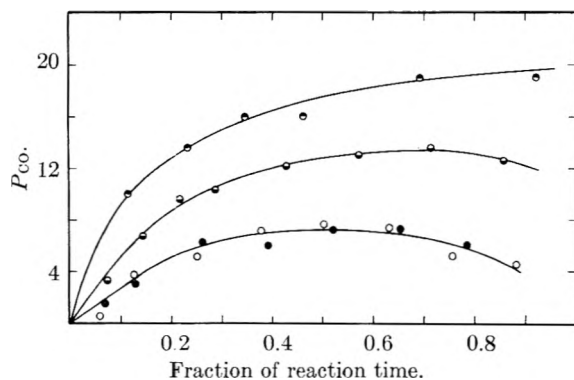


Fig. 3.—The partial pressure of CO, in mm., as a function of reaction time on a variety of surfaces at 550°: ●, O₂-treated surface; ●, run following a run on an O₂-treated surface; ●, oxide surface; ○, H₂-treated surface. There is essentially no difference between an oxide and a H₂-treated surface. Initial NO pressure in each case was approximately 150 mm.

initial reaction product is only N₂ at temperatures below 200°, or at higher temperatures N₂ along with insufficient CO₂ to account for all the NO decomposed.

2. Carbon-oxygen surface complexes are important intermediates in the reaction, as evidenced by the fact that (a) the rate on a H₂-treated surface is slowest, (b) the initial important process on a H₂-treated surface is the production of N₂ without CO₂, (c) there is an excess of oxygen in the products (over that contained in the NO which decomposed) if the reaction is carried out on an oxygen-treated surface.

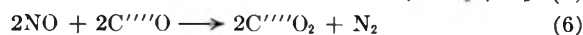
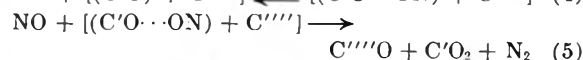
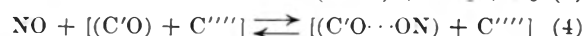
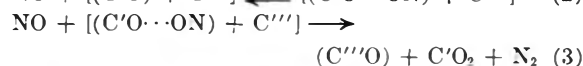
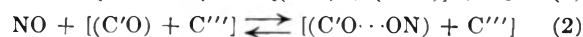
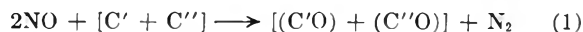
3. The complexes from which CO is produced must be more stable or less reactive than those from which CO₂ is produced as evidenced by the fact that (a) CO is produced only at temperatures above 500° on H₂-treated surfaces, whereas CO₂ production on similar surfaces commences at about 200°, (b) less CO is always produced than CO₂, (c) in the thermal decomposition of carbon-oxygen surface complexes CO₂ is the predominant product at lower temperatures and CO at higher temperatures.

4. CO does not arise from the thermal decomposition of carbon-oxygen surface complexes, for a well-outgassed oxidized surface which has resided in a closed system for several hours at a given temperature without giving any gaseous products will subsequently react with NO to give CO.

5. CO, once produced, may react with NO to produce N₂ and CO₂ as evidenced by the fact that (a) CO will not react at the temperatures of this study with carbon or with carbon possessing carbon-oxygen surface complexes, (b) CO is consumed when mixed with NO and passed over carbon at these temperatures, especially readily when CO is in excess, (c) the CO content of the reaction mixture increases during the initial part of the reaction, and then decreases during the latter part of the reaction when the CO becomes large relative to the NO.

6. The carbon-oxygen complexes made by oxygen seem to be somewhat greater in quantity and somewhat different in nature from those produced by NO as evidenced by the fact that (a) the reaction goes fastest on an O₂-treated surface, (b) with an O₂-treated surface there is an excess of oxygen in the products over that available in the initial NO used, (c) the ratio of CO to CO₂ in the gas products from the O₂-treated surface is greater, and that (d) in a succession of reactions, the first being over an O₂-treated surface, the reaction rate and the CO-to-CO₂ ratio approach those observed with a non-oxygen-treated surface in about three runs.

These six reaction steps appear to account for all of the observed experimental data



Step 1 occurs readily at temperatures from below -80° and up, and below 200° it is the only step which leads to the formation of N₂. [C' + C'] represents two adjacent surface carbon atoms, and [(C'O) + (C''O)] represents the oxygen complex on C' and C''. The oxygen complexes may then serve as sites for physical adsorption of NO, and thus steps 2 and 4 are reversible. It is believed that it is the oxygen atom of the NO molecule which is held to the surface. The only difference between steps 2 and 4 is in the nature of the adjacent carbon atoms, C''' and C'''''. It is not known just what the real difference between C''' and C'''' is, but it is postulated here that C'''' will yield CO gas, whereas C''' will form just another surface complex, (C''''O), with the same properties as (C'O) and (C''O). If no CO gas were formed, steps 1, 2 and 3 would be sufficient to explain the reaction at temperatures above 200°. Since considerably less CO is formed than CO₂ it is apparent that C'''' atoms are not the most common, and perhaps they are located at corners, edges, or cracks. Step 6 will not take place homogeneously at the temperature studied for it

has an activation energy of 49.6 kcal./mole.⁵ It is catalyzed by carbon surfaces and hence step 6 is really a summary step for a reaction which needs further study. Steps 4 and 5 represent a minor fraction of the over-all reaction, and step 6 involves only part of the CO produced in steps 4 and 5.

Steps 3 and 5 seem reasonable if NO is adsorbed by the oxygen end of the molecule and if the carbon atoms C' and C''' or C' and C'''' are adjacent. In this way two nitrogen atoms may conveniently unite, oxygen atoms from two different NO molecules are available to a single carbon atom for CO₂, and the necessary intermediate carbon-oxygen surface complex is regenerated for further reaction by steps 2 and 4. This mode of adsorption of NO and the decomposition of the resulting complex is different from that which Shah⁶ suggested to explain the low-temperature formation of a trace of NO₂.

This mechanism also satisfactorily accounts for the first-order nature of the reaction. On a surface which has not been H₂-treated step 1 is unimportant because the complexes (C'O) and (C''O) have already been made in previous reactions, and step 6 is also unimportant in the over-all picture. Omitting steps 1 and 6 from serious consideration, then, leads to the rate expression

$$-\frac{dP}{dt} = k_1\theta'P + K_1\theta''P \quad (1)$$

where P is the partial pressure of NO, and θ' and θ'' are the fractions of the surface holding NO by the [(C'O) + C'''] and [(C'O) + C''''], respectively. Applications of the simple Langmuir concept for the fraction of the surface covered leads to

$$-\frac{dP}{dt} = \frac{k_2P^2}{1 + k_3P} + \frac{K_2P^2}{1 + K_3P} \quad (2)$$

If k_3P and K_3P are both substantially greater than unity, then equation 2 reduces to the simple first-order expression

$$-\frac{dP}{dt} = k_4P + K_4P = KP \quad (3)$$

Step 1 is interesting in that it goes quite rapidly, even at very low temperatures, but at each temperature below 200° it comes to a standstill when the surface carbon atoms which are capable of form-

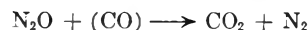
ing oxygen complexes at the given temperature have obtained their oxygen. In the temperature range of this study, the total amount of nitrogen produced by step 1 is small compared to that produced by steps 2 to 5 of the continuing reaction. Thus, even on a H₂-treated surface, step 1 is not important in the total picture for the continuing reaction of NO. An additional term should be added to equation 3 to include the removal of NO by step 6 but, as pointed out earlier, this step plays a minor role (in the later stages of the reaction) in the over-all reaction, and the nature and order of this reaction are not sufficiently well-known to include such a term.

When the surface has been treated with oxygen (and outgassed) prior to the addition of NO, the surface has more than the usual concentration of (C'O) and (C''O) and the rate is greater. In addition there are apparently more sites involving C'''' atoms because the rate of production of CO is greater.

It is of some interest to compare NO with N₂O with respect to oxidation of carbon. Though both processes require carbon-oxygen surface complexes as intermediates, the N₂O oxidation mechanism is far simpler.⁷ This is due primarily to the fact that in N₂O both nitrogen atoms are already joined together and the reaction is merely a two-step transfer of oxygen atoms to carbon to form CO₂. The first step is



and the second is



Physical adsorption of N₂O does not seem to be involved as it is with NO.

The oxidation of CO by N₂O over carbon² involves the physical adsorption of CO at some "active carbon" atom, not a carbon-oxygen complex, and it may be that the oxidation of CO by NO requires a similar active site. Further study will be needed to determine this.

Acknowledgment.—The authors gratefully acknowledge the support of the Office of Naval Research for this work which was done under contract N8onr54700. Production in whole or in part is permitted for any purpose of the United States Government.

(5) C. P. Fenimore, *J. Am. Chem. Soc.*, **69**, 3143 (1947).

(6) M. S. Shah, *J. Chem. Soc.*, 2676 (1929).

(7) R. N. Smith, D. Lesnini and J. Mooi, *THIS JOURNAL*, **61**, 81 (1957).

A CONVENIENT NEW FORM OF ONSAGER'S EQUATION FOR THE DIELECTRIC CONSTANT OF POLAR SOLUTIONS¹

BY RICHARD N. WORK

Department of Physics, The Pennsylvania State University, University Park, Pa.

Received August 15, 1958

Onsager's equation for the dielectric constant of solutions of polar molecules in polar or non-polar solvents has been recast to express the relation between the dipole moments of the polar molecules present and $\epsilon_s - \epsilon_\infty$ the orientational contribution to the dielectric constant, where ϵ_s is the static dielectric constant and ϵ_∞ is the high frequency dielectric constant. The new form of Onsager's equation is convenient to use and is valid over the whole range of solution concentrations, within the limitations of Onsager's model. The effect of the free volume of the solution has been included. It is shown that serious errors can be introduced by the usual assumption that the volume actually occupied by the molecules is equal to the volume of the solution. The new equation is particularly useful in studies of short-range forces that lead to directional correlations between polar molecules, or in studies of the asphericity of molecules.

Introduction

A new form of Onsager's² equation for the dielectric constant of solutions of polar molecules has been developed in connection with a study of the detailed structure of copolymers.³ It is believed that the new equation presents sufficient advantage under wide enough circumstances to justify a separate discussion. The result obtained previously has been generalized to include cases where the volume fraction actually occupied by the molecules of the solution is less than unity, and it is presented here with revised notation.

There are several advantages in the use of Onsager's equation for the determination of dipole moments of molecules in solution.

First, the equation is derived rigorously from a model, which, though incomplete in certain respects, is clearly defined. Hence, differences which are observed in the values of the dipole moment of a given polar molecule, when measured in the vapor phase and in various solvents can be attributed to factors not included in the model, *viz.*, molecular asphericity and directional correlations arising out of short-range intermolecular forces, instead of attributing them to "solvent-effects," a term which is not very meaningful.

Secondly, Onsager's equation is valid over the whole range of solution concentrations. This simplifies the experimental task of determining dipole moments by permitting measurements in solutions of sufficient concentration that the dipolar contribution to the dielectric constant be large enough to be measured easily. In addition, the dependence of the measured value of the dipole moment on concentration can be used to study short-range forces⁴ in the liquid and molecular shape.⁵ In contrast to this, equations⁶ based on

the Mossotti internal field do not take into account the dipole-dipole interaction force, and hence they are valid only in the limiting case of dilute solutions of polar molecules in non-polar solvents. This leads to certain difficulties. First, the orientational contribution to the dielectric constant of the polar molecules in a dilute solution is small, making difficult the measurement of this quantity. This difficulty is partially alleviated by methods⁶ making use of several measurements in the region of higher concentration and extrapolating to infinite dilution. But, the extrapolation laws are uncertain because there is no clear way to separate the effects of dipole-dipole interactions, short range forces and molecular shape. Finally, the requirement that measurements be made only in dilute solutions eliminates the possibility of using the variation of the dipole moment with concentration to study molecular association.

Onsager's equation has not been widely used for the calculation of dipole moments from measurements on solutions because the calculations, involving Onsager's eq. 35 or 36,² are rather cumbersome. In addition, the question of how to take into account the free volume of the solution has been left open.

In the following, a new form of Onsager's equation is derived that is relatively easy to use and the question of the free volume is examined quantitatively.

Derivation

Onsager's equation is derived from a model in which each molecule of the *j*th kind is represented as a homogeneous and isotropic sphere of radius a_j , having an index of refraction n_j , corresponding to the atomic and electronic polarizabilities of the sphere, immersed in a medium of dielectric constant ϵ_s , and containing a rigid dipole $\mu_j = \mu_{jv}(n_j^2 - 2)/3$ at its center. Here, μ_{jv} is the dipole moment of an isolated molecule.

In the following it will be necessary to distinguish between the moment μ_{jv} and $(\mu_{jv})_{0n}$ the latter being the value obtained by applying Onsager's equation to measurements of the dielectric constant of solutions.

The new equation was developed to express $\langle(\mu_{jv}^2)_{0n}\rangle_{Av}$ in terms of the orientational contribution to the dielectric constant $\epsilon_s - \epsilon_\infty$ rather than $\epsilon_s - 1$. The average-square dipole moment is given by the expression $\langle(\mu_{jv}^2)_{0n}\rangle_{Av} = \sum x_j$

(1) The research reported here was started at the Plastics Laboratory, Princeton University, Princeton, New Jersey, under joint sponsorship of the Army and Navy under Signal Corps Contract No. DA-36-039sc-70154; ONR 356-375. Sponsorship has been continued at The Pennsylvania State University by the Atomic Energy Commission under Contract No. AT-(30-1)-1858.

(2) L. Onsager, *J. Am. Chem. Soc.*, **58**, 1486 (1936).

(3) R. N. Work and Y. Tréhu, *J. Appl. Phys.*, **27**, 1003 (1956).

(4) J. G. Kirkwood, *J. Chem. Phys.*, **7**, 911 (1939).

(5) F. Buckley and A. A. Maryott, *J. Research Natl. Bur. Standards*, **53**, 229 (1954).

(6) C. J. F. Böttcher, "Theory of Electric Polarization," Elsevier Publishing Co., Houston, Texas, 1952; C. P. Smyth, "Dielectric Structure and Behavior," McGraw-Hill Book Co., Inc., New York, N. Y., 1955. These authors give comprehensive reviews of the many equations for the static dielectric constant of solution of polar molecules in non-polar solvents.

$(\mu_{jv}^2)_{0n}$, where x_j is the mole fraction of component j . The static dielectric constant ϵ_s is determined by making measurements at frequencies sufficiently low that the distribution of dipolar vectors is always in equilibrium with the applied alternating field; while the high frequency dielectric constant ϵ_∞ is determined at a sufficiently high frequency that the distribution of dipolar vectors does not change under the influence of the field.

In deriving the new equation, we begin with Onsager's² eq. 35. This gives the static dielectric constant ϵ_s of a solution containing $j = 1, 2, \dots, n$ molecular species, each having a dipole moment as determined in the vapor phase of μ_{jv} , and a concentration of N_j molecules per unit volume. Fröhlich⁷ has re-expressed the equation as

$$\epsilon_s - 1 = \frac{3\epsilon_s}{2\epsilon_s + 1} \sum \left[\frac{4\pi(\mu_{jv}^2)_{0n}}{3kT} N_j \left(\frac{2\epsilon_s + 1}{2\epsilon_s + n^2_j} \times \frac{n^2_j + 2}{3} \right) + \frac{2\epsilon_s + 1}{2\epsilon_s + n^2_j} (n^2_j - 1) \frac{4\pi}{3} a^3 N_j \right] \quad (1)$$

where k is the Boltzmann constant and T is the absolute temperature. We will use the symbol $\epsilon_{j\infty}$ to represent n_j^2 , and $(\mu_{jv}^2)_{0n}$ to emphasize the fact that the conditions of Onsager's model are not always fulfilled.

Representing $(4/3)\pi a_j^3 N_j$, the volume fraction actually occupied by the j th kind of molecule by v_j , and defining the apparent moment $(\mu_j)_{app}$ by the relation

$$(\mu_j)_{app} \equiv (\mu_{jv})_{0n} \frac{2\epsilon_s + \epsilon_\infty}{2\epsilon_s + \epsilon_{j\infty}} \frac{\epsilon_{j\infty} + 2}{3} \quad (2)$$

we have, with some rearrangement of the terms in eq. 1

$$\epsilon_s - 1 = \frac{3\epsilon_s}{2\epsilon_s + \epsilon_\infty} \sum \left[\frac{4\pi(\mu_{j,app}^2) N_j}{3kT} \frac{2\epsilon_s + 1}{2\epsilon_s + \epsilon_\infty} + \frac{2\epsilon_s + \epsilon_\infty}{2\epsilon_s + \epsilon_{j\infty}} (\epsilon_{j\infty} - 1) v_j \right] \quad (3)$$

where ϵ_∞ is the high frequency dielectric constant of the solution. The quantity $(\mu_j)_{app}$ has no simple interpretation in terms of a physical model. By making use of the identity

$$\frac{2\epsilon_s + \epsilon_\infty}{2\epsilon_s + \epsilon_{j\infty}} (\epsilon_{j\infty} - 1) = \epsilon_\infty - 1 + \frac{2\epsilon_s + 1}{2\epsilon_s + \epsilon_{j\infty}} (\epsilon_{j\infty} - \epsilon_\infty) \quad (4)$$

Eq. 3 can be rearranged to yield the expression

$$\epsilon_s - \epsilon_\infty = \frac{3\epsilon_s}{2\epsilon_s + \epsilon_\infty} \left[\sum \frac{4\pi(\mu_{j,app}^2) N_j}{3kT} + (2\epsilon_s + \epsilon_\infty) \sum v_j \frac{(\epsilon_{j\infty} - \epsilon_\infty)}{2\epsilon_s + \epsilon_{j\infty}} + \frac{2\epsilon_s + \epsilon_\infty}{2\epsilon_s + 1} (\epsilon_\infty - 1)(\bar{V} - 1) \right] \quad (5)$$

where $\bar{V} \equiv \sum v_j$ is the volume fraction actually occupied by the molecules. Finally, using the relations $N_j = N_A (\bar{\rho}/\bar{M}) x_j$ and $\langle (\mu_j^2)_{app} \rangle_{Av} = \sum x_j (\mu_j^2)_{app}$ where $\bar{\rho}$ is the density of the solution, \bar{M} is its average molecular weight, N_A is Avogadro's number, and x_j is the mole fraction of component j , we have, on rearranging eq. 5

$$\langle (\mu_j^2)_{app} \rangle_{Av} = \frac{3kT\bar{M}}{4\pi N_A \bar{\rho}} \frac{2\epsilon_s + \epsilon_\infty}{3\epsilon_s} \left[\epsilon_s - \epsilon_\infty + \frac{3\epsilon_s}{2\epsilon_s + 1} (1 - \bar{V})(\epsilon_\infty - 1) - 3\epsilon_s \sum v_j \frac{\epsilon_{j\infty} - \epsilon_\infty}{2\epsilon_s + \epsilon_{j\infty}} \right] \quad (6)$$

(7) H. Fröhlich, "Theory of Dielectrics," Oxford University Press, London, 1949, eq. 6.38.

Discussion

The discussion of eq. 6 given here is divided into three parts. First, suitable methods are described for evaluating the quantities in eq. 6 which are not directly measurable. Second, the error that is introduced by assuming that the sum of the molecular volumes is equal to the volume of the solution is considered quantitatively. Finally, some further advantages in the use of the modified version of Onsager's equation are pointed out.

Evaluation of $\epsilon_{j\infty}$ and \bar{V} .—In eq. 6, the quantities v_j , and hence \bar{V} , and $\epsilon_{j\infty}$ are the only ones that are not directly measurable. Now, the molecular radius a_j and the high frequency dielectric constant $\epsilon_{j\infty}$ of the molecular sphere can be treated as constants, since they depend only slightly on temperature. Hence, a single determination of the value of a_j or $\epsilon_{j\infty}$, for each pure liquid, at a convenient temperature suffices to establish these quantities for any mixture. Hence, the ratio of the density of the pure liquid at the temperature of interest to the density of the pure crystalline phase can be taken as an adequate approximation of V_j , the volume actually occupied by the molecules in the pure liquid at the given temperature.

The relation between V_j , ϵ_∞ and $\epsilon_{j\infty}$ can be established by considering eq. 6. Since we are interested here only in the atomic and electronic contributions to the dielectric constant, we can set $\epsilon_s = \epsilon_\infty$ and obtain the relation

$$\frac{(1 - \bar{V})(\epsilon_\infty - 1)}{2\epsilon_\infty + 1} = \sum v_j \frac{\epsilon_{j\infty} - \epsilon_\infty}{2\epsilon_\infty + \epsilon_{j\infty}} \quad (7)$$

Whence, it follows that

$$(\epsilon_\infty - 1) = 3\epsilon_\infty \sum v_j \frac{(\epsilon_{j\infty} - 1)}{2\epsilon_\infty + \epsilon_{j\infty}} \quad (8)$$

and hence for a pure liquid

$$(\epsilon_{j\infty} - 1) = (\epsilon_\infty - 1) \frac{1}{1 - 3\epsilon_\infty(1 - V_j)/(2\epsilon_\infty + 1)} \quad (9)$$

Thus, using eq. 9, an estimate of V_j from density measurements, and a measurement of ϵ_∞ of the pure liquid, one can obtain an estimate of $\epsilon_{j\infty}$. The relation $\bar{V} = \sum x_j V_j$, establishes the value of \bar{V} .

Magnitude of the Free Volume Effect.—In order to simplify the calculations whenever possible, it is of interest to determine the conditions under which the effect of the free volume can be neglected.

By making use of eq. 8 and 9, it is possible to recast eq. 6 into the form

$$\langle (\mu_j^2)_{app} \rangle_{Av} = \frac{3kT\bar{M}}{4\mu\bar{\rho}N_A} \frac{2\epsilon_s + \epsilon_\infty}{3\epsilon_s} (\epsilon_s - \epsilon_\infty)(1 - C) \quad (10)$$

where

$$C = 2 \frac{3\epsilon_s(\epsilon_\infty - 1)^2(1 - \bar{V})}{(2\epsilon_s + \epsilon_\infty)(2\epsilon_s + 1)(2\epsilon_\infty + 1)} + \frac{2}{2\epsilon_s + \epsilon_\infty} \sum v_j \frac{(\epsilon_{j\infty} - \epsilon_\infty)^2}{(2\epsilon_\infty + \epsilon_{j\infty})(2\epsilon_s + \epsilon_{j\infty})}$$

Also the left-hand-side of eq. 10 can be written as

$$\begin{aligned} \langle (\mu_j^2)_{app} \rangle_{Av} &= \sum x_j (\mu_{jv}^2)_{0n} \left(\frac{2\epsilon_s + \epsilon_\infty}{2\epsilon_s + \epsilon_{j\infty}} \frac{\epsilon_{j\infty} + 2}{3} \right)^2 \\ &= \sum x_j (\mu_{jv}^2)_{0n} \left(\frac{\epsilon_{j\infty} + 2}{3} \frac{2\epsilon_s + \epsilon_\infty}{2\epsilon_s + \epsilon_{j\infty}} \right)^2 (1 + C_j)^2 \end{aligned} \quad (11)$$

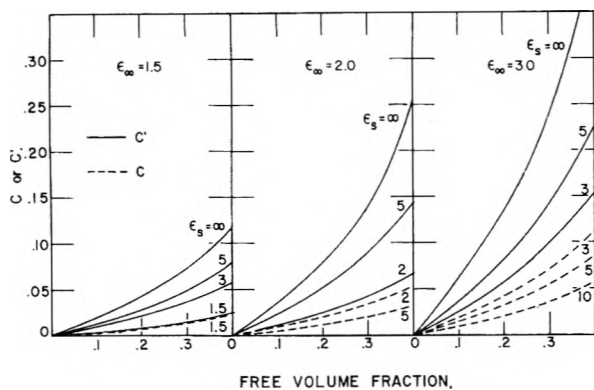


Fig. 1.—Values of C and C' (see eq. 12) for a pure polar liquid as a function of the free volume fraction for various values of the high frequency ϵ_∞ and static ϵ_s dielectric constants.

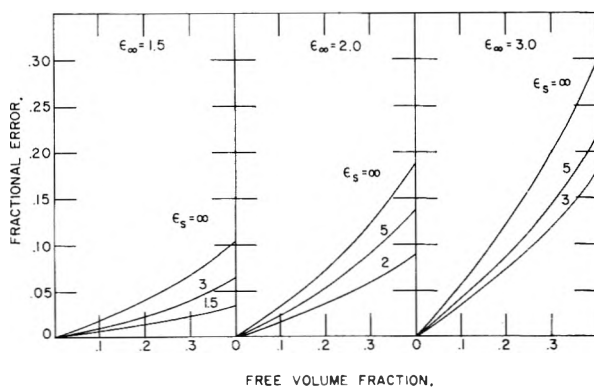


Fig. 2.—Values of the fractional error in the dipole moment introduced by the usual assumption that the volume of the liquid equals the sum of the molecular volumes as a function of the actual free volume in the liquid.

where

$$C'_j = \frac{A'_j(1 - V_j)/V_j}{1 - B_j(1 - V_j)/V_j}$$

$$A'_j = \frac{2(\epsilon_s - 1)(\epsilon^{j_\infty} - 1)3\epsilon^{j_\infty}}{(2\epsilon^{j_\infty} + 1)(\epsilon^{j_\infty} + 2)(2\epsilon_s + \epsilon^{j_\infty})}$$

and

$$B_j = \frac{2(\epsilon_s - \epsilon^{j_\infty})(\epsilon^{j_\infty} - 1)}{(2\epsilon^{j_\infty} + 1)(2\epsilon_s + \epsilon^{j_\infty})}$$

Here ϵ^{j_∞} is the macroscopic high-frequency dielectric constant of the pure liquid j .

It will be seen later that in many, but by no means in all, cases the factor C and sometimes even C' are negligible leading to a considerable simplification of the computations. In intermediate cases the second term in C (eq. 11) is negligible leading to a lesser simplification.

To investigate the magnitude of the terms C and C' , it is convenient to consider a pure polar liquid. Then eq. 11 can be simplified by using eq. 8 and 9 to express ϵ^{j_∞} in terms of V_j . The result is

$$(\mu^{j_v})_{0n} = \left(\frac{3}{\epsilon_\infty + 2} \right)^2 \frac{3kTM}{4\pi f N_A} \frac{2\epsilon_s + \epsilon_\infty}{3\epsilon_s} (\epsilon_s - \epsilon_\infty) \frac{1 - C}{(1 + C')^2} \quad (12)$$

with now, the factors C and A , given by the expressions

$$C = \frac{A(1 - \bar{V})/\bar{V}}{1 - B(1 - \bar{V})/\bar{V}}$$

and

$$A = 2 \frac{3\epsilon_s(\epsilon_\infty - 1)^2}{(2\epsilon_s + \epsilon_\infty)(2\epsilon_s + 1)(2\epsilon_\infty + 1)}$$

The significance of B and C' is the same as in eq. 11 except that ϵ^{j_∞} and ϵ_∞ are here identical.

Values of C and C' are shown in Fig. 1 as a function of the free volume fraction V_f for different values of ϵ_s and ϵ_∞ . Curves for $\epsilon_s = \infty$ and $\epsilon_s = \epsilon_\infty$ give the limiting values of the factors C' and C for the cases of very large and very small dipole moments, respectively. The limit of C , as ϵ_s becomes large, is zero in all cases. In Fig. 2 values are given of C'' where $1 - C'' \equiv [(1 - C)/(1 + C')]^{1/2}$. The quantity C'' represents the fractional contribution to $(\mu^{j_v})_{0n}$ obtained by taking into account the free volume of the pure liquid.

The calculation of the factor C for solutions can often be simplified by neglecting the second term in C (eq. 11). This term is important only if ϵ_s is not much larger than ϵ_∞ and the free volume fraction V_f is large. In addition, the term C itself rapidly becomes negligible with respect to C' as ϵ_s becomes large. The factor C represents the dependence on molecular size of the enhancement of the molecular polarization in the direction of the applied field due to the polarization of the surroundings. Its magnitude depends on the values of ϵ_s , ϵ_∞ and each ϵ^{j_∞} , and in the case of mixtures, C is the weighted sum of the contributions of all molecular species present. The factor C'_j represents the enhancement of the dipole moment of the j th species through the polarization of the molecule in the direction of the dipole vector by the dipole part of the internal field. That is, the dipole μ_j , by polarizing the surroundings, produces an additional electric field at the molecule which further polarizes the molecular sphere of dielectric constant ϵ^{j_∞} , thus increasing the moment of the molecule. This factor depends only on ϵ_s , ϵ_∞ and ϵ^{j_∞} of the particular molecule of the j th kind. Therefore the correction C'_j is calculated separately for each species of molecule in the solution.

It is true that the free volume error is not the only source of the difference between μ_{jv} and $(\mu_{jv})_{0n}$. In fact, deviations of molecular shape from the assumed spherical shape can lead to errors of up to 40%,⁴ and short range forces that are responsible for directional correlations between polar groups can also introduce considerable difference between μ_{jv} and $(\mu_{jv})_{0n}$. Hence, unless the latter effects are known, there is still no assurance that the correction for free volume will lead to true values of the dipole moment. The use of the corrected value will however usually lead to a significantly better value of the dipole moment. In studies of molecular shape or molecular association a knowledge of the correction is important.

Further Advantages.—As mentioned previously the ratio of $(\mu^{j_v})_{0n}$ to (μ^{j_v}) can be used to study molecular shape factors and short-range intermolecular forces. These effects can be separated because they depend in different ways upon solution compositions. The shape factors depend only upon ϵ_s , and they are essentially constant for values of $\epsilon_s > 10$. On the other hand, the effect of di-

rectional correlations arising out of short-range intermolecular forces depends only upon the average separation of the interacting molecules, and hence upon their concentration. Thus, by appropriate variations of solution compositions, either effect can be made constant (or negligible in the case of interactions) while the other can be varied. The validity of Onsager's equation for any solution composition makes its use highly desirable in such studies, and the relative simplicity of the new form makes its application practicable.

Since the new form of Onsager's equation relates $(\mu_{jv})_{0n}$ to $\epsilon_s - \epsilon_\infty$ in a way that is nearly linear, *i.e.*, by a linear equation with nearly constant coefficients, the quantities ρ , ϵ_s and ϵ_∞ in the coefficients, need only be determined to precisions corresponding to that of $\epsilon_s - \epsilon_\infty$. This contrasts with the requirements of methods⁶ using increments of molar polarization where ρ and x_j must be deter-

mined to unusually high precisions because the increment is usually a small difference of two large numbers. In any case, the quantities $\epsilon_{j\infty}$ and V need be determined only to nominal precisions since C and C' are usually small compared to one.

Sometimes ϵ_s and ϵ_∞ can both be determined from measurements of a single specimen in a single cell, *e.g.*, bulk polymers. In this case, the difference ($\epsilon_s - \epsilon_\infty$) can be determined to an accuracy comparable with that of ϵ_s or ϵ_∞ leading to improved accuracy of the result in spite of the fact that ($\epsilon_s - \epsilon_\infty$) represents a small difference between two larger numbers. This is because the same cell constants apply in the calculation of ($\epsilon_s - \epsilon_\infty$) from a capacitance increment as in the calculation of ϵ_s or ϵ_∞ separately, and the capacitance increment can be calibrated to the same accuracy (about 1 part in 1000) as the total capacitance, providing it is of the order of 1 $\mu\mu\text{f.}$ or greater.

THEORY OF THE DONNAN MEMBRANE EQUILIBRIUM. II. CALCULATION OF THE OSMOTIC PRESSURE AND OF THE SALT DISTRIBUTION IN A DONNAN SYSTEM WITH HIGHLY CHARGED COLLOID PARTICLES¹

BY D. STIGTER² AND TERRELL L. HILL

Department of Chemistry, University of Oregon, Eugene, Oregon

Received August 18, 1968

As shown earlier,³⁻⁵ the McMillan-Mayer statistical theory enables one to express the osmotic pressure and the salt distribution in a Donnan system in terms of expansions in powers of the colloid concentration. The (virial) coefficients in these expansions are formulated with the help of "cluster integrals" depending on the potential of average force between the relevant particles. In this paper the second and third virial coefficients in the above expansions are evaluated by numerical integration for the case of spherical, highly charged colloid particles, surrounded by a Gouy-Chapman type of ionic double layer. It is shown that the value of the virial coefficients depends mainly on the (Debye-Hückel) potential field in the outer part of the double layer. This justifies the use of an approximate Debye-Hückel type of potential of average force in evaluating the cluster integrals. The calculations are put in "corresponding states" form which generalizes the applicability of the results.

1. Introduction

In a recent paper,³ various approaches to the osmotic pressure, salt distribution and membrane potential in a Donnan system were compared, all charged species being treated as point charges. In particular, the application of the statistical theory of McMillan and Mayer⁴ to the Donnan equilibrium was discussed.

In another paper,⁵ the McMillan-Mayer treatment was applied to the more general situation in which *two* species, though present on both sides of the membrane, are not in equilibrium across the membrane, while the other species are in equilibrium. Specialization of the general results led to the (equilibrium) salt distribution in a more conventional Donnan system (one non-equilibrium species).

The present work deals with calculations of the

osmotic pressure and of the salt distribution in a Donnan system, using the McMillan-Mayer approach and a model for highly charged colloid particles. Features of particular interest are: (1) unlike the treatment in Section 4 of I, we are able here, through the use of reference 5, to express both the osmotic pressure and the equilibrium salt distribution in terms of appropriate cluster integrals. Thus, the entire discussion is put on a firm statistical mechanical foundation. (2) A consequence of this situation is that the concept of "membrane potential" does not enter the discussion at all. (3) The calculations below can be put in "corresponding states" form and hence are rather general in applicability (though restricted, of course, to the model chosen).

We consider two solutions separated by a semi-permeable membrane. The solvent and the ionic species 1, 2 . . . j have the same chemical potentials in both solutions, but colloid particles are present on one side of the membrane only (the "inside" solution). The concentrations (number densities) of small ions are denoted $\rho_1, \rho_2, \dots, \rho_j$ and $\rho_1^*, \rho_2^*, \dots, \rho_j^*$ in the inside and in the outside solution, respectively. In the inside solution the

(1) This work was supported by a research grant from the Heart Institute of the U. S. Public Health Service.

(2) Western Utilization Research and Development Div., Albany 10, Calif.

(3) T. L. Hill, *Faraday Soc. Disc.*, **21**, 31 (1956). Hereafter denoted by I.

(4) W. G. McMillan and J. E. Mayer, *J. Chem. Phys.*, **13**, 276 (1945).

(5) T. L. Hill, *J. Am. Chem. Soc.*, **80**, 2923 (1958).

colloid concentration ρ gives rise to an osmotic pressure π . The small ions are considered as point charges and the colloid particles as spheres whose charges are compensated by ionic double layers of the Gouy-Chapman type.

2. Review of Statistical Results

The osmotic pressure can be expressed in the form of a virial expansion in ρ . McMillan and Mayer⁶ have shown that the virial coefficients in such an expansion depend on "cluster integrals" (as in imperfect gas theory) in which the intermolecular potential is here the potential of average force between colloid particles in the limit $\rho \rightarrow 0$ (i.e., in the outside salt solution of the Donnan system). Thus

$$\frac{\pi}{kT} = \rho + B_2\rho^2 + B_3\rho^3 + \dots \quad (1)$$

where ρ is expressed as the number of colloid particles per unit volume. The virial coefficients are functions of the temperature and of the chemical potentials of the species in the outside salt solution.

Let W_{12} be the potential of average force between two spherically symmetrical colloid particles in positions \mathbf{r}_1 and \mathbf{r}_2 , respectively. Then

$$B_2 = -\frac{1}{2V} \int_V \int_V (e^{-W_{12}/kT} - 1) d\mathbf{r}_1 d\mathbf{r}_2 \quad (2)$$

where V is the volume of the system. The third virial coefficient concerns the interaction between three colloid particles. If the interaction is assumed to be pairwise additive

$$B_3 = -\frac{1}{3V} \int_V \int_V \int_V (e^{-W_{12}/kT} - 1)(e^{-W_{23}/kT} - 1)(e^{-W_{13}/kT} - 1) d\mathbf{r}_1 d\mathbf{r}_2 d\mathbf{r}_3 \quad (3)$$

The virial coefficients B_n also suffice to determine the (number density) activity coefficient of the colloid ions in the inside solution⁴

$$\ln \gamma = \frac{2}{1} B_2\rho + \frac{3}{2} B_3\rho^2 + \dots$$

The McMillan-Mayer method does not give direct, explicit information on any equilibrium species, as these are treated as part of the suspending medium for the non-equilibrium species. In treating the equilibrium distribution⁵ of small ions, therefore, it is necessary to assume first that, besides the colloid species, one species of small ions, say the k th species, is not in equilibrium. Subsequently one considers the limiting case in which the activity difference of species k across the membrane vanishes. This procedure permits one to express the equilibrium ratio ρ_k/ρ_k^* as a power series in ρ (viz., eq. 27 of reference 3 with $\rho^* = 0$)

$$\frac{\rho_k}{\rho_k^*} = 1 + b_{11}\rho + (b_{21} - 2b_{20}b_{11})\rho^2 + \dots \quad (4)$$

As in eq. 1, the coefficients in expansion 4 are related to cluster integrals. b_{11} depends on the interaction between one colloid particle and one small ion, integrated over positions \mathbf{r}_1 and \mathbf{r}_3 , respectively. Using definitions in reference 5 one obtains

(6) Compare T. L. Hill, "Statistical Mechanics," McGraw-Hill Book Co., Inc., New York, N. Y., 1956, eq. (25, 21) and p. 278.

$$b_{11} = \frac{1}{V} \int_V \int_V (e^{-W_{13}'/kT} - 1) d\mathbf{r}_1 d\mathbf{r}_3 \quad (5)$$

where W_{13}' is the potential of average force between a colloid particle and a small ion in the limit $\rho \rightarrow 0$ (outside solution).

The coefficient of ρ^2 in eq. 4 relates to an integral of the interaction between two colloid particles, say at \mathbf{r}_1 and \mathbf{r}_2 , and one small ion, at \mathbf{r}_3 . With the help of the relevant expressions of reference 5 and, as in B_3 , the assumption that interaction forces are pairwise additive, we find

$$b_{31} - 2b_{20}b_{11} = \frac{1}{2V} \int_V \int_V \int_V (e^{-W_{13}'/kT} - 1)(e^{-W_{23}'/kT} - 1)e^{-W_{12}/kT} d\mathbf{r}_1 d\mathbf{r}_2 d\mathbf{r}_3 \quad (6)$$

Incidentally, we have used eq. 5 and 6 to check the corresponding coefficients (obtained by a method which included the use of the membrane potential) in eq. 89 of I. In this case $W = W' = e^2 e^{-\kappa r} / \epsilon r$, where ϵ is the dielectric constant.

It should, perhaps, be emphasized that, except for the assumption of pair-wise additivity, eq. 1 to 6 are formally exact in classical statistical mechanics. Further errors are introduced on adopting a model and approximating W and W' for the model.

3. The Potentials of Average Force

Our choice of the interaction potentials is based upon detailed consideration of the electrostatic potential field around a colloid particle. Let us consider a spherical colloid particle with radius a and surface potential ψ_0 immersed in a salt solution containing ρ_i^* ions of valency z_i per unit volume. For sufficiently low values of ψ_0 , the electrostatic potential at a distance r from the center of the particle is given by the well known Debye-Hückel expression

$$\psi = \psi_0 \frac{a}{r} e^{-\kappa(r-a)} \quad (7)$$

κ is the reciprocal thickness of the ionic double layer defined by

$$\kappa^2 = \frac{4\pi e^2}{\epsilon kT} \sum_i \rho_i^* z_i^2 \quad (8)$$

For high surface potentials, expression 7 is no longer valid. For some values of $e\psi_0/kT$ and κa the potential-distance relation has been evaluated by Hoskin⁷ with the help of an electronic computer. The results are fairly well represented by an analytical expression of the form

$$\psi = \frac{\psi_0}{\gamma} \frac{a}{r} e^{-\kappa(r-a)} \{1 + (\gamma - 1)e^{-2\kappa(r-a)}\} \quad (9)$$

The parameter γ is somewhat larger than unity and depends on $e\psi_0/kT$ and on κa . Far from the particle surface, where $2\kappa(r-a) \gg 1$, the factor in brackets approaches unity and expression 9 simplifies to

$$\psi = \frac{\psi_0}{\gamma} \frac{a}{r} e^{-\kappa(r-a)} \quad (10)$$

This equation is consistent with the fact that in the outer part of the double layer, where the potential is low, the potential is indeed correctly represented by a Debye-Hückel field. In relating this field to the electric properties of the colloid particle the

(7) N. E. Hoskin, *Trans. Faraday Soc.*, **49**, 1471 (1953).

proportionality constant is to be adjusted properly, that is, in eq. 7, ψ_0 is replaced by ψ_0/γ to obtain eq. 10. In an earlier paper⁸ an accurate method was developed for interpolating γ between Hoskin's values.

The electrostatic interaction between two colloid particles at large distances may now be dealt with on the basis of expressions developed by Verwey and Overbeek.⁹ They derive for the potential of average force $W(R)$ between two identical colloid particles surrounded by a Debye-Hückel potential field

$$W(R) = \epsilon a^2 \psi_0^2 \frac{e^{-\kappa(R-2a)}}{R} f \quad (11)$$

where R is the distance between the centers of the particles. f is a factor less than unity, the value of which depends on κR and on the assumption made when the particles approach, constant ψ_0 or constant particle charge. At large distances of separation, $\kappa(R - 2a) \gg 1$, one has $f = 1$.

In view of eq. 7 and 10 we adapt eq. 11 to the case of high surface potentials by substituting ψ_0/γ for ψ_0

$$W(R) = \epsilon a^2 \left(\frac{\psi_0}{\gamma}\right)^2 \frac{e^{-\kappa(R-2a)}}{R} f \quad (12)$$

We turn now to the virial coefficients in eq. 1. It will be noted in eq. 2 and 3 that the interaction appears in factors of the form $(e^{-W/kT} - 1)$. These factors take the value -1 for close approach, when $W/kT \gg 1$, or particle overlap, $W/kT = \infty$. Thus the virial coefficients are very insensitive to the actual value of $W(R)$ in this range. In physical terms, the probability of close approach is very small and hence even an appreciable error in $W(R)$ in this range does not change the over-all distribution significantly.

In the next section, eq. 12 for $W(R)$ with $f = 1$ is used to evaluate B_2 and B_3 numerically. We now discuss the errors resulting from this approximation to $W(R)$.

As stated above, the factor f in eq. 12 differs from unity significantly for small values of $R - 2a$. The effect on B_2 can be illustrated with a numerical example. We consider particles with a radius of 20 Å. in an aqueous 0.025 M solution of a 1-1 electrolyte at 25°. Then $\kappa = 5 \times 10^6 \text{ cm.}^{-1}$ and $\kappa a = 1$. Furthermore we assume $e\psi_0/kT = 4$, corresponding to $\psi_0 \approx 100 \text{ mv.}$ For these data the value $\gamma = 1.145$ can be derived from Hoskin's tables,⁷ and eq. 12 becomes

$$\frac{W(R)}{kT} = 252.6 \frac{e^{-\kappa R}}{\kappa R} f$$

In Fig. 1, $W(R)/kT$ is plotted vs. κR . To obtain curve 1, values of f were taken from the work of Verwey and Overbeek (ref. 9, table XVII) for the case that ψ_0 remains constant when two particles approach. Curve 2 was constructed with $f = 1$ in the entire range. If it is assumed that not ψ_0 but the particle charge remains constant, the corresponding $W(R)$ curve lies between curves 1 and 2. Figure 2 shows the function $1 - e^{-W(R)/kT}$,

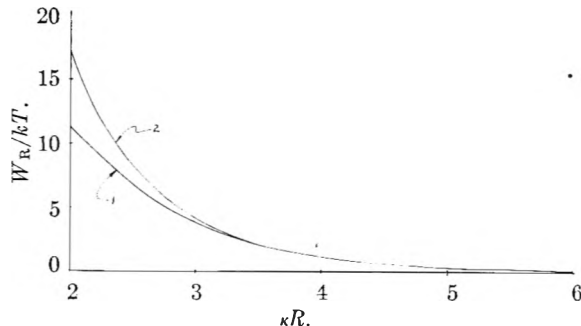


Fig. 1.— W_R/kT vs. κR according to eq. 12: curve 1, f for ψ_0 constant; 2, $f = 1$.

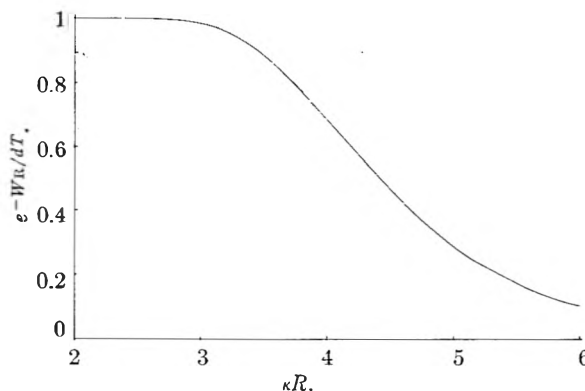


Fig. 2.—Plot of $1 - e^{-W_R/kT}$ vs. κR for W_R/kT from Fig. 1

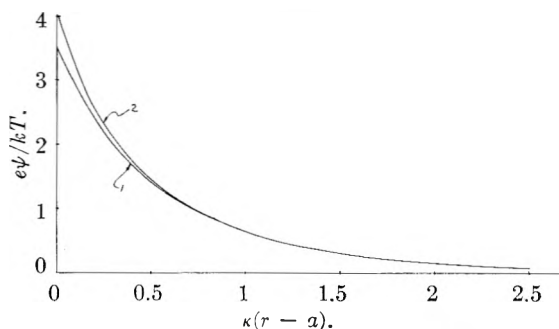


Fig. 3.—Potential distance plots for $e\psi_0/kT = 4$ and $\kappa a = 1$: curve 1, eq. 10, Debye-Hückel; 2, eq. 9, Hoskin.

which is virtually the same for the three $W(R)$ curves under discussion. In fact, changing from curve 1 to curve 2 in Fig. 1 increases B_2 by only 1%. The correction is somewhat larger for lower surface potentials when the particles may approach more closely.

In addition there is a second error to consider. Equation 12 assumes a Debye-Hückel potential field around the colloid particles, as illustrated by curve 1, Fig. 3, for the data discussed above. Actually the potential in the interior of the double layer is somewhat higher since it reaches the value ψ_0 at the surface, curve 2 in Fig. 3, instead of ψ_0/γ . Now, changing from the actual potential-distance curve to the Debye-Hückel potential, implicit in eq. 12, lowers B_2 slightly. The relative error is small compared with $\gamma^2 - 1$ and is expected to be of the order of a per cent.

In summary, the use of eq. 12 for $W(R)$, with $f = 1$, introduces two minor errors of opposite sign in the virial coefficients.

(8) D. Stigter and K. J. Mysels, THIS JOURNAL, 59, 45 (1955).

(9) E. J. W. Verwey and J. Th. G. Overbeek, "Theory of the Stability of Lyophobic Colloids," Elsevier Publishing Co., Inc., Amsterdam, 1948.

We now turn to the coefficients in eq. 4. b_{11} resembles the mixed second virial coefficient in a two component gas mixture. For the potential of average force between an ion with charge z_1e and a colloid particle, $W_{13}' = z_1e\psi$ is introduced, where ψ is given by eq. 10. Only the distribution of co-ions is considered, $W_{13}' > 0$. This suffices to determine also the distribution of counter ions ($W_{13}' < 0$) from the colloid charge and the condition of electroneutrality.

The use of eq. 10 instead of the correct potential causes a slight error, similar to the one in B_2 discussed above. For the data in Fig. 3, the relevant error in b_{11} was found to be only 0.5%.

In the interaction between three particles (the coefficients of ρ^3 in eq. 1 and 4) the conventional but approximate assumption of pairwise additivity of interaction potentials impairs somewhat the precision of our results. This error, though difficult to assess, is not expected to be large.

4. Calculations and Results

In the preceding section it was demonstrated that the virial coefficients are insensitive to the high part of the interaction potential curve. This justifies the use of eq. 12, with $f = 1$, for $R \geq 0$ and of eq. 10 for $r \geq 0$, which means in fact that the colloid particles are treated as point charges. This feature is convenient for generalizing the results. Specifically, in the case of eq. 1, it leads to a two parameter "law of corresponding states."

In the case of spherical particles, with $\kappa R = x$ as the dimensionless variable, eq. 2 for B_2 (in cc./molecule) is transformed into

$$\kappa^3 B_2 = 2\pi \int_0^\infty (1 - e^{-W(x)/kT}) x^2 dx \quad (13)$$

where

$$\frac{W(x)}{kT} = F \frac{e^{-x}}{x} \quad (14)$$

and

$$F = \frac{\epsilon \kappa a^2}{kT} \left(\frac{\psi_0}{\gamma} \right)^2 e^{2\kappa a}$$

$\kappa^3 B_2$ has been computed from eq. 13 by numerical integration. The results for a number of F values are presented in Table I.

TABLE I

F	0.5	1	2	5	10	20	50
$\kappa^3 B_2$	2.86	5.38	9.8	21.2	36.1	57.5	102
F	100	200	500	1000	2000	5000	10,000
$\kappa^3 B_2$	150	216	332	447	589	825	1040

The equation for B_3 , given in (3), may be converted into (see I)

$$\kappa^6 B_3 = \frac{8\pi^2}{3} \int_0^\infty (1 - e^{-W(x)/kT}) x dx \int_0^\infty (1 - e^{-W(y)/kT}) y dy \int_{|x-y|}^{x+y} (1 - e^{-W(z)/kT}) z dz \quad (15)$$

where x , y and z are the interparticle distances expressed in units of $1/\kappa$. As for B_2 , we use (14), and analogous expressions for $W(y)$ and $W(z)$.

The triple integral in (15) was evaluated numerically for a number of F values and the results are given in Table II.

For hard spheres the ratio $B_3/B_2^2 = 0.625$. It is seen in Table II that for increasing F this ratio

TABLE II

F	10	20	50	100
$\kappa^6 B_3$	338	1014	3830	9330
B_3/B_2^2	0.259	0.307	0.369	0.413
F	300	1000	3000	10,000
$\kappa^6 B_3$	31,700	100,700	248,000	596,000
B_3/B_2^2	0.466	0.504	0.529	0.548

approaches slowly the hard sphere value, as expected. For intermediate values of F , B_2 and B_3 may be obtained from the above data by interpolation on logarithmic plots.

For calculating b_{11} , eq. 5 is written as

$$\kappa^3 b_{11} = -4\pi \int_0^\infty (1 - e^{-W'(x)/kT}) x^2 dx \quad (16)$$

where

$$\frac{W'(x)}{kT} = G \frac{e^{-x}}{x} \quad (17)$$

and

$$G = \frac{z_1 e \kappa a}{kT} \frac{\psi_0}{\gamma} e^{\kappa a}$$

As pointed out earlier only the interaction between colloid particles and co-ions is considered, $G > 0$. Comparison with eq. 13 and 14 shows that the integrals for B_2 and b_{11} are of the same form, the difference being a factor -2 and the substitution of G for F . Thus Table I may be used for reading $-1/2\kappa^3 b_{11}$ (instead of $\kappa^3 B_2$) as a function of G (instead of F). From eq. 14 and 17, the relation between G and F is

$$G = z_1 e \sqrt{\frac{F\kappa}{\epsilon kT}} \quad (18)$$

The coefficient of ρ^2 in eq. 4 follows from eq. 6, which reads, after transformation of co-ordinates

$$\kappa^6 (b_{21} - 2b_{20}b_{11}) = 4\pi^2 \int_0^\infty (1 - e^{-W'(x)/kT}) x dx \int_0^\infty (1 - e^{-W'(y)/kT}) y dy \int_{|x-y|}^{x+y} e^{-W(z)/kT} z dz \quad (19)$$

x/κ and y/κ are the distances between the small co-ion and the centers of the two colloid particles, respectively, while z/κ is the distance between the centers of the colloid particles. $W'(x)$ is given in eq. 17, $W'(y)$ is of the same form, and eq. 14 defines $W(z)$ (substituting z for x). The results of the numerical integration of eq. 19 are shown in Table III. The parameters were chosen so that in the case of a 1-1 electrolyte in water at 25° the set of G values for each F corresponds to $\kappa = 3 \times 10^5, 10^6, 3 \times 10^6$ and 10^7 cm.⁻¹.

In the case of hard sphere colloid particles $b_{21} - 2b_{20}b_{11}$ vanishes. This agrees with the results in Table III where the ratio $(b_{21} - 2b_{20}b_{11})/b_{11}^2$ tends to zero for F and $G \rightarrow \infty$.

Discussion

It is interesting to compare our results for the ion distribution with a less general approach, first advanced by Davis¹⁰ and by Klaarenbeek,^{11,12} which

(10) L. E. Davis, *Soil Science*, **54**, 199 (1942); **59**, 379 (1945).

(11) F. W. Klaarenbeek, Thesis, Utrecht, 1946.

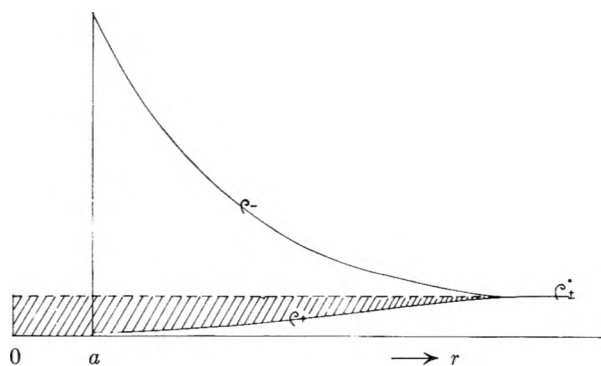


Fig. 4.—Local ion concentrations near positively charged colloid particle.

$$\rho_{\pm}^0 \int (1 - e^{-e\psi/kT}) dr$$

The average concentration of co-ions, $\bar{\rho}_+$, in a solution containing ρ colloidal particles per unit volume, is therefore

$$\bar{\rho}_+ = \rho_{\pm}^0 [1 + \rho \int (e^{-e\psi/kT} - 1) dr] \quad (\rho \rightarrow 0) \quad (20)$$

The comparison of eq. 20 with eq. 4 and 5 shows that ρ_{\pm}^0 is to be identified with ρ_k^* and $z_i e \psi$ with W'_{13} .

In order to demonstrate the relative importance of the terms in eq. 4 we have calculated the ion distribution in the case of colloid particles with $e\psi_0/kT = 3$ and $a = 25 \times 10^{-8}$ cm., and immersed in an aqueous 1-1 electrolyte solution at 25°. Figure 5 shows the ratio ρ_k/ρ_k^* of co-ions versus ρ

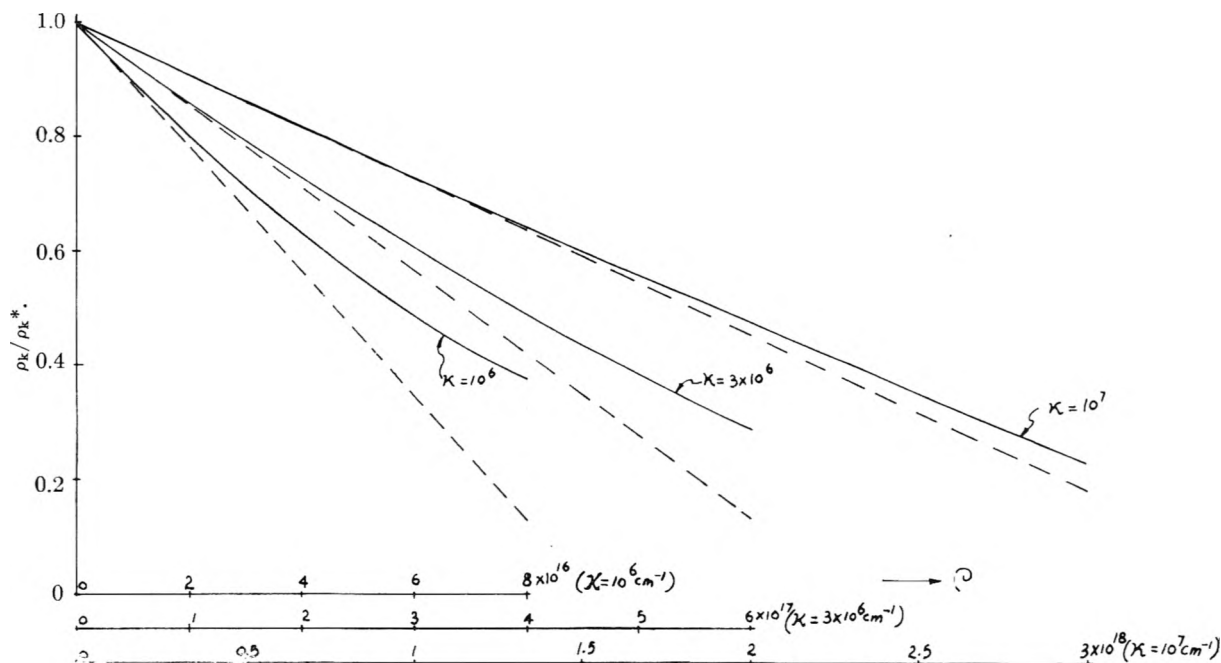


Fig. 5.—Distribution of coions for colloid particles with $a = 25 \times 10^{-8}$ cm., $e\psi_0/kT = 3$ and aqueous 1-1 electrolyte solution at 25°.

TABLE III

	VALUES OF $\kappa^6(b_{21} - 2b_{20}b_{11})$ AND, IN BRACKETS, OF $(b_{21} - 2b_{20}b_{11})/b_{11}^2$ AS A FUNCTION OF F AND G									
$G \rightarrow$	0.463	0.845	1.464	2.67	4.63	8.45	14.64	26.7	46.3	84.5
$F \ 10$	9.49	29.5	81.5	235						
\downarrow	(0.328)	(0.336)	(0.347)	(0.362)						
100			39.5	123	320	906				
			(0.169)	(0.189)	(0.203)	(0.230)				
1000					117.6	341	875	2370		
					(0.075)	(0.086)	(0.101)	(0.125)		
10000							247	718	1830	4820
							(0.028)	(0.038)	(0.049)	(0.065)

considers the local ion concentrations in the vicinity of a colloid particle in the limit $\rho \rightarrow 0$. In Fig. 4 this situation is sketched for a 1-1 electrolyte and a positively charged colloid particle. Far from the colloid the concentration of the ions is ρ_{\pm}^0 . In the double layer the counter ions are accumulated and the concentration of co-ions is decreased, the local concentrations being $\rho_{\pm}^0 e^{e\psi/kT}$ and $\rho_{\pm}^0 e^{-e\psi/kT}$, respectively. The deficit of co-ions (the "negative adsorption"), as indicated by the shaded area in Fig. 4, is

for various values of κ which correspond roughly to salt concentrations of $10^{-1} M$ ($\kappa = 10^7 \text{ cm}^{-1}$), 10^{-2} and $10^{-3} M$. As seen in Fig. 5, the linear term, $b_{11}\rho$, in eq. 4 describes the ion distribution down to rather small values of ρ_k/ρ_k^* , in particular for high salt concentrations. This agrees with Klaarenbeek's experiments on the Donnan equilibrium of gum arabic and NaBr (or NaCl).^{11,12} Since gum arabic is a (branched) long chain polyelectrolyte, quantitative agreement with the present model was not obtained.

Some results on the osmotic pressure, calculated with eq. 1 for the numerical data used in Fig. 5,

(12) J. Th. G. Overbeek, "Progress in Biophysics and Biophysical Chemistry," Vol. 6, Pergamon Press, London, 1956, p. 57.

indicated that the quadratic term becomes important at colloid concentration about 1/10 as large as is the case in eq. 4. This also is in qualitative agreement with Klaarenbeek's results on gum arabic.⁹

The present results for B_2 may be compared with earlier work based on a hard sphere model, where the surface of the sphere, replacing the colloid particle and its double layer, was defined as the surface on which the interaction energy $W(R)$ equals kT .¹³ In Table IV the results for $(N_0M)/B_2$ are given in the case of micelles of sodium lauryl sulfate in aqueous NaCl solutions at 25°, N_0 being Avogadro's number and M the micellar weight. It will be observed in Table IV that the hard sphere values of B_2 are consistently too low, showing that the hard sphere cut off should have been

(13) D. Stigter, *Rec. trav. chim.*, **73**, 593 (1954).

chosen at some surface where $W(R) < kT$. In any case, the hard sphere model is rather poor since $W(R)$ decreases with R over a considerable range.

TABLE IV

COMPARISON OF DIFFERENT CALCULATIONS OF B_2 FOR NaLS MICELLES

C_{NaCl} , mole/l.	$(N_0/M)B_2$, cc./g.	
	Hard sphere	Present work
0	80	143
.03	24	34.8
.1	12	15.6

Finally, it should be recalled that the McMillan-Mayer (virial expansion) approach fails at very low ionic strength. In the limit $\kappa \rightarrow 0$, the potentials of interaction $W(R)$ and $W'(r)$ fall off as $1/R$ and $1/r$, respectively and, as a consequence, the virial coefficients become infinitely large.

VAPORIZATION CHARACTERISTICS OF *p*-DIBROMOBENZENE

By J. H. STERN AND N. W. GREGORY

Contribution from the Department of Chemistry, University of Washington, Seattle, Washington

Received August 19, 1958

Vapor pressures of *p*-dibromobenzene have been measured in the temperature range -45 to 74° using effusion, gas saturation and static techniques: $\log P_{atm} = -3850T^{-1} + 8.80$. Condensation coefficients, estimated from effusion pressure dependence on cell geometry, range from near unity at the lowest temperatures to ca. 0.025 at 13° .

Recently the use of the effusion method as a means of determining the condensation coefficient of iodine has been described.¹ A similar study of *p*-dibromobenzene has been made to test further the applicability of the method. Its properties are well-suited for an effusion study. Only a limited study of its vapor pressure appears in the literature² (there is a general paucity of low vapor pressure data for simple aromatic compounds). In the present work effusion, gas saturation (transpiration), rate of vaporization and static vapor pressure measurements have been made in the temperature interval -45 to 74° .

Experimental

Samples of *p*-dibromobenzene from two sources (Matheson, Coleman and Bell, Reagent Grade; Eastman Kodak, White Label) were used. Melting points of both samples, before and after recrystallization from 95% ethanol, were the same, $86-87^\circ$. The small quantities transported at low vapor pressures in the dynamic methods were determined by spectrophotometry, using solutions of *p*-dibromobenzene in 95% ethanol. Quantities of the order of a micromole were determined at 2710 \AA . (Beckman D.U.); the more strongly absorbing region at 2400 \AA . was used for smaller amounts; as little as 5×10^{-8} mole easily could be determined within 5% uncertainty. Beer's law appeared valid at both wave lengths.

Effusion.—Measurements were made with the same cells and technique described fully in the recent publication on iodine. Cell numbers on Fig. 4 and cited in the discussion correspond to those listed in ref. 1.

Gas Saturation.—The first measurements using this technique were made in the very low vapor pressure range, 10^{-5} atmosphere or less; poor reproducibility and an apparent dependence on carrier gas was noted. These difficulties disappeared at higher vapor pressures, but the carrier

gas dependence was examined fully, using helium, argon, chlorotrifluoromethane (F-13), hydrogen and air. All gases (except air) were taken directly from commercial reagent grade tanks. Air was displaced from a five liter flask, driven at a constant rate by adding water from a constant level column above the flask. The carrier gases were dried, passed through a flow meter for qualitative indication of rate, into a thermal equilibration tube and then through the saturator. The latter two were immersed in a thermostat; the saturator column consisted of a simple Pyrex trap, about 20 mm. o.d. and 20 cm. in length, with the inner surface of the outer walls coated with *p*-dibromobenzene, previously sublimed in under high vacuum. The saturated gas mixture then left the thermostat region *via* a heated tube leading to a U tube where the vapor was condensed (U tube cooled with liquid oxygen, or with a diethyl malonate slush bath (-55°) when F-13 was used as the carrier gas). The carrier gas then passed through an additional drying tube, to prevent back diffusion of water, and into a Mariotte flask where it displaced a measured volume of water. The latter was used to determine the flow rate. The sample collected from a given run was dissolved in ethanol and removed from the U tube for analysis.

The saturation column was evacuated before changing flow gas and flushed each time with gas flowing in reverse to the normal direction before initiating a run. Carrier gas pressures were kept near atmospheric pressure. Flow rates were varied between 4 and 84 ml./minute without noticeable variation in the calculated vapor pressures. Most runs were for periods less than one hour.³

Static Pressure Measurements.—*p*-Dibromobenzene was not observed to react with mercury at temperatures below its melting point. A modification of a mercury gauge suggested by Pearson,⁴ Fig. 1, was used to make direct measurements of the vapor pressure in the range around one millimeter. Tube A, containing the sample, was connected by a multiple bore stopcock, lubricated with Apiezon T, to B, the null-point reference tube of the gauge. B is also connected to C, a precision bore tube of diameter 25.42 mm ,

(3) Details of these and other experiments may be found in the Doctoral Thesis of John Hanus Stern, University of Washington, Seattle, 1958.

(4) T. G. Pearson, *ibid.*, **A156**, 86 (1931).

(1) J. H. Stern and N. W. Gregory, *THIS JOURNAL*, **61**, 1226 (1957).

(2) F. W. Küster, *Z. physik. Chem.*, **51**, 222 (1905).

a uniform capillary tube D, 2.68 mm. diameter, and a mercury reservoir E. The entire gauge was initially evacuated and the level of the mercury adjusted by a stainless steel valve F so as to just close an electrical circuit between vertical and horizontal tungsten electrodes in the null-point tube. The electrodes were attached to an electronic indicating device. The entire apparatus was immersed in a water thermostat. To measure the vapor pressure, the sample vapor was allowed to enter B, depressing the level of mercury. Air was then admitted to D to displace sufficient mercury to restore the initial level in B. The volume of mercury displaced from D is equal to that added to C; from the known ratio of cross-sectional areas of the two tubes (giving a multiplication factor of 90) the small pressure may be calculated from the relatively large change in height observed in D. The mercury and glass must be cleaned carefully to minimize abnormal capillary displacement effects.

Rates of Free Vaporization.—A limited number of measurements of the rate of vaporization into vacuum of powder and pressed tablets was made in the same manner as described for iodine.¹ The irregular surface changes on single crystals undergoing free evaporation were recorded at various intervals by macrophotography.³

Results and Discussion

P_s values, calculated from the equation¹

$$P_s(\text{atm}) = n(MT)^{1/2}(44.38A_0tK)^{-1} \quad (1)$$

where n is the number of moles of molecular weight M collected in time t at T° (Kelvin), A_0 the orifice area and K the cell geometry factor, from effusion cells 3, 4, 5 and 6 are shown in Fig. 2. Between $ca.$ -13 and -45° results from all cells were indistinguishable, indicating that the condensation coefficient is near unity in this low temperature range. At higher temperatures a dependence of steady-state pressures on cell geometry becomes apparent; data from the various cells may be correlated with the equation¹

$$P_s = P_e - fP_s/\alpha \quad (2)$$

where f is the ratio of cell orifice area to cross-sectional area, P_e the apparent equilibrium pressure and α the condensation coefficient. P_e values selected to give the most consistent set of α values for all cells were only a few per cent. larger than steady-state pressures observed in cell 6. Condensation coefficients so determined are summarized in the table

Cell	47	30	13	$\alpha \times 10^4$		
				0	-6	-15°C.
3		23	28	50		
4		21	25	60	110	>200
5	16	19	32	90	180	>200
6	16	18	29			

Effusion measurements were made up to the millimeter pressure range (1.5×10^{-3} atm.). At pressures above 10^{-5} atmosphere ($ca.$ 10°), however, P_s for cells 3 and 6 calculated from equation 1 lie above those indicated by gas saturation and static measurements as equilibrium pressures, shown as the dotted line on Fig. 2. This appears to be a manifestation of the breakdown of molecular flow conditions; it is concluded that P_e values based on (2) are too high at temperatures above 13° leaving doubt as to the validity of α values tabulated at 30 and 47° .

Results of the gas saturation and static pressure measurements are shown in Fig. 3. Ideal gas behavior was assumed. The various carrier gases all gave vapor pressures in good mutual accord

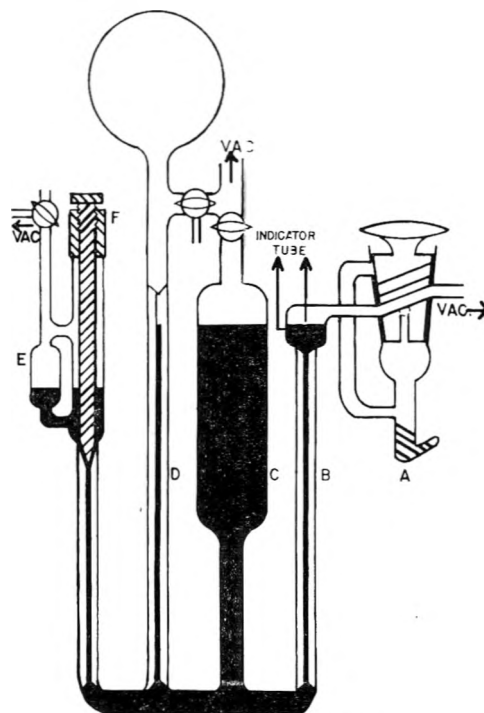


Fig. 1.—Static pressure gauge.

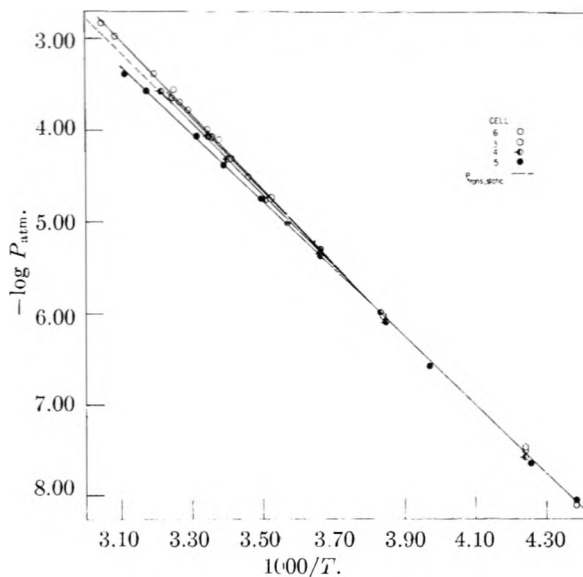


Fig. 2.—Vapor pressures measured by effusion: 6, \circ ; 3, \triangle ; 4, \square ; 5, \diamond ; $P_{\text{trans, static}}$, ---.

above 20° (v.p. $ca.$ 5×10^{-5} atm. and higher) and are seen to be in excellent agreement with the static pressure measurements. An extrapolation of the line shown in Fig. 3 correlates very well with effusion data between -13 and -45° , the range in which α is near unity; the combined data lead to the equation

$$\log P(\text{atm}) = -3850T^{-1} + 8.80 \quad (3)$$

giving a mean standard heat and entropy of sublimation of 17,650 cal. mole⁻¹ and 40.3 cal. deg.⁻¹ mole⁻¹, respectively. P_s from cell 6 is shown at two temperatures on Fig. 3 to indicate its relationship to the equilibrium line in the high pressure region.

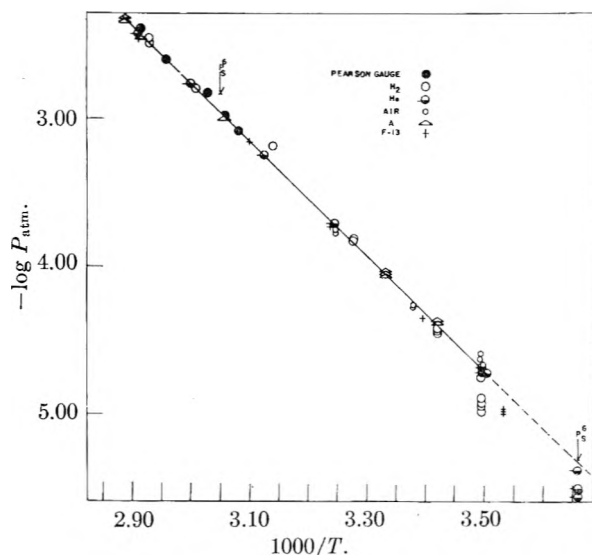


Fig. 3.—Vapor pressures measured by gas saturation and static methods.

Pressures reported by Küster are considerably lower than those predicted by equation 3.

The continuous rise of the effusion: apparent equilibrium vapor pressure curve above the correct line (at higher temperatures), 30% higher for cell 6 at 55° ($p = 1.1$ mm.) is in contrast to the behavior observed with iodine. Iodine cell 6 pressures agreed closely with transpiration data of Baxter, Hickey and Holmes⁵ in the pressure region near one millimeter. At higher temperatures a rather sudden fall-off, or flattening, of the $\ln P$ vs. $1/T$ curve was observed; the pressure at which this occurred was a function of cell geometry, 1.2 mm. for cell 6, 0.1 mm. for cell 5. The fall-off in the case of iodine is thought to be due principally to the self-cooling of the sample at the relatively large net rates of vaporization from the effusion cells at the highest pressures; however, a similar phenomenon was not observed with *p*-dibromobenzene. Molecular diameters, mean free paths and heats of vaporization are quite similar for the two substances; hence the fall-off in the case of iodine seems to be determined by solid characteristics rather than a molecular flow problem. It is concluded that the breakdown of the Knudsen equation at pressures above 10^{-2} mm. may result in a rise of apparent pressures above the actual values as viscous flow becomes more important, as predicted by Dushman,⁶ or, depending on the heat conduction properties of the solid, a fall-off due to lowered surface temperatures produced by self-cooling. A fortuitous combination of these effects may result in close correspondence of effusion pressures with correct values at pressures up to the millimeter range.

The condensation coefficient of *p*-dibromobenzene, like that of iodine, appears to decrease as the temperature is increased. Equation 2 is of little value for its estimation below temperatures of 0°, where α becomes materially larger than 0.1, because of the small difference between P_e and P_s . While

effusion data at temperatures higher than 13° appear to correlate well with equation 2, the breakdown of the Knudsen equation at the higher pressures makes the significance of the α values questionable (the deviation from molecular flow conditions would be different in each cell). A plot of the apparent α values vs. $1/T$ shows considerable curvature and does not give a suitable basis for estimation of activation energy and entropy. The

EFFUSION DATA

Cell 3

($A_0 24.2 \times 10^{-3}$ cm.²; $f 25.0 \times 10^{-4}$; $K 0.97$)

Temp., °C.	Time (min.)	$P \times 10^2$ (atm.)
35.1	15.49	22.4
25.3	19.82	8.57
11.2	13.33	1.88
0	33.65	0.473
0	22.77	.476
-12.9	47.25	.0927
-37.5	91.03	.00349
-37.4	49.19	.00328
-45.2	124.78	.000777

Cell 4

($A_0 13.3 \times 10^{-3}$ cm.²; $f 51.8 \times 10^{-4}$; $K 0.98$)

Temp., °C.	Time (min.)	$P \times 10^2$ (atm.)
38.3	14.65	26.8
26.2	19.01	8.82
21.0	21.88	4.93
11.5	34.07	1.72
0	48.88	0.445
0	55.12	.458
-12.6	56.01	.101
-37.3	77.74	.00269

Cell 5

($A_0 16.7 \times 10^{-3}$ cm.²; $f 135 \times 10^{-4}$; $K 0.96$)

Temp., °C.	Time (min.)	$P \times 10^2$ (atm.)
48	21.37	41.4
42	13.86	27.2
28.5	30.76	8.91
21.5	33.55	4.29
17	21.60	2.65
13.1	17.38	1.84
7.2	36.18	0.946
0	26.89	.443
-12.8	35.52	.0821
-21	91.30	.0263
-45	156.64	.000868

Cell 6

($A_0 4.23 \times 10^{-3}$ cm.²; $f 5.97 \times 10^{-4}$; $K 0.97$)

Temp., °C.	Time (min.)	$P \times 10^2$ (atm.)
55	28.68	147
51	19.28	106
40	12.80	42
36.7	29.79	28.9
33	33.60	20.4
31	16.78	16.9
26	26.45	10.5
23	31.39	8.15
20	35.38	5.04
20	24.92	4.94
5	33.00	0.832
0	35.10	.504
0	39.14	.502
-13.1	62.37	.0800
-13.1	62.93	.0800
-38	86.80	.00222

(5) G. P. Baxter, C. H. Hickey and W. C. Holmes, *J. Am. Chem. Soc.*, **29**, 127 (1907).

(6) S. Dushman, "Vacuum Technique," Chapt. 2, John Wiley and Sons, Inc., New York, N. Y., 1949.

general behavior is comparable to that found for iodine, however, with a somewhat more rapid change of α with temperature.

As with iodine, it does not seem possible to attribute the deviation of P_s values in the various effusion cells to surface cooling effects. For example the net rate of vaporization from cell 3 is larger than cell 5; yet the former yields P_s values larger than the latter. Furthermore even in cell 3, which has the highest rate of effusion (moles sec.⁻¹), radiation transfer alone is sufficient to keep surface temperatures within less than a degree of the walls at temperatures as high as 0°. Hence the P_s to P_e relationship has been interpreted as an α effect. It should be emphasized that the absolute value of α depends on the value selected for the sample area, A_s ; the latter has been taken as the cross-sectional area of the cell; if in reality it is only proportional to this, possibly much larger, then α may have a

much smaller value, as averaged over the total surface area. Photographs of freely vaporizing crystals show vaporization occurs more rapidly at crystal edges than on the faces.³ The condensation coefficient may well be different on the various crystal surfaces.

The surfaces of freely vaporizing crystals were seen to undergo irregular and chaotic disintegration; a reliable area of vaporization cannot be estimated under these extreme non-equilibrium conditions. This area must be known if quantitative interpretation of free vaporization data is to be attempted for evaluation of vapor pressures or condensation coefficients by the free evaporation method.

Acknowledgment.—Financial support of this work by the Research Corporation and the Office of Ordnance Research, U. S. Army, is acknowledged with thanks.

DEVIATIONS FROM PLATE THEORY IN THE ION-EXCHANGE SEPARATION OF TECHNETIUM AND RHENIUM¹

BY R. N. SEN SARMA,^{2a} EDWARD ANDERS^{2b} AND J. M. MILLER^{2c}

Contribution from the Department of Chemistry and the Enrico Fermi Institute for Nuclear Studies of the University of Chicago, Chicago, Ill., and the Department of Chemistry, Columbia University, New York, N. Y.

Received August 21, 1958

Technetium and rhenium in their highest oxidation states can be separated by ion-exchange chromatography on the synthetic resin Dowex 1, using perchlorate ion as the elutriant. In 0.1 and 0.2 *f* HClO₄ solutions, the peak elution volumes (in units of free column volumes) are 43.0 ± 0.8 and 23.6 ± 0.4 for ReO₄⁻, and 85.2 ± 1.9 and 43.7 ± 0.7 for TcO₄⁻, respectively. The trailing edges of the elution curves deviate markedly from the predicted Gaussian shape, and the observed separation factors differ from those calculated from the plate theory of Mayer and Tompkins, and Glueckauf, by factors of 10² to 10¹⁸. Part of the discrepancy is due to a chemical cause, presumably radiocolloid formation, and can be eliminated by appropriate chemical treatment. In addition, there appears to be a "residual" tailing-effect which can be reduced, but not eliminated, by changing the experimental variables. This effect, which appears to arise from the infrequent occurrence of a second, slow exchange process, limits the maximum separation factors attainable to 10⁴–10⁵, irrespective of the number of theoretical plates. The mechanism of this process could not be established with certainty, although its dependence on flow rate was consistent with the behavior expected if the chemical exchange reaction with the exchange site, rather than film or particle diffusion was the rate-determining step. It appears that the "residual" tailing-effect is not limited to the two elements studied, but occurs in other systems as well. At high acid concentrations, a broadening and distortion of the technetium peaks was observed, indicating oxidation of the resin by pertechnetate.

Introduction

In conjunction with a search³ for naturally occurring Tc⁹⁸, a highly efficient method was needed for the separation of trace quantities of Tc and Re. Separations of these elements had been described by Perrier and Segrè,⁴ Sugarman and Richter,⁵ Rogers,⁶ and Atteberry and Boyd.⁷

As shown previously,^{3a} these methods suffered from one or more of the following shortcomings: low separation factors, low yields and failure at trace

concentrations. For this reason, a new ion-exchange procedure was developed^{3a} using the synthetic resin Dowex-1 as the exchanger, and perchlorate ion as the elutriant. Upon application of this procedure, it was found, however, that the rhenium content of the technetium fractions, as determined by neutron activation analysis, was frequently about 10²–10⁸ times higher than predicted by the plate theory of Mayer and Tompkins⁸ and Glueckauf.⁹ For example, in the experiment illustrated in Fig. 1, the technetium fraction cut at 71.5 free column volumes would have contained >2.1 × 10⁻⁴ of the initial amount of rhenium, compared to values of 1.1 × 10⁻⁹ and 3.0 × 10⁻⁷ calculated from the theories of Mayer and Tompkins, and Glueckauf, respectively. (An even more drastic case is shown in Fig. 4, where discrepancies by factors of 2.4 × 10¹⁸ and 1.3 × 10¹⁴, respectively are found.)

(8) S. W. Mayer and E. R. Tompkins, *ibid.*, **69**, 2866 (1947).

(9) (a) E. Glueckauf, *Trans. Faraday Soc.*, **61**, 34 (1955); (b) E. Glueckauf in "Ion Exchange and Its Applications," Society of Chemical Industry, London, 1955, pp. 34–45.

(1) Presented before the 130th National Meeting of the American Chemical Society, Atlantic City, September 19, 1956. This work was supported in part by the U. S. Atomic Energy Commission.

(2) (a) Department of Chemical Engineering, Jadavpur University, Calcutta, India; (b) Department of Chemistry and the Enrico Fermi Institute for Nuclear Studies of the University of Chicago, Chicago, Illinois; (c) Department of Chemistry, Columbia University, New York, N. Y.

(3) (a) E. Alperovitch, Ph.D. Dissertation, Columbia University (January 1954); U. S. Atomic Energy Commission Report NYO-6139. (b) E. Alperovitch and J. M. Miller, *Nature*, **176**, 299 (1955).

(4) C. Perrier and E. Segrè, *J. Chem. Phys.*, **7**, 155 (1939).

(5) N. Sugarman and H. Richter, *Phys. Rev.*, **73**, 1411 (1948).

(6) L. B. Rogers, *J. Am. Chem. Soc.*, **71**, 1507 (1949).

(7) R. W. Atteberry and G. E. Boyd, *ibid.*, **72**, 4805 (1950).

TABLE I
 ELUTION PARAMETERS OF PERRHENATE AND PERTECHNETATE

Resin type	Resin cross linkage (% DVB)	Resin capacity (meq./dry g.)	Elutriant	$C_{\text{TcO}_4^-}$	$C_{\text{ReO}_4^-}$	$\frac{C_{\text{TcO}_4^-}}{C_{\text{ReO}_4^-}}$
Dowex-1	4	3.5	0.1 f NH_4ClO_4 + 0.1 f NH_3	93.5 ± 2.0	49.0 ± 1.0	1.91 ± 0.06
Dowex-1	8	3.25	.2 f HClO_4	43.7 ± 0.7	23.6 ± 0.4	1.85 ± .041
Dowex-1	8	3.25	.2 f NH_4ClO_4 + 0.1 f NH_3	41.7 ± .5	23.5 ± .4	1.78 ± .04
Dowex-1	8	3.25	.1 f HClO_4	85.2 ± 1.9	43.0 ± .8	1.98 ± .06
Dowex-1	8	3.25	.1 f NH_4ClO_4 + 0.1 f NH_3	79.8 ± 2.0	42.4 ± 1.0	1.88 ± .06
Dowex-1	8	3.25	.2 f Na salicylate	170		
Dowex-1	10	3.11	.2 f HClO_4	44.2 ± 0.6	24.2 ± 1.2	1.83 ± .09
Dowex-2	10	3.0	.1 f HClO_4		57 ± 2	

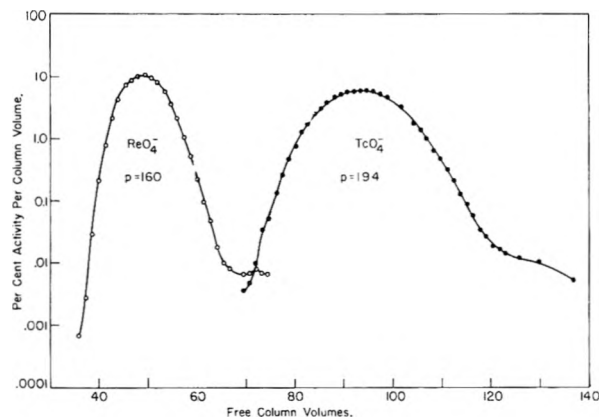


Fig. 1.—Discrepancy between calculated and observed cross-contamination. If a cut is taken at 71.5 v., the rhenium content of the technetium fraction will be $>2.1 \times 10^{-4}$, compared to calculated values of 1.1×10^{-9} (Mayer and Tompkins) and 3.0×10^{-7} (Glueckauf). Carrier-free pertechnetate and 10 mg. of perrhenate refluxed with 0.5 f H_2SO_4 for 21 hours and made basic to pH 9 before absorbing on column. Dowex 1-X4, ClO_4^- -form, 200–400 mesh; column 23.0 cm. \times 0.204 cm.². Eluted with 0.1 f NH_4ClO_4 ; flow rate 0.75 cm./min.

This observation raised the question whether the discrepancy was due to intrinsic shortcomings of the theory, or to unfavorable experimental conditions. We have been able to show that part of the deviation was indeed caused by a number of controllable experimental factors, and have succeeded in reducing the discrepancy by factors of 10^2 to 10^3 . Beyond that, however, there appear to exist at least two other effects. One of these is peculiar to technetium, and apparently involves a reduction of pertechnetate ion by the resin. The other one, observed with both ReO_4^- and TcO_4^- , is independent of nearly all experimental variables except the flow rate, and appears to arise from the presence of two different types of exchange sites on the resin.

Experimental

Resins.—The synthetic anion-exchange resins Dowex-1 and Dowex-2¹⁰ were used in all experiments. The characteristics of these resins are listed in the first three columns of Table I and in the figure captions. Unless otherwise specified, a fraction between 270 and 325 mesh was used. The mesh sizes refer to wet-screened resin in the chloride form. In several cases, the particle size of the perchlorate form of the resin was measured directly by means of a microscope equipped with a micrometer eyepiece.

Columns.—Glass columns of 0.49 to 0.51 cm. i.d., 10–60 cm. long, were used. The resin was held in place by glass

wool plugs at the top and bottom of the column. The fractional void space of the columns was 0.40 ± 0.01 .

Tracers.—Carrier-free $\text{Re}^{183,4}$ and Tc^{95} , prepared by deuterium irradiation of tungsten and molybdenum, respectively, in the Washington University cyclotron, were purified by distillation and ion exchange, and coprecipitated with CuS . The CuS was dissolved in $\text{NH}_3 + \text{H}_2\text{O}_2$, the Cu^{++} removed by cation exchange, the solution evaporated to dryness to remove NH_3 , and the residue taken up in water. Before use, the solutions were stored for a period long enough to ensure complete decay of Re^{186} , Tc^{96} and other short-lived activities.

Determination of Elution Curves.—One to four ml. of TcO_4^- or ReO_4^- solution was adsorbed on the column, and eluted with 60–150 free column volumes of perchlorate solution. The effluent fractions (about 1–2 free column volumes each) were collected in glass vials on a RINCO automatic fraction collector, and counted on a low-level scintillation spectrometer. The radiations counted were the 201 kev. γ -ray of Tc^{95} , and the K X-ray of $\text{Re}^{183,4}$. At these energies the instrumental backgrounds ranged from 5–7 counts per minute. In elutions of mixtures of ReO_4^- and TcO_4^- , the cross-contaminated fractions were counted in both the rhenium and technetium channels, and the amount of each species calculated by means of simultaneous equations. In this manner, fractions containing the two species in ratios of 500:1 readily could be analyzed. The resolving time of the circuit was so short as to make coincidence losses negligible even at the highest counting rates encountered ($\sim 4 \times 10^4$ counts per minute).

Elution Parameters.—The experimental data were analyzed according to the plate theory of Mayer and Tompkins⁸ and Glueckauf.⁹ From the elution curve, such as the one shown in Fig. 1, two quantities were determined: (1) the peak elution volume C and (2) the number of plates p .

Some observed values of C are given in Table I. As expected, the value of C for a given ion is roughly inversely proportional to the elutriant concentration. In addition, the ratio $C_{\text{TcO}_4^-}/C_{\text{ReO}_4^-}$ appears to be slightly dependent on pH and elutriant concentration, possibly due to activity coefficient variations and polyfunctional character of the resin.

Flow Rate.—It had been shown by Mayer and Tompkins⁸ and by Glueckauf^{9b} that the number of plates increased with decreasing particle size, and, under most conditions, with decreasing flow rate. Although it soon became apparent that the limiting factor in our separations was the residual tailing-effect rather than the nominal number of plates, we attempted nevertheless to choose experimental conditions favorable to the attainment of high values of p . Most experiments with the 270–325 mesh resin were conducted at flow rates of ca. 0.3 cm./min., which was about the lowest value attainable by gravity flow. Even at twice this flow rate, the elution peaks were symmetrical, indicating that the column was operating at near-equilibrium conditions.

Chemical Form of Resin.—When the resin was in the perchlorate rather than in the chloride form at the start of the experiment, the initial adsorption bands of both rhenium and technetium were broadened sufficiently to cause a marked decrease in the number of theoretical plates (*e.g.*, from 410 to 136). For this reason, many of the earlier experiments were performed with chloride-form resin, although this practice resulted in asymmetric elution curves, as discussed in a later section.

(10) Processed by the Bio-Rad Laboratories, Berkeley, California.

Results

(1) Freshly prepared rhenium tracer gives an asymmetric elution curve with considerable tailing. (Up to 25% of the total activity is found in the tail.) The tailing sets in when the concentration has fallen to about 0.6% of the total amount of tracer per column volume (curve I, Fig. 2). About the same degree of tailing is obtained when the sulfide precipitate is dissolved in cold concd. HNO_3 instead of $\text{NH}_3 + \text{H}_2\text{O}_2$. In either case, it can be greatly reduced, but not eliminated, by refluxing the tracer with dilute H_2SO_4 for several hours (curve II, Fig. 2). Still, about 0.1% of the total activity remains in the tail. Addition of oxidizing agents, such as HNO_3 , Ce^{4+} , MnO_4^- , IO_4^- , H_2O_2 and $\text{S}_2\text{O}_8^{2-}$ during the refluxing produced no perceptible improvement. The tailing-effect diminished with aging of the tracer solution, and was reduced by about an order of magnitude after four months. Technetium behaves almost identically in all of these respects.

(2) When the tracer is redistilled from concentrated sulfuric acid, the distillate still gives some tailing, about 0.01% of the activity per column volume. Technetium again behaves similarly.

(3) When some inactive rhenium is added to the tracer solution, and the mixture put through another sulfide precipitation cycle to facilitate exchange between active and inactive rhenium, the resulting solution still shows tailing at a concentration of about 0.002% per column volume (Fig. 3). A "residual" tailing-effect of this order of magnitude persists in all rhenium and technetium elutions, regardless of the presence or absence of carrier, the type and duration of chemical treatment, and the pH of the elutiant.

(4) Essentially the same degree of residual tailing is observed when resin of different cross-linkage (Dowex-1-X4, 8, 10; Figs. 1, 3, 4), or different type (Dowex-2-X10), is used.

(5) Resin of larger particle size gives about the same or a slightly lower degree of tailing (Fig. 3). A definite conclusion could not be drawn, since the flow rate and the width of the peak changed drastically when the particle size was changed.

(6) When perrhenate is eluted from the same column at two different flow rates, the degree of tailing is higher at the lower flow rate, although the nominal number of plates increases at the same time (Fig. 4).

(7) If the resin is initially in the chloride form, the rhenium peak is asymmetric, the leading edge being sharpened and the trailing edge broadened. If technetium is eluted in the same experiment, its peak is appreciably less asymmetric, indicating that the effect is not due to incomplete attainment of equilibrium (Fig. 5).

(8) If the initial tracer solution is more than 1 normal in H^+ , the technetium peak shows considerable flattening and broadening, while the rhenium peak is much less affected (Fig. 6). Moreover, at all acidities a small and nearly constant amount of technetium (0.005% of the activity per column volume) leaks from the column long before the leading edge of the peak appears

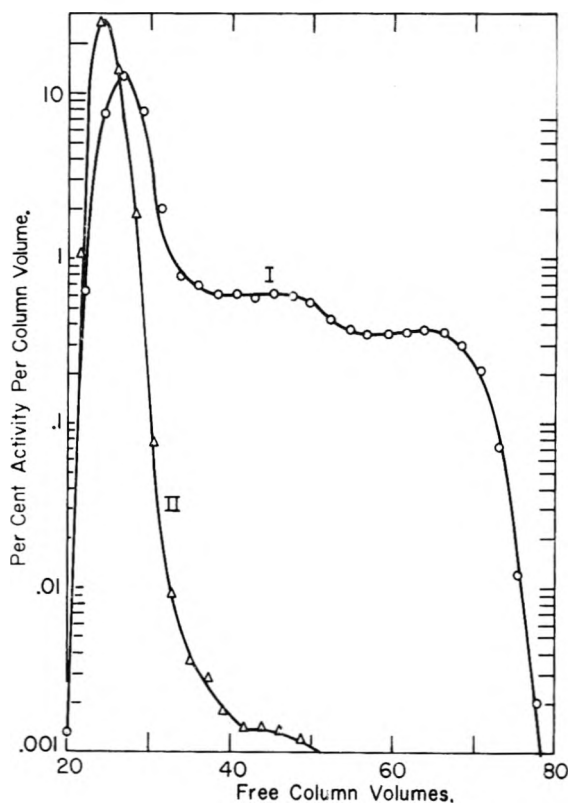


Fig. 2.—Reduction of tailing-effect by chemical treatment: curve I, untreated Re^{184} tracer; curve II, tracer refluxed with 0.5 f H_2SO_4 for 6 hours.

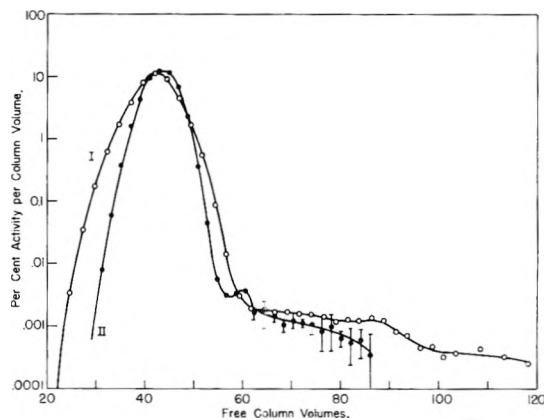


Fig. 3.—Dependence of tailing-effect on particle size of resin. $\text{Re}^{184}\text{O}_4^- + 0.5$ mg. stable ReO_4^- refluxed with 0.5 f H_2SO_4 for 21 hours; adsorbed on Dowex 1-X8, ClO_4^- -form. Curve I, average particle size 48 μ , column 12.1 cm. $\times 0.204$ cm^2 ; eluted with 0.1 f HClO_4 ; flow rate 0.30 cm./min. Curve II, average particle size 56 μ ; column 59.3 cm. $\times 0.197$ cm^2 ; eluted with 0.1 f NH_4ClO_4 ; flow rate 0.51 cm./min.

(Figs. 5, 6, 7). Rhenium shows no such behavior.

(9) When untreated TcO_4^- is eluted with 0.2 f HClO_4 instead of ammoniacal NH_4ClO_4 , the tailing-effect is immediately reduced by about an order of magnitude, e.g., from 0.4 to 0.04% per column volume, whereas any further reduction requires prolonged heating at higher acid concentrations.

Discussion

Any interpretation of the above experiments must account for these four phenomena: (1)

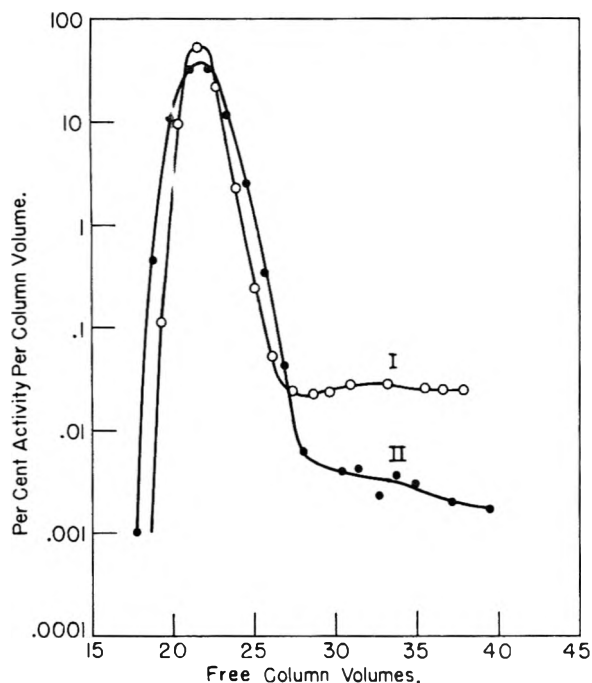


Fig. 4.—Increase in tailing-effect with decreasing flow rate. $\text{Re}^{185}\text{O}_4^-$ — 0.5 mg. stable ReO_4^- refluxed with 0.5 *f* H_2SO_4 for 21 hours. Dowex 1-X10, ClO_4^- -form, average particle size 21 μ , column 30.0 cm. \times 0.204 cm^2 ; elutriant, 0.2 *f* HClO_4 . Curve I, flow rate 0.072 cm./min.; Curve II, flow rate 0.193 cm./min.; 310 plates.

If a cut is taken at 28.8 v. (Curve I), the rhenium content of the technetium fraction will be $>2.5 \times 10^{-3}$, compared to calculated values of 1.0×10^{-21} (Mayer and Tompkins) and 1.9×10^{-17} (Glueckauf).

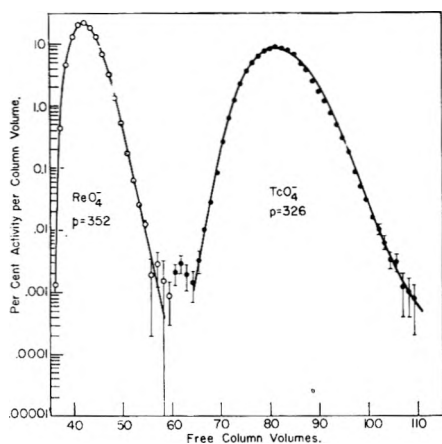


Fig. 5.—Elution of ReO_4^- and TcO_4^- with 0.1 *f* NH_4ClO_4 . Tracer refluxed with 0.5 *f* H_2SO_4 for 6 hours, but made basic to pH 9 before absorbing on column. Dowex 1-X8, Cl^- -form; column 24.5 cm. \times 0.202 cm^2 ; flow rate 0.25 cm./min.

the decrease of the tailing-effect upon chemical treatment; (2) persistence of a "residual" tailing-effect; (3) asymmetry of the rhenium peaks; and (4) pH-dependence of the technetium peaks. For the sake of simplicity, each of these phenomena will be discussed separately.

1. Decrease of Tailing-effect by Chemical Treatment.—It is proposed that this part of the tailing-effect is caused by a radiocolloid, a thioanion, or both.

One can explain the observed shape of the elu-

tion curves by assuming that rhenium and technetium sulfides coprecipitated on CuS are not completely converted to ReO_4^- and TcO_4^- , respectively, by NH_3 and H_2O_2 . Instead, a sizable fraction of the sulfide remains in the form of a radiocolloid or a slowly hydrolyzable thioanion such as ReO_3S^- . This species, whatever its nature, is more strongly held by the resin than ReO_4^- , and remains at the top of the column, where it is slowly attacked and converted to one or several less strongly held species, e.g., ReO_4^- , by the influent perchlorate solution. Such a gradually decreasing retention of activity at the top of the column was actually observed in a high activity level tracer experiment.

Although the presence of a thioanion cannot be ruled out with complete certainty, most available evidence is strongly in favor of a radiocolloid. In particular, the decrease of the effect by two orders of magnitude upon addition of carrier rhenium (Results, § 3) is in far better accord with the expected properties of a radiocolloid than with those of a thioanion.

2. Residual Tailing.—In the experiments described under "Results," § 1 to 6 (cf. also Figs. 1, 3 and 4), a "residual" tailing-effect of 0.001 to 0.02% has persisted under a wide variety of experimental conditions. At least five different explanations, only one of which is in accord with all experimental observations, may be advanced to account for this phenomenon.

a. Non-linearity of Exchange Isotherm.—Asymmetric elution curves with long trailing edges are obtained when the exchange isotherms are non-linear. However, when the column is loaded to only a small fraction of its capacity (less than 1% in most of our experiments), only the linear region of the isotherm is utilized, and symmetrical elution curves should result.

b. Multiplicity of Chemical Species.—Originally, the residual tailing was thought to be due to yet another chemical species, but all subsequent experiments have failed to lend support to this assumption. For example, about the same degree of residual tailing was observed in 10^{-14} and 10^{-6} *f* perrhenate solutions that had been treated with 0.5 to 9 *f* H_2SO_4 , 1 to 15 *f* HNO_3 , KMnO_4 , KIO_4 and Ce(IV) ; redistilled from concd. sulfuric acid or scavenged with Fe(OH)_3 prior to adsorption on the resin; regardless of whether the resin columns were initially in the perchlorate or chloride form. Even more surprising was the fact that *pertechnetate* solutions treated similarly again gave nearly the same degree of residual tailing. However, this fact may not be relevant, since, as will be shown below, TcO_4^- probably oxidizes the resin and exhibits other anomalies as well.

c. Instrumental Effect.—One must also consider the possibility that the residual tailing was caused by an instrumental effect, for example, retention of activity by the fraction collector siphon. However, this interpretation has been ruled out by control experiments wherein fractions were collected manually without use of the siphon. Essentially the same degree of residual tailing was observed.

d. **Chemical Reaction with the Resin.**—It is conceivable that a small fraction of the adsorbed anions will be reduced by the resin during elution. If the reaction product, presumably the dioxide, were to migrate at a slower rate than the anions themselves, tailing will result. In order to account for the near-independence of the residual tailing-effect of concentration, pH and nature of the adsorbed species (e.g., ReO_4^- or TcO_4^-), this interpretation leads to the implausible assumption that the rate of the reaction is independent of all these variables, and is the same for both elements under discussion. The latter assumption is at variance with experimental evidence, since conditions have been found where TcO_4^- but not ReO_4^- reacts with the resin (e.g. Results, § 8 and Fig. 6). Similarly, treatment of perchlorate-form resin with NaOH causes very severe distortion of the technetium but not the rhenium peak.¹¹

e. **Two Exchange Processes.**—One can explain the observed shape of the elution curves by assuming that in addition to the regular exchange process, a second type of process takes place at a very much slower rate. An equivalent description is the postulation of two types of exchange sites, which we may denote by the symbols A and B. Either because of their location in the resin structure,¹² or the chemical nature of the exchanging group,¹³ the rarer B-sites undergo exchange at a much slower rate than the A-sites. Due to the scarcity and slow rate of exchange of the B-sites, only a few perrhenate ions will ever interact with them. Those that do, however, will remain at their sites much longer than the ions adsorbed at the normal A-sites, and will consequently appear in the effluent some time after the main peak. It should be noted that this model contains the implicit requirement that the B-sites do not, at any time, reach equilibrium with the surrounding solution.

We may now inquire into the nature of the postulated slow exchange process. Boyd, Adamson and Myers¹⁷ have pointed out that three processes can be rate-controlling in ion-exchange reactions: diffusion through the liquid film surrounding the resin particle, diffusion into the resin particle, and the chemical reaction with the exchange group. The first of these mechanisms, film diffusion, cannot account for the occurrence of two types of exchange processes without invoking the existence of two types of liquid films. Since the "normal" films are believed to be of a thickness comparable to the diameter of the resin particles used in our experiments,¹⁷ it is difficult to see how films of even greater thickness, as required for a slow exchange

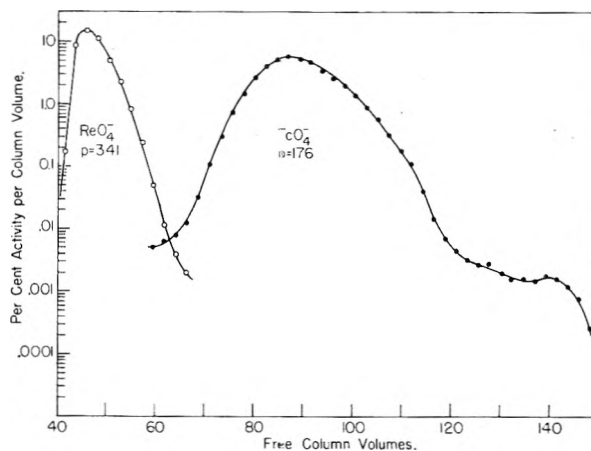


Fig. 6.—Elution of ReO_4^- and TcO_4^- with 0.1 *f* HClO_4 . Tracer refluxed with 3 *f* H_2SO_4 for 6 hours before adsorbing on column. Dowex 1-X8, Cl^- -form; column 14.0 cm. \times 0.190 cm.²; flow rate 0.27 cm./min.

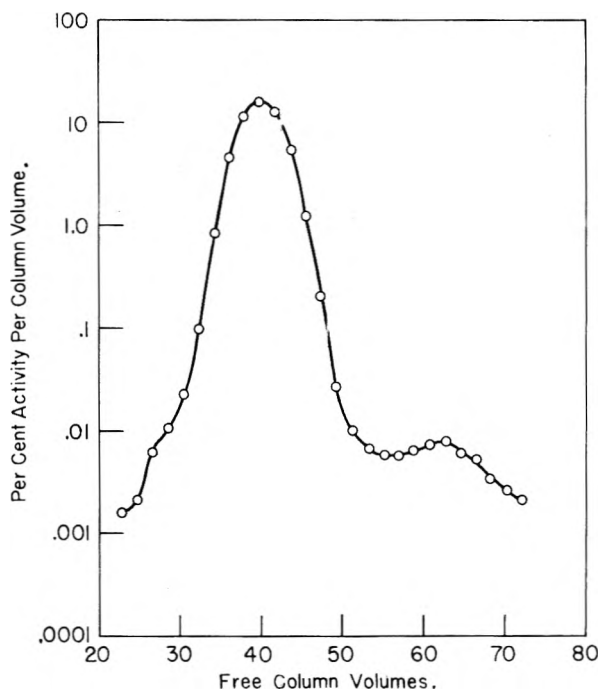


Fig. 7.—Elution of perrhenate at low acidity. Tracer refluxed with 0.5 *f* H_2SO_4 for 6 hours. Dowex 1-X8, Cl^- -form; column 13.5 cm. \times 0.197 cm.². Eluted with 0.2 *f* HClO_4 ; flow rate 0.25 cm./min.

process, could arise in a tightly packed column.

The second mechanism, particle diffusion, does indeed permit the existence of two types of exchange sites. It is conceivable that a small fraction of the sites is situated in highly cross-linked regions of the resin, where the diffusion constant is smaller than in the regions of normal cross-linkage.¹² If only a single exchange site is located in each of these inaccessible regions, the situation is mathematically indistinguishable from one in which the chemical reaction with the exchange site, rather than diffusion to the site, is the rate-determining step. Only in the event that a large number of exchange sites is situated within an inaccessible region would particle diffusion have to be treated as a separate process. This possibility

(11) R. N. Sen Sarma and C. A. Lovejoy, unpublished.

(12) D. Reichenberg and D. J. McCauley, *J. Chem. Soc.*, 2741 (1955).

(13) It is known that quaternary ammonium type anion-exchange resins contain weakly basic ternary and binary ammonium groups.¹⁴⁻¹⁶ Conceivably, these groups might react at slower rates than the quaternary groups.

(14) R. M. Wheaton and W. C. Bauman, *Ind. Eng. Chem.*, **43**, 1088 (1951).

(15) H. P. Gregor, J. Belle and R. A. Marcus, *J. Am. Chem. Soc.*, **76**, 1984 (1954).

(16) H. A. Strobel and R. W. Gable, *ibid.*, **76**, 5911 (1954).

(17) G. E. Boyd, A. W. Adamsor and L. S. Myers, Jr., *ibid.*, **69**, 2836 (1947).

is rendered very unlikely by the observed near-independence of the tailing-effect on resin cross-linkage and particle size (Results, §§4, 5), whereas none of the observed facts seems to contravene the third mechanism: chemical reaction with the exchange group. However, since the experiments reported in this paper were not particularly designed to establish the mechanism of the slow exchange process, we shall confine ourselves to a qualitative comparison of our experimental data with a general feature of the proposed mechanism: the dependence of the tailing-effect upon flow rate (Results, §6).

The concentration of perrhenate in the tail will be a function of both the amount of perrhenate adsorbed by the B-sites, and the rate of desorption. It is therefore convenient to regard the history of the B-sites during elution as consisting of two separate stages, during neither of which is equilibrium reached. In the first stage, from the arrival of the leading edge of the adsorption band until some time after the passage of the peak, the perrhenate concentration in solution will be greater than the amount that would be in equilibrium with perrhenate on the B-sites. The net effect during this stage will therefore be *adsorption* of perrhenate by the B-sites. During the second stage, from some time after the passage of the peak until the end of the elution, the reverse condition will apply: the perrhenate concentration in solution will be smaller than the amount in equilibrium with the perrhenate on the B-sites, and the net effect during this stage will be *desorption* of perrhenate from the B-sites.

For a given column, the quantity of perrhenate that will be adsorbed on the B-sites during the passage of the perrhenate band through the column will be inversely proportional to the flow rate. After the passage of the perrhenate band, the amount desorbed *per unit volume* from the B-sites by the elutriant will also be inversely proportional to the flow rate. Therefore, the concentration of perrhenate in the tail should be approximately inversely proportional to the *square* of the flow rate. That this is in fact observed may be seen in the experiments depicted in Fig. 4 where a decrease in the flow rate by a factor of 2.7 resulted in an increase of the perrhenate concentration in the tail of the order of 10.

It is clear that the $\text{ReO}_4^-/\text{TcO}_4^-$ separation factors calculated from plate theory will remain meaningless until the residual tailing-effect has been eliminated. One may also wonder whether this effect is limited to the two elements studied, or whether it occurs in other systems as well. It definitely has been observed in the elution of chloroplatinate with perchlorate ion¹⁸ and in the ion-exchange separation of the lithium isotopes by Glueckauf, Barker and Kitt.¹⁵ The first of these systems again involves perchlorate ion, and it may not be unreasonable to suppose that the large size of the exchanging ions and the extreme degree of dehydration of perchlorate-form resin¹⁵

combine to accentuate differences in the accessibility¹² or reactivity of exchange sites. In the lithium isotope separation, these factors do not apply; instead, the appearance of a tailing-effect may well be a matter of observational selection, since the experiment was designed specifically to detect very minute effects. It is quite possible that the tailing-effect is a very general phenomenon, but has been overlooked by previous investigators, since it becomes noticeable in the systems studied only after the concentration of the eluted species has fallen to $<10^{-3}$ of its peak value. Most published elution curves terminate before this point. Similarly, the fact that none of the published rate studies show evidence for the presence of slowly-reacting sites, may again be a matter of observational selection. None of these were performed with perchlorate-form resin, nor were they designed to detect effects as small as the ones under discussion.

3. Asymmetry of the Peaks.—This effect was always observed when the resin was initially in the chloride form (Fig. 5). It was definitely not due to non-equilibrium operation of the column, since, under identical conditions, perchlorate-form resin always gave symmetric peaks.

A clue to the above behavior is provided by the observation that the volume of the resin bed shrank by about 18–20% during the elution, during and after the conversion of the resin from the chloride to the perchlorate form. This contraction also has been observed by Gregor, Belle and Marcus.¹⁵ If particle diffusion is the rate-determining step in the exchange process with the A-sites, then the decrease in the internal diffusion constant during the contraction and dehydration accompanying the conversion of the resin to the perchlorate form will decrease the rate of desorption to a greater extent than the rate of adsorption. This will cause a sharpening of the leading edge and a broadening of the trailing edge, in accord with observation.

4. pH-Dependence of Technetium Peaks.—The distortion and broadening of the technetium peak at high acid concentrations (Fig. 6) may be attributed to reduction of TcO_4^- at low pH values. Oxidation of the resin by oxyanions such as molybdate, chromate and permanganate has been reported,²⁰ and in view of the fact that the $\text{TcO}_2-\text{TcO}_4^-$ potential²¹ is about 0.2 v. more negative than the $\text{Mo(V)}-\text{Mo(VI)}$ potential in acid solution, it seems reasonable to assume oxidation of the resin by pertechnetate ion. The exact pH dependence cannot be predicted without knowing the stoichiometry of the oxidation half-reaction; however, it was found empirically that the broadening was considerable when the adsorbate was $\geq 3 f$ in H_2SO_4 , and negligible at $\leq 0.5 f$ H_2SO_4 (Figs. 6, 7). No further improvement was observed when both adsorption and elution were performed in ammoniacal solution (Fig. 5).

In addition to this pH-dependent broadening, the technetium peaks exhibited a residual tailing-

(18) (a) S. S. Berman and W. A. E. McBryde, *Can. J. Chem.*, **36**, 835 (1958). (b) R. A. Naumann, private communication. (c) G. G. Goles, unpublished.

(19) E. Glueckauf, K. H. Barker and G. P. Kitt, *Disc. Faraday Soc.*, **7**, 199 (1949).

(20) O. Samuelson, "Ion Exchangers," John Wiley and Sons, Inc., New York, N. Y., 1953, p. 93.

(21) G. H. Cartledge and W. T. Smith, Jr., *This Journal*, **59**, 1111 (1955).

effect completely analogous to that observed in the case of rhenium and, like the latter, independent of pH . However, in contrast to rhenium, a small and nearly constant amount of technetium also appeared *ahead* of the main peak in every elution (e.g., Figs. 5, 6, 7). The appearance of this activity could not be correlated with any of the experi-

mental variables.

Acknowledgment.—We wish to thank Miss Carolyn A. Lovejoy for performing several of the experiments. One of us (E.A.) is also indebted to E. I. du Pont de Nemours and Company for the award of a pre-doctoral fellowship during the early stages of this investigation.

THE EFFECT OF ADJACENT BONDS ON BOND DISTANCES IN HYDROCARBONS

BY H. J. BERNSTEIN

Division of Pure Chemistry, National Research Council, Ottawa, Canada

Received September 8, 1958

The CC and CH bond distances in non-aromatic molecules are correlated with the π -bond orders of adjacent bonds, and CC bond distances in condensed aromatic molecules with the bond order evaluated by weighting Kekulé structures equally. The agreement between observed and calculated distances is within about ± 0.01 Å.

From the accumulating structural data derived from X-ray and electron diffraction, and rotation-vibration and microwave spectroscopy, it is apparent that the CC single bond distance in hydrocarbons is not constant but varies from 1.54 Å. in diamond to 1.38 Å. for the central bond in biacetylene (see upper field of Table I). Further, the CH bond distance is longest in saturated hydrocarbons and shortest when adjacent to a triple bond as in alkynes, with the distance in the vinyl group being intermediate. The other CC distances of interest are those in aromatic and condensed ring compounds.

It is the purpose of this note to show that CC and CH distances in hydrocarbons can be systematized on the basis of two simple notions—one for all hydrocarbons other than the condensed aromatics, and the other for the aromatics. In the case of the non-aromatic hydrocarbons as may be seen from Table I, the shortening of a CC bond adjacent to a multiple bond is additive and seems to depend only on the π -bond order of the adjacent bond. The effect of the neighbor bonds on CC single bond lengths has already been pointed out by Herzberg and Stoicheff.¹ If p_1 and p_2 are the π -bond orders of the carbon bonds adjacent to the C-C "single" bond under consideration, the CC "single" distances for the situations given in Table I may be represented to about ± 0.01 Å. by the equation²

$$R_{CC} = 1.542 - 0.042(p_1 + p_2) \quad (1)$$

Here, it is assumed that all single bonds whether CC or CH have zero bond order and do not affect the CC distance, and also that the effect of non-adjacent bonds is negligible. Since we write a Kekulé structure for the benzene ring its effect on an adjacent bond is considered to be the same as that of a double bond. It is apparent that the agreement between the observed values and those estimated from equation 1 is satisfactory.

(1) G. Herzberg and B. P. Stoicheff, *Nature*, **175**, 79 (1955).

(2) The shortening of a CC bond by 0.04 Å. per unit of bond order in its adjacent bonds also has been recognized by McHugh. I am grateful to Prof. V. Schomaker for sending me the Ph.D. thesis of J. P. McHugh, Calif. Inst. of Technology, 1957.

Walsh³ proposed that increasing the s character of a carbon hybrid orbital as one proceeds from sp^3 to sp hybridization accounts for a stronger and shorter bond. Analogous to equation 1 one could write then

$$R_{CC} = 1.542 - 0.042[6 - m - n] \quad (2)$$

where sp^m and sp^n are the states of hybridization of the orbitals of the C atoms forming the CC bond under consideration. According to the above notion then, non-aromatic CC single bond distances do not take any value between 1.38 and 1.54 Å. but are grouped very closely around the "magic" distances 1.38, 1.42, 1.46, 1.50 and 1.54 Å.

For double bonds of the type $\begin{array}{c} \diagup \\ \text{C}=\text{C} \\ \diagdown \end{array}$ the π -bond

orders of the adjacent bonds are zero, so that a linear relation of the above type would predict all CC double bonds of this kind to have the same length, namely, 1.34 Å. As far as one can ascertain from the literature,⁴ no experimental determination of CC double bond lengths of this type in a variety of molecules has given a length significantly different⁵ from 1.34 Å. There are two other kinds of double bonds, one kind as in allene, and the other, the central bond in butatriene. The observed distances⁶ can be represented by the equation

$$R_{C-C} = 1.34 - 0.03(p_1 + p_2) \quad (3)$$

where $p_1 + p_2 = 1$ for allene, and 2 for the central bond of butatriene.

On the basis of this notion, there is only one bond length to be expected for the CC triple bond since

(3) A. D. Walsh, *Disc. Faraday Soc.*, **2**, 18 (1947).

(4) Molecular orbital (MO) calculations yield a bond order of 0.894 for the double bond in butadiene.⁵ From the conventional bond order/bond distance plot⁴ a significant lengthening of the CC double bond would be expected. However, a more recent self-consistent molecular orbital (SCMO) treatment of butadiene⁷ gives a value of 0.96 for the bond order of the double bonds which would predict a very small change in the CC double bond length.

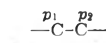
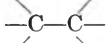
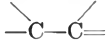
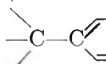
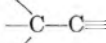

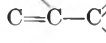
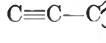
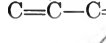
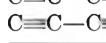
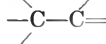
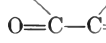
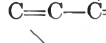
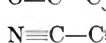
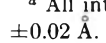
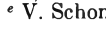
(5) C. A. Coulson, "Valence," Clarendon Press, Oxford, 1952, p. 254.

(6) G. Wheland, "Resonance in Organic Chemistry," John Wiley and Sons, Inc., New York, N. Y., 1955.

(7) J. A. Pople, *Trans. Faraday Soc.*, **49**, 1375 (1953).

(8) B. P. Stoicheff, *Can. J. Phys.*, **33**, 811 (1955); **35**, 837 (1957).

TABLE I
C-C BOND DISTANCES

	p_1	p_2	Σp	R_{calcd}	R_{obsd}^a	Molecule
	0	0	0	1.54	1.54	Alkanes, diamond
	0	1	1	1.50	1.50 ^c	Propene, isobutene
	0	1	1	1.50	1.50	<i>p</i> -Xylene
	0	2	2	1.46	1.47	Methylacetylene
	1	1	2	1.46 ^d	1.48	Biphenyl
	1	1	2	1.46	1.44	<i>trans</i> -Stilbene 1,10-diphenyl-1,3,5,7,9-decapentane
	2	1	3	1.42	1.40	Toluene
	1	1	2	1.46	1.47	1,3-Butadiene
	2	1	3	1.42	1.42	Perylene
	2	2	4	1.38	1.376 ^b	Biacetylene
	0	1	1	1.50	1.50 ^{e,e}	Acetaldehyde
	1	1	2	1.46	1.47	Glyoxal
	1	1	2	1.46	1.46	Acrolein
	1	1	2	1.46	1.48	Nicotinic acid
	2	2	4	1.38	1.37	Cyanogen

^a All internuclear distances unless otherwise indicated are from reference 4 and are usually quoted with an accuracy of ± 0.02 Å. ^b J. H. Calloman and B. P. Stoicheff, *Can. J. Phys.*, **35**, 373 (1957). ^c R. W. Kilb, C. C. Lin and E. B. Wilson, Jr., *J. Chem. Phys.*, **26**, 1695 (1957). ^d This distance may be greater than 1.46 Å. if the two phenyl rings are not coplanar. ^e V. Schomaker, private communication, 1957.

its adjacent bonds have zero bond order. This expectation⁹ is borne out by the experimental results.^{10,6}

It might be possible to extend these notions to molecules other than hydrocarbons. In the first instance, one might consider the effect of atoms other than C and H on CC bond lengths. In some cases (see the lower field of Table I) the CC distances are not too dependent on the nature of the other atom. In oxalic acid, however, the carboxyl groups do not have the same effect as in glyoxal, the central CC bond⁶ being 1.54 Å. This suggests that electrons are withdrawn from the CC bond into the carboxyl groups in keeping with the short C=O and CO distances observed.⁶

A discussion of CN and CO bonds is less satisfactory than for the CC bonds due primarily to mesomeric effects and the lack of equally reliable experimental data.¹¹

The aromatic distances such as in benzene and

(9) Again MO theory gives a bond order of 1.92 for the triple bond in diacetylene.¹⁰ It is probable that a SCMO treatment for the molecule would result in a higher bond order corresponding to very little lengthening.

(10) B. Pullman and A. Pullman, "Les Théories Electroniques de la Chimie Organique," Masson et Cie, 1952, p. 371.

(11) C. H. Townes and A. H. Schawlow, "Microwave Spectroscopy," McGraw-Hill Book Co., New York, N. Y., 1955.

graphite, and the different CC distances in naphthalene for example may be systematized on the basis of the following simple notion. A bond order is calculated considering only Kekulé structures (all weighted equally), and neglecting all formally bonded structures.^{6,12-14} This is essentially the Pauling bond order (P). We assume also that the CC distance under consideration may be given by an equation of the type

$$R_{\text{CC}} = P(\text{double bond distance}) + (1 - P)(\text{single bond distance}) \quad (4)$$

Mesomerism between the two Kekulé structures for benzene yields a bond order of $1/2$. In (i) bond *a* is the same as the central CC bond in butadiene and in (ii) it is a double bond. This



indicates that the value for the single bond dis-

(12) L. Pauling, L. O. Brockway and J. Y. Beach, *J. Am. Chem. Soc.*, **57**, 2705 (1935).

(13) L. Pauling and L. O. Brockway, *ibid.*, **59**, 1223 (1937).

(14) C. K. Ingold, "Structure and Mechanism in Organic Chemistry," Cornell University Press, Ithaca, N. Y.

tance to be used¹⁵ in equation 4 should be 1.46 Å. (corresponding to $P = 0$), and that for the double bond distance, 1.34 Å. (corresponding to $P = 1$). The equation for aromatic CC distances is then

$$R_{CC} = 1.34P + 1.46(1 - P) \quad (5)$$

which produces the observed distance of 1.40 Å. for benzene. A further test of this relation is obtained for graphite. The bond order evaluated from the Kekulé structures is $1/3$, which upon substitution in equation 5 gives a value of 1.42 Å. for the bond distance, in excellent agreement with the experimentally determined value.⁶ In the Kekulé structures for naphthalene the bond orders obtained by weighting structures equally are $a = 1/3$, $b = 1/3$, $c = 2/3$ and $d = 1/3$. The observed CC distances for naphthalene are compared with the calculated ones in Table II. The values calculated from equation 5 have a root mean square (r.m.s.) deviation intermediate to that calculated by MO and SCMO methods. A similar comparison for anthracene shows that there is about the same agreement between the results calculated by either equation 5 or the SCMO method and the observed data.¹⁷ The MO estimates are not in as good agreement, however.

It is instructive to compare the relation between Pauling bond orders and those obtained by MO and SCMO methods. In Fig. 1 this bond order correlation is shown. For ethylene, benzene and graphite the SCMO and MO bond orders are the same, but they are quite different for the central CC bond of butadiene. One might expect therefore to be able to estimate about the same values for CC distances by either equation 5 or a SCMO bond order plot.¹⁸ A significant difference would be expected for SCMO bond orders below 0.28 since equation 5 predicts the largest possible CC distance in condensed aromatic hydrocarbons to be 1.46 Å. whereas a SCMO bond order/bond distance plot indicates a value of 1.47₆ Å.

A reasonably reliable quantitative relation can be developed for aromatic CN bonds as well. From the CN distance of 1.34 Å. observed in pyridine¹⁹ and symmetrical triazine²⁰ (corresponding to a bond order of $1/2$), and the value of 1.28 Å. usually adopted for the CN double bond distance, the

(15) This differs from previous considerations of this type in which the single bond distance was taken to be that found in ethane, viz., 1.54 Å.

(18) There is a small curvature in a SCMO bond order/bond distance plot whereas the P vs. R plot is linear. The departure from linearity of the former plot, however, does not affect significantly the conclusion drawn.

(19) B. Bæk, W. Hansen and J. Rastrup-Andersen, *J. Chem. Phys.*, **22**, 2013 (1954).

(20) J. E. Lancaster and B. P. Stoicheff, *Can. J. Phys.*, **34**, 1016 (1956).

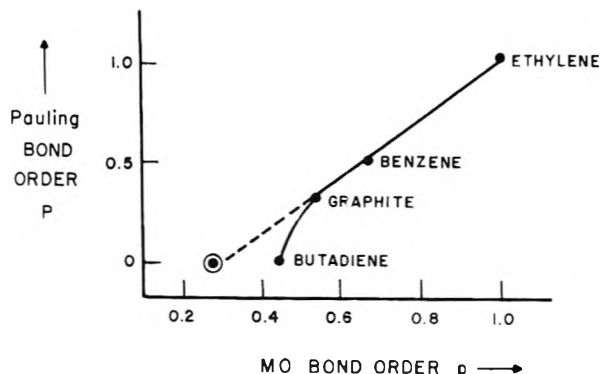
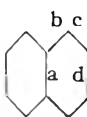


Fig. 1.—The relation between Pauling bond order and those given by molecular orbital theory: \odot , SCMO bond order for butadiene.

TABLE II
CALCULATED AND OBSERVED BOND DISTANCES FOR NAPHTHALENE

Bond order	Pauling bond order	Obsd. ^{a,c}	Calcd.		
			Eq. 5	MO ^b	SCMO ^c
a	1/3	1.41 ₀	1.42	1.42	1.40
b	1/3	1.42 ₅	1.42	1.41	1.42
c	2/3	1.36 ₁	1.38	1.38	1.36
d	1/3	1.42 ₁	1.42	1.40	1.42
r.m.s. dev.			0.011	0.017	0.006

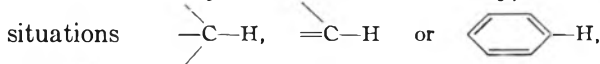


^a Ref. 17, D. W. Cruickshank, *Acta Cryst.*, **9**, 915 (1956).
^b Ref. 16, H. O. Pritchard and F. H. Sumner, *Proc. Roy. Soc. (London)*, **A226**, 128 (1954). ^c SCMO calculations given in ref. 16.

equation for aromatic CN bonds analogous to equation 5 for aromatic CC bonds may be written as

$$R_{CN} = 1.28P + 1.40(1 - P) \quad (6)$$

CH Bonds.—From the above considerations, the CH distance may have three values only, in the situations



and $\equiv\text{C}-\text{H}$. The experimental distances⁷ can be represented by the equation

$$R_{CH} = 1.10 - 0.02p \quad (7)$$

where p is the π -bond order of the bond adjacent to the CH bond, or by

$$R_{CH} = 1.10 - 0.02(3 - m) \quad (8)$$

where sp^m is the state of hybridization of the C atom. It is probable that equations analogous to (7) and (8) also may be written for C-halogen bonds.

Acknowledgment.—Helpful and illuminating discussions with Drs. B. Bæk, D. W. J. Cruickshank, J. A. Pople and B. P. Stoicheff are gratefully acknowledged.

F¹⁹ NUCLEAR MAGNETIC RESONANCE OF VARIOUS METAL-FLUORIDE COMPLEXES IN AQUEOUS SOLUTION

BY ROBERT E. CONNICK AND RICHARD E. POULSON

Contribution from the Department of Chemistry and the Radiation Laboratory, University of California, Berkeley, Cal.

Received September 8, 1958

The chemical shifts of F¹⁹ have been observed for a number of metal fluoride complexes in aqueous solution. No simple correlation was found with the electronegativity of the metal ion or the stability of the complex formed. It appears that metal cations of high atomic number produce a strong decrease in the magnetic shielding and a rough correlation was obtained with A/d , *i.e.*, ratio of the atomic number of the metal ion to the interatomic distance in the complex. In several cases separate resonances were observed, and assuming that they represent species which exchange fluorines only slowly, lower limits to the lifetime for exchange were calculated.

The position of the F¹⁹ nuclear magnetic resonance in a number of metal fluoride complexes in aqueous solution was investigated to determine whether there was a correlation of the chemical shifts with such properties as the stability of the complex, electronegativity of the metal atom, its charge, radius, etc. The results are shown in Table I. Included are several measurements from the literature and values for the reference compounds used in the present work. The data are reported in terms of the chemical shift σ , defined as

$$\sigma = 10^6 \frac{(H_c - H_r)}{H_r}$$

where H_c and H_r are the field strengths at resonance for the sample and the reference solutions, respectively. The reference compound was fluorine gas. Where possible, the formulas of the principal species were deduced from known complexing constants from the references cited.

In a few cases more than one resonance was observed and these have been interpreted as arising from different fluorine-containing species which do not exchange fluorines rapidly. From the separation of the lines a lower limit can be set to the exchange lifetime^{1,2} from the equation

$$\tau_e > \frac{1}{\Delta\omega} = \frac{10^6}{2\pi\nu\Delta\sigma}$$

where τ_e is the exchange lifetime, $\Delta\omega$ is the difference in angular precession frequencies, ν is the resonance frequency, and $\Delta\sigma$ is the difference in chemical shifts of the two species. These lower limits to the exchange lifetimes are given in the last column of Table I. In the case of aluminum the two species are known to be AlF₂⁺ and AlF⁺⁺, respectively.³ The σ values of 550 and 552 for titanium and zinc, respectively, almost certainly arise from fluoride ion. The 574 value for the second silicon solution is likely an average of F⁻, HF and HF₂⁻. The species corresponding to the two tin resonances are unidentified.

The observed line widths at half intensity were approximately the same as for the two aluminum fluoride complexes³, *i.e.*, 0.6 p.p.m., except in the case of the silver solutions where they were approximately 5.5 p.p.m. at 10⁴ gauss. This broadening with silver ion might be caused by an ap-

propriate rate of exchange between F⁻ and AgF, although other explanations are possible.

Saika and Slichter⁴ have proposed that the chemical shift in fluorine compounds is due primarily to the second-order paramagnetic term of the electrons on the fluorine. Using this hypothesis they explain the empirical correlation of Gutowsky and Hoffman⁵ of the F¹⁹ shifts with electronegativity. The present work gives no evidence for such a correlation.⁶ Our experiments differ from those of Gutowsky and Hoffman in that aqueous solutions rather than pure liquids were used and the compounds were more ionic than theirs.

An examination of the data reveals no obvious correlation with stability of the complexes. For example, ThF⁺³ and AlF⁺⁺ are much more stable complexes than ZnF⁺ although the resonance of the latter lies between those of the first two. Neither does there appear to be a simple correlation with the charge or radius of the metal ions, or combinations of these two.

Perhaps the most striking effect is the large decrease in shielding observed with thorium and uranyl ions. It seems probable that the large number of electrons in these atoms is somehow producing a strong decrease in the shielding of the F¹⁹ nucleus. An even larger decrease in shielding has been found for F¹⁹ in UF₆.⁷ Van Dyke Tiers⁸ has reported somewhat analogous effects for iodine, etc., altering the F¹⁹ resonance in substituted alkyl halides, although he interpreted the results in terms of steric interactions.

A plot of σ vs. the ratio of the atomic number of the metal ion and the approximate interatomic separation of the metal and fluorine nuclei measured in ångström units, *i.e.*, A/d is shown in Fig. 1 for the complex ions in aqueous solution. There is a rough correlation but its physical significance is not apparent. Superimposed on the A/d dependence, there may be an electronegativity dependence. The silicon point deviates from that of its more electropositive neighbors in the direction of smaller shielding, as would be expected from

(4) A. Saika and C. P. Slichter, *J. Chem. Phys.*, **22**, 26 (1954).

(5) H. S. Gutowsky and C. J. Hoffman, *ibid.*, **19**, 1259 (1951).

(6) For a discussion of this point see R. E. Poulson, Thesis, University of California, Nov. 16, 1956; printed as University of California Radiation Laboratory Report UCRL-3567. These various electronegativity values are given by Haissinsky (*J. Phys. Rad.*, [8] **7**, 7 (1946); Si, 1.8; Ag, 1.8; Sb(III), 1.8; Sn(II), 1.65; Ti(IV), 1.6; Be, 1.5; Al, 1.5; Zn, 1.5; U(IV), 1.3; Th, 1.1.

(7) J. N. Shoolery and H. E. Weaver, *Ann. Rev. Phys. Chem.*, **6**, 440 (1955).

(8) G. Van Dyke Tiers, *J. Am. Chem. Soc.*, **78**, 2914 (1956).

(1) H. S. Gutowsky and A. Saika, *J. Chem. Phys.*, **21**, 1688 (1953).

(2) P. W. Anderson, *J. Phys. Soc. Japan*, **9**, 317 (1954).

(3) R. E. Connick and R. E. Poulson, *J. Am. Chem. Soc.*, **79**, 5153 (1957).

TABLE I
CHEMICAL SHIFTS OF F¹⁹ IN METAL FLUORIDE COMPLEXES IN AQUEOUS SOLUTIONS

Principal fluoride species	Solution	σ^d	Lower limit for exchange time, τ (msec.)
ThF ^{+3a}	1.0 M Th(NO ₃) ₄ , 0.5 M NaF	336	
UO ₂ F ^{+b}	2.0 M UO ₂ (NO ₃) ₂ , 2.0 M NaF	395	
UO ₂ F ₂ ?	1.3 M UO ₂ (NO ₃) ₂ , 2.6 M NaF	401	
CF ₃ CO ₂ H	Pure CF ₃ CO ₂ H	(507.6) ^g	
SnF ⁺ , SnF ₂ ? ^c	0.8 M SnCl ₂ , 1 M NaF, 0.3 M HF	527, 588	0.07
F ⁻	Dilute NaF or KF	547.7	
F ⁻	13.3 M KF	(549.2)	
AgF, F ^{-d}	1 M AgNO ₃ , 1 M NaF	550 (very broad)	
AgF, F ^{-d}	2 M AgNO ₃ , 1 M NaF	550 (very broad)	
SiF ₆ ⁻²	(NH ₄) ₂ SiF ₆ (satd.)	(557.3) ^h	
SiF ₆ ⁻² , HF, F ⁻ , HF ₂ ⁻	0.1 M (NH ₄) ₂ SiF ₆ , 0.4 M HF, 0.4 M NaF	557.3, 574	0.3
TiF _n ⁺⁴⁻ⁿ , F ^{- ?}	K ₂ TiF ₆ (satd.)	573, 550	0.2
ZnF ⁺ , F ⁻	ZnF ₂ (satd.)	579, 552	0.2
BF ₃	Dissolved in ether	(583.2) ^h	
AlF ₂ ⁺ , AlF ^{+2e}	1 M Al(NO ₃) ₃ , 1 M NaF	587.0, 587.5	8
AlF ₂ ⁺ , AlF ^{+2e}	2 M Al(NO ₃) ₃ , 2 M NaF	588.0, 588.8	5
HF	48-51% aq. HF	(596.9) ^h	

^a H. W. Dodgen and G. K. Rollefson, *J. Am. Chem. Soc.*, **71**, 2600 (1949). ^b R. A. Day, Jr., and R. M. Powers, *ibid.*, **76**, 3895 (1954). ^c R. E. Connick and Armine D. Paul, unpublished. Some Sn(IV) also present. ^d I. Leden and L. Marthen, *Acta Chem. Scand.*, **6**, 1125 (1952). ^e Reference 3. ^f See "Experimental" for accuracy. The more intense line is italicized. ^g Reference solution, H. S. Gutowsky, D. W. McCall, B. R. McGarvey and L. H. Meyer, *J. Am. Chem. Soc.*, **74**, 4809 (1952). ^h Reference solution, H. S. Gutowsky and C. J. Hoffman, *Phys. Rev.*, **80**, 110 (1950).

Gutowsky and Hoffman's⁵ correlation. The remainder of the data, except perhaps for silver, are consistent with such an hypothesis but provide little substantiation for it.⁵

Experimental

The apparatus used is described elsewhere.³ The value of 507.6 for σ of CF₃CO₂H⁹ was used to refer all values to F₂. Values of σ for the reference solutions SiF₆⁻, BF₃(ether), and HF(aq.) were obtained in the following way. The position of CF₃COOH on Gutowsky and Hoffman's BeF₂ scale¹⁰ was established as 102.6 p.p.m. by comparing the σ 's of the organic fluorides reported in references 9 and 10, making allowance for the correction reported in footnote 23 of reference 5. The positions of SiF₆⁻, BF₃(ether), and HF(aq.) were then known from reference 10. The consistency of the assignment was checked by recording on the same chart, using a 1.5 gauss sawtooth sweep, the resonances of SiF₆⁻, BF₃(ether), HF(aq) and CF₃CO₂H, the solutions being contained in 2 mm. o.d. glass tubes simultaneously inserted in a sample tube. Taking the BF₃(ether) and CF₃CO₂H values as fix points, the SiF₆⁻ and HF(aq.) values were 0.6 p.p.m. less and 0.5 p.p.m. greater than Gutowsky and Hoffman's values, respectively. The values for the latter two solutions given in Table I are those measured here. The above procedure also calibrated the 1.5 gauss sweep field.

Where the sample resonance was within 10 p.p.m. of a reference solution, the chemical shift between the two was determined as described in reference 3. In other cases, *i.e.*, ThF⁺³, UO₂F⁺ and SnF⁺, the calibrated 1.5 gauss sweep was used to refer the sample to trifluoroacetic acid. The 13.3 M KF solution also was measured by the latter procedure. This solution and UO₂F⁺ were subsequently used as secondary reference solutions. The shifts relative to the nearest primary or secondary reference solutions are believed to be correct to about ± 1 p.p.m., except for aluminum and dilute NaF and KF solutions where they are probably within ± 0.3 p.p.m. and for ThF⁺³ and UO₂F⁺ where the uncertainty is ± 10 and ± 5 p.p.m., respectively.

(9) Footnote g, Table I.

(10) Footnote h, Table I.

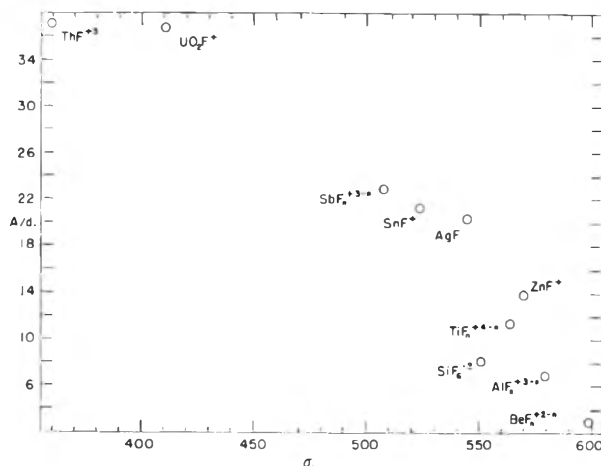


Fig. 1.—Correlation of σ of metal fluoride complexes with ratio of atomic number A of metal ion to interatomic distance d in ångström units. The beryllium and antimony points are from reference 5.

The relative accuracy of the reference solutions depends on Gutowsky and Hoffman's work¹⁰ to which they assigned a probable error of ± 1.5 p.p.m. The accuracy of all results on the F₂ scale depends on the accuracy of the value for trifluoroacetic acid.⁹ The authors gave no statement of accuracy but it may be $\pm 1\%$ as given in some earlier work.⁵ Some earlier chemical shift values given for the present work⁶ are in error because of oversight of the correction given in footnote 23 of reference 5.

In some cases the samples were contained in 15 mm. i.d. Lusteroid test-tubes rather than in Pyrex tubes. These tubes gave a 30% increase in sample volume over the glass tubes. They also fitted the Varian rf. probe insert snugly. Positioning of the sample inside the receiver coil has a marked effect on the balancing of the nuclear induction circuit when large tubes are used and the circuit can be balanced more readily if the tubes fit the probe insert well.

TERNARY ISOTHERMAL DIFFUSION AND THE VALIDITY OF THE ONSAGER RECIPROcity RELATIONS¹

BY DONALD G. MILLER

University of California Radiation Laboratory, Livermore, Cal.

Received September 8, 1958

Equations are derived relating experimentally measured ternary diffusion coefficients D_{ij} with the appropriate phenomenological coefficients L_{ij} of the thermodynamic theory of irreversible processes. The necessary and sufficient condition that the Onsager reciprocity relations be satisfied is also given. These equations, together with the measured values of D_{ij} and approximations for the required—but unavailable—activity data, permit a preliminary test of the Onsager Reciprocity Relations. It is found that these relations are satisfied within the estimated error for eight of the nine cases for which D_{ij} have been experimentally determined. The activity coefficient approximations and their probable errors are discussed.

I. Introduction

In almost all non-equilibrium situations where thermodynamic variables have meaning, the Thermodynamic Theory of Irreversible Processes² (TIP) can be applied successfully.³ In brief, this theory says (1) the rate at which entropy is produced inside a system undergoing dissipative processes σ can be written as

$$T\sigma = \sum J_i X_i \quad (1)$$

where T denotes the absolute temperature; J_i generalized flows, such as matter (moles cm.^{-2} sec.^{-1}), electricity (faradays cm.^{-2} sec.^{-1}), or heat (cal. cm.^{-2} sec.^{-1}); and X_i generalized thermodynamic forces such as temperature gradients, e.m.f.s, or chemical potential gradients in terms of moles. (2) The flows J_i of equation 1 are related linearly to the forces X_i of (1), *i.e.*

$$J_i = \sum_j L_{ij} X_j \quad (2)$$

where L_{ij} are the phenomenological coefficients. These coefficients are related to electrical resistances, diffusion coefficients, heat conductivities, etc. (3) If the J_i are mutually independent, or the X_i are, or both sets are,⁴ then the L_{ij} satisfy the following relations, known as the Onsager Reciprocity Relations (ORR); namely

$$L_{ij} = L_{ji} \quad (3)$$

The ORR's reduce considerably the number of experimental quantities necessary to describe the irreversible flows, and therefore the experimental verification of (3) is of considerable interest. This verification is at hand in a number of cases: *e.g.*, heat conduction in anisotropic crystals, thermoelectricity, electrokinetic effects and e.m.f. and transference in electrolyte solutions.⁵

The one outstanding case for which the ORR's have not been tested experimentally is isothermal diffusion.⁶ Although there is a great quantity

(1) This work was performed under the auspices of the U. S. Atomic Energy Commission. The derivations and some of the discussion are given in more expanded form in a UCRL Report, No. 5332.

(2) S. R. De Groot, "Thermodynamics of Irreversible Processes," Interscience Publishers Inc., New York, N. Y., 1951.

(3) Chemical reactions are the only really poor cases since they do not satisfy the linear laws (2) below.

(4) G. J. Hooyman and S. R. De Groot, *Physica*, **21**, 73 (1955).

(5) These cases are discussed in more detail by D. G. Miller, *Am. J. Phys.*, **24**, 433 (1956); *Chem. Revs.*, in preparation.

(6) This case is particularly interesting in view of the controversy over whether concentration gradients or chemical potential gradients are the true driving forces for diffusion. Since the chemical potential gradient characterizes diffusion in the TIP theory, the verification of

of excellent data for binary diffusion, there are no ORR in this situation.² Consequently, the test must come from diffusion experiments in systems of three or more components. In the past, there have been no suitable data available. However, some relatively good data on ternary solution systems have been published recently. Therefore, it seems worthwhile to set forth the necessary and sufficient condition that the ORR be satisfied, as well as the equations to determine the L_{ij} , all in terms of reported experimental quantities.⁷ Once these equations are at hand, the diffusion data together with suitable activity coefficient data will provide an experimental test of the ORR.

Unfortunately, activity coefficient data for the ternary systems studied are not at hand. Consequently, a rigorous test of the ORR cannot be made yet. However, a significant preliminary test of this important relation can be made by approximating activity coefficients. We shall find that with such approximations, the ORR are verified within the accuracy of the data and the estimated error of the activity assignments.

The systems involved are of three types: two electrolytes with a common ion in a neutral solvent; one electrolyte and one non-electrolyte in a neutral solvent; and two non-electrolytes in a neutral solvent. The last is clearly a ternary system. The other two are also, as will be shown in Appendix I.⁸

II. Derivations

We shall now derive equations for the L_{ij} in terms of the reported diffusion coefficients D_{ij} , some useful miscellaneous relations valid for multi-component systems, and expressions for the $\partial\mu_{iTP}/\partial c_j$ in terms of various tabulated quantities. The quantity μ_{iTP} is the chemical potential per mole at constant T and constant pressure P , and c_j is the concentration in moles per liter (molarity).

(a) **Equations for L_{ij} in Terms of D_{ij} .**—Assume one dimensional flow for convenience, and restrict the considerations to ternary diffusion. Let 1, 2 and 3 refer to solute 1, solute 2 and the solvent, respectively. Then the entropy production becomes

the ORR's in this case would settle the argument in favor of chemical potentials once and for all.

(7) This condition and the results to be described in detail below were reported in a brief preliminary communication: D. G. Miller, *THIS JOURNAL*, **62**, 767 (1958).

(8) A system such as $\text{NaCl-KBr-H}_2\text{O}$, however, is *not* a ternary system for diffusion, although it is a ternary system with respect to equilibrium properties; *cf.* B. R. Sundheim, *J. Chem. Phys.*, **27**, 791 (1957).

$$T\sigma = J_1X_1 + J_2X_2 + J_3X_3 \quad (4)$$

In isothermal diffusion, the thermodynamic force for each component is given by²

$$X_i = \frac{\partial\mu_{iTP}}{\partial x} \quad (5)$$

where x represents the position coordinate.

To obtain the ORR, the J_i or X_i or both must be independent. However, owing to the Gibbs-Duhem equation, the forces (5) are subject to the linear relation

$$\sum c_i X_i = 0 \quad (6)$$

Furthermore, these experiments are usually done in such a way that there is essentially no volume change during the course of the experiment. This second condition may be written

$$\sum \bar{V}_i J_i = 0 \quad (7)$$

where \bar{V}_i is the partial molal volume⁹ in cc./mole.

Consequently, equation 4 as it stands consists of dependent J_i and X_i , and is thus unsuitable for setting up linear laws (2) to which the ORR apply. By eliminating solvent terms, using equations 6 and 7, equation 4 can be brought to the form

$$T\sigma = J_1Y_1 + J_2Y_2 \quad (8)$$

where

$$Y_1 = \left[1 + \frac{c_1\bar{V}_1}{c_3\bar{V}_3} \right] X_1 + \left[\frac{c_2\bar{V}_1}{c_3\bar{V}_3} \right] X_2 = \alpha X_1 + \beta X_2 \quad (9)$$

$$Y_2 = \left[\frac{c_1\bar{V}_2}{c_3\bar{V}_3} \right] X_1 + \left[1 + \frac{c_2\bar{V}_2}{c_3\bar{V}_3} \right] X_2 = \gamma X_1 + \delta X_2$$

and α, β, γ and δ denote the corresponding square brackets. These J 's and Y 's are now independent, and the linear laws (2) may be written

$$\begin{aligned} J_1 &= L_{11}Y_1 + L_{12}Y_2 \\ J_2 &= L_{21}Y_1 + L_{22}Y_2 \end{aligned} \quad (10)$$

For this set, the theory states that $L_{12} = L_{21}$.

Owing to the difficulty in measuring chemical potential gradients directly, ternary diffusion data ordinarily are based on concentration (molarity) gradients. The following generalizations of Fick's law have been used,^{10,11} and fully take interaction effects into account

$$J_1 = -D_{11} \frac{\partial c_1}{\partial x} - D_{12} \frac{\partial c_2}{\partial x} \quad (11)$$

$$J_2 = -D_{21} \frac{\partial c_1}{\partial x} - D_{22} \frac{\partial c_2}{\partial x}$$

where D_{ij} are the (molarity) diffusion coefficients whose numerical values are reported. These D_{ij} have the units l./cm.sec. and are 1/1000.027 of the coefficients given in cm.²/sec.

Extensive use will be made of the identity

$$\frac{\partial f}{\partial t_i} = \sum_j \left(\frac{\partial f}{\partial x_j} \right)_x \left(\frac{\partial x_j}{\partial t_i} \right)_x \quad (12)$$

where $f = f(x_1 \dots x_n)$, and $x_i = x_i(t_1 \dots t_m)$.

To obtain the L_{ij} in terms of the D_{ij} , we write

(9) An alternative restriction on the J_i is the condition of no mass flow. In this case $\sum J_i M_i = 0$, where M is the molecular weight. The equations derived below will be valid for this case when M_i is substituted for \bar{V}_i .

(10) R. L. Baldwin, P. J. Dunlop and L. J. Gosting, *J. Am. Chem. Soc.*, **77**, 5235 (1955).

(11) P. J. Dunlop and L. J. Gosting, *ibid.*, **77**, 5238 (1955).

equation 10 in terms of $\partial c_i/\partial x$ and then compare coefficients. By equation 12, X_i can be written

$$X_i = \frac{\partial\mu_{iTP}}{\partial x} = \sum_j \mu_{ij} \frac{\partial c_j}{\partial x} \quad (13)$$

where μ_{ij} denotes $(\partial\mu_{iTP}/\partial c_j)$. Upon substituting equation 13 into 10, rearranging and equating the appropriate coefficients of $(\partial c_i/\partial x)$ in equations 11 we obtain

$$\begin{aligned} -D_{11} &= [\alpha\mu_{11} + \beta\mu_{21}]L_{11} + [\gamma\mu_{11} + \delta\mu_{21}]L_{12} = \\ &\qquad\qquad\qquad aL_{11} + bL_{12} \quad (14) \\ -D_{12} &= [\alpha\mu_{12} + \beta\mu_{22}]L_{11} + [\gamma\mu_{12} - \delta\mu_{22}]L_{12} = cL_{11} + dL_{12} \\ -D_{21} &= aL_{21} + bL_{22} \\ -D_{22} &= cL_{21} + dL_{22} \end{aligned}$$

where $a, b, c,$ and d denote the corresponding square brackets. Solution of these equations for L_{ij} yields

$$\begin{aligned} L_{11} &= \frac{bD_{12} - dD_{11}}{ad - bc} & L_{12} &= \frac{cD_{11} - aD_{12}}{aa - bc} \quad (15) \\ L_{21} &= \frac{bD_{22} - dD_{21}}{ad - bc} & L_{22} &= \frac{cD_{21} - aD_{22}}{aa - bc} \end{aligned}$$

Clearly the necessary and sufficient condition that $L_{12} = L_{21}$ is

$$\begin{aligned} aD_{12} + bD_{22} &= cD_{11} + dD_{21} \quad (16) \\ ad - bc &\neq 0 \end{aligned}$$

The chemical potential of the i th constituent can be written as

$$\mu_i = \mu_i^0 + RT \ln a_i \quad (17)$$

where μ_i^0 is a function of T only, R is the gas constant, and a_i the activity. Hence the expressions for $a, b, c, d,$ given for completeness, are

$$\begin{aligned} a &= RT \left[\left(1 + \frac{c_1\bar{V}_1}{c_3\bar{V}_3} \right) \frac{\partial \ln a_1}{\partial c_1} + \left(\frac{c_2\bar{V}_1}{c_3\bar{V}_3} \right) \frac{\partial \ln a_2}{\partial c_1} \right] \\ b &= RT \left[\left(\frac{c_1\bar{V}_2}{c_3\bar{V}_3} \right) \frac{\partial \ln a_1}{\partial c_1} + \left(1 + \frac{c_2\bar{V}_2}{c_3\bar{V}_3} \right) \frac{\partial \ln a_2}{\partial c_1} \right] \quad (18) \\ c &= RT \left[\left(1 + \frac{c_1\bar{V}_1}{c_3\bar{V}_3} \right) \frac{\partial \ln a_1}{\partial c_2} + \left(\frac{c_2\bar{V}_1}{c_3\bar{V}_3} \right) \frac{\partial \ln a_2}{\partial c_2} \right] \\ d &= RT \left[\left(\frac{c_1\bar{V}_2}{c_3\bar{V}_3} \right) \frac{\partial \ln a_1}{\partial c_2} + \left(1 + \frac{c_2\bar{V}_2}{c_3\bar{V}_3} \right) \frac{\partial \ln a_2}{\partial c_2} \right] \\ ad - bc &= (RT)^2 \left[1 + \frac{c_1\bar{V}_1 + c_2\bar{V}_2}{c_3\bar{V}_3} \right] \\ &\qquad\qquad\qquad \left[\left(\frac{\partial \ln a_1}{\partial c_1} \right) \left(\frac{\partial \ln a_2}{\partial c_2} \right) - \left(\frac{\partial \ln a_1}{\partial c_2} \right) \left(\frac{\partial \ln a_2}{\partial c_1} \right) \right] \end{aligned}$$

It will be shown in appendix III that

$$b = c \quad (19)$$

in all cases, and this relation is useful in checking the calculations.

Exactly the same equations are valid for the molality gradient description (*i.e.*, $\partial m_i/\partial x$) when c_1, c_2 and c_3 are replaced by m_1, m_2 and $1000/M_3$ wherever they appear in equations 6 through 18. The quantity m_i is the number of moles of i per kilo of solvent.

Hooymann¹² and Sundheim¹³ have derived certain related results in a more general but less direct way. Agar¹⁴ also has obtained some similar equations.

(12) G. J. Hooymann, *Physica*, **22**, 751 (1956); *Supp. Nuovo Cim.*, **1**, 166 (1955).

(13) B. R. Sundheim, *J. Chem. Phys.*, **27**, 791 (1957).

(14) J. Agar, private communication.

(b) **Some Useful Equations for Multi-component Solutions.**—In an n -component solution, only $n - 1$ of the concentrations c_i are independent. Thus in a ternary system, c_3 can be written as a function of c_1 and c_2 in these two ways, among many others

$$1000 = c_1 \bar{V}_1 + c_2 \bar{V}_2 + c_3 \bar{V}_3 \quad (20)$$

$$1000\rho = c_1 M_1 + c_2 M_2 + c_3 M_3 \quad (21)$$

where ρ is the density in grams/cc. and M_i the molecular weight of the i th constituent in grams/mole. The solvent will henceforth be considered as the n th component and its concentration as the dependent variable.

Note also that m_i and c_i can be written in terms of each other in several ways

$$m_i = \frac{1000c_i}{c_n \bar{M}_n} \quad (22)$$

$$c_i = \frac{1000\rho m_i}{1000 + \sum_{i=1}^{n-1} m_i M_i} \quad (23)$$

$$c_i = \frac{1000m_i}{1000 \frac{\bar{V}_n}{\bar{M}_n} + \sum_{i=1}^{n-1} m_i \bar{V}_i} \quad (24)$$

The derivation of the seven useful relations (25) to (31) will now be sketched

$$\sum_{i=1}^n c_i \left(\frac{\partial \bar{V}_i}{\partial c_j} \right) = 0, \quad j = 1, \dots, n-1 \quad (25)$$

$$\left(\frac{\partial c_n}{\partial c_j} \right)_c = - \frac{\bar{V}_j}{\bar{V}_n} \quad (26)$$

where c means that all the other independent c_k , $k \neq j$, n are held constant

$$1000 \left(\frac{\partial \rho}{\partial c_j} \right)_c = M_j - \frac{M_n \bar{V}_j}{\bar{V}_n} \quad (27)$$

$$\left(\frac{\partial m_i}{\partial c_j} \right)_c = \frac{1000}{c_n \bar{M}_n} \left[\delta_{ij} + \frac{c_i \bar{V}_i}{c_n \bar{V}_n} \right] = \frac{m_i}{c_i} \left[\delta_{ij} + \frac{c_i \bar{V}_i}{c_n \bar{V}_n} \right] \quad (28)$$

where δ_{ij} is the Kronecker delta

$$\left(\frac{\partial c_i}{\partial m_j} \right)_m = \frac{c_n \bar{M}_n}{1000} \left[\delta_{ij} - \frac{c_i \bar{V}_j}{1000} \right] = \frac{c_i}{m_i} \left[\delta_{ij} - \frac{c_i \bar{V}_j}{1000} \right] \quad (29)$$

where m means that all the other independent m_k are kept constant

$$\left(\frac{\partial \rho}{\partial m_i} \right)_m = \frac{M_i - \bar{V}_i \rho}{\bar{V}_m} \quad (30)$$

where \bar{V}_m is the denominator of equation 24, and finally

$$\mu_{21} = \frac{\mu_{12} c_{22} + \mu_{11} c_{12} - \mu_{22} c_{21}}{c_{11}} \quad (31)$$

where c_{ij} is the abbreviation for $(\partial c_i / \partial m_j)_m$. Similarly, $(\partial m_i / \partial c_j)_c$ will henceforth be denoted by m_{ij} .

Equations 25 are obtained from Duhem's equation for \bar{V} with $d\bar{V}_i$ written in terms of the independent dc_1, \dots, dc_{n-1} . But this result is a null linearly independent form whose coefficients, equations 25, must therefore be zero.

Differentiation of equation 20 and application of 25 yield equation 26. Analogously, the same order of operations with equations 21 and 26 yields 27, and with equations 22 and 26 yields 28.

It can be shown from equations 22 and 20 that $\bar{V}_m = 1000^2 / c_n \bar{M}_n$. Equation 29 then comes from the differentiation of 24 followed by the application of Duhem's equation, the above result for \bar{V}_m , and 22.

If the denominator of 23 is denoted by W_m , then $\rho = W_m / \bar{V}_m$. Differentiation of this plus Duhem's equation for \bar{V} yields equation 30.

It is well known that

$$\left(\frac{\partial \mu_i}{\partial m_j} \right)_m = \left(\frac{\partial \mu_j}{\partial m_i} \right)_m \quad (32)$$

a form not valid for derivatives with respect to the molarity c . Equation 31 is derived by expanding both sides of (32) by equation 12 and solving for μ_{21} . Note that by means of (29), equation 31 can be written

$$\mu_{21} = \frac{\mu_{12} \left(1 - \frac{c_2 \bar{V}_2}{1000} \right) - \mu_{11} \left(\frac{c_1 \bar{V}_2}{1000} \right) + \mu_{22} \left(\frac{c_2 \bar{V}_1}{1000} \right)}{\left(1 - \frac{c_1 \bar{V}_1}{1000} \right)} \quad (33)$$

Thus μ_{21} will be nearly equal to μ_{12} only if the \bar{V}_i are small or in dilute solutions.

Hooyma^{12,15} has presented some of these equations, but in gram units instead of mole units.

(c) **Expressions for μ_{ij} .**—From equation 17

$$\mu_{ij} = RT \frac{\partial \ln a_i}{\partial c_j} \quad (34)$$

(1) **Non-electrolytes.**—For non-electrolytes, the activity may be written in several ways; in terms of molarities c_i , molalities m_i , mole fractions N_i , etc. Concentration units are convenient here since equations 11 are in terms of concentration gradients. Thus, the activity will be written

$$a_i = c_i y_i \quad (35)$$

where y_i is the concentration (molarity) activity coefficient. In n -component systems, y_i will be a function of the concentrations of all the constituents. Thus

$$\mu_{ij} = RT \frac{\partial \ln a_i}{\partial c_j} = RT \left[\frac{\delta_{ij}}{c_j} + \frac{\partial \ln y_i}{\partial c_j} \right] \quad (36)$$

(2) **Binary Electrolytes.**—For binary electrolytes, the activity of the i th constituent is given in general by

$$\begin{aligned} a_i &= a_{ic} r_{ic} c_{ia} r_{ia} \\ a_{ic} &= c_{ic} y_{ic} \\ a_{ia} &= c_{ia} y_{ia} \end{aligned} \quad (37)$$

where a_{ic} is the activity of the cation, r_{ic} is the number of cations resulting from the dissociation of the electrolyte, c_{ic} is the concentration of the cations, and y_{ic} is the cation activity coefficient. Similarly, the ia subscripts apply to the anion. Since y_{ic} and y_{ia} are not experimentally attainable by themselves, the mean activity coefficient y_i must be employed. Thus

$$a_i = c_{ic} r_{ic} c_{ia} r_{ia} y_i^{r_i} \quad (38)$$

where $r_i = r_{ic} + r_{ia}$ and $y_i^{r_i} = y_{ic}^{r_{ic}} y_{ia}^{r_{ia}}$

Restricting ourselves to ternary systems, there are two cases: (i) No common ions—in this case

$$c_{ic} = r_{ic} c_i, \quad c_{ia} = r_{ia} c_i \quad (39)$$

where c_i is the concentration of the electrolyte-as-a-whole. Consequently

(15) G. J. Hooyma, *Physica*, **22**, 761 (1956).

$$a_i = r_{ic} r_{ie} r_{ie} r_{ia} c_i r_i y_i r_i \quad (40)$$

and

$$\mu_{ij} = RT \left[\frac{r_i \delta_{ij}}{c_j} + r_i \frac{\partial \ln y_i}{\partial c_j} \right] \quad (41)$$

This analysis includes the systems non-electrolyte-electrolyte or two binary electrolytes in a neutral solvent. However, the latter is not a ternary system for diffusion.⁸

(ii) Common ion—suppose for definiteness that the common ion is the anion. Then

$$c_{1a} = c_{2a} = r_{1a} c_1 + r_{2a} c_2 \quad (42)$$

$$c_{ic} = r_{ic} c_i$$

and consequently

$$a_i = r_{ic} r_{ie} c_{ic} r_{ie} [r_{1a} c_1 + r_{2a} c_2] r_{ia} y_i r_i \quad (43)$$

The differentiation of this expression yields

$$\mu_{ij} = RT \left[\frac{r_i \delta_{ij}}{c_j} + \frac{r_{ia} r_{ja}}{r_{1a} c_1 + r_{2a} c_2} + r_i \frac{\partial \ln y_i}{\partial c_j} \right] \quad (44)$$

If the common ion is the cation, interchange subscripts *a* and *c*.

(3) $\partial \ln y_i / \partial c_j$ in Terms of Tabulated Quantities.—Ordinarily, activity coefficients are tabulated in terms of the molality *m* and the molality activity coefficient γ . To get $\partial \ln y_i / \partial c_j$ in terms of γ , equations 2.23 of Robinson and Stokes¹⁶ are used. Thus y and γ are connected by this relation

$$y_i = \frac{\gamma_i \rho_0}{\rho - \sum_{k=1}^{n-1} \frac{c_k M_k}{1000}} = \frac{1000 \rho_0 \gamma_i}{c_n M_n} \quad (45)$$

The differentiation of equation 45 and application of (26) yields

$$\frac{\partial \ln y_i}{\partial c_j} = \frac{\partial \ln \gamma_i}{\partial c_j} + \frac{\bar{V}_j}{c_n \bar{V}_n} \quad (46)$$

By equation 12

$$\frac{\partial \ln \gamma_i}{\partial c_j} = \sum_{k=1}^{n-1} m_{kj} \frac{\partial \ln \gamma_i}{\partial m_k} \quad (47)$$

$$\frac{\partial \ln \gamma_i}{\partial m_j} = \sum_{k=1}^{n-1} c_{kj} \frac{\partial \ln \gamma_i}{\partial c_k} \quad (48)$$

Therefore

$$\frac{\partial \ln y_i}{\partial c_j} = \frac{\bar{V}_j}{c_n \bar{V}_n} + \sum_{k=1}^{n-1} m_{kj} \frac{\partial \ln \gamma_i}{\partial m_k} \quad (49)$$

using equation 47. Expressions for m_{kj} were given in equation 28.

The following results, useful in other connections, are easily derived from equations¹⁶ similar to equation 45

$$\frac{\partial \ln f_i}{\partial c_j} = \frac{\partial \ln y_i}{\partial c_j} + \frac{r_i - (\bar{V}_j / \bar{V}_n)}{\sum_{i=1}^n r_i c_i} \quad (50)$$

$$\frac{\partial \ln f_i}{\partial m_j} = \frac{\partial \ln \gamma_i}{\partial m_j} + \frac{r_j M_n}{1000 + M_n \sum_{i=1}^{n-1} r_i m_i} \quad (51)$$

where f_i is the mole fraction activity coefficient. Note that for non-electrolytes, $r_i = 1$. Equations 45-51 are not restricted to ternary systems.

(16) R. A. Robinson and R. H. Stokes, "Electrolyte Solutions," Butterworth Publications, London, 1953.

With the foregoing equations, we can make use of the D_{ij} data to compute the L_{ij} as well as both sides of equation 16. Partial molal volumes and approximations for the as yet unmeasured activity coefficients will also be required.

We consider the systems

- (I) LiCl-KCl-H₂O¹¹
- (II) LiCl-NaCl-H₂O¹¹
- (III) NaCl(0.25)-KCl(0.25)-H₂O¹⁷
- (IV) NaCl(0.5)-KCl(0.25)-H₂O¹⁷
- (V) NaCl(0.25)-KCl(0.5)-H₂O¹⁷
- (VI) NaCl(0.5)-KCl(0.5)-H₂O¹⁷
- (VII) Raffinose-KCl(0.5)-H₂O¹⁵
- (VIII) Raffinose-KCl(0.1)-H₂O⁸
- (IX) Raffinose-urea-H₂O¹⁹

each system having components 1, 2, 3, in the order as written above.²⁰

The D_{ij} used for I and II are from method IV of Fujita and Gosting.²¹ Dunlop's^{18,19} data (VII, VIII and IX) have been recalculated to give mole units; the d_{ij} in gram units by the relation $D_{ij} = M_j d_{ij} / M_i$ (see Appendix II).

III. Calculations of α , β , γ and δ

All concentrations are in moles/liter; the apparent molal volumes ϕ_v as well as \bar{V} are in cc./mole. The quantity c_3 was computed using the relation

$$c_3 = \frac{1000 - c_1 \phi_{v1} - c_2 \phi_{v2}}{\bar{V}_3^0} \quad (52)$$

where \bar{V}_3^0 was taken as 18.07 cc./mole.

The quantities $\phi_{v\text{KCl}}$, $\phi_{v\text{NaCl}}$, $\phi_{v\text{LiCl}}$ were taken from reference 11, and the ϕ_v 's for raffinose and urea were calculated from the values in reference 19. The quantities \bar{V}_1 and \bar{V}_2 were calculated using the approximate relation (53) (based on substituting *c* for *m*)

$$\bar{V}_i = \phi_{vi} + c_1 \frac{\partial \phi_{v1}}{\partial c_1} + c_2 \frac{\partial \phi_{v2}}{\partial c_1} \quad (53)$$

It was assumed in I-VI that ϕ_i was a function of the ionic strength ($c_1 + c_2$) only, and in VII and VIII that ϕ_2 was a function of ionic concentration c_2 only. The quantity \bar{V}_3 was computed from equation 20. These approximations do not affect the results much since the \bar{V} correction is relatively small, and the same approximations were used in the calculations of the D_{ij} from the raw data.^{11,17-19}

The \bar{V} data permit the computation of α , β , γ and δ , and the relevant quantities are given in Table I.

IV. Activity Coefficient Approximations

Unfortunately, there are no activity coefficient data for these systems, and consequently approximations are necessary to compute μ_{ij} . These approximations are the weakest links in the present calculations.

Since the calculations of the L_{ij} are sensitive to the values of activity coefficients, it is necessary to discuss in some detail the approximations used in the three types of ternary systems.

(a) **Two Binary 1-1 Electrolytes with One Ion in Common.**—Cases I-VI are of this type. Although some ternary activity coefficient data exist for these six systems, it is all at much higher concentrations than those used in the diffusion measurements.

(17) I. J. O'Donnell and L. J. Gosting, Enlarged Abstracts of Symposium on the Structure of Electrolytic Solutions, Electrochemical Society Meeting, May, 1957, Washington, D. C.

(18) P. J. Dunlop, *THIS JOURNAL*, **61**, 994 (1957).

(19) P. J. Dunlop, *ibid.*, **61**, 1619 (1957).

(20) There also exist two sets of D_{ij} for glucose in 60% aqueous sucrose; F. E. Weir and M. Dole, *J. Am. Chem. Soc.*, **80**, 302 (1958). However, their solutions were so concentrated that there is no hope of any reasonable activity approximation.

(21) H. Fujita and L. Gosting, *ibid.*, **78**, 1099 (1956).

TABLE I
 DATA FOR NINE TERNARY DIFFUSION SYSTEMS

	I	II	III	IV	V	VI	VII	VIII	IX
c_1	0.25	0.25	0.25	0.5	0.25	0.5	0.0149	0.0149	0.0149
c_2	0.20	0.20	0.25	0.25	0.5	0.5	0.5	0.1	0.5
c_3	54.8	54.8	54.69	54.43	54.29	54.02	54.2	54.9	53.9
M_1	42.40	42.40	58.45	58.45	58.45	58.45	504.4	504.4	504.4
M_2	74.56	58.45	74.56	74.56	74.56	74.56	74.56	74.56	60.06
M_3	18.02	18.02	18.02	18.02	18.02	18.02	18.02	18.02	18.02
I	0.45	0.45	0.5	0.75	0.75	1.0	0.5	0.1	...
\sqrt{I}	0.6708	0.6708	0.7071	0.8660	0.8660	1.0	0.707	0.317	...
$D_{11} \times 10^8$	1.134	1.099	1.372	1.414	1.343	1.389	0.4309	0.4303	0.421
$D_{12} \times 10^8$	-0.001	0.100	-0.0053	-0.0116	-0.0010	-0.0102	0.000975	0.000325	0
$D_{21} \times 10^8$	0.215	0.198	0.1429	0.0959	0.2053	0.1536	0.221	0.0636	0.0924
$D_{22} \times 10^8$	1.811	1.351	1.826	1.824	1.838	1.841	1.815	1.828	1.321
\bar{V}_1	18.62	18.60	18.71	19.22	19.25	19.67	307.2	307.2	307.2
\bar{V}_2	28.70	18.44	28.96	29.49	29.52	29.97	27.34	26.52	44.29
\bar{V}_3	18.05	18.08	18.07	18.06	18.06	18.05	18.09	18.08	18.07
α	1.005	1.005	1.005	1.010	1.005	1.010	1.005	1.005	1.005
β	0.00376	0.00376	0.00473	0.00489	0.00982	0.01008	0.1568	0.0311	0.1575
γ	0.00725	0.00465	0.00733	0.01500	0.00753	0.01537	0.000415	0.000309	0.000677
δ	1.006	1.004	1.007	1.008	1.015	1.0154	1.014	1.003	1.023
$c_2 M_3$	987.50	987.50	985.51	980.82	978.31	973.44	976.68	989.30	971.28
$c_3 \bar{V}_3$	989.14	990.78	988.26	983.02	980.43	975.18	980.47	992.59	973.97
m_1	0.253	0.253	0.2537	0.5098	0.2555	0.5136	0.01525	0.01506	0.01534
m_2	0.2025	0.2025	0.2537	0.2549	0.5111	0.5136	0.5122	0.1017	0.5143
S	0.4555	0.4555	0.5074	0.7647	0.7666	1.0273	0.5122	0.1017	...

At the ionic strengths used in the diffusion measurements (0.45–1.0), the Debye-Hückel theory is well outside its region of validity, calculated values often having the wrong sign. Therefore, the best approximation for electrolyte activity coefficients in ternary systems is based on Harned's Rule.^{16,22} This rule is valid to good approximation at constant total molality $m = m_1 + m_2$, and is written

$$\begin{aligned} \ln \gamma_1 &= \ln \gamma_1^0 - 2.303 \alpha_1 m_2 \\ \ln \gamma_2 &= \ln \gamma_2^0 - 2.303 \alpha_2 m_1 \end{aligned} \quad (54)$$

where γ_1^0 and γ_2^0 are the activity coefficients of each salt in pure water at molality m . The α_i , denoted by α_{ij} in Harned and Owen,²² are functions only of the total molality m .

The problem of estimating α_i is discussed in Robinson and Stokes,¹⁶ Chapter 15, and the most general approximation for α_i in terms of data for the pure salts is

$$2.303 \alpha_i = \frac{\phi_i^0 - \phi_j^0}{m} \quad (55)$$

where ϕ_k^0 are the molality osmotic coefficients of the pure salts at molality m . Equation 55 is strictly valid only if $\alpha_1 = -\alpha_2$. This will not be the case in general, but no better approximation is available.²³

Thus from (54) and (55), we have

$$\ln \gamma_i = \ln \gamma_i^0 - \frac{(\phi_i^0 - \phi_j^0)m_j}{m} \quad (56)$$

The differentiation of equation 56 yields the required expressions for $\partial \ln \gamma_i / \partial m_j$; namely

(22) H. S. Harned and B. B. Owen, "Physical Chemistry of Electrolyte Solutions," Third Edition, Reinhold Publ. Corp., New York, N. Y., 1958.

(23) An estimate of γ_i can be obtained from just γ_i^0 data as follows. Under the further assumption that $\gamma_{01} = \gamma_{02}$, it can be shown¹⁶ that

$$2.303 \alpha_i = \frac{\phi_i^0 - \phi_j^0}{m} = \frac{\ln (\gamma_i^0 / \gamma_j^0)}{2m}$$

where γ_{01} is the activity coefficient of component 1 infinitely dilute in a solution of component 2 at molality m , and similarly for γ_{02} . Upon substitution of this equation into (54), one obtains

$$\ln \gamma_i = \frac{m_i}{m} \ln \gamma_i^0 + \frac{m_j}{m} \left(\frac{\ln \gamma_1^0 + \ln \gamma_2^0}{2} \right)$$

This equation ordinarily gives a fairly reliable estimate.

$$\begin{aligned} \frac{\partial \ln \gamma_1}{\partial m_1} &= \frac{\partial \ln \gamma_1^0}{\partial m} - \frac{m_2}{m^2} \Delta \phi + \frac{m_2}{m} \frac{\partial \Delta \phi}{\partial m} \\ \frac{\partial \ln \gamma_1}{\partial m_2} &= \frac{\partial \ln \gamma_1^0}{\partial m} + \frac{m_1}{m^2} \Delta \phi + \frac{m_2}{m} \frac{\partial \Delta \phi}{\partial m} \\ \frac{\partial \ln \gamma_2}{\partial m_1} &= \frac{\partial \ln \gamma_2^0}{\partial m} - \frac{m_2}{m^2} \Delta \phi - \frac{m_1}{m} \frac{\partial \Delta \phi}{\partial m} \\ \frac{\partial \ln \gamma_2}{\partial m_2} &= \frac{\partial \ln \gamma_2^0}{\partial m} + \frac{m_1}{m^2} \Delta \phi - \frac{m_1}{m} \frac{\partial \Delta \phi}{\partial m} \end{aligned} \quad (57)$$

where $\Delta \phi = \phi_2^0 - \phi_1^0$.

By means of the relation¹⁶

$$\frac{d \ln \gamma}{dm} = \frac{\phi - 1}{m} + \frac{d\phi}{dm} \quad (58)$$

equations 57 can be shown to satisfy the condition

$$\frac{\partial \ln \gamma_1}{\partial m_2} = \frac{\partial \ln \gamma_2}{\partial m_1} \quad (59)$$

derivable from equation 32 and valid for the 1-1 electrolyte mixtures considered here. In the calculations, equation 58 is used as a check on the differentiations of the experimental data and (59) as a check on the arithmetic of (57).

The values of $\partial \ln \gamma_i^0 / \partial m$, $\partial \phi_i^0 / \partial m$ and ϕ_i were obtained numerically by means of Bessel's or Stirling's interpolation and differentiation formulas²⁴ up to third differences. All data were taken from the compilation of Robinson and Stokes.²⁵ The value of m at which the derivatives were evaluated was obtained from values of m_1 and m_2 calculated with equation 22.

The estimated error of the numerical differentiations is 0.001, based on the spread of values obtained from Newton's Forward, Newton's Backward, Bessel's, and Stirling's interpolation formulas for the same derivative. Besides this, there is of course the error resulting from employing the approximation of equation 55, possibly 10%. Consequently, the over-all error in $\partial \ln \gamma_i / \partial m_j$ is assumed to be 0.001 or 10%, whichever is larger.

(24) K. S. Kunz, "Numerical Analysis," McGraw-Hill Book Co., Inc., New York, N. Y., 1957.

(25) Reference 16, appendices 8.3 and 8.10. Inspection of the differences shows that these data are not as smooth as might be desired. Thus, the NaCl and KCl data, ostensibly good to 4 significant figures, resulted in deviations from equation 58 as high as 0.001. Similarly the values of $\partial \ln \gamma / \partial m$ for LiCl evaluated at the values of $m = 0.1, 0.2$, etc., did not form a very smooth curve.

The values of μ_{ij} are now obtained from the values of $\partial \ln \gamma_i / \partial m_j$ by means of equations 49 and 44.

(b) **One Non-electrolyte—One Binary Electrolyte.**—The raffinose-KCl-H₂O systems (VII and VIII) are of this type. No experimental data exist for this system. Therefore, to determine the required four μ_{ij} , it is necessary to approximate three of them or three related quantities such as $\partial \ln \gamma_i / \partial m_j$.

We shall assume that, although $\ln \gamma_1$ and $\ln \gamma_1^0$ are no doubt different in KCl-H₂O and in pure H₂O, the curves of $\ln \gamma_1$ and $\ln \gamma_1^0$ vs. m_1 will be almost parallel at constant m_2 . Consequently

$$\frac{\partial \ln \gamma_1}{\partial m_1} = \frac{\partial \ln \gamma_1^0}{\partial m_1} \quad (60)$$

the derivative being evaluated at the same ionic strength in the binary system as in the ternary mixture. A similar assumption is made about component two; *i.e.*

$$\frac{\partial \ln \gamma_2}{\partial m_2} = \frac{\partial \ln \gamma_2^0}{\partial m_2} \quad (61)$$

Here this approximation is very reasonable indeed, since raffinose is quite dilute (0.015 mole/l.), and consequently the system is for all practical purposes KCl dissolved in "almost pure" H₂O.

The data for KCl-H₂O are available,²⁵ and the value of $\partial \ln \gamma_2^0 / \partial m$ was obtained numerically as described in section (a) above with an estimated error of 10%.

Unfortunately, there are no suitable measurements on the raffinose-H₂O system. A few osmotic pressures were determined by Hess and Suranyi,²⁶ but these are not sufficiently precise to yield significant values of $\partial \ln \gamma_i^0 / \partial m$.

However, an approximation for $\partial \ln \gamma_i^0 / \partial m$ can be obtained from an estimate of the hydration number of raffinose. It has been shown^{27,28} that the activity coefficients of certain non-electrolytes in pure water can be described fairly well up to 2-3 molal by the expression

$$\ln \gamma_i^0 = -\ln [1 - 0.018(h - 1)m] \quad (62)$$

where h is an empirically determined hydration number. Thus

$$\frac{\partial \ln \gamma_i^0}{\partial m} = \frac{0.018(h - 1)}{1 - 0.018(h - 1)m} \quad (63)$$

Ikeda²⁷ noted that for solutions of other sugars such as glucose, sucrose, etc., h was approximately equal to the number of free hydroxyl groups. Raffinose has 11 such groups. Assuming that this correspondence is valid for raffinose too, at 0.015 molal we find

$$\frac{\partial \ln \gamma_i^0}{\partial m} \cong 0.20 = \frac{\partial \ln \gamma_i}{\partial m_1} \quad (64)$$

Here the absolute error is assumed to be 0.1.

It still remains to get a cross derivative such as $\partial \ln \gamma_1 / \partial c_2$. This can be obtained if the salting out coefficient of the non-electrolyte is known. This coefficient k_s , a measure of the effect of an electrolyte on the activity of a non-electrolyte, is given by the empirical relation²⁹

$$\log y_1 = k_s c_2 + k_1 c_1 \quad (65)$$

where k_1 is a numerically small coefficient. It is found experimentally that k_1 and k_s are nearly independent of concentration. Consequently

$$\left(\frac{\partial \ln y_1}{\partial c_2} \right)_{c_1} = 2.303 k_s \quad (66)$$

Unfortunately, k_s for the raffinose-KCl-H₂O system has never been determined; moreover, no other sugar systems have been investigated either.³⁰ However, examination of various non-electrolyte-KCl-H₂O systems listed in Long and McDevit²⁹ shows that k_s varies between 0.05 and 0.3. As a

representative value, we have chosen k_s to be approximately 0.1, or more exactly³¹

$$2.303 k_s = 0.25 \quad (67)$$

This choice is further supported by consideration of the following equation, due to McDevit and Long.³² In our notation, it is

$$2.303 k_s = \frac{V_1^0(V_{21} - V_2^0)}{\beta_0 RT} \times \left(\frac{d_2}{d_1 + d_2} \right) \quad (68)$$

where V_1^0 and V_2^0 are the partial molal volumes of pure components 1 and 2 at infinite dilution, V_{21} is the "liquid" salt volume, β_0 is the compressibility of the solvent, d_1 and d_2 are the diameters of solutes 1 and 2, respectively. If we approximate $d_2/(d_1 + d_2)$ by $(V_2^0)^{1/3}/[(V_1^0)^{1/3} + (V_2^0)^{1/3}]$ and use the value 10 for the $(V_{21} - V_2^0)$ of KCl,³² then (68) yields

$$2.303 k_s = 0.83 \quad (69)$$

However, this equation is valid only for non-polar non-electrolytes. Polar non-electrolytes have values of k_s smaller by a factor of 2-3. Thus the polarity correction brings the value of 2.303 k_s estimated from equation 69 close to the previously estimated value. An error of 0.1 has been assumed for 2.303 k_s .

We may now obtain μ_{12} from equations 67 and 36.

We compute $\partial \ln y_1 / \partial c_1$ by means of equations 46, 64 and 48 with $i = j = 1$. Equation 36 and $\partial \ln y_1 / \partial c_1$ yield μ_{11} .

The calculation of μ_{22} is more complicated. From equations 47, 32, 48 and 46, an expression for $\partial \ln y_2 / \partial c_2$ can be obtained

$$\frac{\partial \ln y_2}{\partial c_2} = \left\{ r_1 \left[\left(\frac{\partial \ln y_1}{\partial c_1} - \frac{\bar{V}_1}{c_3 \bar{V}_3} \right) c_{12} + \left(\frac{\partial \ln y_1}{\partial c_2} - \frac{\bar{V}_2}{c_3 \bar{V}_3} \right) c_{22} \right] m_{12} + \frac{\partial \ln \gamma_2}{\partial m_2} m_{22} \right\} + \frac{\bar{V}_2}{c_3 \bar{V}_3} \quad (70)$$

in which all the quantities are in Table I or were given or computed above. From this result and equation 36, μ_{22} is obtained.

Finally μ_{21} is obtained from μ_{11} , μ_{12} and μ_{22} by means of equation 31.

(c) **Two Non-electrolytes.**—The raffinose-urea-H₂O system (IX) is of this type.

We assume, for the same reasons as in the previous case, that

$$\frac{\partial \ln \gamma_i}{\partial m_1} = \frac{\partial \ln \gamma_i^0}{\partial m} \quad (71)$$

The value for raffinose is that given in equation 64 with the same estimated error. The $\partial \ln \gamma_2^0 / \partial m$ for urea was evaluated numerically from the data of Scatchard, *et al.*,³³ at the same molality of urea (0.5143) in the binary system as in the ternary system. A 10% error is assumed.

The estimation of a cross derivative such as $\partial \ln \gamma_2 / \partial m_1$ is more difficult. We reason crudely as follows. Assume that components 1 and 2 do not interact with each other except indirectly through their respective interactions with the solvent. It has been shown^{27,28} that a positive hydration number can be assigned to non-electrolytes whose activity coefficients increase with increasing concentration. In section (b) above, it was estimated as approximately 11 for component 1. Thus if component 1 is added to a solution of component 2, part of the water formerly available for dissolving component 2 is now solvated with component 1. Consequently the "effective" concentration of component 2 is larger than would be considered otherwise. The activity coefficient of component 2 will thus be that characteristic of the "effective" concentration. Hence in our system, the activity coefficient of urea is smaller in the presence of the solvated raffinose, since the γ of urea decreases as its concentration increases. Thus, $\partial \ln \gamma_2 / \partial m_1$ should be negative.³⁴ A similar conclusion would be reached if there

(26) K. Hess and L. Suranyi, *Z. physik. Chem.*, **184A**, 327 (1939).

(27) T. Ikeda, Repts. Lib. Arts. Fac., Shizuoka Univ., Series B, No. 1, (1950); *Bull. Chem. Soc. Japan*, **24**, 101 (1951).

(28) D. G. Miller, *This Journal*, **60**, 1296 (1956).

(29) A comprehensive review of the salting out effect has been given by F. A. Long and W. F. McDevit, *Chem. Revs.*, **51**, 119 (1952).

(30) The freezing point measurements of A. C. D. Rivett, *Medd. Vetenskapskad. Nobelinst.*, 2, No. 9 (1911), are insufficient to calculate k_s for sucrose-KCl-H₂O, the only sugar system recorded by Long and McDevit.²⁹

(31) After 0.1 was chosen as approximately correct, the value in equation 67, equivalent to $k_s = 0.109$, was taken because it gave good agreement in system VIII.

(32) W. F. McDevit and F. A. Long, *J. Am. Chem. Soc.*, **74**, 1733 (1952).

(33) G. Scatchard, W. Hamer and S. Wood, *ibid.*, **60**, 3061 (1938).

(34) The same sort of argument predicts that if γ_1^0 and γ_2^0 both increase or else both decrease as the concentration increases, then $\partial \ln \gamma_2 / \partial m_1$ will be positive in the ternary (non-electrolyte) mixture.

TABLE II
QUANTITIES INVOLVED IN THE CALCULATION OF μ_{ij}

	II	III	IV	V	VI	VII	VIII	IX	
m_{11}	1.0177	1.0177	1.0195	1.0295	1.0272	1.0377	1.0290	1.0159	1.0347
m_{12}	0.00734	0.00471	0.00744	0.01529	0.00770	0.01579	0.00425	0.000402	0.000697
m_{21}	0.00381	0.00381	0.00480	0.00499	0.01004	0.01036	0.1605	0.0314	0.1622
m_{22}	1.0187	1.0167	1.0221	1.0272	1.0376	1.0431	1.0382	1.0138	1.0532
c_{11}	0.9826	0.9826	0.981	0.971	0.9736	0.964	0.972	0.984	0.966
c_{12}	-.00708	-.00455	-.00714	-.01446	-.00722	-.0146	-.000398	-.000391	-.000640
c_{21}	-.00367	-.00367	-.00461	-.00471	-.009416	-.00957	-.1501	-.0306	-.1490
c_{22}	.9816	.9836	.978	.9736	.964	.959	.963	.986	.950
$\frac{\partial \ln y_1}{\partial c_1}$.0238	0.1090	-.1208	-.0435	-.0401	-.0041	.553	.553	.516
$\frac{\partial \ln y_1}{\partial c_2}$	-.0974	-.0666	-.1550	-.0746	-.0714	-.0331	.250	.250	.00348
$\frac{\partial \ln y_2}{\partial c_1}$	-.1085	-.0670	-.1650	-.08501	-.0818	-.0440	.389	.397	.262
$\frac{\partial \ln y_2}{\partial c_2}$	-.2304	-.1526	-.1994	-.1165	-.1134	-.0735	-.1916	-.8106	-.0346
μ_{11}/RT	6.270	6.260	5.758	3.246	5.253	-2.992	67.85	67.85	67.811
μ_{12}/RT	2.028	2.089	1.690	1.184	1.191	0.9337	0.250	0.250	0.00348
μ_{21}/RT	2.005	2.088	1.670	1.163	1.170	0.9119	0.779	0.794	0.262
μ_{22}/RT	6.762	6.917	5.601	5.100	3.107	2.853	3.617	18.38	1.965

TABLE III
QUANTITIES INVOLVED IN THE CALCULATION OF L_{ij}

	I	II	III	IV	V	VI	VII	VIII	IX
a^a	6.309	6.299	5.793	3.284	5.290	3.031	68.31	68.21	68.19
b	2.063	2.126	1.724	1.221	1.227	0.9719	0.8179	0.8237	0.3136
c	2.063	2.126	1.727	1.221	1.227	0.9719	0.8184	0.8228	0.3131
d	6.817	6.954	6.115	5.185	3.162	2.911	3.668	18.43	2.011
$ad - bc^b$	38.75	39.29	32.45	15.44	15.22	7.88	249.89	1256.4	137.00
$-L_{11}^c$	0.200	0.189	0.259	0.473	0.279	0.514	0.00632	0.00631	0.00618
$-L_{12}$	-.0605	-.0434	-.0739	-.114	-.109	-.175	-.00114	-.000265	-.00096
$-L_{21}$	-.0586	-.0380	-.0702	-.112	-.105	-.170	-.00269	-.000264	-.00166
$-L_{22}$.283	.206	.318	.380	.622	.689	.495	.0992	.657

^a RT has been factored out in a, b, c, d . ^b $(RT)^2$ has been factored out. ^c $10^{-8}/RT$ has been factored out of all L_{ij} quantities. The L_{ij}/RT have the units, moles/em. sec.

is some direct interaction, such as hydrogen bonding, between the N of the urea and the O of the raffinose hydroxyl groups. The numerical value is probably somewhere between zero and $\partial \ln \gamma_2 / \partial m_2 = -0.076$. We choose

$$\frac{\partial \ln \gamma_2}{\partial m_1} = \frac{\partial \ln \gamma_1}{\partial m_2} = -0.04 \quad (72)$$

with an estimated error of ± 0.04 .

The values of μ_{ij} were calculated by means of equations 47, 49 and 36, and checked using equation 31.

V. Results and Discussion

The values of $\partial \ln y_i / \partial c_j$ based on the foregoing approximations are given in Table II along with the values of c_{ij} , m_{ij} and the resulting values of μ_{ij}/RT . The calculated values of a, b, c and d , as well as $ad - bc$ and the L_{ij} , are in Table III. The computations of b and c were checked by equation 19.

In Table IV are the assumed errors in the D_{ij} . Finally in Table V are desired values of the rhs and lhs of the necessary and sufficient condition, equation 16. Included also are the differences between the rhs and lhs as well as the probable error based on estimated errors in the measured D_{ij} and the approximated activity derivatives.

Electrolyte mixtures are more complex since $\ln \gamma_i^0$ goes through a minimum, but the hydration part of the argument seems to be qualitatively correct here as well in predicting the sign of $\partial \ln \gamma_i / \partial m_j$.

The probable error in equation 16 was determined as follows. Let R be defined as

$$R = (aD_{12} + bD_{22}) - (cD_{11} + dD_{21}) \quad (73)$$

Then R is a function of the experimental quantities e_k such as the \bar{V}_i , D_{ij} , $\partial \ln \gamma_i / \partial m_j$ or $\partial \ln y_i / \partial c_j$, and the c_i . If δe_k is the probable error in e_k , then the probable error δR of (16) is given by³⁵

$$\delta R = \sqrt{\sum_k \left[\left(\frac{\partial R}{\partial e_k} \right)^2 \delta e_k^2 \right]} \quad (74)$$

A typical term of the sum in (74) is $(a\delta D_{12})^2$, for example. No errors were assumed for the \bar{V}_i and c_i .

TABLE IV

	ERRORS ASSUMED FOR D_{ij}								
	I	II	III	IV	V	VI	VII	VIII	IX
D_{11}	0.02	0.02	0.01	0.01	0.01	0.01	0.01	0.01	0.01
D_{12}	.01	.02	.01	.01	.01	.01	.0002	.0001	.001
D_{21}	.02	.02	.01	.01	.01	.01	.02	.01	.02
D_{22}	.01	.02	.01	.01	.01	.01	.02	.02	.02

Of the nine systems considered, the activity approximations are the best in the electrolyte systems, I-VI, and it is felt that the test of the ORR

(35) H. Margenau and G. Murphy, "Mathematics of Physics and Chemistry," D. Van Nostrand Co., New York, N. Y., 1943, p. 498.

TABLE V

	TEST OF THE ONSAGER RECIPROCALITY RELATIONS								
	II	III	IV ^b	V	VI	VII	VIII	IX	
$lhs (16)^a$	3.73	3.50	3.12	2.19	2.25	1.76	1.55	1.53	0.41 ^c
$rhs (16)^a$	3.80	3.71	3.24	2.22	2.30	1.80	1.16	1.53	.32 ^c
Difference	0.07	0.21	0.12	0.03	0.05	0.04	0.39	0	.09
Probable error	.17	.20	.12	.08	.07	.05	.21	.27	.10

^a $10^{-2} RT$ has been factored out. ^b An error in activity coefficient derivatives has been corrected. The corrected values in column IV differ slightly from those reported in reference 7. ^c An improved estimate of activity coefficients gives these values, differing slightly from those reported earlier.⁷

here is more significant than in the other examples. Equation 16 is clearly verified very well for systems I, IV, V, VI and is just on the border line for systems II and III. Note, however, that the comparison of fringe deviation graphs for I and II (Figs. 3 and 4, reference 21) shows that the reported D_{ij} give a much poorer fit for the borderline case II. Unfortunately, fringe deviation graphs are not as yet available for III-VI.

For the non-electrolyte-electrolyte cases, VII and VIII, the verification for VIII is good, with a reasonable value of the salting out coefficient.³¹ Case VII, however, is off somewhat more than the estimated error. Since the same value of k_s should be valid for both systems and since the error in $\partial \ln \gamma_2 / \partial m_2$ is not large, a simultaneous solution of the equations $L_{12} = L_{21}$ for both systems should lead to values of k_s and $\partial \ln \gamma_1 / \partial c_1$. The resulting values, however, give $\partial \ln \gamma_1 / \partial c_1$ an enormously large and completely unreasonable value. From this, it must be concluded that VII and VIII are inconsistent.³⁶ Again inspection of the fringe deviation graphs (Fig. 2, ref. 18) shows that the assumed D_{ij} for VII give a very poor fit for the bad case VII, whereas for VIII the fit is quite good. It seems reasonable to assume, therefore, that the errors in D_{ij} for VII are much larger than the estimates given in Table IV; how much larger is not known.

For case IX, the verification is quite adequate considering the complete lack of knowledge of activity coefficients. The fringe deviation graphs show a reasonably good fit for the reported D_{ij} . Consequently, one expects the inexact assignment of activity coefficients to be the principal cause of error. This case is especially sensitive to the values of D_{12} and $\partial \ln \gamma_1 / \partial m_2$.

It may thus be concluded that the agreement of both sides of equation 16 within the estimated error for 8 of the 9 cases considered constitutes the preliminary justification of Onsager Reciprocity Relations in ternary diffusion.

It should be emphasized that an absolute test still remains to be accomplished. At present, systems or concentrations for which activity data are available and systems or concentrations for which diffusion data are available form mutually exclusive sets. For the rigorous test, it would be very desirable for experimentalists to (a) supply activity data for the nine systems investigated so far, or (b) do the diffusion experiments on

(35) In fact a backwards computation on VII, using any reasonable value of $\partial \ln \gamma_1 / \partial c_1$, indicates raffinose is salted in rather than salted out. ADDED IN PROOF.—Dr. P. J. Dunlop has stated (private communication) that errors in D_{ij} for VII are in fact somewhat larger than were assumed in Table IV, which helps explain the discrepancy between VII and VIII.

systems in the range of concentrations for which activity data are known.

NOTE ADDED IN PROOF:—Recently P. J. Dunlop and L. J. Gosting, THIS JOURNAL, 63, 56 (1959), here reported similar calculations on systems III-VI. Their work also involves activity coefficient estimates, since they assume the value of $\beta (=0)$ valid from 2-5 molal is also valid from 0.25-1 molal. It is gratifying that our numbers are so close and our conclusions the same.

Appendix I

The Ternary Systems for Diffusion.—There are eight types of ternary system with respect to equilibrium properties which can be formed from non-electrolytes (n) and binary electrolytes (e). These are (i) 3n, (ii) 2n - 1e, (iii) 1n - 2e (ion in common), (iv) 1n - 2e (no common ion), (v) 3e (ion common to all 3), (vi) (ion common to 2), (vii) 3e (2 common ions each common to 2), and (viii) 3e (no common ion). The first four are exemplified by the systems we have been considering; the last four by molten salt mixtures. Cases (i), (ii), (iii) and (v) are ternary systems for diffusion and are characterized by three or four diffusing species. The remaining cases are *not* ternary systems for diffusion, even though (vii) has 4 diffusing species also.

Case (i), like raffinose-urea-H₂O, is clearly a ternary system for diffusion. In this appendix, we will show in detail that case (ii) is also. The arguments for cases (iii) and (v) are analogous and will be indicated very briefly.

Case (ii), like the raffinose-KCl-H₂O system, has four diffusing species: the non-electrolyte solvent, the non-electrolyte solute and the two ions. It is intuitively clear that owing to electroneutrality the cations and anions must move together in their stoichiometric ratios. The formal justification, easily generalized to cases (iii) and (v), is given.

From equation 1

$$T\sigma = J_c X_c + J_a X_a + J_1 X_1 + J_3 X_3 \quad (1A)$$

where c refers to the cation and a refers to the anion, 1 is the neutral solute and 3 is the solvent. Suppose component 2, the electrolyte, ionizes as



where CA represents the electrolyte-as-a-whole, τ_c and τ_a the stoichiometric coefficients of C and A, and z_c and z_a the charges on C and A with due regard to sign. Then

$$\mu_{CA} = \mu_2 = \tau_c \mu_c + \tau_a \mu_a \quad (3A)$$

$$0 = \tau_c z_c + \tau_a z_a \quad (4A)$$

Furthermore, since no current I flows in this system

$$0 = I = z_c J_c + z_a J_a \quad (5A)$$

Equation 5A is equivalent to electroneutrality. Finally, for a charged particle, the thermodynamic force is given by¹

$$\bar{X}_i = \frac{\partial \mu_i}{\partial x} + z_i F \frac{\partial \phi}{\partial x} \quad (6A)$$

where F and ϕ are the value of the faraday and the electrical potential, respectively.

Now consider only the ionic terms. By equation 6A

$$J_c X_c + J_a X_a = J_c \frac{\partial \mu_c}{\partial x} + J_a \frac{\partial \mu_a}{\partial x} + (z_c J_c + z_a J_a) F \frac{\partial \phi}{\partial x} \quad (7A)$$

However, by (5A), the electrical term vanishes. The substitution of (5A) solved for J_a yields

$$J_c \left[\frac{\partial \mu_c}{\partial x} - \frac{z_c}{z_a} \frac{\partial \mu_a}{\partial x} \right] \quad (8A)$$

The application of (4A) and (3A) to (8A) now yields

$$J_c X_c + J_a X_a = \frac{J_c}{r_c} \frac{\partial \mu_c}{\partial x} \quad (9A)$$

But J_c/r_c is precisely the amount of cation which would flow if it were tied up as the compound CA. Consequently

$$\frac{J_c}{r_c} = J_2 \quad (10A)$$

Thus the ionic terms have reduced to $J_2 (\partial \mu_2 / \partial x)$. Hence $T\sigma$ may be written as $J_1 X_1 + J_2 X_2 + J_3 X_3$, which was the starting point of the derivations in section II.

Cases (iii), like NaCl-KCl-H₂O, and (v), like NaCl-KCl-LiCl, are verified in the same way. Thus the generalized form of (5A) is used to get rid of the ϕ terms and to solve for J_a . Then the equations like (3A) and those like (4A) are substituted in, and again the flows will be in the form of (10A), yielding the desired results.

Appendix II

Relations between Gram and Mole Descriptions of Diffusion.—Some of the diffusion data^{18,19} have been reported in gram units instead of mole units. In this appendix we investigate the equations in terms of gram units.

For the i th component, let j_i be the flow in g./cm.² sec., J_i the flow in moles/cm.² sec., μ_i^g the chemical potential per gram, μ_i^m the chemical potential per mole, v_i the partial specific volume,

\bar{V}_i the partial molal volume, c_i^g the concentration in g./l., c_i the concentration in moles/liter, x_i the thermodynamic force in gram units, X_i the thermodynamic force in mole units, M_i the molecular weight, d_{ij} the diffusion coefficient in gram units, D_{ij} the diffusion coefficient in mole units, l_{ij} the Onsager coefficients in gram units, and L_{ij} the Onsager coefficients in mole units. Then we have immediately

$$J_i = j_i/M_i \quad (11A) \quad \mu_i = M_i \mu_i^g \quad (14A)$$

$$\bar{V}_i = M_i \bar{v}_i \quad (12A) \quad X_i = M_i x_i \quad (15A)$$

$$c_i = c_i^g/M_i \quad (13A)$$

From these equations, one can very easily prove by substitution that

$$T\sigma = \sum J_i X_i = \sum j_i x_i \quad (16A)$$

$$\sum c_i d\mu_i = \sum c_i^g d\mu_i^g \quad (17A)$$

$$\sum J_i \bar{V}_i = \sum j_i \bar{v}_i \quad (18A)$$

$$D_{ij} = d_{ij}(M_j/M_i) \quad (19A)$$

$$L_{ij} = l_{ij}(M_j M_i) \quad (20A)$$

The gram unit expressions of (16A), (17A) and (18A) are identical in form to the mole unit ones. Hence, all the results obtained earlier in terms of mole units are equally valid for gram units upon substitution of gram quantities for mole quantities. The relation between gram coefficients and mole coefficients is given by (19A) and (20A). Equation (19A) was originally stated by P. J. Dunlop.³⁷

Appendix III

Proof that $b = c$.—We prove that for ternary systems, the b and c of equations 18 are equal.

From the definitions of b , c , α , β , γ , δ , equations 14 and 9 and equation 20, we have

$$c_3 \bar{V}_3 b = c_1 \bar{V}_2 \mu_{11} + (1000 - c_1 \bar{V}_1) \mu_{21} \quad (21A)$$

The substitution of the *rhs* of equation (33) for μ_{21} and cancellation of $(1000 - c_1 \bar{V}_1)$ yields

$$c_3 \bar{V}_3 b = c_1 \bar{V}_2 \mu_{11} + [(1000 - c_2 \bar{V}_2) \mu_{12} - c_1 \bar{V}_2 \mu_{11} + c_2 \bar{V}_1 \mu_{22}] \quad (22A)$$

Again the use of (20) yields

$$c_3 \bar{V}_3 b = (c_3 \bar{V}_3 + c_1 \bar{V}_1) \mu_{12} + c_2 \bar{V}_1 \mu_{22} = c_3 \bar{V}_3 [\delta \mu_{12} + \beta \mu_{22}] = c_3 \bar{V}_3 c \quad (23A)$$

Cancellation of $c_3 \bar{V}_3$ gives the desired result.

(37) Cf. Reference 20, footnote 6.

CARBON FORMATION IN AN ACETYLENE-AIR DIFFUSION FLAME

BY M. E. MILBERG

Scientific Laboratory, Ford Motor Company, Dearborn, Michigan

Received September 11, 1968

The rate of soot issue from an acetylene-air diffusion flame has been measured as a function of pressure and air/fuel ratio. The soot has been analyzed for soluble and volatile constituents by infrared and ultraviolet absorption spectroscopy and mass spectrometry. The rate measurements can be explained on the basis of a soot formation rate which varies linearly with pressure and is independent of air/fuel ratio. The analyses showed the presence of polynuclear aromatics and oxygenated aliphatics. The rate and analytical results are consistent with a pyrolysis mechanism of carbon formation involving polymerization of acetylene to large aromatic molecules followed by carbonization. Oxygen may be involved in the pyrolysis process.

Introduction

Considerable interest in the nature of the mechanism of combustion deposit formation has been evidenced for quite some time. This interest

has, in part, manifested itself in efforts to elucidate the mechanism of carbon formation in explosions and burner flames, principally by flame spectroscopy and analysis of soot for intermediates in the forma-

tion process. Although the rate of carbon formation would be expected to provide some information of value toward elucidation of the formation mechanism, relatively little work along these lines has been reported. There are no reports of measurements of sooting rate as a function of pressure and air/fuel ratio for diffusion flames, although measurements of soot yield have been made in premixed flames.¹

In the present work the rate of soot issue from an acetylene-air diffusion flame has been measured as a function of pressure and air/fuel ratio. Concomitant with the rate measurements, some analyses of the soot and its solvent extracts have been made. Acetylene was chosen as the fuel because of its chemical simplicity and high C/H ratio, and because of its rather special position as a common intermediate in Porter's suggested mechanism of carbon formation,² recently contradicted by the results of Ferguson.³

Sooting rates were measured by collecting the soot issuing from the flame for a measured time interval and determining the weight collected. Several methods of analysis were employed. These included extraction of the collected soot with organic solvents, followed by infrared and ultraviolet spectral analysis of the extracts, mass spectrometric analysis of distillate from the soot, and infrared and ultraviolet spectral analysis of condensate from the flame exhaust. The experimental results can be explained on the basis of a soot formation rate which is linear with pressure and independent of air/fuel ratio and are consistent with a mechanism involving polymerization of acetylene to polynuclear aromatic structures with subsequent degradation to a carbonaceous residue.

Experimental

The prime consideration in setting up the burner system was that it permit the collection of soot in an essentially complete and reproducible manner under controlled conditions. The burner, which was similar to that of Parker and Wolfhard,⁴ is shown in Fig. 1. It consisted of two concentric tubes whose diameters were such that at the desired air/fuel ratio, the linear flow rates of fuel and air were essentially equal. The burner proper was enclosed by a shield which permitted operation at pressures other than atmospheric. Three interchangeable stainless steel burner tube assemblies providing equal linear flow rates at air/fuel volume ratios of 15.1, 12.3 and 9.0, respectively, were used. The tube diameters are given in Table I. A small point was provided on the inside of the top edge of each outer tube to permit a spark to be jumped from the outer to the grounded inner tube for ignition. The stainless steel block with two 24/40 standard taper holes for holding the soot collecting tubes was arranged to slide between guide strips on the top plate in such a manner that at each end of its travel one of the collecting tubes was aligned with a concentric hole in the top plate. Each collecting tube, as shown in Fig. 2, had a shoulder ground into the inside of the standard taper joint, against which a soot collecting cartridge, also shown in Fig. 2, was sealed by means of an O ring. All glass wool packing was delubricated before use. The flow, purification, metering and exhaust system, as well as the burner, is represented schematically in Fig. 3.

The rate measurements were made as a function of pres-

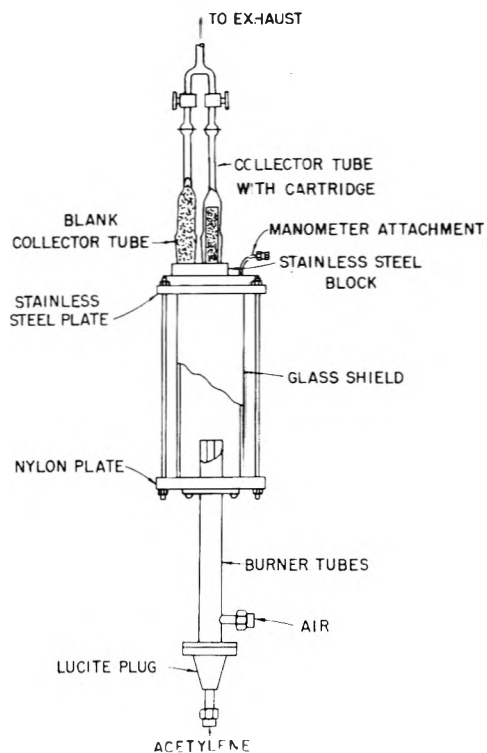


Fig. 1.—Burner assembly.

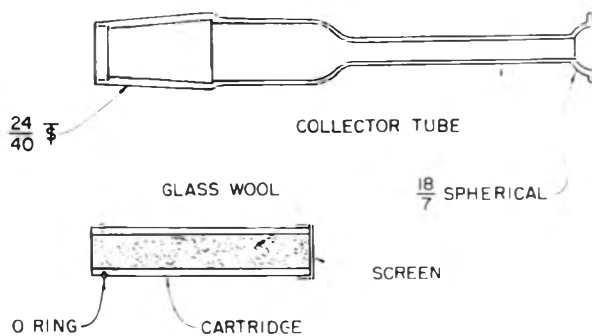


Fig. 2.—Soot collecting tube.

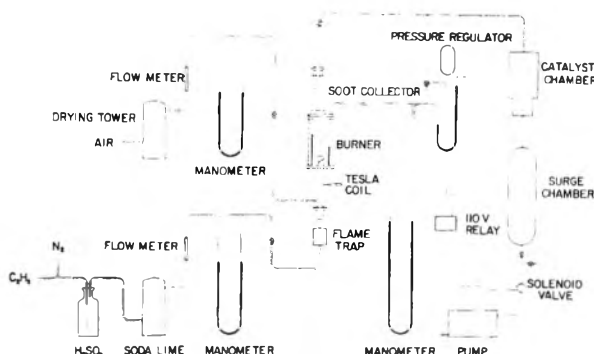


Fig. 3.—Schematic diagram of complete experimental setup.

TABLE I
BURNER TUBE DIAMETERS

Air/fuel ratio for equal linear flow rates	Inner tube, in.		Outer tube, in.	
	O.d.	L.d.	O.d.	I.d.
15.1	0.250	0.180	0.875	0.745
12.3	.315	.243	1.0	.908
9.0	.313	.249	1.0	.810

(1) C. P. Fenimore, G. W. Jones and G. E. Moore, "Sixth Symposium (International) on Combustion," Reinhold Publ. Corp., New York, N. Y., 1957, p. 242.

(2) G. Porter, "Fourth Symposium (International) on Combustion," The Williams and Wilkins Co., Baltimore, Md., 1953, p. 248.

(3) R. E. Ferguson, *Combustion and Flame*, **1**, 431 (1957).

(4) W. G. Parker and H. G. Wolfhard, *J. Chem. Soc.*, 2038 (1950).

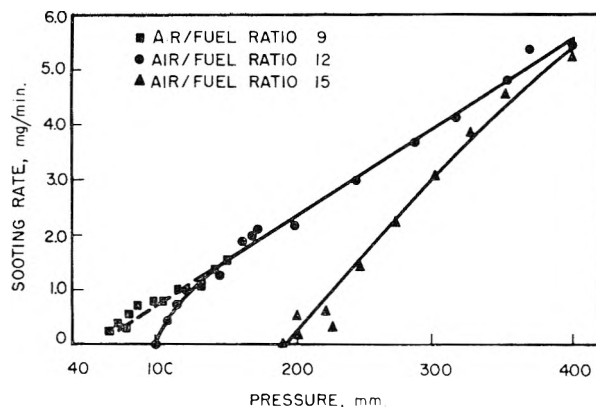


Fig. 4.—Pressure dependence of sooting rate.

pressure at air/fuel volume ratios of 9.0, 12.0 and 15.0. For each air/fuel ratio the mass flow rates were maintained constant, the acetylene flow rate being kept at 60 cc./min. STP throughout. The rate measurement technique was the same throughout the investigation. The system was flushed with nitrogen and brought to the desired pressure, the air and acetylene flow rates adjusted to their proper values, and the igniter spark coil turned on. Until the flame reached its stable configuration, a blank collector tube packed with glass wool was maintained in position over the flame. When the flame became stable, a collector tube containing a packed, dried and weighed cartridge was positioned over the flame by means of the sliding block. Soot was collected for a measured time interval of from five to ten minutes, generally eight minutes, in the cartridge. Next, the blank tube was repositioned over the flame and the cartridge replaced with a fresh one. By repetition of this procedure three or four collections were made at each pressure. The cartridges then were dried and reweighed, and the sooting rate determined from the weight increase and the known collection time. All weighings were made with an analytical balance. The rates are the averages, then, of three or four measurements. Rates were measured from the cut-off pressure to 401 mm. for the 12.0 air/fuel ratio, to 153 mm. for the 9.0 air/fuel ratio, and to 402 mm. for the 15.0 air/fuel ratio. The 12.0 ratio maximum pressure was limited by the tendency of the soot to clump and become difficult to collect above about 400 mm. At the 9.0 ratio, the naturally open shape of the underventilated flame prevented soot from issuing in a fine stream at pressures much above 150 mm., thus preventing complete collection. The maximum pressure for air/fuel ratio 15.0 was maintained approximately the same as that for air/fuel ratio 12.0. The low pressure cut-off was not actually observed for air/fuel ratio 9.0 because the flame blew off the burner below 66 mm. For the other air/fuel ratios, the cut-off pressure was taken as that at which a visible but unweighable quantity of soot was obtained.

For soot extract analysis, the soot containing cartridges were extracted with organic solvents in modified Soxhlet extractors and the extracts were subjected to infrared and ultraviolet absorption spectral analysis. The solvents used were acetone, carbon tetrachloride and benzene. One acetone extract was separated into three fractions with the aid of chromatography before the analysis. The extract was evaporated to a oily yellow material which was treated with 10 ml. of boiling benzene. The benzene solution was poured onto a 0.8×2 cm. column of 50–200 mesh alumina and eluted with 20 ml. of benzene followed by 15 ml. of methanol. The portion of the original material which was insoluble in boiling benzene was dissolved in acetone. It was noted that several of the extracts showed a blue fluorescence in ultraviolet light and that the fluorescence of the benzene eluate from the chromatographed extract was quite strong. From five to ten per cent. of the soot was extracted by the solvents. The quantity extracted was quite insensitive to the production and collection conditions.

Two soot samples heated at 500–550° in a stream of nitrogen for 3.5 hours lost 13% of their weight, somewhat more than the weight loss on extraction. In order to obtain additional information concerning the nature of this relatively volatile portion of the soot, samples were examined mass

spectrometrically with the aid of a heated inlet system for the mass spectrometer. The examination consisted of heating the soot samples from about 100 to about 450° in several stages, and analyzing the material evolved from the soot at each stage.

Since it was considered that a knowledge of the nature of constituents of the products from a sooting flame which were too volatile to be retained on the soot would also be of value, the flame exhaust was passed through a cold trap at about -150° , and the collected material was subjected to analysis by infrared and ultraviolet absorption spectroscopy. For infrared analysis, the water had to be evaporated from the sample beforehand, probably causing the loss of the most volatile fraction.

Examination of the soot with the electron microscope indicated that the particle size ranged from 200 to 500 Å. and seemed to be independent of formation conditions.

Results and Discussion

The rates of soot issue, hereafter referred to as sooting rates, in mg./min. as a function of pressure in mm. for air/fuel ratios of 9.0, 12.0 and 15.0 are represented graphically in Fig. 4. It will be noted that the curve for the ratio 12.0 is essentially linear down to a pressure of 145 mm. and then turns down sharply to zero at a pressure of 101 mm. The dashed portion of the curve is a continuation of the linear portion of the 12.0 ratio curve, and not one drawn as the best fit for the 9.0 ratio points. Nevertheless, the points for the air/fuel ratio of 9.0 do fit fairly well this extrapolated line. The curve for the air/fuel ratio of 15.0 cuts off at the much higher pressure of 195 mm. and appears to approach the 12.0 curve gradually.

The linearity of the curves for air/fuel ratios 12.0 and 9.0 is reminiscent of the inverse linearity of maximum smoke-free fuel flow with pressure reported by Schalla and McDonald.⁵ However, their explanation, based on the inverse proportionality of the diffusion coefficient to pressure, is not applicable to the present case because the mass flow rates of fuel and air were maintained constant and the diffusion rates should have been essentially independent of pressure. Furthermore, since the measured sooting rate represents the difference between the rates of soot formation and consumption in the flame, the pressure dependence of the rate of soot formation is not necessarily the same as that of the sooting rate. However, the fact that the rate curve for the underventilated flame is essentially an extension of the linear portion of the stoichiometric curve to lower pressures, and that the rate curve for the overventilated flame seems to approach the stoichiometric curve at higher pressures, makes somewhat attractive the hypothesis that the formation rate is essentially independent of air/fuel ratio.

It is indeed possible to account qualitatively for the curves on the basis of a soot formation rate which varies linearly with pressure and is independent of air/fuel ratio. The deviations from linearity of the sooting rate curves are then accounted for as resulting from the variation of the soot consumption rate with pressure and air/fuel ratio. Considering the stoichiometric curve on this basis, the greater slope at low pressures than at high pressures would be reflection of a smaller increase

(5) R. L. Schalla and G. E. McDonald, "Fifth Symposium (International) on Combustion," Reinhold Publ. Corp., New York, N. Y., 1955, p. 316.

in soot consumption rate with pressure at low pressures than at high pressures.

Now, it would be expected that the soot consumption rate should increase regularly with pressure, provided that the residence time of the soot in the region where it is consumed were either independent of pressure or increased regularly with pressure. It is, however, known that as a result of the balance between combustion reaction and diffusion rates, the reaction zone of a diffusion flame is quite thick at low pressures, and that the thickness of this zone decreases with increasing pressure to a very small essentially constant value at moderate and high pressures. At low pressures, then, the thickened reaction zone can provide a greater residence time for soot consumption than at high pressures, and this residence time will decrease with increasing pressure to a constant value. The result of superimposing this residence time effect on the chemical consumption rate is a net consumption rate which increases more slowly (or perhaps even decreases) with pressure at low pressures than at high pressures, and a pressure dependence of sooting rate of the type observed in the stoichiometric case. An increase in air/fuel ratio might be expected to increase the consumption rate generally, thereby decreasing the sooting rate and moving the low pressure cut-off to a higher pressure. A decrease in air/fuel ratio would be expected to move the cut-off to a lower pressure and perhaps change the pressure dependence at low pressures, since the open shape of the reaction zone of an underventilated diffusion flame⁶ undoubtedly affects the residence time available for soot consumption.

It must be emphasized that these considerations are extremely qualitative. The picture of the process as consisting of two separate steps, production and consumption, is an obvious oversimplification. It is quite probable that reactions tending to prevent soot formation, such as combination of soot intermediates with oxygen, occur, and that these reactions have the net effect of soot consumption. Furthermore, the omission from consideration of the effect of temperature on the reaction and diffusion rates may certainly lead to error, particularly since not only the temperature, but the spatial temperature distribution, varies with experimental conditions. Nevertheless, it is believed that the qualitative picture given may be of some utility in working back toward the mechanism.

The infrared absorption spectra of the soot extracts and chromatographic fractions were very similar to those reported by Thorp, Long and Garner⁷ and by Arthur and Napier.⁸ They were consistent with those of fairly large saturated aliphatic hydrocarbons containing carbonyl and hydroxyl substituents and ester groups along with unsaturated and aromatic constituents, or, perhaps, aromatics with substituted aliphatic side chains. The infrared absorption spectrum of the cold trap

condensate, after evaporation of water, was quite similar to those of the extracts. Ultraviolet absorption spectra of the extracts and the cold trap condensate showed only a broad continuous absorption with no well defined maxima. No indication of fulvic constituents was observed.

The mass spectrometric analysis of the soot indicated strongly that the major species present in the material volatilized from the soot were polynuclear aromatic hydrocarbons with 2, 3, 4 and 5 rings and related materials, such as acenaphthylene. There was some evidence of aliphatic and alicyclic fragments. Indications were that there was a greater quantity of 4 ring species than 3 ring, and more 3 ring than 2 ring, but with 5 rings, the quantity decreased again. However, the relatively low volatility of the 5 ring compounds may account for the smaller quantity observed.

The detection of polynuclear aromatics and related compounds brings to mind the mechanism proposed by Rummel and Veh,⁹ wherein soot was formed by the laydown of polycyclic structures formed by the pyrolysis and dehydrogenation of fuel hydrocarbons. The work of Parker and Wolfhard³ on benzene-air diffusion flames, in which it was found that the benzene band spectrum disappeared low in the flame and was not replaced by those of naphthalene, anthracene, etc., apparently contradicts this proposed mechanism. However, Campbell and Johnson¹⁰ have shown this to be a temperature effect and not susceptible to interpretation in terms of the absence of aromatic constituents. In addition, Norrish, Porter and Thrush¹¹ have observed spectra characteristic of polynuclear aromatics in carbon-forming explosions of acetylene. In view of this, it seems quite likely that the observed aromatic hydrocarbons are indeed intermediates in the process of carbon formation. It is then necessary to consider that the oxygen containing compounds detected were formed from the reaction of soot intermediates with oxygen, either in competition with or as a part of the pyrolysis process. This is in essential agreement with the results of Arthur and Napier on reversed flames,⁸ since they found oxygen containing compounds in soot formed under conditions where contact of oxygen with the soot itself was very unlikely. It is perhaps also possible that aromatic intermediates were formed by condensation of oxygen containing aliphatics, in the manner of the condensation of acetone to mesitylene.

The sooting rate data themselves do not permit a definite decision to be made on the question of oxygen involvement in the mechanism. However, if the hypothesis that the rate of soot formation is independent of air/fuel ratio is accepted, then the indication is that oxygen is not involved in a rate controlling step of the process.

Conclusions

Measurements of the rate of soot issue from an acetylene-air diffusion flame and the results of

(6) S. P. Burke and T. E. W. Schumann, *Ind. Eng. Chem.*, **20**, 998 (1928).

(7) N. Thorp, R. Long and F. H. Garner, *Fuel*, **34**, S1 (1955).

(8) J. R. Arthur and D. H. Napier, "Fifth Symposium (International) on Combustion," Reinhold Publ. Corp., New York, N. Y., 1955, p. 303.

(9) K. Rummel and P. O. Veh, *Arch. Eisenhüttenwesen*, **14**, 489 (1941).

(10) C. E. Campbell and I. Johnson, *J. Chem. Phys.*, **27**, 316 (1957).

(11) R. G. W. Norrish, G. Porter and B. A. Thrush, *Proc. Roy. Soc. (London)*, **227A**, 423 (1955).

analysis of the soot for soluble and volatile constituents are consistent with a pyrolysis mechanism of carbon formation involving polymerization of acetylene to large aromatic molecules. The question of oxygen involvement in the mechanism cannot be settled on the basis of this work, but there are indications that it does not take part in

a rate-controlling step of the mechanism.

Acknowledgment.—The author wishes to thank Dr. C. E. Welling of this Laboratory for several helpful discussions and Messrs. J. L. Parsons and J. C. Neerman for performing, respectively, the infrared and ultraviolet and the mass spectrometric analyses reported herein.

MICROWAVE ABSORPTION AND MOLECULAR STRUCTURE IN LIQUIDS. XXVI. THE DIELECTRIC RELAXATION TIMES OF TWO LARGE OBLATE ELLIPSOIDAL MOLECULES IN BENZENE SOLUTION^{1,2}

BY DONALD A. PITT AND CHARLES P. SMYTH

Contribution from the Frick Chemical Laboratory, Princeton University, Princeton, N. J.

Received September 11, 1968

The dielectric relaxation times of metal-free heptaphenylchlorophenyl-porphyrizine and of ferric octaphenylporphyrizine chloride have been determined in benzene solution, based on dielectric constant data at 1.25, 3.22, 10.0, 25.0 and 50.0 cm. wave lengths at temperatures of 20, 40 and 60°. The dipole moment of the chloroporphyrizine lies in the plane of the great ring, while that of the ferric complex is perpendicular to the molecular plane. The relaxation time of the former is close to that calculated by equations taking into account the microscopic viscosity. The ferric complex, with a relaxation time 5/2 that of the chloroporphyrizine, is better described by a relation involving the macroscopic solvent viscosity. It is evident that relaxation occurs through two different modes of orientation. The dipole moments, atomic polarizations and the energies and entropies of activation for dielectric relaxation are given. A new dielectric measuring apparatus is described, consisting of a coaxial line resonant cavity. The transmission-line equations provide a simple derivation of the transmission of power through the cavity as a function of the cavity dimensions and of the dielectric properties of the liquid filling the cavity. The apparatus is usable over a wide frequency range and is especially applicable to measurements of the dielectric constant and loss of dilute solutions.

The theoretical model³ for dielectric relaxation of a solute molecule orienting in a continuum can be approached through investigations of solutions in which the molecular size of the solute is much greater than that of the solvent. In the past, solubility considerations have limited such studies to polymeric materials. While aqueous solutions of proteins⁴ behave electrically as large rigid ellipsoids in a continuous medium, polymers in non-polar solvents show predominantly segmental orientation. The octaphenylporphyrizine complexes possess adequate solubility in benzene to allow the measurement of their dielectric relaxation, and are of well-defined, roughly ellipsoidal shape.

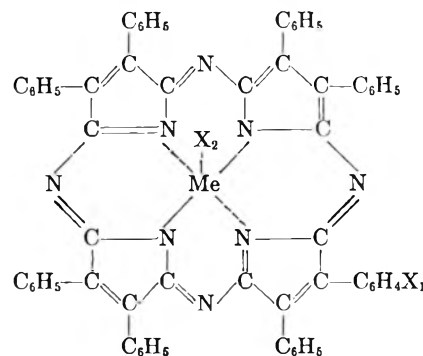
Two of these complex planar molecules have been prepared. The dipole moment is located in the plane of I and perpendicular to the plane of II. The dielectric relaxations in benzene solutions of these ellipsoids of revolution have been investigated and will be discussed in terms of their shapes and the positions of their dipole moments.

(1) This research has been supported by the Office of Naval Research. Reproduction, translation, publication, use and disposal in whole or in part by or for the United States Government is permitted.

(2) This article represents a portion of the work submitted by Donald A. Pitt to the Graduate School of Princeton University in partial fulfillment of the requirements for the degree of Doctor of Philosophy.

(3) P. J. W. Debye, "Polar Molecules," Chemical Catalog Co., New York, N. Y., 1929.

(4) J. L. Oncley, "The Electric Moments and the Relaxation Times of Proteins . . ." in E. J. Cohn and J. T. Edsall, "Proteins, Amino Acids, and Peptides," Reinhold Publ. Corp., New York, N. Y., 1943.



Experimental Methods

The static dielectric constant ϵ_0 was measured with heterodyne-beat apparatus⁵⁻⁸ at a wave length of 577 meters, and the density was determined with an Ostwald-Sprengel pycnometer.⁹ Wave guide measurements of dielectric constant and loss at 1.25 and 3.22 cm. wave length were carried out on apparatus previously described,^{10,11} using the standing wave ratio technique.

Resonant Coaxial Cavity Apparatus.—The cavity, as illustrated in Fig. 1, consists of a water-jacketed $5/8$ inch

(5) C. P. Smyth and S. O. Morgan, *J. Am. Chem. Soc.*, **60**, 1547 (1938).

(6) G. L. Lewis and C. P. Smyth, *J. Chem. Phys.*, **7**, 1085 (1939).

(7) L. M. Kushner and C. P. Smyth, *J. Am. Chem. Soc.*, **71**, 1401 (1949).

(8) A. J. Petro, C. P. Smyth and L. G. S. Brooker, *ibid.*, **78**, 3040 (1956).

(9) G. R. Robertson, *Ind. Eng. Chem., Anal. Ed.*, **11**, 464 (1939).

(10) H. L. Laquer and C. P. Smyth, *J. Am. Chem. Soc.*, **70**, 4097 (1948).

(11) W. M. Heston, A. D. Franklin, E. J. Hennelly and C. P. Smyth, *ibid.*, **72**, 3443 (1950).

i. d. tube, lapped after fabrication for uniform bore, a short-circuit fitting, and $\frac{5}{32}$ inch o.d. inner conductor, all silver plated. The center conductor is drilled and tapped for a polytetrafluoroethylene spacer which provides an open-circuit termination of low loss. While a short-circuit could also have been used, the cavity length necessary for a given number of resonances would thereby be increased. Energy is introduced and sampled for detection, through two small rotatable magnetic coupling loops very near the short-circuit. The degree of coupling is kept as low as possible, consistent with a detectable output signal. The cell is fitted with a standpipe to allow filling from the bottom, with flow through perforations in the polytetrafluoroethylene plug and the short-circuit fitting. The micrometer system, Fig. 2, utilizes a 12 inch precision-ground hardened steel screw of 1 mm. pitch, and a similarly ground bronze bushing. A revolution counter, reading in mm., is provided, and the head is divided to allow estimation to 10^{-4} cm. The assembly is mounted on a heavy supporting member with guide rods and a loading device to minimize backlash.

Four square-wave modulated high-frequency generators are in use with this cavity. Two are tuned concentric-line oscillators, the Hewlett-Packard Model A (range 500-1300 Mc.p.s.) and the Hazeltine Model 1050-B (range 900-1300 Mc.p.s.), the latter having greater R.F. power. Their frequency is adjusted to give a minimum audio beat frequency with the 50 Mc.p.s. signal of the Hazeltine Model 1134 frequency calibrator. This unit contains a 10 Mc.p.s. crystal-controlled oscillator and a quintupler circuit, and is calibrated by beating against the 10 Mc.p.s. transmission of radio station WWV, National Bureau of Standards, Washington, D.C. Two klystrons, a type 707B (ca. 3,000 Mc.p.s.) and a type 2K23 (ca. 4,850 Mc.p.s.), are operated at fixed frequencies from stabilized power supplies. The 2K23 feeds into a wave guide section having a tunable capacitive feed to coaxial cable. The cavity is matched to each generator and to the 1N21 crystal detector with triple stub tuners, and the transmitted power is measured with a Hazeltine Model 1052-A tuned amplifier.

Cavity Transmission Function.—The weak coupling between the coupling loops and the cavity cell, with negligible loop-loop interaction, permits the analysis of the microwave circuit in terms of an equivalent low-frequency circuit having a constant coefficient of mutual inductance. By this means, it can be shown¹² that the output meter of the tuned amplifier will show a deflection proportional to the square of the cavity admittance seen at the short-circuit, looking toward the open circuit. The part of the cell past the center conductor appears as a circular wave guide beyond cut-off, and the use of the spacer gives a low termination loss essentially independent of the loss of the liquid dielectric. The resonating portion of the cell is, therefore, only that part between the short-circuit and the end of the sliding contact fingers. The cavity admittance, for an inner conductor depth d , and a characteristic admittance Y_0 of the coaxial line, is

$$Y \cong Y_0(Y_{oc} + Y_0 \tanh \gamma d)/(Y_0 + Y_{oc} \tanh \gamma d) \cong \frac{Y_{oc} \tanh \gamma d}{Y_0 + Y_{oc} \tanh \gamma d} \quad (1)$$

As a result of the open-circuit design, its admittance Y_{oc} is neglected. In these expressions, $\gamma = \alpha + j\beta$ is the propagation constant of the wave in the medium, α is the attenuation constant, and $\beta = 2\pi/\lambda$ is the phase constant.

The cavity resonates when the susceptance given by eq. 1 is equal in magnitude and opposite in sign to the susceptance in the direction of the short-circuit. This occurs when

$$d_n = (2n - 1) \pi / 2\beta = (2n - 1)\lambda / 4 \quad (2)$$

where d_n is the depth, measured from the short-circuit, at the n th resonance. This is applicable when d_n is considerably greater than 25 mm., the length of the sliding contact fingers. The admittance at the point of resonance is given by

$$Y_n \cong Y_0 \coth \alpha d_n \quad (3)$$

The power transmission through the cavity may be expressed as the function T_n , the ratio of the power at a depth d to that transmitted at the n th resonance peak,

$$T_n \cong \tanh^2 \gamma d \tanh^2 \alpha d_n \quad (4)$$

Measurement Technique.—The distance between resonance peaks, from eq. 2, is $\lambda/2$, a half-wave length in the di-

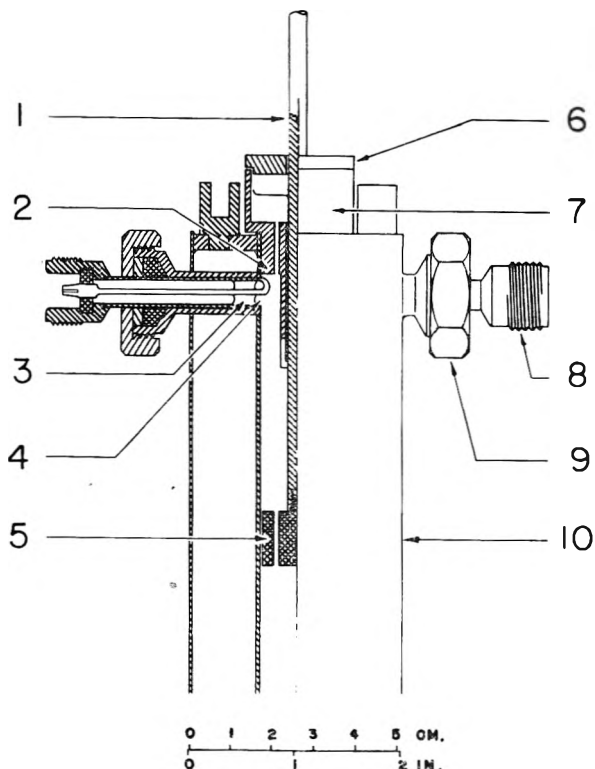


Fig. 1.—Half section view of the coaxial resonant cavity cell: 1, inner conductor; 2, short circuit; 3, glass-Kovar liquid seal; 4, rotatable magnetic coupling loop; 5, polytetrafluoroethylene open circuit fitting; 6, reservoir cover; 7, sample reservoir; 8, type N coaxial fitting; 9, stuffing box; 10, water jacket.

electric. Measurements must be conducted at depths well beyond the contacting fingers of the short-circuit fitting. Dielectric loss in the medium introduces a slight asymmetry of the resonance peak, and hence some error in locating d_n . This may be neglected within the limitations on attenuation mentioned below.

While the peak is sharp only for low-loss media, the phase change through a resonance is seen from eq. 4 to be rapid, and largely independent of losses. The interferometric technique of Branin¹³ may be applied for materials of $\tan \delta > 0.05$ by the introduction of a phase reference signal between the cavity output stub tuner and the crystal detector.

The half-power widths of these resonance peaks are used to evaluate ϵ'' for low-loss dielectrics. The distance $(\delta d)_n$ between d_n and the points at which $T_n = 0.5$ is found by expansion of eq. 4. This gives, for $(\delta d)_n \ll d_n$

$$\sin[2\beta(\delta d)_n] = \sin(2\alpha d_n) \quad (5)$$

Neglecting terms in $\beta(\delta d)_n$ and αd_n higher than the first order, this simplifies to

$$(\delta d)_n = \kappa d_n \quad (6)$$

where $\kappa = \alpha/\beta$ is the absorption index. This approximation may be used to 1% accuracy for $\alpha d < 0.1$, and to 5% for $\alpha d < 0.2$. Since the termination losses and coupling losses are independent of n , while the loss of the medium and cavity walls κ_{total} increases with d , the absorption index of the dielectric κ is found from

$$(2\delta d/\lambda)_n = 2(\delta d/\lambda)_{n-1} = \frac{\kappa_{total}}{\kappa + \kappa_c} \quad (7)$$

where κ_c is the wall loss, obtained from measurements on the empty cell.

The complex dielectric constant, $\epsilon = \epsilon' - j\epsilon''$, is related to the propagation constants by the equations

$$\epsilon' = (\lambda_0/\lambda_d)^2(1 - \kappa^2) \quad (8)$$

$$\epsilon'' = 2(\lambda_0/\lambda_d)\kappa^2 \quad (9)$$

(12) D. A. Pitt, Ph.D. Dissertation, Princeton University, 1957.

(13) F. H. Branin, *J. Appl. Phys.*, **23**, 990 (1952).

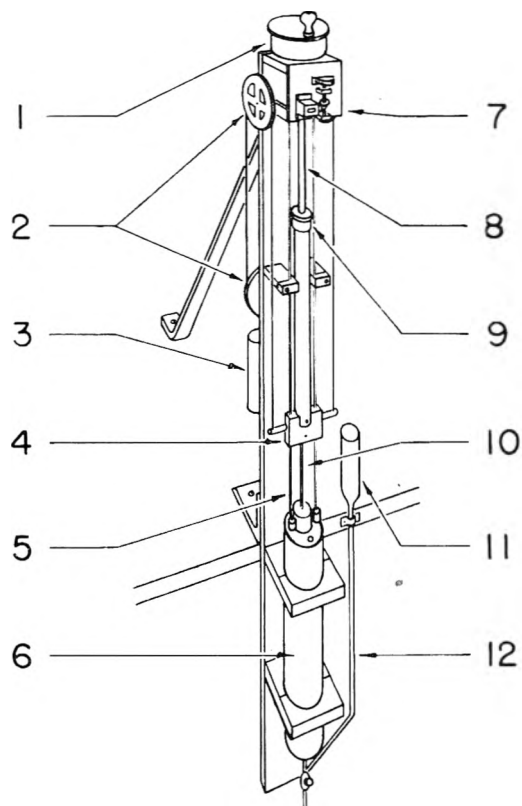


Fig. 2.—The resonant cavity cell, micrometer and mounting: 1, micrometer divided head; 2, pulleys; 3, counterweight; 4, inner conductor guide; 5, guide rods; 6, resonant cavity; 7, revolution counter; 8, micrometer screw; 9, micrometer bushing; 10, inner conductor; 11, glass sample reservoir; 12, fill and drain pipes and valve.

where λ_d is the measured wave length of the high-frequency wave in the dielectric, and λ_0 is the equivalent free-space wave length.

The data necessary to characterize the dielectric constant of low-loss liquids are the micrometer readings at the half-power points at as many resonances as are within the range of the cell and micrometer. The intercomparison of the peak positions (the average of a pair of half-power points) gives values of $\lambda_d/2$ (eq. 2) while a plot of $2\delta d$ vs. the ordinal number of the resonance, n , has a slope of $\lambda_d \kappa_{\text{total}}$, which is then corrected to yield κ (eq. 7).

Dilute Solution Technique.—A differential technique for dilute solutions, in which the solvent used to make up the solutions is measured at each temperature and frequency immediately before or after the solution measurements, yields a considerable increase in precision. For a wave length and absorption λ_1 and κ_1 of the pure solvent, and λ_{12} and κ_{12} of the solution, the complex dielectric constant of eq. 8 and 9 may be expressed as

$$\epsilon'_{12} = \epsilon'_1 (\lambda_1/\lambda_{12})^2 (1 - \kappa_{12}^2) / (1 - \kappa_1^2) \quad (10)$$

$$\cong \epsilon'_1 (\lambda_1/\lambda_{12})^2 \quad (11)$$

$$\epsilon''_{12} = 2\epsilon'_1 (\lambda_1/\lambda_{12})^2 \kappa_{12} / (1 - \kappa_1^2) \quad (12)$$

$$\cong 2\epsilon'_{12} \kappa_{12} \quad (13)$$

where ϵ'_1 is the real part of the dielectric constant of the solvent. Alternatively, the slopes a' and a'' (*vide infra*, eq. 18 and 19) may be obtained directly from the following relations, in which c_2 is the concentration of solute.

$$a' = \epsilon'_1 \left[\left(\frac{\lambda_1}{\lambda_{12}} \right)^2 \left(\frac{1 - \kappa_{12}^2}{1 - \kappa_1^2} \right) - 1 \right] / c_2 \quad (14)$$

$$\cong \epsilon'_1 [(\lambda_1/\lambda_{12})^2 - 1] / c_2 \quad (15)$$

$$a'' = 2\epsilon'_1 [(\lambda_1/\lambda_{12})^2 \kappa_{12} - \kappa_1] / c_2 (1 - \kappa_1^2) \quad (16)$$

$$= 2(\epsilon'_{12} \kappa_{12} - \epsilon'_1 \kappa_1) / c_2 \quad (17)$$

This procedure removes the effect on the slope of variations in the electrical quality of the solvent used, and obviates the determination of λ_0 , for which effective cell thermostating is difficult.

Preparation of Materials.—Diphenylmaleonitrile, the intermediate from which the porphyrzines were prepared, was synthesized from phenylacetoneitrile according to the procedure of Cook and Linstead.¹⁴

Metal-free heptaphenylchlorophenylporphyrzine was prepared by heating four parts diphenylmaleonitrile with one part of freshly prepared cuprous chloride. A salt-bath of 1:1 NaNO_3 : KNO_3 was used to maintain a temperature of 250–260°. The ground reaction product was extracted in a Soxhlet with pyridine, from which the porphyrzine was obtained by precipitation in boiling water. This was taken up in a minimal amount of benzene, extracted with alkali and washed. After filtering and drying, it was placed on a column containing alumina treated according to Weitz, *et al.*¹⁶ Material from the main band was recovered and recrystallized from benzene into shining black platelets giving opaque green solutions. Before use, the porphyrzine was thoroughly dried *in vacuo* at 100° in an Abderhalden pistol. The molecular weight of the monochlorinated compound is 957.5. *Anal.* Calcd.: C, 80.28; H, 4.32; N, 11.70; Cl, 3.70. Found: C, 82.17; H, 4.06; N, 11.38; Cl, 2.39.

The ferric octaphenylporphyrzine chloride condensation was carried out at 280–295° with 3 parts of hydrated ferric chloride per 8 parts of diphenylmaleonitrile. This was purified by the same procedure, but crystalline material could not be obtained from the benzene solution, which had a dark brownish green color. The calculated molecular weight is 1012.4. *Anal.* Calcd.: C, 75.93; H, 3.98; N, 11.07; Cl, 3.50; Fe, 5.52. Found: C, 79.41; H, 4.41; N, 9.00; Cl, 2.26; Fe, 4.83.

The benzene used as solvent was the Baker and Adamson reagent grade product. It was carefully protected from exposure to the atmosphere, but was not further purified. The measured physical properties at 20, 40 and 60° are n_D 1.50094, 1.48874, 1.47625; n_D 2.2854, 2.2454, 2.2055; d 0.8783, 0.8572, 0.8358.

Experimental Results

The dielectric relaxation properties of solutions of the porphyrzine complexes in benzene were obtained by determining the slopes of dielectric constant and loss as a function of the mole fractions of solute. Denoting solvent by the subscript 1, solute by 2, and solution by 12, the slope of the linear plot at each wave length is given by

$$\epsilon'_{12} = \epsilon_1 + a'c_2 \quad (18)$$

$$\epsilon''_{12} = a''c_2 \quad (19)$$

where the concentration c_2 is in mole fraction. Solutions measured were in the concentration range of 0.0003 to 0.001 mole fraction. All slopes, as given in Table I, were calculated with the use of the static dielectric constants of benzene. The solution technique described above (eq. 15 and 17) was used.

The dependence of the static dielectric constant and specific volume on concentration are given by a_0 and β' according to

$$\epsilon_0 = \epsilon_1 + a_0 c_2 \quad (20)$$

$$v_{12} = v_1 + \beta' c_2 \quad (21)$$

The most probable relaxation time τ is obtained graphically from the Argand diagram of the slopes.^{16,17} The spread of relaxation times about τ is indicated by the parameter α , and a_∞ is the infinite frequency arc intercept. Both are obtained from the plot. These constants are shown in Table II.

(14) A. H. Cook and R. P. Linstead, *J. Chem. Soc.*, 929 (1937).

(15) E. Weitz, F. Schmidt and J. Singer, *Z. Elektrochem.*, **46**, 222 (1940).

(16) K. S. Cole and R. H. Cole, *J. Chem. Phys.*, **9**, 341 (1941).

(17) A. D. Franklin, W. M. Heston, E. J. Hennelly and C. P. Smyth, *J. Am. Chem. Soc.*, **72**, 3447 (1950).

TABLE I

SLOPES FOR THE DEPENDENCE OF DIELECTRIC CONSTANT AND LOSS OF BENZENE SOLUTIONS ON MOLE FRACTION OF SOLUTE

λ_0	20°		40°		60°	
	a'	a''	a'	a''	a'	a''
Metal-free porphyrzine complex						
1.25	9.6	0.8	10.0	0.7	10.0	0.8
3.22	10.1	1.1	10.2	1.3	10.5	1.2
10.0	11.2	2.3	11.4	2.5	11.7	2.3
25.0	12.8	3.0	13.2	2.9	13.5	2.7
50.0	14.4	3.3	14.8	2.9	14.9	2.6
Iron porphyrzine complex						
1.25	12.2	2.2	12.5	2.1	12.9	2.3
3.22	13.6	3.4	13.5	3.9	14.5	3.7
10.0	16.4	6.1	17.2	6.0	17.7	6.4
25.0	21.1	9.0	21.9	9.6	22.5	9.8
50.0	25.8	10.7	27.0	10.7	27.9	10.7

TABLE II

SLOPES FOR THE DEPENDENCE OF STATIC DIELECTRIC CONSTANT AND SPECIFIC VOLUME ON MOLE FRACTION, WITH INFINITE FREQUENCY INTERCEPTS, DISTRIBUTION PARAMETERS, RELAXATION TIMES (10^{-12} SEC.) AND DIPOLE MOMENTS (10^{-18} E.S.U.-CM.)

$t, ^\circ\text{C.}$	a_0	a_∞	β'	α	τ	μ
Metal-free porphyrzine						
20	20.53	9.0	-3.745	0.35	302	2.92
40	19.20	9.4	-3.875	.31	212	2.78
60	18.07	9.6	-4.075	.28	159	2.73
Iron porphyrzine complex						
20	58.04	10.7	-4.861	0.38	706	5.79
40	53.85	10.9	-4.993	.36	500	5.82
60	49.89	11.3	-5.275	.34	367	5.82

In the calculation of the dipole moment, the Halverstadt-Kumler¹⁸ equation was used to extrapolate for the total polarization P from the variation of ϵ_0 with concentration. The distortion polarization, P_D , was found by a similar calculation from a_∞ values. The dipole moment is then given by

$$\mu = 0.01281 \times 10^{-18} [(P - P_D)T]^{1/2}$$

Direct measurement of the electronic polarization of these substances was not possible due to the opacity of the solutions. The D-line molar refractions were evaluated from the atomic refractions given by Fajans¹⁹ and from the molar refraction of pyrrole (20.40 cc.) and of benzene (26.14 cc.), as determined in this Laboratory. Exaltation was neglected in view of the possible effects of resonance in the great ring^{20,21} and of the omission of extrapolation to infinite wave length. The calculated molar refraction values are 280.55 cc. for the metal-free porphyrzine, and 290.1 cc. for the ionic

structure of the ferric complex. The refractions due to the central ferric atom are by Fajans and co-workers.²² The total polarizations, distortion polarizations and atomic polarizations P_A are given in Table III.

TABLE III

Solute	MOLAR POLARIZATIONS (CC.)			
	$t, ^\circ\text{C.}$	P	P_D	P_A
Metal-free porphyrzine	2)	538	368	87
	4)	530	379	99
	6)	524	387	107
Iron porphyrzine complex	2)	1075	386	96
	4)	1049	396	106
	6)	1020	407	117

Discussion of Results

The dipole moment of the metal-free porphyrzine complex, which was calculated by extrapolation from the relaxation data, exceeds by a considerable margin the dipole moment of chlorobenzene,²³ 1.58×10^{-18} . In the reaction of cuprous chloride with diphenylmaleonitrile, Cook and Linstead¹⁴ conclude that the monochlorinated porphyrzine is the only product. While both *ortho* and *para* positions would be expected to be reactive, the *ortho* substitution is sterically hindered by the adjacent phenyl groups, especially when coplanar with the great ring. The dipole moment will therefore be in the plane of the porphyrzine ring independent of the degree of the chlorination. The planarity of quadridentate ligands of the porphyrzine structure has been established by X-ray diffraction studies.²⁴

The dipole moment of the iron compound as given in Table II is of the magnitude to be expected from the iron-chlorine bond. By analogy to the structure of the ferriheme chloride molecule,²⁵ the dipole moment should be perpendicular to the large ring, with ionic bonding.

The values of atomic polarization given in Table III may be considered as approximate since the extrapolation of the points on the Cole-Cole arc to infinite frequency could involve an error of several cc. in P_D . The apparent increase in P_A with temperature is, therefore, without significance. The values observed, 87-117 cc., are considerably higher than the atomic polarizations reported for smaller chelate compounds, such as 67.8 cc. for thorium acetylacetonate.²⁶

The dispersion region of these complexes is characterized by a rather large distribution of relaxation times. Such distribution is contrary to the Perrin theory, which deduces a single relaxation time.²⁷ The departure of these molecules from spherical symmetry may be the cause of the finite distribution,²⁸ even though the dipole moment lies parallel to a principal axis of the molecule.

(18) I. F. Halverstadt and W. D. Kumler, *ibid.*, **64**, 2988 (1942).
 (19) N. Bauer and K. Fajans, "Refractometry," in "Physical Methods of Organic Chemistry," Vol. I (A. Weissberger, editor), Interscience Publishers, Inc., New York, N. Y., 2nd ed., 1949, chap. XX.
 (20) G. D. Dorough and K. T. Shen, *J. Am. Chem. Soc.*, **72**, 3939 (1950).
 (21) J. A. Leermakers and A. Weissberger, "Constitution and Physical Properties of Organic Compounds," in "Organic Chemistry" (H. Gilman, editor), John Wiley and Sons, Inc., New York, N. Y., 2nd ed., 1943, chap. XXIII.

(22) K. Fajans and G. Joos, *Z. Physik*, **23**, 1 (1924); K. Fajans and R. Lühdemann, *Z. Physik. Chem.*, **B29**, 150 (1935).
 (23) C. P. Smyth, "Dielectric Behavior and Structure," McGraw-Hill Book Co., Inc., New York, N. Y., 1955.
 (24) J. M. Robertson, *J. Chem. Soc.*, 1195 (1936).
 (25) L. Pauling and C. D. Coryell, *Proc. Natl. Acad. Sci.*, **22**, 159 (1936).
 (26) A. E. Finn, G. C. Hampson and L. E. Sutton, *J. Chem. Soc.*, 1254 (1938).
 (27) R. C. Miller and C. P. Smyth *THIS JOURNAL*, **60**, 1354 (1956).
 (28) N. E. Hill, *Proc. Phys. Soc. (London)*, **67B**, 149 (1954).

The relaxation times to be expected of these molecules may be calculated by several equations. The method of Spornol, Gierer and Wirtz²⁹ and two methods of Chau, LeFèvre and Tardif³⁰ have been reasonably successful in calculating the relaxation times of smaller ellipsoidal solutes.³¹ The molecular dimensions of the porphyrazines shown in Table V are based on the X-ray measure-

TABLE V

MOLECULAR DIMENSIONS (Å.) AND ACTIVATION ENERGIES, KCAL./MOLE, AND ENTROPIES FOR DIELECTRIC RELAXATION

	Metal-free porphyrazine	Iron porphyrazine complex
A	6.25	7.15 ^a
B	20.3 ^a	19.0
C	19.0	19.0
$\Delta H\epsilon$	2.5	2.6
$\Delta S\epsilon$	-6.4	-7.9

^a Axis parallel to the dipole moment.

ments by Robertson^{24,32} of structures in the phthalocyanine series, with additional data from Stuart-Briegleb models. An equation of Chau, *et al.*, involves the mean polarizability, which was derived from the infinite frequency intercept a_∞ as measured from the arc plots obtained in this study. The calculated relaxation times as indicated on lines 1, 2 and 3 of Table VI are somewhat below the observed values for the metal-free compound, and much below those for the iron compound.

TABLE VI

RELAXATION TIMES (10^{-12} SEC.) CALCULATED BY THE METHODS OF SPORNOL, GIERER AND WIRTZ,²⁹ OF CHAU, LEFÈVRE AND TARDIF,^{30,34} AND OF FISCHER⁴

$t, ^\circ\text{C.}$	Equation	Metal-free porphyrazine	Iron porphyrazine complex
20	1	206	223
	2	218	232
	3	149	200
	4	1016	889
	Obsd.	302	706
40	1	143	154
	2	156	166
	3	110	148
	4	719	629
	Obsd.	212	500
60	1	104	112
	2	117	125
	3	85	114
	4	537	470
	Obsd.	159	367

The relaxation equation derived by Debye³ for spherical molecules was modified by Perrin³³ and Fischer³⁴ to

$$\tau = 4\pi\eta abc f / kT$$

where a , b and c are the semi-axes of an ellip-

soidal molecule, η_μ is the microscopic viscosity coefficient, and f is a friction factor due to the geometry of the ellipsoid. When η_μ is set equal to η_1 , the solvent viscosity, the relaxation behavior of proteins is adequately described.⁴ With the dimensions of Table V, values of f from the tabulations of Budo, Fischer and Miyamoto,³⁵ and $\eta_\mu = \eta_1$, the relaxation times on lines 4 of Table VI were calculated. These are somewhat higher than the experimental values for the iron complex, and very much higher than those for the metal-free porphyrazine.

The position of the dipole moment perpendicular to the plane of the great ring necessitates turning of the iron complex molecule about an axis in the molecular plane. Since this involves displacement of the neighboring solvent molecules, the macroscopic viscosity of the solvent may be expected to have importance in determining the relaxation time.³⁶ It may thus be expected that with the use of the macroscopic viscosity coefficient, the Fischer equation should be applicable.

The chloroporphyrazine has its dipole moment in the molecular plane, and orientation can take place about any axis in the plane perpendicular to the moment direction. At one extreme this entails the same motion required of the iron complex, and at the other involves wheeling of the molecular ellipsoid on its axis of revolution. The latter process depends primarily on the much weaker internal friction forces predominant in the relaxation of smaller and more nearly spherical molecules,³⁷ and calculation methods 1-3 are apropos.

The orientation of the ferric compound involves a factor not taken into account in the Debye theory, *viz.*, the work of displacement of solvent molecules by the rotation of the solute. One would expect the metal-free ligand to orient predominantly by rotation in the molecular plane with a shorter relaxation time, since such displacement is involved to a lesser extent. Considerable differences in the relaxation behavior of the polar metal-free and ferric porphyrazines would not be expected on the basis of over-all molecular size and shape. The disparity in relaxation times by a factor of 5/2 evidences a fundamental difference in the modes of orientation of the two molecules arising from the different positions of their dipole moments. This disparity is similar in size and cause to that found³⁸ between the relaxation times of paraldehyde and collidine.

In a paper published after the initial completion of the present paper, Meakins³⁹ has concluded that when the solute molecule is at least three times as large as the solvent molecule, the solutions give good agreement with Debye's simple equation, which is based upon a system of spheres moving in a uniform viscous medium. The use of this equation with a molecular volume calculated as an additive quantity⁴⁰ gives 410×10^{-12} sec. for the re-

(29) A. Spornol and K. Wirtz, *Z. Naturforsch.*, **8A**, 522 (1953); A. Gierer and K. Wirtz, *ibid.*, **8A**, 532 (1953).

(30) J. Y. H. Chau, R. J. W. LeFèvre and J. Tardif, *J. Chem. Soc.*, 2293 (1957).

(31) D. A. Pitt and C. P. Smyth, *J. Am. Chem. Soc.*, **80**, 1061 (1958).

(32) J. M. Robertson and I. Woodward, *J. Chem. Soc.*, 36 (1940).

(33) F. Perrin, *J. phys. Radiat.*, **5**, 497 (1934).

(34) E. Fischer, *Physik. Z.*, **40**, 645 (1939).

(35) A. Budo, E. Fischer and S. Miyamoto, *ibid.*, **40**, 337 (1939).

(36) A. J. Curtis, P. L. McGeer, G. B. Rathmann and C. P. Smyth, *J. Am. Chem. Soc.*, **74**, 644 (1952).

(37) C. P. Smyth, *This Journal*, **58**, 580 (1954).

(38) R. C. Miller and C. P. Smyth, *ibid.*, **60**, 1354 (1956).

(39) R. J. Meakins, *Trans. Faraday Soc.*, **54**, 1160 (1958).

(40) J. T. Edward, *Chem. and Ind.*, 774 (1956).

laxation time at 20° of the metal-free porphyrine molecule in benzene solution, which agrees with the observed value 302×10^{-12} as well as or better than any of the calculated values in Table VI. Since the volume of the iron porphyr-

zine complex is almost the same as that of the metal-free molecule, the relaxation time calculated for this molecule by the Debye equation is considerably too small, but not as much too small as three of the four different calculated values in Table VI.

DISSOCIATION PRESSURE AND STABILITY OF BERYLLIUM CARBIDE¹

By B. D. POLLOCK

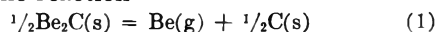
Contribution from Atomics International, A Division of North American Aviation, Inc., Canoga Park, California

Received September 11, 1958

Equilibrium pressures for the reaction $\frac{1}{2}\text{Be}_2\text{C}(s) = \text{Be}(g) + \frac{1}{2}\text{C}(s)$ were measured in the temperature range 1430–1669°K. by the Knudsen technique. The dissociation pressure in this temperature range is given by the equation $\log P(\text{atm.}) = 7.026 \pm 0.347 - (19,720 \pm 537)/T$. The heat and free energy of formation of beryllium carbide were derived from the above equation in combination with the literature vapor pressure data for solid beryllium.

Introduction

Beryllium carbide is of potential interest in atomic power applications because of its nuclear properties; however, experimental thermodynamic data concerning it are meager. Krikorian² estimates heat, free energy and entropy of formation of Be_2C at 298°K. to be -13.0 ± 5 kcal., -12.4 ± 5 kcal., and -2.0 ± 1.0 entropy units, respectively, and Quirk³ estimates -7.83 kcal. for the free energy of formation at 2400°K. However, the latter quotes, for various temperatures, estimated vapor or dissociation pressures of beryllium carbide⁴ which are equal to or greater than those of pure liquid beryllium.^{5,6} These pressures are inconsistent with a negative free energy of formation for a compound having no stable gaseous carbide species.⁷ The absence of such species and the observation that beryllium carbide loses beryllium preferentially at elevated temperatures with deposition of graphite³ indicate that the carbide dissociates according to the reaction



Thus a determination of the dissociation pressure as a function of temperature for this compound would yield results which could be combined with data on the vapor pressure of beryllium metal from the literature to obtain the free energy and heat of formation of the solid compound.

Experimental

Dissociation pressures were measured by the Knudsen method and the experiments were performed in the vacuum induction furnace illustrated in Fig. 1. The power source was a 6 kilowatt arc-type high frequency converter. The vacuum system was capable of maintaining residual gas pressures in the range 10^{-6} – 10^{-6} mm. during the major part of each run following the initial warm-up. Knudsen cells and orifice plates were turned from National Carbon Company ATZ grade graphite. Temperatures were read with a

disappearing-filament type optical pyrometer by sighting into black-body holes in the bottom of the Knudsen cell, through a prism and optical window. The instrument, made by the Pyrometer Instrument Company of Bergenfield, New Jersey, was calibrated against a secondary standard which consisted of a tungsten ribbon lamp for which current *versus* temperature data had been obtained at the National Bureau of Standards. The window and prism correction was checked periodically. These corrections did not change significantly during the investigation. The over-all uncertainty in temperature measurements was estimated to be about 10°.

A layer of beryllium carbide was formed on the interior of the effusion cell prior to a group of experiments by heating a few pellets of metallic beryllium in the apparatus to about 1400° for a few minutes and then removing the excess metal. The carbide formed in this manner was hard, dense and adherent to the graphite. Spectroscopic examination showed only trace amounts of iron and silicon and X-ray diffraction showed Be_2C and no detectable amount of BeO . The interior of the cell was inspected visually after each run to ensure the presence of a large evaporating surface of beryllium carbide throughout each experiment. The surface area of the carbide layer was estimated to be at least 100 times the orifice area in all cases.

Vapor effusing from the cell was condensed on the interior of the quartz vacuum cell and no detectable deposit was found on the glass below the level of the top of the graphite cell. This observation showed that no error occurred by virtue of diffusion of beryllium through the graphite. It was found that the deposit adhered to the glass if it were less than about 3 mg., otherwise there was a tendency to flake off. Accordingly, variables were chosen so as to obtain beryllium losses of about 1 mg. After the run, the deposit was dissolved easily in a few cc. of dilute HCl and the amount of beryllium determined by a spectrophotometric method⁸ with an estimated accuracy of 2–3%.

Results and Discussion

The vaporization data are summarized in Table I. The pressure of beryllium was calculated by use of the equation

$$P(\text{atm.}) = 0.02254(m/at)(K)^{-1}(T/M)^{1/2} \quad (2)$$

where (m/at) is the rate of effusion in g./cm.²-second, K is the Clausing orifice correction, and T and M are the temperature in degrees Kelvin and the atomic weight of beryllium, respectively. Results of these calculations are listed in the last column of Table I and also shown in Fig. 2.

A least squares treatment of the data yielded the equation

$$\log P(\text{atm.}) = (7.026 \pm 0.347) - (19,720 \pm 537)/T \quad (3)$$

the slope of which corresponds to a mean enthalpy

(8) M. E. Smith, "A Spectrophotometric Method for Determining Small Amounts of Beryllium in Uranium" LA-1585, August, 1953.

(1) This work was carried out as part of Contract AT-11-1-GEN-8 with the United States Atomic Energy Commission.

(2) O. H. Krikorian, "High Temperature Studies: Part II, Thermodynamic Properties of the Carbides" UCRL 2888, Apr. 1955, p. 82.

(3) J. F. Quirk, "Beryllium Carbide," *AEC-TIS Reactor Handbook*, 3, Section 1, Ch. 1.5 (1955).

(4) Jacob Kjielland and Leif Tronstad, "Det Kongelige Norske Videnskabers Selskab," Vol. VIII, No. 42, 1935, pp. 147, 150.

(5) R. B. Holden, R. Speiser and H. L. Johnston, *J. Am. Chem. Soc.*, 70, 3897 (1948).

(6) E. A. Gulbransen and K. F. Andrew, *J. Electrochem. Soc.*, 97, 383 (1950).

(7) W. A. Chupka, J. Berowitz, C. F. Giese and M. G. Inghram, *This Journal*, 62, 611 (1958).

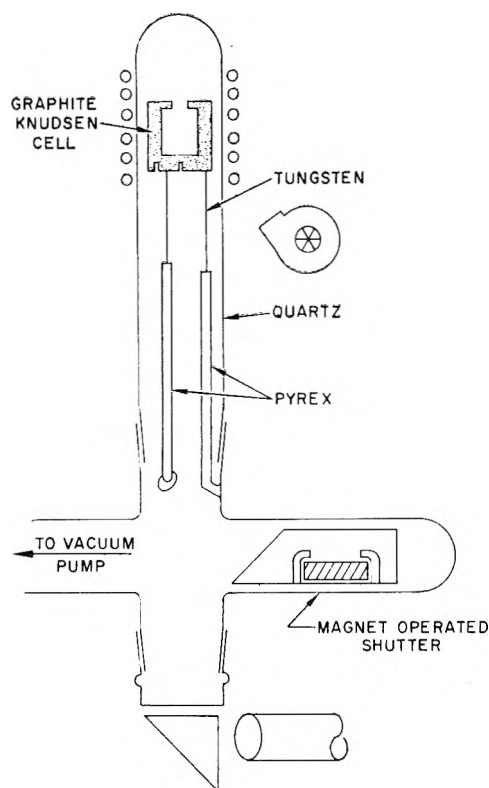
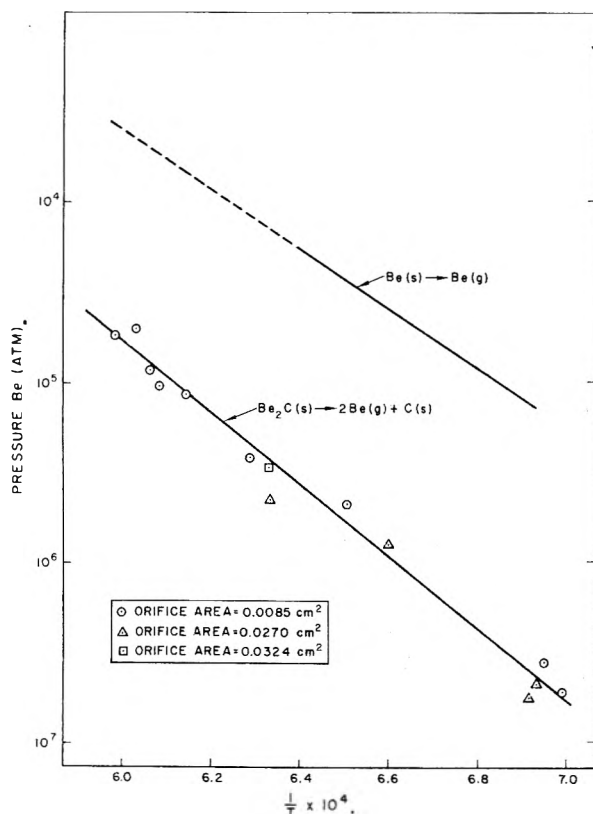


Fig. 1.

Fig. 2.—Dissociation pressure of Be_2C .

change of 90.2 ± 2.5 kcal. for reaction 1 in the temperature range 1430–1669°K.

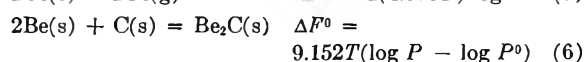
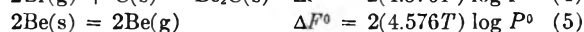
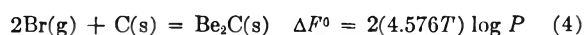
For the data to be used for calculation of thermodynamic quantities, the identity of the gaseous

TABLE I

Expt. no.	Temp., °K.	Time, sec.	Wt. loss Be, mg.	Orifice area, cm^2	Clausing factor	P (atm.)
2	1669	4680	1.60	0.0085	0.69	1.79×10^{-6}
1	1659	4260	1.50	.0085	.69	1.83×10^{-6}
4	1647	4500	0.94	.0085	.69	1.08×10^{-6}
3	1643	6120	1.00	.0085	.69	8.5×10^{-6}
13	1628	4980	0.83	.0085	.69	8.6×10^{-6}
11	1590	6720	0.50	.0085	.69	3.80×10^{-6}
16	1580	9660	2.80	.0324	.81	3.3×10^{-6}
12	1578	4200	0.45	.0270	.65	2.18×10^{-6}
7	1536	10,800	.45	.0085	.69	2.08×10^{-6}
6	1515	12,600	.95	.0270	.65	1.25×10^{-6}
8	1446	27,600	.29	.0270	.65	1.72×10^{-7}
14	1442	26,900	.33	.0270	.65	2.00×10^{-7}
10	1424	25,000	.14	.0085	.69	2.72×10^{-7}
9	1430	23,450	.09	.0085	.69	1.86×10^{-7}

and condensed phases must be known and the existence of equilibrium between the solid and vapor during the experiment must be shown. Chupka, Berkowitz, Giese and Inghram showed in a mass spectrometric study that Be(g) is the only important gaseous species above Be_2C at approximately 1900°K.⁷ This was confirmed by an experiment performed at 1580°K. in this Laboratory in which the gross weight loss of a Knudsen cell was found to be equal to the amount of beryllium in the sublimate. Solid solubility in beryllium carbide is assumed to be negligible. The existence of equilibrium is shown by the non-dependence of measured pressures on orifice area. Thus, equation 3 may be used for thermodynamic calculations.

The standard free energy of formation of beryllium carbide may be obtained by combining the data for reaction 1 with data for the vapor pressure of beryllium by the usual thermodynamic treatment



The vapor pressure of solid beryllium is⁵

$$\log P^0(\text{atm.}) = 6.186 + 1.454 \times 10^{-4} T - \frac{16,734 (\pm 80)}{T} \quad (7)$$

If equations 3 and 7 are substituted in (6) one obtains for the free energy of formation of Be_2C

$$\Delta F^0(f) = (7.688 \pm 3.176)T - 1.331 \times 10^{-3} T^2 - 27,328 (\pm 500) \quad (8)$$

The heat of formation may be obtained from the expression

$$\frac{\partial(\Delta F^0/T)}{\partial T} = \frac{-\Delta H^0}{T^2}$$

which gives

$$\Delta H^0(f) = 1.331 \times 10^{-3} T^2 - 27,328 (\pm 5000)$$

The entropy of formation may be obtained from the expression

$$\Delta H^0 = \Delta F^0 + T\Delta S^0$$

At 1500°K., the approximate mid-point of the experimental temperature range, these equations give -18.8 kcal. for $\Delta F^0(f)$, -24.3 kcal. for $\Delta H^0(f)$ and

-3.7 e.u. for $\Delta S^0(f)$. For reactions in which reactants and products are solids entropy changes are usually small, *i.e.*, 1-2 e.u. per gram atom of constituents. Thus the value found above indicates that the magnitude and temperature dependence of the pressures measured in this investigation are consistent.

To obtain values of ΔF^0_{298} and ΔH^0_{298} in the ab-

sence of high temperature heat capacity data it is assumed that ΔC_p for reaction 6 is zero and the approximate expression

$$\Delta F(T) = \Delta H_{298} - T(\Delta S_{298})$$

will be used together with Krikorian's estimate of $\Delta S^0_{298}(f)$. These assumptions lead to a value of -21.8 ± 5.0 kcal. for ΔH^0_{298} , and -21.2 ± 5.0 for ΔF^0_{298} .

HEATS OF MIXING IN THE SYSTEM CARBON TETRACHLORIDE-CYCLOHEXANE-BENZENE

BY J. REX GOATES, RALPH J. SULLIVAN AND J. BEVAN OTT

Contribution from the Department of Chemistry, Brigham Young University, Provo, Utah

Received September 11, 1958

Heats of mixing were measured calorimetrically for the three binary solutions that can be formed from carbon tetrachloride, cyclohexane and benzene at several temperatures in the range of 10-40°. The heats of mixing in the two systems containing benzene varied appreciably with temperature, $(\partial \Delta H^0_M / \partial T)_p$ at the equal mole fraction composition being 0.33 cal. mole⁻¹ deg.⁻¹ for CCl_4 - C_6H_6 , and -2.00 cal. mole⁻¹ deg.⁻¹ for C_6H_{12} - C_6H_6 . The heat of mixing of CCl_4 - C_6H_{12} was independent of temperature over the 25° range investigated. Analytical expressions for the heats of mixing as a function of temperature and composition were derived. These equations were combined with free energy data from the literature to obtain free energy expressions from which all the thermodynamic properties at constant pressure can be calculated. Heats of mixing at 25° are also reported for the two ternary systems CCl_4 - C_6H_{12} - C_6H_6 and CCl_4 - CHCl_3 - CH_2Cl_2 . In the first system a ternary term that accounts for 3-4% of the total heat of mixing is necessary to adequately describe the data. The heats of mixing in the second system were found to be within 1% of the values predicted from the properties of the binaries. Freezing point measurements of the binary solutions of CCl_4 , C_6H_{12} and C_6H_6 were made, from which partial phase diagrams could be constructed. The CCl_4 - C_6H_6 diagram showed the existence of a 1:1 addition compound, with a heat of dissociation of approximately 3.5 kcal./mole. It is suggested that π -bonding between the aromatic ring and the empty 3-d level of chlorine may be responsible for this complex. Replacing benzene with *p*-xylene to increase the electron density of the ring increased the heat of dissociation of the resulting complex to a value of approximately 6.3 kcal./mole. On the other hand, either decreasing the electron density of the ring by using nitrobenzene, or decreasing the electronegativity of the chlorine atoms by substituting CHCl_3 for CCl_4 prevented complex formation.

Some years ago Scatchard, Wood and Mochel¹ made a careful study of the vapor-liquid equilibria of the three binary systems that can be formed from carbon tetrachloride, cyclohexane and benzene. From these data they calculated the thermodynamic properties at constant pressure and expressed this information analytically as functions of both composition and temperature.

Later Wood, *et al.*,² measured the volumes of mixing of these systems over a wide temperature range, making possible the calculation of the thermodynamic properties at constant volume. Very extensive use of the information obtained in these two studies has been made in the evaluation of theories of solutions. We felt that additional data on the heats of mixing, especially the effect of temperature on the heat of mixing, were needed; and have measured calorimetrically the heats of mixing for these systems in the temperature range of 10-40°. The heats of mixing in the systems containing benzene were found to vary appreciably with temperature, while CCl_4 - C_6H_{12} showed no detectable change over the 25° range that was investigated.

Solid-liquid equilibria also were investigated. Our original intention was to calculate the free energies of mixing from these data. Formation of solid solutions, however, precluded the use of the

freezing point measurements for this purpose. This part of the study did, however, prove to be rewarding, for the phase diagrams show the formation of a compound in the system CCl_4 - C_6H_6 . The phase diagram evidence of compound formation, together with the effect of temperature on the heat of mixing, shows that this system is considerably less ideal than it was formerly thought to be.

Experimental

Reagent grade chemicals were purified by both fractional crystallization and distillation and then stored under an atmosphere of dry nitrogen gas. Indices of refraction of the final products agreed to the fourth decimal place with those given in the Dow Chemical tables³; and the mole per cent. impurities, calculated from freezing points, were less than 0.02%.

The calorimeter consisted of two 15-ml. stainless steel compartments separated by an aluminum or tin foil disc. Mixing was accomplished by causing a steel plunger inside one of the compartments to pierce the metal foil. The calorimeter is so constructed that no vapor phase needs to be present; however, by purposely leaving a small (approximately 2% vapor space) changes in pressure brought about by volume changes in mixing are minimized, and the effect of pressure on the heat of mixing becomes insignificant. The heat effects produced by change in composition of the vapor during mixing are calculated to be less than 0.1 cal./mole. Further details have been published previously.⁴ The over-all uncertainty of these calorimetric measurements is calculated to be less than either one calorie, or one per cent., whichever is larger.

The freezing point data were obtained from cooling curves. A calibrated 10 junction thermocouple connected to a 10

(1) (a) G. Scatchard, S. E. Wood and J. M. Mochel, *THIS JOURNAL*, **43**, 119 (1939); (b) *J. Am. Chem. Soc.*, **61**, 3206 (1939); (c) **62**, 712 (1940).

(2) (a) S. E. Wood and J. P. Brusie, *ibid.*, **65**, 1891 (1943); (b) S. E. Wood and A. E. Austin, *ibid.*, **67**, 480 (1945); (c) S. E. Wood and J. A. Gray, III, *ibid.*, **74**, 3729 (1952); (d) **74**, 3733 (1952).

(3) R. R. Dreisbach, "Physical Properties of Chemical Substances," Dow Chemical Co., Midland, Michigan, 1952.

(4) J. R. Goates and R. J. Sullivan, *THIS JOURNAL*, **62**, 188 (1958)

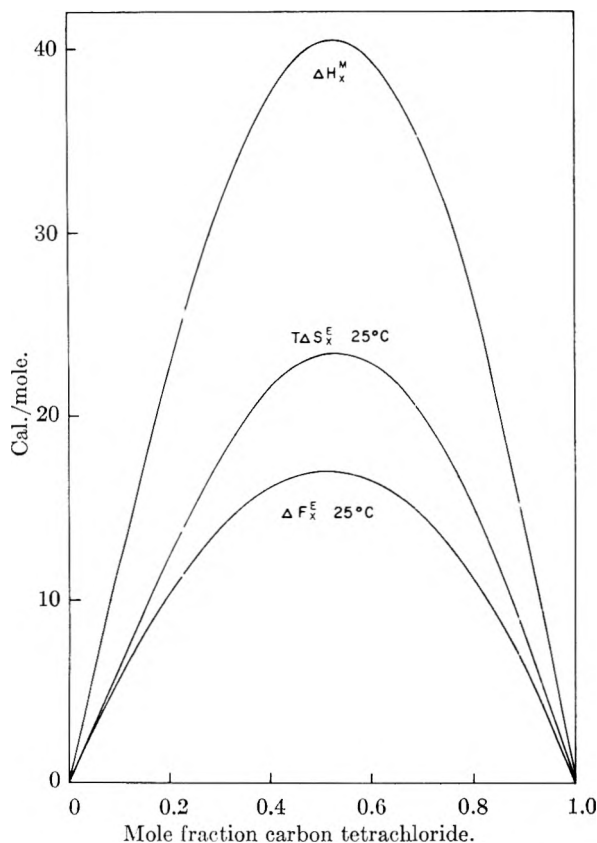


Fig. 1.—Thermodynamic properties of $\text{CCl}_4\text{-C}_6\text{H}_{12}$.

mv. recorder made possible equilibrium temperature measurements to within 0.05° . The solution to be frozen was sealed from the atmosphere to prevent evaporation and, more important, to prevent condensation of water vapor into the system.

Results and Discussions

Carbon Tetrachloride-Cyclohexane.—Of the three binary systems $\text{CCl}_4\text{-C}_6\text{H}_{12}$ was the least complex. The heats of mixing per mole of solution, ΔH_x^M , at 15, 25, 35 and 40° are recorded in Table I. When these data are plotted *versus* mole fraction, they fall nicely on the slightly distorted parabola of equation 1, in which x_1 is mole fraction of CCl_4 , and x_2 is mole fraction of C_6H_{12} .

$$\Delta H_x^M = x_1 x_2 [160.8 + 18.9(x_1 - x_2) - 20.2(x_1 - x_2)^2] \quad (1)$$

The deviations of the experimental points from the plot are given in Table I. Within the limits of the experimental data, ΔH_x^M of this system is independent of temperature over the range $15\text{-}40^\circ$. This fact, together with the relatively low values of ΔH_x^M , shows the system to be fairly close to an ideal solution.

If the excess free energy of mixing per mole, ΔF_x^E , data at 40° of Scatchard, *et al.*,¹ are expressed in the same form as equation 1, and then combined with equation 1 in such a way that $[\partial(\Delta F/T)/\partial T]_p = -\Delta H/T^2$ an equation for ΔF_x^E as a function of both composition and temperature (eq. 2) is obtained that is based on the directly determined ΔH_x^M data of this study.

$$\Delta F_x^E = x_1 x_2 [160.8 - 0.3117T + (18.9 - 0.9489T)(x_1 - x_2) - (20.2 - 0.0645T')(x_1 - x_2)^2] \quad (2)$$

TABLE I
CALORIMETRIC HEATS OF MIXING OF
CARBON TETRACHLORIDE (1)-CYCLOHEXANE (2)

t , $^\circ\text{C.}$	x_1	ΔH_x^M , cal./mole	Dev. from eq. 1, cal./mole	
15	0.4221	39.0	0.6	
	.6185	38.9	.2	
	25	0.2714	29.2	.0
		.4542	39.8	.4
		.5019	40.1	.1
35	.5599	39.9	.0	
	.7746	28.9	.1	
	0.4011	37.2	.3	
40	0.4138	37.9	.2	
	0.4073	37.1	.7	
CYCLOHEXANE (2)-BENZENE (3)				
t , $^\circ\text{C.}$	x_2	ΔH_x^M , cal./mole	Dev. from eq. 3, cal./mole	
15	0.2066	145.8	1.2	
	.3551	193.6	3.7	
	.3843	194.0	0.6	
	.4460	199.7	.4	
	.4766	201.4	.2	
	.4795	202.8	1.6	
	.5292	199.3	0.6	
	.5434	199.3	0.4	
	.5504	197.4	1.0	
	.5710	196.4	0.2	
	.7324	161.3	1.0	
	25	0.2359	137.7	1.6
		.2511	141.2	0.1
		.4253	177.9	.2
		.4721	181.0	.0
.5086		182.3	.9	
.5616		178.9	.2	
.6941		157.7	.3	
35	0.4323	159.2	1.9	
	.4403	161.4	3.4	
	.4866	160.1	0.9	
CARBON TETRACHLORIDE (1)-BENZENE (3)				
t , $^\circ\text{C.}$	x_1	ΔH_x^M , cal./mole	Dev. from eq. 5, cal./mole	
10	0.1803	11.9	0.5	
	.2056	12.6	.1	
	.3590	18.6	.3	
	.3595	19.1	.2	
	.4204	20.1	.2	
	.5238	21.0	.0	
	.5703	20.7	.0	
	.5859	20.1	.3	
	.7172	16.9	.0	
	.7761	14.5	.2	
	.7774	14.5	.2	
	.8175	12.4	.2	
	.8377	11.0	.0	
	25	0.2313	16.6	0.2
		.4113	24.7	.1
.4460		25.3	.2	
.5456		25.9	.1	
.7056		21.9	1.1	
40	0.4566	30.8	0.2	
	.6084	28.0	1.2	
	.5899	29.3	0.5	
	.3621	28.8	1.4	

Such an equation represents a summary of the thermodynamic properties at constant pressure, since the other thermodynamic properties of mixing and the relative partial molar quantities may be obtained from it by differentiation with respect to either temperature or composition. Graphs of three of these thermodynamic properties are shown in Fig. 1.

Strictly speaking, equations 1 and 2 apply only in the temperature range of 15–40°. However, since the change in ΔH_x^M with temperature is so small in this system, one would expect to be able to extrapolate fairly accurately to higher and lower temperatures. For example, equation 2 fits the 70° measurements of Scatchard, *et al.*,¹ to within 0.1–0.4 cal./mole.

The heat of mixing at the equal mole fraction composition found in this study is 40.2 cal./mole, which is 2.2 cal./mole higher than the calorimetric value reported by Scatchard, *et al.*,⁵ at 20°, and 0.8 cal./mole lower than that reported by Noordtzijs⁶ at 15 and 30°.

Cyclohexane-Benzene.—The heats of mixing for C_6H_{12} - C_6H_6 are several times higher than those of the previous system, less symmetrical with mole fraction and highly dependent on temperature. Table I contains the ΔH_x^M data and the deviations of the experimental points from analytical equation 3.

$$\Delta H_x^M = x_2x_3[3105.0 - 7.9800T - (1303.0 - 4.3700T)(x_2 - x_3) + (1738.0 - 5.4860T)(x_2 - x_3)^2] \quad (3)$$

The form of equation 3 (ΔH_x^M linear with temperature) is based on the assumption that the *difference* in heat capacity before and after mixing remains constant over the 25° temperature range. Since the shape of the ΔH_x^M versus mole fraction curve changed with temperature, all three parameters were expressed as linear functions of temperature.

Using the same procedure as described in the previous system, we combined the 40° vapor-liquid data¹ with equation 3 to obtain equation 4, which applies over the temperature range of 15–40°

$$\Delta F_x^E = x_2x_3[3105.0 - 54.877T + 7.9800T \ln T - (1303.0 - 29.229T + 4.3700T \ln T)(x_2 - x_3) + (1738.0 - 37.062T + 5.4860T \ln T)(x_2 - x_3)^2] \quad (4)$$

Plots of equations 3 and 4 and the excess entropy of mixing calculated from (3) and (4) are shown in Fig. 2.

Scatchard, *et al.*,⁵ reported the value of 196.5 cal./mole for the heat of mixing of the equal mole fraction composition at 20°. For the same temperature and composition, equation 3 gives 191.5 cal./mole. Noordtzijs⁶ reported the value of 200 cal./mole at 15°, which should be compared with the value of 201.3 from equation 3. The close agreement here, however, would appear to be partly fortuitous, since the experimental points in reference 6 are widely scattered. In an early study of this system, Baud⁷ reported 188 cal./mole at temperatures somewhere between 15 and 20°.

Carbon Tetrachloride-Benzene.—The ΔH_x^M data

(5) G. Scatchard, L. B. Ticknor, J. R. Goates and E. R. McCartney, *J. Am. Chem. Soc.*, **74**, 3721 (1952).

(6) R. M. A. Noordtzijs, *Helv. Chim. Acta*, **39**, 637 (1956).

(7) E. Baud, *Bull. soc. chim.*, [IV] **17**, 329 (1915).

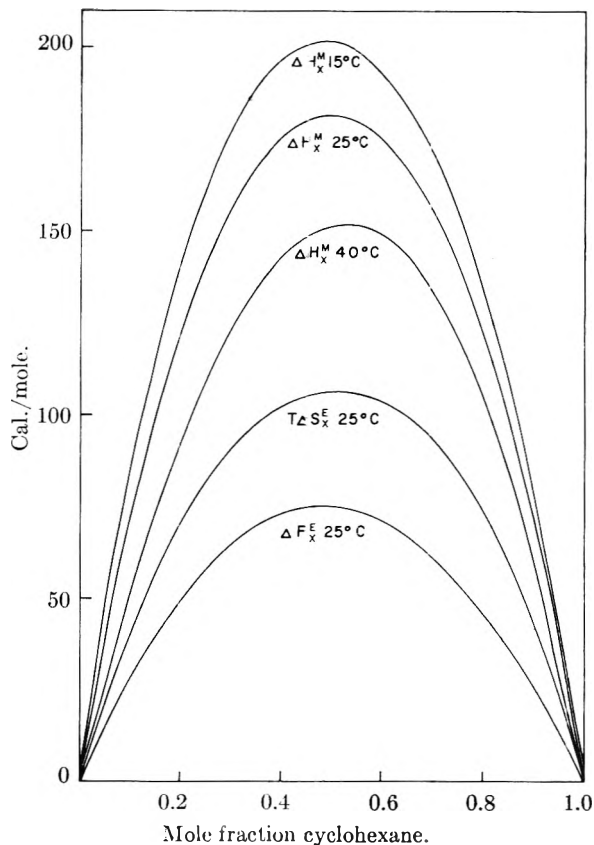


Fig. 2.—Thermodynamic properties of C_6H_{12} - C_6H_6 .

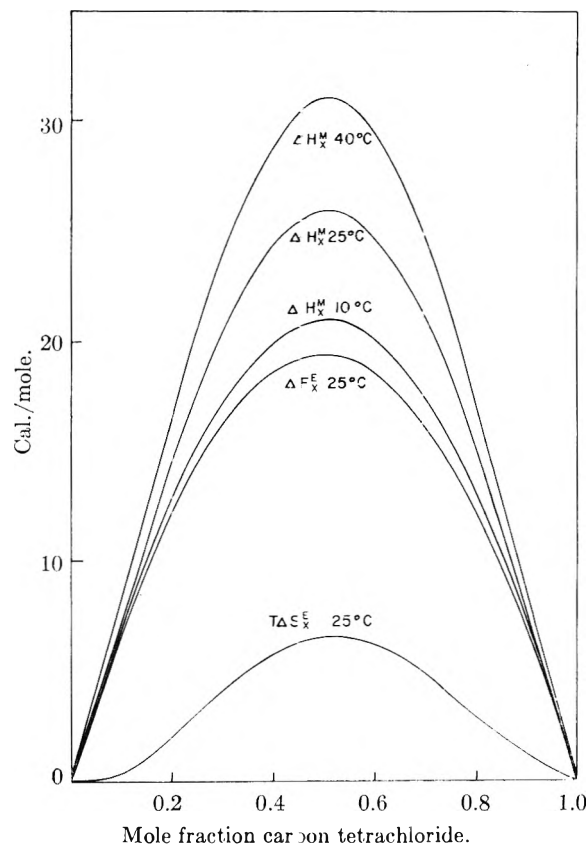
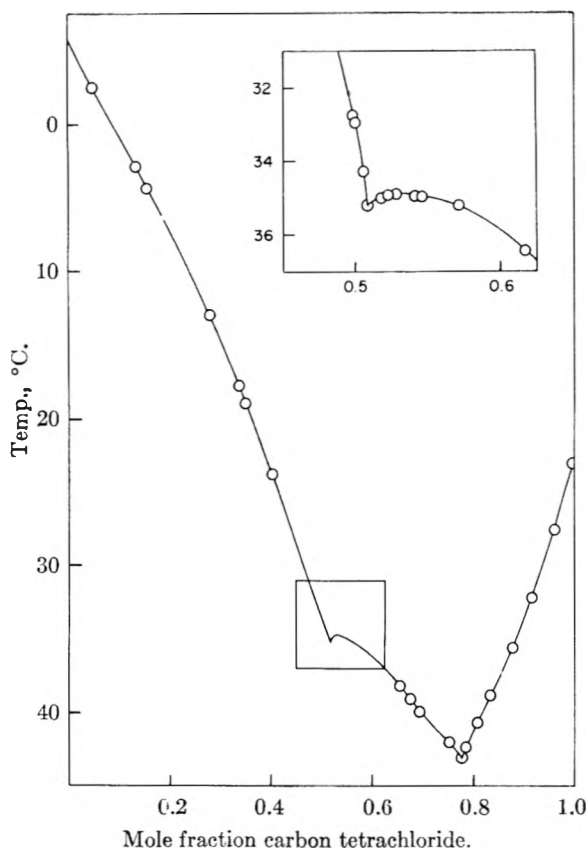
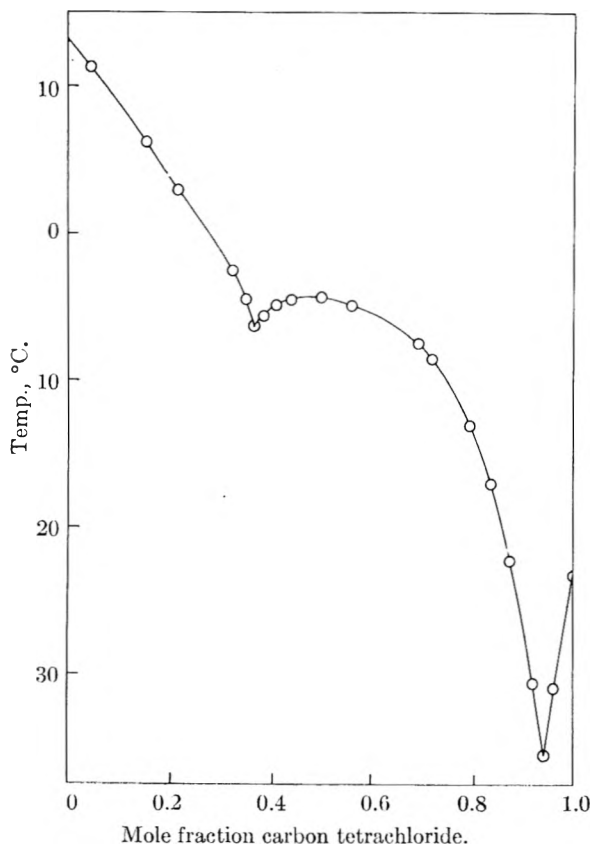


Fig. 3.—Thermodynamic properties of CCl_4 - C_6H_6 .

Fig. 4.—Freezing points of $\text{CCl}_4\text{-C}_6\text{H}_6$.Fig. 5.—Freezing points of $\text{CCl}_4\text{-}p\text{-(CH}_3)_2\text{C}_6\text{H}_4$.

for $\text{CCl}_4\text{-C}_6\text{H}_6$ are given in Table I, and are summarized by equation 5

$$\Delta H_x^M = x_1x_2[-293.5 + 1.3333T - (8.04 - 0.04137T) \times (x_1 - x_2) + (375.6 - 1.3667T)(x_1 - x_2)^2] \quad (5)$$

Several studies of the heat of mixing of $\text{CCl}_4\text{-C}_6\text{H}_6$ have been made.^{10,5-11} The results at 25° range from 21–30 cal./mole at the equal mole fraction composition. Our data are in best agreement with those of Cheesman and Whitaker.¹¹ Equation 5 deviates from their experimental data at both 17.80 and 24.70° by an average of somewhat less than 0.5 cal./mole.

Proceeding as with the two previous systems, we obtained equation 6 which applies over the range 10–40°.

$$\Delta F_x^E = x_1x_2[-293.5 + 8.8434T - 1.3333T \ln T - (8.04 - 0.2612T + 0.04137 \ln T)(x_1 - x_2) + (375.6 - 9.0558T + 1.3667T \ln T)(x_1 - x_2)^2] \quad (6)$$

Figure 3 shows a plot of equations 5 and 6. The ΔH_x^M values are the lowest of the three systems studied, which fact considered by itself suggests near-to-ideal behavior. The drop in ΔH_x^M as the temperature decreases, however, suggests the formation of an exothermic complex.

The results of the freezing point measurements on this system do show the existence of such a complex. Figure 4 is the phase diagram constructed from the freezing point data. The compound peak is at a mole fraction of 0.524 CCl_4 , roughly 1 CCl_4 to 1 C_6H_6 . Calculated on the assumption that the compound was present in an ideal solution,¹² the heat of dissociation is 3.5 kcal./mole.

Figure 4 is in general agreement with phase diagrams that were obtained previously by Baud¹³ and Linard.¹⁴ The freezing points of the pure components that were found in these early investigations, however, are as much as 1° lower than the presently accepted values, so no more detailed comparison can be made.

Spectrophotometric evidence for complexes between aromatic compounds and I_2 ,^{15,16} Br_2 ^{17a} and ICl ^{17b} has been reported. In such complexes the aromatic compound appears to be an electron donor to the halogen molecule. It may be that the same explanation applies to the $\text{CCl}_4\text{-C}_6\text{H}_6$ complex. Here there might be π -bonding between the electron cloud of the benzene ring and the empty 3-d level of the chlorine atoms in CCl_4 .

Assuming such bonding, one would predict that the formation of the complex would be enhanced by substituents in the benzene ring that would increase the electron density of the ring and be hindered by

(8) H. Hirobe, *J. Faculty Sci. Imp. Univ. Tokyo*, **1**, 155 (1925).

(9) R. D. Vold, *J. Am. Chem. Soc.*, **59**, 1515 (1937).

(10) C. G. Boissonnas and M. Cruchaud, *Helv. Chim. Acta*, **27**, 934 (1944).

(11) G. H. Cheesman and A. M. B. Whitaker, *Proc. Roy. Soc., (London)*, **A212**, 406 (1952).

(12) I. Prigogine and R. Defay, "Chemical Thermodynamics," Longmans Green & Co., London, 1954, p. 375.

(13) E. Baud, *Ann. chim. phys.*, **29**, 124 (1913).

(14) J. Linard, *Bull. soc. chim. Belg.*, **34**, 363 (1925).

(15) (a) H. A. Benesi and J. H. Hildebrand, *J. Am. Chem. Soc.*, **70**, 2832 (1948); (b) **71**, 2703 (1949).

(16) J. H. Hildebrand, H. A. Benesi and L. M. Mower, *ibid.*, **72**, 1017 (1950).

(17) (a) R. M. Keefer and L. J. Andrews, *ibid.*, **72**, 4677 (1950); (b) **72**, 5170 (1950).

substituents that withdraw electrons from the ring. As one check on these predictions, we made freezing point measurements on the systems carbon tetrachloride-*p*-xylene and carbon tetrachloride-nitrobenzene. The freezing point data for the first system are in Fig. 5, which shows that the predicted behavior was realized. The pronounced compound peak occurs at the equal mole fraction composition. The heat of dissociation of the complex was found to be 6.3 kcal./mole, almost twice the value for the CCl₄-C₆H₆ complex. Also in agreement with the predictions, CCl₄-C₆H₅NO₂ did not form a complex.

Freezing points of CHCl₃-*p*-(CH₃)₂C₆H₄ solutions were also taken. No complex was evident in this system. Since the size of the CCl₄ molecule is just right for three of the chlorine atoms to sit on a flat side of a benzene ring, one might expect—if such were the structure—that the three chlorine atoms in chloroform would do likewise. The explanation may be based on the difference in the electronegativities of the chlorine atoms in CCl₄ and CHCl₃. On the basis of an inductive effect one would predict that the net negative charge of a Cl atom in CHCl₃ would be greater than that in CCl₄. Smith and Eyring's¹⁸ quantitative calculations of this difference shows that it is quite significant. This larger negative charge may prevent the Cl atom from accepting further electrons.

Equal Mole Fraction Mixtures.—Table II gives the values of some heat content and entropy functions of the three binary systems at the equal mole fraction composition. The heats of mixing for both of the systems containing benzene are shown to be appreciably dependent on temperature. The -2 cal. mole⁻¹ deg.⁻¹ change for the C₆H₁₂-C₆H₆ system, on a percentage basis, is actually slightly less than that found in the CCl₄-C₆H₆ system. The drop in ΔH_x^M as the temperature is lowered in the CCl₄-C₆H₆ system is in agreement with what one would expect as the amount of the exothermic complex that was found in this system increased at the lower temperature.

TABLE II

HEAT CONTENT AND ENTROPY FUNCTIONS FOR THE EQUAL MOLE FRACTION MIXTURES AT 25°

	CCl ₄ - C ₆ H ₁₂	C ₆ H ₁₂ - C ₆ H ₆	CCl ₄ - C ₆ H ₆
ΔH_x^M (15°), cal./mole	40.2	201.4	22.7
ΔH_x^M (25°), cal./mole	40.2	181.5	26.0
ΔH_x^M (40°), cal./mole	40.2	151.5	31.0
$(\partial \Delta H_x^M / \partial T)_p$, cal./mole, deg.	0.0	-2.00	0.333
ΔS_x^E (25°), e.u.	0.0778	0.356	0.0221
\bar{L}_{CCl_4} (25°), cal./mole	44.9	...	27.1
$\bar{L}_{C_6H_{12}}$ (25°), cal./mole	35.5	181.5	...
$\bar{L}_{C_6H_6}$ (25°), cal./mole	...	181.5	24.9
$S_{CCl_4}^E$ (25°), e.u.	0.0902	...	0.0258
$S_{C_6H_{12}}^E$ (25°), e.u.	0.0657	0.367	...
$S_{C_6H_6}^E$ (25°), e.u.	...	0.345	0.0181

The symmetry of the ΔH_x^M versus composition curves of the solutions containing C₆H₆ is also measurably affected by temperature. As the temperature increases, the maximum in the ΔH_x^M -mole frac-

tion curve shifts toward the benzene-poor composition in both systems.

Since the ΔH_x^M and ΔS_x^E versus mole fraction curves are fairly symmetrical at 25° in all three systems, there are no large differences in either the \bar{L} or S_x^E values of the two components of any of the equal mole fraction solutions. The contribution of CCl₄ to both ΔH_x^M and ΔS_x^E is slightly higher than that of the other component; and the contribution of C₆H₆ is either equal to, or lower than, that of the other component in each of the binary solutions.

Ternary Systems.—(a) **Carbon Tetrachloride-Cyclohexane-Benzene.**—Heats of mixing for six compositions of the ternary system CCl₄-C₆H₁₂-C₆H₆ are reported in Table III. Scatchard, *et al.*,^{1c,5} and Redlich and Kister¹⁹ have proposed that the thermodynamic properties of symmetrical systems may be obtained as the sum of the properties of the binaries. The fourth column in Table III is the difference between the experimental value for the ternary and the value predicted from the binaries. Inasmuch as there is a fair amount of asymmetry in the binary solutions containing benzene, the agreement between the measured and estimated heats is fairly good; the greatest deviation observed is less than 5%. A ternary term, such as has been added in equation 7, is necessary to describe the data more accurately.

$$\Delta H_{123}^M = \Delta H_{12}^M + \Delta H_{13}^M + \Delta H_{23}^M + x_1 x_2 x_3 [128 + 161(x_1 - x_2) - 1636(x_1 - x_2)^2] \quad (7)$$

The fifth column in Table III is the difference in the experimental values and this equation.

TABLE III
CALORIMETRIC HEATS OF MIXING OF
TWO TERNARY SYSTEMS AT 25°

x_1	x_2	ΔH_x^M , cal./mole	Dev. from sum of binaries, %	Dev. from eq. 7, %
Carbon tetrachloride (1)-Cyclohexane (2)-Benzene (3)				
0.213	0.574	109.7	3.6	0.2
.233	.534	115.3	0.8	.9
.280	.440	120.5	2.7	.9
.306	.388	118.2	2.7	1.3
.325	.350	117.2	4.6	0.7
.500	.000	25.8	0.0	.0
x_1	x_2	ΔH_x^M , cal./mole	Dev. from eq. 8, %	
Carbon tetrachloride (1)-Chloroform (2)- Methylene Chloride (3)				
0.0000	0.5000	4.3		0.0
.1870	.4065	63.2		.2
.3146	.3427	87.3		.6
.4128	.2936	96.2		.0
.4966	.2517	100.9		2.6
.4968	.2516	99.9		1.6
.5500	.2250	95.8		0.9
.5512	.2244	96.9		.2
.8178	.0911	57.0		.4

(b) **Carbon Tetrachloride-Chloroform-Methylene Chloride.**—Cheesman and Whitaker¹¹ have reported ΔH_x^M values for the binaries that can be

(18) R. P. Smith and H. Eyring, *ibid.*, **74**, 229 (1952).

(19) O. Redlich and A. T. Kister, *Ind. Eng. Chem.*, **40**, 431 (1948).

formed from $\text{CCl}_4\text{-CHCl}_3\text{-CH}_2\text{Cl}_2$. Since these binary solutions were reported as very nearly symmetrical, we were interested in the ternary solution. The third column of Table III reports our experimental heats for the ternary, and the fourth column is the deviation of these values from the sum of the binary data of Cheesman and Whitaker, which is given in equation 8.

$$\Delta H_{123}^M = 220.4x_1x_2 + x_1x_2[565 - 33.1(x_1 - x_2)] + 17.0x_2x_3 \quad (8)$$

The deviation is about the order of the experimental error. It is possible, therefore, to predict ΔH_{123}^M values for this ternary as accurately as the binaries were measured.

Acknowledgment.—The authors gratefully acknowledge the support given this project by the National Science Foundation. We also wish to thank Miss Norene McClellan, who assisted with the freezing point measurements.

HEATS OF IMMERSION. I. THE SYSTEM SILICA-WATER

By A. C. MAKRIDES AND N. HACKERMAN

Department of Chemistry, The University of Texas, Austin, Texas

Received September 19, 1958

The heat of wetting of SiO_2 by water depends on temperature of evacuation and on thermal treatment of the SiO_2 powder. Available data suggest that the heat of wetting may depend on the specific surface area of the powder.

Introduction

A number of heats of wetting of silica powders with water have been reported.¹⁻⁷ Values for relatively coarse powders ($<3 \text{ m.}^2/\text{g.}$) are generally greater than those obtained with powders of large specific surface area ($>100 \text{ m.}^2/\text{g.}$) and with gels by a factor of about 2 or more. Data for coarse powders are restricted, however, to a single temperature of evacuation and, in a number of cases, refer to powders of unspecified impurity content. Heats of wetting of silica powders variously pretreated are reported here.

Experimental

Calorimeter.—Heats of wetting were measured with a twin microcalorimeter similar to the instrument of Evans and Richards.⁸ A major modification was the use of thermistors for measuring temperature changes (see below).

Two closely similar Dewar flasks of 500-cc. capacity served as the calorimeter vessels. They were attached to a nickel-plated brass plate with aluminum rings equipped with Neoprene gaskets. Both vessels were enclosed by a bright nickel-plated jacket which was also attached to the brass plate through an intervening gasket.

The calorimeter assembly, suspended with Bakelite rods from an aluminum plate, was immersed in a constant temperature bath. A thyatron circuit temperature controller with a thermistor as one arm of an a.c. (60 c.p.s.) bridge regulated the bath temperature within $\pm 0.001^\circ$ over 24-hour periods.

Heat exchange between vessels and bath took place across the brass plate. Heat transfer across the air space between vessels and jacket was comparatively negligible. A Neoprene sheet and a Lucite plate, inserted between the brass plate and the Dewar flasks, reduced heat exchange to a desirable level.

Each vessel included a heater, a stirrer, a sample holder and breaker and a thermistor.

The calorimeter heaters were wound non-inductively from manganin wire. They were coated with Glyptal resin and enclosed in gold containers friction-fitted on Teflon plugs inserted in the brass plate. Transformer oil increased thermal conductivity between heater and container.

Both calorimeter stirrers were driven at 150 r.p.m. by a single Bodine precision motor with attached reduction gear. A Gilmer positive-drive belt, with associated pulleys, was used to ensure constancy of stirring.

A Bakelite section, threaded at both ends, reduced heat conduction along the stirrer shaft. Bakelite gave air-tight seals with Neoprene O-rings placed in recesses drilled in the brass plate. The Bakelite sections were replaced every two or three runs, while O-rings were changed after every run.

The breaker rods were in two parts, both ending in Bakelite sections. The upper part rested against the Neoprene sheet, while the lower end extended from just beneath the sheet to the bulb. The bulb was broken by pressing the upper section against the flexible Neoprene sheet.

Electrical Circuits.—The calorimeter vessels were calibrated electrically. The potential drop across the heater and across a series standard resistance was measured with a precision (0.05 mv.) Rubicon potentiometer. Current was drawn from a Willard cell which had been stabilized by discharge, for at least 3 hours, through a resistance equal to that of the heating circuit. A double-throw, double-pole microswitch closed the heating circuit and simultaneously actuated a precision timer (0.01 sec. sensitivity). The timer was driven by a constant frequency (60 c.p.s.) source.

The electrical circuit used in conjunction with the thermistors consisted of a Müller bridge, a 70 ohm input impedance Liston-Becker DC 14 breaker amplifier and a Brown potentiometer. The initial (small) difference in resistance between thermistors was compensated on the bridge, the output of which was fed to the amplifier and the signal recorded on the potentiometer. With the amplification ratio generally used, a resistance difference of 0.01 ohm gave 100 mv. deflection. The corresponding temperature sensitivity was $20 \times 10^{-6} \text{ }^\circ\text{C./mv.}$ and the equivalent heat input sensitivity 0.01 cal./mv.

Thermistors.—The high sensitivity of thermistors as compared to other temperature-sensitive devices offers a major advantage in calorimetric application. Microcalorimeters employing thermistors have been described.^{8,9} Thermistors sometimes lack stability, particularly over long periods of use. With some precautions, however, stable and reproducible behavior was obtained.

Disk-shaped thermistors of 100 ohm nominal resistance were used in pairs matched within 0.1%. They were prepared by Victory Engineering Corporation by aging in a constant temperature bath (25°) for about 3 months. They were coated with Glyptal resin, air-dried and then baked at

(1) G. E. Boyd and W. D. Harkins, *J. Am. Chem. Soc.*, **64**, 1190 (1942); W. D. Harkins and G. E. Boyd, *ibid.*, **64**, 1195 (1942).

(2) F. L. Howard and J. L. Culbertson, *ibid.*, **72**, 1185 (1950).

(3) A. C. Zettlemoyer, G. J. Young, J. J. Chessick and F. H. Healy, *This Journal*, **57**, 649 (1953).

(4) A. V. Kiselev, N. N. Mikos, M. A. Romanchuk and K. D. Shcherbakova, *Zhur. Fiz. Khim.*, **21**, 1223 (1947).

(5) W. A. Patrick, quoted by R. K. Iler, "The Colloid Chemistry of Silica and Silicates," Cornell University Press, Ithaca, N. Y., 1955, pp. 240-242.

(6) F. E. Bartell and R. M. Suggitt, *This Journal*, **58**, 36 (1954).

(7) M. E. Egorov, K. G. Krasil'nikov and E. A. Sysoev, *Doklady Akad. Nauk S.S.S.R.*, **108**, 103 (1956).

(8) D. F. Evans and R. E. Richards, *J. Chem. Soc.*, 3932 (1952).

TABLE I

Powder	% Al ₂ O ₃	% Fe ₂ O ₃	% TiO ₂	% Loss ignition	% min. SiO ₂	Other
A ^a	0.22	0.05	0.034	0.13	99.56	Trace MgO, CaO
B ^b	.04	.016	.008	.09	99.92	Trace MgO, CaO
C	.049	.019	99.82	0.031% MgO
D ^c	Fe ₂ O ₃ + Al ₂ O ₃	.01	...	0.2-1.0	99.0-99.7	...
E ^d	.014	.0017	Nil	CaO < 0.0003; MgO < 0.0007

^a Supplied by New Jersey Silica Sand Corporation (200-mesh Silica Flour). ^b Supplied by C. A. Wagner, Inc. (No. 111 Silica). ^c Supplied by Godfrey L. Cabot, Inc. (Cab-O-Sil). ^d Supplied by Cleveland Quartz Works, General Electric Company (Quartz Crystal Powder).

120° for 1 hour. The electrically-insulated thermistors were inserted in gold containers having a "pocket" at one end with about 0.1 mm. clearance on each side. Wood's metal filled this space and covered the thermistor to a depth of about 1 cm.

Stability of thermistors prepared and mounted in this fashion was satisfactory. Calibrations over a three-month period showed a mean deviation of 0.8% with no apparent trend. The deviation is within the range expected from the precision with which the amplified voltage was recorded (0.5 mv. for total changes of 50 to 100 mv.).

Operation of the Calorimeter.—The calorimeter was left to equilibrate overnight in the constant temperature bath. A reference line with a drift of about 20×10^{-6} °C./min. generally was obtained. Three calibrations were performed before a sample bulb was broken and three after. Changes of drift during a run generally were small. Corrections for drift did not exceed 10% of total deflection. Uncertainties in drift correction because of changes of slope were less than 1% of total deflection. Oscillation of the reference line about its mid-point was $\pm 0.5\%$ of total deflection.

Heat of Bulb Breaking.—Some difficulty was experienced in preparing sample bulbs. It was required that bulbs break in a manner promoting complete wetting of the powder and that the heat of bulb breaking be small and reproducible. Attempts to prepare bulbs of thin, uniform wall thickness by etching in hydrofluoric acid proved fruitless. Thin-walled bulbs blown from Pyrex glass in groups of 24 or more finally were used. Bulbs of nearly equal volumes and volume-weight ratios were selected. Even with these precautions, however, the reproducibility of the heat of bulb breaking was only 30%.

The heat of bulb breaking made a small but significant contribution to the over-all heat effect observed. The heat of bulb breaking, Δh , was approximated by

$$\Delta h = (\Delta h)_{\text{obsd}} - C\Delta V$$

where $(\Delta h)_{\text{obsd}}$ is the total heat (absorption) for breaking an empty bulb, ΔV the volume of the bulb (~ 18 cc.) and $C = -0.0561$ joule/cc., a constant calculated from the heat of vaporization of water. The average for six runs with empty bulbs was $\Delta h = 0.40 \pm 0.14$ joule. This may be compared with 3.2 joules⁶ and 0.2 to 0.4 joules³ obtained by others.

All measurements of heats of wetting were corrected by adding to the observed heat evolution the quantity $-(C\Delta v + 0.40)$, where $\Delta v = \Delta V - (\text{wt. sample}/\text{density SiO}_2)$. The correction amounted to about 0.3 joule.

Material.—The reported bulk impurity content of the silica powders is given in Table I.

Powder C was prepared by sedimentation from water from powder available under the trade name Super-X-Microsil. The fraction in suspension after 10 minutes was retained. The filter pad was washed with MeOH.⁹ The powder subsequently was heated in air at 800° for 24 hours¹⁰ to remove any adsorbed MeOH. It then was rehydrated by exposure to saturated water vapor for two weeks.

Powder E was treated with hydrochloric acid to remove iron particles apparently introduced in the crushing operation. It subsequently was washed repeatedly with triply distilled water, the total volume of water used being about

(9) The powder was fractionated and washed by Dr. J. W. Whalen of the Magnolia Petroleum Co. Field Research Laboratory and he kindly supplied us with a sample.

(10) W. Stöber, G. Bauer and K. Thomas, *Ann.*, **604**, 104 (1957); N. N. Avgul, O. M. Dzhitig, A. A. Isirikyan, A. V. Kiselev, and K. D. Shecherbakova, *Doklady Akad. Nauk S.S.S.R.*, **77**, 625 (1951).

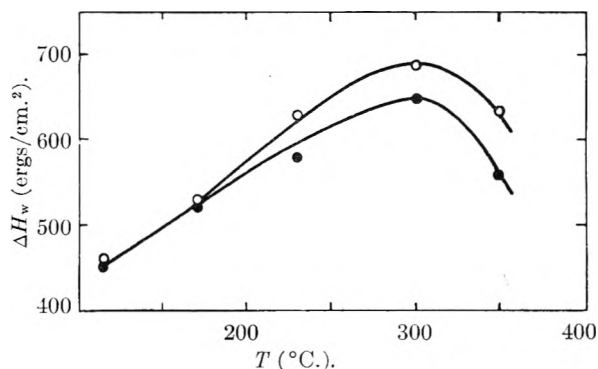


Fig. 1.—The heat of wetting of powdered quartz as a function of temperature of evacuation: open circles, powder A; full circles, powder B.

4 liters per g. of powder. The powder was dried at 110° for weighing.

Samples were selected to give a total area of 10–20 m.². Their weight varied from 0.1 to 25 g., while total heat evolution was 3 to 8 joules. The calorimeter vessels contained 450 cc. of water in all cases.

Samples were evacuated for 24 hours at 10^{-5} mm. Water was triply distilled, one distillation being out of dilute KMnO₄ solution.

Heats of wetting, per unit area, of 5-, 10- and 20-g. samples of powder A were the same within experimental error. Dispersion of sample into the liquid presented some difficulty at first. Use of thin-walled bulbs described above eliminated this difficulty. The bulbs shattered on breaking and the powder was dispersed completely in the stirred liquid.

Reproducibility was generally better than $\pm 4\%$. Thus, the heat of wetting of powders A, B and C evacuated at 120° was, respectively, 460, 450 ergs/cm.²; 450, 445 ergs/cm.²; 300, 275 ergs/cm.². The uncertainty in the heat measurement (including corrections for the heat of bulb breaking) was about $\pm 3\%$. The probable error did not exceed 5%. The accuracy of the absolute value for the heat of wetting is probably less since it includes an uncertainty in the absolute area. Specific surface areas were determined from Kr adsorption using the BET method. Although this method is the best now available, it yields values that are probably uncertain to within 10%.

Results and Discussion

The total heat change observed on immersion of silica powder in water is the sum of the heat of wetting and heat of dissolution. Both the solubility and the solution rate of silica are small.¹¹ Therefore, unless the heat of dissolution is particularly large, its contribution may be neglected.¹⁻³ This assumption is supported by the observation that heat evolution on dispersing a sample in water was complete in about 1 min. No significant changes in drift, expected if dissolution were appreciable, occurred after immersion.

Heats of wetting by water at 25° of powders A

(11) P. F. Holt and D. T. King, *J. Chem. Soc.*, 773 (1955).

TABLE II
HEATS OF WETTING OF SILICA POWDERS BY WATER AT 25°

Powder	Specific surface area (m. ² /g.)	Thermal pretreatment	Heat of wetting (ergs/cm. ²) at temp. (°C.) of evacuation				
			115°	170°	230°	300°	360°
A	0.91	None	460	530	630	690	635
B	.91	None	450	520	570	650	560
B	.85	Heated in air at 700° for 24 hr. ^a	440	410	550	425	...
B	.83	Heated in air at 1100° for 48 hr. ^a	...	425	600	320	260

^a Rehydrated by exposure to saturated water vapor for 1 week.

and B evacuated at temperatures between 120 and 360° are given in Table II. The heat of wetting shows a broad maximum at about 300° (Fig. 1). Differences between powders A and B are small and are evident only on evacuation at temperatures above 200°.

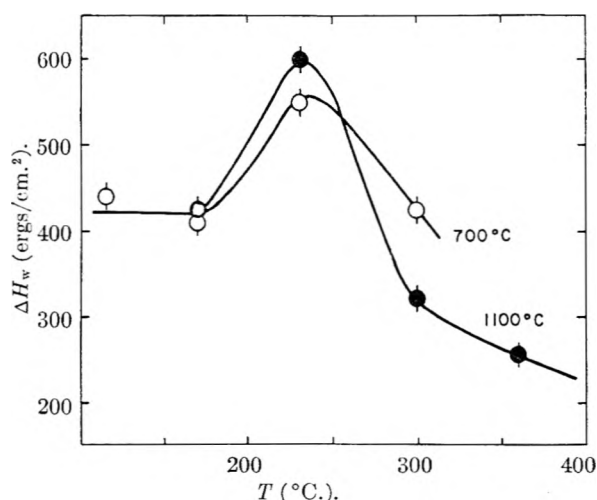


Fig. 2.—The heat of wetting of powdered quartz (powder B) as a function of temperature of evacuation: open circles, powder pretreated by heating in air at 700° for 24 hours; full circles, powder pretreated by heating in air at 1100° for 48 hours. In both cases, samples were rehydrated by exposure to saturated water vapor for 1 week.

Heats of wetting of powder B, pretreated by heating in air at 700° for 24 hours and at 1100° for 48 hours, followed by rehydration by exposure to saturated water vapor for 1 week and subsequent evacuation at indicated temperatures, are also given in Table II. Comparison of Figs. 1 and 2 shows that thermal pretreatment changed little the heat of wetting of powders degassed at 115°. However, significant differences appeared at higher temperatures. The maximum in the heat of wetting was displaced to a lower temperature (ca. 230°) and was more sharply defined. The heat of wetting for temperatures of evacuation above 230° was considerably less than for powders which had not been thermally pretreated.

It is interesting to note that even at 1100° no appreciable loss of surface area occurred. It may be concluded that any decrease in surface area for samples evacuated at temperatures up to 360° was negligible. The thermal stability of these powders may be contrasted with that of SiO₂ gels, the area of which decreases appreciably on heating above 700°.⁷

Heats of wetting of powders C and D evacuated at 120° are given in Table III together with results of other investigators.

The heat of wetting of silica powders varies within wide limits (Tables II and III). It is apparent that surface structure and composition not only differ from powder to powder but are also significantly modified by the conditions under which samples are prepared. Some of the factors that may be responsible for this diversity of results are discussed below.

Impurities.—The influence of impurities has not been studied in any detail. Figure 1 suggests that the heat of wetting is not a sensitive function of impurity content for bulk impurity concentrations of about 0.08 to 0.4%.

There is little doubt (see below) that SiO₂ surfaces chemisorb -OH groups and that subsequent adsorption is dependent on the extent of surface coverage by hydroxyl groups. Surface trivalent ions (Fe⁺³, Al⁺³) also have tightly bound hydroxyl groups. With a more or less fully hydroxylated surface, obtained at low temperatures of evacuation, the effect of impurity cations should be secondary. At higher temperatures the surface is progressively dehydrated and impurities are expected to have a proportionately larger effect. Results presented in Fig. 1 show this general behavior.

The significantly higher heat of wetting of powder E is probably not associated with its somewhat higher purity. Trivalent impurity ions are generally expected to increase the heat of wetting (compare powders A and B) rather than decrease it. A possible cause for the higher heat of wetting of powder E is discussed below.

Surface Hydration.—As noted above, recent experimental work^{12,13} has substantiated Carman's¹⁴ suggestion that SiO₂ surfaces adsorb hydroxyl groups irreversibly. The extent of surface coverage by hydroxyl groups has a pronounced influence on subsequent reversible adsorption of polar adsorbates. For example, the extent of adsorption of water vapor diminishes with increasing dehydration of the surface.¹²⁻¹⁵ The decrease is approximately equal to the loss of hydroxyl groups, suggesting a one to one correspondence between adsorbed H₂O molecules and surface hydroxyl groups.¹⁵

SiO₂ surfaces may be dehydrated by heating

(12) S. P. Zhdanov, *Doklady Akad. Nauk S.S.S.R.*, **100**, 1115 (1955).

(13) S. P. Zhdanov, *ibid.*, **115**, 938 (1957).

(14) P. C. Carman, *Trans. Faraday Soc.*, **36**, 964 (1940).

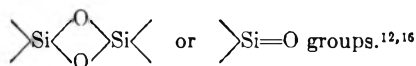
(15) V. A. Dzis'ko, A. A. Vishnevskaya and V. S. Chesalova, *Zhur. Fiz. Khim.*, **24**, 1416 (1950).

TABLE III
 HEATS OF WETTING OF SILICA POWDERS AND GELS

	Material	Specific surface area (m. ² /g.)	Degassing conditions		ΔH_w (ergs/cm. ²)
			T (°C.)	P (mm.)	
Boyd and Harkins ¹	a	2.33	400-600	10 ⁻⁵	600
Howard and Culbertson ²	b	2.13	300	"	880
Zettlemoyer, Young, Chesick and Healy ³	c	0.96	400	"	560
This work	d	.082	115	10 ⁻⁵	1450
This work	e	.91	115	10 ⁻⁵	450
			300	10 ⁻⁵	650
This work	f	5.5	115	10 ⁻⁵	290
This work	g	190 ⁴	115	10 ⁻⁵	160
Kiselev, Mikos, Pomanshuk and Sheherbakova ⁴	Gel ^h	300	400	10 ⁻⁵	220
Patrick ⁵	i	188	"	"	175 ⁶
	j	240			130
	Gel ^k	800			160
Bartell and Suggitt ⁶	l	328	300-350	10 ⁻⁵	260
	Gel ^m	366	300-350	10 ⁻⁵	260
Egorov, Krasil'nikov and Sysoev ⁷	Gel ⁿ	275	300	5 × 10 ⁻⁴	200 ⁸
	Gel ^o	400	300	5 × 10 ⁻⁴	175
	Gel ^p	695	300	5 × 10 ⁻⁴	150

^a Described only as "powdered crystalline quartz." ^b Prepared from "carefully selected natural quartz crystals." ^c New Jersey Silica Sand "silica flour" (same as powder A of Table I). ^d Powder E of Table I. ^e Powder B of Table I. ^f Powder C of Table I. ^g Powder D of Table I. ^h Coarse silica gel obtained by washing commercial silica gel with hydrochloric acid solution and water; subsequent calcining at 500°. Pore volume, 0.87 cc./g. Mean pore diameter, 100 Å. ⁱ Linde Silica from burning chlorosilanes. ^j Flarox Silica prepared by burning ethyl silicate. ^k An otherwise unspecified silica xerogel. ^l Linde Silica powder (#2669-95B). ^m Commercial silica gel (Davison Chemical Company) digested with HNO₃, washed and dried at 300°. ⁿ Silica gel from hydrolysis of SiCl₄. ^{o,p} "Purified" commercial silica gels. ^q Sample preparation prior to wetting unspecified. ^r The heat of wetting decreased with dehydration of silica. Values given are averages. Iler¹⁰ calculates from these data 190 ergs/cm.² for a completely hydrated surface and 130 ergs/cm.² for a completely dehydrated surface. ^s The heat of wetting was a maximum at 300°. For temperatures less than 300°, ΔH_w decreased by not more than 25 ergs/cm.². At higher temperatures (up to 800°), a decrease up to 50 ergs/cm.² was noted. ^t Specific surface area supplied by the manufacturer (see Powder D of Table I). ^u Pressure not specified.

above 200-300°. ¹⁵ It has been postulated that at higher temperatures \rightarrow Si-OH groups are replaced by



The first of the last two structures appears unlikely from crystallographic considerations.¹⁷ However, its existence has some experimental support.¹⁸

Rehydration of thermally dehydrated SiO₂ does not restore completely the surface to its original condition.^{12,13} A permanent decrease occurs in the maximum number of hydroxyl groups per cm.².⁷ Precise kinetic data on the rehydration reaction are not available. It is known, however, that rehydration proceeds slowly.^{7,12,13}

Heat of Wetting and Surface Hydration.—Adsorption energies for water vapor on the two types of surface at least present on thermally treated SiO₂ differ significantly, as is indicated by difference in extent of adsorption.^{12,13,15} The heat of wetting, which includes the integrated heat of adsorption, necessarily reflects these differences.

The dependence of the heat of wetting of powdered quartz on temperature of evacuation and thermal pretreatment parallels that for silica gels⁷ and may be accounted for in a similar way.

The large specific surface area of gels makes relatively simple the determination of the number

of chemisorbed -OH groups per unit area. With thermally pretreated gels, subsequently rehydrated to varying degrees and evacuated at 300°, the heat of wetting is a linear function of the number of hydroxyl groups per unit surface area.⁷ With gels not thermally pretreated, the heat of wetting is a maximum on evacuation at 300°. ^{7,20} The heat of wetting on evacuation at $T < 300^\circ$ is smaller and at temperatures above 300° larger, than expected from the linear relation. The maxima (at 300°) lie on the straight line portion. These results suggest that on evacuation at temperatures below 300°, not all molecularly adsorbed water is removed, leading to smaller than expected heats of wetting. At higher temperatures, an additional heat effect from reaction of water with a partially dehydrated surface is included in the over-all heat effect observed.

Powdered quartz gives similar results, in spite of the fact that its absolute heat of wetting is greater than that of gels by a factor of 2 to 3.²¹

The maxima in Figs. 1 and 2 probably correspond to fully hydroxylated surfaces with all molecularly adsorbed H₂O removed. The decrease of the heat of wetting on evacuation at higher temperatures is attributed to increasing dehydroxylation of the surface. An undetermined, but probably small, heat evolution from rehydration is included

(19) R. K. Iler, "The Colloid Chemistry of Silica and Silicates," Cornell University Press, Ithaca, New York, p. 241.

(16) S. P. Zhdanov and A. V. Kiselev, *Zhur. Fiz. Khim.*, **31**, 2213 (1957).

(17) W. A. Weyl, *Research*, **3**, 230 (1950).

(18) A. Weiss and A. Weiss, *Z. anorg. allgem. Chem.*, **276**, 95 (1954).

(20) A maximum in the heat of wetting vs. temperature of pretreatment of gels also was observed by Bartell and Almy.³¹

(21) F. E. Bartell and E. G. Almy, *This Journal*, **36**, 475 (1932).

in the apparent heat of wetting of powders evacuated at temperatures above 200–300°.

Thermal pretreatment at 700 and 1100°, followed by rehydration, displaces the maximum to a lower temperature (*ca.* 230°), indicating easier removal of molecularly adsorbed water. The curves are also displaced toward lower values for the heat of wetting, suggesting that thermal pretreatment, followed by rehydration, results in a surface having fewer hydroxyl groups per unit area than the original one.

Specific Surface Area and Heat of Wetting.—The heat of wetting apparently decreases sharply when the specific surface area, s , exceeds about 3 m.²/g. (Table III). Heats of wetting of powders with $s < 3$ m.²/g. generally are between 450 and 700 ergs/cm.²; corresponding values for powders with $s > 100$ m.²/g. and for gels are in the range 100–250 ergs/cm.².

Egorov, Krasil'nikov and Sysoev⁷ found that the heat of wetting of a group of gels, evacuated at the same temperature, decreased with increasing specific surface area. The number of hydroxyl groups per unit area also decreased with area. If this relation is assumed to be general, the larger heats of wetting of small specific surface area powders may be attributed to a greater number of hydroxyl groups per unit area.

A variation in the maximum number of chemisorbed hydroxyl groups implies differences in the spacing of surface Si atoms. X-Ray studies indicate that the surface of quartz crystals is disturbed appreciably by grinding or abrading.^{22–25} The presence of partially amorphous surface layers on powdered quartz is also suggested from solubility, solution rate, density and differential thermal analysis studies.^{25,26,27} The extent of departure from what might be termed a "crystalline surface" increases with prolonged grinding.²⁸ It is, therefore,

(22) D. D'Eustachio, *Phys. Rev.*, **70**, 522 (1946).

(23) D. D'Eustachio and S. Greenwald, *ibid.*, **69**, 532 (1946).

(24) E. J. Armstrong, *Bell. System Tech. J.*, **25**, 136 (1946).

(25) J. G. Gibb, P. D. Ritchie and J. W. Sharpe, *J. Appl. Chem.*, **3**, 213 (1953).

(26) D. W. Clelland, W. M. Cumming and P. D. Ritchie, *ibid.*, **2**, 31 (1952).

(27) P. B. Dempsted and P. D. Ritchie, *ibid.*, **3**, 182 (1953).

likely that surface layers with structures approaching amorphous silica are present on powders, and that the degree of amorphicity depends on the method of preparation. The existence of partially amorphous layers would lead to differences in spacing of surface hydroxyl atoms and, consequently, to differences in the heat of wetting.

It is uncertain whether the substantially higher heat of wetting of powder E is associated with its relatively small specific surface area. In this instance, the powder was washed with hydrochloric acid prior to evacuation. It has been suggested¹¹ that silica powders exposed to acid solutions adsorb silicic acid. The effect, if any, of adsorbed silicic acid on the heat of wetting is not known. Further experimental work on this point would be of interest.

Conclusions.—The heat of wetting of silica depends, among other factors, on temperature of evacuation and thermal pretreatment of the powder. The heat of wetting of powders used here has a broad maximum at about 300°. Thermal pretreatment at 700 and 1100°, followed by rehydration, displaces the maximum to approximately 230° and leads to smaller heats of wetting at evacuation temperatures above 230°.

Data for a wide variety of powders and gels show that for any temperature of evacuation, the heat of wetting of powders with $s > 100$ m.²/g. is not much different from that of gels. For $s < 3$ m.²/g., the heat of wetting is greater by a factor of 2 to 3. It is not possible to decide from available data whether the transition from large to small heats of wetting is gradual or abrupt.

Acknowledgment.—This work is a contribution from Project 47d of the American Petroleum Institute at the Department of Chemistry, University of Texas. Dr. H. L. Wang initiated the work on the microcalorimeter. A. C. Hall and R. D. O'Bryan carried out the surface area measurements. We are happy to take this opportunity to express our appreciation to the American Petroleum Institute for the support, financial and otherwise, of this work.

(28) D. W. Clelland and P. D. Ritchie, *ibid.*, **2**, 42 (1952).

EFFECT OF STRUCTURE AND CRYSTALLINITY ON WATER SORPTION OF DEXTRANS

BY N. W. TAYLOR, H. F. ZOBEL, N. N. HELLMAN AND F. R. SENTI

Contribution from the Cereal Crops Laboratory, Northern Utilization Research and Development Division,¹ Peoria, Illinois

Received September 22, 1958

Water absorption and desorption isotherms were determined for 17 dextrans differing in their contents of 1,6-like, 1,4-like and 1,3-like linked units, but all initially amorphous as demonstrated by X-ray diffraction patterns. The absorption isotherms were identical up to 85% relative humidity, thus demonstrating no specific sorption effect assignable to the known structural elements. Above 85% relative humidity, water absorption varied with dextran type. X-Ray diffraction experiments showed that high water absorption above 85% humidity corresponded to a continued amorphous state, while depressed water absorptions corresponded to crystallization of the dextrans. Generally, the presumably less branched dextrans with high proportions of 1,6-like linked units crystallized at high humidity. All amorphous dextrans which did not crystallize at high humidity were nearly identical both in absorption and desorption isotherms; above 75% humidity no water sorption hysteresis was observed.

A large number of dextrans from various strains of microorganisms were prepared and examined recently by A. Jeanes, *et al.*² Dextrans are bacterial polysaccharides composed of glucose joined predominantly as α -1,6-glucosidic linked units. It is clear from their periodate oxidation analysis that dextrans as a group show wide variation in the proportions of 1,6-like, 1,4-like and 1,3-like linked units. The term "like" indicates an uncertainty of alternative structures in interpretation of the analyses.³ These dextrans are a source of variable chemical structures with which some of the effects of structure on water sorption may be investigated.

The following factors might be expected to influence water sorption in this comparison: the nature of the water-binding groups or sites, the presence of a crystalline component in the sense used for high polymers, molecular branching and association of molecular groups in the polymer. Because the general water solubility of these dextrans indicates that they are not strongly associated when amorphous, the effects of chemical structure and crystallinity on water sorption should not be obscured by this factor.

Periodate oxidation analyses indicated that variable proportions of 2-, 3-, 4- and 6-hydroxyl groups were present in individual dextrans. It was anticipated that the proportion of 6-hydroxyl groups might affect water sorption. Assaf, *et al.*,⁴ suggested that in glucose polymers, specifically cellulose, the primary 6-hydroxyl group formed stronger hydrogen bonds than any others, and was assumed by them to be the main site for binding water at low humidities.

Northcote⁵ determined the water sorption isotherms of several polysaccharides, including a dextran. He found similar water sorption behavior at low relative humidity in the dextran, which contained few primary hydroxyls, and in several glycogens which contained a relatively larger number. This similarity is suggestive that the primary hydroxyl group is not a markedly stronger water-bonding group. There is some uncertainty,

however, in this conclusion. A principal difficulty in a comparison of water sorption behaviors is that any relatively permanent association between water-sorbing groups might obliterate behavior characteristic of the particular groups. Therefore, comparison should be among samples that are all amorphous to minimize influence on sorption of the specific associations which exist in the crystalline state. The profound effect of crystallinity in cellulose on its water-sorbing capacity⁶ is well known.

The extent of crystallinity in Northcote's dextran remains unknown. It is known⁷ that by appropriate treatment some dextrans develop crystalline material, as shown by X-ray diffraction patterns. It was desirable, therefore, to investigate the sorption properties of known amorphous samples to define more clearly the relative contribution of the primary hydroxyl.

In addition to the effects of specific water-absorbing groups, molecular branching might also influence water sorption. The structure analyses² allow the possibility of large variations in degree and types of branching among the individual dextrans. Methylation and hydrolysis studies⁸ of a few dextrans show clearly that both degree and types of branching are important variables in the structures of dextrans. It was desirable also to investigate the influence of branching as a factor in water sorption, although to some extent the contributions of branching and water-absorbing groups might be undifferentiable in these dextrans.

Experimental

Dextrans.—The 17 different types and subfractions of native dextrans were selected for this investigation and made available by Dr. Allene Jeanes of this Division. They were purified² and fractionated⁹ as previously reported. They were dehydrated in ethanol or by lyophilization. All had amorphous X-ray diffraction patterns except one (dextran type NRRL B-1433).

Sorption Isotherms.¹⁰—About 0.5 to 1.0 g. of each dextran was weighed into each of two bottles. The bottles

(6) P. H. Hermans, "Contributions to the Physics of Cellulose Fibres," Elsevier, Amsterdam 1946.

(7) A. Jeanes, N. C. Schieltz and C. A. Wilham, *J. Biol. Chem.*, **176**, 617 (1948).

(8) R. J. Dimler, R. W. Jones, W. C. Schaefer and J. W. Van Cleve, *Abstr. Papers Am. Chem. Soc.*, **129**, 2D (1956).

(9) C. A. Wilham, B. H. Alexander and A. Jeanes, *Arch. Biochem. Biophys.*, **59**, 61 (1955).

(10) The water sorption measurements were made by Mrs. Mary Rose.

(1) One of the Divisions of the Agricultural Research Service, U. S. Department of Agriculture. Article not copyrighted.

(2) A. Jeanes, *et al.*, *J. Am. Chem. Soc.*, **76**, 5041 (1954).

(3) J. C. Rankin and A. Jeanes, *ibid.*, **76**, 4435 (1954).

(4) A. G. Assaf, R. H. Haas and C. B. Purves, *ibid.*, **66**, 66 (1944).

(5) D. H. Northcote, *Biochim. Biophys. Acta*, **11**, 471 (1953).

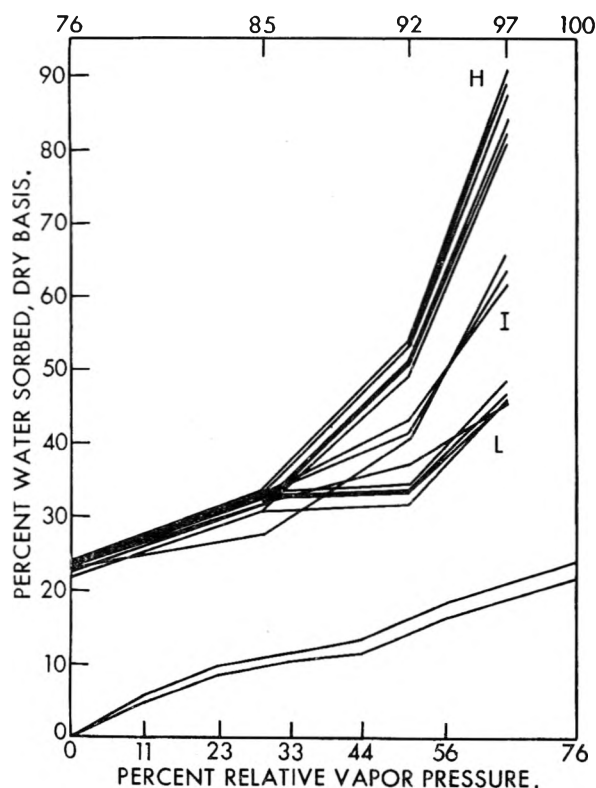


Fig. 1.—Water absorption (ascending) sequences of dextrans: upper diagram, humidity range 76 to 100%, as shown on the upper scale; lower diagram, humidity range 0 to 76%, as shown on the lower scale. The numbers on the scales indicate the humidities investigated.

were separated into two sets, undergoing absorption (consecutively higher humidities) and desorption (consecutively lower humidities) experiments. No duplicates were made because of the scarcity of some of the dextrans. All the samples were dried to constant weight in a vacuum oven at 105°. About 5 mg. of sodium pentachlorophenate was added to each sample to minimize growth of organisms.

Relative humidity (relative vapor pressure) was controlled by using saturated salt solutions in evacuated desiccators which were set in an insulated box in a room controlled at $25 \pm 1^\circ$. Although this arrangement does not give the highest precision, the data should allow comparison between samples. The insulated box retarded temperature fluctuations, and it can be assumed that samples and salt solutions were at the same temperature within a few tenths of a degree; fluctuations in relative humidity consequently should be small. Except for the highest and lowest humidities, water sorption results are estimated to be accurate within about 1% water content.

Weighings were made twice a week until weights were constant within 2 mg. The weights became constant in 2 to 6 weeks depending on the relative humidity. The absorption set was placed successively in desiccators at higher humidities. Desorption samples were first wet with an excess of water, placed in the highest humidity and then successively in the lower humidities.

X-Ray Diffraction Patterns.—X-Ray diffraction patterns were taken using a conventional powder diffraction unit, with flat film technique: 5-cm. film to sample distance, 1.5 hours exposure, with Ni filtered Cu radiation. Patterns were termed "amorphous" if only broad, diffuse halos could be seen, "crystalline" if the line pattern was more evident than the halo and "trace of crystallinity" if the line pattern was weak compared to the halo. Even a fairly strong X-ray line pattern does not imply more than about 30% of the crystalline material, and weak line patterns can result from only small fractions of crystalline material.

Results and Discussion

Water Absorption Isotherms.—Absorption data for all samples are presented for comparison in

Fig. 1. Data obtained at 76% and higher humidities are shown in the upper part of the figure. The lines connect data from each sample of dextran, to indicate individuality of dextran types and not the estimated isotherm. All data obtained below 76% humidity are included between the two lines shown in the lower part of Fig. 1. The most salient feature of the isotherms in the humidity region below 85% is their close similarity. Differences between samples are nearly insignificant up to 85% humidity, except for the lowest sorbing sample at 85% humidity (dextran B-1355 Frac. S). In this relative humidity range it would appear that the considerable variability in physical and chemical properties² among the various dextrans is not reflected in absorption behavior. This point will be discussed further below.

At humidities over 85% the water-absorption data (Fig. 1) diverge markedly. Although all dextrans cannot be distinguished in Fig. 1, the samples can be divided rather arbitrarily into 8 highly absorptive dextrans (H), 6 low-absorbing dextrans indicated by the essentially horizontal lines joining water sorption values at 85 and 92% humidity (L) and 3 of intermediate absorption (I). In view of the known crystallizability of some types of dextran⁷ it appeared likely that the lowered absorption of some of the dextrans at high humidity was the result of crystallization of dextran in these samples as humidity was increased.

Crystallization of Dextrans.—In line with the above reasoning the crystallization of the dextrans was investigated. A separate set of dextran samples was dried and given a sequence of humidity treatments of 1 week each at 85, again at 85 and finally at 92% relative humidity (R.H.). X-Ray diffraction patterns of the dextran samples were obtained in the condition as received, and again after each humidity treatment. Results of this experiment are given in Table I, which lists the dextrans in order of descending absorption at 92% R.H. The first 8 dextrans compose the group (H) in Fig. 1, the last 6 dextrans are the group (L) and the other 3 are in group (I).

The patterns were either amorphous (A in Table I) or crystalline. The crystalline-type L-1 patterns were identical to those previously reported⁷ by others. The L-3 patterns were identical to the previously reported patterns except that the diameters of the diffraction rings on the films were about 3% smaller. Two other patterns were observed, which were termed L-5 and L-6. The L-5 pattern appeared to be identical to the pattern observed for dextran B-523 by Jeanes, *et al.*,⁷ but was more intense. It had Bragg spacings at 9.7-(m), and 4.2-(m) Å. and an additional diffuse ring at 5.2-(m) Å. The L-6 pattern was very diffuse and had spacings at 20.6(s), 11.1(m), 8.4(w), 4.5(s), 3.8(w) and 3.3(w) Å. The letters s, m and w indicate relative intensities of strong, medium and weak.

It is evident that all the dextran samples except B-1433 were initially amorphous. This one dextran had the L-5 pattern. The observed pattern was weak, indicating only a trace of observable crystallinity.

TABLE I
 X-RAY DIFFRACTION PATTERNS OF HUMIDIFIED NATIVE DEXTRANS

Water absorption at 92% R.H.	Dextran		X-Ray diffraction patterns ^a				Linkages ^b		
	NRRL strain	Fraction	Before humidification	85% R.H. 7 days	85% R.H. 14 days	92% R.H. 7 days	1-6	1-4	1-3
High									
54	B-1424		A	A	A	A	72	28	0
53	B-1377		A	A	A	A	84	7	9
53	B-1525		A	A	A	A	83	17	0
51	B-742	L	A	A	A	A	81	19	0
51	B-1299	L	A	A	A	A	58	36	6
51	B-1433		tr L-5	tr L-5	..	tr L-5	63	30	7
50	B-1398		A	A	A	tr L-3	70	11	19
49	B-1254	L	A	A	A	A	69	31	0
Intermediate									
43	B-742	S	A	A	tr L-3	L-3	57	17	26
42	B-1254	M-R	A	A	A	tr L-1	90	4	6
41	B-1355	S	A	L-6	L-6	L-6	58	6	36
Low									
37	B-1355	L	A	tr L-1	L-1	L-1	89	11	0
34	B-1254	B-4F	A	tr L-1	L-1	L-1	94	4	2
34	B-512-E		A	A	A	L-1	95	5	0
34	B-1146		A	A	L-1	L-1	97	3	0
33	B-1064		A	tr L-1	L-1	L-1	96	4	0
32	B-1308		A	A	L-1	L-1	94	6	0

^a A, amorphous; tr denotes a trace of pattern.

Over the course of the equilibration the diffraction patterns of the high absorption dextrans remained the same, or developed only very faint traces of crystallinity. The diffraction pattern of dextran B-1433 remained weak.

In contrast, all other dextrans developed crystallinity on continued exposure to water vapor, and most developed good crystalline patterns. It is evident that the depressed water-absorbing power shown by the intermediate and low-absorbing dextrans at high R.H. is directly correlated with the development of X-ray diffraction crystallinity. It can be inferred, therefore, that the main observable factor which affected water sorption in dextrans was the presence of crystalline material; the various structural types appear to be nearly equivalent in water-sorption power, except as they affect crystallinity.

There are some points of comparison between water sorption and crystallinity of individual dextrans. After 1 week at 85% R.H. dextran B-1355 Frac. S developed relatively good crystallinity, in agreement with the observed lowest water sorption at 85% R.H. visible in Fig. 1. In contrast after 2 weeks at 85% R.H. 6 dextrans developed at least moderately good crystallinity, but only 1 dextran, the B-1355 Frac. S, showed relatively lower water sorption than most dextrans at 85% R.H. Thus, there are some minor exceptions to the parallelism of depressed water sorption and crystallinity. It is possible that the very small samples used for the X-ray analyses might have reached equilibrium more quickly, or possibly humidities were not controlled sufficiently accurately. Further, at lower humidities crystallization should be slower; therefore, the apparent break in the isotherms of the dextrans which crystallize may be mainly a matter of comparing

the time duration of the sorption experiments with the time for an appreciable amount of crystallization to occur.

Data in Table I show there is some correlation between structure, as given by the proportions of different linked units, and the crystallizability of the dextrans. In general, the dextrans which crystallized best were the most nearly "linear"; *i.e.*, they contained the highest proportions of 1,6-linked units. Further, "branching," as indicated by lowered proportions of 1,6-linked units, appeared to hinder crystallization, as might be expected. In general highly branched high polymers crystallize poorly.

Dextran B-1355 Frac. S developed crystallinity on humidification, although the proportion of 1,6-linked units was low. Evidence from complex formation with cuprammonium¹¹ and from methylation techniques⁸ has been offered that this dextran has some 1,3-linked units in the linear chain segments and contains roughly as many branch points as dextran B-512. Thus, this dextran is less branched than the maximum consistent with the periodate analysis. Its crystallizability is consistent with this relative linearity.

The behavior of dextran B-742 Frac. S was unexpected. It crystallized on humidification and the water sorption was depressed; yet it had a relatively low content of 1,6-like linked units, and tentative methylation evidence⁸ indicated that this dextran was highly branched, and even had some doubly branched units. There appeared to be only about 28% of 1,6-linked units; the remainder were end units and branch points. Information from hydrolysis experiments⁸ suggested a large number of short branches. The question, then, arises as

(11) T. A. Scott, N. N. Hellman and F. R. Senti, *J. Am. Chem. Soc.*, **79**, 1178 (1957).

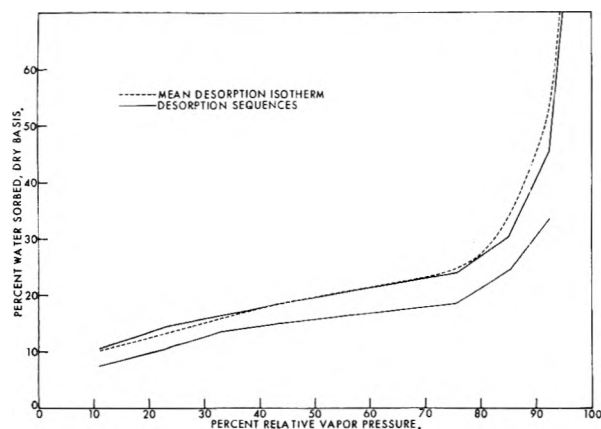


Fig. 2.—Water desorption sequences of dextrans which crystallized at high humidity compared to the mean amorphous desorption isotherm. The two solid lines enclose the data of all crystallizable dextrans.

to what structure could crystallize in this dextran. Perhaps the molecular structures composing crystalline regions are regular sequences of single unit branches arranged along the main chains. The observed L-3 pattern raises the question whether the crystalline regions might in fact be composed of 1,6'-linked chains because this type of pattern was observed in B-512 dextran preparations.⁷ This alternative scheme requires that the relatively few 1,6-linked units be disposed consecutively in segments long enough and numerous enough to crystallize. Molecular heterogeneity is a third possibility to explain this anomalous behavior.

Water Sorption of Amorphous Dextrans.—X-Ray studies showed that the eight dextrans which absorbed the most water at high humidities did not crystallize appreciably. This evidence for no structural changes during humidification indicates that the water sorption data for these dextrans were near the true equilibrium values at all humidities. Because of the experimental identity of their water absorption sequences as evident in Fig. 1, these "amorphous" dextrans can be most simply described by their mean absorption values at each humidity, which are given in Table II. Since all dextrans were initially amorphous, the absorption means up to 75% relative humidity include all dextran data. At higher humidities the absorption values include only data for the highly absorbing, "amorphous" dextrans. Means of the data (\bar{X}) and their coefficients of variation $100 S/\bar{X}$ (percentage of mean value) are given in Table II. Standard deviations (S) were computed with allowance for small numbers of samples. Coefficients of variation of the mean absorption isotherm, only a few per cent. at each humidity, demonstrate the nearly identical behavior of the dextrans on absorption.

Desorption data of the eight amorphous dextrans were also similar.¹² Their mean desorption values appear in Table II. The coefficients of variation of the desorption data are larger than the absorption values. This may be the result of maintaining

(12) The desorption isotherm of dextran B-1377 was exceptional. It was higher by approximately 3% of water sorbed over the entire measured range. This discrepancy is probably an error of measurement as only one sample was involved.

the desorption samples at high moisture content with subsequent development either of traces of crystallinity or of compact masses which lost water too slowly to observe.

TABLE II

R.H., %	Absorption		Desorption	
	\bar{X} , % water, dry basis	$100 S/\bar{X}$, % of \bar{X}	\bar{X} , % water, dry basis	$100 S/\bar{X}$, % of \bar{X}
11.2	5.4	4	10.1	12
22.6	9.0	3	13.3	9
32.5	11.0	3	16.0	8
43.5	13.1	3	18.4	7
56.4	17.7	3	20.6	7
75.4	23.5	2	24.0	6
85.0	32.5	3	33.1	5
92.5	51.7	3	52.9	5
97.0	84.6	5	88.6	5

Considerable hysteresis in water sorption at low humidities is apparent in the data in Table II but virtually none was present at 75% R.H. or higher. The mean of the differences between individual desorption and absorption pairs is 0.3% water sorbed at 75% R.H., if one dextran is ignored,¹² and 2.6% water sorbed at 56% R.H. Thus, the character of sorption changes abruptly in this humidity range. The disappearance of hysteresis above 75% R.H. is one indication of essentially solution behavior. Most of the dextrans examined were in fact water soluble. Other experiments¹³ have shown that the high humidity sorption can be interpreted according to the theory developed by Flory and Huggins to describe random coil high polymers in solution.¹⁴

The continuation of such solution behavior to as low as 24% water (dry basis) probably means that the dextran molecules associate only slightly, even in concentrated solutions, or that they are relatively flexible.

Water Sorption of Crystallizable Dextrans.—The crystallizability of the intermediate and low water-absorbing dextrans is well correlated with their diminished water absorptions at high humidity. Their desorption isotherms were obtained after wetting the samples with excess water; presumably these isotherms represent the behavior of the partly crystallized dextrans. The two solid lines in Fig. 2 enclose all the desorption data of the intermediate and lower absorbing dextrans. The dashed line shows the mean desorption isotherm of the "amorphous" dextrans. Most data fall below the average amorphous dextran desorption isotherm. Such depressed sorption would be expected if the samples had crystallized.

Northcote's⁵ recently reported absorption and desorption isotherms of a dextran showed considerably less water absorption at high humidities than the amorphous dextrans reported here. This difference may be the result of crystallinity present in Northcote's dextran. His desorption isotherm lies within 1% water content of our lowest observed desorption isotherms, indicated by the lower solid line in Fig. 2.

(13) N. W. Taylor, J. E. Cluskey and F. R. Senti, observations to be published.

(14) M. L. Huggins, *Ann. N. Y. Acad. Sci.*, **44**, 431 (1943).

Site-bound Water and Relationship to Dextran Structure.—The general interpretation of the convex (to the humidity axis) portion of the isotherm at low humidities is that in this region water is absorbed on some localized "surface" or hydration sites. Various theoretical treatments give measures of these sorption sites in the sample. The treatment developed by Hailwood and Horrobin¹⁵ can be applied in the region of the lower half of the humidity scale, and it was used by Northcote⁵ in characterizing his polysaccharides.

In the Hailwood-Horrobin treatment, three parameters are determined by a curve fitting procedure.¹⁶ From these can be deduced the weight of dextran associated with 1 mole of theoretical water-binding sites. From our mean "amorphous" isotherms were determined the values of 177 g. from absorption and 123 g. from desorption. These values are only approximate; because of a rather irregular shape of the isotherm, curve fitting was not precise. When these values are compared with the molecular weight of the glucose residue, 162, the calculated figures roughly agree with the concept that every glucose residue is accessible

(15) A. J. Hailwood and S. Horrobin, *Trans. Faraday Soc.*, **42B**, 84 (1946).

(16) C. H. Nicholls and J. B. Speakman, *J. Textile Inst.*, **46**, T264 (1955).

and can form a hydrate with 1 molecule of water. However, the significance of this agreement is obscure.

The fact that the absorption isotherms of all dextran samples were nearly identical at low humidities is evidence in agreement with Northcote⁵ and contrary to the concept that the primary 6-hydroxyl groups are the principal water-binding sites. From the analyses of Jeanes, *et al.*,² presented in Table I, these dextrans range in primary hydroxyl content from as low as 5% to at least 40% of the number of glucose residues, if it is assumed that the various types of linked units have the meanings suggested by Rankin and Jeanes.³ A directly proportional variation should be found in numbers of sorption sites and, hence, in water absorption at low humidities if the primary hydroxyls were the principal binding sites for water.

This investigation does not rule out a relatively stronger hydrogen bond in primary hydroxyl interactions. First, the most reactive groups should be saturated at low humidities, and perhaps an investigation of lower humidities would discover differences in sorptive power among the dextrans before saturation is complete. Moreover, it is possible that the most reactive water-binding groups are satisfied to a correspondingly greater extent by bonding to other polymer groups.

HEAT STABILITIES AND VOLATILITIES OF METAL CHELATES DERIVED FROM 8-HYDROXYQUINOLINE

BY ROBERT G. CHARLES AND ALOIS LANGER

Westinghouse Research Laboratories, Pittsburgh 35, Pennsylvania

Received September 24, 1958

The behavior of eighteen metal 8-hydroxyquinolates upon heating *in vacuo* has been investigated. Many of the compounds were observed to sublime completely, without appreciable decomposition, over fairly narrow temperature ranges. The temperature range of volatilization was found to be a function of metal ion electronegativity for the divalent metal 8-hydroxyquinolates. In contrast to this behavior, nearly all of the trivalent metal 8-hydroxyquinolates volatilized over the same temperature range, 250 to 350°. Sublimation of the Ca(II) and Bi(III) 8-hydroxyquinolates was accompanied (or preceded) by significant decomposition, while the Ba(II), Sr(II) and La(III) compounds did not sublime appreciably, but decomposed at sufficiently high temperatures.

Recent interest¹⁻³ in metal chelate polymers has made desirable a more complete knowledge of the heat stabilities characteristic of the various metal chelate ring systems which might be incorporated into such polymers. A number of workers^{4,5} have investigated the heat stabilities, in air, of the metal 8-hydroxyquinolates I, chiefly from the standpoint of establishing suitable drying temperatures for these compounds. Under the conditions used by these authors the chelates may be subjected to oxidative attack as well as to pyrolysis. It was the purpose of the present investigation to determine the behavior of the 8-hydroxyquinolates when heated in the absence of oxygen.

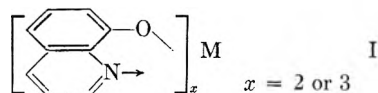
(1) W. C. Fernelius, Wright Air Development Center, Report WADC 56-203 (Oct. 1956).

(2) J. P. Wilkins and E. L. Wittbecker, U. S. Patent 2,659,711 (Nov. 17, 1953).

(3) K. V. Martin, *J. Am. Chem. Soc.*, **80**, 233 (1958).

(4) C. Duval, "Inorganic Thermogravimetric Analysis," Elsevier Pub. Co., New York, N. Y., 1953.

(5) M. Borrel and R. Paris, *Anal. Chim. Acta*, **4**, 267 (1950).



The experimental method used in this work involved following sample weight loss *in vacuo* as a function of temperature, as the temperature was increased linearly with time. Because of the apparent non-volatility of most of the 8-hydroxyquinolates in air, it was hoped that, under the present conditions, decomposition would occur at temperatures below those required to volatilize the unchanged chelates. In practice this has been found to be true for only a small number of the compounds examined.

Experimental

Preparation of Compounds.—The metal 8-hydroxyquinolates were prepared in high purity by precipitation from aqueous solution, using conventional analytical procedures.⁶

(6) R. G. W. Hollingshead, "Oxine and Its Derivatives," Vols. I and II, Butterworths Publications, London, 1954.

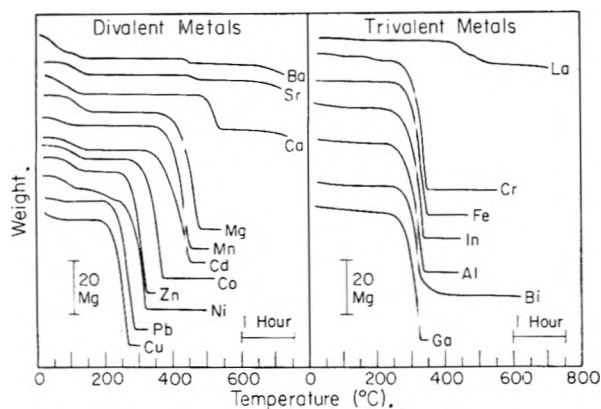


Fig. 1.—Weight loss curves for metal 8-hydroxyquinolates *in vacuo*. Fifty-mg. samples were used. For clarity curves are displaced along the ordinate.

The chelates were collected in sintered glass crucibles and washed thoroughly with hot water to remove excess 8-hydroxyquinoline. To facilitate handling, the chelates were dried by allowing to stand at room temperature in the open air for a period of one week (protected from dust and strong light) and then stored in stoppered vials. Most of the compounds contained water of hydration after this period, although the amount of water may not have been the same as initially present in the air-dried precipitates. The water contents for a number of the compounds were established by drying weighed portions of the hydrated compounds in air in an oven maintained at the approximate midpoint of the temperature ranges recommended by Duval⁴ to obtain the anhydrous compounds. Per cent. weight losses obtained were: Cu, 5.8; Ni, 9.9; Co, 9.7; Zn, 9.4; Cd, 9.7; Mn, 5.0; Mg, 11.5; Ca, 12.6; Al, 3.1; In, 1.9; Fe, 0.5; Cr, 1.9; La, 1.0.

Apparatus.—An automatic recording vacuum thermobalance constructed in these laboratories was used for the present studies. The sample to be heated was contained in a shallow platinum crucible which was suspended by a fine nichrome wire from one end of a light quartz beam. This load was balanced at the other end of the beam by a small cylindrical permanent magnet suspended within a solenoid. The beam was supported by jewel bearings. Weight changes were recorded automatically as a function of time in terms of the current supplied to the solenoid to maintain balance. Weight changes of 0.1 mg. could be detected readily.

The entire balance, and the sample, were surrounded by a glass and quartz envelope which could be evacuated to 10^{-6} mm. The tube surrounding the sample was of quartz and was contained in a cylindrical tube furnace mounted vertically. Temperature was plotted automatically as a function of time, using a thermocouple in close proximity to the sample. The temperature of the tube furnace was varied with time by means of a Variac variable transformer driven by a synchronous motor and reducing gear system. By starting a run at a voltage setting of 30, a nearly linear temperature-time plot was obtained.

Procedure.—The apparatus was assembled using a 50.0-mg. sample of the 8-hydroxyquinolate (finely powdered as obtained by precipitation). The system was evacuated and heating begun. After the run was completed any appreciable residue remaining in the sample container was stored in a desiccator for analysis. Where possible, any sublimate on the walls of the tube surrounding the sample was scraped into a vial with a wire. The sublimate was then dried in a vacuum oven at 100° for an hour to remove any water adsorbed from the air during the scraping procedure and finally the infrared spectrum ($3\text{--}15\ \mu$) of the sublimate was determined in KBr. The resulting spectra were compared with those of the authentic anhydrous 8-hydroxyquinolates. The latter were obtained by drying the chelates in air at the temperatures recommended by Duval.^{4,7}

(7) Duval⁴ does not give suitable drying temperatures for the Pb and Ga compounds. In the present work these were dried in a vacuum oven at 100° .

The weight-time and temperature-time curves obtained from the runs were used to construct the curves given in Fig. 1. The latter curves are very different from those reported for the same chelates in air.^{4,5} Duplicate curves were reproducible to about $\pm 4^{\circ}$ throughout their more vertical portions, when plotted as in Fig. 1.

Results and Discussion

Figure 1 shows the weight loss-temperature curves obtained for the metal 8-hydroxyquinolates *in vacuo*. These curves are very different from those reported for the same chelates in air.^{4,5}

Weight losses up to a temperature of about 200° in Fig. 1 are due in all cases to loss of water of hydration. That this is true is shown by close correspondence of the weight losses up to 200° in Fig. 1 with the weight loss data obtained by heating the compounds to constant weight in air (Experimental section). Similar initial weight losses due to water of hydration are observed in the curves obtained in air by other workers.^{4,5}

The nature of the curves above 200° in Fig. 1 permits dividing the 8-hydroxyquinolates into two classes. The first group of compounds, derived from Cu, Ni, Co, Zn, Cd, Mg, Pb, Al, Ga, In, Fe and Cr volatilize almost completely over fairly narrow temperature ranges. The remaining 8-hydroxyquinolates volatilize only partially over the temperature range studied.

The volatilization of the first class of chelates involves simple sublimation of the unchanged 8-hydroxyquinolates. For all of these runs apparently homogeneous but non-crystalline sublimate formed on the quartz tube above the furnace throughout the temperature ranges corresponding to weight loss in Fig. 1. The sublimate had the colors expected for the anhydrous 8-hydroxyquinolates. Only traces (0.5 mg. or less) of black residue remained in the sample containers at the end of the runs.

The design of the apparatus, and the small size of the samples, made recovery of the sublimed compounds difficult. For the Cu, Co, Mn, Zn, Cd, Mg, Pb, Al, Ga, In, Fe and Cr compounds, however, sufficient sublimed material was recovered to permit obtaining infrared spectra. These spectra were found to be essentially identical with the spectra of authentic samples of the anhydrous 8-hydroxyquinolates which had been dried in air.⁷ With the exception of the copper compound no additional peaks were noted in the spectra of the sublimed compounds which could be ascribed to decomposition products. A small absorption peak at 726 cm.^{-1} was present in the spectrum of the sublimed copper chelate which was not found in the spectrum of the air-dried material. Since the remainder of the two spectra were identical, this peak may be due to a difference in crystal structure between the two samples rather than to the presence of impurities in the sublimed material.

The Ca and Bi 8-hydroxyquinolates also sublimed to some extent, but for these compounds significant amounts of black residue were left in the sample container at the conclusion of the runs. Large amounts of black residue were left by the Sr, Ba and La chelates. The latter three compounds were not observed to sublime appreciably and the weight losses observed were due to decomposition.

Elemental analyses were obtained for the residues from the Ca, Sr, Ba, La and Bi compounds.⁸ Unlike the results found in air,^{4,5} where the ultimate residues are usually the metal oxides, the residues obtained here contained considerable amounts of carbon and nitrogen, and some hydrogen, as well as metal. An attempt was made to determine the infrared spectra of the Ba and Ca residues in KBr pellets. No recognizable absorption peaks were observed in the wave length region 3 to 15 μ , indicating that complete destruction of the starting chelates had occurred. It is striking that decomposition of the Ba and Sr chelates proceeds with only a small loss of weight. Most of the decomposition products must therefore be non-volatile.

Because of the observed volatilities of the unchanged chelates it is difficult to compare the heat stabilities of the 8-hydroxyquinolates among themselves under the conditions used here. It is also difficult to compare the stabilities *in vacuo* with those observed in air.^{4,5} It is interesting, however, that some of the 8-hydroxyquinolates (notably the Mg and Mn compounds) show no decomposition at temperatures in excess of 400°. Insofar as a comparison is possible, the 8-hydroxyquinolate chelates appear less stable in air than *in vacuo*. This is reasonable in view of the possibilities of reaction with molecular oxygen in air.

From Fig. 1 it will be noted that, for the divalent metal chelates which sublime, the temperature range over which sublimation takes place is a function of the metal present. In contrast to this behavior the trivalent metal 8-hydroxyquinolates all sublime in the same temperature range, 250 to 350°.

According to the Langmuir equation⁹ the rate of evaporation of a subliming substance *in vacuo*

(8) Elemental analyses of the residues left by the 8-hydroxyquinolates of the indicated metals (% C, H and N, respectively): Ca, 63.1, 3.1, 7.6; Sr, 53.5, 1.6, 5.5; Ba, 43.1, 2.1, 6.1; La, 50.7, 1.7, 2.0; and Bi, —, —, 3.1. Only N was determined for the Bi residue.

(9) A. Weissberger, ed., "Technique of Organic Chemistry," Vol. IV, Interscience Pub., Inc., New York, N. Y., 1951, p. 501.

at a given temperature should be a function of the vapor pressure, molecular weight and surface area of the substance. Since the molecular weights of many of the divalent metal 8-hydroxyquinolates are similar, the observed differences in temperature range for these compounds in Fig. 1 must be due primarily to differences in vapor pressure and/or surface area.

$$Q = P/\sqrt{2\pi MRT} \quad (1)$$

where Q is the evaporation rate per unit area, P is the vapor pressure of the compound, M is the molecular weight, R is the gas constant and T is the absolute temperature.

It is interesting that a relationship appears to exist between the temperature range of sublimation for the divalent metal 8-hydroxyquinolates and the electronegativities¹⁰ (X_M) of the bonded metal ions. The order of decreasing X_M for these metals is Cu > Ni > Co > Pb > Zn, Cd > Mn > Mg > Ca. With the exceptions of Pb and Zn this is also the order of increasing temperature of sublimation. Since no relation between X_M and surface area would be expected, the observed relation between X_M and sublimation temperature probably is the consequence of a relationship between X_M and vapor pressure for these compounds. Since the vapor pressure is determined, at least in part, by intermolecular forces in the solid compounds, these forces must decrease with increasing values of X_M . The lack of dependence upon X_M of the sublimation temperature range for the trivalent metal 8-hydroxyquinolates may be due to the additional shielding of the metal atom by the third 8-hydroxyquinolate residue present in these molecules.

Acknowledgments.—The writers are grateful to Mrs. M. A. Pawlikowski for the preparation of some of the 8-hydroxyquinolates, to Dr. H. Lady for the infrared determinations, and to Miss M. A. Knuth for help with some of the sublimation studies.

(10) W. Gordy and W. J. O. Thomas, *J. Chem. Phys.*, **24**, 439 (1956).

HEATS OF FORMATION OF FERROUS CHLORIDE, FERRIC CHLORIDE AND MANGANOUS CHLORIDE

By MARY F. KOEHLER AND J. P. COUGHLIN¹

Contribution from the Minerals Thermodynamics Experiment Station, Region II, Bureau of Mines, United States Department of the Interior, Berkeley, Cal.

Received September 27, 1958

Heats of formation from the elements of anhydrous ferrous chloride, ferric chloride and manganous chloride were determined by measuring appropriate heats of solution and reaction in hydrochloric acid. The results obtained are as follows: ferrous chloride, -81.86 ± 0.12 ; ferric chloride, -95.7 ± 0.2 ; and manganous chloride, -115.19 ± 0.12 (kcal./mole at 298.15°K.).

Previously existing^{2,3} values of the heats of formation of the chlorides of iron and manganese are

(1) Formerly physical chemist, Minerals Thermodynamics Experiment Station, Bureau of Mines, Region II, Berkeley, Calif.

(2) F. D. Rossini, D. D. Wagman, W. H. Evans, S. Levine and I. Jaffe, Natl. Bur. Standards Circ. 500, 1952.

(3) O. Kubaschewski and F. L. Evans, "Metallurgical Thermochemistry," John Wiley and Sons, Inc., New York, N. Y., 1956.

based upon rather old and somewhat uncertain thermochemical measurements. It is difficult to appraise the accuracy of these values. (Selected data in the two references cited differ by as much as 3.3 kcal./mole.) As a consequence, new determinations appeared desirable. The present paper reports new values for anhydrous ferrous chloride,

ferric chloride and manganous chloride, obtained by solution calorimetry.

Materials.—Iron powder was prepared from ferric hydroxide, obtained by dissolving pure iron wire in sulfuric acid and precipitating with ammonia. The ferric hydroxide was washed, dried at 140° and crushed to -100 mesh. It then was reduced with hydrogen for 5.5 hr. at 500°, after which the metallic clumps were broken up and again treated with hydrogen for 5.5 hr. at 500°. The oxygen content of the product as it was used in the measurements ranged from 0.10 to 0.22%.

The ferrous chloride was prepared by Kelley and Moore.⁴ It was retreated before use in the present measurements by drying in a stream of hydrogen chloride for 5 hr. at 450° and 6 hr. at 460–475°. Tests for ferric iron (thiocyanate method) indicated 0.005% (equivalent to 0.015% ferric chloride). Analysis gave 44.06% iron and 56.10% chlorine, as compared with the theoretical 44.06 and 55.94%.

Ferric chloride was prepared by the reaction of high-purity iron wire and dry hydrogen chloride gas near 350°. The ferric chloride sublimed in the hot zone and condensed downstream on the cooler parts of the tube wall. The condensate was removed and resublimed in dry hydrogen chloride. Tests for ferrous iron indicated 0.006% (equivalent to 0.014% ferrous chloride). Analysis gave 34.41% iron and 62.42% chlorine, as compared with the theoretical 34.43 and 65.57%.

Reagent grade hydrogen peroxide was used at concentrations of 12.76 to 13.73%. Analysis of the hydrogen peroxide will be discussed later.

The manganese was an electrolytic product furnished by the Boulder City, Nev., Station of the Bureau of Mines. The purity was stated to be 99.92%. It was degassed by heating in a stream of pure helium for 1.5 hr. at 990–1020°.

Manganous chloride was prepared from reagent grade manganous carbonate by K. C. Conway of this Laboratory. The carbonate was dissolved in hydrochloric acid and the solution was filtered and then evaporated until a good crop of crystals of the hydrated chloride was obtained. The crystals were transferred to a Pyrex tube and dehydrated by prolonged treatment with a stream of hydrogen chloride and nitrogen at 350°. Analysis of the product gave 43.71% manganese and 56.37% chlorine (theoretical values, 43.66 and 56.34%).

Methods and Results

The heats of formation of ferrous and manganous chlorides were obtained by calorimetric reaction schemes involving solution of the chlorides and the metals in hydrochloric acid. In the case of ferric chloride, an additional reaction step (the oxidation of ferrous ion by hydrogen peroxide) was necessary.

All measurements were made with previously described apparatus.^{5,6} The results are expressed in defined calories (1 cal. = 4.1840 abs. joules). All sample weights were corrected to vacuum and all formula weights accord with the 1954–1955 Report on Atomic Weights.⁷

All reactions were conducted in 1936.2 g. of 4.360 *m* hydrochloric acid; the preparation and standardization were discussed previously.⁸ The amounts of the other substances were 0.03 mole for the reactions used to obtain the heats of formation of the iron compounds and 0.02 mole for the reactions used to obtain the heat of formation of manganous chloride.

Each individual heat of reaction measurement was accompanied by a calibration of the calorimetric system. The calorimeter surroundings were

maintained 30.00 ± 0.01°, and all results were corrected to exactly 30.00° (303.15°K.).

Ferrous Chloride.—Table I gives the equations for the reactions used to determine the heat of formation of ferrous chloride and the mean values of the heats and the precision uncertainties. Reactions 1 and 2 were measured consecutively in the same batch of acid; reactions 3 and 4 were measured consecutively in another batch of acid. Thus the final solutions after conducting reactions 1 and 2, and after conducting reactions 3 and 4, are identical and $\Delta H_1 + \Delta H_2 - \Delta H_3 - \Delta H_4$ yields the heat, ΔH_5 , of the resultant over-all calorimetric reaction.

TABLE I
HEAT OF FORMATION OF FERROUS CHLORIDE

Reaction	$\Delta H_{303.15^\circ}$, cal.
(1) $\text{Fe}(\alpha) + 2\text{H}^+(\text{soln}) = \text{Fe}^{++}(\text{soln}) + \text{H}_2(\text{g})$	-20,820 ± 40
(2) $2(\text{HCl} \cdot 12.731\text{H}_2\text{O})(\text{l}) = 2\text{H}^+(\text{soln}) + 2\text{Cl}^-(\text{soln}) + 25.462\text{H}_2\text{O}(\text{soln})$	0 ± 10
(3) $\text{FeCl}_2(\text{c}) = \text{Fe}^{++}(\text{soln}) + 2\text{Cl}^-(\text{soln})$	-15,000 ± 20
(4) $25.462\text{H}_2\text{O}(\text{l}) = 25.462\text{H}_2\text{O}(\text{soln})$	-2,030 ± 20
(5) $\text{Fe}(\alpha) + 2(\text{HCl} \cdot 12.731\text{H}_2\text{O})(\text{l}) = \text{FeCl}_2(\text{c}) + \text{H}_2(\text{g}) + 25.462\text{H}_2\text{O}(\text{l})$	-3,790 ± 50

At 298.15°K.; $\Delta H_5 = -3,790 - 270 = -4,060 \pm 50$

Six determinations of reaction 1 were made, yielding -20,860, -20,780, -20,780, -20,850, -20,810 and -20,870 cal. These results contain a correction of -338 cal. for heat absorbed in vaporizing water and hydrogen chloride by the escaping hydrogen and a correction of 4 cal. for the heat evolved in reducing a small amount of chloroplatinic acid used as a catalyst for the reaction. The correction for the oxygen content of the metal ranged from -3 to -8 cal., depending upon the time of storage of the sample.

Reaction 2 is necessary to maintain stoichiometry. Only a single heat measurement was made to confirm previous work⁹ in which substantially this same reaction was measured and found to have virtually zero heat effect.

Six measurements of the heat of reaction 3 were conducted, the values being -14,980, -14,980, -15,000, -15,000, -15,010 and -15,000. The calculated correction for the ferric chloride content of the ferrous chloride is about 1 cal., a negligible amount.

Substantially the same reaction as reaction 4 has been investigated previously.⁹ Two additional heat determinations were made to confirm the previous results. In the first, the water was added to the calorimeter in three equal portions. The measured heats were -676, -672 and -666 cal., making a total of -2,014 cal. for 25.462 moles of water. In the second, the total required amount of water was added in one step, and -2,060 cal. was the measured heat effect. These two measurements and the three previous ones⁹ lead to -2,030 ± 20 cal. as the heat of reaction 4.

Reaction 5 represents the formation of ferrous

(4) K. K. Kelley and G. E. Moore, *J. Am. Chem. Soc.*, **65**, 1264 (1943).

(5) J. C. Southard, *Ind. Eng. Chem.*, **32**, 442 (1940).

(6) J. P. Coughlin, *J. Am. Chem. Soc.*, **77**, 868 (1955).

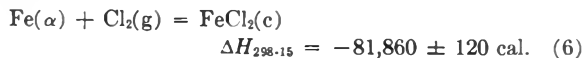
(7) E. Wichers, *ibid.*, **78**, 3235 (1956).

(8) J. P. Coughlin, *ibid.*, **78**, 5479 (1956).

(9) J. P. Coughlin, *THIS JOURNAL*, **62**, 419 (1958).

chloride, water and hydrogen from iron and hydrochloric acid. The heat was corrected to 298.15°K. by means of the heat capacity data of Kelley¹⁰ and Rossini.¹¹

The heat of formation of ferrous chloride from the elements was obtained from the heat of reaction 5 and the literature value² of the heat of formation of the hydrochloric acid ($-38,900 \pm 50$ cal./mole).



Ferric Chloride.—Table II summarizes the reactions used to obtain the heat of formation of anhydrous ferric chloride. Reactions 7–10 were conducted consecutively in the same batch of hydrochloric acid and reactions 11 and 12 likewise were conducted in another batch of acid. The summation, $\Delta H_7 + \Delta H_8 + \Delta H_9 + \Delta H_{10} - \Delta H_{11} - \Delta H_{12}$, gives ΔH_{13} for the over-all calorimetric reaction.

TABLE II
HEAT OF FORMATION OF FERRIC CHLORIDE

Reaction	$\Delta H_{298.15}$, cal.
(7) $\text{Fe}(\alpha) + 2\text{H}^+(\text{soln}) = \text{Fe}^{++}(\text{soln}) + \text{H}_2(\text{g})$	$-20,820 \pm 40$
(8) $2(\text{HCl} \cdot 12.731\text{H}_2\text{O})(\text{l}) = 2\text{H}^+(\text{soln}) + 2\text{Cl}^-(\text{soln}) + 25.462\text{H}_2\text{O}(\text{soln})$	0 ± 10
(9) $\text{Fe}^{++}(\text{soln}) + \frac{1}{2}(\text{H}_2\text{O}_2 \cdot 12.580\text{H}_2\text{O})(\text{l}) + \text{H}^+(\text{soln}) = \text{Fe}^{+++}(\text{soln}) + 7.290\text{H}_2\text{O}(\text{soln})$	$-31,350 \pm 40$
(10) $(\text{HCl} \cdot 12.731\text{H}_2\text{O})(\text{l}) = \text{H}^+(\text{soln}) + \text{Cl}^-(\text{soln}) + 12.731\text{H}_2\text{O}(\text{soln})$	0 ± 10
(11) $\text{FeCl}_3(\text{c}) = \text{Fe}^{+++}(\text{soln}) + 3\text{Cl}^-(\text{soln})$	$-24,460 \pm 20$
(12) $45.483\text{H}_2\text{O}(\text{l}) = 45.483\text{H}_2\text{O}(\text{soln})$	$-3,630 \pm 10$
(13) $\text{Fe}(\alpha) + 3(\text{HCl} \cdot 12.731\text{H}_2\text{O})(\text{l}) + \frac{1}{2}(\text{H}_2\text{O}_2 \cdot 12.580\text{H}_2\text{O})(\text{l}) = \text{FeCl}_3(\text{c}) + \text{H}_2(\text{g}) + 45.483\text{H}_2\text{O}(\text{l})$	$-24,080 \pm 70$

$$\text{At } 298.15^\circ\text{K.}, \Delta H_{13} = -24,080 - 410 = -24,490 \pm 70$$

Reactions 7 and 8 are identical with reactions 1 and 2 of Table I, and the same heats apply.

In studying reaction 9 (the oxidation of ferrous ion by hydrogen peroxide) weighed amounts of the peroxide solution were sealed in glass bulbs, which were broken in the calorimeter at the proper time. It was arranged that the amount of peroxide was slightly less than that required to oxidize all of the ferrous ion present. Determinations of the ferrous ion content of the calorimeter solution before the peroxide was added, and immediately after reaction 9 was complete, served to determine the actual amount of peroxide used in reaction 9. This procedure was necessary because of the inherent instability of the peroxide. There always was some decomposition during filling, sealing and storing of the bulbs. This made it impossible to know their exact peroxide contents, even though accurate weighings were conducted. Six measurements of the heat of reaction 9 gave $-31,340$, $-31,370$, $-31,410$, $-31,370$, $-31,280$ and $-31,350$ cal.

Reaction 10 involves the necessary additional

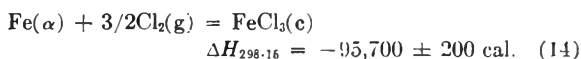
acid makeup after reaction 9, to maintain rigid stoichiometry. A single measurement was made to confirm that the heat of reaction 10 was virtually zero, as for the similar reaction 8.

Six measurements of reaction 11 gave $-24,440$, $-24,470$, $-24,450$, $-24,480$, $-24,460$ and $-24,440$ cal. The calculated correction for the ferrous chloride content of the ferric chloride is negligible (*ca.* 1 cal.).

Three measurements of reaction 12 gave $-3,630$, $-3,620$ and $-3,630$ for 45.483 moles of water.

Reaction 13 represents the formation of ferric chloride, hydrogen, and water from iron, hydrochloric acid and hydrogen peroxide solution. Correction of the heat to 298.15°K. was made by means of the heat capacity data of Kelley,¹⁰ Rossini,¹¹ and Giguere and co-workers.¹²

The heat of formation of ferric chloride from the elements was obtained from the heat of reaction 13 and literature values² of the heats of formation of hydrochloric acid ($-38,900 \pm 50$ cal./mole), water ($-68,320 \pm 10$ cal./mole), and hydrogen peroxide solution ($-45,660 \pm 200$ cal./mole).



Manganous Chloride.—Table III summarizes the measurements for obtaining the heat of formation of anhydrous manganous chloride. Reactions 15 and 16 yield the same end products and concentrations as reactions 17 and 18. Consequently, $\Delta H_{19} = \Delta H_{15} + \Delta H_{16} - \Delta H_{17} - \Delta H_{18}$.

TABLE III
HEAT OF FORMATION OF MANGANOUS CHLORIDE

Reaction	$\Delta H_{298.15}$, cal.
(15) $\text{Mn}(\alpha) + 2\text{H}^+(\text{soln}) = \text{Mn}^{++}(\text{soln}) + \text{H}_2(\text{g})$	$-51,610 \pm 40$
(16) $2(\text{HCl} \cdot 12.731\text{H}_2\text{O})(\text{l}) = 2\text{H}^+(\text{soln}) + 2\text{Cl}^-(\text{soln}) + 25.462\text{H}_2\text{O}(\text{soln})$	0 ± 10
(17) $\text{MnCl}_2(\text{c}) = \text{Mn}^{++}(\text{soln}) + 2\text{Cl}^-(\text{soln})$	$-12,470 \pm 20$
(18) $25.462\text{H}_2\text{O}(\text{l}) = 25.462\text{H}_2\text{O}(\text{soln})$	$-2,010 \pm 10$
(19) $\text{Mn}(\alpha) + 2(\text{HCl} \cdot 12.731\text{H}_2\text{O})(\text{l}) = \text{MnCl}_2(\text{c}) + \text{H}_2(\text{g}) + 25.462\text{H}_2\text{O}(\text{l})$	$-37,130 \pm 50$

$$\text{At } 298.15^\circ\text{K.}, \Delta H_{19} = -37,130 - 260 = -37,390 \pm 50$$

Six measurements of the heat of reaction 15 gave $-51,650$, $-51,540$, $-51,650$, $-51,590$, $-51,620$ and $-51,590$ cal. These results include a -329 cal. correction for vaporization of water and hydrogen chloride by the escaping hydrogen.

The heat of reaction 16 would be expected to be virtually zero, in view of results for similar reaction 2. A single measurement was made to confirm this.

Six heat determinations were made of reaction 17. The results were $-12,470$, $-12,450$, $-12,460$, $-12,460$, $-12,480$ and $-12,490$ cal.

Three determinations of the heat of reaction 18 were made, $-2,010$, $-2,000$ and $-2,000$ cal. It is to be expected that the heat of this reaction would be virtually identical with that of similar reaction 4.

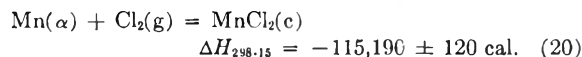
Correction of the heat of reaction 19 to 298.15°K.

(10) K. K. Kelley, U. S. Bur. Mines Bull. 477, 1950.

(11) F. D. Rossini, J. Research Natl. Bur. Standards, 4, 313 (1930).

(12) P. A. Giguere, B. G. Morissette, A. W. Olinas and O. Knop, Can. J. Chem., 33, 804 (1955).

was made, using heat capacity data from the literature.^{10,11} Combination of heat of reaction 19 with the heat of formation of hydrochloric acid² yields the heat of formation of manganous chloride from the elements.



Discussion of Results

It is believed that these new heat of formation values are an improvement over previously existing data, especially from the viewpoint of assigning uncertainties. The value for ferrous chloride is -360 cal./mole more negative than the result listed in previously mentioned compilations.^{2,3} However,

it is virtually identical with the value ($-81,900$ cal./mole) selected previously in connection with thermochemical measurements of fayalite,¹³ ferrous oxide¹⁴ and ilmenite.¹⁵ The value for ferric chloride is identical with the selection of Kubaschewski and Evans,³ but 1,100 cal./mole more positive than that of Rossini and co-workers.² On the other hand, the value for manganous chloride checks the selection of the latter workers and is 3,190 cal./mole more negative than that of the former.

(13) E. G. King, *J. Am. Chem. Soc.*, **74**, 4446 (1952).

(14) G. L. Humphrey, E. G. King and K. K. Kelley, U. S. Bur. Mines Rept. of Investigations 4870, 1952.

(15) K. K. Kelley, S. S. Todd and E. G. King, U. S. Bur. Mines Rept. of Investigations 5059, 1954.

EQUATION OF SOLUBILITY OF NONELECTROLYTES WHICH POSSESS A SPECIFIC INTERACTION

BY S. V. R. MASTRANGELO

Research Division Contribution No. 276, Jackson Laboratory, Organic Chemicals Department, E. I. du Pont de Nemours and Company, Wilmington, Delaware

Received September 29, 1953

An equation of solubility has been derived for two component systems which possess one or more similar interactions per molecule. The equation predicts the number, f , of interactions per molecule and the equilibrium constant, K . Good agreement with experimental data on the solubility of chlorofluoromethanes and ethanes in tetraethylene glycol dimethyl ether and of chloroform in acetone is shown.

The solubilities of a number of simple chlorofluorocarbons have been measured in tetraethylene glycol dimethyl ether. Interaction presumably occurs by formation of hydrogen bonds. All of the systems studied gave a linear plot when the activity coefficient, γ_r , of the solute was plotted against its activity, a_r (defined as the ratio (P/P_0) of its vapor pressure above the solution to the vapor pressure of the pure liquid solute at the same temperature). This linear relationship held in the region: $0 < a_r < 0.5$. When $a_r > 0.5$, a downward curvature was noted in most cases. Assuming two experimental parameters, this suggests an equation of the form shown by equation 1.

$$\gamma_r = K_1 + K_2 a_r + f(K_1, K_2) a_r^2 \quad (1)$$

where K_1 and K_2 are constants. Since an equation of this type allows experimental solubility data to be plotted directly and correlated very simply, it was felt that some theoretical justification might not only yield some needed insight on solubility theory in general but also provide a useful interpretation of the constants of equation 1.

Statistical Model.—The model which fits the systems studied regards the solvent as a number, fN_s , of energetically identical sites, where N is the total number of solvent molecules in solution and f is the number of active sites per molecule. For example, the solvent used was tetraethylene glycol dimethyl ether. This molecule has a theoretical maximum functionality, f , of 5, one for each unhindered ether link, when a simple solute such as dichlorofluoromethane (CHCl_2F) is used. The total number of solute molecules in solution is taken as N_r , of which Z are bound to some of the

fN_s solvent sites and $(N_r - Z)$ are free to occupy positions near the bound molecules in a manner that is energetically and statistically equivalent to that of the pure solute liquid.

It is to be noted that in this rather simplified model, the elements of the solvent molecule which are not part of the active sites, *e.g.*, the methylene groups in tetraethylene glycol dimethyl ether, are ignored. The fN_s available ether oxygens are considered as separate entities. Use of a coordination number is thus avoided.

Derivation of the Solubility Equation.—Derivation of the solubility equation follows simply by application of standard methods of statistical thermodynamics. For this purpose, the "quasi-chemical" treatment of Fowler and Guggenheim (p. 358)² was used with the "harmonic oscillator model" (p. 325)² for the liquid. The details of this treatment, using the proposed model, are straightforward after stating the partition functions for the bound and free solute molecules. These may be written according to equations 2 and 3, respectively.

$$Q = \frac{(fN_s)!}{(fN_s - Z)!(Z)!} \left[J \exp \frac{x + kT}{kT} \right]^Z \quad (2)$$

$$Q_0 = \frac{(N_r - 1)!}{(N_r - Z)!(Z - 1)!} \left[J_0 \exp \left(\frac{x_0 + kT}{kT} \right) \right]^{(N_r - Z)} \quad (3)$$

where

$$J \equiv \left[\frac{kT}{h\nu} \right]^3 J' \quad (4)$$

(1) E. A. Guggenheim, "Mixtures," Chapter XI, Oxford University Press, Amen House, London, 1952.

(2) R. H. Fowler and E. A. Guggenheim, "Statistical Thermodynamics," Cambridge University Press, Cambridge, 1939.

Except for the symbols defined previously, the nomenclature is essentially that of Fowler and Guggenheim.² By application of standard methods, it can be shown that the "quasi-chemical" type equation (cf. eq. 409.1)² for this system is given by equation 5.

$$(fN_s - Z_m)(N_r - Z_m) = \eta Z_m^2 \quad (5)$$

where $\eta \equiv J_0/J \exp((X_0 - X)/kT)$ and Z_m is the value of Z which maximizes the partition function. It also can be shown that equation 6

$$\frac{N_r - Z_m}{N_r} = P/P^0 \equiv a_r \quad (6)$$

results simply from expressions for the chemical potentials of the solute in solution and of the pure liquid solute derived from the partition functions. Substitution of equation 6 into equation 5 results in equation 7.

$$(K + 1)a_r[fN_s - N_r(1 - a_r)] = N_r(1 - a_r)^2 \quad (7)$$

where $(K + 1) \equiv 1/\eta$. Equation 7 is homogeneous in N_r , so that the following substitutions may be made easily after dividing both sides by $N_r + N_s$.

$$X_r \equiv \frac{N_r}{N_r + N_s} \quad (8)$$

$$X_s \equiv \frac{N_s}{N_r + N_s} = 1 - X_r \quad (9)$$

$$\gamma_r \equiv a_r/X_r \quad (10)$$

This leads to the solubility relationship given by equation 11

$$\gamma_r = K_1 + K_2 a_r + (1 - K_1 - K_2) a_r^2 \quad (11)$$

where

$$K_1 = \frac{1}{f(1 + K)} \quad (12)$$

and

$$K_2 = 1 + \frac{K - 1}{f(1 + K)} \quad (13)$$

Equation 11 is exactly the expression (equivalent to equation 1) which has been sought.

Refinements.—One obvious refinement of this treatment is to consider that the free solute molecules move in a potential field that is different from that of the pure liquid. It can be shown then that an additional parameter is required in the solubility expression such that equation 15 now obtains.

$$g\gamma_r = K_1 + K_2 g a_r + (1 - K_1 - K_2)(g a_r)^2 \quad (15)$$

where $g \equiv J_0/J_1 \exp(\chi_0 - \chi_1/kT)$. The zero subscripts refer to the free solute molecules and the "1" subscripts refer to the pure liquid solute. If the interactions become non-specific, $f = 1$ and $K = 1$, so that this treatment becomes equivalent to Guggenheim's (p. 30)¹ zeroth approximation for regular solutions. This leads to the familiar logarithmic relationship shown by equation 16.

$$\ln \gamma_r = B_r (1 - X_r)^2 \quad (16)$$

where B_r is a constant.

Ordinary Thermodynamic Treatment.—Equation 11 can be derived by application of ordinary thermodynamics. Consider the equilibrium specified by equation 17



such that

$$K = \frac{a_{rs}}{a_r a_s} \quad (18)$$

where r and s represent $(N_r - Z)$ moles of solute and $(fN_s - Z)$ moles of solvent, respectively, and rs represents Z moles of the bonded species. The values of a_{rs} , a_r and a_s are defined below as effective concentrations.

$$a_r = \frac{N_r - Z}{N_r + fN_s - Z} = \frac{X_r - \bar{Z}}{f + (1 - f)X_r - \bar{Z}} \quad (19)$$

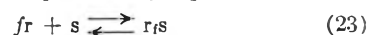
$$a_s = \frac{fN_s - Z}{N_r + fN_s - Z} = \frac{fX_s - \bar{Z}}{f + (1 - f)X_r - \bar{Z}} \quad (20)$$

$$a_{rs} = \frac{Z}{N_r + fN_s - Z} = \frac{\bar{Z}}{f + (1 - f)X_r - \bar{Z}} \quad (21)$$

where $\bar{Z} \equiv Z/N_r + N_s$. The right-hand terms of equations 19 to 21 were obtained by multiplying numerator and denominator by $N_r + N_s$ and making the substitutions prescribed by equation 8 and 9. This treatment differs from the usual chemical equilibrium treatment³ in that the probability expression, eq. 18, for the equilibrium constant does not distinguish between solute collisions with reacted and unreacted molecules. The usual expression for this latter situation is given by equation 22

$$K = \frac{a_{rs}}{a_r a_r'} \quad (22)$$

for the equilibrium expressed by equation 23



Equations 22 and 23 lead to rather complex expressions for the solubility relationships. However, the very simple expression, given by equation 11, may be derived by substituting equations 20 and 21 into equation 18 to yield equation 24

$$\bar{Z} = \frac{KfX_s a_r}{1 + Kc_r} \quad (24)$$

and eliminating \bar{Z} between equations 19 and 24. The expression for the activity coefficient of the solvent can be derived in an analogous manner. This is given by equation 25.

$$\gamma_s = \frac{f}{K + 1} + \left[1 + \frac{f(K - 1)}{K + 1} \right] a_s - \frac{Kf}{K + 1} a_s^2 \quad (25)$$

Experimental Plots of Activity Coefficient vs. Activity.—Equation 11 shows that a plot of γ_r vs. a_r will yield a straight line in regions of low activity ($0 \leq a_r \leq 0.5$). Table I lists the least squares values of K_1 (intercept) and K_2' (slope) obtained by application of equation 1 to a series of chlorofluorohydrocarbons in tetraethylene glycol dimethyl ether. The quadratic term was ignored. These data appear in another publication.⁴ The number of experimental points, their average and maximum per cent. deviation and the range of activity also are listed. In most cases, the data fit a straight line to within the experimental error of $\pm 2\%$.

In order to calculate the functionality, f , and the equilibrium constant, K , it is necessary to know the initial slope of the curve. This may be accomplished simply by calculating the quadratic coefficient of equation 11 and extrapolating back over

(3) J. H. Hildebrand and R. L. Scott, "The Solubility of Non-electrolytes," Reinhold Publ. Corp., New York, N. Y., 1955, Chap. XI.

(4) S. V. R. Mastrangelo, *Refrig. Engr.*, submitted for publication.

TABLE I

LINEAR SOLUBILITY RELATIONSHIPS FOR SOME SIMPLE CHLOROFLUOROHYDROCARBONS IN TETRAETHYLENE GLYCOL DIMETHYL ETHER

Solute	<i>t</i> , °C.	<i>P</i> ^o , p.s.i.a.	<i>K</i> ₁	<i>K</i> ₂ '	<i>f</i>	Calcd. slope ^a	Initial slope ^b	Dev., % Av. ^c	Max. ³	No. of points	Range of <i>a</i> _r
CHCl ₂ F	28.6	29.3	0.148	0.991	3	1.037	1.061	2.6	5.9	6	0-0.5
	56.0	66.5	.190	.983	3	0.953	0.983	0.2	0.8	5	0-0.3
CHClF ₂	28.6	169.7	.166	.919	3	1.010	.979	0.8	1.9	11	0-0.7
	56.0	326.1	.201	.904	3	0.932	.904	3.1	6.3	12	0-0.3
	86.0	609.1	.243	.874	3	.847	.874	1.4	3.2	17	0-0.15
	91.0	669.8	.253	.820	3	.827	.820	0.7	1.6	8	0-0.15
CH ₂ ClF	35.0	71.2	.240	.925	2	1.02	.991	.3	0.4	8	0-0.4
	54.4	123.5	.260	.925	2	0.980	.972	.2	0.3	6	0-0.25
	73.9	202.5	.276	.925	2	0.948	.925	.8	1.6	3	0-0.15
CHF ₂ CHF ₂	28.6	85.8	.213	1.057	2	1.074	1.057	1.5	2.9	9	0-0.2
	56.0	184.4	.285	0.925	2	0.931	0.925	0.5	0.7	6	0-0.3
	86.0	348	.364	.811	2	.771	.811	0.1	0.4	4	0-0.2
CHF ₂ CClF ₂	35.0	70.6	.374	.682	2	.751	.721	1.0	3.9	16	0-0.7
	54.4	119.7	.444	.594	2	.612	.617	0.9	3.9	17	0-0.5
	73.9	190.6	.505	.508	2	.490	.514	0.3	0.5	7	0-0.5

^a Calcd. slope = $1 + K_1(1/fK_1 - 2) = f + 1/f - 2K_1$. ^b Initial slope = $K_2' - (1 - K_1 - K_2)(\text{range } a_r)$; correction for curvature when the range extended beyond $a_r = 0.4$ or when the range of a_r was small. ^c Average and maximum per cent. deviation of the experimental points from the equation $\gamma_r = K_1 + K_2'a_r$.

half of the range of a_r . This leads to the expression given by equation 26

$$K_2 = \text{initial slope} = K_2' - (1 - K_1 - K_2)a_r' \quad (26)$$

where a_r' is the maximum value of activity over which the data were plotted (or least squared). This correction is small and is probably required when the range of activity treated is 0.4 or greater. The values of f and K may then be calculated by simultaneous solution of equations 12 and 13.

A simpler procedure for determining f and K is to fit K_1 and K_2 to the theoretical lines of K_1 versus K_2

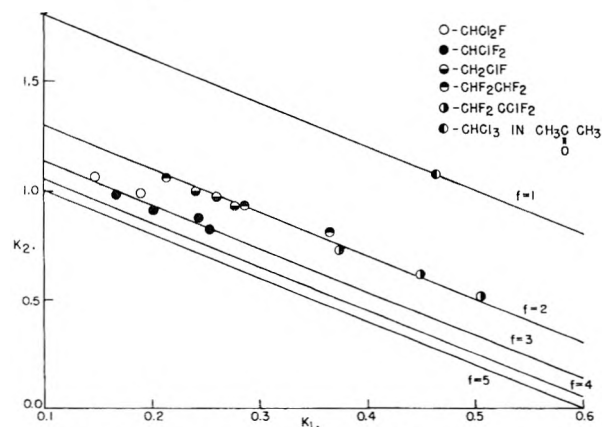


Fig. 1.—Comparison of experimental slopes and intercepts with theoretical values at different values of the functionality.

for various values of f as shown in Fig. 1 or by interpolation in Table II. The theoretical values were calculated by equation 27

$$K_2 = 1 + K_1 \left(\frac{1}{fK_1} - 2 \right) = \frac{f+1}{f} - 2K_1 \quad (27)$$

Figure 1 shows the experimental values of K_1 vs. K_2 for the various systems listed in Table I. These points fall near the $f = 3$ curve for CHCl₂F and CHClF₂ and near the $f = 2$ curve for the remaining systems. The actual values calculated for the slope when f takes on integral values of 2.0 or 3.0

TABLE II

THEORETICAL RELATIONSHIP BETWEEN K_1 , K_2 AND f

$K_1/f \rightarrow$	0.1	0.2	0.3	0.4	0.5
1	1.8000	1.6000	1.4000	1.2000	1.0000
2	1.3000	1.1000	0.9000	0.7000	0.5000
3	1.1333	0.9333	.7333	.5333	.3333
4	1.0500	.8500	.6500	.4500	.2500
5	1.0000	.8000	.6000	.4000	.2000

are listed in Table I along with values calculated for the initial slope by equation 26 when $a_r \geq 0.4$ or when the range of a_r was small. The agreement between these values of calculated and observed initial slope is considered good in view of the uncertainty of $\pm 2\%$ in the experimental data.

The classical data of Zawidzki⁵ for chloroform-acetone was fitted to equation 11 and the resulting expression is shown by equation 28.

$$\gamma_r = 0.462 + 1.076a_r - 0.538a_r^2 \quad (28)$$

Table III lists the results of applying equation 28 to Zawidzki's data and compares these with the Hildebrand³ expression. The agreement is shown to be at least as good as the Hildebrand expression at the ends and somewhat better in the middle. This, of course, does not justify our model over any other model since, as Hildebrand states (p. 18),³ solubility equations derived from various models frequently agree with each other better than with the experimental data. It is felt, however, that equation 11 does allow a greater insight into the mechanism of solubility than the logarithmic expression and that the direct plots of γ_r vs. a_r are used more easily for treating data and making correlations. It should be noted that the slope-intercept relationship for the chloroform-acetone data is plotted in Fig. 1 where it is shown to fall on the line of $f = 1.0$ as it should.

Discussion of Results

Dichlorofluoromethane and chlorodifluoromethane in tetraethylene glycol dimethyl ether yielded

(5) J. Zawidzki, *Z. physik. Chem.*, **35**, 129 (1908).

TABLE III

COMPARISON OF SOLUBILITY EQUATIONS WITH DATA ON THE SYSTEM CHLOROFORM-ACETONE

X_r	a_r	γ_r (obsd.) Zawadzki ⁴	γ_r (calcd.) eq. 28	γ_r (calcd.) Hildebrand, ³ Chapter XI
0.000	0.000	(0.462)	(0.462)	(0.44)
.060	.0306	.51	.494	.48
.184	.1086	.59	.573	.56
.263	.1710	.65	.630	.61
.361	.2491	.69	.696	.69
.424	.3053	.72	.740	.74
.508	.3911	.77	.800	.81
.581	.476	.82	.852	.86
.662	.583	.88	.906	.91
.802	.762	.95	.970	.97
.918	.909	.99	.996	.99
1.000	1.000	1.00	1.000	1.00

values of 3 for the functionality. This indicates that two of the five ether-oxygens of the ether are sterically hindered (or deactivated due to hydrogen-bonding at the other three oxygen sites). This is in agreement with the conclusion deduced intuitively by Zellhoeffer and Copley⁶ from the position of the maximum in the heat of mixing curve for dichlorofluoromethane in tetraethylene glycol dimethyl ether. Values of the heat of mixing, ΔH^m , were interpolated from a graph given in Zellhoeffer's paper⁶ and listed in Table IV. These are compared with values for the heat of mixing calculated by equation 29 for our model.

TABLE IV

HEAT OF MIXING OF CHCl_2F IN $\text{CH}_3\text{O}(\text{C}_2\text{H}_4\text{O})_n\text{CH}_3$

ΔH^m (first approx.)						
X_1	X_1X_2	$X_1 + 3X_2$	$\frac{\Delta H_r/K}{X_1 + 3X_2}$	$X_1 + 3X_2$	$\frac{\Delta H^m}{\Delta H_r}$	Cal./mole soln. ΔH^m (ref. no. 6)
0.0	0.00	3.0	0	3.00	0	0
.1	.09	2.8	240	2.73	250	250
.2	.16	2.6	460	2.47	490	525
.3	.21	2.4	640	2.22	710	750
.4	.24	2.2	820	1.98	910	950
.5	.25	2.0	940	1.74	1100	1125
.6	.24	1.8	1000	1.52	1190	1300
.7	.21	1.6	990	1.33	1190	1350
.8	.16	1.4	860	1.16	1030	1280
.9	.09	1.2	570	1.05	680	900
1.0	.00	1.0	0	1.00	0	0

(6) G. F. Zellhoeffer and M. J. Copley, *J. Am. Chem. Soc.*, **60**, 1343 (1937).

$$\Delta H^m = \Delta H_r \frac{fK}{1 + K} \frac{X_r X_s}{X_r + fX_s - \bar{Z}} \quad (29)$$

where

$$\Delta H_r = kT \left[\frac{d \ln K}{d \frac{1}{T}} \right]_f \quad (30)$$

and

$$\bar{Z} = \frac{\Delta H^m}{\Delta H_r} \quad (31)$$

Equation 29 requires the application of successive approximations until a constant value of \bar{Z} is obtained by equation 31. The values of f , K and ΔH_r determined from our data⁴ were 3.0, 2.201 and -3.65 kcal./mole, respectively, at 3.5° . Table IV shows that the agreement in magnitude and position of the maximum calculated by equations 29 to 31 and the experimental data of Zellhoeffer and Copley⁶ is good.

The value of $f = 2$ for the other solutes in tetraethylene glycol dimethyl ether is believed to be caused by greater steric effects due to the larger size of these molecules. Also, two out of three of these compounds have two hydrogens which may be capable of forming hydrogen bonds. This, of course, would reduce the apparent functionality of the solvent since two solvent sites may be satisfied by only one solute molecule. The fact that the functionality is 2 rather than 1.5 for these solutes results from steric considerations again. These effects can be seen readily by constructing models. It should be noted also that when different proton acceptors (or donors) are present in the same molecule or when the first interaction influences the degree of the second interaction, equilibria of the type described by equations 22 and 23 are likely to occur. Under these conditions, the value of f is likely to be non-integral. The value of $f = 1$ obtained for the chloroform-acetone system is in agreement with theoretical considerations.

In conclusion, it is believed that, because of its simplicity, equation 11 will be useful for correlating and treating solubility data, especially for complex or polymeric solvents which interact with simple solutes. Also, the possibility of using solubility techniques for investigating the structure of polymers or polymer solutions of polyethers, polyamides, polyamines, etc., is apparent.

DATA FOR DIFFUSION IN A CONCENTRATED SOLUTION OF THE SYSTEM NaCl-KCl-H₂O AT 25°. A TEST OF THE ONSAGER RECIPROCAL RELATION FOR THIS COMPOSITION

By PETER J. DUNLOP¹

Contribution from the Department of Chemistry, University of Wisconsin, Madison, Wisconsin

Received October 1, 1958

The four diffusion coefficients which are necessary to describe the solute flows in a ternary solution have been measured for the system NaCl-KCl-H₂O with each solute concentration equal to 1.5 molar. These data together with previously measured activity coefficients for this system are used to test the Onsager reciprocal relation for ternary diffusion. The Onsager relation is verified within 8%, and this value is less than the maximum expected error which is calculated from estimated individual errors in the various experimental data.

In a recent paper² four tests were made of the Onsager reciprocal relation³⁻⁵ for ternary diffusion in relatively dilute solutions of the system NaCl-KCl-H₂O. In no case was the total salt concentration of the system greater than one molar. Previously measured diffusion⁶ and thermodynamic^{7,8} data were employed in these tests and in each case the Onsager relation was verified within the expected experimental error of about 8%. Miller⁹ has also reported several tests of the Onsager relation, but he used certain estimated, rather than experimental, values for the solute activity coefficients.

The diffusion measurements reported in this paper were undertaken to test the Onsager relation for two reasons. Firstly, at high concentrations it was hoped that the *cross-term* diffusion coefficients¹⁰ would be larger than those in the previous measurements.⁶ Secondly, at high concentrations the derivatives of the logarithms of the activity coefficients contribute a greater proportion of the chemical potential derivatives, which appear in the Onsager relation for a three-ion system (see equations 1 of ref. 2), than they do at low concentrations. Thus at the high salt concentrations used in this study these chemical potential derivatives are not as accurately known as they are at lower concentrations.

This paper must be read in conjunction with two previous publications^{2,11} since frequent reference will be made to certain equations and tables in those works. When the letters D or F follow equation and table numbers in this paper, they refer to references 1 and 11, respectively.

Experimental

The Gouy diffusimeter used to measure the reduced height-area ratios, \mathcal{D}_A , and the differential refractive incre-

ments, R_i , has been previously described,^{12,13} as have also the necessary experimental conditions and methods^{10,14} used to obtain the \mathcal{D}_A , the R_i and the graphs of the fringe deviations, Ω , versus the reduced fringe numbers $f(\xi)$. The reader is referred to previous publications^{10,14} for definitions of these experimental quantities.

A single quartz Tiselius cell, 9 cm. in height, was used in all experiments. The cell dimension, a , along the optic axis was 2.5062 cm. and the optical lever arm, b , of the Gouy diffusimeter was 306.86 cm. All diffusion measurements were made with the 5460.7 Å. mercury line isolated from a G.E. A-H4 lamp with a Wratten 77A filter.

Materials and Solutions.—The sodium and potassium chlorides used in these experiments had been recrystallized and fused previously.^{10,14} All solutions were prepared by weight using doubly-distilled water, saturated with air, as solvent. The weight fraction of each solute, corrected to vacuum, was converted to the corresponding molarity, C_i , by means of densities, ρ , in g./ml., measured in triplicate in 30-ml. Pyrex pycnometers. The molecular weights of NaCl and KCl were taken to be 58.448 and 74.557, respectively.

To facilitate preparation of solutions, an equation was derived for predicting solution densities in the region $C_1 = C_2 = 1.5$ by using the empirical relation

$$V = N_0 \bar{V}_0^0 + N_1 \phi_1 + N_2 \phi_2 \quad (1)$$

where V is the total volume of solution, N_0 , N_1 , and N_2 are the number of moles of water, NaCl and KCl, respectively, and \bar{V}_0^0 is the volume of a mole of water at 25°. The dependences on concentration of ϕ_1 and ϕ_2 , the apparent molar volumes for binary systems, are given approximately by¹⁵

$$\phi_1 = 16.40 + 2.153\sqrt{C_1} \quad (2)$$

$$\phi_2 = 26.52 + 2.327\sqrt{C_2} \quad (3)$$

For this ternary system C_1 and C_2 in these expressions were replaced by the total solute concentration ($C_1 + C_2$).¹⁶ The resulting expression in the region of $C_1 = C_2 = 1.5$ is

$$\rho = 1.120786 + 0.03644(C_1 - 1.5) + 0.04216(C_2 - 1.5) \quad (4)$$

The density of water was taken to be 0.997075 g./ml. in this calculation. This equation predicts solution densities with an accuracy of about 6 parts in the fifth decimal place (see Table I) and it was used for preparing solutions of the desired concentration for each experiment.

Results

All the experimental quantities for the determination of the four diffusion coefficients are summarized in Table I. Lines 2-9 give the solution concentrations used in each experiment together

(12) L. J. Gosting, E. M. Hanson, G. Kegeles and M. S. Morris, *Rev. Sci. Instr.*, **20**, 209 (1949).

(13) P. J. Dunlop and L. J. Gosting, *J. Am. Chem. Soc.*, **75**, 5073 (1953).

(14) D. F. Akeley and L. J. Gosting, *ibid.*, **75**, 5685 (1953).

(15) H. S. Harned and R. B. Owen, "The Physical Chemistry of Electrolytic Solutions," 3rd Ed., Reinhold Publ. Corp., New York, N. Y., 1958, p. 253.

(16) H. E. Wirth, *J. Am. Chem. Soc.*, **59**, 2549 (1937).

(1) Department of Chemistry, University of Adelaide, South Australia.

(2) P. J. Dunlop and L. J. Gosting, *THIS JOURNAL*, **63**, 86 (1959).

(3) (a) L. Onsager, *Phys. Rev.*, **37**, 405 (1931); (b) **38**, 2255 (1931).

(4) L. Onsager and R. M. Fuoss, *THIS JOURNAL*, **36**, 2689 (1932).

(5) L. Onsager, *Ann. N. Y. Acad. Sci.*, **46**, 241 (1945).

(6) I. J. O'Donnell and L. J. Gosting, a paper presented in a Symposium at the 1957 meeting of the Electrochemical Society in Washington, D. C.; the Symposium papers are to be published as a monograph by John Wiley and Sons, New York.

(7) R. A. Robinson, in "Electrochemical Constants," National Bureau of Standards Circular 524, 1953.

(8) R. A. Robinson and R. H. Stokes, "Electrolyte Solutions," Appendix 8.3, Butterworths Scientific Publications, London, 1955.

(9) D. G. Miller, *THIS JOURNAL*, **62**, 767 (1958).

(10) P. J. Dunlop and L. J. Gosting, *J. Am. Chem. Soc.*, **77**, 5238 (1955).

(11) H. Fujita and L. J. Gosting, *ibid.*, **78**, 1099 (1956).

TABLE I^a

DATA FROM EXPERIMENTS IN WHICH NaCl AND KCl DIFFUSED SIMULTANEOUSLY IN WATER AT 25°

1 = NaCl, 2 = KCl; $\bar{C}_1 = 1.5$, $\bar{C}_2 = 1.5$

1	Exp. no.	1	2	3	4
2	(C ₁) _A	1.37536	1.50007	1.40071	1.47534
3	(C ₂) _A	1.49996	1.37497	1.47496	1.39960
4	(ρ_{exp}) _A	1.116292	1.115584	1.116180	1.115727
5	(ρ_{calc}) _A ^b	1.116242	1.115518	1.116111	1.115654
6	(C ₁) _B	1.62516	1.49996	1.59976	1.52482
7	(C ₂) _B	1.49997	1.32509	1.52534	1.60028
8	(ρ_{exp}) _B	1.125390	1.126122	1.125552	1.125974
9	(ρ_{calc}) _B	1.125346	1.126059	1.125489	1.125918
10	\bar{C}_1	1.50026	1.50002	1.50024	1.50008
11	\bar{C}_2	1.49996	1.50003	1.50015	1.49994
12	ΔC_1	0.24980	-0.00011	0.19905	0.04948
13	ΔC_2	0.00001	0.25012	0.05038	0.20068
14	J_{exp}	97.71	96.01	97.22	96.40
15	J_{calc}	97.72	96.00	97.21	96.42
16	α_1	1.0000	-0.0004	0.8010	0.2007
17	$\mathcal{D}_A \times 10^6$	1.6797	1.9142	1.7259	1.8641
18	$\mathcal{D}_{2m} \times 10^6$	1.7046	1.9039	1.7520	1.8646
19	$\Omega(\sqrt{2}) \times 10^4$	14.8	-5.0	15.0	0.4
		$R_1 \times 10^3 = 8.523$	$I_A \times 10^{-2} = 2.2854$	$I_{2m} \times 10^6 = 1.9044$	
		$R_2 \times 10^3 = 8.367$	$S_A \times 10^{-2} = 0.1535$	$S_{2m} \times 10^6 = -0.1961$	

^a Units in Table I: concentrations, C_i, moles/l.; densities, ρ , g./ml.; reduced height-area ratios, \mathcal{D}_A , and reduced second moments, \mathcal{D}_{2m} , cm.²/sec. ^b Calculated using equation 4.

with the measured densities and those predicted by means of equation 4. The subscripts A and B on these data denote the upper and lower initial solutions, respectively, used in each diffusion experiment. Lines 10-13 list the mean solute concentrations, \bar{C}_i , and the concentration increments, ΔC_i , across the initial diffusion boundaries. Concentration increments are considered positive if a solute's concentration in a given lower solution is greater than its value in the corresponding upper solution. The total number of Gouy fringes, J , obtained in each experiment is given in line 14. Using these values of J and the corresponding values of the ΔC_i , values for the differential refractive increments, R_i , were calculated.⁶ These values are reported at the bottom of Table I and were used, together with the ΔC_i , to calculate the values of J_{calc} in line 15 and also the solute fractions on the basis of refractive index (see equations 45F-47F), α_i , in line 16. Lines 17-19 give the measured height-area ratios; the values of the reduced second moments, \mathcal{D}_{2m} , which were calculated¹⁰ from the \mathcal{D}_A and the fringe deviation graphs (see Fig. 1); and the values of the fringe deviations at $f(\zeta) = 0.73854$. The values of I_A , S_A , I_{2m} and S_{2m} in Table I were obtained from the quantities $1/\sqrt{\mathcal{D}_A}$ and \mathcal{D}_{2m} by the method of least squares. These latter quantities are linear functions of α_1 (see equations 55F and 60F); their average deviations from straight lines were 0.03 and 0.13%, respectively.

Evaluation of the Four Diffusion Coefficients

The methods used to evaluate the four diffusion coefficients which appear in the flow equations for diffusion in ternary solutions¹⁰ have been described in detail in two previous papers.^{6,11} Approximate values for these coefficients were first obtained from the \mathcal{D}_A and the \mathcal{D}_{2m} (see method iii of Table IIF) and then final values were computed by means of method iv of Table IIF. These values of the

(D_{ij})_v are given in Table III and it is estimated that they are accurate to $\pm 0.03 \times 10^{-5}$. The double subscripts on the values of the (D_{ij})_v are retained only for calculating predicted values of the \mathcal{D}_A , the \mathcal{D}_{2m} and the fringe deviations. Although both these figures are in doubt, they are necessary in these calculations because of certain restrictions which exist between the values of the four diffusion coefficients if they are determined by the method used in this paper. The (D_{ij})_v were rounded to the third decimal place for use in testing the Onsager relation. Because of the relatively small concentration increments used in each diffusion experiment, it is believed that any errors in the four diffusion coefficients due to their concentration dependences are negligible when compared to the errors of $\pm 0.03 \times 10^{-5}$ which were estimated from the expected errors of $\pm 2 \times 10^{-4}$ in the experimental deviation graphs. The subscript V has been given to the values of the D_{ij} in Table III because they correspond to a volume-fixed frame of reference which becomes identical with the cell frame of reference (a) if the partial molal volumes of all components are independent of concentration or (b) in the limit that the ΔC_i are all zero.

Using the four (D_{ij})_v in Table III, the values of the α_i in Table I and in addition Table IV of reference 14, values for the \mathcal{D}_A , the \mathcal{D}_{2m} and the fringe deviations were calculated for each experiment by means of equations 30F, 31F, 50F, 51F, 55F, 60F-63F and 72F. Table II lists the calculated and experimental values of \mathcal{D}_A and \mathcal{D}_{2m} together with values for the intermediate quantity Γ_+ (see equation 50F). The agreement is seen to be not unsatisfactory. Figure 1 gives the fringe deviations calculated by means of equation 72F (dashed lines); they are to be compared with the average experimental points denoted by crosses. Inspection of Table II and Fig. 1 shows that the four values of (D_{ij})_v will reproduce, within the error of measurement, not only the height-area ratios and the reduced second moments, but also the deviations of the refractive index gradient curves from Gaussian shape.

TABLE II

COMPARISON OF CALCULATED WITH EXPERIMENTAL VALUES OF \mathcal{D}_A AND \mathcal{D}_{2m} $T = 25^\circ$; 1 = NaCl, 2 = KCl

α_1	Γ_+	$\mathcal{D}_A \times 10^6$		$\mathcal{D}_{2m} \times 10^6$	
		Expt.	Calcd.	Expt.	Calcd.
-0.0004	-0.0624	1.9142	1.9147	1.9039	1.9039
.2007	.0081	1.8641	1.8640	1.8646	1.8652
.8010	.2185	1.7259	1.7240	1.7520	1.7499
1.0000	.2882	1.6797	1.6811	1.7046	1.7117

The Test of the Onsager Reciprocal Relation

A complete description of the methods used to evaluate the diffusion coefficients with respect to the solvent frame of reference, (D_{ij})₃, the chemical potential derivatives and the expected error in a given test of the Onsager relation already has been given²; only a short summary will be given here.

Diffusion Coefficients for the Solvent Reference Frame.—Diffusion coefficients for the solvent frame of reference were obtained from the values for the

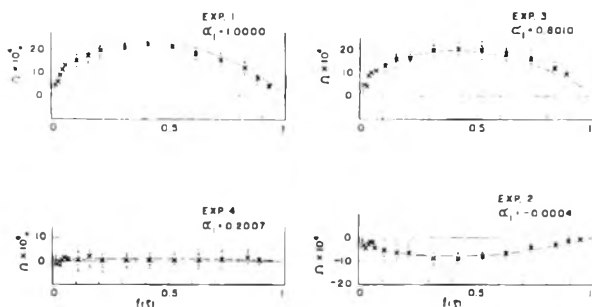


Fig. 1.—Fringe deviation graphs for the system NaCl-KCl-H₂O. The mean solute concentrations are $C_1 = C_2 = 1.5$ molar. At a given value of $f(\xi)$ crosses indicate the average of the experimental points (dots) obtained from ten different photographs of the same boundary. The dashed curve indicates values of Ω predicted by equation 72F. Individual experimental points have not been included for values of $f(\xi)$ less than 0.1. However, in this region the average deviation of such points from their mean value is about the same as at higher values of $f(\xi)$.

volume-fixed frame in Table III by means of equation 2D. The partial molal volumes for this composition of the system were calculated by means of equations 3D-5D and the relation

$$\rho = 1.12084_6 + 0.0364_2 (C_1 - 1.5) + 0.0421_2 (C_2 - 1.5) \quad (5)$$

to represent the measured density data in the region of $C_1 = C_2 = 1.5$. Equation 5 was obtained by the method of least squares and reproduces the experimental density data in Table I with an average deviation of $\pm 0.0006\%$. It is interesting to note that the coefficients of $(C_1 - 1.5)$ and $(C_2 - 1.5)$ in equations 4 and 5 agree to 0.1%. The values of the $(D_{ij})_0$ are given in Table III.

Derivatives of the Chemical Potentials.—The four derivatives of the two solute chemical potentials, μ_i , which are required for testing the Onsager relation in a three-component system are²

$$\mu_{ij} = (\partial\mu_i/\partial C_j)_{T,P,C_k \neq 0,j} = \sum_{k=1}^2 A_{ik} B_{kj} \quad \left(\begin{matrix} i = 1,2 \\ j = 1,2 \end{matrix} \right) \quad (6)$$

where

$$A_{ik} = (\partial\mu_i/\partial m_k)_{T,P,m_l \neq k} \quad (6a)$$

and

$$B_{kj} = (\partial m_k/\partial C_j)_{T,P,C_k \neq 0,j} \quad (6b)$$

In these relations T is the absolute temperature P is the pressure and the molalities, m_k , are related to the C_k by equation 7D. The B_{kj} for this composition of the system are listed in Table III and were calculated by means of equations 8D. The A_{ik} were calculated by first computing the Γ_{ik} (see equations 19D) from the data in Table III and then using equations 10D and the values for the molalities m_i . Equations 6 were then employed to compute the μ_{ij} . Values for the Γ_{ik} and μ_{ij} are given in Table IV. The methods used to obtain the experimental quantities in Table III already have been given,² as have also the references for the primary experimental data.⁶⁻⁸

The values of the μ_{ij} and the $(D_{ij})_0$ were then substituted into equations 1D and the four $(L_{ij})_0$ computed. If the Onsager relation is valid $(L_{12})_0$ should equal $(L_{21})_0$; inspection of Table IV shows that this condition is approximately satisfied. The experimental percentage dif-

TABLE III

DATA FOR TESTING THE ONSAGER RECIPROCAL RELATION FOR THE SYSTEM NaCl-KCl-H₂O AT 25°

C_1 (moles/l.) ^a	1.50000	B_{11}	1.12430
C_2 (moles/l.)	1.50000	B_{12}	0.03892
C_0 (moles/l.)	51.140	B_{21}	0.05732
m_1 (molality)	1.62807	B_{22}	1.14270
m_2 (molality)	1.62807	$d \log \gamma_{1(0)}/dm$	0.0383
m (molality)	3.25614	$d \log \gamma_{2(0)}/dm$	0.0047
\bar{V}_1 (ml./mole)	21.96	Φ	0.0158
\bar{V}_2 (ml./mole)	32.34	K_α	0.0168
\bar{V}_0 (ml./mole)	17.961	β_1	0
$(D_{11})_v \times 10^{10}$	1.3908	β_2	0
$(D_{12})_v \times 10^6$	0.1015	M_1	58.448
$(D_{21})_v \times 10^5$	0.3269	M_2	74.557
$(D_{22})_v \times 10^6$	1.8004	M_0	18.0160
$(D_{11})_0 \times 10^6$	1.458		
$(D_{12})_0 \times 10^6$	0.201		
$(D_{21})_0 \times 10^6$	0.394		
$(D_{22})_0 \times 10^6$	1.899		

^a The numbers 0, 1 and 2 denote water, NaCl and KCl, respectively. ^b Diffusion coefficients are expressed as cm.²/sec.; they correspond to amounts of solutes expressed in moles.

ference, $\% \Delta_{\text{exp}}$, calculated by equation 21D is 7.4%. Values of $(L_{11})_0$ and $(L_{22})_0$ are included in Table IV to indicate their magnitude.

The following equation previously has been derived and used² to estimate the maximum percentage error, $\% \Delta_{\text{est}}$, in a given test of the Onsager relation for a three-ion system.

$$\% \Delta_{\text{est}} = 100 \frac{[10(RT)^2/S]}{\left[\frac{(L_{12})_0 + (L_{21})_0}{2} \right] \times RT \times 10^6} \sum_{i=1}^8 \psi_i \delta_i \quad (7)$$

It should be noted that this relation does not give the absolute error in $(L_{12})_0$ and $(L_{21})_0$. Equations 22D and 24D indicate how the coefficients ψ_i may be calculated from the experimental quantities in Tables I, III and IV. The F_i ¹⁶ for this system when $C_1 = C_2 = 1.5$ are $F_1 = 0.29$, $F_2 = -0.63$, $F_3 = -0.78$ and $F_4 = 0.31$. The estimated errors, δ_i , in the various experimental quantities (see Table V) are the same as in reference 2 except that $\pm 0.03 \times 10^{-5}$ is assigned to δ_1 and δ_2 , and δ_5 is now ± 0.0003 since Φ (equation 15D) is inversely proportional to m and the assumed error of ± 0.001 in the osmotic coefficients for the binary systems, NaCl-H₂O and KCl-H₂O, is assumed to be independent of concentration.

TABLE IV^a

SUMMARY OF THE TEST OF THE ONSAGER RELATION FOR THE SYSTEM NaCl-KCl-H₂O AT 25°

$C_1 = 1.5 = C_2$			
Γ_{11}	0.0373	$\mu_{11}/(RT)$	1.2500
Γ_{12}	.0131	$\mu_{12}/(RT)$	0.4624
Γ_{21}	.0131	$\mu_{21}/(RT)$	0.4674
Γ_{22}	.0057	$\mu_{22}/(RT)$	1.0971
$(L_{12})_0 \times RT \times 10^9$	-3.66	$(L_{11})_0 \times RT \times 10^9$	13.03
$(L_{21})_0 \times RT \times 10^9$	-3.94	$(L_{22})_0 \times RT \times 10^9$	18.97
$\% \Delta_{\text{exp}}^b$	7.4		

^a The coefficients $(L_{ij})_0$ reported here are for flow equations expressed in moles of components 1 and 2. ^b Calculated by means of equation 21D.

(16) See equations 23D and ref. 33 of ref. 2.

The same two cases for estimating errors are discussed here as in reference 2, (a) when $\beta_1 = \beta_2 = 0$ (i.e., Harned's rule¹⁷ is perfectly valid) and (b) when β_1 and β_2 are allowed values of ± 0.001 .¹⁸ Table V summarizes the analysis of errors for this composition of the system. The $\% \Delta_{est}$ at the bottom were calculated by summing the eight products $\psi_i \delta_i$ for cases (a) and (b) and substituting the results into equation 7; the values of $(L_{12})_0$ and $(L_{21})_0$ are in Table IV and the value of S for this calculation is obtained from the μ_{ij} by using equations 1D.

TABLE V^a

MAXIMUM ESTIMATED ERRORS FOR THE TEST OF THE ON-SAGER RECIPROCAL RELATION

	$C_1 = 1.5 = C_2$		
$(\delta_i)_{def}$	$(\delta_i)_{exp}$	ψ_i	$\psi_i \delta_i$
$\delta_1 = \delta[(D_{12})_V \times 10^5]$	± 0.03	-0.75	0.022
$\delta_2 = \delta[(D_{21})_V \times 10^5]$	$\pm .03$.66	.020
$\delta_3 = \delta \left(\frac{d \log \gamma_1(0)}{dm} \right)$	$\pm .002$	-.67	.001
$\delta_4 = \delta \left(\frac{d \log \gamma_2(0)}{dm} \right)$	$\pm .002$	-.67	.001
$\delta_5 = \delta \Phi$	$\pm .0003$	-2.35	.001
$\delta_6 = \delta K_{\alpha a}$	$\pm .001$	1.07	.001
b	$\pm .004$.004
$\delta_7 = \delta \beta_1$	a	-6.96	0
b	$\pm .001$.007
$\delta_8 = \delta \beta_2$	a	-4.41	0
b	$\pm .001$.004
$\% \Delta_{est}$	a		± 10.5
b			± 13.7

^a Because the δ_i may be either positive or negative, values of $\psi_i \delta_i$ are reported without regard to sign; the $\% \Delta_{est}$ in the last two lines were obtained from equation 7 by assuming that these products all have the same signs. In practice some of the products $\psi_i \delta_i$ probably have opposite signs, causing some cancellation of errors, and some experimental errors will be less than the assigned values, δ_i . Therefore it is not unreasonable that the above values of $\% \Delta_{est}$ are greater than the observed value of $\% \Delta_{exp}$ in Table IV.

Discussion

Comparison of the value of $\% \Delta_{exp}$ in Table IV with the values for the $\% \Delta_{est}$ in Table V indicates

(17) See references 17-19 of ref. 2.
 (18) See ref. 37 of ref. 2.

that the Onsager relation is verified within the expected experimental error. The fact that the value of $\% \Delta_{exp}$ is greater than the corresponding four values in reference 2 is due mainly to two reasons, (a) the $(D_{ij})_V$ are slightly less accurate than those in reference 2 because the number N (see equation 11 of reference 6) for this composition of the system is 30% lower than its value at the lower concentrations⁶ and (b) because the derivatives of the logarithms of the activity coefficients now contribute a much greater proportion of the μ_{ij} than they do at lower solute concentrations. In reference 2 the activity coefficient data played a rather small part in the tests of the Onsager relation; the assumption that the activity coefficients were constant in each case actually improved the agreement between $(L_{12})_0$ and $(L_{21})_0$. However for this composition of the system NaCl-KCl-H₂O ($C_1 = C_2 = 1.5$) the $\% \Delta_{exp}$ is 7.4% when the experimental activity data are used and -17.6% when the activity coefficients on the molarity scale are assumed to be constant.

It is interesting to note in Table V that the errors of ± 0.001 in β_1 and β_2 , which in Table IIID contributed a relatively small fraction of the total $\% \Delta_{est}$, here contribute about 20% of the maximum expected error of 13.7%.

The Onsager reciprocal relation has now been verified, within the expected experimental error, over a large concentration range for isothermal diffusion in the system NaCl-KCl-H₂O. In addition, using certain approximations to evaluate the μ_{ij} , Miller⁹ has reported tests for the systems NaCl-LiCl-H₂O, KCl-LiCl-H₂O, KCl-raffinose-H₂O and KCl-urea-H₂O. Because the values of μ_{12} and μ_{21} (see equations 6) depend only on the derivatives of logarithms of activity coefficients for the latter two systems, experimental activity coefficients for such systems would enable tests of the Onsager relation to be made which may be more sensitive to experimental errors in the activity coefficients than are the tests reported for the above three-ion systems. It is hoped that such thermodynamic data soon will become available.

Acknowledgments.—It is a pleasure to thank Professor L. J. Gosting for helpful discussions and advice during the course of this work. This study was supported by a grant from the National Science Foundation.

RARE EARTH METAL "DISILICIDES"¹

BY JOHN A. PERRI, IRA BINDER AND BEN POST

Polytechnic Institute of Brooklyn, Brooklyn, N. Y.

Received October 2, 1958

Disilicides of Ce, Pr, Nd, Sm, Eu, Gd, Dy and Y have been prepared. The Ce, Pr and Nd compounds are tetragonal as previously reported; the Sm, Gd, Dy and Y compounds are orthorhombic, space group Imma. Their structures are slightly distorted versions of the tetragonal MeSi₂ structure. The magnitude of the distortion appears to increase with decreasing size of the metal atom. Chemical and X-ray diffraction studies of "GdSi₂" indicate that the composition is actually close to GdSi_{1.4}. EuSi₂ crystallizes in the tetragonal system apparently due to the anomalously large size of the metal atom.

Introduction

Brauer and Haag² have described the isomorphous disilicides formed by La, Ce, Pr and Nd. The unit cells are tetragonal; there are four formula weights per unit cell, and the space group is I4₁/amd. Dimensions of the unit cells, as given by Brauer and Haag, are listed in Table I.

The structure may be described in terms of linear arrays of atoms of the type Si-Me-Si-Si-Me-Si-, parallel to the "c"-axis. One such line is placed at $x = 0$ and $y = 1/4$; the operation of the fourfold screw axis generates three additional lines at $x = 0, y = 3/4$; $x = 1/2, y = 1/4$; and $x = 1/2, y = 3/4$. This arrangement is shown schematically in Fig. 1.

In terms of a unit cell whose origin is at a center of symmetry, atomic positions are

4 metal atoms in 4b:

$$0, 1/4, 3/8; 0, 5/4, 5/8; 1/2, 3/4, 7/8; 1/2, 1/4, 1/8$$

8 silicon atoms in 8c:

$$0, 1/4, z; 0, 3/4, \bar{z}; 1/2, 3/4, 1/2 + z; 1/2, 1/4, 1/2 - z; 0, 3/4, 1/4 + z; 0, 1/4, 3/4 - z; 1/2, 1/4, 3/4 + z; 1/2, 3/4, 1/4 - z$$

There are two types of Si-Si bonds in this structure, *i.e.*

$$(a) \text{ from } 0, 1/4, z \text{ to } 0, 1/4, 3/4 - z$$

$$(b) \text{ from } 0, 1/4, 3/4 - z \text{ to } 0, 3/4, 1/4 + z$$

Brauer and Haag postulated an "ideal" MeSi₂ structure in which both types of Si-Si bonds are equal in length. Simple geometrical considerations show that in this "ideal" structure the variable positional parameter of the silicon atoms is $z = 0.792$. Brauer and Haag found that calculated and observed diffraction intensities showed fairly good agreement in the cases of LaSi₂ and CeSi₂ when z was assumed equal to this value. They also reported the doubling of some weak reflections on the powder diffraction patterns of SmSi₂ and YSi₂ and suggested the possibility that the symmetry of the unit cell deviated from tetragonal in these compounds, and that it was possibly orthorhombic.

The present investigation was undertaken to study more closely the structures of these and other rare earth disilicides.

Sample Preparation.—Disilicides of La, Ce, Pr, Nd, Sm, Eu, Gd, Dy and Y were prepared. These compounds were produced readily by direct silicon reduction of the metal oxides, either *in vacuo* or in a protective atmosphere such as hydrogen. Some reductions also were carried out using mixtures of carbon and silicon with the metal oxides. The oxides were 99–99.9% pure except in the case of neodymium where an oxide of 95% purity was used.

Reactions carried out in alumina boats under vacuum (with continuous pumping) generally gave the best products. The silicon monoxide which was formed in the reaction between the metal oxide and the silicon was quickly and completely removed from the reaction mass. When reactions were carried out under a protective layer of hydrogen, the silicon oxides appeared to form coatings about the silicide particles. These coatings were never completely removed and all lots produced in reactions carried out in hydrogen contained some oxygen. For this reason each of the disilicides also was prepared *in vacuo*.

Reaction temperatures of the order of 1100 to 1600° were used. Preparations fired at temperatures above 1600° usually yielded relatively impure products due to chemical attack on the container. In the case of yttrium and dysprosium, reactions were carried out most successfully in the temperature range 1400–1550°; for SmSi₂, a temperature range of 1200–1300° was found most suitable. The exact temperatures did not appear to be critical in other cases.

As a check on the procedure, lanthanum metal was heated with silicon *in vacuo*; a pure disilicide was obtained identical with that produced in the reaction between the metal oxide and silicon.

X-Ray Results. Powder Data.—X-Ray diffraction examination of the powdered products indicated that the La, Ce and Pr compounds were tetragonal with lattice constants differing slightly from those reported by Brauer and Haag (see Table I). It should be noted that Brauer and Haag's measurements were made on films taken in a small (57.3 mm. diameter) Debye-Scherrer camera. Our measurements were made with a Geiger counter diffractometer, making possible far better precision of measurement and resolution of lines than are generally obtainable with small film cameras.

TABLE I
LATTICE CONSTANTS OF RARE EARTH AND YTTRIUM DISILICIDES

Brauer and Haag ²			The present work		
a	c		a	b	c
4.272	13.72	LaSi ₂	4.31	...	13.80
4.148	13.81	CeSi ₂	4.27	...	13.88
4.140	13.64	PrSi ₂	4.29	...	13.76
4.103	13.53	NdSi ₂	4.18	4.15	13.56
		SmSi ₂	4.105	4.035	13.46
		GdSi ₂	4.09	4.01	13.44
		DySi ₂	4.04	3.95	13.34
		YSi ₂	4.04	3.95	13.23

The powder patterns of Nd, Sm, Gd, Dy and Y disilicides could be indexed only on the basis of a slightly distorted (orthorhombic) version of the LaSi₂ tetragonal type. (The europium disilicide preparation will be discussed separately below.) Unit cell dimensions of these compounds are included in Table I; powder data are listed in Table II.

(1) Supported by Air Force Office of Scientific Research.

(2) V. G. Brauer and H. Haag, *Z. anorg. allgem. Chem.*, **267**, 198 (1952).

TABLE II

PARTIAL POWDER DIFFRACTION DATA FOR ORTHORHOMBIC DISILICIDES

NdSi ₂		SmSi ₂		GdSi ₂		DySi ₂		YSi ₂	
<i>hkl</i>	<i>d</i> (Å.)	<i>I</i>	<i>d</i> (Å.)	<i>I</i>	<i>d</i> (Å.)	<i>I</i>	<i>d</i> (Å.)	<i>I</i>	<i>d</i> (Å.)
101	4.00 ^a		3.93	30	3.91	25	3.86	30	3.89 ..
011	3.97 ^b	35	3.86	25	3.84	25	3.77	30	3.79 ..
004	3.39	35	3.37	50	3.36	30	3.33	35	3.33 ..
103	3.06	65	3.03	35	3.02	25	2.99	35	3.00 ..
013			3.01	40	2.99	30	2.95	40	2.96 ..
112	2.70	100	2.65	100	2.62	100	2.60	100	2.60 ..
105	2.274	50	2.252	35	2.25	20	2.225	30	2.23 ..
015			2.241	35	2.23	20	2.21	25	2.21 ..
200	2.048	18	2.052	25	2.047	14	2.021	20	2.021 ..
020	2.074	18	2.017	20	2.005	12	1.974	15	1.975 ..

^a Overlapping peaks (additional peaks were not recorded). ^b Several peaks of this phase coincided with peaks of another phase and intensities are not considered reliable.

X-Ray Results. Single Crystal Data.—Systematic absences of reflections from the powder patterns indicated that the space group of the orthorhombic silicides was either *Imma* or *Im2a*.

A few small single crystals of GdSi₂ were found in one of the preparations. Two of these were examined by single crystal techniques. The crystals were tiny rhombs having maximum dimensions of less than 0.1 mm. X-Ray photographs taken with the precession camera, using Mo K radiation, confirmed that the space group was either *Imma* or *Im2a* and that, within the limits of experimental error, $I_{hkl} = I_{khl}$. This also was indicated, for fewer reflections, by the powder diffractometer data. It was therefore felt that *Imma*, in which the same symmetry elements are associated with both the "a" and "b"-axes, is the more probable space group.

In order to determine the positional parameters in the orthorhombic phase, careful measurements were made of eight observable *00l* reflections (004, 008, 0012, 0020, 0024, 0028 and 0032). The crystal was mounted along [100] and the intensities of the diffracted beams were recorded with a scintillation counter. Filtered Mo K radiation was used. A voltage and current stabilized source of X-radiation was used. The counter was kept in a fixed position, with the window open, and the diffracted beam was recorded as the crystal was turned slowly through the diffracting position. The window on the scintillation counter covered a range of 4° (2θ) and the crystal was rotated at 1/4° (θ) per min. The diffracted peaks were recorded on a strip chart and their areas were subsequently measured with a planimeter.

The usual Lorentz and polarization corrections were applied in order to convert the measured (integrated) intensities to numbers proportional to |F²|. No absorption correction was applied; approximate calculations showed that, for all but the (004) reflection, the absorption factor varied linearly with sin²θ/λ² and could therefore be absorbed into the usual "temperature factor."

No signs of *00l* reflections with $l \neq 4n$ were detected either with the scintillation counter or on highly over-exposed precession photographs.

In the tetragonal unit cell (*I*4₁/amd) the metal atom has a fixed value of *z* ($z_m = 0.375$) and the arrangement of the silicon atoms is such that they lie at eight different levels; i.e., if $z = 0.786$, then

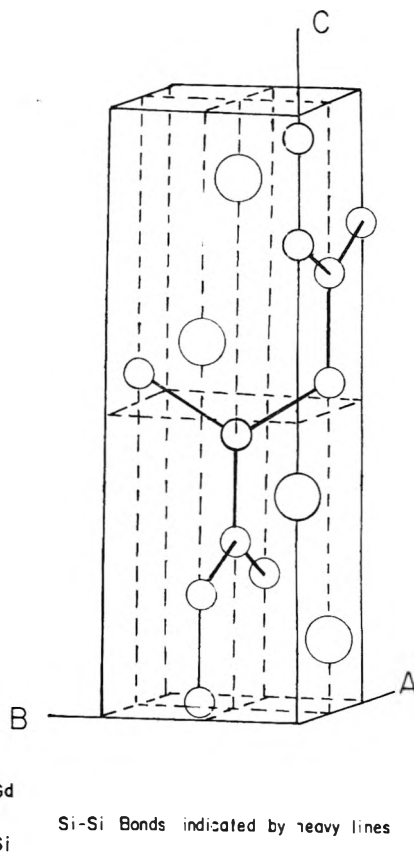


Fig. 1.—Arrangement of atoms in *MiSi*₂ unit cell.

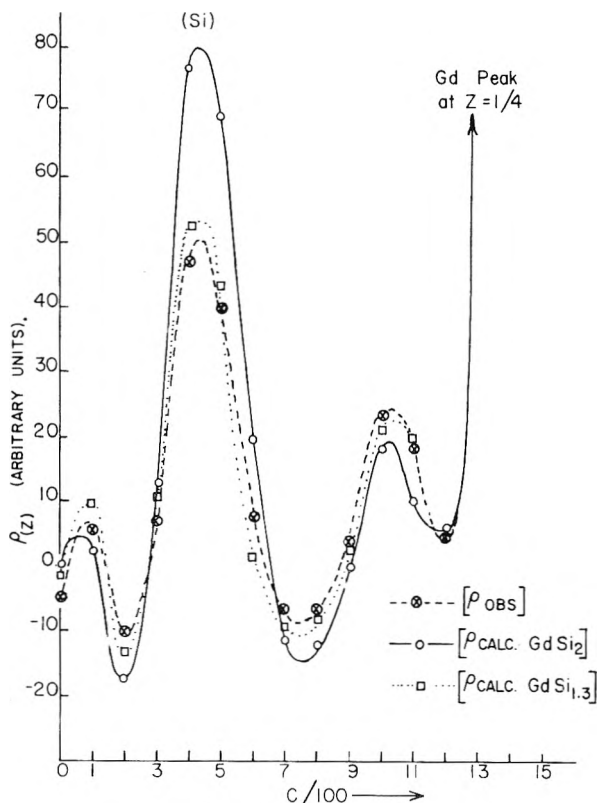


Fig. 2.—(*z*) calcd. and obsd.

there are silicon atoms at $z = 0.786, 0.214, 0.036, 0.964, 0.286, 0.714, 0.536, 0.464$.

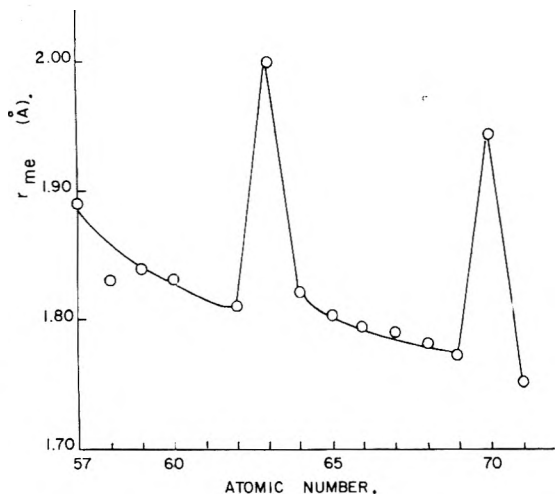
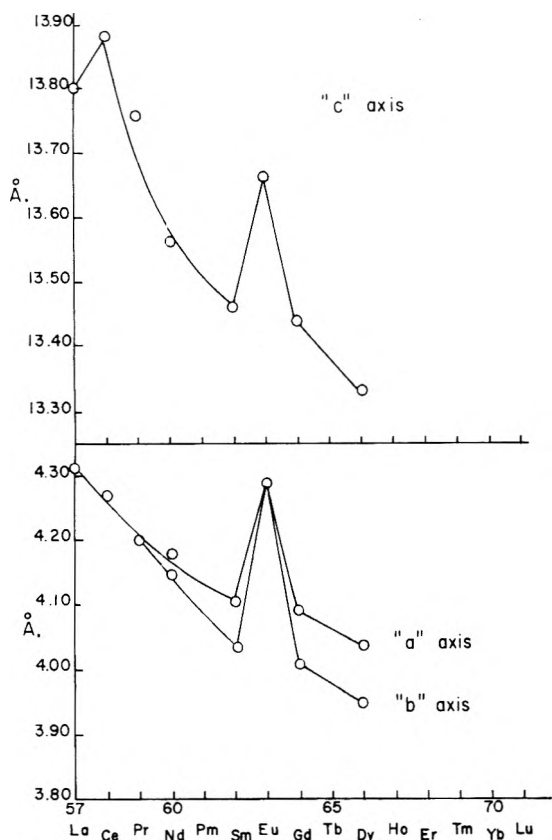
Fig. 3.—Atomic radii of rare earth metals.³

Fig. 4.—Axial lengths of rare earth "disilicides."

In view of the close similarity between the orthorhombic and tetragonal structures it was clear that the silicon atoms in the orthorhombic unit cell (Imma) also lie at eight different levels along the *c*-axis. The available eightfold positions in Imma place atoms in only four different levels along *c*. It is therefore necessary to place the silicon atoms in two distinct sets of fourfold positions. The only suitable ones having variable *z* parameters are the positions $4e$

$$0, \frac{1}{4}, z, \quad 0, \frac{3}{4}, \bar{z}$$

$$\frac{1}{2}, \frac{3}{4}, \frac{1}{2} + z, \quad \frac{1}{2}, \frac{1}{4}, \frac{1}{2} - z$$

In the tetragonal cell the metal atoms must be in special positions, *i.e.*, at $z = \frac{3}{8}$ when the origin

is at a center of symmetry. No such restrictions are imposed on the *z* parameters of either the Si or the Gd in the orthorhombic unit cell. However, a study of the diffracted intensities indicates that restrictions are present even though not required by the space group.

In Imma, $F_{00l} = \sum_i f_i \cos 2\pi lz_i$. If a Gd atom is at $z = \frac{3}{8}$, it will contribute only to reflections having $l = 4n$. If it is shifted to $\frac{3}{8} + \epsilon$ its contribution to $00l$ reflections is $f_{\text{Gd}} \cos 2\pi l(\frac{3}{8} + \epsilon)$; this is equivalent to $f_{\text{Gd}} (\cos 2\pi l \frac{3}{8} \cos 2\pi l\epsilon - \sin 2\pi l \frac{3}{8} \sin 2\pi l\epsilon)$. For l even, but not equal to $4n$, this gives $-f_{\text{Gd}} \sin 2\pi l\epsilon$. On the basis of the observed intensities of high order reflections, it has been estimated that if $\epsilon \geq 0.001$, reflections of the type (0026) and (0030) should have been readily detectable. No such reflections were observed. We may conclude that in the orthorhombic cell the value of z_{Gd} lies within the range $z = 0.375 \pm 0.001$. Similar arguments may be used to limit the extent to which the distance from a gadolinium atom to a silicon atom "above" it differs from that to a silicon atom "below" it; the difference, if it exists, cannot exceed 0.02 Å.

Electron density maps were computed to determine $\rho(z)$. These are shown in Fig. 2. "Observed" values of F_{00l} were used as coefficients for one summation; for the other summations shown, calculated values of F_{00l} were used as coefficients of the Fourier series. It was assumed that a gadolinium atom was located at $z = 0.375$ and that silicon atoms were at 0.375 ± 0.411 .

It will be noted that peaks not attributable to either the silicon or gadolinium atoms appear on both maps (at $z = 0.008$ and $z = 0.087$). Since only gadolinium and silicon atoms were included in the F_{calcd} summation it is clear that these are spurious peaks resulting from the use of a small number of terms in the Fourier summations.

In the electron density summations, intensities of (00*l*) reflections other than those having $l = 4n$ were taken to be equal to zero. It is probable that these do not exactly equal zero, but were merely below the level of detection. However, as a result of taking (00*l*) $l \neq 4n$ reflections equal to zero, the gadolinium atoms must be found at $z = \frac{1}{8}, \frac{3}{8}, \frac{5}{8}, \frac{7}{8}$ and the silicon atoms at $Z_{\text{Gd}} \pm \alpha$.

The parameters of the silicon atoms as derived from the electron density map shown in Fig. 2, after application of the "back-shift" correction, are $z = 0.3750 \pm 0.4112$. As noted previously, the possibility that the distances of the two silicon atoms from the metal atom between them differ slightly cannot be ruled out.

A calculation of the discrepancy factor

$$R = \frac{\sum |F_o| - |F_c|}{\sum |F_c|}$$

where F_{calcd} was based on $Z_{\text{Si}} = Z_{\text{Gd}} \pm 0.4112$, with two silicon atoms per metal atom, led to a value of $R = 8.3\%$. It was evident that no adjustment of z could greatly improve the agreement between F_{obsd} and F_{calcd} . Slight shifts in either direction improved some values of F_{calcd} and made others worse. It was then assumed that the silicon to metal atom ratio was not exactly two, and R was

computed for GdSi , $\text{GdSi}_{1.25}$, $\text{GdSi}_{1.50}$ and $\text{GdSi}_{2.00}$. For all the calculations $z_{\text{Gd}} = 0.3750$ and $z_{\text{Si}} = z_{\text{Gd}} = 0.4112$. The calculation for GdSi , for example, implied that half the available Si positions were randomly unoccupied. A minimum in R occurs near $\text{GdSi}_{1.3}$ where R is somewhat less than 2.7% (Table III). It was felt that there would be little point in attempting to refine this value further.

TABLE III
VALUES OF "R" FOR VARIOUS Si/Gd RATIOS

Si/Gd	R, %
1.00	4.8
1.25	2.7
1.50	4.3
2.00	8.3

It should also be noted that the calculated silicon peaks computed on the basis of a Si/Gd ratio of two are considerably higher than those on the F_{obsd} summation. A summation computed on the basis of a Si/Gd ratio of 1.3 is also shown in Fig. 2. The height of the silicon atom peak on this map is in far better agreement with that on the F_{obsd} map.

Pycnometric measurements of the density of powdered " GdSi_2 " gave a value of 5.94 g./cc.; the density calculated for GdSi_2 is 6.43 g./cc.; for $\text{GdSi}_{1.4}$ it is 5.92 g./cc. A chemical analysis indicated a Si/Gd atom ratio of 1.47, in good agreement with X-ray and density measurements. It is clear that the composition of " GdSi_2 " is actually close to $\text{GdSi}_{1.4}$. It was not possible to establish whether a range of homogeneity exists for this compound.

Europium Disilicide.—The ionic radii of the trivalent rare earth ions decrease regularly as we proceed from La^{+++} (1.06 Å.) to Lu^{+++} (0.85 Å.).³ The atomic radii of the elementary metals also decrease with increasing atomic number, with the conspicuous exceptions of Eu and Yb, whose atomic radii are about 10% greater than those of neighboring elements (Fig. 3).⁴ This anomaly is associated with the abnormal valencies of these atoms; most of the rare earth metals are essentially trivalent, but Eu and Yb show a large amount of divalent character which usually is attributed to the withdrawal of one electron from the outermost orbit ($5d^1$) to fill a gap in an inner one ($4f^6$). This leads also to an increase in the effective sizes of these atoms.

(3) D. H. Templeton and C. H. Dauben, *J. Am. Chem. Soc.*, **76**, 5327 (1954).

(4) F. H. Spedding, D. H. Daane and K. W. Herrmann, *Acta Cryst.*, **9**, 559 (1956).

It was felt that the anomaly mentioned above might affect the size of the metal atom in europium disilicide. It has been seen (Table I) that, as we proceed from LaSi_2 to the silicides of metals of higher atomic numbers (and smaller effective sizes) the unit cell decreases progressively in size and the symmetry changes from tetragonal to orthorhombic. In the case of EuSi_2 the size anomaly could lead to crystallization in the tetragonal system.

This proved to be the case. Europium disilicide, prepared by heating Eu_2O_3 and silicon under vacuum, is tetragonal with $a = 4.29$ Å., $c = 13.66$ Å. Powder diffraction data for this compound are shown in Table IV. Both "a" and "c" are substantially larger than the corresponding axes in either SmSi_2 or GdSi_2 . Figure 4 also shows the "a," "b" and "c" axial lengths of the compounds described above.

TABLE IV
PARTIAL POWDER PATTERN OF EuSi_2 TETRAGONAL
 $a = 4.29$ Å., $c = 13.66$ Å.

<i>hkl</i>	<i>d</i> , Å.	<i>I</i>
101	4.09	50
004	3.41	38
103	3.12	Coincides with Si(111) peak
112	2.75	100
105	2.305	4
200	2.147	28
211	1.901	31
116	1.819	25
108	1.779	38
213	1.773	38
008	1.708	13
215	1.523	31
220	1.518	19

It is considered very probable that ytterbium disilicide, when prepared, will be found to crystallize in the tetragonal system.

Similar behavior is manifested by the cubic hexaborides of the rare earth metals. These show decreases in unit cell sizes with increasing atomic number of metal atom except for europium and ytterbium hexaborides.⁵

Acknowledgment.—The authors wish to thank the American Electro Metal Division of the Firth Sterling Company, Yonkers, New York, for preparing the silicide samples used in this investigation and for valuable technical assistance rendered in the course of the work.

(5) B. Post, D. Moscovitz and F. W. Glaser, *J. Am. Chem. Soc.*, **78**, 1800 (1956).

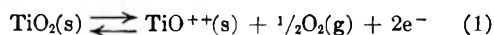
INTERACTION OF OXYGEN WITH TITANIUM DIOXIDE

BY A. W. CZANDERNA¹ AND J. M. HONIG*Richard B. Wetherill Laboratory of Chemistry, Purdue University, W. Lafayette, Indiana**Received October 2, 1958*

Reversible oxygen adsorption has been measured on commercial grade titanium dioxide powder at 500, 700 and 900° as a function of the ambient pressure by a weighing technique. No oxygen adsorption is detectable in highly purified TiO₂ in the same temperature range. Mass losses have been recorded in a dynamic high vacuum as a function of temperature for highly purified TiO₂ "bulk" and also for purified TiO₂ containing various quantities of BaO, TiF₄ and Na₂O. Details of the techniques employed for carrying out the measurements are discussed. Interpretation of the mass changes observed in the bulk material indicates that "dehydration" of TiO₂ is complete at 800° and that incipient decomposition of bulk TiO₂ occurs at 875° in a dynamic vacuum of 10⁻⁵ mm. The reversible oxygen adsorption is believed to occur at surface impurity centers.

Introduction

It has been recognized for some time that the oxides of many metals are non-stoichiometric compounds in which the oxygen to metal ratio is variable. This fact is of great interest because such oxides are generally semi-conducting. In TiO₂, the relation between the defect structure and the electronic properties may be exhibited by the over-simplified quasichemical relation



The "reaction" shows that as oxygen is evolved upon heating, defect centers, TiO⁺⁺(s), are generated and quasi-free electrons are released in the crystal. These are responsible for the extrinsic semi-conducting properties of the partially reduced oxides. Equations of this type have been discussed by a number of authors and, in particular, by Hauffe.² Such equations form the basis of a quantitative correlation between the electrical properties of the material and the oxygen pressure to which the sample is exposed.² In some cases, the extent of the defect structures can be inferred from measurements of electrical properties. In the case of TiO₂, such a correlation would be especially useful since existing chemical methods of analysis of the Ti to O ratio are, at best, accurate to ±0.4%.³

One of the principal difficulties in applying the correlation procedures arises from the fact that small traces of impurities may completely vitiate the results. This matter has been discussed at great length²; in the presence of such impurities, the ion defect concentration as well as the electrical properties of the oxide are greatly altered. In the case of TiO₂, most of the electrical measurements have been carried out on relatively impure samples (impurity content in the range 0.03 to 0.20%).⁴⁻¹² Also, while there have been a number of reports

providing chemical evidence that TiO₂ is a non-stoichiometric oxide,^{13,14} the samples were again impure. Thus, it seemed of interest to initiate a study concerning the defect stoichiometry of TiO₂, utilizing a weighing procedure to monitor changes in composition.

Two types of experiments were carried out on bulk and powdered TiO₂ samples of different purity. The first was to investigate the mass losses from TiO₂ in a dynamic high vacuum as a function of temperature, thus providing information about the stability of this compound. The second was to measure oxygen uptake by TiO₂ at elevated temperatures as a function of the ambient pressure and, if present, to determine whether the uptake was reversible or irreversible. Finally, surface areas were measured on all powdered samples.

Experimental

Description of Equipment.—Mass changes were determined by means of a vacuum quartz microbalance, which was connected to a vacuum system, as shown in Figs. 1 and 2. The changes in mass were compensated by adjusting the current passing through a solenoid that acted on a magnetic wire suspended from the balance. The e.m.f. developed by the compensation current across a standard resistor was measured with a potentiometer. A detailed description of the construction, operation, calibration and limitations of the equipment has been reported.¹⁵ In the present set of experiments, the operating reproducibility was ±0.1 μg. in high vacuum and ±1 μg. in the pressure range studied. The apparent decrease in accuracy arises because corrections must be introduced for the thermomolecular flow of gases in the pressure region 10⁻³ to 15 mm.

Oxygen was prepared by thermal decomposition of chemically pure potassium permanganate dried with magnesium perchlorate and stored in bulbs. Nitrogen was prepared by the decomposition of sodium azide, stored in a vacuum bulb and dried over phosphorus pentoxide prior to admission to the balance system.

Preparation of Samples.—Several types of titanium dioxide samples were studied.

(1) Spectroscopically pure material, prepared by oxidizing commercially pure titanium metal with 90% H₂O₂ in an ammoniacal solution; the impurities were removed by filtering and the filtrate was evaporated to dryness. The yellow peroxidized material was converted to anatase by heating at 200°; the chemically analyzed composition of the material was in the range TiO_{1.98} to TiO_{2.01}, which is within experimental error of the stoichiometric composition TiO₂. Since the material passed through the peroxidized form before conversion to anatase, it is likely that the composition of the starting material was quite close to the stoichiometric formula. Details of the procedure, the analysis of the product for purity, the sample composition and its

(1) National Carbon Research Laboratories, P. O. Box 6116, Cleveland 1, Ohio.

(2) K. Hauffe, "Reaktionen in und an festen Stoffen," Springer, Berlin, 1955.

(3) H. R. Hoekstra and J. J. Katz, *Anal. Chem.*, **25**, 1608 (1955).

(4) R. Breckenridge and W. Hosler, *Phys. Rev.*, **91**, 793 (1953).

(5) D. Cronmeyer, *ibid.*, **87**, 876 (1952).

(6) M. Foex, *Bull. soc. chim.*, **11**, 6 (1944).

(7) R. Breckenridge and W. Hosler, *J. Research Natl. Bur. Standards*, **49**, 65 (1952).

(8) H. Henisch, *Elec. Comm.*, **25**, 163 (1948).

(9) B. K. Boltaks, F. K. Vasenin and A. E. Salunina, *Zhur. Tekh. Fiz.*, **21**, 532 (1951) (*Phys. Ab.*, **55**, No. 3588 (1951)).

(10) K. Abe and T. Tanaka, *Repts. inst. chem. res., Kyoto Univ.*, **17**, 47 (1949) (*C. A.*, **46**, 1368 (1951)).

(11) Ya. M. Kaenzov, *Zhur. Tekh. Fiz.*, **20**, 117 (1950).

(12) M. Earle, *Phys. Rev.*, **61**, 56 (1942).

(13) E. Whalley and E. R. S. Winter, *J. Chem. Soc.*, 1170 (1950).

(14) L. H. Reyerson and J. M. Honig, *ibid.*, **75**, 3920 (1953).

(15) A. W. Czanderna and J. M. Honig, *Anal. Chem.*, **29**, 1206 (1957).

(16) A. W. Czanderna, A. F. Clifford and J. M. Honig, *J. Am. Chem. Soc.*, **79**, 5407 (1957).

TABLE I
 PROPERTIES OF TiO₂ POWDERS

	MP-980-1 ^a	MP-980-2 ^a	MP-980-5 ^a	MP-532-2 and MP-532-3 ^b	Highly purified ^c
Crystal form	Anatase ^d	Rutile ^d	Rutile ^d	Rutile ^d	Anatase
Heat treatment					
Hours	16	16	1	...	16
Temp., °C.	120	120	600	...	180
Area, sq. in./g. (BET)	87.7 ± 0.7 ^e	175 ± 3.5 ^e
	82 ± 0.8 ^f	123 ± 2.5 ^f	21.9 ± 0.8 ^f	...	41.0
Apparent particle size, μ	0.01-0.1	0.01	0.03-0.3
Particle shape ^g	Irregular Acicular	Agglomerated	Irregular
Color	White	White	Yellow	White	White
pH	9.2	8.9	7.2
Chemical anal., %					
TiO ₂	94.4	91.4	99.1	...	99.3
Loss on ignition	5.1	8.6	0.8	...	0.7
Chlorides (Cl ⁻)	0.08	0.04	0.09
Spectrographic anal., %					
SiO ₂	0.15 ^h	0.15 ^h	0.18 ^h	0.3	~0.01
Fe ₂ O ₃	.002	.001	.003	Unknown	< .001
Al ₂ O ₃	.015	.001	.02	Unknown	< .001
SnO ₂	.01	.004	.004	Minor	< .001
Cu	.0005	.0001	.0008	Unknown	< .001
Mn	.00001	.00001	.00001	Unknown	< .001
W	.005	.005	.005	Unknown	< .001
Na ₂ O	1-2	< .001
B	~.001

^a Reported by National Lead Company. ^b From Ph.D. Thesis, J. M. Honig, University of Minnesota. ^c Determined in this Laboratory. ^d By electron diffraction methods. ^e Degassed 4 hours at 200°. ^f Degassed 4 hours at 400°. ^g From electron micrographs. ^h Nb and ZnO are <0.01; Sb₂O₃, V and Cu are <0.001; Mg and Pb are <0.0005.

structure have been described in a recent publication.¹⁶ The resulting material was quite coarse (see below).

(2) Anatase, prepared as above but doped with varying quantities of sodium hydroxide, barium hydroxide or titanium tetrafluoride just prior to precipitation of the peroxidized titania gel.¹⁵ The sample compositions are indicated in Fig. 4.

(3) Samples prepared as in (1), but ground to a powder in a clean glass mortar.

(4) Commercial powders of high surface area containing various impurities. The known properties of the commercial grade powders are given in Table I.

Determination of Surface Areas of Powders.—A weighed quantity of the powder was placed in a sample bulb, suspended from the balance and counterweighted to an approximate null position. After evacuation and outgassing at the temperatures listed in Table II, the sample and compensation bulbs were cooled *in vacuo* to 78°K. by immersing the sample and compensation tubes in liquid nitrogen. Helium was admitted to a pressure of 2 mm. to accelerate the attainment of thermal equilibrium. The helium was evacuated; evacuation was continued until no change in the balance null position was observed for 30 minutes. Dry nitrogen, which is customarily used in surface area determinations,¹⁷ then was admitted in pressure increments. The compensation e.m.f. required to maintain the balance in the null position was plotted as a function of pressure. A typical isotherm obtained in this manner is shown in Fig. 3 for a rutile sample (MP-980-5) that had been outgassed at 500° until no further mass loss was observed. The isotherm was retraced upon evacuating the nitrogen in pressure decrements.

The surface area was computed using the BET value¹⁶ for the area per nitrogen molecule (16.2 Å.²) and assuming that monolayer coverage was complete at the point labeled as B on the isotherm shown in Fig. 3. Since the surface areas were obtained for rough comparisons, it did not seem worthwhile to utilize the BET procedure to locate point B more precisely.

(17) S. Brunauer and P. H. Emmett, *ibid.*, **59**, 2682 (1937).

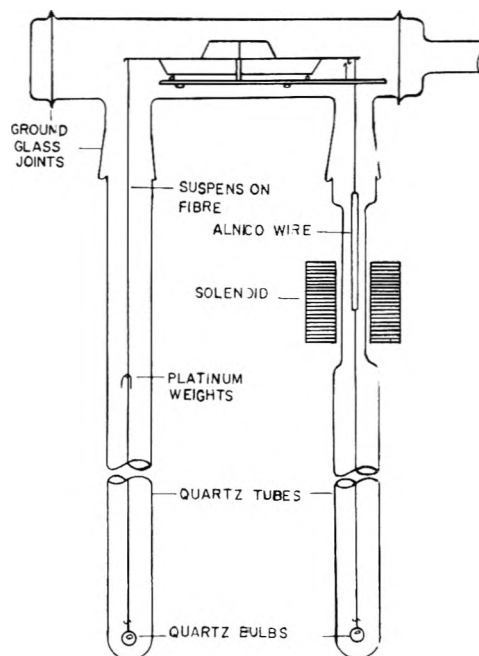


Fig. 1.—Schematic representation of microbalance used to determine changes in high vacuum.

Procedure for the Determination of Loss in Mass of a Material as a Function of Temperature in High Vacuum.—A weighed quantity of the TiC₂ crystals was suspended from the microbalance in a quartz bulb. The balance was counterweighted to an approximate null position; the system was then sealed and a vacuum drawn. Two hinged furnaces were mounted about the sample and dummy bulb (sus-

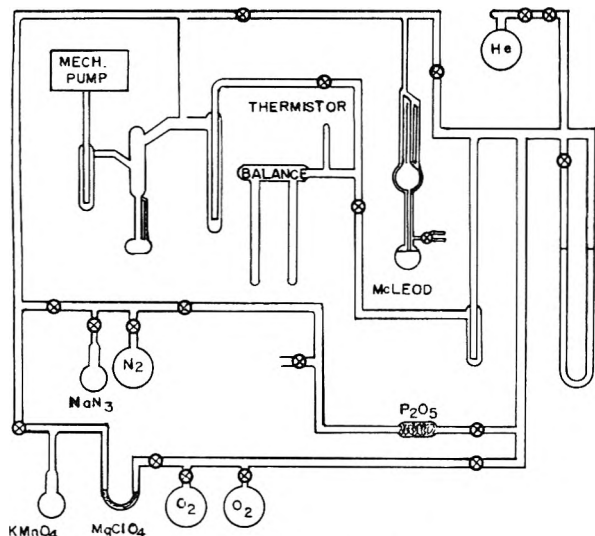


Fig. 2.—Vacuum system.

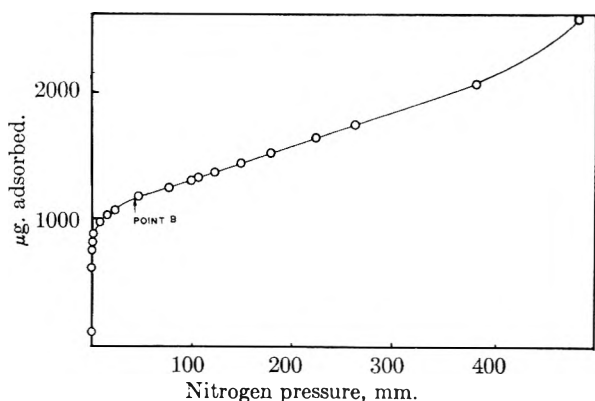


Fig. 3.—Nitrogen adsorption isotherm on rutile powder (MP-980-5) at 78°K.

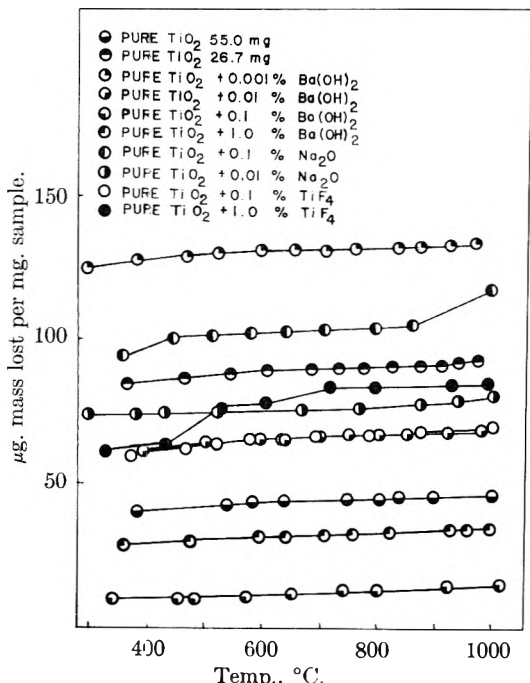


Fig. 4.—Decremental mass changes in high vacuum for TiO_2 and doped TiO_2 as a function of temperature. All curves originate at zero at 25°.

TABLE II

SUMMARY OF THE TOTAL OXYGEN UPTAKE, SURFACE AREA, AND OXYGEN UPTAKE PER UNIT SURFACE AREA OF COMMERCIAL TiO_2 SAMPLES AT VARIOUS TEMPERATURES^a

Mass of sample, mg.	Temp., °C.	Total O ₂ uptake, μg.	N ₂ adsorption, μg.	BET Surface area, m. ² /g.	Column 3 ÷ Column 5 μg./m. ²	O ₂ pressure, mm.
Anatase						
151.5	Room T	...	1224	28.1
151.5	500	... ^{b,c}	1022	23.42	... ^{a,b}
151.5	800	36	85.6	1.96	121	10
45.1	700	33	158.4	12.22	60.0	20
172.6	500	23 ^c	1120	22.6	5.9	30
172.6	700	30 ^d	120	2.41	72	12
172.6	800	35.5 ^d	165	3.31	62.4	21
172.6	915	29 ^d	54	1.09	154	16
163.5	800	52 ^c	172	3.66	87	22
Rutile MP-980-5						
206.1	Room T	...	771.2	15.38
206.1	504	19.8 ^c	1116.0	22.25	4.32	22
206.1	695	10.0 ^d	732.8	14.62	3.32	6
206.1	930	45.8 ^d	167.2	3.30	67.5	17
Rutile MP-532-3						
102.6	Room T	...	1926.3	65.31
102.6	520	42.5 ^c	1683.0	57.07	7.25	14
102.6	710	81.3 ^d	473.2	16.04	67.3	2.2
102.6	895	33 ^d	84.2	2.85	113	0.010
Rutile MP-532-2						
90.5	691	35.7 ^c	419.5	16.15	24.5	.006
90.5	896	34.8 ^d	223.0	8.60	44.8	.0014
Rutile MP-980-2						
98.0	713	59.2 ^c	176.3	6.26	96.5	.0013
98.0	920	24.4 ^d	74.8	2.66	93.5	.007
202.9	504	50.1 ^d	3190	54.6	4.52	18
Anatase (highly purified and crushed in glass mortar)						
142.9	Room T	...	1695.0	41.1
142.9	500	0	268.0	6.5	0
142.9	700	0	8.2	0.2	0
142.9	900	0	<2	<0.05	0

^a Column 1, mass of sample; column 2, temperature at which sample was outgassed to constant mass prior to the admission of oxygen; column 3, total oxygen uptake by the sample at the outgassing temperature; column 4, nitrogen adsorption on the sample at 78°K. as determined from the BET point B. After outgassing and adsorbing oxygen on the sample, it was cooled *in vacuo* from the outgassing temperature to 78°K; column 5, BET surface area, see Section IIB for method of calculation; Column 6, column (3) ÷ column (5) to obtain the oxygen of adsorption per unit area; column 7, oxygen pressure, above which no further sorption could be detected. ^b The oxygen uptake was completely masked by a prolonged drift in the balance at low pressures. ^c The sample turned grey during outgassing and white after the first admission of oxygen. Thereafter, the sample remained white (or yellow at high temperatures) even after prolonged outgassing at 915°. This oxygen adsorption was reversible. ^d This oxygen adsorption occurred reversibly.

pended from the counterweight side). The voltage input to each furnace, and hence its temperature, was regulated by fused Variacs. The latter were powered by a constant voltage transformer. In the absence of thermal drafts, temperature control to ±1° was achieved. The sample temperature was determined from the e.m.f. of a calibrated chromel-alumel thermocouple.

A precise null reading was obtained prior to evacuation at room temperature. A subsequent determination of the buoyancy slope in nitrogen thus allowed a very precise correction to be applied to the apparent mass loss on evacuation. While maintaining a continuous dynamic high vacuum of 10⁻⁴ mm. or better, the sample was heated to progressively higher temperatures. When no further change in mass could be detected in a period of eight hours at each temperature, an "equilibrium" reading was taken. The mass changes shown in Fig. 4 thus were obtained.

The readings below 300° are omitted from this figure because, as will be shown later, they pertain to the desorption of water vapor and not to changes in sample composition.

In an independent experiment, the above procedure was carried out utilizing an empty quartz sample bulb. No mass change could be detected at the highest temperature over a three-day period. Thus, if there was any volatilization of quartz at 1000° in high vacuum, it was either too slow to be detected or it occurred at nearly identical rates from the sample and compensation bulbs.

Procedure for the Determination of Oxygen Uptake by TiO₂ Powders as a Function of Pressure.—At elevated temperatures, the procedure utilized for carrying out this measurement is complicated by the existence of thermomolecular flow of gases in the pressure range $10^{-3} < P < 15$ mm. The gas flow, which results from a temperature gradient in a closed system, exerts a "drag" on the suspension fiber causing an apparent mass change.¹⁵ This effect is reproducible for a given geometry, temperature gradient and pressure, but the amount of drag depends on the properties of the ambient gas. It was determined experimentally that the drag effect could be minimized¹⁵ and calibrated with little effort. Nitrogen was used as the calibrating gas. For work of the highest precision, account should be taken of the slight difference in thermomolecular flow behavior between N₂ and O₂. However, it was established in an experiment utilizing an empty sample bulb that plots of apparent mass change against oxygen or nitrogen pressure nearly superimposed; the deviation between the two curves was less than the over-all experimental uncertainty.

The procedure for outgassing the sample was the same as described in the preceding section. After the thermomolecular flow effect was minimized,¹⁵ a plot of the apparent mass change of the sample as a function of nitrogen gas pressure was obtained; the gas then was removed in decrements as a further check on the curve. When the balance position became constant in high vacuum, oxygen was introduced to the balance system; again, the compensation current required to keep the balance in the null position was plotted against pressure. For the temperatures studied, oxygen uptake was completed in less than two to five minutes at each pressure. A typical set of data is plotted in Fig. 5. The difference between the two curves corresponds to the mass gain by the sample at various oxygen pressures. This is shown in the inset of Fig. 5.

Results

Mass Loss by Highly Purified and Doped "Bulk" Samples.—The results of a number of investigations of the loss in mass by various purified and doped TiO₂ samples (of type 1 or 2 as described earlier) are plotted in Fig. 4. All points represent equilibrium values, with the exception of the 1000° point for the TiO₂ sample containing 0.1% Na₂O. This run was terminated when the sample container dropped off the suspension. As can be seen the mass loss per unit sample mass varied widely up to 400° but was relatively constant beyond this temperature except for the samples containing 0.1% sodium oxide and 1% titanium tetrafluoride.

The mass change below 400° presumably is due to the desorption of water and of other condensable vapors from the surface and adjoining regions of the sample. This hypothesis is supported in a separate experiment carried out on the TiO₂ sample containing 0.1% sodium oxide. In this experiment, 80 μg. of water vapor per mg. of sample was collected in a microanalytical absorption tube containing a CaSO₄ getter. This compares with a mass loss of about 96 μg. per mg. of the aliquot suspended from the balance. The difference can be ascribed to variations in the surface areas of the two aliquots and to the presence of other adsorbed or trapped vapors such as carbon dioxide which are not collected in the absorption tube.

The material containing TiF₄ exhibited a marked

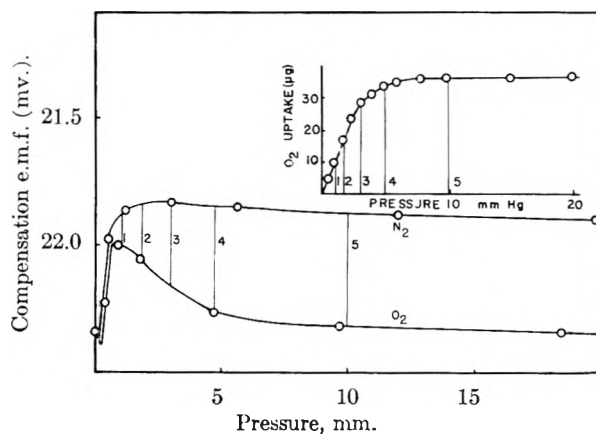


Fig. 5.—Graphical method for determining oxygen uptake on TiO₂ powders as a function of pressure.

change of mass in the region from 400 to 800°. The changes observed here probably resulted from volatilization of the gaseous titanium tetrafluoride. In support of this statement, it should be noted that the equilibration time at each temperature below 700° ranged from one to four days, whereas, in other samples, equilibrium generally was established in 8–12 hours. Furthermore, a negative test was obtained for fluoride ion¹⁸ for both of the samples doped with TiF₄ after they had been heated *in vacuo* to 1000°. This indicated that not more than 1% of the original impurity remained in the sample.

Likewise, the material doped with sodium oxide exhibited marked changes in mass at temperatures exceeding 900°. These changes were probably due to the sublimation of the sodium and/or sodium oxide. This was established by observing: (a) an excessively long equilibration time at 1000° (seven days for the 0.1% sodium oxide sample); (b) a chemical attack, not encountered in any other run, on the silica sample bulb and on the Vycor suspension fiber; and (c) a negative flame test for sodium in the samples heated to 1000° *in vacuo*.

Oxygen Uptake on Highly Purified and Doped "Bulk" TiO₂ Samples.—After reaching the highest sample temperature (~1000°) in measuring the mass loss *in vacuo* of the highly purified and doped TiO₂ samples, oxygen was admitted up to a pressure of 150 mm. No uptake was observed over a 24-hour period at 1000° with any of the samples. Additional runs were carried out in which new aliquots of several of the bulk samples were heated at 500 or 700° until no further change in mass was observed. Oxygen then was admitted at these lower temperatures up to a pressure of 150 mm., but again no uptake could be detected within a 24-hour period. The surface area of the "bulk" material was 0.2 m.²/g. or less in all cases.

Oxygen Uptake on Commercial TiO₂ Powders.—The interaction of oxygen with commercial TiO₂ powders (of type 4 as described earlier) then was studied as a function of pressure at various temperatures. After the oxygen uptake has been determined at a given temperature, the oxygen was

(18) F. Feigl, "Spot Tests," 3rd English Edition, Elsevier Publishing Co., Inc., New York, N. Y., 1946, p. 252.

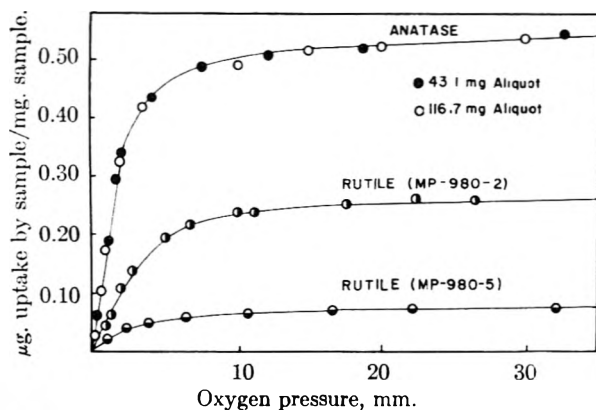


Fig. 6.—Oxygen adsorption isotherms on TiO_2 powders at 504° .

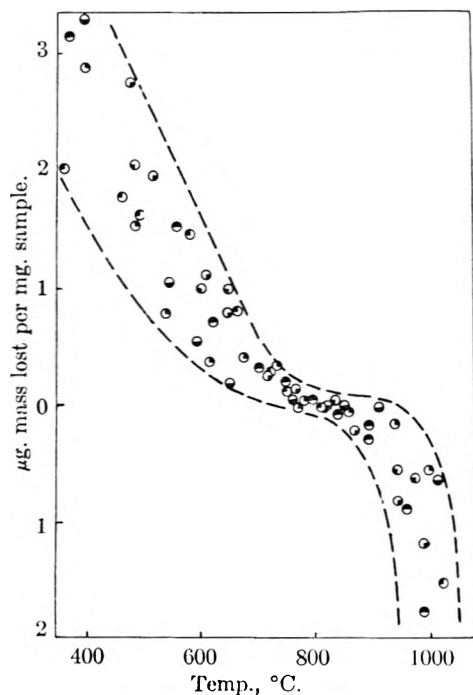


Fig. 7.—Magnification of the $400\text{--}1000^\circ$ temperature region for the pure TiO_2 and $\text{Ba}(\text{OH})_2$ doped TiO_2 data plotted in Fig. 4. See Fig. 4 for the key to the symbols. All curves are plotted relative to zero at 800° .

evacuated. In these experiments, oxygen uptake or loss was complete in two to five minutes at each pressure. High vacuum was maintained until a constant sample mass again was achieved. The sample then was cooled *in vacuo* to liquid nitrogen temperature and the surface area was determined. The sample was reheated to a higher temperature in vacuum until no further mass change was observed. The oxygen uptake and surface area then were measured following the same procedure as described above; this cycle was repeated several times for each sample. The total oxygen uptake, the surface area and the pressure, above which no further oxygen uptake could be measured for the various samples at different temperatures, are summarized in Table II. Adsorption isotherms, similar to the one shown in the inset of Fig. 5, were obtained in each case.

In addition to the above systematic cycle of experiments, a second aliquot of sample MP-

532-3 was outgassed to constant mass at 700 and 900° . After cooling to 78°K . *in vacuo*, oxygen was admitted in increments up to the saturation pressure and then evacuated. A reversible desorption process was observed, thus indicating no net oxygen uptake at 78°K . One of the isotherms from this experiment was presented as Fig. 6 in reference 15.

Sorption data were obtained at 504° for two aliquots of anatase (43.1 and 116.7 mg., see Table II) and the uptake per unit sample mass was plotted as a function of pressure. As can be seen in Fig. 6, the resulting isotherms superpose within experimental error. Results for two of the rutile samples are also plotted on this figure for the purpose of comparison.

Oxygen Uptake by Highly Purified TiO_2 Powder.—The results of the determination of the oxygen uptake of highly purified TiO_2 powder (of type 3 as described earlier) also are summarized in Table II. These data were obtained utilizing the same systematic cycle of tests employed for the commercial grade powders.

Discussion

As a first approximation, it can be stated that the sample composition of bulk TiO_2 remains constant above 400° ; however, a number of interesting features are revealed in Figs. 7 and 8 in which mass changes relative to the sample mass at 800° are plotted as a function of temperature on a very much larger scale. In these figures, it is evident that for *all* samples there is a gradually diminishing mass loss up to 875° , beyond which a gradually increasing loss of mass again is observed. Upon bracketing the experimental results with the dotted envelopes, an inflection point at 875° is clearly indicated.

The loss in mass up to the inflection point is probably a result of the expulsion of entrapped water vapor. In other systems, such as aluminum oxide and silicon dioxide, it is known that samples must be heated to over 900° in order to expel all water vapor.¹⁹⁻²¹ The divergence in mass losses at lower temperatures undoubtedly indicates that the mass change up to the inflection point depends on the sample history and composition.

The increasing mass loss above 875° is probably the result of an incipient decomposition of the sample, perhaps of the general type expressed in equation 1. This is supported by the following observations: (a) samples heated to 800° and cooled to room temperature in vacuum retain their ivory appearance, whereas (b) samples heated to 1000° assume a grey color, not only on the surface but also in the interior. It is well known from experiments involving a partial reduction of TiO_2 that the creation of oxygen vacancies is accompanied by the appearance of a bluish color.

It is of interest to compare the above properties with those of high area commercial grade powder (anatase). Both types of samples exhibit con-

(19) W. Blum, *J. Am. Chem. Soc.*, **38**, 1282 (1916).

(20) W. Mielr, P. Koch and J. Kratzert, *Z. angew. Chem.*, **43**, 250 (1930).

(21) J. N. Frers, *Z. anal. Chem.*, **95**, 131 (1933).

siderable mass loss in the temperature region below 400° *in vacuo*, but no drastic change in composition occurs between 400 and 1000°. However, while reversible oxygen sorption isotherms were obtained in the temperature range 500–900° for the commercial samples, these were not encountered in the pure material. It might be postulated that the difference is a result of surface effects. In Table II, column 3, it can be seen that the maximum oxygen uptake in all cases was in the range 20 to 80 μg . The *minimum* surface area, A , encountered with these commercial samples, was of the order 2 m^2/g . Since A for the bulk material was at least one order of magnitude less than the above value, the expected uptake of oxygen would be diminished to a *maximum* of 2 to 8 μg . This quantity is barely above the experimental error associated with the most careful use of the balance at elevated temperatures. However, it can be seen in Table II that no oxygen uptake was detected even in the case where the pure bulk anatase was crushed to a comparably high surface area. In an additional experiment, no oxygen uptake could be detected on a crushed sample of a doped material containing bulk impurities. Thus, it would seem that impurities on the surface of TiO_2 strongly influence the ease of oxygen adsorption or desorption for this material and that, in the absence of impurities, no appreciable oxygen losses occur from the surface in the temperature range studied.

While marked sintering is exhibited by the commercial samples in the temperature range 500–900°, the quantity of oxygen uptake remained essentially constant (column 3, Table II). Thus, the relative amount of oxygen uptake per unit surface area increased greatly during sintering. It may be postulated that this increase was the result of diffusion of additional impurity centers to the surface. Or one could argue that the impurity centers on the surface became more active at higher temperatures. In any event, it remains to be established to what extent the reversible oxygen uptake on the surface depends on the nature of the impurities and on their distribution. The impurity additions to the pure bulk material had no apparent effect on the incipient decomposition, but this does not mean that impurity centers on the surface would not affect the oxygen loss. The surface area of the doped samples was too small for any effect, if present, to be observed.

As can be seen in Table II, the properties of the rutile samples MP-980-2, MP-980-5, MP-532-2 and MP-532-3 were essentially the same as for the anatase powder (MP-980-1). However, there were differences in the initial slopes of some of the sorption isotherms; it was not possible to establish a correlation with the impurity content of the sample.

At this point, it should be mentioned that the blue color observed upon original outgassing of the commercial samples has been observed by others.^{22–24} We believe that the discoloration is a result of slight oxygen loss from the TiO_2 . Re-

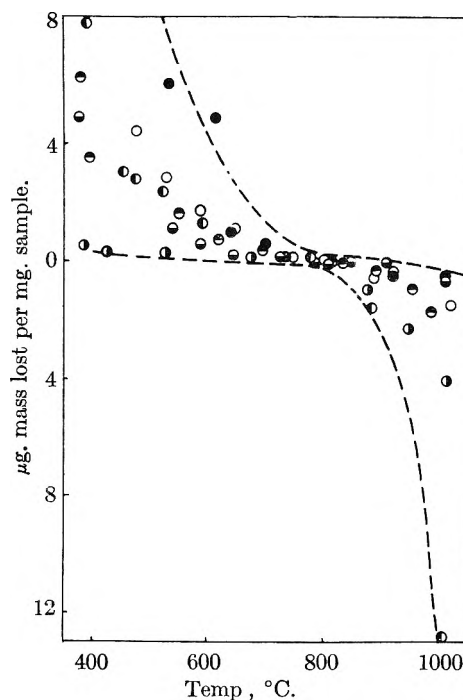


Fig. 8.—Same as Fig. 7 but for pure TiO_2 and TiF_4 and Na_2O doped TiO_2 data. See Fig. 4 for the key to the symbols.

cently, Gebhardt²⁴ reported that the discoloration in commercial rutile powders resulted principally from organic contamination of the surface in a "dirty" vacuum system. If an organic material were oxidized from the surface, an apparent loss in sample mass would be observed. We did not observe such an effect in any of our experiments. Further, in some cases, *i.e.*, rutile MP-532-2 and -3, oxygen uptake was completed at pressures of 10 μ . In these cases, a continuous decrease in gas pressure was recorded as long as there was a continuous increase in sample mass. Equilibrium was attained within a few minutes. We therefore conclude that our vacuum system was "clean" in the definition of Gebhardt. We cannot overemphasize that once oxygen was admitted to a commercial grade discolored sample, the discoloration could not be made to reappear ever though the solid was heated to as high as 1000° in a dynamic high vacuum.

There is an interesting coincidence between the temperature of incipient decomposition of the bulk material (875°) and the temperature at which a sharp break in the resistivity of rutile single crystals was observed (900°) by Cronmeyer.⁵ However, no convincing explanation can be advanced that correlates the observed irreversible creation of defects from the incipient decomposition with the reversible change in resistivity of the single crystals.

Finally, an interesting correlation exists between the temperature above which marked sintering of the powders occurred (500°) and the temperature at which a reversible oxygen uptake was first detected (500°) (see Table II). It is generally accepted that the oxygen loss from a titanium dioxide surface is equivalent to the creation of surface vacancies or defects. Thus, for the

(22) L. H. Reyerson and J. M. Honig, *J. Am. Chem. Soc.*, **75**, 3917 (1953).

(23) Y. L. Sandler, *This Journal*, **58**, 54 (1954).

(24) J. Gebhardt and K. Herrington, *ibid.*, **62**, 120 (1958).

powders studied, the temperature at which sintering set in corresponds roughly with the temperature at which surface defects are formed. Recently Parravano²⁵ proposed that the sintering mechanism in metal oxides consists of welding crystallites together by "bridges" which emerge from surface defects. Our results tend to support this hypothesis.

Conclusions

Several conclusions can be cited from this work.

(1) Reversible oxygen adsorption seems to occur at surface impurity centers in commercial grade titanium dioxide at temperatures between 500 and 900°. This finding is in agreement with reports that isotopic oxygen exchange is obtained with commercial and/or reagent grade samples of NiO, CaO, MnO₂, TiO₂, ThO₂ and γ -Al₂O₃.²⁶⁻²⁹ at temperatures as low as one-fourth the melting point of the bulk phase.

(2) The temperature of incipient decomposition of highly purified TiO₂ in a dynamic vacuum of

about 10⁻⁵ mm. is approximately 875°. Reversible oxygen adsorption, if present, is too small to be detected.

(3) Nearly all water vapor and other condensable vapors appear to be desorbed at 800° in high vacuum. Presumably, an analysis of the composition of low area titanium dioxide subjected to these conditions should yield a compound close to the stoichiometric composition.

(4) Neither conclusion (2) nor (3) was altered by doping the purified TiO₂ with various amounts of BaO, Na₂O or TiF₄. However, Na₂O incorporated in the lattice is volatile above 875° and incorporated TiF₄ is volatile between 400 and 800°.

NOTE ADDED IN PROOF.—Under the conditions of our experiment, the Na₂O undoubtedly vaporized from the doped TiO₂ samples as sodium atoms and oxygen molecules.³⁰

Acknowledgments.—The authors thank the National Lead Company and the Electro Metallurgical Company for contribution of the TiO₂ powder and granular titanium metal, respectively. They also thank the Research Corporation for its financial support of this study and the National Science Foundation for its grant to A. W. Czanderna. Finally, thanks are due to Dr. A. F. Clifford and Mr. Q. W. Choi for consultation and suggestions.

(30) Leo Brewer, personal communication.

(25) G. Parravano, personal communication.

(26) J. A. Allen and I. Lauder, *Nature*, **164**, 142 (1949).

(27) N. Morita, *Bull. Chem. Soc. Japan*, **15**, 1 (1940).

(28) E. R. S. Winter, *J. Chem. Soc.*, 1170 (1950).

(29) E. Whalley and E. R. S. Winter, *ibid.*, 1175 (1950).

A MASS SPECTROMETRIC STUDY OF THE VAPORIZATION OF FERROUS BROMIDE¹

BY RICHARD F. PORTER AND RICHARD C. SCHOONMAKER

Department of Chemistry, Cornell University, Ithaca, New York

Received October 2, 1958

A mass spectrometer has been used to analyze the vapors effusing from a Knudsen cell containing FeBr₂(s). In the temperature interval 620–665°K., the monomer is the predominant vapor species; but at the melting point the dimer concentration becomes significant. Thermochemical data have been determined for the reactions: 2FeBr₂(s) = Fe₂Br₄(g), $\Delta H_{645}^{\circ} = 59.5 \pm 6$ kcal./mole dimer; Fe₂Br₄(g) = 2FeBr₂(g), $\Delta H_{640}^{\circ} = 34.7 \pm 4$ kcal./mole dimer.

Introduction

Unlike the iron(III) bromide which is known to vaporize largely as gaseous dimers, the iron(II) bromide is believed to vaporize primarily as the monomer, FeBr₂(g). Evidence that FeBr₂ is not appreciably associated as dimers in the vapor phase has been obtained in the vapor pressure studies of MacLaren and Gregory.² Employing effusion, transpiration and diaphragm methods of measurement, these investigators determined vapor pressures of solid and liquid FeBr₂ in the temperature range 400–909°. Based on the three independent methods their data give reasonably concordant vapor pressures if the monomer is assumed to be the major vapor species. The authors point out, however, that in the higher temperature range near the melting point of the solid, the presence of about 15% dimer cannot be excluded. In order to obtain information on the possible

existence of polymeric species, we have analyzed, mass spectrometrically, the vapors effusing from a Knudsen cell containing solid, anhydrous ferrous bromide. Earlier mass spectrometric studies on ferrous chloride² indicated that FeCl₂ is associated to some extent as dimers in the saturated vapor.

Experimental

Descriptions of the experimental method and the furnace assembly for a 12-inch, direction-focusing mass spectrometer have been given earlier.^{3a,b} The method involves electron bombardment of the vapor leaving an effusion cell and the subsequent identification and study of the positive ions produced. The experimental conditions closely approximated those previously reported for FeCl₂. Effusion cells were constructed of high purity iron and the ratio of orifice area to total sample surface area was less than 5×10^{-4} . The temperature range investigated was between 300 and 400°. Temperatures were measured with a chromel–alumel thermocouple calibrated at the melting point of zinc. Samples of FeBr₂ were prepared by passing anhydrous HBr over red hot iron wire in a Vycor tube. Yellow flakes of FeBr₂, collected on the cooler portion of the tube, were used. Results from the first few experiments were discarded be-

(1) This research was supported by the U. S. Air Force through the Air Force Office of Scientific Research of the Air Research and Development Command under contract No. AF 18 (603)-1.

(2) R. O. MacLaren and N. W. Gregory, *THIS JOURNAL*, **59**, 184 (1955).

(3) (a) R. C. Schoonmaker and R. F. Porter, *J. Chem. Phys.*, **29**, 116 (1958); (b) R. F. Porter and R. C. Schoonmaker, *THIS JOURNAL*, **62**, 234 (1958).

cause of interfering hydrolysis of the samples. This was recognized by the high HBr^+ background and a black residual surface layer on the samples after heating. With sufficient precautions to keep the samples dry during preparation and rapid transfer of the freshly prepared material to the mass spectrometer, hydrolysis was diminished and satisfactory results could be obtained. At temperatures above 400° ion current ratios were not, in general, very reproducible. This condition probably was caused by failure to attain complete vapor saturation due to surface contamination of the solid resulting from hydrolysis. A large, discontinuous and non-reproducible increase in the ratio $I_{\text{FeBr}^+}/I_{\text{FeBr}_2^+}$ was observed at higher temperatures during several runs. At present, this anomalous behavior remains unexplained.

Results and Discussion

A typical mass spectrum of ferrous bromide vapor is shown in Table I. Identification of ionic species with masses below 200 was obtained by counting from known background masses (primarily residual hydrocarbon). Ions with mass over 200 were checked with a Rotating Coil Gaussmeter. Final identification of all ions was made by comparison of observed intensities of isotopic species with those calculated from the natural abundances of Fe and Br isotopes. Since all of the isotopic masses are two units apart, no difficulty was encountered in resolving the heaviest isotopic species. Masses containing three or four atoms of Fe were not detected. Appearance potentials for the principal ions in the vapor, calibrated against the ionization potential of HBr^+ , are presented in Table I. The ions observed fall

TABLE I
MASS SPECTRUM OF FeBr_2 VAPOR ($T = 392^\circ$)

Ion	Mass no.	Intensity; ^a	Appearance potential ^b (v.)
Fe^+	56	45.0	16.6 ± 0.5
FeBr^+	135	63.5	$12.9 \pm .5$
FeBr_2^+	216	100.0	$10.7 \pm .5$
Fe_2Br^+	191	0.8
Fe_2Br_2^+	272	0.3
Fe_2Br_3^+	351	9.3	$13.6 \pm .5$
Fe_2Br_4^+	431	5.6	$12.6 \pm .5$

^a Relative units; ionizing electron energy = 50 volts.

^b Obtained by linear extrapolation of appearance potential curves, calibrated against $A(\text{HBr}^+) = 13.2$ volts.

into two classes: those containing one atom of Fe, and those containing two atoms. Below 400° , the ratios $I_{\text{FeBr}^+}/I_{\text{FeBr}_2^+}$ and $I_{\text{Fe}_2\text{Br}_4^+}/I_{\text{Fe}_2\text{Br}_3^+}$ had only a slight dependence on temperature (see Fig. 1) indicating that FeBr^+ and Fe_2Br_3^+ are probably formed primarily from the parent molecules of FeBr_2^+ and FeBr_4^+ , respectively. The slight temperature dependence of these ratios may be due to a temperature dependent dissociative ionization cross section, or, in the case of $I_{\text{Fe}_2\text{Br}_4^+}/I_{\text{Fe}_2\text{Br}_3^+}$, to a small contribution from a second process, e.g., dissociative ionization of the dimer. The presence of stable molecules with iron in an oxidation state lower than two (i.e., $\text{FeBr}(\text{g})$, $\text{Fe}_2\text{Br}_3(\text{g})$, etc.) is more or less ruled out since the solid vaporizes stoichiometrically as FeBr_2 . The intensity ratio of FeBr_2^+ to Fe_2Br_3^+ varied considerably with temperature as indicated in Fig. 1. This is taken as sufficient evidence that FeBr_2^+ is not formed primarily from the parent of Fe_2Br_3^+ or Fe_2Br_4^+ . The observations are consistent with

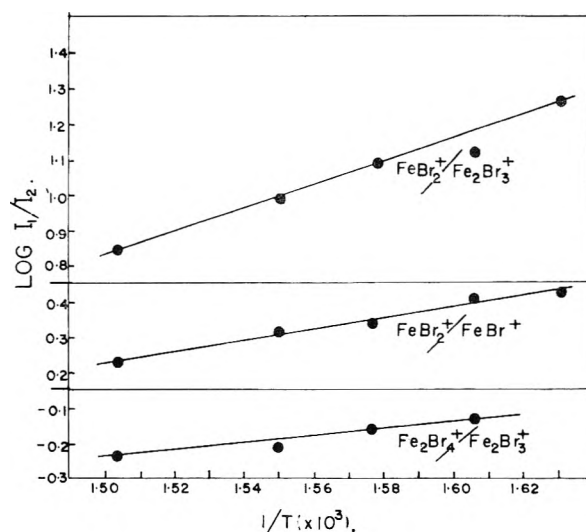
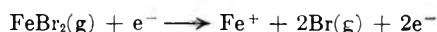


Fig. 1.

the presence of two molecules, $\text{FeBr}_2(\text{g})$ and $\text{Fe}_2\text{Br}_4(\text{g})$, in the vapor phase. The high appearance potential (~ 16.6 volts) of the Fe^+ ion leads to the conclusion that it is formed by fragmentation. A possible process for the formation of Fe^+ is



The mechanisms by which Fe_2Br_2^+ and Fe_2Br_3^+ are formed could not be determined due to the low intensities of these species. However, it seems reasonable to attribute their formation to dissociative ionization of $\text{Fe}_2\text{Br}_4(\text{g})$.

Since our temperature range overlaps the effusion data of MacLaren and Gregory, we can use their vapor pressures to calibrate the mass spectrometer. For our instrument,^{3a} $P_{x_i} = TK_{x_i}I_{x_i}^+$, where P_{x_i} is the partial pressure of species x_i in the effusion cell, $I_{x_i}^+$ is the total intensity of the ion species x_i^+ corrected for isotopic abundance, T is the absolute temperature, and K_{x_i} is an instrument sensitivity factor incorporating ionization cross section and ion detection efficiency terms. Thus, for a given temperature

$$\frac{P_{\text{FeBr}_2}}{P_{\text{Fe}_2\text{Br}_4}} = \left[\frac{\sigma(\text{Fe}_2\text{Br}_4)}{\sigma(\text{FeBr}_2)} \right] \left[\frac{S(\text{Fe}_2\text{Br}_4^+)}{S(\text{FeBr}_2^+)} \right] \left[\frac{I_{\text{FeBr}_2^+}}{I_{\text{Fe}_2\text{Br}_4^+}} \right]$$

In this expression $\sigma(\text{Fe}_2\text{Br}_4)/\sigma(\text{FeBr}_2)$ is the ratio of relative partial ionization cross sections for $\text{Fe}_2\text{Br}_4(\text{g})$ and $\text{FeBr}_2(\text{g})$; and $S(\text{Fe}_2\text{Br}_4^+)/S(\text{FeBr}_2^+)$ is the ratio of relative electron multiplier detection efficiencies for FeBr_2^+ and Fe_2Br_4^+ . If the ionization cross section ratio, $\sigma(\text{Fe}_2\text{Br}_4)/\sigma(\text{FeBr}_2)$, is taken to be 2 and the multiplier efficiency term to be approximately $1/\sqrt{2}$,⁴ then

$$P_{\text{Fe}_2\text{Br}_4} \cong \frac{P_{\text{FeBr}_2}}{\sqrt{2}} \left[\frac{I_{\text{Fe}_2\text{Br}_4^+}}{I_{\text{FeBr}_2^+}} \right]$$

Equilibrium pressures of $\text{FeBr}_2(\text{g})$ and $\text{Fe}_2\text{Br}_4(\text{g})$ at several temperatures, calculated from our ion intensity ratios and the effusion data of MacLaren and Gregory, are presented in Table II. Since

$$\Delta F^0_T = -RT \ln \left(\frac{P_{\text{FeBr}_2}}{I_{\text{Fe}_2\text{Br}_4}} \right)^2$$

for the reaction $\text{Fe}_2\text{Br}_4(\text{g}) = 2\text{FeBr}_2(\text{g})$, a heat of

dissociation may be determined if an entropy is evaluated for the reaction. Experimental reaction entropies have been determined² for the dimerization of $\text{FeCl}_2(\text{g})$, $\text{FeCl}_3(\text{g})$ and $\text{FeBr}_3(\text{g})$. The values are not widely divergent, and from them we estimate -28 ± 5 e.u. for the entropy of dimerization of $\text{FeBr}_2(\text{g})$. Using this entropy and values of ΔF^0_T , we have calculated the heats of dissociation for $\text{Fe}_2\text{Br}_4(\text{g}) = 2\text{FeBr}_2(\text{g})$ presented in Table II. Combination of the heat of dissociation of $\text{Fe}_2\text{Br}_4(\text{g})$ with a value of 47.1¹ kcal./mole for the process $\text{FeBr}_2(\text{s}) = \text{FeBr}_2(\text{g})$ yields the heats of

TABLE II

THERMOCHEMICAL DATA FOR THE REACTIONS: (a) $\text{Fe}_2\text{Br}_4(\text{g}) = 2\text{FeBr}_2(\text{g})$; (b) $2\text{FeBr}_2(\text{s}) = \text{Fe}_2\text{Br}_4(\text{g})$

T (°K.)	$p_{\text{FeBr}_2}(\text{atm.})$	$p_{\text{Fe}_2\text{Br}_4}(\text{atm.})$	ΔF_T^0	ΔH_T^0 , ^a	ΔH_T^0 , ^b
			kcal./ mole dimer reac-	kcal./ mole dimer reac-	kcal./ mole dimer reac-
622	2.76×10^{-8}	1.08×10^{-9}	17.4	34.8	59.4
635	6.05×10^{-8}	2.54×10^{-9}	17.0	34.8	59.4
645	1.07×10^{-7}	4.54×10^{-9}	16.5	34.6	59.6
665	3.3×10^{-7}	1.95×10^{-8}	16.0	34.6	59.6

^a $\Delta S_T^0 \approx 28$ e.u.; $\Delta H_{640}^0(\text{av.}) = 34.7 \pm 4$ kcal. ^b ΔH_T^0 [$\text{FeBr}_2(\text{s}) = \text{FeBr}_2(\text{g})$] = 47.1 kcal./mole. See ref. 1; $\Delta H_{640}^0(\text{av.}) = 59.5 \pm 6$ kcal.

sublimation for $\text{Fe}_2\text{Br}_4(\text{g})$ shown in Table II. The uncertainties are due mainly to the entropy and ionization cross section terms. The difference in heats of sublimation for $\text{Fe}_2\text{Br}_4(\text{g})$ and $\text{FeBr}_2(\text{g})$ may be calculated from the slope of the $I_{\text{FeBr}_2^+}/I_{\text{Fe}_2\text{Br}_4^+}$ vs. $1/T$ curve shown in Fig. 1. In this plot $I_{\text{Fe}_2\text{Br}_4^+}$ is used instead of $I_{\text{FeBr}_2^+}$ in order to gain a factor of approximately 1.5 in sensitivity. The difference in heats of sublimation, 14.2 kcal., determined by a least squares treatment of the graphical points is in good agreement, considering the uncertainties involved, with the value of 12.4 determined by the third law method. This agreement establishes some degree of confidence in the estimated value for the entropy of dimerization for $\text{FeBr}_2(\text{g})$.

The data in Table III represent an extrapolation of our calculated pressures to higher temperatures using a heat of sublimation of $\text{FeBr}_2(\text{g})$ of 47.1 kcal./mole and a heat of fusion of $\text{FeBr}_2(\text{s})$ of 11 kcal./mole from ref. 1, a heat of sublimation of

$\text{Fe}_2\text{Br}_4(\text{g})$ of 59.5 kcal./mole determined in the present work, and assuming that ΔC_p (sublimation) for $\text{FeBr}_2(\text{g})$ and $\text{Fe}_2\text{Br}_4(\text{g})$ are approximately equal to those estimated^{1,2,4,5} for $\text{FeCl}_2(\text{g})$ and $\text{Fe}_2\text{Cl}_4(\text{g})$, respectively. At the melting point of FeBr_2 , we obtain a total vapor pressure of 3.0×10^{-2} atm. which, though perhaps fortuitous, is in good agreement with the value 2.95×10^{-2} atm. calculated from the vapor pressure equation of MacLaren and Gregory which was obtained from diaphragm gauge measurements where no assumption was necessary concerning the vaporizing species. The data in Table III indicate approxi-

TABLE III

MONOMER/DIMER PRESSURE RATIO FOR FERROUS BROMIDE

VAPOR AT VARIOUS TEMPERATURES

T, °K.	$p_{\text{FeBr}_2}/p_{\text{Fe}_2\text{Br}_4}$
645	24.6
964 (m.p.) ^a	1.1
1215 (b.p.) ^b	1.1

^a Reference 2. ^b Extrapolated value, this work.

mately equal partial pressures of monomer and dimer in the saturated vapor over $\text{FeBr}_2(\text{l})$. This dimer concentration is somewhat larger than that estimated as an upper limit (15%) by MacLaren and Gregory from a comparison of their transpiration and diaphragm measurements in an overlapping temperature range near the melting point. It is interesting to note, however, that, with the aid of the previously estimated ΔC_p (sublimation) of $\text{FeBr}_2(\text{g})$, the extrapolation of their vapor pressure curve obtained from effusion experiments at low temperatures, where the monomer is the major vapor species, gives a monomer vapor pressure at the melting point which is closer to 50% of the total pressure obtained from their diaphragm measurements. The accuracy in calculation of the monomer-dimer ratio in our work is subject to the uncertainty in the heat of dimerization of the monomer. With the present results, it is only possible to set the limits of 30-70% for the dimer concentration at the melting point of FeBr_2 where the total pressure is taken to be 3×10^{-2} atmosphere.

(4) M. G. Inghram, R. Hayden and D. Hess, "Mass Spectroscopy in Physics Research," Nat. Bur. Standards Cir. 522, 1952.

(5) K. K. Kelley, U. S. Bur. Mines Bull. No. 476, 1949.

LIGHT SCATTERING INVESTIGATION OF ORDERING EFFECTS IN SILICOTUNGSTIC ACID SOLUTIONS

BY M. J. KRONMAN AND SERGE N. TIMASHEFF

Eastern Regional Research Laboratory,² Philadelphia 18, Pennsylvania

Received October 9, 1958

A light scattering investigation was carried out on silicotungstic acid in the presence and absence of salt. In the presence of 0.300 M NaCl, the dependence of $H(C/\tau)$ on C was normal and the intercept corresponded to the formula molecular weight. In the absence of salt, at concentrations above 20 g./l., the points fell on a straight line that seemed to extrapolate to $1/2$ the formula weight. Below 20 g./l., the $H(C/\tau)$ values curved strongly downward toward the formula weight. This behavior is interpreted in terms of ordering effects in the solution, due to electrostatic repulsion.

Introduction

In addition to the use of the light scattering technique for the determination of molecular weights,^{3,4} it has been of special value in the study of physico-chemical properties of proteins⁵⁻⁷ and in the elucidation of processes in which they are involved, such as enzyme inactivation,⁸ enzyme-substrate interaction^{9,10} and aggregation-disaggregation phenomena.¹¹⁻¹⁷ The latter types of studies, however, are complicated by the fact that often the best experimental conditions for the investigation of the given process may be poor from the standpoint of light scattering work, with the result that the data cannot be interpreted in an unambiguous manner.

For a system composed of water, protein and a salt, for example, multi-component theory¹⁸⁻²⁰ yields the following expression for the variation of the excess turbidity, τ , with concentration

$$H \frac{C_2}{\tau} = \frac{1}{1+D} \left\{ \frac{1}{M_2} + \left[\frac{A_{22}}{M_2} - \frac{A_{12}}{M_1} \left(\frac{A_{12}}{\frac{2}{C_1} + A_{11}} \right) \right] C_2 \right\}$$

$$H = \frac{32\pi^3 n^2 (\partial n / \partial C_2)^2}{3\lambda^4 N}$$

$$D = \frac{-2\alpha A_{12}}{\frac{2}{C_1} + A_{11}} + \left(\frac{\alpha A_{12}}{\frac{2}{C_1} + A_{11}} \right)^2 \quad (1)$$

$$A_{ij} = \frac{1}{kT} \frac{\partial \mu_i^{(e)}}{\partial C_j}$$

$$\mu_i = RT \log C_i - \mu_i^{(e)} + \mu_i^0(T, p)$$

$$\alpha = \frac{\partial \epsilon}{\partial C_1} / \frac{\partial n}{\partial C_2}$$

where water is component 0, a 1-1 salt is component 1 and protein is component 2. C_i is the concentration of component i in grams per ml., n is the refractive index of the solution, M_i is the molecular weight of component i , and $\mu_i^{(e)}$ is the excess chemical potential of that component. It is apparent from this equation that in systems involving strong salt-protein interaction the zero concentration intercept does not give the molecular weight of the protein. Attraction between protein and salt leads to values of $(HC_2/\tau)_{C_2=0}$ lower than those corresponding to the molecular weight, while repulsion results in values which are too high.

In cases where salt-protein interactions are sufficiently small and can be neglected, equation 1 can be transformed⁷ to

$$H \frac{C_2}{\tau} = \frac{1}{M_2} + \frac{1000}{M_2^2} C_2 \left(\frac{Z_2^2}{2m_1} + \beta_{22} \right) \quad (2)$$

where m is the molarity of the salt and β_{22} is $\partial \ln \alpha_2 / \partial C_2$, i.e., the derivative of the activity coefficient of the protein with respect to its own concentration. Here, extrapolation to infinite dilution yields the correct molecular weight within the above approximation. In many cases, however, the extrapolation cannot be performed, and it is necessary to calculate the molecular weight *directly* from the light scattering data obtained at finite concentrations. Under such conditions serious difficulties may arise.

For moderate protein concentrations, under conditions of low charge and high ionic strength, the value of $H(C_2/\tau)$ is a reasonable approximation of the reciprocal of the weight average molecular weight. At low ionic strength and high charge this approximation can lead to very serious errors. The use of salt-free systems, in which the light scattering expression is formally simpler, does not eliminate these difficulties. For a two-component system, the light scattering equation is

$$H \frac{C_2}{\tau} = \frac{1}{M_2} \left[1 + \frac{C_2}{RT} \left(\frac{\partial \mu_2^{(e)}}{\partial C_2} \right)_{T,p} \right] \quad (3)$$

(1) This work was presented in part at the Second Delaware Valley Regional Meeting of the Am. Chem. Soc., February, 1958, and at the 133rd Meeting of the American Chemical Society, San Francisco, April, 1958.

(2) Eastern Utilization Research and Development Division, Agricultural Research Service, U. S. Department of Agriculture.

(3) M. Halwer, G. C. Nutting and B. A. Brice, *J. Am. Chem. Soc.*, **73**, 2786 (1951).

(4) M. J. Kronman and M. D. Stern, *THIS JOURNAL*, **59**, 969 (1955).

(5) S. N. Timasheff and I. Tinoco, *Arch. Biochem. Biophys.*, **66**, 427 (1957).

(6) S. N. Timasheff, H. M. Dintzis, J. G. Kirkwood and B. D. Coleman, *J. Am. Chem. Soc.*, **79**, 782 (1957).

(7) J. T. Edsall, H. Edelhoch, R. Lontie and P. R. Morrison, *ibid.*, **72**, 4641 (1950).

(8) H. Edelhoch, *ibid.*, **79**, 6100 (1957).

(9) D. S. Yasnoff and H. B. Bull, *J. Biol. Chem.*, **200**, 619 (1953).

(10) M. J. Kronman and M. D. Stern, manuscript in preparation.

(11) J. E. Fitzgerald, N. S. Schneider and D. F. Waugh, *J. Am. Chem. Soc.*, **79**, 601 (1957).

(12) J. F. Foster and R. C. Rhees, *Arch. Biochem. Biophys.*, **40**, 437 (1952).

(13) S. N. Timasheff and R. J. Gibbs, *ibid.*, **70**, 547 (1957).

(14) R. Townend and S. N. Timasheff, *J. Am. Chem. Soc.*, **79**, 3613 (1957).

(15) M. J. Kronman, M. D. Stern and S. N. Timasheff, *THIS JOURNAL*, **60**, 829 (1956).

(16) I. Tinoco, *Arch. Biochem. Biophys.*, **68**, 367 (1957).

(17) M. Bier and F. F. Nord, *Proc. Natl. Acad. Sci., U. S.*, **35**, 17 (1949).

(18) J. G. Kirkwood and R. J. Goldberg, *J. Chem. Phys.*, **18**, 54 (1950).

(19) W. H. Stockmayer, *ibid.*, **18**, 58 (1950).

(20) H. C. Brinkman and J. J. Hermans, *ibid.*, **17**, 574 (1949).

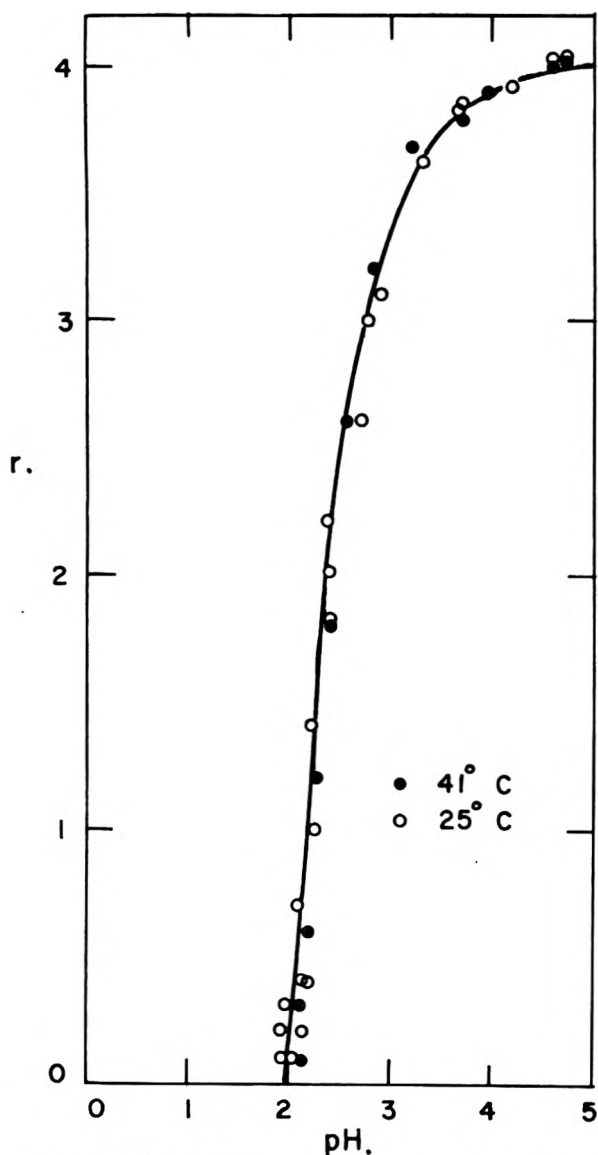


Fig. 1.—The titration curve of STA in the presence of 0.300 *M* NaCl: —, curve calculated assuming STA to be a strong acid. *r* represents moles of base added per mole of STA.

In this case extrapolation of $H(C_2/\tau)$ to infinite dilution does yield $1/M_2$. This extrapolation, however, may be difficult or practically impossible due to the strong and often complicated concentration dependence of $H(C_2/\tau)$. Such is the case found for isoionic proteins^{5,6,21} and for highly charged macromolecules.^{13,22,23}

It is this problem of the interpretation of light scattering data from very low ionic strength solutions of highly charged particles that is considered in this paper. This problem has been examined previously by Doty and Steiner²² for the case of serum albumin at low *pH*'s. The study of such a protein involves certain innate difficulties, since it cannot be considered unequivocally from the viewpoint of a definite physical model, because its shape

(21) J. G. Kirkwood and S. N. Timasheff, *Arch. Biochem. Biophys.*, **66**, 50 (1956).

(22) P. Doty and R. F. Steiner, *J. Chem. Phys.*, **20**, 85 (1952).

(23) A. Oth and P. Doty, *This Journal*, **56**, 43 (1952).

is not truly spherical and its electric charge and charge distribution at any set of conditions may be somewhat uncertain.

The work to be reported in this communication was carried out on silicotungstic acid (STA) which is known to be a spherical molecule,²⁴ 5.5 Å. in radius. Its charge of -4 corresponds to a charge density comparable to that of proteins distant from their isoelectric point. Because of these properties it seemed like a good model system for studying the effect of high charge on the light scattering behavior of macromolecules.

Experimental

Material.—Reagent grade, General Chemical silicotungstic acid (STA) was dried to constant weight over calcium chloride and the residual moisture determined by the Karl Fischer method. Concentrated stock solutions were prepared for light scattering measurements by dissolving the appropriate amount of STA in doubly distilled water and titrating to *pH* 4.5 to 5 with the calculated amount of sodium hydroxide solution.

Light Scattering Measurements.—Measurements of excess turbidity at 436 *mμ* were made with the Brice photometer²⁵ equipped with the narrow slit system. Measurements were made by the Dintzis procedure^{5,26} paying particular attention to the exclusion of dust. Stock solutions were clarified using an ultrafine filter of the type designed by Bier.^{27,28}

The absence of fluorescence was demonstrated by the method described by Brice, Nutting and Halwer.²⁹ Depolarizations were determined in the usual way and found to be negligibly small.^{29,30} Refractive index increments were determined with a photoelectric differential refractometer.³¹

***pH* Measurements.**—The titration curve of STA was determined using a Beckman GS³² differential *pH* meter together with a thermostated electrode assembly similar to that described by Tanford.³³ Standards for these measurements were freshly prepared HCl solutions having the same salt concentration as the solutions with which they were being compared, as well as a *pH* within one unit of that of the solution. Other *pH* measurements were made with a Beckman G *pH* meter.

Electrophoresis Experiments.—Electrophoretic measurements were carried out with a Model 38-A Perkin-Elmer apparatus at 0°. Mobilities were calculated from enlarged projected tracings.

Results

Silicotungstic Acid Charge.—One of the most important parameters in this study being the average net charge of the macro-ion, it was important to determine the *pH* dependence, if any, of the ionization of silicotungstic acid.

Shown in Fig. 1 are results of titration experiments carried out at constant final STA and NaCl concentrations of 0.00197 and 0.300 *M*, respectively.

(24) M. C. Baker, P. A. Lyons and S. J. Singer, *J. Am. Chem. Soc.*, **77**, 2011 (1955).

(25) B. A. Brice, M. Halwer and R. Speiser, *J. Opt. Soc. Amer.*, **40**, 768 (1950).

(26) H. M. Dintzis, in preparation.

(27) M. Bier, Doctoral Dissertation, Fordham University, 1950.

(28) F. F. Nord, M. Bier and S. N. Timasheff, *J. Am. Chem. Soc.*, **73**, 289 (1951).

(29) B. A. Brice, G. C. Nutting and M. Halwer, *ibid.*, **75**, 824 (1953).

(30) E. P. Geiduschek, *J. Polymer Sci.*, **13**, 408 (1954).

(31) B. A. Brice, to be published.

(32) The mention of commercial products throughout this paper does not imply that they are endorsed or recommended by the Department of Agriculture over others of a similar nature not mentioned.

(33) C. Tanford in T. Shedlovsky, ed., "Electrochemistry in Biology and Medicine," John Wiley and Sons, Inc., New York, N. Y., 1955.

The experimental points obtained at 25 and 40° are shown by the circles, while the solid line was calculated on the assumption that the acid is completely dissociated over the entire pH range. It is thus evident that STA is a strong acid having four ionizable hydrogens, and is completely dissociated over the pH range studied.

A further determination of the variation of charge with pH was obtained from the pH dependence of the electrophoretic mobility. These experiments were carried out at an STA concentration of $1.1 \pm 0.09 \times 10^{-2}$ g./ml. and yielded an average mobility of $-1.56 \pm 0.1 \times 10^{-4}$ over the pH range of 1.71 to 4.64. Making use of the Henry equation³⁴ and properly taking into account the size of the gegenions,³⁵ it was found that this corresponds to a net charge of -3.4 ± 0.3 with no pH variation characteristic of ionization. If one allows for the fact that the experiments were carried out at a finite STA concentration and for the limitations of the Henry equation, the charge of -3.4 obtained from electrophoresis can be considered in satisfactory agreement with the value of -4.0 obtained from the titration curve.

High Ionic Strength Experiments.—Light scattering data on STA obtained in the presence of 0.300 M NaCl are shown in Fig. 2. $H(C_2/\tau)$ was found to be linear in STA concentration with a slope, $2B$, of 1.22×10^{-2} , corresponding to a reduced slope $BM^2/1000$ of 51.5. The latter value is comparable to those reported by Edsall, *et al.*,⁷ for serum albumin at low charge and high ionic strength.

The molecular weight obtained from the intercept of the curve was found to be 2860. In Table I it is compared with values obtained by other methods. The agreement is found to be excellent, especially in view of the errors inherent in the molecular weight determination of relatively small molecules by the light scattering technique.

As is shown in eq. 1 for a three component system, where strong interactions are absent, A_{12} tends to zero. In such a case D is also zero and the intercept yields the correct molecular weight. The fact that the light scattering intercept corresponds to the formula molecular weight of STA, therefore, is evidence that salt-STA interactions are not significant.

TABLE I

MOLECULAR WEIGHT OF SILICOTUNGSTIC ACID

$M \times 10^{-3}$	Method	Ref.
2.86	Light scattering	This study
2.875	Formula weight
2.91	Sedimentation-diffusion	Baker, <i>et al.</i> ²⁴
2.8	Sedimentation-Archibald procedure	Kronman and Timasheff Unpublished results

The positive slope is indicative of repulsive interactions between quadruply charged silicotungstate ions. Its sign and magnitude are as would be expected from the screening provided by an ionic strength of 0.300.

Salt-free Solutions.—Light scattering data ob-

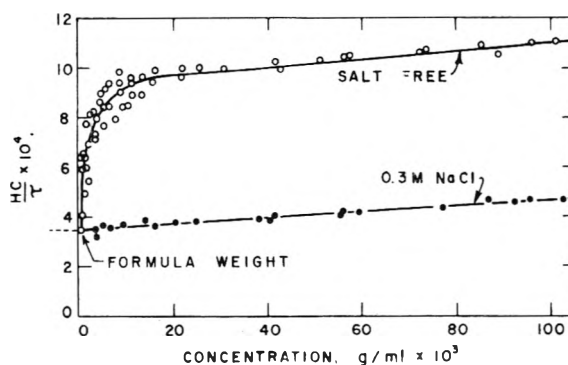


Fig. 2.— $H(C_2/\tau)$ as a function of STA concentration in the presence and absence of neutral salt.

tained in the absence of salt are shown also in Fig. 2. In the region above a concentration of 20 g./l. the data appear to fall on a straight line that would extrapolate to an intercept corresponding to about $1/3$ of the formula molecular weight. At concentrations below 20 g./l. the scattering shows a marked dependence upon concentration, $H(C_2/\tau)$ decreasing almost threefold in the concentration range of 1 to 10 g./l.³⁶

Examination of equation 3 indicates that for a constant M_2 the observed variation of $H(C_2/\tau)$ must be due to either a concentration dependence of $\partial\mu_2^{(e)}/\partial C_2$ or of H . The only portion of H that need be considered is the refractive index increment $\partial n/\partial C_2$. The latter quantity was determined as a function of concentration over the range of 8.57 to 82.3 g./l. The value obtained for 436 m μ was 0.1065 ± 0.0014 with no significant concentration variation. The refractive index increment for STA in the presence of 0.300 M NaCl was the same as for the salt-free acid within experimental error. Therefore, the variation of $H(C_2/\tau)$ with concentration in terms of equation 3 leads to the conclusion that $\partial\mu_2^{(e)}/\partial C_2$ is a strong function of the STA concentration and that the rapid increase of $H(C_2/\tau)$ with concentration is the result of strong repulsive forces between the silicotungstate ions.

Discussion

Quantitative Representation of the Data.—The large positive values of $\partial\mu_2^{(e)}/\partial C_2$ observed for STA in the absence of salt testify to the presence of strong repulsive forces between the STA particles. This is not surprising since STA is a tetravalent ion and in the absence of salt the screening is extremely weak. The gradual leveling off of the light scattering curve with an increase in STA concentration can be attributed to the growth of screening as the STA concentration increases since the Debye-Hückel factor κ increases directly with the square root of STA concentration. Taking the univalent gegenion concentration into account

$$\kappa^2 = \frac{4\pi N e^2}{DkT} \left(\frac{20C_2}{M_2} \right) \quad (4)$$

where e is the protonic charge, D is the dielectric constant of the medium, k is Boltzmann's constant,

(36) The high scatter of experimental points at low concentrations is not surprising, since in that range the excess turbidity represents only a few per cent. of the apparent turbidity of the pure solvent.

(34) D. C. Henry, *Proc. Roy. Soc. (London)*, **A193**, 106 (1931).

(35) M. H. Gorin, *J. Chem. Phys.*, **7**, 405 (1939).

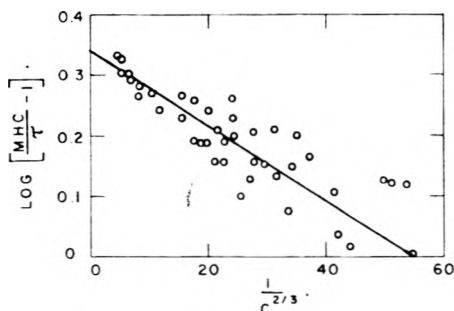


Fig. 3.— $(M_2HC_2/r - 1)$ as a function of $1/C_2^{2/3}$ (see eq. 6).

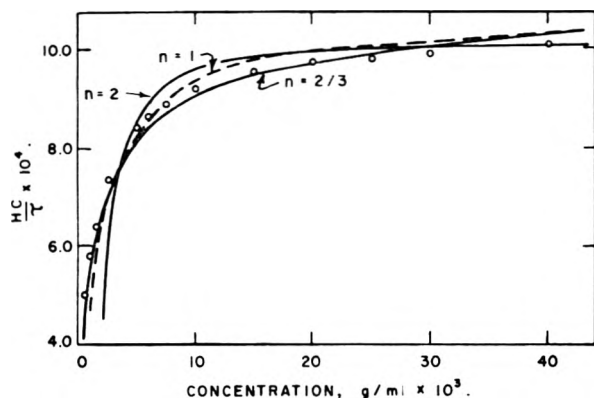


Fig. 4.—Comparison of the smoothed experimental data (circles) with semi-empirical curves obtained from $1/C_2^{2/3}$, $1/C_2$ and $1/C_2^2$ fits.

T is the thermodynamic temperature, C_2 is the STA concentration in g./l. and M_2 is its molecular weight.

A strong repulsive force of the magnitude existing in this system should result in an ordering effect and thus a non-random arrangement of the scattering centers.^{37,38} Qualitatively, one would expect this to result in a diminution of scattered intensity as compared to that from an isolated particle. A quantitative treatment of the problem has been made by Doty and Steiner²² in their study of serum albumin at high charge and very low ionic strength.

Making use of the Fournet radial distribution function³⁹ together with suitable expressions for the repulsive ionic potential, they have derived light scattering equations which describe the observed marked concentration dependence of the scattering for serum albumin under the above stated conditions. For a "soft" exponential potential they obtain the expression

$$\left[\frac{M_2HC_2}{\tau} - 1 \right] = \frac{\pi^{3/2}N_0C_2r_0^3}{M_2} \exp(-h^2r_c^2/4) \quad (5)$$

where $h = 4\pi\lambda' \sin \theta/2$, r_0 is the distance of closest approach of the scattering centers, N_0 is Avogadro's number, λ' is the wave length of the light in the medium and θ is the angle of scattering. It is quite apparent that the greater the screening against electrostatic repulsion the smaller will be r_0 . Thus, in a salt-free solution, r_0 will be some function of the gegenion and hence the macro-ion con-

centration. If it is assumed, as Doty and Steiner have done, that the distance is proportional to $1/C_2^{1/2}$, equation 5 in logarithmic form becomes

$$\log \left[\frac{M_2HC_2}{\tau} - 1 \right] = \log \left(\frac{\pi^{3/2}N_0k^3}{M_2} \right) - \left(\frac{hk}{2C_2^{1/2}} \right)^2 \log e \quad (6)$$

where k is the proportionality constant between r_0 and $1/C_2^{1/2}$.

A plot of the data in the form of equation 6 is shown in Fig. 3. While the plot of $\log ((M_2HC_2/\tau) - 1)$ versus $1/C_2^{2/3}$ appears to be a reasonable fit, plots made versus $1/C_2$ and $1/C_2^{1/2}$ were equally good. The $1/C_2^2$ fit was noticeably poorer. A comparison of the smoothed experimental data with curves calculated using the empirical constants of the $1/C_2^{2/3}$, $1/C_2$ and $1/C_2^2$ fits is given in Fig. 4. While the curves for the exponent of C_2 equal to $2/3$ and 1 seem to describe the data reasonably well at moderately high concentrations, the data fall below the curve at higher values of C_2 . Nonetheless, the form of the curve suggested by equation 5 appears to be adequate.

While it seems possible to predict the shape of the light scattering curve using equation 5, it is by no means as certain that, at the present time, the curve can be calculated theoretically from molecular data. Involved in such a calculation would be an exact evaluation of the relationship between r_0 and macro-ion concentration.

In relating r_0 and C_2 , Doty and Steiner²² made use of equation 2 for a three component system neglecting salt-macro-ion interaction, and assuming β_{22} to be negligibly small. In such a case, a comparison of the coefficients of C_2 in equation 5 and the Donnan term of equation 2 resulted in the previously cited cube root relationship between C_2 and r_0 . Leaving out the β_{22} term in equation 2 is equivalent to assuming that the Donnan term makes the more important contribution to the slope and that the system is close to being ideal. Examination of literature data^{6,7} for serum albumin indicates that this need not be so. Indeed, for most of the conditions cited, $Z_2^2/2m_1$, and β_{22} were of comparable magnitude.

Furthermore, as Doty and Steiner have pointed out,²² equation 2 is inapplicable to a salt-free system. For such a case, multicomponent light scattering theory yields equation 3 which contains no Donnan term and only a β_{22} contribution. No simple relationship can be written, however, between β_{22} and C_2 . Thus, at the present time the problem of the rigorous elimination of r_0 in terms of C_2 from equations, such as eq. 5, must be regarded as unsolved.

A further difficulty, which may or may not be related to the problem discussed above, can be seen when the factor k is calculated using eq. 6 and the experimental data. Such a calculation results in two significantly different values of k : the one obtained from the slope is 8.81×10^{-7} , while the intercept yields 1.23×10^{-7} . This difference is well outside the experimental error. At the present time, it is impossible to state whether this discrepancy is due to the difficulty of relating r_0 and C_2 or to the question of the applicability of the potential functions used to obtain eq. 5 and similar

(37) J. G. Kirkwood and J. Mazur, *J. Polymer Sci.*, **9**, 519 (1952).

(38) J. G. Kirkwood and J. Mazur, *Compt. rend. 8^e Reunion Chim. Phys. Paris*, 143 (1952).

(39) G. Fournet, *Compt. rend.*, **228**, 1421 (1949).

expressions.⁴⁰ In all probability both factors made a significant contribution.

Doty and Steiner²² have found further that in systems displaying a non-random distribution of scattering centers, external interference should result in negative dissymmetries in light scattering. Calculations, however, have shown that in the case of STA, the last would be significant only in the very low concentration range, at which the excess turbidity is very small. Attempts at such measurements have met with failure so far, as the experimental error was found to be greater than the expected difference in scattering at angles of 45 and 135°.

Light Scattering from Other Heteropoly Acids.—Kerker, Lee and Chou⁴² have reported light scattering data for the 9 and 12 phosphotungstic acids which seem to exhibit the same extreme dependence of $H(C_2/\tau)$ on C_2 . In the absence of salt, the apparent molecular weight of the 12 acid was found to be 35% lower than the formula weight, while for the 9 acid it was 25% lower than the monomer weight. In the case of the 12 acid, the failure of $H(C_2/\tau)$ to decrease sharply with C_2 or even to deviate markedly from linearity is probably

(40) It is interesting to point out that calculation of k from a light scattering expression involving the Verwey-Overbeek potential⁴¹ also results in a discrepancy. In this case, however, the intercept yields a value of k much larger than that obtained from the slope.

(41) E. J. W. Verwey and J. T. G. Overbeek, "Theory of the Stability of Lyophobic Colloids," Elsevier Publishing Co., Inc., Amsterdam, 1948.

(42) M. Kerker, D. Lee and A. Chou, *J. Am. Chem. Soc.*, **80**, 1539 (1958).

due to the fact that the measurements were not carried to concentrations sufficiently low to detect the strong curvature. As Fig. 2 indicates, at a concentration of 20 g./l., which is comparable to the lowest concentration employed by Kerker, Lee and Chou, $H(C_2/\tau)$ for STA is still linear in C_2 .

In the case of the 9 acid, the slight curvature that Kerker, Lee and Chou observed at low values of C_2 is consistent with our results and the expectations from the theory.²² Quantitative comparisons of our results with those obtained for the phosphotungstic acids is impossible since the latter measurements do not extend to sufficiently low concentrations for the use of expressions such as eq. 5.

Conclusion

The above-described light scattering measurements on silicotungstic acid can be considered as good experimental evidence for the non-random arrangement in solutions of macro-ions under conditions of low screening. Although no rigorous quantitative treatment of the experimental data is available at the present time, the theory of Doty and Steiner can be used as a first approach for the analysis of such systems. It yields good agreement with experimental data within the limits of the assumptions in its derivation. A more exact theoretical analysis of the situation would seem desirable, and work to that effect has been initiated.

Acknowledgment.—The authors wish to thank Professor S. J. Singer for suggesting this problem and Dr. B. A. Brice for his encouragement in the course of these studies.

THE VELOCITY FIELD IN ELECTROLYTIC SOLUTIONS

BY RAYMOND M. FUOSS¹

Contribution from l'Istituto di Chimica Fisica dell' Università di Roma, Rome, Italy

Received October 24, 1958

The velocity field produced in an electrolytic solution by an external electrical field has been studied further. Both the hydrodynamic term in the relaxation field and the Onsager electrophoresis term can be derived from the Navier-Stokes equation, specialized to the conductance problem. It is shown that the hydrodynamic radius which appears in the analysis must be identified with a , the center-to-center distance at contact between ions of opposite charge. If the ions are represented as spheres of diameter a , then the hydrodynamic radius R is twice the electrostatic radius; this result follows from the facts that no charge except that of the reference ion can penetrate a sphere of radius a around the latter and that information concerning size can only be detected conductimetrically from the consequences of interionic contacts.

In a recent² derivation of the limiting curvature of the conductance function, it was necessary to calculate the velocity field which an ion sets up in the surrounding solvent when an external electrical field causes the ion to move. If the ions are assumed to have non-zero volume, the simplest model which can be used is that of spheres-in-continuum. For this model, an external field will cause the "ion" to move with uniform velocity; "solvent" will be pushed away in the direction of motion in front of the moving ion and will pour in to fill the space vacated by it as it moves. In a plane through the center of the sphere, perpendicular to the field direction, no radial displacement of the solvent will

occur, while solvent just ahead or behind the ion on the line of the diameter parallel to the field will move parallel to the field with the ionic velocity. In other directions, the velocity of the solvent will be a vector quantity with components in both radial and field directions. A nearby ion will therefore be moving, not in a stationary medium, but in a medium which is in motion. The problem therefore may be stated: given the above model, what is the velocity of the solvent at a point $P(r, \theta)$ as a function of distance r from the reference ion and the angle θ between P , the reference ion and the field direction?

This problem was considered by Debye and Hückel³ in their first treatment of the conductance problem; their solution was stated in terms of the

(1) On sabbatical leave from Yale University, second semester 1957-1958. Grateful acknowledgment is made for a Fulbright grant.

(2) R. M. Fuoss and L. Onsager, *THIS JOURNAL*, **61**, 668 (1957).

(3) P. Debye and E. Hückel, *Physik. Z.*, **24**, 305 (1923).

Stokes radius R which entered through the boundary condition that the relative velocity of the solvent be zero at the surface of the ion. By means of a different approach to the problem, Fuoss and Onsager² succeeded in eliminating the Stokes radius from all but a small term in the relaxation field; the electrostatic diameter a appeared everywhere else in their conductance equation as the distance parameter which necessarily must be introduced when the next approximation beyond point charges is used to represent the ions. In order to avoid two arbitrary distance parameters, a and R , Fuoss and Onsager replaced R by $a/2$, arguing that the term in which it appeared was at most only one-twelfth of the radial component of total velocity and that the whole velocity term ΔX_v in the relaxation field was itself small compared to the other higher terms, and therefore that any error made in replacing the hydrodynamic radius by the electrostatic radius would be insignificant. This arbitrary solution of the problem of two parameters by simply ignoring it is aesthetically unappealing, however satisfactory it may be from the practical point of view of numerical calculation.

The previous derivation of the conductance equation also contains another unsatisfying element: the electrophoresis term (which is by far the largest of the interionic force terms), as derived originally by Onsager and Fuoss,⁴ was simply grafted on to the relaxation term in order to obtain the final result. A more direct approach would have been to derive both of the hydrodynamic terms (electrophoresis and ΔX_v) directly from the velocity field. It is the purpose of this paper to present a more thorough study of the velocity field. As expected, both hydrodynamic terms are derivable from the Navier-Stokes equation. An unexpected by-product is the fact that, *as far as conductance is concerned*, the hydrodynamic radius turns out to be equal to a , the center-to-center distance of anion and cation at contact if we require that the velocity of the reference ion at vanishing concentration be given by Stokes law

$$\mathbf{v}_0 = Xe/6\pi\eta R$$

Reflection shows that this result is consistent with the model and with the conductance phenomenon: the only way that we can tell experimentally that ions are not point charges is by observing the consequences of interionic collisions, and it obviously takes two ions to make a collision. Hence only an average distance can appear.

In order to save space, we shall take as given equations 5.5, 5.15, 5.19 and 5.21 of ref. 2, which are, respectively

$$\eta\mathbf{v} = \nabla(\nabla \cdot \mathbf{u}) - \Delta \mathbf{u} \quad (1)$$

$$\mathbf{u}_A = (Xe/4\pi)[r/2 + B/r - \frac{e^{\kappa(a-r)}}{\kappa^2 r(1+\kappa a)}] \quad (2)$$

$$\eta\mathbf{v}_A = \frac{Xe}{4\pi} \left\{ \mathbf{r}_1 \cos \theta \left(\frac{3B}{r^3} - \frac{1}{2r} - \frac{3e^{\kappa(a-r)}(1+\kappa r + \kappa^2 r^2/3)}{\kappa^2 r^3(1+\kappa a)} \right) + \mathbf{i} \left(-\frac{B}{r^3} - \frac{1}{2r} + \frac{e^{\kappa(a-r)}(1+\kappa r + \kappa^2 r^2)}{\kappa^2 r^3(1+\kappa a)} \right) \right\} \quad (3)$$

and

(4) L. Onsager and R. M. Fuoss, *THIS JOURNAL*, **36**, 2686 (1932).

$$\mathbf{u}_S = (Xe/4\pi)(-r/2 + E/r) \quad (4)$$

The symbols are defined as follows: η is viscosity, X is field strength, e is elementary charge, κ is the Debye-Hückel parameter, \mathbf{u} is an auxiliary vector from which the total velocity \mathbf{v} in the liquid at a distance r from the reference ion can be computed by (1), and \mathbf{u}_A and \mathbf{u}_S are the contributions to \mathbf{u} from the atmosphere and charge, respectively, of the reference ion. The constants B and E were found² to have the values

$$B = (1 + \kappa a + \kappa^2 a^2/2 + \kappa^3 a^3/6)/\kappa^2(1 + \kappa a) \quad (5)$$

and

$$E = -R^2/6 \quad (6)$$

The constant B was evaluated by requiring that the first derivative of \mathbf{u}_A be continuous at $r = a$, i.e., at the surface of the sphere which never may contain any charge except that of the reference ion. The constant E was evaluated by the condition that the velocity of the liquid relative to the ion must vanish at $r = R$; in terms of the sphere-in-continuum model, this simply means that the liquid wets the sphere perfectly. The necessity for the appearance of two distance parameters, one of electrostatic nature and one of hydrodynamic nature, is thus inherent in the problem. As we shall see later, the limiting form of the velocity equation for vanishing concentration requires that a equal R .

Substitution of (4) in (1) evaluates \mathbf{v}_S

$$\eta\mathbf{v}_S = \frac{Xe}{4\pi} \left\{ \mathbf{r}_1 \cos \theta \left(\frac{1}{2r} - \frac{R^2}{2r^3} \right) + \mathbf{i} \left(\frac{1}{2r} + \frac{R^2}{6r^3} \right) \right\} \quad (7)$$

and this result, combined with (3), gives for the total velocity

$$\eta\mathbf{v} = \frac{Xe}{4\pi} \left\{ \mathbf{i} \left(\frac{R^2}{6r^3} - \frac{B}{r^3} + \frac{e^{\kappa(a-r)}(1+\kappa r + \kappa^2 r^2)}{\kappa^2 r^3(1+\kappa a)} \right) + \mathbf{r}_1 \cos \theta \left(-\frac{R^2}{2r^3} + \frac{3B}{r^3} - \frac{3e^{\kappa(a-r)}(1+\kappa r + \kappa^2 r^2/3)}{\kappa^2 r^3(1+\kappa a)} \right) \right\} \quad (8)$$

At $r = a$, (8) reduces to

$$\eta\mathbf{v}(a) = \frac{Xe}{4\pi} \left\{ \mathbf{i} \left(\frac{R^2}{6a^3} + \frac{1 - \kappa a/3}{2a(1 + \kappa a)} \right) + \mathbf{r}_1 \cos \theta \left(\frac{1}{2a} - \frac{R^2}{2a^3} \right) \right\} \quad (9)$$

The x -component of (9) can be rearranged to give

$$\eta v_x(a) = \frac{Xe}{4\pi} \left(\frac{R^2}{6a^3} + \frac{1}{2a} - \frac{2\kappa}{3(1 + \kappa a)} \right) \quad (10)$$

The concentration dependent term of (10) is immediately recognized as the electrophoresis term in the velocity

$$\Delta v_x(a) = -Xe\kappa/6\pi\eta(1 + \kappa a) \quad (11)$$

At concentration equal to zero, (10) reduces to

$$v^0_x(a) = \frac{Xe}{4\pi\eta} \left(\frac{R^2}{6a^3} + \frac{1}{2a} \right) \quad (12)$$

which must be the velocity which the field imparts to an isolated ion because (12) is the velocity in the liquid at $r = a$ and must simultaneously be the velocity of the ion of diameter a contained in the sphere of radius a . If we assume that this velocity is given by the Stokes equation

$$v^0_x(a) = Xe/6\pi\eta R \quad (13)$$

then equating (12) and (13) leads to a relation be-

tween R and a

$$R^3 + 3a^2R - 4a^3 = 0 \tag{14}$$

which can only be satisfied if

$$R = a \tag{15}$$

Finally, substitution of $R = a$ in the radial term of (9) gives

$$v_r(a) = 0 \tag{16}$$

i.e., the radial component of $\mathbf{v}(a)$ vanishes, as it should.

The result (15) might be interpreted as follows. As long as an ion is free (not in contact with another ion), electrostatics can tell us nothing about its size. For the idealized model of a sphere in a continuum, hydrodynamics can give us a relation between size and single ion conductance; since, however, Walden's product is known to vary even for a given electrolyte in mixtures of two solvents,⁵ the radius calculated in this way can only be an approximation. In the conductance problem, this difficulty is irrelevant for symmetrical electrolytes, because individual ionic radii are not needed; only the center-to-center distance at contact appears in the equations. Hence it is not surprising that, as far as the velocity term in the relaxation field is concerned, the average value a alone appears. Stated alternatively, it makes no difference what the individual radii are before (or after) contact, and at contact only the sum can appear. But the sum $(a_1 + a_2)/2$ is the center-to-center distance.

The parameter a entered the theory by explicit use of the Debye-Hückel potential

$$\psi^0_j(r) = (e^{-\kappa r} e_j / Dr) [\exp(\kappa a_j) / (1 + \kappa a_j)] \tag{17}$$

for ions of non-zero size in the equation of continuity. Actually a_j in (17) was replaced by a in the derivation. Let us recall the definition of a in terms of a_1 and a_2 . Formal theory gives for the activity coefficient of an ion of species j

$$-\ln f_j = \beta' c^{1/2} / 2(1 + \kappa a_j) \tag{18}$$

But since single ion activities cannot be measured, the quantity in square brackets in (19)

$$-\ln f_{\pm} = (\beta' c^{1/2} / 2) [(1 + \kappa a)^{-1} + (1 + \kappa a_2)^{-1}] \tag{19}$$

must be replaced by $2/(1 + \kappa a)$, whereby a is perforce defined, and so defined, is a function of concentration. Algebraic rearrangement of the expression

$$2/(1 + \kappa a) = [(1 + \kappa a)^{-1} + (1 + \kappa a_2)^{-1}] \tag{20}$$

gives

$$a_1 + a_2 - 2a = \kappa(aa_1 + aa_2 - 2a_1a_2) \tag{21}$$

If we want a value of a which is independent of concentration, (21) must reduce to the identity $0 = 0$, which will be true only if simultaneously

$$a_1 + a_2 = 2a \tag{22}$$

and

$$a(a_1 + a_2) = 2a_1a_2 \tag{23}$$

Eq. 22 states that a is the arithmetic mean a_m of a_1 and a_2 , and substitution of (22) in (23) gives the result that a must also be the geometric mean $(a_1a_2)^{1/2}$ of the two diameters. These two means

(5) H. Sadek and R. M. Fuoss, *J. Am. Chem. Soc.*, **72**, 301 (1950); **76**, 5897, 5902, 5905 (1954).

are equal if and only if a_1 and a_2 are equal; that is, the condition that a be a concentration-independent parameter leads to the result that the model must be one for which

$$a = a_1 = a_2 \tag{24}$$

As a matter of fact, the concentration dependence of a , as defined by (20), actually is slight for most practical cases. If we let $a_1 = xa_2$, $0 < x < 1$; then

$$a = a_m \left(\frac{1 + 2\kappa c_2 / (1 + x)}{1 + \kappa a_2 (1 + x) / 2} \right) \tag{25}$$

and the function multiplying a_m in (25) is not at all sensitive to κ . For $\kappa = 0$, a always equals a_m , of course; for the extreme case $x = 1/10 = a_1/a_2$, $a/a_m = 0.965$ for $\kappa c_2 = 0.1$ and for the absurdly high value $\kappa a_2 = 1.0$, $a/a_m = 0.762$. For the cases of real interest where approximately $a_2 > a_1 > 0.3 a_2$ and $\kappa a_2 < 0.2$, the difference between a and the arithmetic mean of a_1 and a_2 is experimentally undetectable and hence not a suitable subject for discussion.

Finally, we consider the consequences of using (15) instead of the original guess $R = a/2$ in ΔX_v . Using $R = a$ in (8), the radial component of the velocity, which is needed for the evaluation of ΔX_v , becomes

$$v_r = (Xe \cos \theta / 2\pi\eta) [p_1 - e^{\kappa(a-r)} / (1 + \kappa r)] / \kappa^2 r^3 (1 + \kappa a) \tag{26}$$

where

$$p_1 = 1 + \kappa a + \kappa^2 c^2 / 3 \tag{27}$$

This differs from the previous equation (5.26) by the appearance of $\kappa^2 a^2 / 3$ in place of $\kappa^2 a^2 / 2$ in the constant term in the square bracket in (26). Integration of the differential equation then gives explicitly

$$\Delta X_v / X = [ab\kappa^2 / 6\pi\eta (1 + \kappa a)^2 (\omega_1 + \omega_2)] \zeta_7 - \kappa^2 a / 36\pi\eta p_2 (1 + \kappa a) (\omega_1 + \omega_2) \tag{28}$$

where

$$\zeta_7 = (13 + 3\sqrt{2}) / 48 p_2 + F(\kappa a) / 2 \tag{29}$$

and $F(\kappa a)$ is the transcendental function which appeared in the previous analysis. Approximating $F(\kappa a)$ as before, the velocity term in the relaxation field is found to reduce to

$$\Delta X_v / X = - [\kappa^2 ab / 6\pi\eta (\omega_1 + \omega_2)] [0.2543 + 0.25 \ln \kappa a + 1 / 6b] = - \kappa H / 6\pi\eta (\omega_1 + \omega_2) \tag{30}$$

As before, this hydrodynamic term is now combined with the electrophoresis term, because (30) shows that they have similar coefficients. The mobility of an ion of species 1 is given by

$$u_1 = \sigma [|e_1| \omega_1 - |e_1| \kappa / 6\pi\eta (1 + \kappa a)] (1 + \Delta X / X) \tag{31}$$

where $\sigma = 1/299.79$ is the factor which converts electrostatic units of field strength to volts/cm. If Λ_h denotes the equivalent conductance, corrected for electrophoresis and the hydrodynamic term (30), *i.e.*, ignoring temporarily all of the relaxation field except the term ΔX_v , (31) and a similar expression for species 2 leads to

$$\Lambda_h = \Lambda_0 - (\sigma F_{ek} / 3\pi\eta) (1 + \kappa a)^{-1} + H / 2 \tag{32}$$

where F is the faraday equivalent and

$$\sigma F_{ek} / 3\pi\eta c^{1/2} = \beta \tag{33}$$

where β is the Onsager electrophoresis coefficient.

Hence

$$\Lambda_h = \Lambda_c - \beta c^{1/2} [1 + \kappa a]^{-1} + H/2 \quad (34)$$

Approximating $(1 + \kappa a)^{-1}$ by $(1 - \kappa a + \kappa^2 a^2)$, (34) can be simplified to

$$\Lambda_h = \Lambda_0 - \beta c^{1/2}(1 - \kappa a + H/2) - \beta c^{1/2} \kappa^2 a^2 \quad (35)$$

The last term of (35) gives the major part of the former term $J_2 c^{1/2}$; comparison with experiment

shows that it usually can be neglected, provided $\kappa a < 0.2$. Replacing H by its explicit value, we have finally

$$\Lambda_h = \Lambda_0 - \beta c^{1/2} + \beta c^{1/2} \kappa a [11/12 - (b/8)(\ln \kappa a + 1.0172)] \quad (36)$$

When combined with the other relaxation terms, (36) will then give the final conductance equation.⁶

(6) R. M. Fuoss, *ibid.*, **80**, 3163 (1958).

NOTES

THE ACTION OF REACTOR RADIATION ON SATURATED FLUOROCARBONS

BY J. H. SIMONS AND ELLISON H. TAYLOR

University of Florida, Gainesville, Florida, and Chemistry Division, Oak Ridge National Laboratory,¹ Oak Ridge, Tennessee

Received September 15, 1955

The extraordinary stability of fluorocarbons to heat and to most reagents led to early hopes of a similar high stability to ionizing radiation. Experiments upon fluorocarbon polymers,² however, indicated a greater than average sensitivity to radiation. Interest in these materials for applications involving radiation therefore waned, despite the fact that non-polymeric saturated fluorocarbons would be expected to act differently. Other radiation studies of fluorocarbons have been motivated by interest in radiation polymerization of some unsaturates, and have shown that these can be polymerized when irradiated in glass.³

On the hypothesis that the observed radiation instability of the polymers and the polymerizable monomers might result from impurities (residual H in impure fluorocarbons), reaction with the container (glass), or from innate instability of particular compounds (polytetrafluoroethylene), the present experiments were initiated. Fluorocarbons and fluorocarbon derivatives of low hydrogen content had become available, and it was therefore thought possible finally to establish the degree of radiation stability of this class of compound.

Experimental

Materials.—C-F₁₆—less than 10⁻³% hydrolyzable F; b.p. 82°; optical density 0.51 at 2700 Å.; 0.23 at 2460 Å.; 0.57 at 2200 Å.

C₈F₁₆O—a mixture of cyclic fluorocarbon oxides of this composition but undetermined structure; b.p. 101° (constant over whole sample); optical density 0.57 at 2536 Å.

(C₄F₉)₃N—purified to remove H-containing compounds; b.p. 177°.

Methods.—Each sample was further purified by evacuation while frozen, melting, refreezing, and further evacuation, followed by distillation through P₂O₅ into the irradiation vessel. This was a 4 inch length of 1-inch aluminum (2 S) tube with a flat bottom and a 3/8-inch aluminum tube at the top, fabricated by heliarc welding. It was attached

to the vacuum system through a Kovar-to-Pyrex seal. After being filled, the vessel was sealed off while frozen, first in the glass and then by pinching and welding the aluminum.

The samples were irradiated for 4 weeks in the Oak Ridge Graphite Reactor at a neutron flux of 5.5×10^{11} cm.⁻² sec.⁻¹ and at a maximum temperature of 110°. The total energy absorption at this position should have been 3.6×10^{-4} cal./g., sec., for a sample composed of graphite, based upon calorimetric measurements by Richardson and Boyle⁴ corrected for the flux ratio between their position of measurement and the present location. About 82% of the energy (in graphite) arises from absorption of γ -rays and the remainder from stopping of fast neutrons.⁴

The samples were opened by attaching them to a vacuum system, cooling in liquid air, and then drilling a small hole in the top of the entrance tube by hand with a steel twist drill. The first sample opened was completely removed from the ampoule by vaporization. Because of the formation of high-boiling substances this became a lengthy procedure. The other samples were similarly opened but, after the low-boiling material was removed, air was admitted, the ampoule removed from the system, and the contents poured into the distillation apparatus.

Results

There was no evidence of corrosion, the inner wall of each capsule being clean and bright after irradiation. There was no large amount of gas in any case, and in particular no F₂ or CF₄. Each irradiated sample was clear and colorless. The results of distillation and other examination of the samples are given in Table I, and the distillation curves (5 to 10 theoretical plates) in Fig. 1.

Discussion

The irradiation effected chemical changes in these three materials. Thermal changes cannot have contributed since the compounds are stable to 500°. The yield, G , can be estimated from the distillation analyses and the energy absorption in graphite, assumed equal to that in the fluorocarbons. This assumption is probably accurate to $\pm 20\%$ except for (C₄F₉)₃N, in which the reaction N¹⁴(n,p)C¹⁴ increases the energy absorption appreciably. For C₇F₁₆, with 35% of the molecules transformed for a total energy absorption of 2.2×10^{22} e.v./g., $G = 2$ to 3 molecules transformed per 100 e.v. absorbed. This value is based only on the total energy absorbed, since such reactor experiments give no way for separating the effects of the different kinds of radiation. If the relatively

(1) Operated by Union Carbide Corporation for the U. S. Atomic Energy Commission.

(2) O. Sisman and C. D. Bopp, Physical Properties of Irradiated Plastics, USAEC Unclassified Report, ORNL-928 (June, 1951).

(3) D. S. Ballantine, A. Glines, P. Colombo and B. Manowitz, "Further Studies of the Effect of Gamma Radiation on Vinyl Polymer Systems," BNL-294 (March, 1954).

(4) D. M. Richardson, A. O. Allen and J. W. Boyle, "Calorimetric Measurement of Radiation Energy Dissipated by Various Materials Placed in the Oak Ridge Pile," USAEC Unclassified Report, ORNL-129 (December, 1948).

TABLE I
EXAMINATION OF IRRADIATED FLUOROCARBONS

Sample	Wt. sample (g.)	Gas	Liquid	—% of product boiling— Below original Near original Above original			B.p. residue, ^b °C.
C ₇ H ₁₆	23.1	Less than 1% of total sample	—	12	65	23	185–192
C ₈ H ₁₆ O	26.5	Acidic. ^a Smells like low mol. wt. fluorinated carboxylic acids	Acidic ^a	12	42	46	300
(C ₄ H ₉) ₃ N	26.2	2 ml. boiling below 25°	Neutral ^a	40	7	53	>300

^a To moist litmus paper. ^b Residues represented about 10% of total sample.

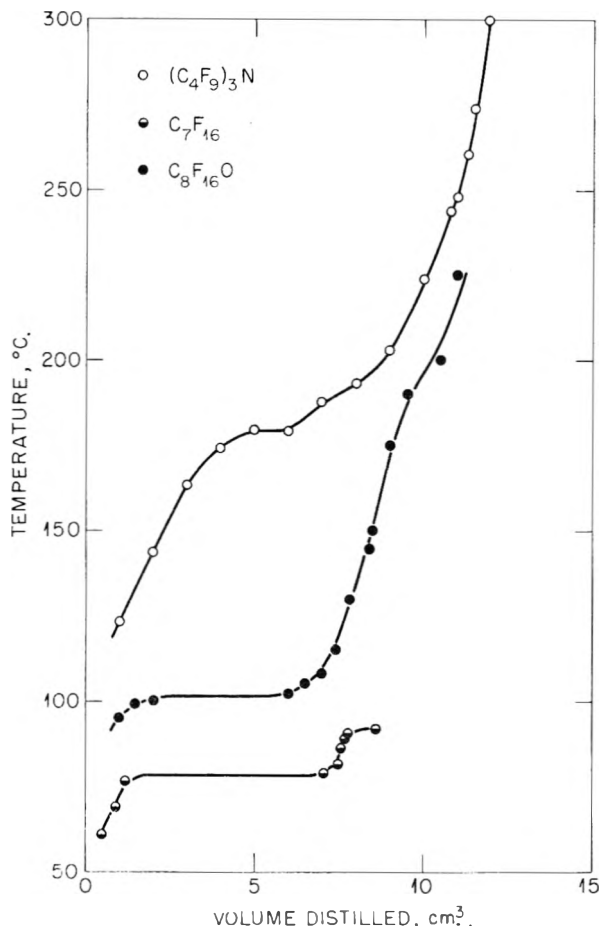


Fig. 1.—Distillation curves for irradiated fluorocarbons.

great stability against γ -rays which has been observed in certain experiments with other fluorocarbons⁵⁻⁷ applies under the present conditions, then of course the G value for neutrons would be proportionately higher.

The absence of F₂ and of CF₄ suggests that the primary chemical effect is the breakage of C—C rather than of C—F bonds. The greater instability of the O- and N-containing compounds can be explained by the lower strength of C—N and C—O bonds compared with C—C, as demonstrated by the relative thermal stabilities of the compounds in question.

Dried, highly pure samples of C₇F₁₆, C₈F₁₆O and (C₄F₉)₃N in aluminum were irradiated in a nuclear reactor. Higher and lower boiling materials were

produced in moderate amounts, without detectable corrosion or production of F₂, CF₄, carbon, or of tars. The chemical changes here reported as the result of reactor radiation have not been reported to be produced in saturated, hydrogen-free fluorocarbons and their derivatives by heat, electromagnetic radiation, or by electrical discharge.

Acknowledgment.—The authors wish to thank the Minnesota Mining and Manufacturing Company for providing the pure samples of hydrogen-free saturated fluorocarbons. The authors also wish to thank Drs. Christie, Dreschner, Shultz and Wethington for permission to refer to the results of their experiments.

FILM AND SUBSTRATE FLOW IN SURFACE CHANNELS¹

BY ROBERT S. HANSEN

Contribution from Institute for Atomic Research and Department of Chemistry, Iowa State College, Ames, Iowa

Received July 8, 1958

LaMer and Blank have recently published two studies of the transfer of monolayers in surface channels^{2,3} in which the transfer rate is interpreted in terms of a geometric resistance factor and a rate constant. Transfer of appreciable quantities of substrate was observed.⁵

The purpose of this note is to point out, as has indeed previously been done by Harkins and Kirkwood⁴ that an idealization of this problem (film flow in a rectangular channel) can be solved by conventional hydrodynamics, and to give results pertinent to experiments such as those performed by LaMer and Blank.

Consider a long rectangular trough of depth h and width $2a$, filled with a liquid of viscosity η on top of which rests a film of surface viscosity μ ; the film is subjected to a film pressure gradient K along the axis of the trough. We choose the film surface as the xy -plane, the y -axis as the trough axis, and the z -coordinate as the depth coordinate. For steady flow, let $U(x,z)$ be the fluid velocity at x,z . Then

$$\nabla^2 U = 0, \quad -a \leq x \leq a, \quad 0 \leq z \leq h \quad (1)$$

$$U(\pm a, z) = U(z, h) = 0 \quad (2)$$

$$U(x, z) = U(-x, z) \text{ (by symmetry)} \quad (3)$$

$$\mu U_{xx}(x, 0) + \eta U_z(x, 0) = -K \quad (4)$$

(1) Work was performed in the Ames Laboratory of the Atomic Energy Commission.

(2) V. K. LaMer and M. Blank, *J. Colloid Sci.*, **11**, 608 (1956).

(3) M. Blank and V. K. LaMer, *This Journal*, **61**, 1611 (1957).

(4) W. D. Harkins and J. G. Kirkwood, *J. Chem. Phys.*, **6**, 53 (1938).

(5) J. A. Wethington and W. H. Christie, personal communication.

(6) R. D. Dreschner, personal communication.

(7) Allan R. Shultz, personal communication.

(Subscripts denote differentiations after variables indicated.)

This boundary value problem can be solved by standard Fourier series methods; we find

$$U(x,z) = \frac{16Ka^2}{\pi^3\mu} \sum_{n=0}^{\infty} \frac{(-1)^n \cos \frac{(2n+1)\pi x}{2a} \sinh \frac{(2n+1)\pi(h-z)}{2a} \left[\frac{\sinh \frac{(2n+1)\pi h}{2a} \right]^{-1}}{(2n+1)^3 \left[1 + \frac{2a\eta}{(2n+1)\pi\mu} \coth \frac{(2n+1)\pi h}{2a} \right]} \quad (5)$$

The area flux of film Q is

$$Q = \int_{-a}^a U(x,0) dx = \frac{64Ka^3}{\pi^4\mu} \sum_{n=0}^{\infty} \frac{1}{(2n+1)^4} \left[1 + \frac{2a\eta}{(2n+1)\pi\mu} \coth \frac{(2n+1)\pi h}{2a} \right]^{-1} \quad (6)$$

The volume flux of substrate F is

$$F = \int_{-a}^a \int_0^h U(x,z) dz dx = \frac{128Ka^4}{\pi^5\mu} \sum_{n=0}^{\infty} \frac{1}{(2n+1)^5} \left\{ \frac{\coth \frac{(2n+1)\pi h}{2a}}{1 + \frac{2a\eta}{(2n+1)\pi\mu} \coth \frac{(2n+1)\pi h}{2a}} \right\} \quad (7)$$

Equation 6 has been given previously by Harkins and Kirkwood.⁴

The series expressions for U , Q and F are rapidly converging; for $\pi h/2a = 1$, $2a\eta/\pi\mu = 1$, for example, the error caused by neglecting all terms beyond the first is 8% in $U(0,0)$; 2% in Q , and 1% in F . Rapidity of convergence is little affected by variation in the group $\pi h/2a$, but is somewhat slower if $2a\eta/\pi\mu$ is large. For long chain organic compounds on water in condensed films $\mu \sim 10^{-3}$ c.g.s. units,⁵ $\eta \sim 10^{-2}$ c.g.s. units, so $2a\eta/\pi\mu \sim 1$ for a ~ 1 mm. Approximate conclusions concerning substrate flow can therefore be obtained by considering only the leading terms in the series. For example

$$\frac{U(x,z)}{U(x,0)} \approx \frac{\sinh \frac{\pi(h-z)}{2a}}{\sinh \frac{\pi h}{2a}} \approx \frac{h-z}{h} \text{ if } \frac{h}{a} \ll 1, \text{ or } e^{-\pi z/2a} \text{ if } \frac{h}{a} \gg 1 \quad (8)$$

so that the variation in substrate flow with distance from surface depends principally on parameters of the trough rather than on parameters of the fluid or film. Similarly, the ratio of fluid flux to film flux is given by

$$\frac{F}{Q} \approx \frac{2a}{\pi} \coth \frac{\pi h}{2a} \quad (8)$$

so that for $h \gg a$ the film will drag with it liquid equivalent to a slab with depth about one third the width of the trough.

It should be noted that the boundary value problem solved here assumes the film parallel to the trough bottom and perpendicular to the sides; it appears unlikely that exact solutions can be obtained for angular troughs and curved films with arbitrarily located centers of film curvature such as those studied by LaMer and Blank. The same comment applies to the capillary viscometer of Myers and Harkins⁶ unless the film is perpendicular

to the walls of the viscometer, and their paper does not make it clear that this condition must be met experimentally before the surface viscosity can be calculated from their approximate formula or the

exact formula of Harkins and Kirkwood.⁴ Neglecting the viscous drag of the substrate, the flux of a film, of constant radius of curvature, making a contact angle φ with the walls of the trough is

$$Q = \frac{2Ka^3}{3\mu} \left(\frac{\pi/2 - \varphi}{\cos \varphi} \right)^3 \quad (9)$$

rather than

$$Q = \frac{2Ka^3}{3\mu} \quad (10)$$

as given by Myers and Harkins.⁶ Neglect of viscous drag of substrate is likely to introduce a serious error in these formulas, particularly if $a\eta/\mu$ is not small.

Finally, it should be noted that if $2a\eta/\pi\mu \gg 1$ the leading terms in the expressions for $U(x,z)$, Q and F (eq. 5, 6 and 7) become independent of μ , and these quantities therefore become insensitive to the composition of the surface film.

EFFECT OF POLYDISPERSITY ON NON-NEWTONIAN VISCOSITY OF POLYMERIC SOLUTIONS

BY M. E. REICHMANN

Chemistry Section, Science Service Laboratory, Canada, Department of Agriculture, Vancouver, B. C.

Received September 26, 1958

Recently some attention has been paid to the specific viscosity and its dependence on velocity gradient and rotatory diffusion constant of solutions of ellipsoidal particles.¹⁻³ Since most of the viscosity measurements are made on polymers with some degree of polydispersity in size, it is of interest to investigate the influence of polydispersity on the $\eta_D/\eta_{D=0}$ vs. α curves.² This is particularly important, if these curves are to be used in conjunction with flow birefringence data for the evaluation of the specific viscosity at zero gradient.³

We have recently tabulated the values of the extinction angle χ as a function of α for a polydisperse system that has undergone random end-to-end aggregation and contained a fraction p of aggregated material.⁴ A similar treatment of $\eta_D/\eta_{D=0}$ (for an axial ratio 300) resulted in the values summarized in Table I, where θ_1 is the rotatory diffusion constant of the monomer. The following assumptions were made.

1. The hydrodynamic volume of the aggregates increases proportionally to the molecular weight. Under these circumstances

$$\eta_D/\eta_{D=0} = \sum c_i (\eta_D/\eta_{D=0})_i / \sum c_i$$

(1) H. A. Seheraga, *J. Chem. Phys.*, **23**, 1526 (1955).

(2) J. T. Yang, *J. Am. Chem. Soc.*, **80**, 1783 (1958).

(3) J. T. Yang, *This Journal*, **62**, 894 (1958).

(4) M. E. Reichmann, *Canad. J. Chem.*, **36**, 1603 (1958).

(5) M. Joly, *J. Colloid Sci.*, **11**, 521 (1956).

(6) R. B. Myers and W. D. Harkins, *J. Chem. Phys.*, **5**, 601 (1937).

TABLE I
 $\eta_D/\eta_{D=0}$ AS A FUNCTION OF α_1 , ($= D/\theta_1$) AT VARIOUS DEGREES OF END-TO-END AGGREGATION p
 (Prolate ellipsoids, axial ratio 300)

$p = 0.05$		$p = 0.10$		$p = 0.15$		$p = 0.20$	
α_1	$\eta_D/\eta_{D=0}$	α_1	$\eta_D/\eta_{D=0}$	α_1	$\eta_D/\eta_{D=0}$	α_1	$\eta_D/\eta_{D=0}$
0.25	0.9903	0.25	.9768	0.25	0.961	0.25	0.939
0.50	.9750	0.50	.9497	0.50	.922	0.50	.889
1.00	.9445	1.00	.9049	1.00	.864	1.00	.820
2.00	.8863	2.00	.8368	2.00	.789	2.00	.734
3.00	.8238	3.00	.7738	3.00	.725	3.00	.675
4.00	.7630	4.00	.7152	4.00	.668	4.00	.621
5.00	.7080	5.00	.6638	5.00	.619	5.00	.574
6.00	.6600	6.00	.6177				
7.00	.6193	7.00	.5793				
8.00	.5842	8.00	.5463				
9.00	.5544	9.00	.5184				
10.00	.5283	10.00	.4939				

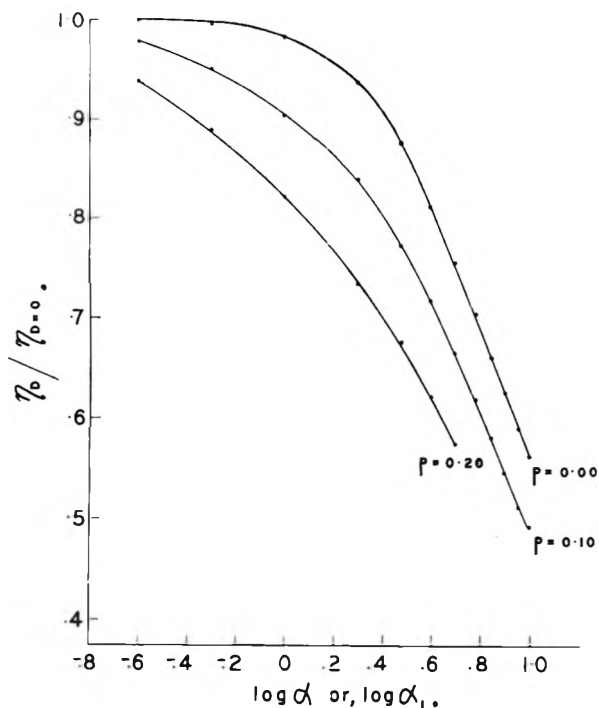


Fig. 1.—Theoretical curves showing viscosity as a function of gradient for monodisperse ($p = 0.00$) and polydisperse system.

2. The parameter α is proportional to the third power of the particle length. This approximation is valid for axial ratios > 5 .³

3. For the evaluation of the contribution of higher terms in the series an extension of Table I in ref. 2 to higher values of α was necessary. A plot of $\log \eta_D/\eta_{D=0}$ showed the latter to be linear in $\log \alpha$ in the range $\alpha = 6 - 60$. The extension of Table I in ref. 2 up to $\alpha = 300$ was made by an extrapolation of this plot. No theoretical justification can be given for this procedure. It should be noticed, however, that in the data in Table I below, the contribution of the terms in which the extrapolated values were used never exceeded 3%. Moreover, for $\alpha = 0-7$ and $p = 0.00-0.10$ the contribution of these terms was 1% or lower.

(5) M. Goldstein, *J. Chem. Phys.*, **20**, 677 (1952).

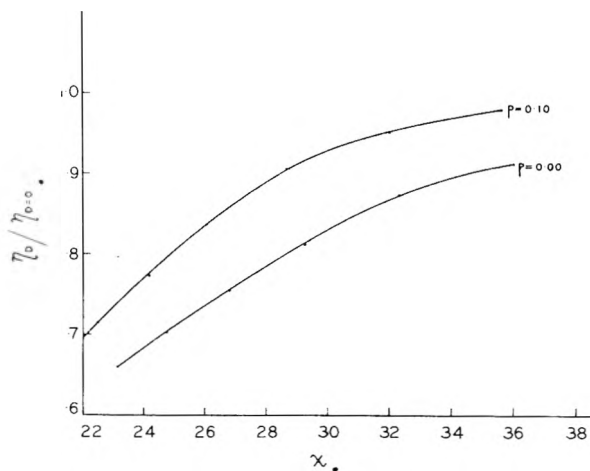


Fig. 2.—Viscosity as a function of extinction angle for monodisperse ($p = 0.00$) and polydisperse systems.

In Fig. 1 $\eta_D/\eta_{D=0}$ is plotted as a function of $\log \alpha$ for a monodisperse system ($p = 0.00$) and for a system containing 10 and 20% aggregated material, respectively. The decrease in $\eta_D/\eta_{D=0}$ at low values of α is sharper for the polydisperse system, resulting in a decrease in curvature. A comparison between the monodisperse and polydisperse system at the same gradients will show that the rotatory diffusion constant of the polydisperse system increases with increasing gradient. This is to be expected since at low gradients the short particles are not yet oriented. The analogy with the χ vs. α curves in flow birefringence is obvious. Quantitatively, however, the effect is not the same as can be seen from Fig. 2. The latter represents a plot of $\eta_D/\eta_{D=0}$ vs. χ for a monodisperse and polydisperse system. At high angles the extinction angle falls off faster with $\eta_D/\eta_{D=0}$ in the polydisperse system, resulting in a divergence of the two curves. At lower angles the two curves converge again. An evaluation of the specific viscosity at zero gradient from combined flow birefringence and viscosity data³ in polydisperse systems would, therefore, lead to erroneous results unless the measurements were made at relatively high gradients.

COMMUNICATION TO THE EDITOR

TWO LIQUID SCINTILLATORS

Sir:

During the course of a systematic study of the relationship between molecular structure and scintillation efficiency, two compounds were observed to exhibit the highly unusual property of scintillating in the pure liquid state. These liquids, methyl anthranilate and ethyl anthranilate, also show marked fluorescence. Dilution with suitable solvents increases the scintillation activity of these compounds as indicated in Fig. 1 which shows the increase in relative pulse height (on an arbitrary

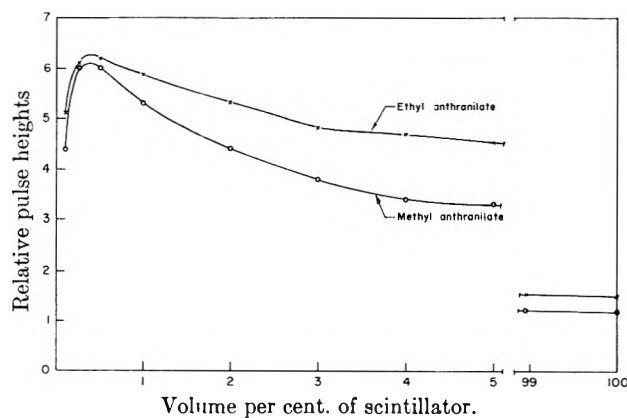


Fig. 1.—Variation in relative pulse heights of liquid scintillators when diluted with toluene.

scale) as these compounds are diluted with toluene. On this same scale, by way of comparison, diphenyloxazole reaches a maximum in relative pulse height of 12.3 in toluene (3 g./l.).

Relative pulse height measurements were made by placing one ml. of the liquid in a one ml. beaker on the face of a Du Mont Type K-1234, 10-stage photomultiplier tube and irradiating with a cesium-137 source which was mounted on a thin Mylar film attached to the top of a hemispherical aluminum reflector.^{1,2}

These compounds offer the interesting possibility of studying the same compound, first, as a solid scintillator, and, second, as a liquid scintillator free from solvent effects. They also afford the opportunity to observe pulse height as a function of temperature as the temperature is varied over a wide range. Of particular interest will be the pulse height variation as the temperature approaches the freezing points.

This work is being supported by the U. S. Atomic Energy Commission under Contract No. AT(11-1)-261.

DEPARTMENT OF CHEMISTRY
UNIVERSITY OF COLORADO
BOULDER, COLORADO

R. N. KELLEHER
JESSE M. CLEVELAND
FRANK BURLINGAME

RECEIVED FEBRUARY 16, 1959

(1) F. Newton Hayes, Donald G. Ott, Vernon N. Kerr and Betty S. Rogers, *Nucleonics*, **13**, No. 12, 38 (1955).

(2) F. Newton Hayes, Northwestern University Conference on Liquid Scintillation Counting, August 20-22, 1957, Evanston, Illinois

New ACS Quarterly

A compilation of fundamental data never before published. Ninety-six pages of material divided into two main subject areas. The first includes articles consisting essentially of data obtained through known concepts, or by known methods, or extensions of such data. The second embraces those articles which list physical properties as an end in themselves, or as aids to other studies or evaluations, and articles characterizing compounds and materials.

Subscription prices:

ACS members \$ 6.00

All others 12.00

Journal of Chemical and Engineering Data

CONTENTS

PART I. PHASE EQUILIBRIA, MOLECULAR TRANSPORT, AND THERMODYNAMICS

- Phase Equilibrium at Elevated Pressures in Ternary Systems of Ethylene and Water with Organic Liquids. Salting Out with a Supercritical Gas.
- Phase Behavior of the System $\text{UO}_2\text{SO}_4\text{-CuSO}_4\text{-H}_2\text{SO}_4\text{-H}_2\text{O}$, at Elevated Temperatures.
- Diffusion Coefficients in Hydrocarbon Systems. Methane in the Liquid Phase of the Methane-Santa Fe Springs Crude Oil System.
- Phase Relations in the Nitric Acid-Nitrogen Dioxide-Water System at Physicochemical Equilibrium.
- Volumetric Behavior of the Methane-Hydrogen Sulfide System at Low Temperatures and High Pressures.
- Thermal Conductivity of Fluids. Nitric Oxide.
- Low Temperature Vapor-Liquid Equilibrium in Light Hydrocarbon Mixtures: Methane-Ethane-Propane System.
- Styrene-Ethylbenzene Vapor-Liquid Equilibria at Reduced Pressures.

PART II. PHYSICAL PROPERTIES AND EVALUATION OF COMPOUNDS AND MATERIALS

- Degradation Studies of Polyethylene Terephthalate.
- Some Anhydride Curing Agents for Epoxy Resins.
- Effect of Temperature on Properties of Aqueous Dispersions of Poly(Vinyl Methyl Ether) Maleic Anhydride Half Amide.
- Solubility of Acidic Gases in Aqueous Monoethanolamine.
- Solubility of Nitrogen in Freon-114.
- Physical Properties of High Molecular Weight Alkylbenzenes and Alkylcyclohexanes.

Back volumes can be purchased from the Special Issues Sales Department, 1155 Sixteenth Street, N.W., Washington 6, D.C.

I/EC



FUNDAMENTALS of PHYSICAL CHEMISTRY

By HORACE D. CROCKFORD, and SAMUEL B. KNIGHT, both of the University of North Carolina. A new treatment that is based upon one of the most successful texts ever written for short courses in physical chemistry. 1959. Approx. 465 pages. Prob. \$7.00.

BIOPHYSICAL SCIENCE

A Study Program

Editor-in-Chief, JOHN L. ONCLEY, Harvard Medical School. Includes new information compiled from the proceedings of the Study Program in Biophysical Science held in Boulder, Colorado in the summer of 1958. 1959. In press.

RESEARCHES in GEOCHEMISTRY

Edited by PHILIP H. ABELSON, Carnegie Institution of Washington. Written by the outstanding men in the field, this book contains discussions on new and important research in geochemistry. 1959. 511 pages. \$11.00.

PRECIPITATION from HOMOGENEOUS SOLUTION

By LOUIS GORDON, Case Institute of Technology; MURRELL L. SALUTSKY, W. R. Grace & Co.; HOBART H. WILLARD, University of Michigan. Gathers together the most important research data on this modern technique. 1959. 187 pages. \$7.50.

BASIC PHYSICS of ATOMS and MOLECULES

By U. FANO and L. FANO, National Bureau of Standards. A systematic treatment of quantum physics which requires no extensive previous knowledge of physical theory or mathematical procedures. 1959. 414 pages. \$8.25.

PHYSICAL LAWS and EFFECTS

By C. F. HIX and R. P. ALLEY, both of General Electric Co. A compilation of physical laws and effects. 1958. 291 pages. \$7.95.

THERMODYNAMICS and STATISTICAL THERMODYNAMICS

By J. G. ASTON and J. J. FRITZ, both of The Pennsylvania State University. First book on thermodynamics to provide new statistical methods for calculating thermodynamic properties of ideally gaseous organic compounds. 1959. Approx. 560 pages. Prob. \$8.25.

HANDBOOK of CHEMICAL MICROSCOPY Vol. I., Third Edition

Principles and Use of Microscopes and Accessories; Physical Methods for the Study of Chemical Problems.

By the late ÉMILE M. CHAMOT, and CLYDE W. MASON, both of Cornell University. The standard text in its field. 1958. 502 pages. \$14.00

ORGANIC SEQUESTERING AGENTS

A Discussion of the Chemical Behavior and Applications of Metal Chelate Compounds in Aqueous Systems.

By STANLEY CHABEREK, Dow Chemical Co. and ARTHUR E. MARTELL, Clark University. 1959. Approx. 596 pages. Prob. \$18.50.

The PHYSICAL CHEMISTRY of STEELMAKING

Edited by JOHN F. ELLIOTT, Massachusetts Institute of Technology. Summary of a 1956 Conference. A Technology Press Book, M.I.T. 1958. 257 pages. \$15.00.

GROWTH and PERFECTION of CRYSTALS

Edited by R. H. DOREMUS, B. W. ROBERTS, and D. TURNBULL, all of General Electric Company. With 51 contributors. 1958. 609 pages. \$12.50.

ELEMENTARY STATISTICAL PHYSICS

By CHARLES KITTEL, University of California, Berkeley. A fundamental exposition of statistical mechanics, including stochastic processes and transport theory. 1958. 288 pages. \$8.00.

Send for examination copies.

JOHN WILEY & SONS, Inc., 440 Fourth Ave., New York 16, N. Y.

1274
9.22